JAERI-M
8971

PROCEEDINGS OF THE US/JAPAN WORKSHOP ON DIVERTORS, FIRST WALL MATERIALS, AND IMPURITY CONTROL

(Exchange A I in the US-Japan Fusion Cooperation Program)

March 17-20, 1980

August 1980

Fusion Research and Development Center

日本原子力研究所
Japan Atomic Energy Research Institute

この報告書は，日本原子力研究所がJAERI-Mレポートとして，不定期に刊行している研究報告書です．入手，複製などのお問合わせは，日本原子力研究所技術情報部（茨城県那珂郡東海村）あて，お申しこしください．

JAERI-M reports, issued irregularly, describe the results of research works carried out in JAERI. Inquiries about the availability of reports and their reproduction should be addressed to Division of Technical Information, Japan Atomic Energy Research Institute, Tokai-mura, Naka-gun, Ibaraki-ken, Japan.

JAERI-M 8971

PROCEEDINGS
OF THE
US/JAPAN WORKSHOP
ON
DIVERTORS, FIRST WALL MATERIALS, AND IMPURITY CONTROL

(Exchange A1 in the US-Japan Fusion Cooperation Program)

March 17 - 20, 1980

Fusion Research and Development Center,
Tokai Research Establishment, JAERI

(Received June 28, 1980)

This proceedings contains the papers presented at the US-Japan workshop "Divertors, First Wall Materials and Impurity Control" which was held at Tokai Research Establishment, JAERI, March 17-20, 1980 under the Auspiece of Science and Technology Agency.

Key words: Divertors, First Wall Materials, Impurity Control, US-Japan Fusion Cooperation Program, Workshop, Proceedings

JAERI－M 8971

報文集：日米作業会「ダイバータ，第一壁材料，不純物制御」

（日米核融合研究協力・交換計画A 1）

日本原子力研究所東海研究所
核融合研究開発推進センター

（1980年6月28日受理）

本報文集は，昭和55年3月17日－20日，科学技術庁主催により，原研東海研究所で行われた日米核融合作業会「ダイバータ，第一壁材料，不純物制御」に提出された論文を集録したものである。

Contents

PROCEEDINGS
OF THE
US/JAPAN WORKSHOP
ON
DIVERTORS, FIRST WALL MATERIALS, AND IMPURITY CONTROL

(Exchange A1 in the US-Japan Fusion Cooperation Program)

March 17 - 20, 1980

Sponsored by

Science and Technology Agency

Hosted by

Japan Atomic Energy Research Institute,
Tokai Research Establishment

FOREWORD

The Divertors, First Wall Materials and Impurity Control Workshop was based on the US-Japan Fusion Cooperation Program which was agreed at the US-Japan Fusion Coordinating Committee last November. The Workshop was sponsored by Science and Technology Agency and held at Japan Atomic Energy Research Institute, Tokai Research Establishment, March 17 - 20, 1980.

This proceedings contains papers and the extended abstracts of presentations and visuals used by the authors. Although we initially intended to allot five pages per paper for Japanese presentations to provide a complete set of notes without overburdening the authors, some of the papers exceeded the allotted pages due to author's enthusiasm.

We would like to express our thanks to all the participants for their active and constructive contributions to the Workshop and to administration staffs of STA and JAERI for their collaborations in carrying out the Workshop successfully. Special thanks are due to Dr. E. Oktay of DOE, Professor A. Miyahara of IPP, Nagoya, and Dr. M. Yoshikawa of JAERI, who provided helpful advices in framing the Workshop.

June 10, 1980

M. Tanaka
Y. Murakami
(Editors, JAERI)

AGENDA

March 17 (Monday) *Chairman: Y. Obata, JAERI*

9:30	- OPENING	Y. Kurihara STA
9:40	- WELCOME	S. Mori JAERI

SESSION I NATIONAL PROGRAM

9:50	- (1-1) Overview of US Programs on Divertors and Impurity Control	E. Oktay DOE
10:35	- (1-2) Overview of Japan Programs	M. Yoshikawa* and A. Miyahara JAERI* and IPP, Nagoya

SESSION II PRESENT AND NEAR-TERM PLASMA EXPERIMENT (I) *Chairman: S. Takamura, Nagoya Univ.*

11:10	- (2-1) ORNL Impurity Studies Program	R. A. Langley ORNL
11:50	- (2-2) Titanium Gettered Wall Experiments on JFT-2	A. Funahashi JAERI

12:30 - LUNCH

SESSION III PRESENT AND NEAR-TERM PLASMA EXPERIMENT (II) *Chairman: N. Inoue, Univ. of Tokyo*

13:30	- (3-1) Impurity Experiments on JIPP T-II	N. Noda IPP, Nagoya
14:10	- (3-2) Monitoring of Radiation Power from HYBTOK-I Plasma with Microchannel Plate	K. Hayashi Nagoya Univ.

14:30 - BREAK

SESSION IV PRESENT AND NEAR-TERM PLASMA EXPERIMENT (III) *Chairman: H. Toyama, Univ. of Tokyo*

14:45	- (4-1) The DIVA Experiment (I)	S. Yamamoto JAERI
15:25	- (4-2) The DIVA Experiment (II)	S. Sengoku JAERI
16:05	- (4-3) Experimental Results on PDX	D. M. Meade PPPL

Chairman: Y. Tanaka, JAERI

16:55 - (4-4) Description of ISX-B Bundle Divertor Experiment — T. Jernigan, ORNL

17:30 - ADJOURNMENT

March 18 (Tuesday)

SESSION V DIVERTOR CONCEPTS AND DESIGN — *Chairman: K. Miyamoto, Univ. of Tokyo*

9:30 - (5-1) Divertor Concept for INTOR-J and its Engineering Feasibility — Y. Shimomura and K. Sako, JAERI

10:20 - (5-2) Poloidal Divertors for Reactors and a Review of INTOR Divertor Studies — D. M. Meade, PPPL

11:10 - (5-3) Bundle Divertor Magnetic Designs for ISX-B, ETF and Reactors — T. Yang, MIT — *Chairman: Y. Gomay, Toshiba*

11:50 - (5-4) Non-Divertor Concepts for Ignition Tokamaks — M. Sugihara, JAERI

12:10 - (5-5) Evaluation of Mechanical Divertors — K. Okamoto, ULVAC Corp.

12:30 - LUNCH

SESSION VI MODELLING — *Chairman: H. Momota, IPP, Nagoya*

13:30 - (6-1) Numerical Simulation of Impurity Transport in Tokamaks — T. Amano, Osaka Univ.

14:10 - (6-2) Numerical Calculations of Helium Ash Enrichment and Exhaust by a Simple Divertor — Y. Seki, JAERI

14:30 - (6-3) Simulation of Scrape-off Plasmas — T. Takizuka, JAERI — *Chairman: M. Wakatani, Kyoto Univ.*

14:50 - (6-4) Analyses of Impurity and α-particle Recyclings in a Tokamak Plasma with Particle Balance Equations — T. Kawamura, IPP, Nagoya

15:10 - BREAK

15:30 - JAERI TOUR

17:30 - RECEPTION

March 19 (Wednesday)

SESSION VII PARTICLE SURFACE INTERACTION — *Chairman: Y. Tuzi, Univ. of Tokyo*

9:30	- (7-1) Overview of US Program on Plasma Wall Interaction	R. A. Langley, ORNL
10:10	- Review Talks from Japanese Institutions	
	(7-2) JAERI (I)	Y. Murakami
	(7-3) IPP, Nagoya	K. Akaishi
	(7-4) Nagoya Univ.	K. Morita
	(7-5) IPCR	Y. Sakamoto
	(7-6) Hokkaido Univ.	M. Mohri
	(7-7) JAERI (II)	K. Kamada
	(7-8) IRI, Nagoya	Y. Ato

Chairman: M. Okada, NRIM

12:30 - LUNCH

SESSION VIII LOW-Z SURFACE COATINGS — *Chairman: Y. Murakami, JAERI*

13:30	- (8-1) Research on Low-Z Material Coatings in National Research Institute for Metals	M. Okada, NRIM
13:50	- (8-2) Review of Low-Z Coating Development Program	R. A. Langley, ORNL

SESSION IX FILM AND POSTER SESSION

14:30	- (9-1) Simultaneous and Continuous Observation of Solid Surfaces under Helium Ion Bombardment (16m/m film)	M. Saidoh, JAERI

14:50 - BREAK

15:10	- (9-2) Measurement of Chemical Sputtering Yield of Various Types of Carbon	R. Yamada, JAERI
	- (9-3) Reduction of Partial Sputtering Yield of Metal Atoms from VC and NbC by Ion Induced Precipitation of Carbon Layer at the Surface	K. Morita, Nagoya Univ.
	- (9-4) Conditioning of Graphite Surface by Atomic Hydrogen	T. Abe, JAERI

(Cont'd)

- (9-5) Conditioning of Graphite Surface by Atomic Hydrogen	K. Akaishi IPP, Nagoya
- (9-6) Physical Vapor Deposition of Low-Z Materials	S. Komiya ULVAC Corp.
- (9-7) Preparation and Properties of Carbon Films with Magnetron Sputtering	H. Kitahara ANELVA Corp.

17:00 - ADJOURNMENT

March 20 (Thursday)

SESSION X FIRST WALL MATERIAL DEVELOPMENT PROGRAM *Chairman: A. Miyahara, IPP, Nagoya*

9:30	- (10-1) Material Studies Related to Divertor Operation and TFTR First Wall	J. Ulrickson PPPL
10:15	- (10-2) Summary of JT-60 First Wall Development Program	H. Nakamura JAERI
11:00	- CLOSING	M. Tanaka* and E. Oktay JAERI* and DOE

11:30 - LUNCH

OPENING REMARK

Y. Kurihara (STA)

Good morning, Gentlemen.

It is our pleasure to have an opportunity to hold this Workshop with many participants including six specialists from the United States of America.

I would like to express our sincere welcome to all participants.

As you know, this Workshop is based on the Exchange Program of Japan-U.S. Cooperation on Fusion Research and Development. I understand that impurity problem is one of the most important barrier to be overcome for a realization of Fusion Power Reactor. So, I hope this Workshop will be significant step on this problem through lively discussion and information exchange among your specialists and accelerate the cooperation between Japan and the United States of America on Fusion Research and Development.

Finally, I would like to express our sincere gratitude to those who have spent a great effort in preparing for this Workshop, especially, to Dr. Oktay, Dr. Tanaka and JAERI staffs.

Thank you.

WELCOME SPEECH

S. Mori (JAERI)

It is my great pleasure to welcome you at this TOKAI Research Establishment.

When I was asked to make a speech of welcome to the US-Japan Workshop on impurities, my first idea was the speech should be in Japanese, which reflects equal participation of United States and Japan.

However, I suppose, it is generally quite unusual to welcome guests with an un-understandable and thus irritating speech.

Thus my choice is to select a third language; that is other than Japanese and English. Fortunately, "broken English", which is quite different from American English and Queen's English, is authorized as common language in over-developed countries.

It is very natural that you have a lot of difficulty in understanding my speech, because it is in broken English.

The themes of this Workshop are impurities, plasma/wall interaction and divertors & impurity control. The impurities are related to phenoma, plasma/wall interaction to physics and divertors & impurity control to counter-measures.

Impurity problems were highlighted some 5 years ago, which were thought to be a major barrier to attain reactor-grade plasmas in tokamaks.

Recent progress on these problems has been very remarkable and, as the results, we are now in the state of the art that we can discuss phenomena, physica and counter-measures simultaneously.

In this connection, I remember and cannot forget a gloomy experience in toroidal confinement study before 1965. We had been blocked by "pumpout" phenomena for about ten years, which has been necessary to pass through the phenomena.

Contrarily, in five years, we have passed through the phenomenological state of impurity research and are able to discuss counter-measures to them; we even could delineate a long-burn scinario in INTOR and ETF, in which impurity control is indispensable.

Now, generally in fusion research, our physics understanding, technology, and experiences have been accumulated to the high level, and thus the progress has become very rapid. It can be expressed as

$$d(\text{progress})/dt = \alpha E ,$$

where E = physics + technology + experiences.
However, as we accumulate E, we have recognized a second negative (decelerating) factor, that is

$$d(\text{progress})/dt = \alpha E - \beta E \times \text{Yen} .$$

The second factor emerges as our devices become larger and more delicate in proportional to E. When our E is small, we did not encounter this second factor. But, our E has become so large that the second factor is now evident.

The objective of this Workshop is to increase E, physics understanding, technology and experiences, on impurity-control by direct discussion of experts in US and Japan.

And, also active spirit of cooperation on both sides in this Workshop, the same as we experienced in every cases under the US-Japan cooperation agreement, will result in decreasing or eliminating this second negative factor by jointly funding big projects.

I hope you will have a stimulating Workshop and pleasant time here at Tokai.

Thank you for your attention.

1 - 1 An Overview of the U.S. Program on Divertors and Impurity Control

Erol Oktay
U.S. Department of Energy

In this overview, I would like to discuss the following:

- A brief review of the U.S. Fusion Program
- Description of the U.S. Tokamak Facilities
- Perspectives on the Workshop topic and on the related issues
- Description of the experimental programs on Divertors and Impurity Control

The U.S. program in fusion is funded and managed primarily by the Office of Fusion Energy, Department of Energy. An organization chart for the OFE is shown in Fig. 1. The Office is under the leadership of Ed Kintner and his deputy, Dr. John Clarke, and it is presently divided into four Divisions:

- Div. of Confinement Systemshas the primary responsibility for planning and operation of major experimental facilities on the Tokamak and Mirror concepts.

- Div. of Development and Technology has the responsibility for materials and component development for the next generation of experiments and test facilities, and for reactor system studies.

- Div. of Applied Physics provides theoretical and computational supports for all of the fusion program. Also, small scale plasma physics experiments, such as those at universities, and Advanced Fusion Concepts such as Reversed Field Pinches, Stellarators, Compact Tori are managed by this Division.

- Div. of Planning and Projects has the responsibility for long term planning and for construction of large projects such as TFTR, MFTF and FMIT. The operation of experimental programs on these devices will be managed by Confinement Systems (TFTR, MFTF) and Development and Technology (FMIT).

All of these Divisions are involved with activities that relate to the subject matter of this Workshop. The broad topic of impurity control, divertors, and first wall materials is a major issue for the tokamak because of its closed geometry. As it will be discussed extensively at this Workshop, tokamak is the concept on which these major issues are being addressed and experimental investigation are being carried out.

Both linear (tandem mirror) and toroidal (bumpy torus) concepts are being pursued in the mirror program. Also, reversed field mirror concept, which is a compact torus and a hybrid between toroidal and linear systems, is being investigated. The impurity issues in these three geometries are different. In the open ended linear systems, the standard impurity concerns of the tokamak system have not been considered as a serious issue. In the bumpy torus system, in which the problems are likely to be similar to those in tokamak, impurity control issues are being discussed and a divertor program is being initiated. The compact torus is in the early stage of concept development and it has not matured to the point where impurity control issues can be identified.

A major topic in this Workshop is surface physics. Programs in this area are managed by the Materials and Radiation Effect branch. Component development for divertors, such as target plate, is being managed by the Components Branch. Design of reactor systems and their divertor systems, managed by the Reactor System and Application Branch provides guidance to the current program on divertors.

Div. of Applied Physics provides theoretical and computational support, and funds university tokamak program, such as that at UCLA, which has made significant contributions to the surface preparation techniques.

Finally, the construction of devices such as TFTR, which requires development of limiter, is providing valuable contribution to the evolution of the impurity control program.

The U.S. laboratories involved significantly with the fusion research and development are as follows:

PPPL - Tokamak Experiments (PLT, PDX, TFTR)
Advanced Fusion Concept Experiment (Spheromak)
Theoretical and Computational Studies

ORNL - Tokamak Experiments (ISX-B)
Bumpy Torus Experiment (EBT)
ETF Design Center
Theoretical and Computational Studies
Major Technology Development Center (superconductor, neutral beams, fueling, etc.)

LLL - Mirror Experiments (MFTF, TMX, BERA-II)
Mirror Theory and Computations
Mirror Technology Development (superconductors, beams, pumping, etc.)

LASL - Advanced Fusion Concepts (RFP, Compact Toroids)
Theoretical and Computational Studies
Technology Development (tritium systems, accelerators for FMIT)
MIT - Tokamak Experiment (ALCATOR)
GAC - Tokamak Experiment (D-III)

Smaller fusion programs are pursued at

- Argonne National Laboratory (reactor studies, materials)
- Sandia Laboratories (materials)
- Brookhaven National Laboratory

and at

- Universities: Univ. of Texas
  UCLA
  Wisconsin
  Colombia Univ.
  Cornell Univ.
  Univ. of Maryland

In addition, various industries are being involved with the fusion program.

The basic machine parameters of the major tokamaks in operation in the U.S. program, and their contributions to the U.S. program on Impurity Control, Divertors and First Wall Materials are shown in Fig. 2.

PLT (PPPL) is the oldest major tokamak in the U.S. program. It has been in operation since Dec. 1975. Major objectives for this device have been to investigate confinement and heating (initially 3 MW of neutral beams and now 5 MW of ICRF and 1 MW of LHH). There has been specific surface physics studies program on this device using a surface analysis station. In addition, a large volume of data has been obtained on various impurity control issues as a part of the effort to achieve high performance on the device. Significant plasma heating (T_i~6 keV, T_e~4 keV) and long confinement time (~100 ms) were achieved on this device. Such achievements have been possible by optimization of impurity control methods (surface preparation, plasma start-up and material choice) without the benefit of an active impurity control system. Therefore, PLT contribution to the basic understandings of the impurity control issues has been significant. We will find in all devices that as they are operated for a number of years and as they reach their goals, their implicit contribution to the program will increase.

ISX-B (ORNL) was initially designed and operated for impurity studies experiments. The initial device, ISX-A, was converted to ISX-B in Oct. 1978

to continue impurity studies and also to investigate high-β issues in tokamaks. There are specific impurity programs on this device which include surface studies, coated-limiters, edge diagnostic development, and impurity flow experiment. The major impurity control program on this device is the investigation of bundle divertors which will be installed in Nov. 1980 - April 1981.

PDX (PPPL) was specifically designed for the investigation of poloidal divertor concept. It has been in operation for about a year. There are other programs such as coated limiters, surface analysis station and surface preparation techniques. The recent result will be discussed by Meade.

Alcator-C (MIT) is a modest-size device designed to investigate high field confinement with toroidal field up to 140 kG. Consequently, it operates at densities ($\sim 10^{15}$ cm^{-3}) higher than the other tokamaks, and relies on surface preparation technique to achieve high purity. Its predecessor, Alcator-A, was the first tokamak to achieve $Z_{eff} \simeq 1$ four years ago, using surface cleaning techniques and also by operating at high density. High-field, high-density characteristics of this device limit plasma heating to ohmic heating and R.F. (LHH and ICRF).

D-III (GAC) was designed to investigate shape optimization to obtain high betas. It produces doublet and Dee-shaped plasmas in addition to circular plasma. This device has been in operation about 18 months. There is an active cooperation between the U.S. and Japan fusion programs on the D-III facility. Like on the other devices, there are a number of investigations of impurity control issues on this device. Some of these are coated limiters and surface preparation techniques. Its unique vacuum chamber has given the motivation for investigation of expanded boundary approach to impurity control.

TFTR (PPPL) is under fabrication and it is scheduled to begin operations at the end of 1981. Since there will be D-T operation and high power neutral beam injection, some of the major issues in heat removal, recycling, limiter design, etc. are being addressed in this program.

In addition to these large tokamaks, there are three smaller devices in the U.S. which are providing useful data to the impurity studies program. These are MACRATOR at UCLA (surface preparation techniques), OCTUPOLE at Wisconsin (E×B and poloidal divertor) and APEX at Argonne National Laboratory (surface physics and diagnostics). These studies on small devices show that there are still a number of issues that are investigated on small devices in order to have maximum flexibility in carrying out the experiments.

The next topic is on the relevance and importance of the Workshop topic to the overall fusion program. Design of impurity control system has been identified as a significant unresolved issue for the next generation of tokamaks such as INTOR and ETF. The economics of fusion reactors depend, among other factors, on the simplicity and effectiveness of the divertor systems.

In fact, impurity problem has been an issue for the fusion systems throughout the development of the fusion program. Solution to these problems, however, at each stage of the fusion development has made it possible to make significant progress. For example, the tokamak concept experienced significant advancement in the USSR in late sixties after change over from dielectric vacuum vessel to metal vessel. Excessive radiation by low-Z impurities (O, Si) from dielectric vessel limited temperature to be low hundred eV. Changing to metal vessel pushed this limit to the keV regime. The temperature limit in the keV regime resulting from high-Z impurities was then exceeded in PLT by going to carbon limiters. While all of the processes in these cases might not be fully understood, their advances are somewhat tied to the solution of the impurity problem peculiar to that stage of the development.

As the fusion program evolves towards the next generation of tokamaks such as TFTR, JT-60, INTOR and ETF, there will be new impurity problems and we have to have new solutions. We have to find ways to reduce impurity levels in order to operate these devices for long pulses to reach ignition, and to be able to remove heat and alpha ash.

The importance of the Workshop topic can also be gauged by the attention it receives. Within the last year there have been several forums on this topic. Some of these are as follows:

- International Workshop on INTOR (Impurity control issues have been discussed extensively and these discussions have provided significant impact to the field.)
- NATO Advanced Summer Institute, Aug. 1979, France, on the topic of "Atomic and Molecular Physics Relevant to Controlled Thermonuclear Fusion Reactors" (Some of the basic atomic and fusion physics of impurity problems were discussed.)
- IAEA Technical Meeting on Impurities in Tokamaks, Oct. 1979, Alushta, USSR (discussion of international programs, identification of issues)
- Workshop on Tokamak Impurity Control Issues, Feb. 1980, Washington, D.C. (discussion of U.S. program, and information exchange)
- Surface Physics Meeting at Garmish to be held in April 1980 (will have significant relevance to the topic of this Workshop.)

The general conclusion from all of these forums is that while there is significant progress being made, much more needs to be done, both experimentally and theoretically on the impurity control issues, and new relevant technologies must be developed. It is through these meetings and workshops that we have the opportunity to discuss what we are doing, what perspectives are on the problems, and how to find solutions. Hopefully, these discussions will lead to a better definition and understanding of the problems which is essential for their timely solution.

What are the Divertors, First Wall Materials, and Impurity Control issues? First of all, the primary objectives in this broad program are to develop methods for

- o exhaust of helium,
- o removal of plasma heat, and
- o reduction of impurity levels in the plasma.

For various reasons, it is desirable to operate reactors for long pulses. Therefore, helium (by-product of D-T reactors) must be removed from the plasma after its energy is reduced; otherwise, plasma-burn can quench by fuel depletion, or by exceeding beta limits resulting from He-contribution to beta.

Ideally, the plasma heat should be removed in a remote chamber in order to avoid impurity generation resulting from plasma-material interaction, and to facilitate heat removal. In present devices, there is evidence of impurity introduction to plasma resulting from plasma-limiter or plasma-wall interactions. In reactors, such impurity production mechanisms should be avoided.

Finally, impurity level should be reduced in the plasma in order to avoid excessive radiation loss which can prevent ignition. This issue has been studied extensively and some of the relevant results [ref. Jensen et al, Nucl. Fusion 17 (1977) 1187, and Jensen et al, Nucl. Sci. 65 (1978) 282] are shown in Fig. 3. These indicate that the required value of $n\tau$ for ignition increases significantly as impurity concentration is slightly increased beyond a certain level. In Fig. 4, tolerable concentrations of impurities for ignition as a function of the value of Z are shown. High-Z impurities must be kept at very low levels.

The objective of reducing impurity levels can be accomplished by

- o identifying the sources of impurities and the mechanisms by which they are produced,
- o understanding physics of impurity transport, and by
- o developing active impurity removal system.

It appears that divertors designed for helium exhaust and heat removal will also remove impurities.

The primary sources of impurities are walls and limiters. The impurities are categorized as low-Z and high-Z impurities. The low-Z impurities (C and O) are present on the material surfaces as surface layers and also at sub-surface layers as oxides. The high-Z impurities are of course from the metal the walls or limiters are made of.

The release of impurities from walls and limiters occurs as a result of numerous activities such as evaporation, melting, arcing, sputtering, etc. The intensity of plasma-wall interaction determines which types of these impurity release mechanisms take place and whether the source of impurities is surface layer or sub-surface layer elements, arcing, etc. Investigation of these topics is the subject of surface study program and they will be reviewed by Langley at this Workshop.

The other factors that contribute to the impurity production mechanism are the manner in which the surface are prepared for plasma discharge. There have been significant amount of development in this area on all devices as a part of their routine programs. Some of the surface preparation techniques include pulsed discharge cleaning, glow discharge cleaning, Taylor discharge cleaning, baking, gettering, and coating.

It should be noted that significant progress has been made in the past four years in the areas of material selection and surface preparation techniques. In 1974 there were only two tokamaks with $Z_{eff} \approx 1$, Alcator (discharge cleaning) and ATC (gettering). Nowadays, almost all of the tokamaks have succeeded operation with $Z_{eff} \approx 1$. Further developments are required, however. Almost each device has its own procedures for surface preparation and operation which cannot yet be characterized as well defined engineering procedures. These procedures should be developed to a level where they can be transferred from one device to another.

A next step control on the plasma impurity concentration involves plasma start-up procedures. For example, it has been shown on PLT [ref. R. Hawryluk et al, Nucl. Fusion 19 (1979) 1307] that rate of gas influx can be used to optimize current profile which affects impurity levels, maximum density, temperature, etc. In these experiments it has also been shown that ultra-soft X-ray emission decreases with a decrease in edge temperature. In Doublet-III it has been shown recently that programming of current rate of rise affects impurity levels in the plasma. The conclusion from these is that there is intimate plasma-wall contact at all times. The effect of

manipulating the intensity of this contact (by edge cooling, profile shaping, current, etc.) is observed on the plasma parameters and in radiation intensity, and in the exact repeatability of the discharge. It is desirable to reduce the effects of plasma-wall contact on plasma operation by reducing recycling and impurity release. To do so, however, requires a better quantification of the plasma-wall contact processes.

Assuming that the above mentioned processes are understood and improved to reduce the impurity levels in plasma, there will still be some level of impurities introduced into the plasma at the plasma edge. The next issue, then, is how these impurities are transported. Some of the impurity particle transport issues are as follows:

- Is the particle diffusion inward or outward?
- Do the impurities cycle through the plasma or do they accumulate?
- How do some procedures such as neutral beam or R.F. heating effect transport?
- How good is the coronal equilibrium model for predicting radial distribution of impurity?

and there are many more theoretical issues.

There is some study on all of the devices that touches on impurity transport. Some of the recent results on this topic were obtained on PLT, ISX-B, and ALCATOR. In ISX-B, there is some indication that neutral beam heating reduces impurity accumulation which is observed in discharges without injection. On the other hand, the experiment on ALCATOR, in which Si is injected into plasma by laser abrasion, there is no accumulation. The impurity confinement is tied to the plasma confinement time. Flow reversal experiment on ISX provides another set of data on the impurity transport [ref. K. Burell]. In ISX-A, there were positive results on the neo-classical behavior of impurities whereas results in ISX-B show an accumulation effect. It appears that surface conditioning (gettering in ISX-A while no gettering in ISX-B) is affecting the results.

All of these activities described above on impurity control are in progress on these devices. Further discussions of these results at this Workshop have not been possible because of the limited representation in the U.S. team. We hope, however, these can be discussed in a follow-on Workshop which we propose to hold in the U.S. next year.

As mentioned before, there will be some impurity level in the plasma. It appears essential that heat removal and helium exhaust be accomplished by a "divertor" and such a system can also sweep out impurities. The primary

issues in this area are as follows:

- o Are magnetic divertors essential, and can the objective be accomplished by non-magnetic approaches?
- o If magnetic divertors are essential, what type (bundle, poloidal, hybrid, and others) can be used? There are a large spectrum of physics issues with all these different divertors.
- o What are the feasibility and physics and technology issues associated with non-magnetic approaches (expanded boundary E×B divertors, large area limiters, streaming pellets, etc.).

In addition, in the issues in helium exhaust and heat removal, there are a variety of questions such as selective helium pumping, fuel and impurity recycling, heat load on divertor plate, etc. These will require experiments with high-power density systems and development of special techniques. The current experimental program on divertors include PDX (to be discussed by Meade) and bundle divertor on ISX-B (to be discussed by Langley) and a general divertor program at MIT (to be discussed by Yang). The limiter studies associated with TFTR will be discussed by Ulrickson. In addition to these, there are studies and activities at GAC, Wisconsin, and UCLA as mentioned at the beginning of this presentation.

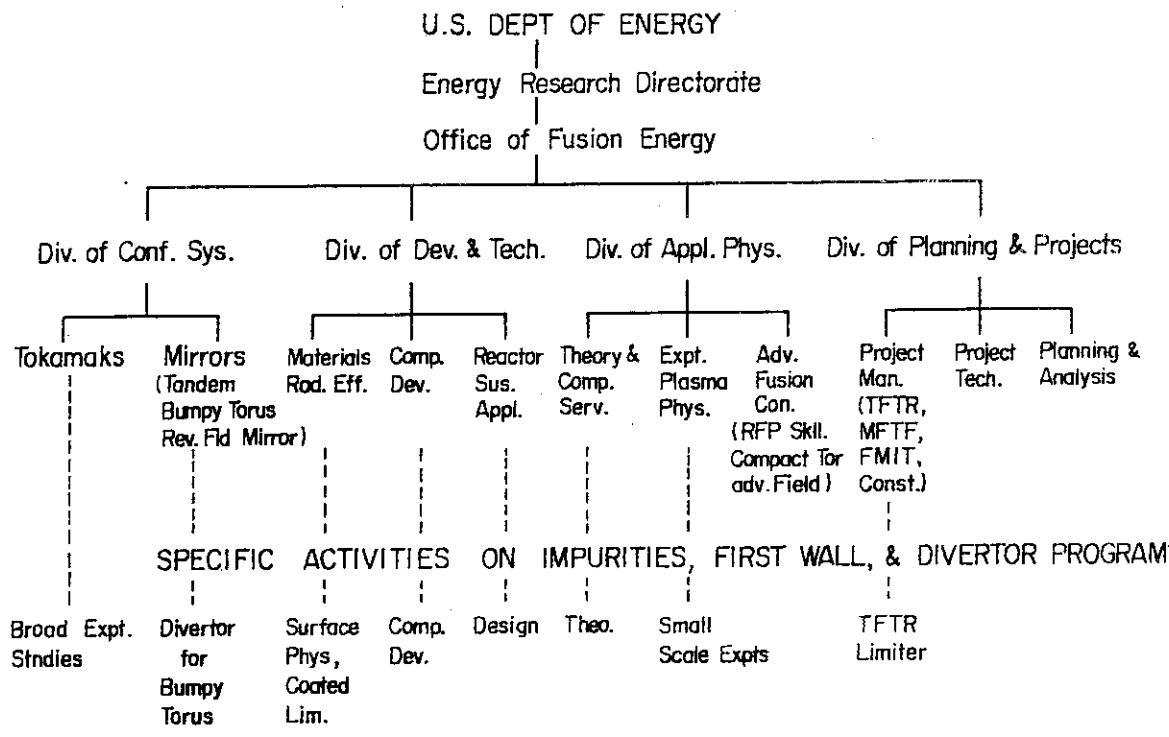

Fig. 1 Organization chart for Office of Fusion Energy, DOE

	a (cm)	R(cm)	B_T (kG)	I_p(kA)	Aux. Htg	Maj. Prog. Obj.	Imp. Related Activities	
PLT (PPPL)	45	130	45(32)	1000 (550)	NB (3MW) ICRF (5MW) LHH (1MW)	Confinement Heating	Surface Phys. Imp. Transport Plasma Startup	Te ~ 4 keV Ti ~ 6 keV τ ~ 0.1 sec
ISX-B (ORNL)	27x54	90	18	200	NB (3MW) ECRH (0.2MW)	Imp. Studies High-β Non-circular	Surface Phys. Coated Limters Flow Reversal Edge Diag. Bundle Div.	$\langle\beta\rangle$ = 2.3 % β_0 ~ 8 %
PDX (PPPL)	45 x	145	24	500	NB(6.5MW) ICRF ECRH	Poloidal Div. High-β	Div. Expts Coated Lim. Surface Phys.	Pol. Div. Config. Established & Sustained
ALCATOR-C A (MIT)	17	64	140	1000	LHH(4MW) ICRF	High Fld Conf. LH heating	Plasma-Wall Int. Coated & Inst. Lim Imp. Transport	$n\tau$ ~ 3×10^{13} cm^{-3}·sec
D-III GAC	45x150	143	26	1000	NB(7MW) ECRH	Shape Opt. for high β	Coated Lim. Imp. Flow	High plasma Current (2.5MA) Coop. w/GOJ
TFTR (PPPL)	85	250	52	2500	NB R.F.	Dem. Q=1 D-T Operation	Limiter & First Wall Mat'l Stud.	Under Const. Op. Dec. 81

Fig. 2 Design parameters and program objectives of major US tokamaks

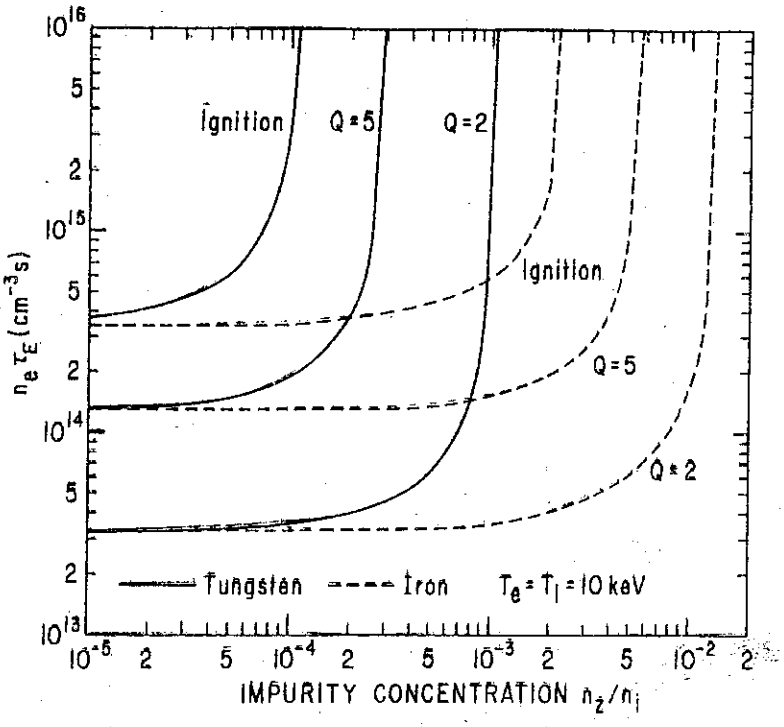

Fig. 3 nτ vs. impurity concentration for Q = 2, 5, and ignition

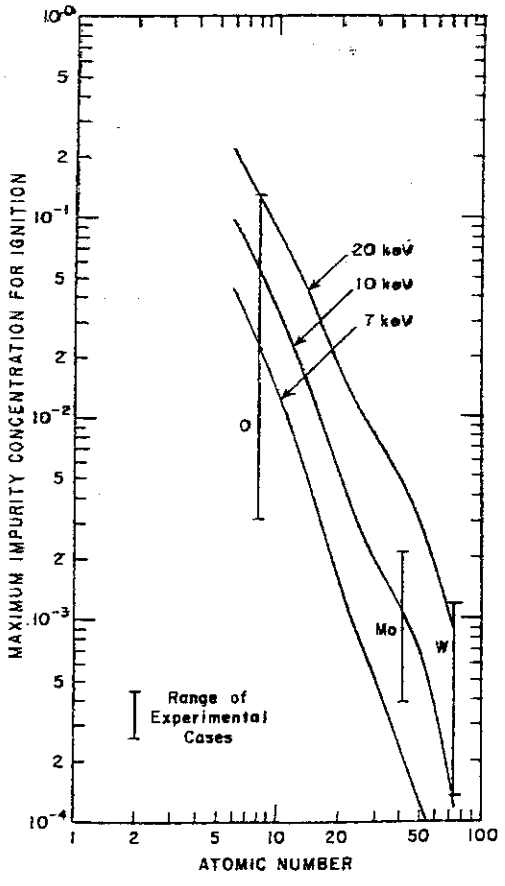

Fig. 4 Tolerable concentration of impurities for ignition as a function of Z.

1 - 2 OVERVIEW OF JAPAN PROGRAMS ON PLASMA WALL INTERACTION UNDER SCIENCE AND TECHNOLOGY AGENCY

Presented by M. Yoshikawa, JAERI

Plasma-Wall Interaction Program under Science and Technology Agency (STA)

— Japan Atomic Energy Research Institute
(JAERI) : 12 + (30) people

— Electrotechnical Laboratory
(ETL) : 10 people

— Institute of Physical and Chemical Research
(IPCR) : 6 people

— National Research Institute for Metals
(NRIM) : 6 people

— Industrial Research Institute, Nagoya
(IRI-Nagoya) : 8 people

Major Devices

	Plasma Devices	Accelerators/Ion Sources (1 MeV — 100keV — 10keV — 1keV)	Coating Devices
JAERI	JFT-2, D-III JFT-2a/DIVA[1] JT-60[2] JVX-1 chamber[2]	HSP (30 - 400 keV) VdG (20 MeV) Hi Cur. Ion Sce (up to 30 keV) LSP (0.1 - 6 keV)	RF In-Situ Coating
ETL		VdG (3 MeV)[1] Ion Source (up to 300 keV) Pelletron (4 MeV)[2] Ion Source (10 keV)	
IPCR	IPCR-1 chamber IPCR-2 chamber	Ion Source (up to 30 keV)	
NRIM			Ion Plating CVD, PVD
IRI-Nagoya		VdG (2 MeV) Ion Source (20 - 200 keV) El. Linac (10 MeV)	

1): shutdown 2) under construction

AES Th.Cycl.

AES μ-pm

AES. Th Cycle) at 1000°C

Tasks for Plasma-Wall Interaction Program

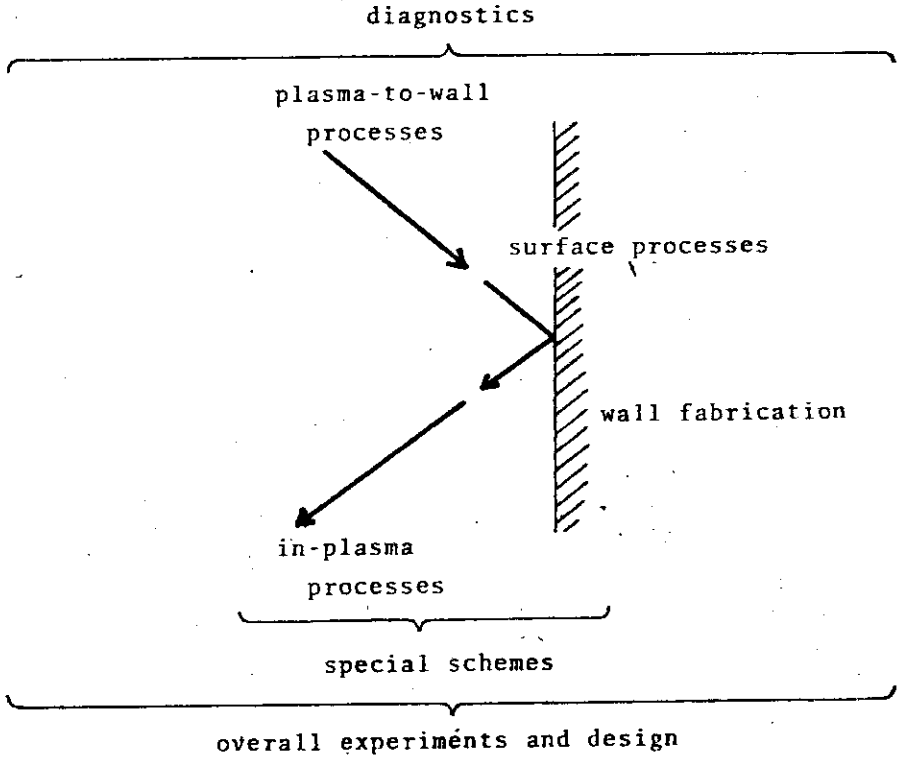

SURFACE PROCESSES

JAERI : SPUTTERING H^+, H^0 : Mo, C, Low Z
BLISTERING etc He^+ H^+ : Mo. C
RECYCLING H^+ : Mo
[REFLECTION/ TRAPPING / REEMISSION/ PCL-INDUCED DESORPTION]

ETL : RECYCLING He^+ : Nb, Mo, V, Al, Cu, N; Ta
[RANGE, RESIDUAL DAMAGE, REEMISSION]
TRAPPING
SURFACE DAMAGE: RARE GAS IONS : CuNi, SS

IPCR : RECYCLING H^+ (IPCR-3 chamber)
[trapping]

NRIM : SPUTTERING

IRI, Nagoya : SPUTTERING : He^+, H_2^+ on SiC, Glassy C.
BLISTERING etc : He^+ on SiC

Overall experiments

— JFT-2 (JAERI)	Ti-Coating C-Limiter Limiter Observation Impurity Transport
— JFT-2a/DIVA (JAERI)	Divertor Ti-Coating C-Limiter C-Coating Gas Injector
— Doublet III	Ti-coating C-limiter/armour

Overall design

— JT-60 (JAERI)	Magnetic Limiter First Wall Low Z Coating
— JT-4 (JAERI)	Divertor Coating
— EPR and INTOR (JAERI)	Divertor Non-Divertor First Wall

Special Schemes

— Divertor Magnetic Limiter	JAERI	JFT-2a/DIVA DOUBLET III (JT-4) JT-60 Doublet IV
— Non-Divertor Special Limiter	JAERI ULVAC	INTOR WS, PETF
Edge Cooling	JAERI	JXFR
— HONEYCOMB	JAERI ULVAC	JT-60 P.E.L.

Wall Fabrication and Conditioning

Coating	JAERI	In-Site Coating by RF Source and Disch. [Mo, Low Z]
		Precoating [Low Z]
	NRIM	CVD, Ion-Plating [SiC, Si_3N_4]
	IRI, Nagoya	CVD [SiC]
Bulk	JAERI	Low Z
Conditioning	JAERI	Oxygen and Hydrogen Gas Cleaning [Mo]
		Taylor Disch. Cleaning
		ECRH Disch. Cleaning
		Active Hydrogen Conditioning [C]
	IPCR	ECRH Disch. Cleaning

PROCESSES IN PLASMA

(JAERI)

TRANSPORT

ATOMIC, MOLECULAR & IONIC PROCESSES

SCRAPE-OFF LAYER

SPECTROSCOPIC

BOLOMETRIC & T/C

NEUTRAL POLES.

GAS PRESSURES AT BOUNDARY

EL. STATIC PROBES

THEORY & COMPUTATION

EXPERIMENT

1 - 2 OVERVIEW OF JAPAN PROGRAMS OF PLASMA WALL INTERACTIONS IN UNIVERSITIES LINKAGE ORGANIZATION

PRESENTED BY AKIRA MIYAHARA

INSTITUTE OF PLASMA PHYSICS

NAGOYA UNIVERSITY, 464 NAGOYA JAPAN

1) Organization

As the oversiew of Japanese activities on plasma wall interaction problems in universities linkage organization, first of all, I have to explain the role of Institute of Plasma Physics, Nagoya University. This institute was founded in 1961, as the key institute of Japanese universities organization by the support of fusion community. The location was determined, closed to the center of gravity of the plasma physicist distribution in NAGOYA city. Since then, IPP was operated as cooperative research facility and in principle, every Japanese plasma physicist can use devices that belongs to IPP. In this sense, IPP is closely related to every university, and in average from one university 150 man-days of exchange has done in fiscal year 1979, only for one subject of surface diagnostics. At the moment, collaborations of JIPP-T-II plasma surface interactions problems and surface characterization studies by various surface diagnostics are main collaboration thema.

Another important facility belongs to IPP is Research

Information Center. One of the objectives of the Research Information Center is to collect, compile and evaluate data on plasma wall interactions relevant to nuclear fusion research. To meet the objective, the Center has organized the Working Group on plasma wall interactions. This Working Group is headed by Prof. N. Itoh of Nagoya University and consists of about twenty scientists belonging to various institutions all over Japan. Four subgroups are now active, each dealing, respectively, with sputtering, blistering, reflection and desorption, and photoelectric effects. Among these subgroups, that for sputtering is ahead of the others.

The detail descriptions of this will be given by Dr. K. Morita later, but I mention the sputtering subgroup has chosen as the first task the collection of the ion-sputtering yield as a function of the incident energy. Experimental data on sputtering yield for all the elements (both for projectiles and for targets) and for a wide range of energies have been already collected and stored in a computer. The subgroup is making an effort to evaluate those collected data and therefrom to derive a semiempirical sputtering formula useful in fusion research. From this result, we recognize that some combinations of projectiles and targets do not fit this formula. These data must be checked by experiments.

Plasma-Wall Interactions problems must be studied from both side of research namely side of plasma physics and material side. About material side, from fiscal year of 1980, special grant-in-aid under the new category of fusion problems will be commenced. Although first year budget is small amount of money of 3×10^7 yen, it will make more tight coupling between university's activities. The first problems we took are,

1) Problem definition of plasma wall interaction
2) Investigation of ion sputtering along the guide line of sputtering working group of Research Information Center. (incl. material coating development)

Further problems of Hydrogen istope recycling, tritium inventory and modified surface will be treated in near future. Besides this, sample characterization group chaired by Prof. G. Tominaga had started including accelerator group and other ultra high vacuum specialist. Preparations of well defined samples at industry of stainless steel sheet and tube are cut and marked at IPP and distributed to universities and national laboratories. The materials are produced not as samples but industrial uses. The surface characterizations of so called the same samples have been done by various universities, and results of analyses are collected and discussed. It turns about this is very good procedure for checking surface diagnostics of each laboratories as the first step. Also surface characterizations of molybdenum as limiter material have been done at IPP by various preparation method. The results shows after the 850°C backing of 1 to 3 min., differences are not serious, but with only low temperature of up to 350°C, differences between them are remarkable. These sample and surface characterization efforts by various universities are very good preparation for further collaborations.

At last I must touch upon the interaction between MOE and STA. The strongest interaction is we took as the reference, DIVA group's interpretation of plasma surface interactions.

The first priority of ion sputtering study at universities linkage organization is started from this. Another examples of interactions can be seen in Wednesday Lecture.

2) Individual activities

Almost all activities of Japan about this problem will be given in this seminar, so I must only mention some items that missed this seminar.

About plasma wall interaction study using Tokamak device at universities are preparation stage during last year. For instance, at JIPP-T-II, surface analysis station has been prepared, together as pilot experiment for Textor international collaboration, which will be installed ISS, AES, MF and Roughness Facter measurement. Also at Kyushu University, TRIAM Tokamak intended to do plasma wall interaction study.

Another topics of plasma surface study has been done by Dr. A. Mohri at IPP. It was experimentally demonstrated that high power irradiation of ions on metal surface can be made by using 'Plasma Anode' for electron beam generation. The irradiation power of 600 keV protons was 50 $MW \cdot cm^{-2}$ which is comparable with pulse power loading of CTR tokamak first wall at a strong major disruption. Damage of 304 stainless steel by this irradiation was different from by usual irradiation of ions at low power level.

3) Conclusion

Surface studies for fusion research have dual aspect of the near and long term projects, because surface conditions have strong influence on plasma situations, vice versa. For this reason, discussions on the problem definitions are very important, since very often, distorted argument of

experimental results and conceptual design studies misled the research directions. This problem takes priority of the next workshop on surface study.

Another points are applications of Tokamak devices for surface studies. At the moment, not sufficient number of Tokamaks are in operation with sufficiently good plasma parameters, and moreover each Tokamak has its specific character.

Tokamaks JIPP-T-II, ISX-B, and TEXTOR must be utilized in the frame work of US-Japan or International collaborations, or else we can not expect rapid development for wall materials. These problems become more serious in future for upgraded Tokamaks. Some irradiation facilities, for instance multi-beam sources, must be considered also, because usually samples are easily transportable.

Sample characterizations are required to compare the results of study between two countries. Perhaps surface characterizations play more essential role but as the first step, sample and pretreatment method must be characterized. Through these efforts, we can also compare and identify surface diagnostics in both countries.

2 - 1 ORNL Impurity Study Program*

Robert A. Langley

Oak Ridge National Laboratory
Oak Ridge, Tennessee 37830 USA

The goal of the Oak Ridge National Laboratory (ORNL) Impurity Study Program is to minimize the amount of impurities in the plasma and to minimize the effect of those that do enter the plasma. To accomplish this goal, it is necessary to identify the controlling mechanisms, understand their relationship to the plasma, and, finally, take the necessary corrective actions using the knowledge acquired. The understanding gained will allow evaluation of the relevance of present-day laboratory experiments and serve as a guide to direct future areas of study. It must be realized that the controlling impurity mechanisms will probably change as tokamaks evolve, but impurity problems with near-term tokamaks must be solved in order to proceed in an orderly and effective manner; also, the solution of these problems, in many cases, will lead to a better understanding of the nature of future problems.

The detrimental effects of plasma impurities in present-day tokamaks have been well documented. Their eventual effect on reactors has been modeled, and it is found that for break-even operation, very low impurity levels are required (see Fig. 1).[1,2] Several means have been suggested to control impurities or to alleviate their effects. Among the proposed solutions to the impurity problem are various divertor configurations,

*Research sponsored by the Office of Fusion Energy (ETM), U. S. Department of Energy under contract W-7405-eng-26 with the Union Carbide Corporation.

impurity flow reversal techniques, low Z coatings for walls, low sputtering walls, and gas blankets. These methods need to be tested to determine their effectiveness in maintaining a low impurity level in the plasma and the cost necessary to accomplish them.

The ORNL program has coordinated efforts in the four main task areas detailed in Fig. 2: *in situ* measurements, the development of new diagnostics, plasma/materials simulation experiments, and basic studies of plasma/materials interactions. *In situ* surface analysis and impurity-correlated plasma diagnostics are essential for identifying the controlling mechanisms. Laboratory simulations of plasma/wall interactions are used to understand impurity mechanisms, determine the effectiveness of cleaning procedures, quantify interactive effects, and study the alteration of material properties due to plasma bombardment. Basic laboratory studies of the phenomena involved are employed to acquire the systematic data and understanding necessary for development and tests of predictive theories and modeling calculations. In these investigations, it is essential to develop theoretical models of the phenomena involved that are suitable for predictive plasma modeling applications, because of the importance of such modeling in future reactor design.

Figure 3 is a flow diagram of the various aspects of the program. In this coordinated program, the Impurity Study Experiment (ISX) and ELMO Bumpy Torus (EBT) serve as test-beds for understanding the relevant plasma/surface phenomena, testing materials and techniques for impurity control, developing improved diagnostics, and relating impurity generation to machine performance.

These techniques and the understanding so developed are used in comparing plasma/wall interactions in a variety of plasma devices via the portable surface analysis station and Doppler-shifted laser fluorescence.

Many studies have been made on ISX-B to date and are expected to continue at an increased rate after the addition of new diagnostics in the near future. Both laboratory and *in situ* tokamak studies of unipolar arcing as an impurity introduction mechanism have been acomplished.[3] Laboratory results indicate that the rate at which arcs occur decreases exponentially with time, that the arcing rate is strongly dependent on surface cleanliness and roughness, and that 10^{16} to 10^{17} atoms are released per arc. *In situ* time-resolved experiments indicate that arcing is most likely to occur during periods of plasma instability and that MHD activity is most likely to occur at the beginning or end of discharges, although the steady-state portion of the tokamak pulses is not immune to arcing phenomena. Segregation of sulfur to the surface of stainless steel samples was observed at crater sites under certain conditions.[4]

Hydrogen recycle is being studied in ISX-B and in a laboratory simulator. It appears that recombination of atomic hydrogen to molecules is the rate limiting step in recycle. Control of recombination is required because order of magnitude changes in tritium inventory are expected.[5]

Experiments on cleanup in tokamaks have led to the use of glow discharge cleaning with hydrogen and helium. Chemical removal of carbon and oxygen appears to be necessary but is not itself sufficient to permit good tokamak plasmas.

Studies using glow discharge cleaning have indicated that significant reduction in arcing may occur.[6,7]

Impurity production and hydrogen species distributions for neutral beam injectors (NBIs) developed by the Plasma Technology Section of ORNL's Fusion Energy Division have been measured by exposing silicon crystal samples to beam pulses and analyzing them by nuclear microanalysis and secondary ion mass spectroscopy (SIMS) techniques. These two important aspects are being studied as a function of beam power, pulse length, and spatial position. Time-resolved measurements will be implemented. The NBIs have been developed for use on the Princeton Large Torus (PLT), the Poloidal Divertor Experiment (PDX), and ISX. Extraction voltages of up to 50 kV are used, and maximum power injected for a 0.5- s pulse is ∿1.2 MW with a design goal of 1.5 MW. The Medium Energy Test Facility (METF) has been used for exposure of single crystal [100] silicon samples. Preliminary results have shown that oxygen is the major atomic impurity and is present at levels of 1.5×10^{-3} O/H. Carbon is the next most abundant impurity, and copper is at or below the sensitivity of the analysis technique. Neutral hydrogen from the injector is expected to have three major energy components, E, E/2, and E/3, arising from the formation of H^+, H_2^+, and H_3^+ in the ion source and subsequent neutralization and dissociation in the gas cell neutralizer. The full energy component (40 keV) is easily separated in the depth analysis, but the E/2 and E/3 components overlap, due mainly to range straggling. SIMS analysis is used to determine the depth profiles of the implanted hydrogen, and the three energy components are determined from this depth profile.

These studies are being continued and new studies started that will utilize new diagnostic capabilities which are now being implemented. These include (a) a UHV transfer system to study hydrogen saturation effects, time-resolved impurity deposition, and *in situ* erosion, (b) a versatile experiment transfer system to allow UHV transfer of complete experimental packages, and (c) *in situ* time resolved Doppler-shifted laser spectroscopy for the study of plasma edge impurities.

Coated limiters have been tested in ISX-B for ohmically heated discharges. Preliminary results indicate satisfactory performance of such limiters in a tokamak environment. Two coatings on POCO graphite substrates of a mushroom shape (replacing the standard stainless steel outer limiter) have been tested: titanium carbide (TiC) and titanium diboride (TiB_2). Initial fear that introduction of new limiters would require a long period of tokamak conditioning (e.g., two weeks for a graphite limiter in ISX-A) was unfounded; the first day of operation with both limiters produced reproducible, clean (Z_{eff}<3) discharges, probably due to baking the limiters at 300°C in a separate vacuum chamber. Under standard conditions very little titanium was present in the discharges; the General Atomic laser-induced fluorescence measurement indicated that titanium density at the plasma edge is less than 6×10^7 cm^{-3}. In order to attain maximum (but controllable) heat load on the limiters, the plasma position was moved out by 3 cm after the discharge was established at the geometrical center, while the limiters were set at 1 cm inside the normal limiter position. As the plasma moved out, radiative power loss increased by a factor of up to three

and titanium line radiation increased sharply in the VUV spectroscopic measurement. Energy deposited on the limiters estimated from water the limiter coolant temperature rise and infrared camera measurements increased to 10 kJ (compared with 2 kJ in the standard case). The maximum heat load corresponds to an average power density of about 0.5 kW/cm^2, which is an order of magnitude less than the maximum expected in beam-heated discharges in which further tests of the coatings will be conducted. Visual inspection of the TiC/C limiter after its removal showed some change in the coating surface, but more detailed metallographical examination is under way. This program is being conducted in collaboration with Sandia Laboratories, Albuquerque.

REFERENCES

1. D. M. Meade, Nucl. Fusion 14, 289 (1974).
2. H. Vernickel, Kerntechnik 19, 279 (1977).
3. P. Mioduzewski, R. E. Clausing, and L. Heatherly, J. Nucl. Mater. 85 & 86, 963 (1979).
4. R. E. Clausing (Oak Ridge National Laboratory), private communication, April 1979.
5. R. E. Clausing, Proc. Workshop on Hydrogen Recycling, p. 17.1-17.5, CONF-791057, (1979).
6. Y. Gomay, R. E. Clausing, R. J. Colchin, L. C. Emerson, L. Heatherly, W. Namkung, and J. E. Simpkins, submitted to J. Vac. Sci. Technol.
7. A. F. Lietzke, S. Ejima, R. E. Clausing, L. C. Emerson, L. Heatherly, S. Halsted, and S. Seki, submitted to J. Nucl. Mater.

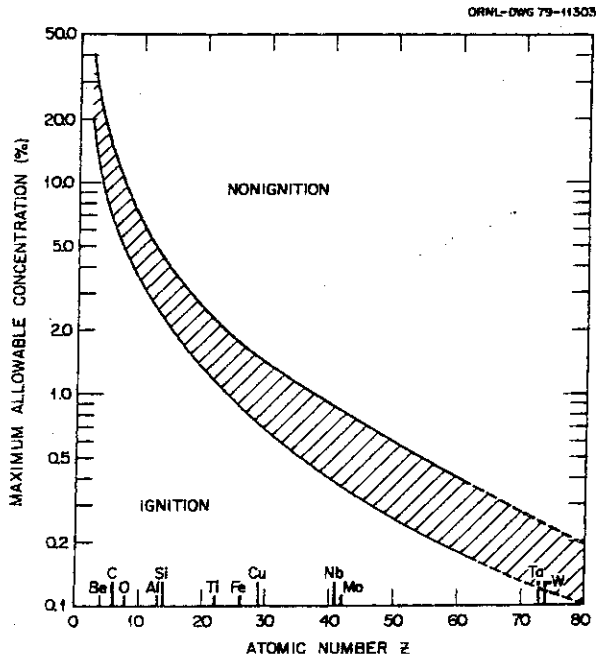

ORNL-DWG 79-2065R3 FED

CHART I. ORNL IMPURITY STUDY TASK ORGANIZATION

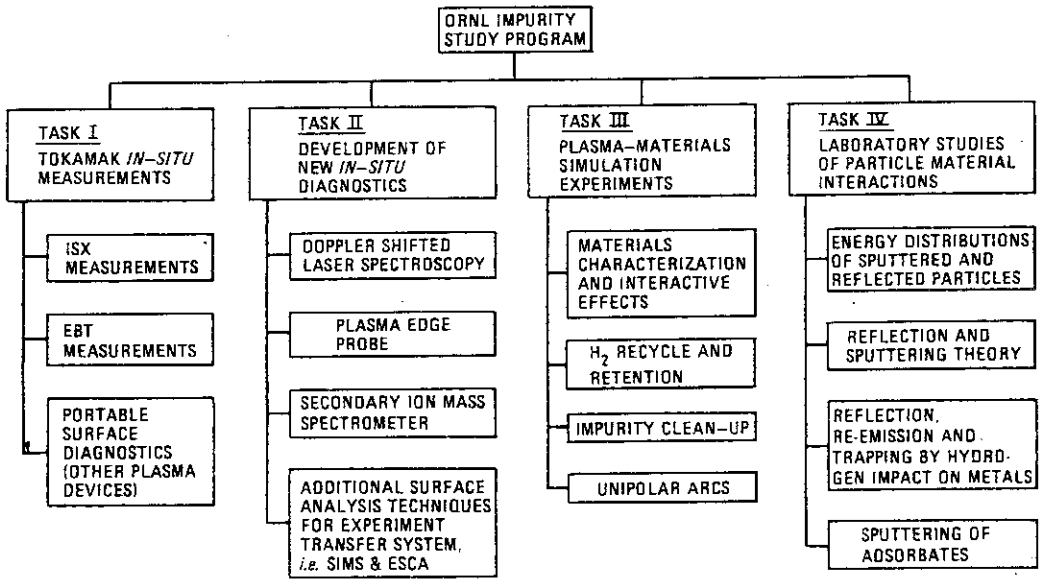

PERSONNEL

R. A. LANGLEY (FED), PROGRAM MANAGER

1. B. R. APPLETON (SSD)
2. R. E. CLAUSING (M&C)
3. R. J. COLCHIN (FED)
4. H. L. DODDS, JR. (UT)
5. L. C. EMERSON (M&C)
6. L. HEATHERLY (M&C)
7. T. J. HOFFMAN (CSD)
8. K. O. LEGG (GIT)
9. J. L. MOORE (SSD)
10. J. B. ROBERTO (SSD)
11. M. T. ROBINSON (SSD)
12. O. S. OEN (SSD)
13. J. E. SIMPKINS (FED)
14. E. W. THOMAS (GIT)
15. S. P. WITHROW (SSD)
16. R. A. ZUHR (SSD)

CSD – COMPUTER SCIENCES DIVISION
FED – FUSION ENERGY DIVISION
GIT – GEORGIA INSTITUTE OF TECHNOLOGY
M&C – METALS AND CERAMICS DIVISION
SSD – SOLID STATE DIVISION
UT – UNIVERSITY OF TENNESSEE

ORNL-DWG 79-2066R FED

CHART II. FLOW DIAGRAM OF IMPURITY STUDY PROGRAM

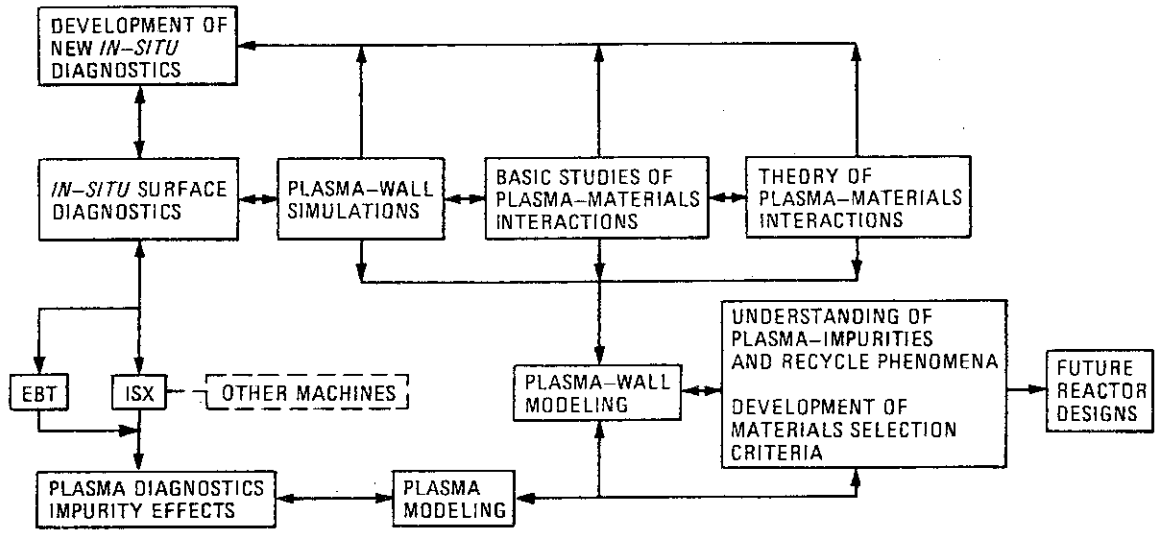

FED/VU 79-188

IMPURITY STUDY PROGRAM CAST

R. A. LANGLEY (FED, COORDINATOR)

R. E. CLAUSING (MCD)
L. C. EMERSON (MCD)
W. R. HUSINSKY (SSD)
J. B. ROBERTO (SSD)
M. T. ROBINSON (SSD)
J. E. SIMPKINS (FED)
S. P. WITHROW (SSD)
R. A. ZUHR (SSD)

H. B. SCHWEER (IPP, JÜLICH)

FED – FUSION ENERGY DIVISION
MCD – METALS AND CERAMICS DIVISION
SSD – SOLID STATE DIVISION

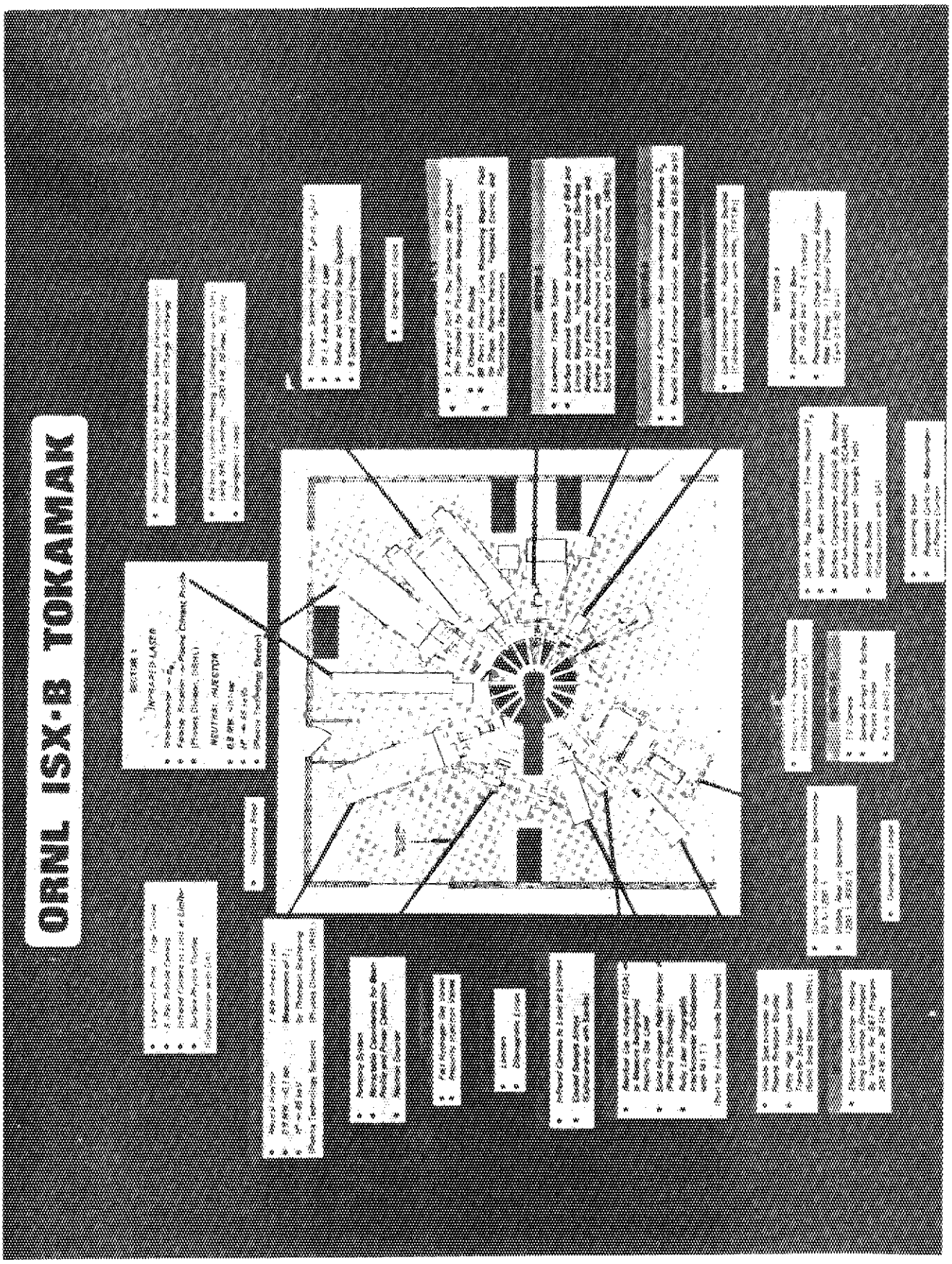
ORNL ISX-B TOKAMAK

ORNL-DWG 78-7208

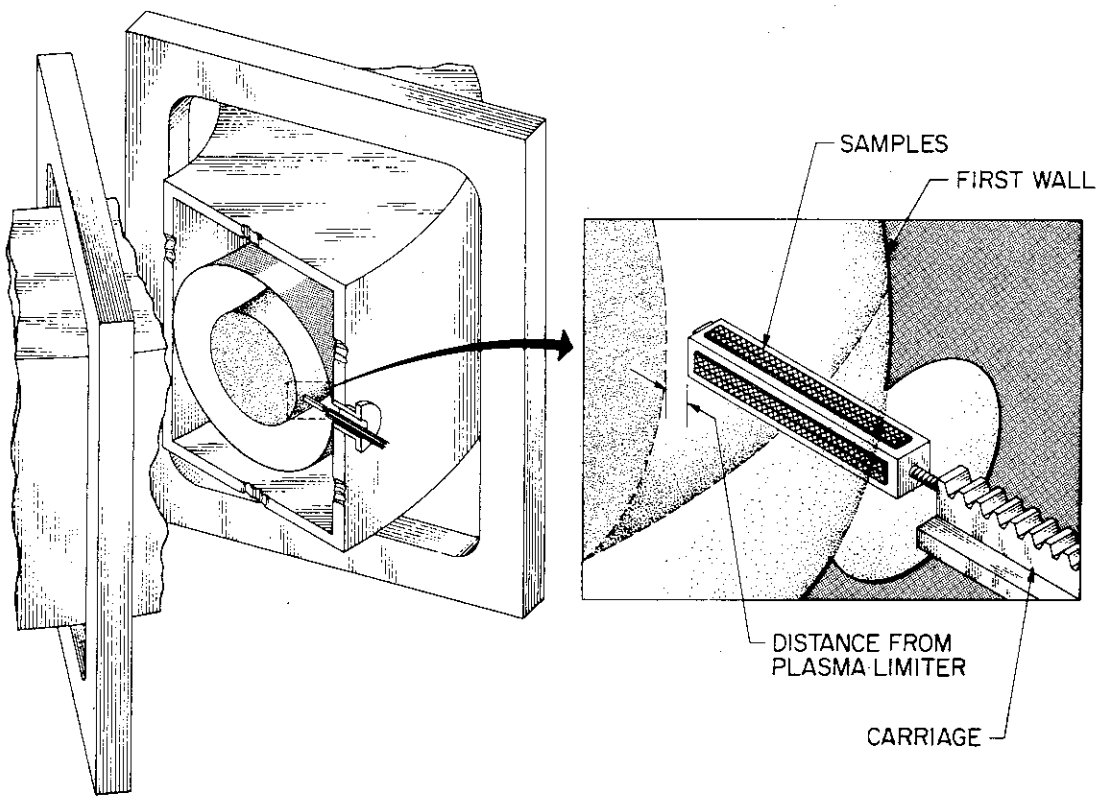

ORNL-DWG 78-9313

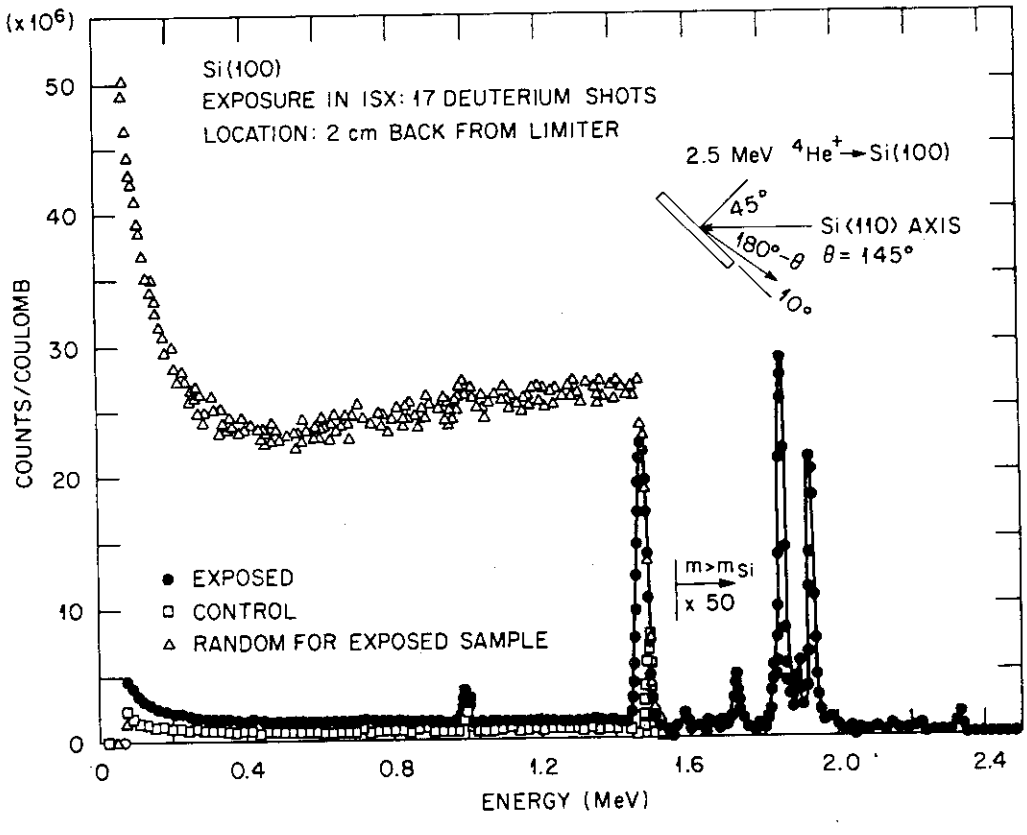

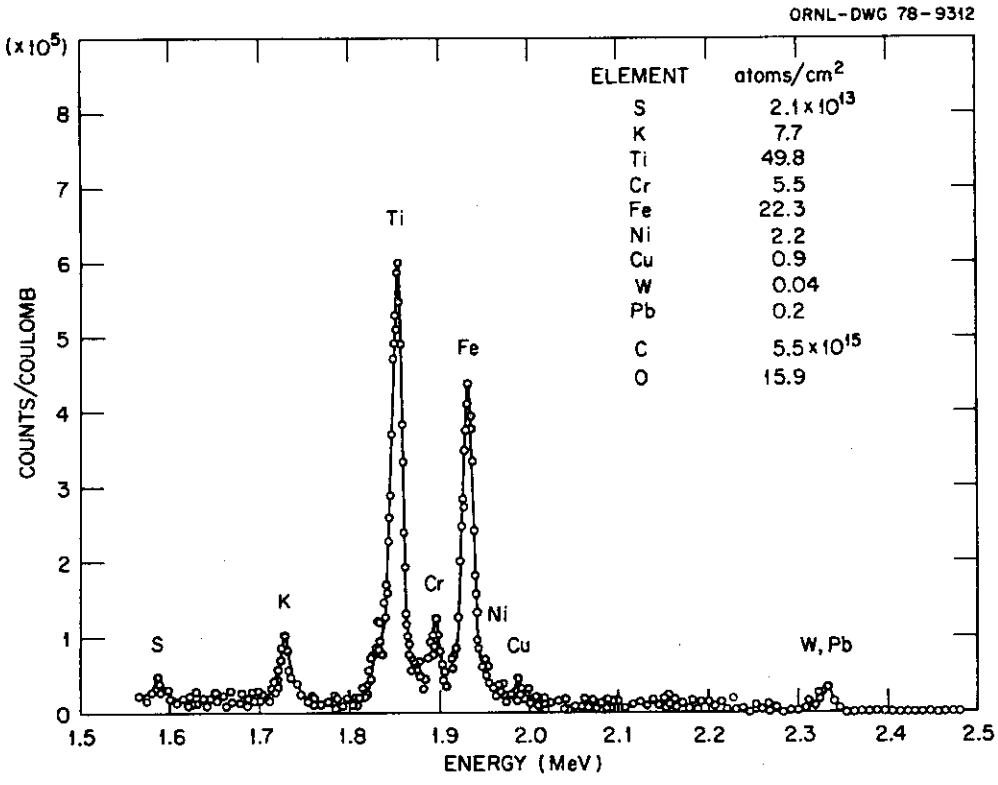
ORNL-DWG 78-9312
(x10^5)
COUNTS/COULOMB
ENERGY (MeV)
ELEMENT atoms/cm^2
S 2.1x10^13
K 7.7
Ti 49.8
Cr 5.5
Fe 22.3
Ni 2.2
Cu 0.9
W 0.04
Pb 0.2
C 5.5x10^15
O 15.9
S
K
Ti
Cr
Fe
Ni
Cu
W, Pb

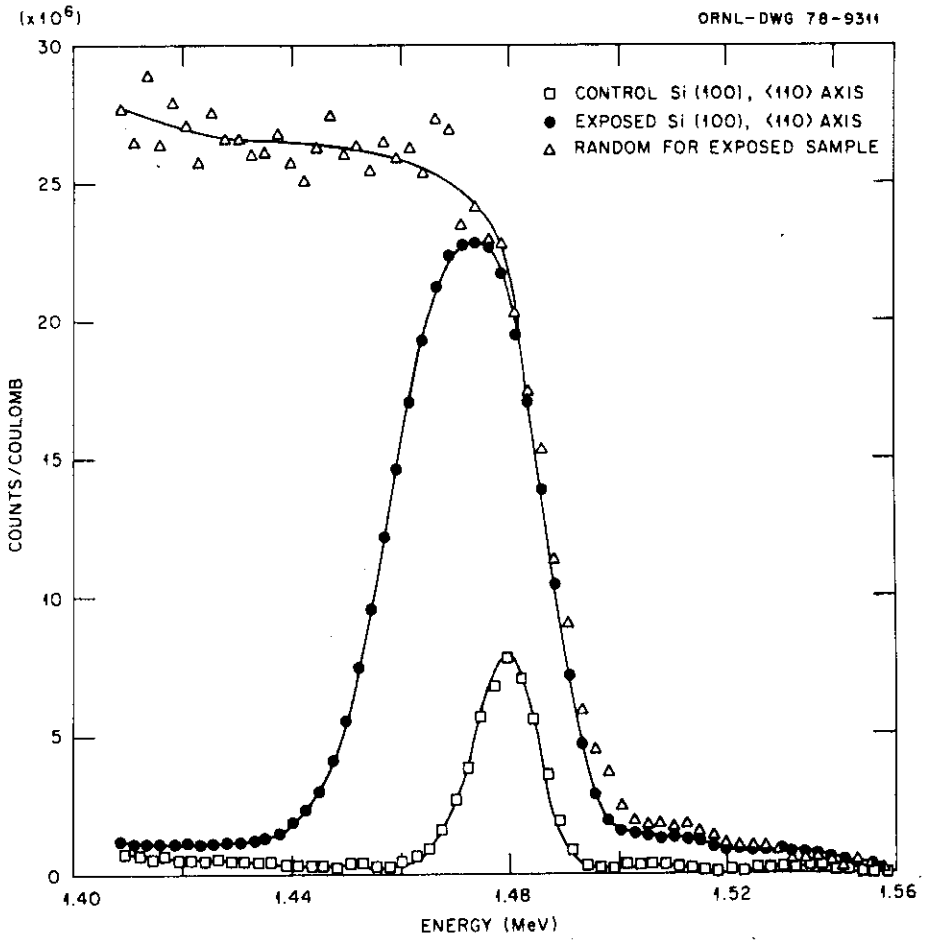
(x10^6)
ORNL-DWG 78-9311
CONTROL Si (100), ⟨110⟩ AXIS
EXPOSED Si (100), ⟨110⟩ AXIS
RANDOM FOR EXPOSED SAMPLE
COUNTS/COULOMB
ENERGY (MeV)

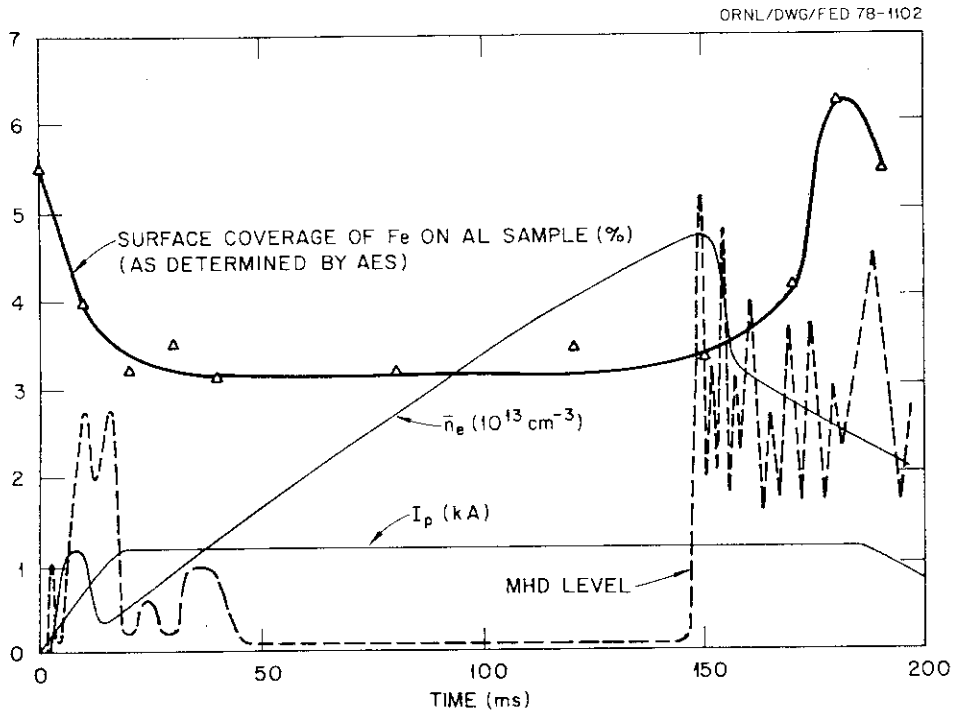
ORNL/DWG/FED 78-1102
SURFACE COVERAGE OF Fe ON AL SAMPLE (%)
(AS DETERMINED BY AES)
$\bar{n}_e$ (10^{13} cm^{-3})
I_p (kA)
MHD LEVEL
TIME (ms)

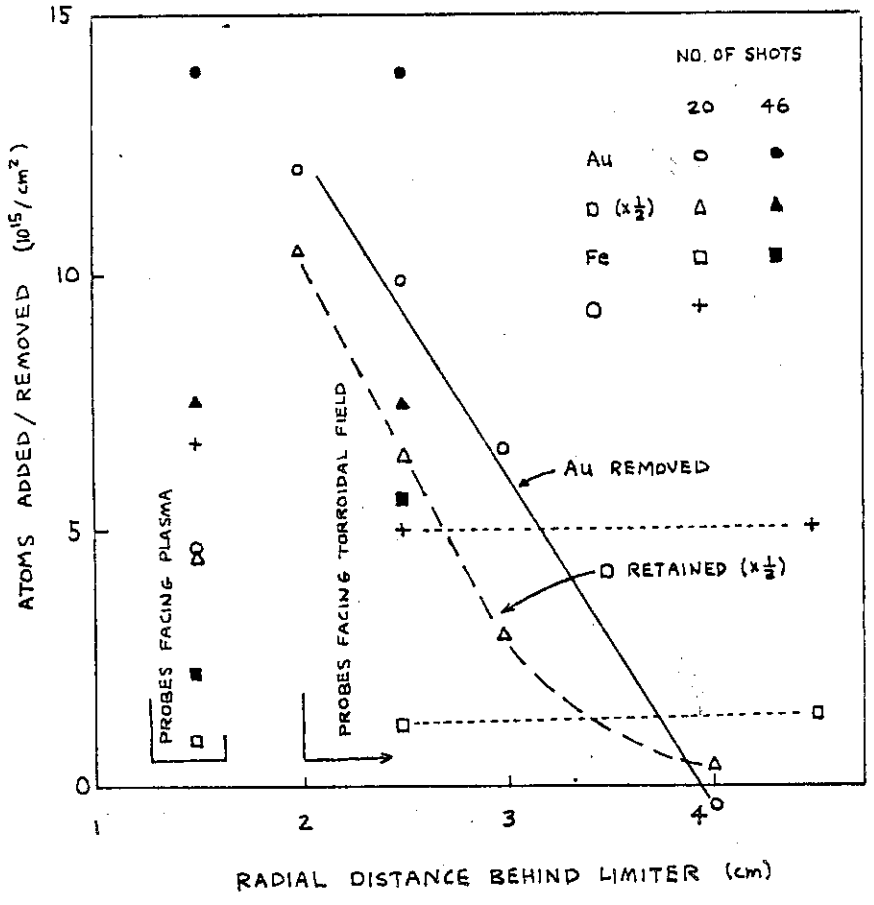
NO. OF SHOTS
20 46
Au
D (x½)
Fe
O
Au REMOVED
D RETAINED (x½)
PROBES FACING PLASMA
PROBES FACING TOROIDAL FIELD
ATOMS ADDED / REMOVED (10^{15}/cm^2)
RADIAL DISTANCE BEHIND LIMITER (cm)

SUMMARY OF D/IMPURITY RESULTS

D/IMPURITY PROFILES SIMILAR FOR OHMIC PLASMAS AND 350 kW INJECTION

D, O SATURATE IN 1-4 SHOTS, HEAVY IMPURITIES DO NOT SATURATE IN 12 SHOTS

D DAMAGE PROFILING, DEPTH PROFILING AND SATURATION BEHAVIOR SUGGEST EDGE TEMPERATURES OF 50-150 eV

MEASURED FLUXES IN THE PLASMA EDGE:

D $\sim 10^{17}/CM^2$ - SHOT

O $\sim 10^{15}$

FE-NI $\sim 3 \times 10^{14}$

ORNL–DWG 78-19775

ARCING STUDIES

1. CHARACTERIZATION OF THE ARC PROPERTIES
   - CURRENT
   - PULSE LENGTH
   - EROSION RATES
2. CORRELATION BETWEEN SURFACE (AND PLASMA) CONDITIONS AND ARCING PROBABILITY
   - POLISHED SURFACES
   - AS RECEIVED SURFACES
   - OXIDE LAYERS
   - ADSORBED GAS LAYERS
   - DIELECTRIC INCLUSIONS
   - OIL CONTAMINATION
3. UNDERSTANDING THE MECHANISMS OF ARCING INITIATION
4. FINDING METHODS TO CONTROL ARCING

ORNL-DWG 78-19778

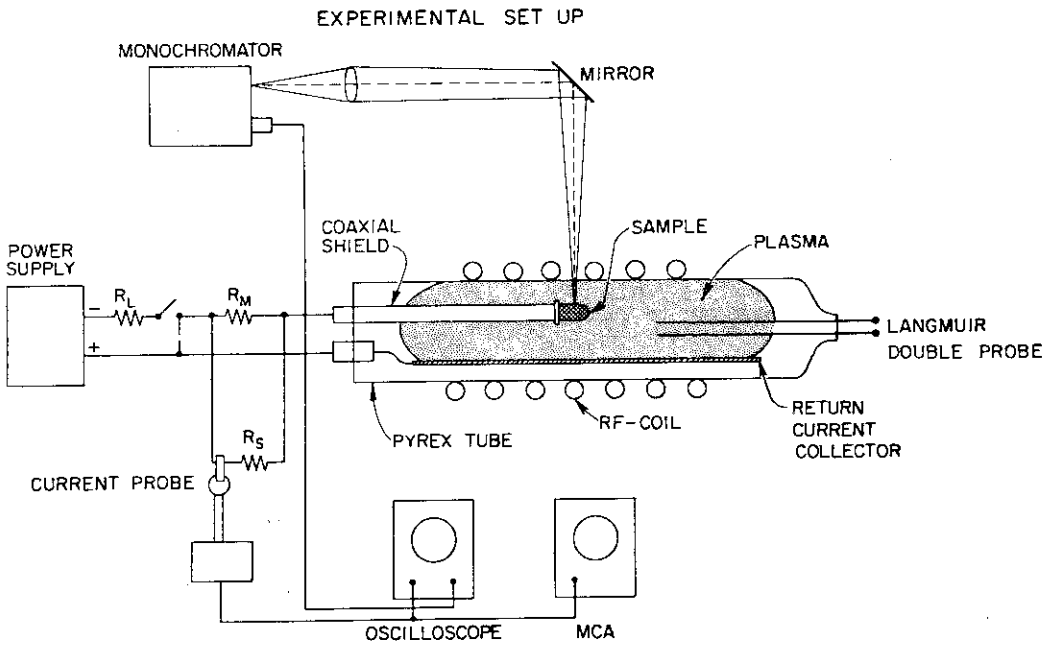

ORNL-DWG 78-19773

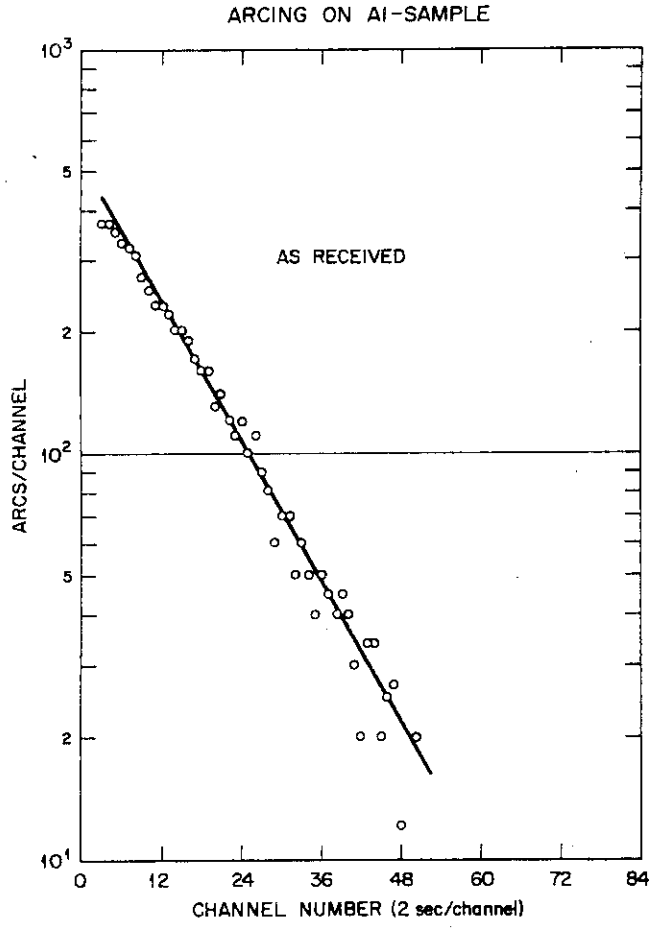

ORNL-DWG 78-19774

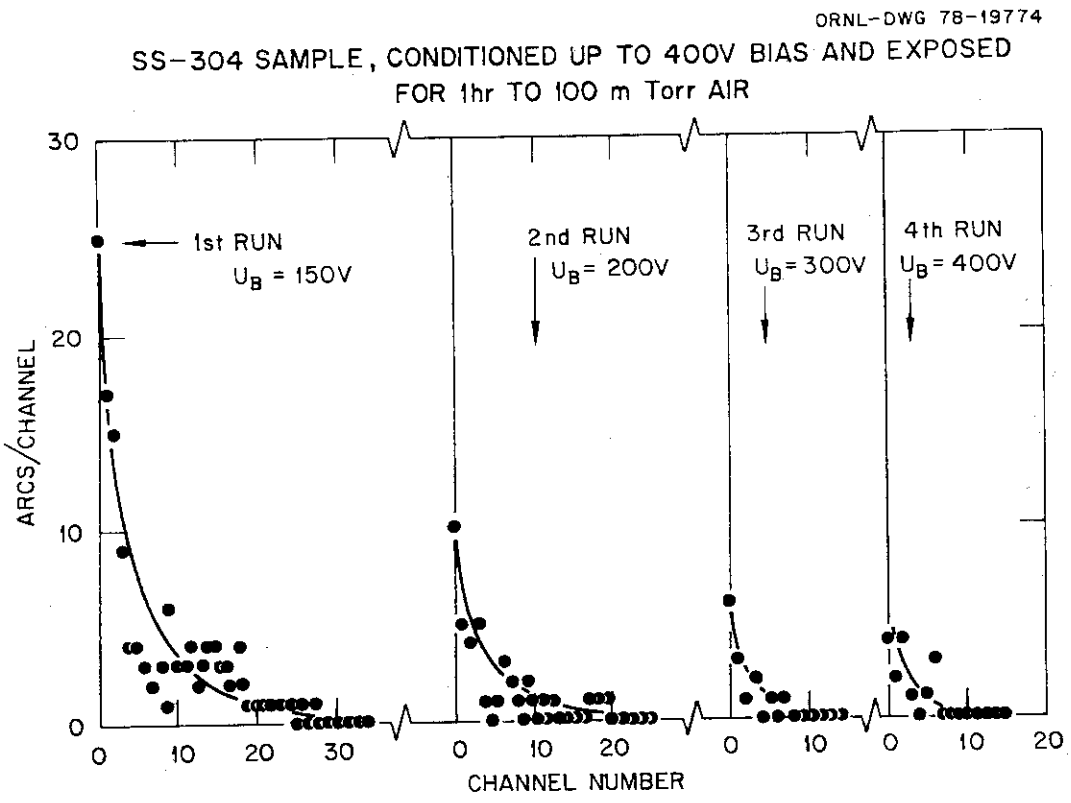

ORNL-DWG 78-19779

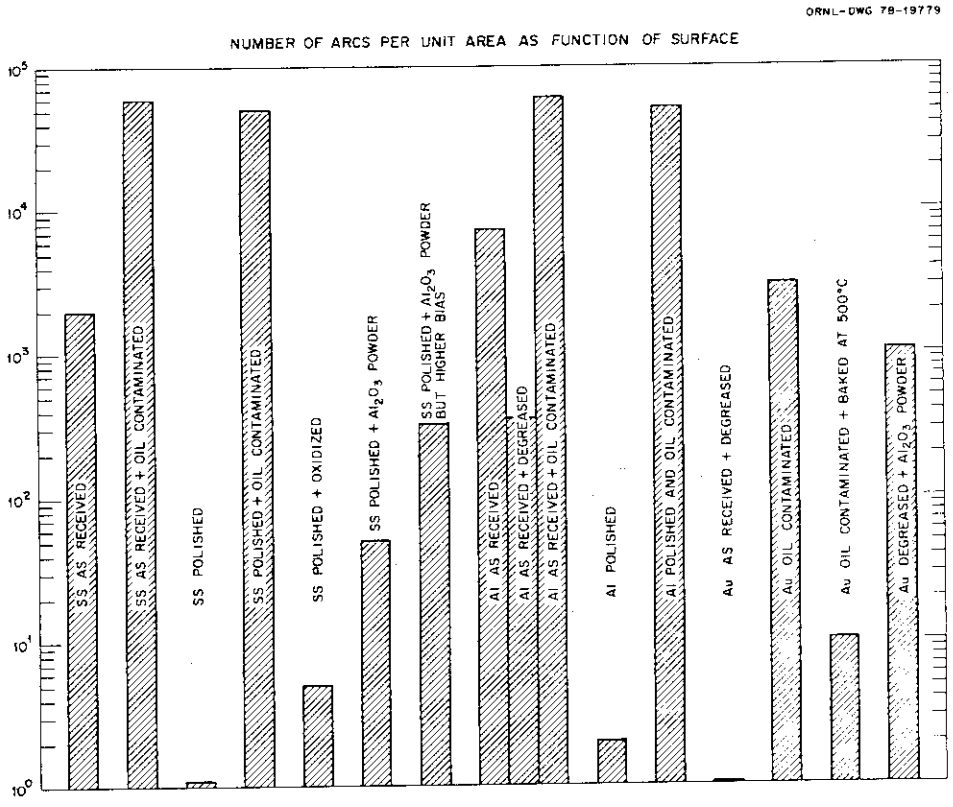

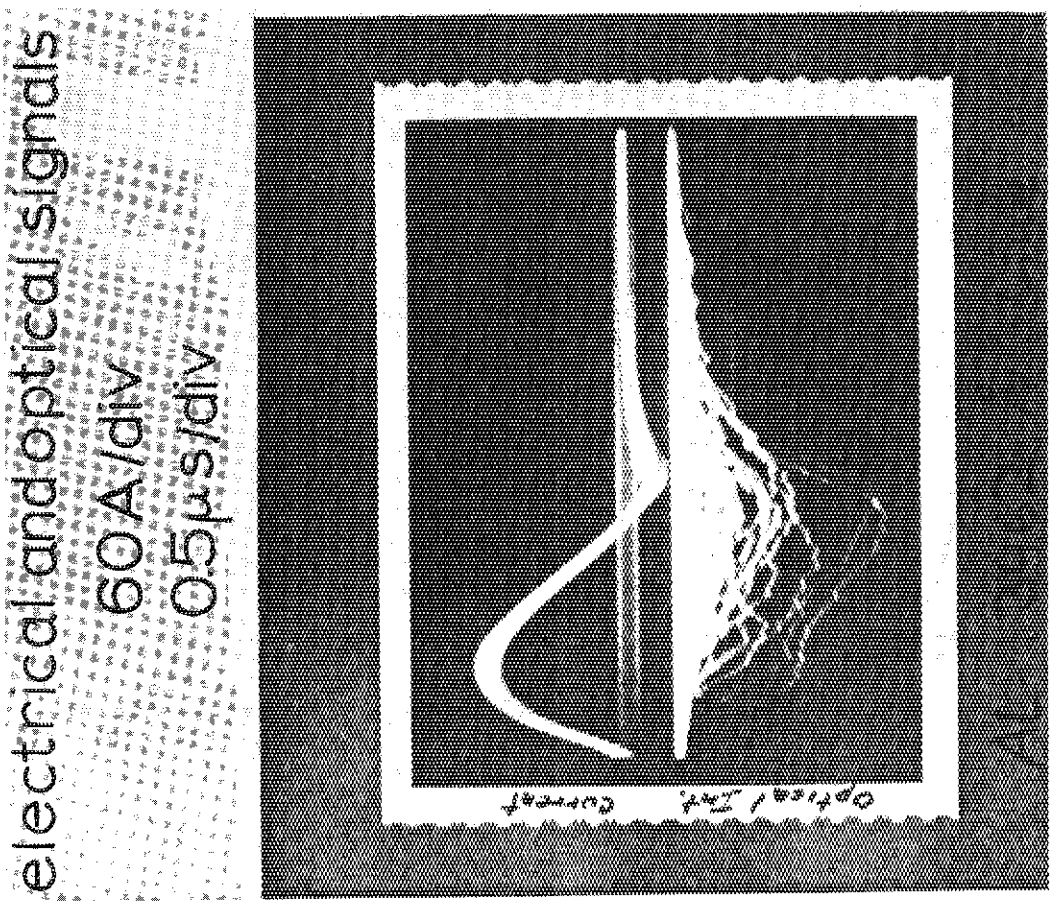
electrical and optical signals
60A/div
0.5μs/div

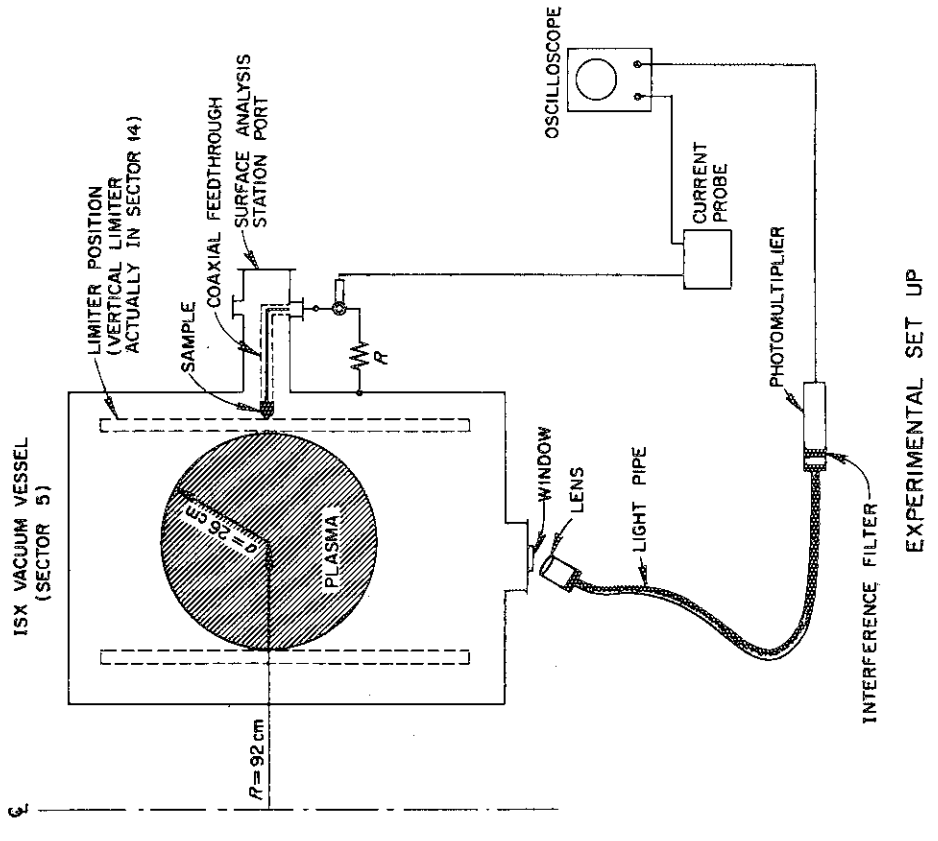
ORNL-DWG 78-22333
ISX VACUUM VESSEL (SECTOR 5)
LIMITER POSITION (VERTICAL LIMITER ACTUALLY IN SECTOR 14)
SAMPLE
COAXIAL FEEDTHROUGH
SURFACE ANALYSIS STATION PORT
R
OSCILLOSCOPE
CURRENT PROBE
PHOTOMULTIPLIER
WINDOW
LENS
LIGHT PIPE
INTERFERENCE FILTER
PLASMA
65
92
51
R=92 cm
EXPERIMENTAL SET UP

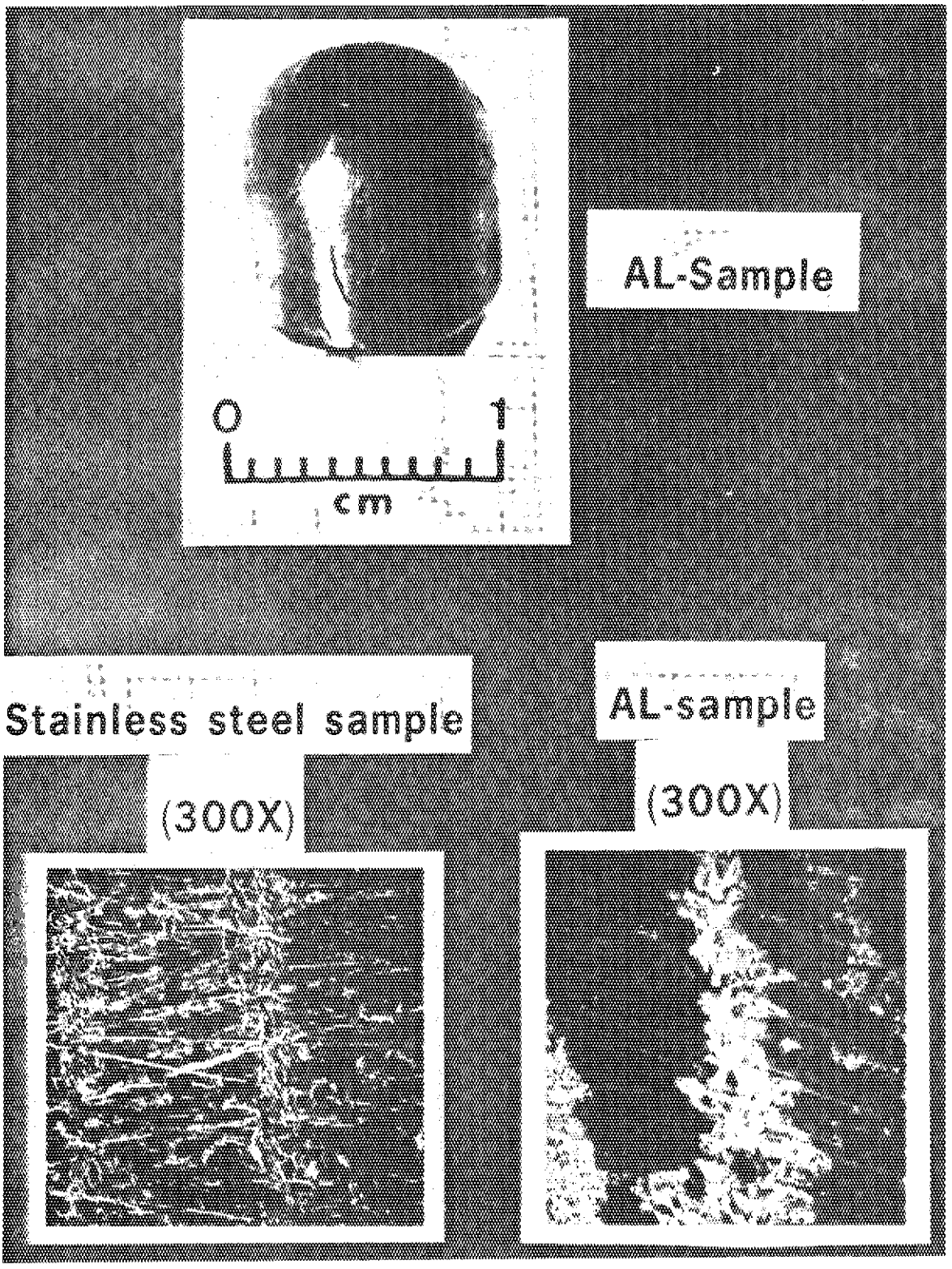
AL-Sample
0
1
cm
Stainless steel sample
(300X)
AL-sample
(300X)

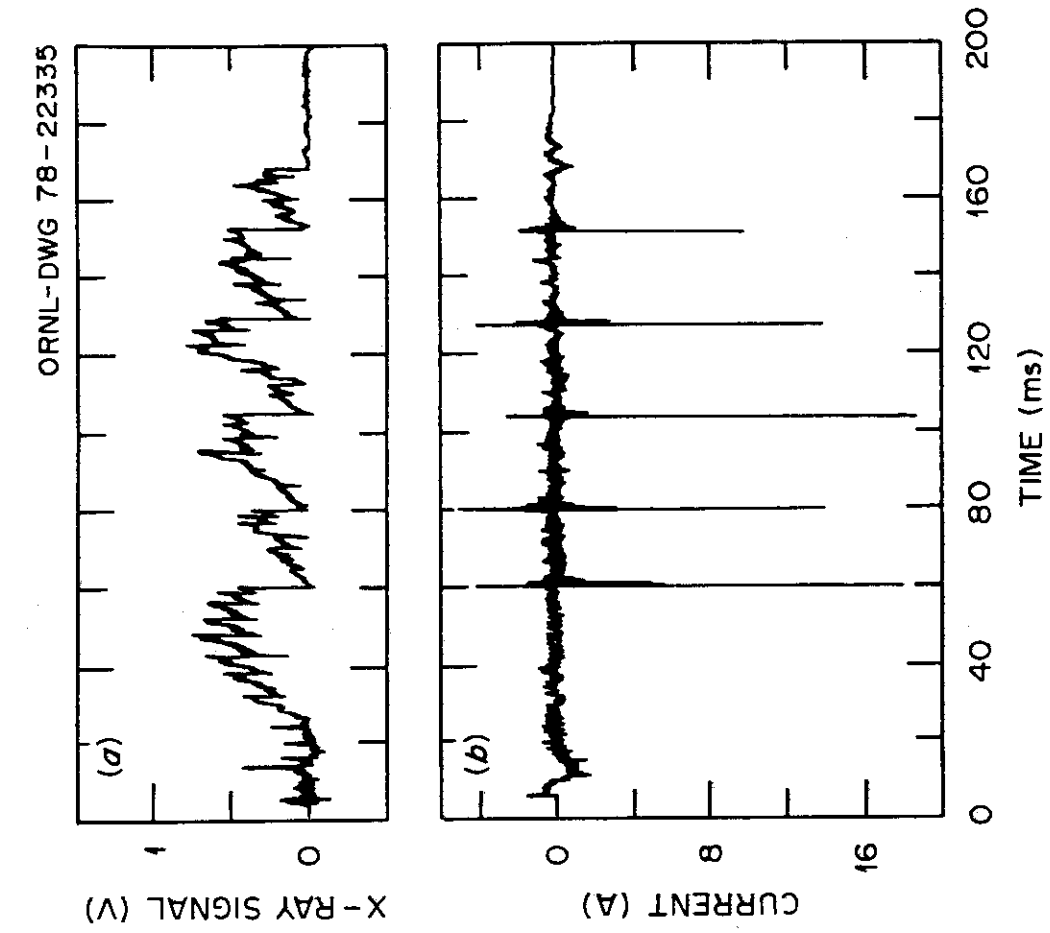
ORNL-DWG 78-22335
(a)
(b)
X-RAY SIGNAL (V)
CURRENT (A)
TIME (ms)

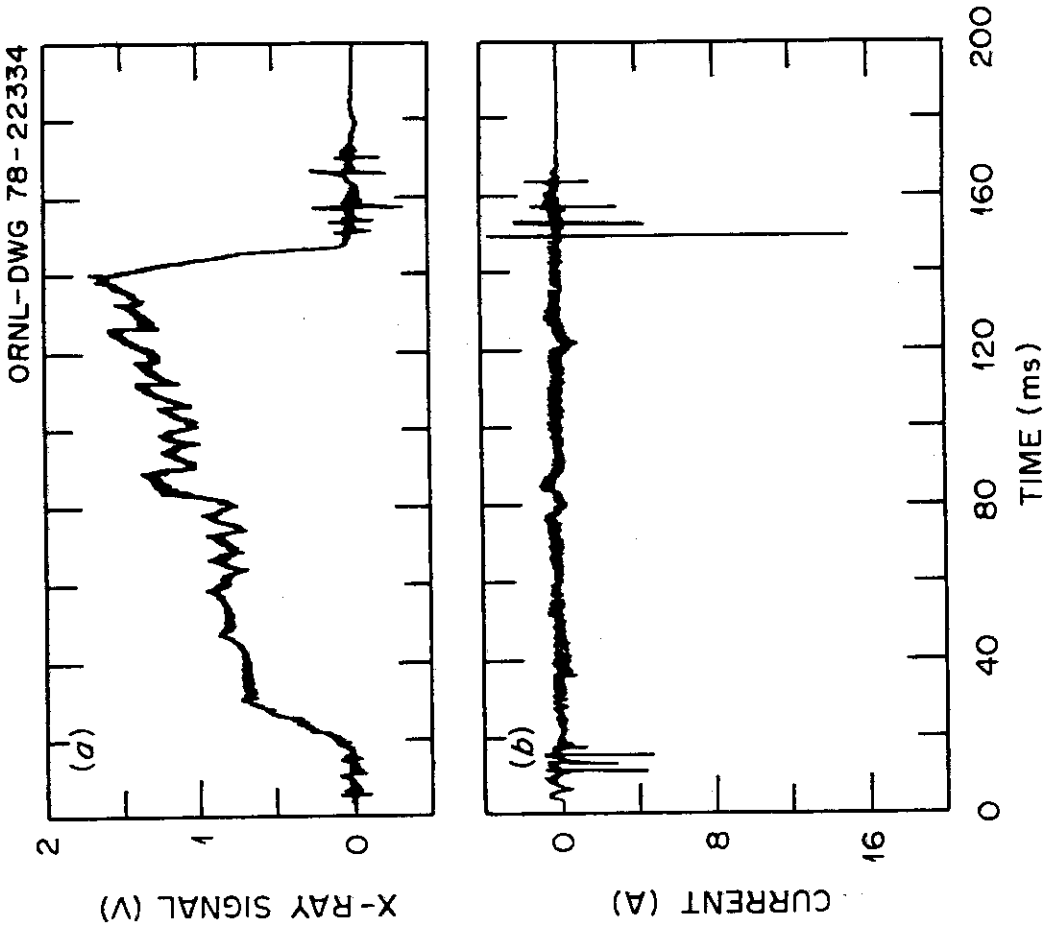
ORNL-DWG 78-22334
(a)
(b)
X-RAY SIGNAL (V)
CURRENT (A)
TIME (ms)

IMPURITY PRODUCTION BY ARCING

ARC TRACKS OBSERVED IN ISX INDICATE AN EROSION OF:

10^{16} ... 10^{17} atoms/arc

COMPARED TO IMPURITY PRODUCTION BY SPUTTERING FOR A MIDSIZE TOKAMAK [1]:

$8 \cdot 10^{16}$ atoms $\cdot$ m^{-1} $\cdot$ sec^{-1}

WITH A WALL SURFACE AREA: $A = 10\ m^2$
AND A PULSE LENGTH: $\tau = 100$ msec

10^{17} atoms/discharge

- ONE SINGLE ARC CAN RELEASE A NUMBER OF IMPURITY ATOMS WHICH IS COMPARABLE TO THE TOTAL NUMBER OF SPUTTERED PARTICLES THROUGHOUT THE DISCHARGE

ORNL-DWG 78-19776

ORNL/DWG/FED 78-272

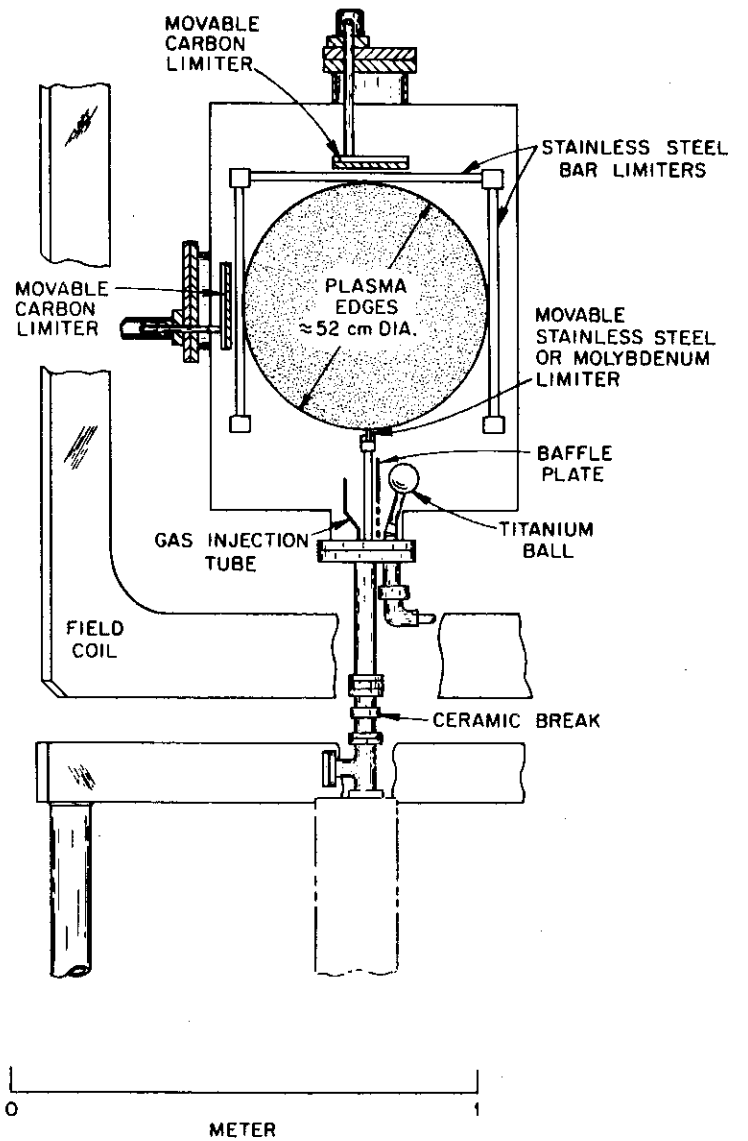

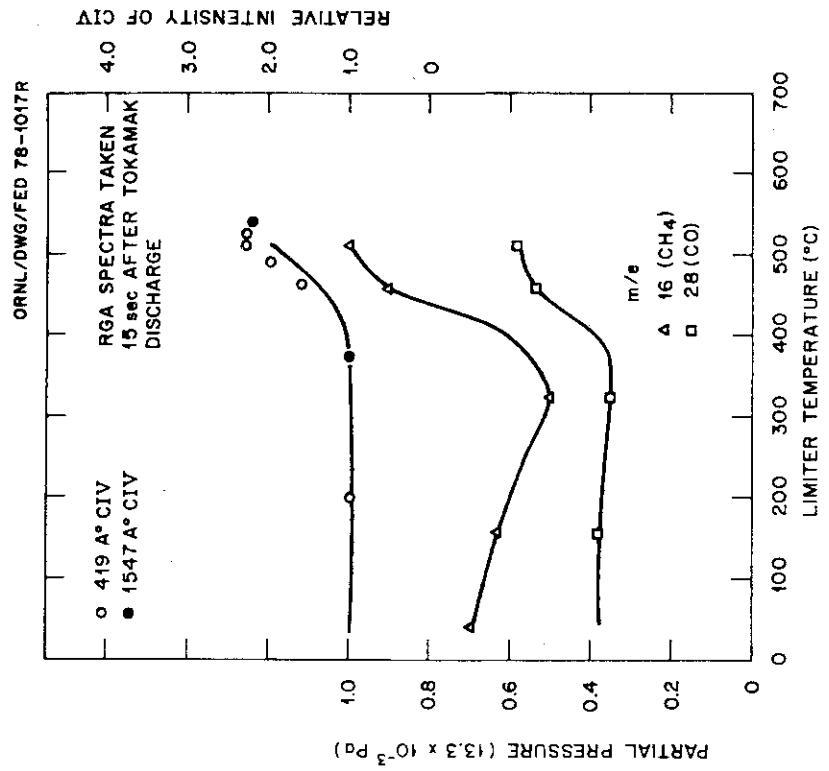
ORNL/DWG/FED 78-1017R
RGA SPECTRA TAKEN
15 sec AFTER TOKAMAK
DISCHARGE
○ 419 A° CIV
● 1547 A° CIV
m/e
△ 16 (CH_4)
□ 28 (CO)
RELATIVE INTENSITY OF CIV
LIMITER TEMPERATURE (°C)
PARTIAL PRESSURE (13.3×10^{-3} Pa)

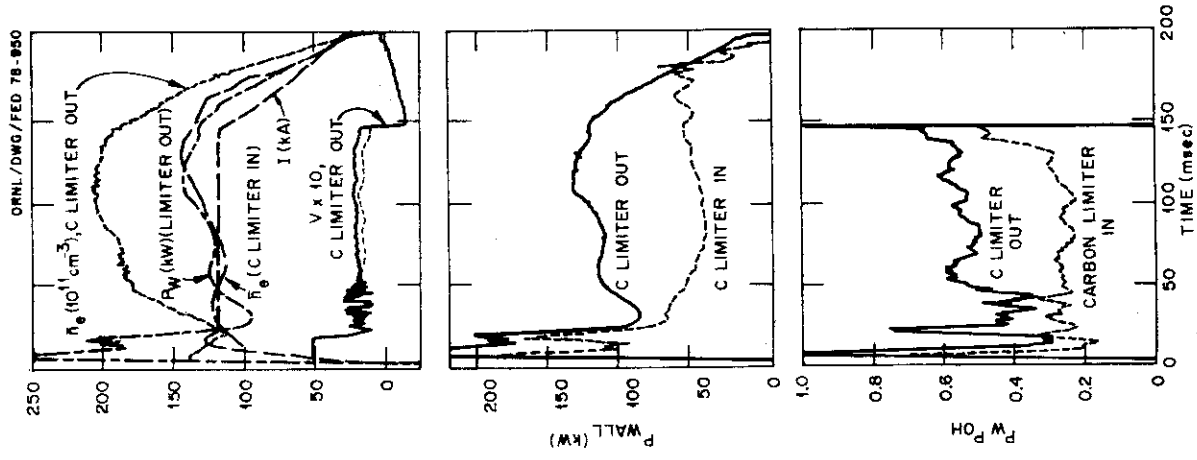
ORNL/DWG/FED 78-950
C LIMITER OUT
C LIMITER IN
CARBON LIMITER IN
TIME (msec)

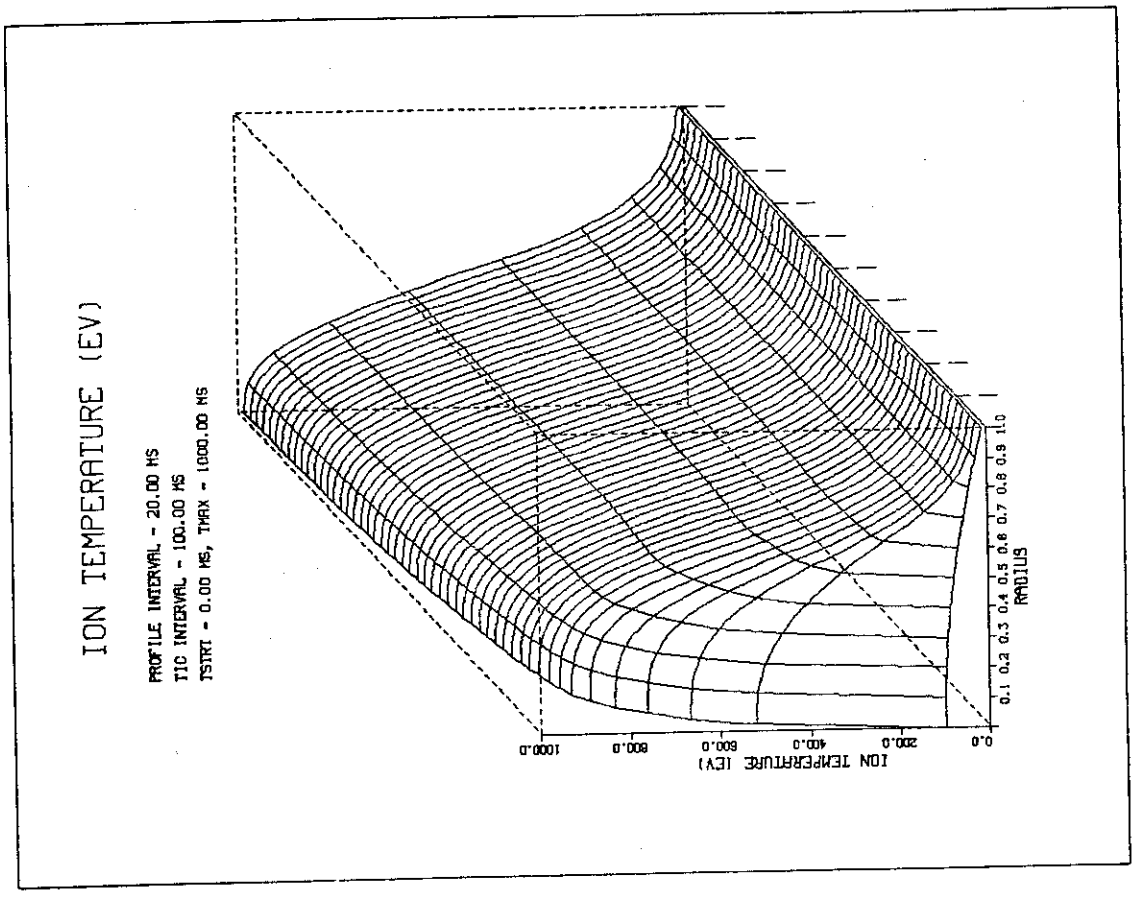
ION TEMPERATURE (EV)
PROFILE INTERVAL = 20.00 MS
TIO INTERVAL = 100.00 MS
TSTRT = 0.00 MS, TMAX = 1000.00 MS
ION TEMPERATURE (EV)
0.0
200.0
400.0
600.0
800.0
1000.0
RADIUS
0.1 0.2 0.3 0.4 0.5 0.6 0.7 0.8 0.9 1.0

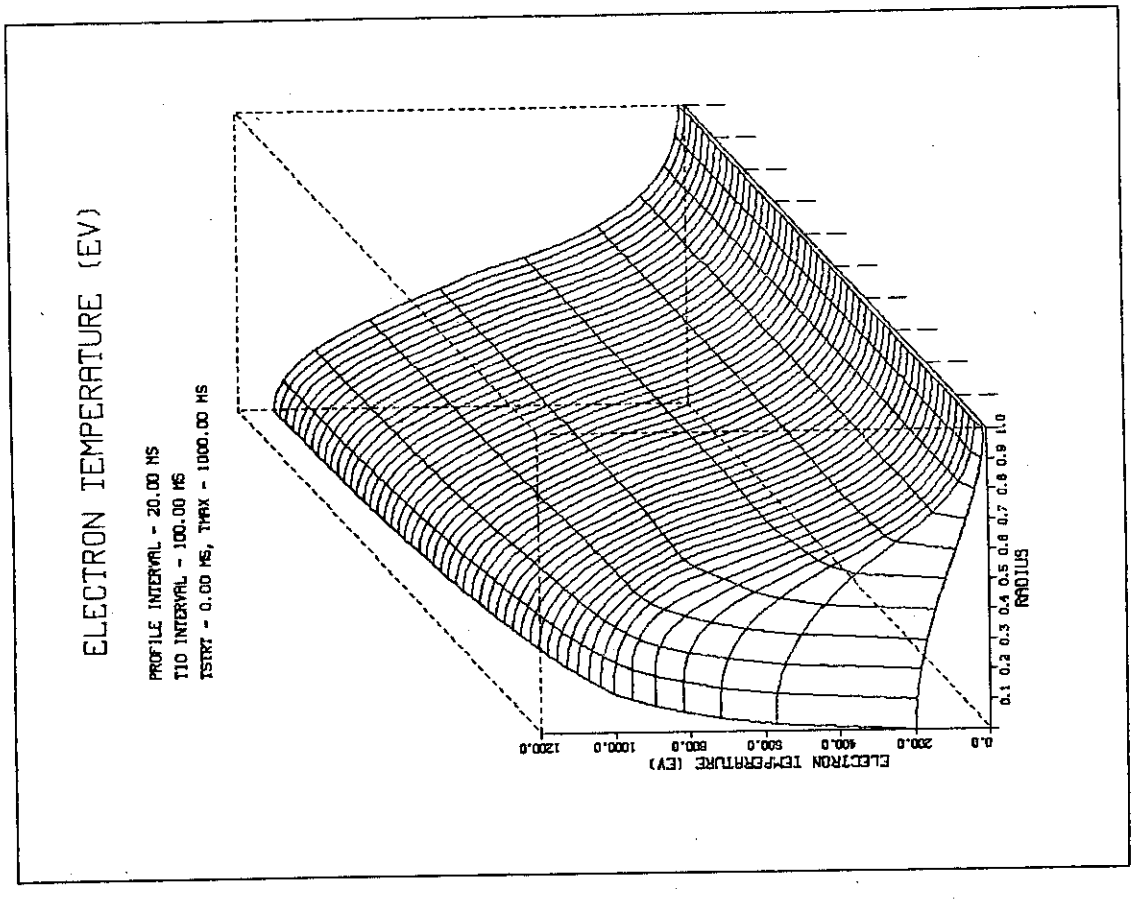
ELECTRON TEMPERATURE (EV)
PROFILE INTERVAL = 20.00 MS
TIO INTERVAL = 100.00 MS
TSTRT = 0.00 MS, TMAX = 1000.00 MS
ELECTRON TEMPERATURE (EV)
0.0
200.0
400.0
600.0
800.0
1000.0
1200.0
RADIUS
0.1 0.2 0.3 0.4 0.5 0.6 0.7 0.8 0.9 1.0

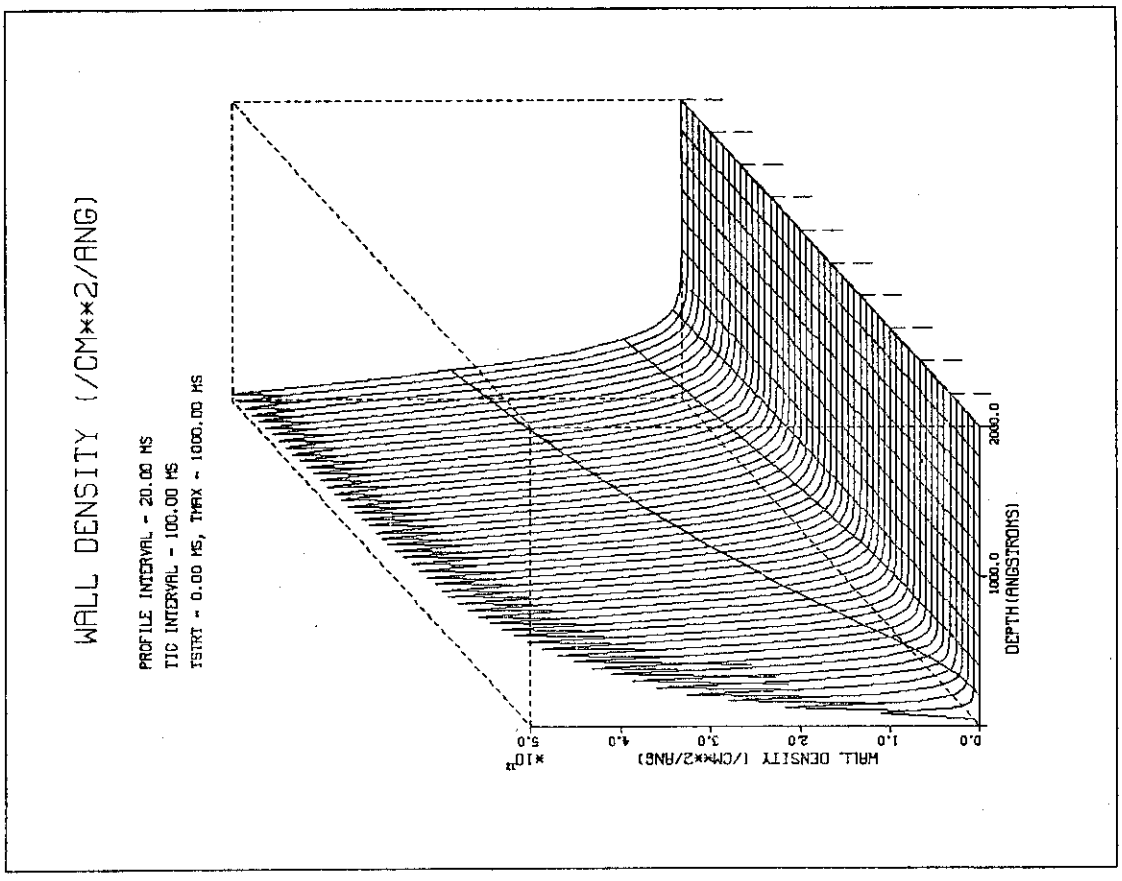
WALL DENSITY (/CM**2/ANG)
PROFILE INTERVAL = 20.00 MS
TIC INTERVAL = 100.00 MS
TSTRT = 0.00 MS, TMAX = 1000.00 MS
WALL DENSITY (/CM**2/ANG)
*10^17
0.0
1.0
2.0
3.0
4.0
5.0
DEPTH(ANGSTROMS)
0.0
1000.0
2000.0

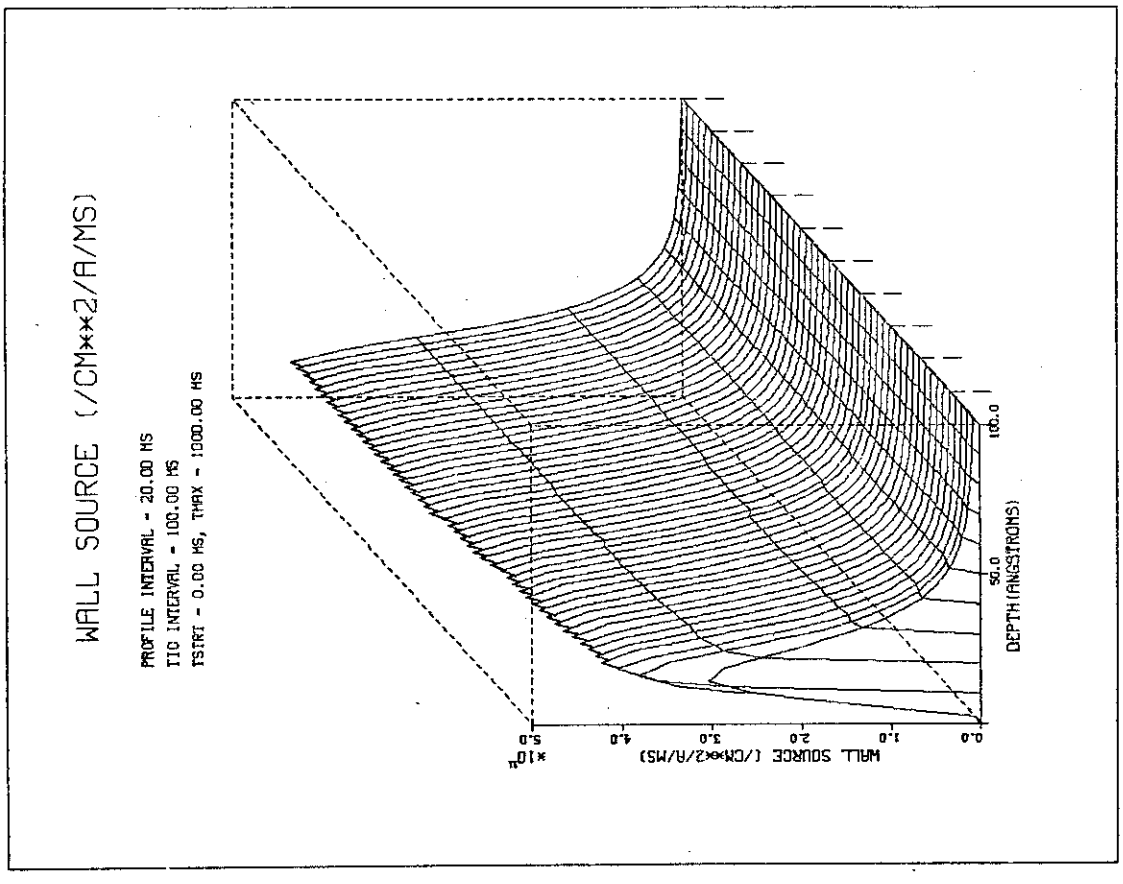
WALL SOURCE (/CM**2/A/MS)
PROFILE INTERVAL = 20.00 MS
TIC INTERVAL = 100.00 MS
TSTRT = 0.00 MS, TMAX = 1000.00 MS
WALL SOURCE (/CM**2/A/MS)
*10^14
0.0
1.0
2.0
3.0
4.0
5.0
DEPTH(ANGSTROMS)
0.0
50.0
100.0

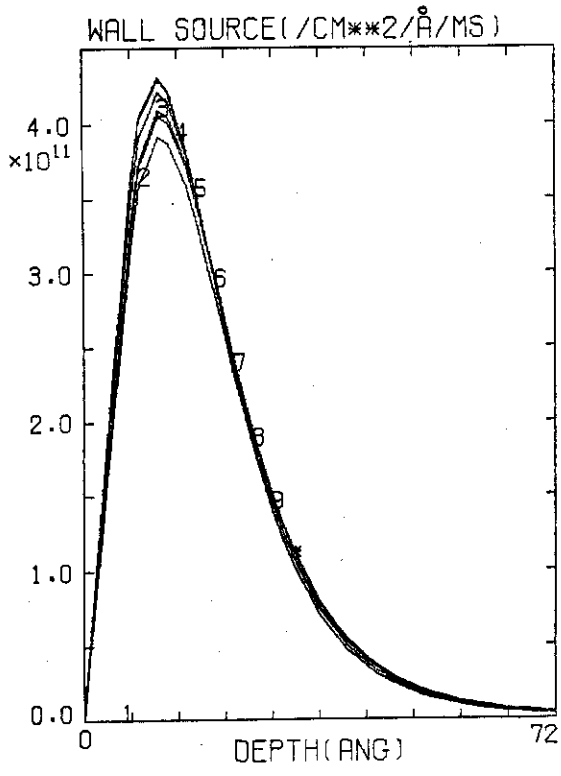
WALL SOURCE(/CM**2/Å/MS)
4.0
×10^11
3.0
2.0
1.0
0.0
0
72
DEPTH(ANG)

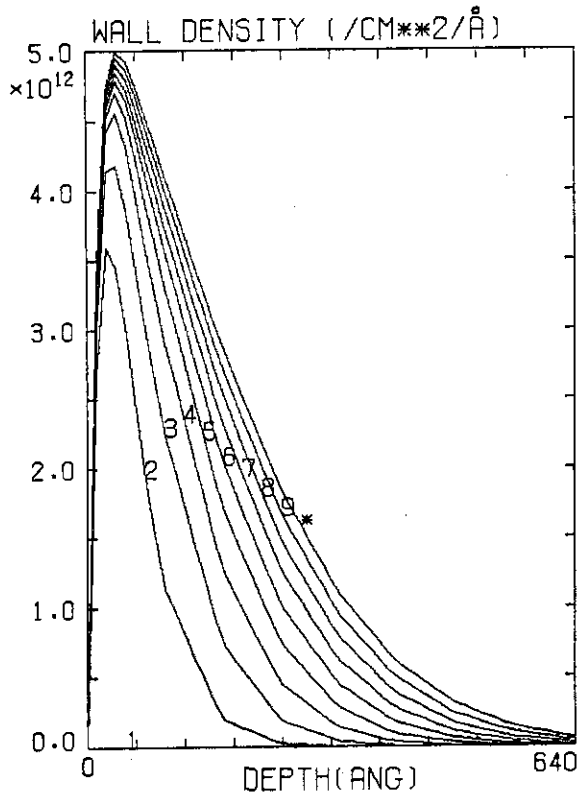
WALL DENSITY (/CM**2/Å)
5.0
×10^12
4.0
3.0
2.0
1.0
0.0
0
640
DEPTH(ANG)

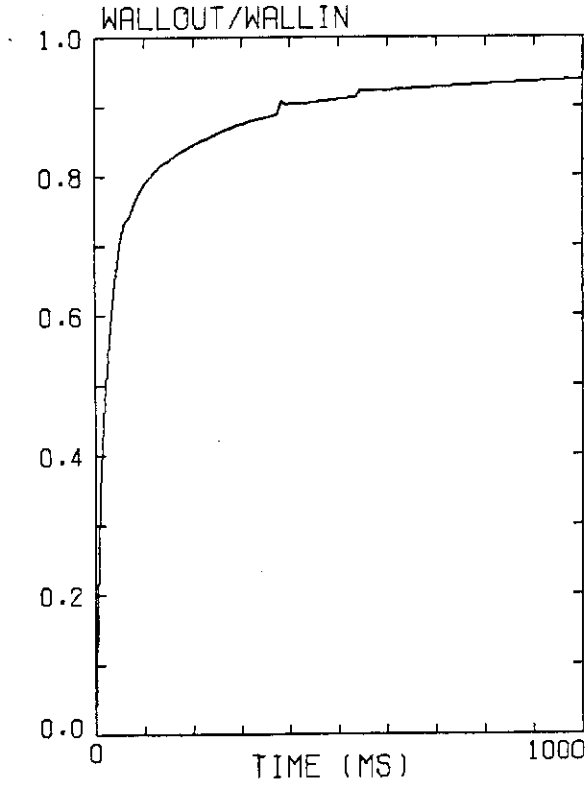
WALLOUT/WALLIN
1.0
0.8
0.6
0.4
0.2
0.0
0
1000
TIME (MS)

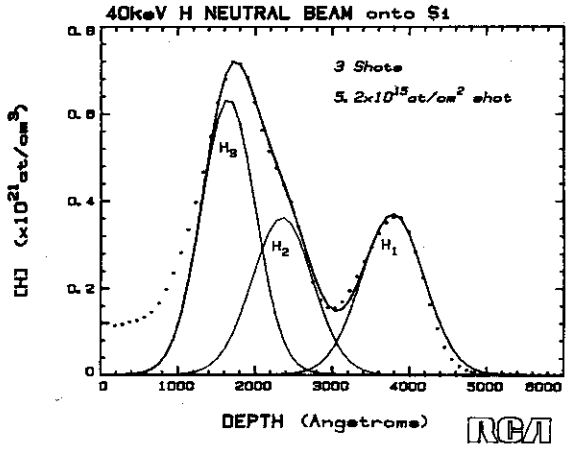
40keV H NEUTRAL BEAM onto Si
3 Shots
5.2x10^15 at/cm^2 shot
H3
H2
H1
[H] (x10^21 at/cm^3)
DEPTH (Angstroms)
RCA

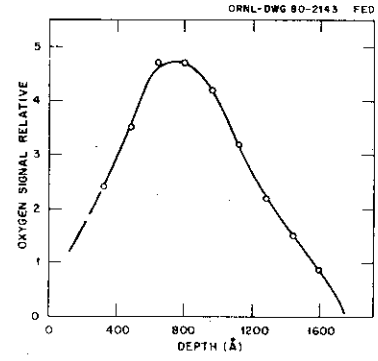
ORNL-DWG 80-2143 FED
OXYGEN SIGNAL RELATIVE
DEPTH (Å)

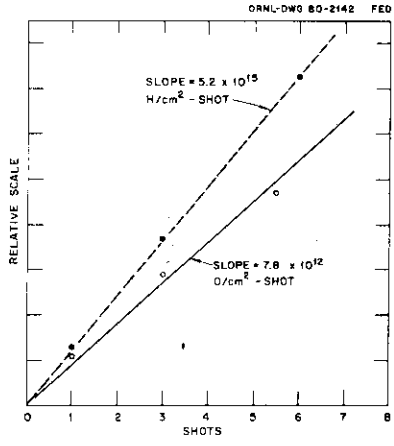
ORNL-DWG 80-2142 FED
SLOPE = 5.2 x 10^15
H/cm^2 - SHOT
SLOPE = 7.8 x 10^12
O/cm^2 - SHOT
RELATIVE SCALE
SHOTS

PRELIMINARY RESULTS

HYDROGEN COMPONENTS OF NEUTRAL BEAM

ENERGY	ATOM %	POWER %
E	29	51
E/2	28	24
E/3	43	25

IMPURITY COMPONENTS OF NEUTRAL BEAM

MASS	ATOM FRACTION (/H)
12 (C)	$< 10^{-3}$
16 (O)	1.5×10^{-3}
HIGHER Z	$< 10^{-5}$

PROBLEM AREAS

1. SAMPLE HEATING EFFECTS
2. ACCELERATING VOLTAGE NOT CONSTANT
3. OTHER (?)

PROPOSED EXPERIMENTS

1. PERFORM MEASUREMENT AS A FUNCTION OF PULSE LENGTH - 40, 100, 150, 200 MS.
2. TIME RESOLUTION - START EXPOSURE AFTER INITIAL 10-15 MS.
3. LATERAL PROFILE (H AND IMPURITIES).
4. CORRELATE PRESENT RESULTS WITH OTHER MEASUREMENTS OF BEAM COMPOSITION FOR SAME SHOTS.
5. OTHER.

2 - 2 TITANIUM GETTERED WALL EXPERIMENTS ON JFT-2

The JFT-2 Group

Japan Atomic Energy Research Institute, Tokai, Japan

Abstract Titanium gettering onto half a torus wall of JFT-2 reduced the oxygen impurity to one percent of electron density, and then improved the energy confinement and maximum density by a factor of 1.6. Origin of metal impurity in the JFT-2 tokamak was investigated experimentally and it was concluded that a predominant mechanism for metal contamination is the sputtering by light impurity ions.

I. Improvement of plasma Parameter[1)]

JFT-2 is a circular tokamak with a major radius of 90 cm. The minor plasma radius, in the present study, was chosen to be 20 cm by using the molybdenum rail limiter. In order to decrease the light impurity, titanium was gettered during each interval between successive discharge shots. Typical parameters of the JFT-2 tokamak are as follows; B_t = 10 - 18 kG, q_a = 2 - 4, $\bar{n}_e$ = 1 - 6 x 10^{13}cm^{-3}, $T_e(0)$ = 0.6 - 1.0 keV and Z_{eff} = 1.5 - 6.

Figure 1 shows typical examples of hydrogen discharge characteristics without and with titanium gettering. An effect of titanium-gettered wall is clearly revealed on a drop of the loop voltage V_L. This voltage drop is coming from that the dominant impurity, oxygen was reduced by a factor of several to 10. Under the titanium-gettering operation the central electron temperature decrease from 800 eV to 630 eV because of a reduction of Joule input power. The radiation power from the plasma decreased down, corresponding to the reduction of oxygen impurity. The titanium gettering successfully reduced the radiation loss and suppressed the peaking of current channel and then improved the energy confinement time by a factor of 1.6 and the maximum density from 4 x 10^{13}cm^{-13} (non-gettering discharge) to 6 x 10^{13}cm^{-3}. With titanium gettering the Z_{eff} value was reduced down to 1.5 in a high-density region.

II. Metal Impurity Contamination[2)]

With titanium gettering, the metal impurity (Mo, Fe) as well as oxygen was reduced by about the same factor as shown in Fig. 2 and Table 1. Titanium impurity was also observed in the gettering case, but its density was the same order of iron density, and so no bad effect on the plasma was observed. It is to be noted that the electron temperature of scrape-off plasma, T_{es} was almost the same in two cases; with and without titanium gettering. This data

is not strange because the reduction of light impurity leads to decrease of Joule input power. The present result is summarized as follows; under the same T_{es} the metal concentration depends on the light impurity one. This phenomenon may be different apparently in comparison with other experiments[3], but a key point in the present experiment is probably that the T_{es} is not so high as to bring about the self-sputtering of metal impurity.

III. Generation of Limiter Metal Impurity[4]

First, thermal evaporation is not a predominant source because the surface temperature of molybdenum limiter measured with an infra-red camera (AGA 680) was 400 - 600 °C at the end of discharges[5] and so it is too low to evaporate molybdenum. The arcing track was not identified on the limiter surface exposed only the stable discharges of 80 shots. On the other hand, the sputtering effect depends strongly on the species of the incident particles and their incident energy. When the sputtering is dominant, the molybdenum content should be a decreasing function of the T_{es}. A scaling on the scrape-off plasma[6] shows that a simple way to change the T_{es} is in control of the peripheral radiation cooling by light impurities. Then the T_{es} was varied by injecting hydrogen (working-gas) pulse during the current plateau phase. Figure 3 shows the relation between the T_{es} and the molybdenum contamination. At a high injection rate as the electron density rise increased the radiation cooling by oxygen atoms, the T_{es} was reduced by 10 eV and the molybdenum impurity was also reduced by a factor 2 or so in the experiment, where the oxygen density was kept constant.

Table 2 shows the comparison among hydrogen, deuterium and helium discharges. It is noted that the helium discharge is fairly different from the others. The molybdenum density in the helium discharge increased to about ten times that of the hydrogen and deuterium discharges. There was no change in both the T_{es} and the oxygen density. The loop voltage rise of from 1.2 to 2.0 volts in the helium discharge comes from helium itself because the oxygen impurity was reduced by the titanium gettering. The rise in the radiation loss is due to the increase of the molybdenum density and the profile of the radiation loss becomes center-peaked. These results show clearly that the sputtering by helium ions was the dominant process of the molybdenum release in the helium discharge. In the hydrogen plasma the molybdenum density can be explained as the sputtering by oxygen ions, because the sputtering yield of oxygen ion $\sim 10^{-1}$, which is necessary to explain the molybdenum density in comparison with the sputtering yield of helium ion, seems a reasonable value. The sputtering by oxygen ions can explain the simultaneous reduction of the metal impurity and oxygen impurity, which was

observed under the gettering operation. The self-sputtering of metal impurity is a sub-process because the T_{es} is rather low; 10 - 30 eV.

References

1) S. Konoshima, et al., J. Nucl. Mater. 76 (1978) 581.
2) S. Kasai, et al., to be submitted to Nucl. Fusion.
3) E. B. Meservey, et al., MATT 1175 (1975), TFR Group, Nucl. Fusion 17 (1977) 1297, J. Hugill, et al., Proc. 8th Eur. Conf., Prague, 1977, p. 39.
4) N. Suzuki, et al., to be presented at 9th European Conference on Controlled Fusion and Plasma Physics, Oxford (September 1979).
5) Y. Gomay, et al., Nucl. Fusion 18 (1978) 849.
6) DIVA Group, Nucl. Fusion 18 (1978) 1619.

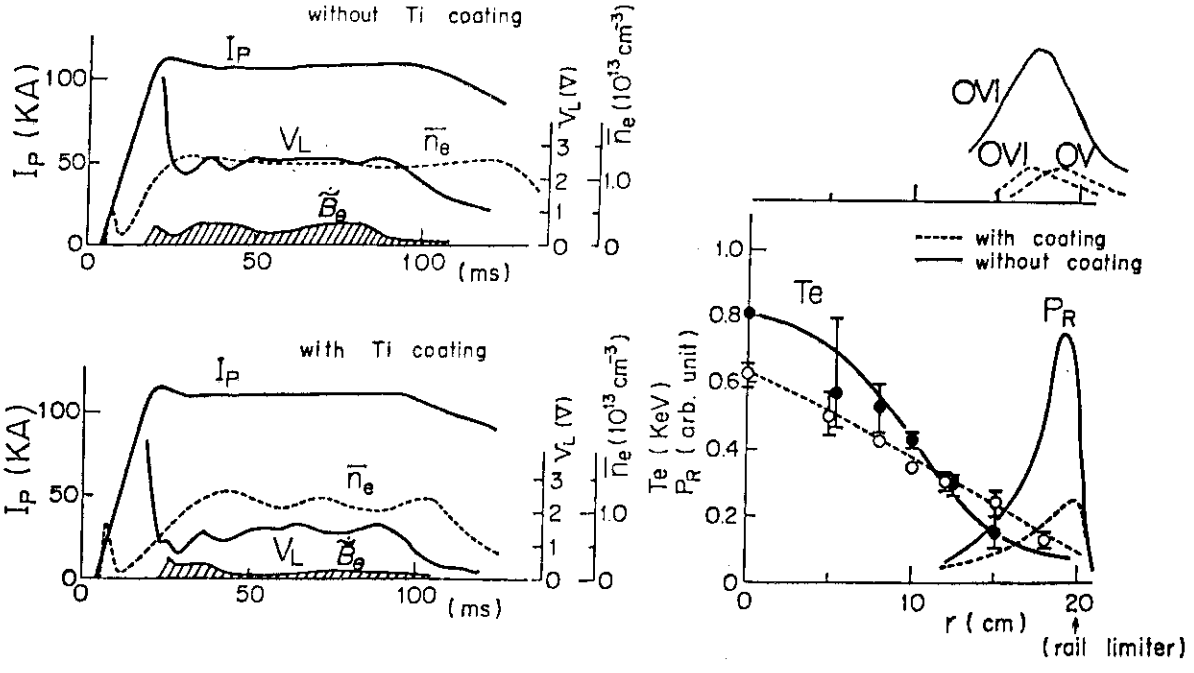

Fig.1 Hydrogen discharge characteristics without and with titanium gettering.

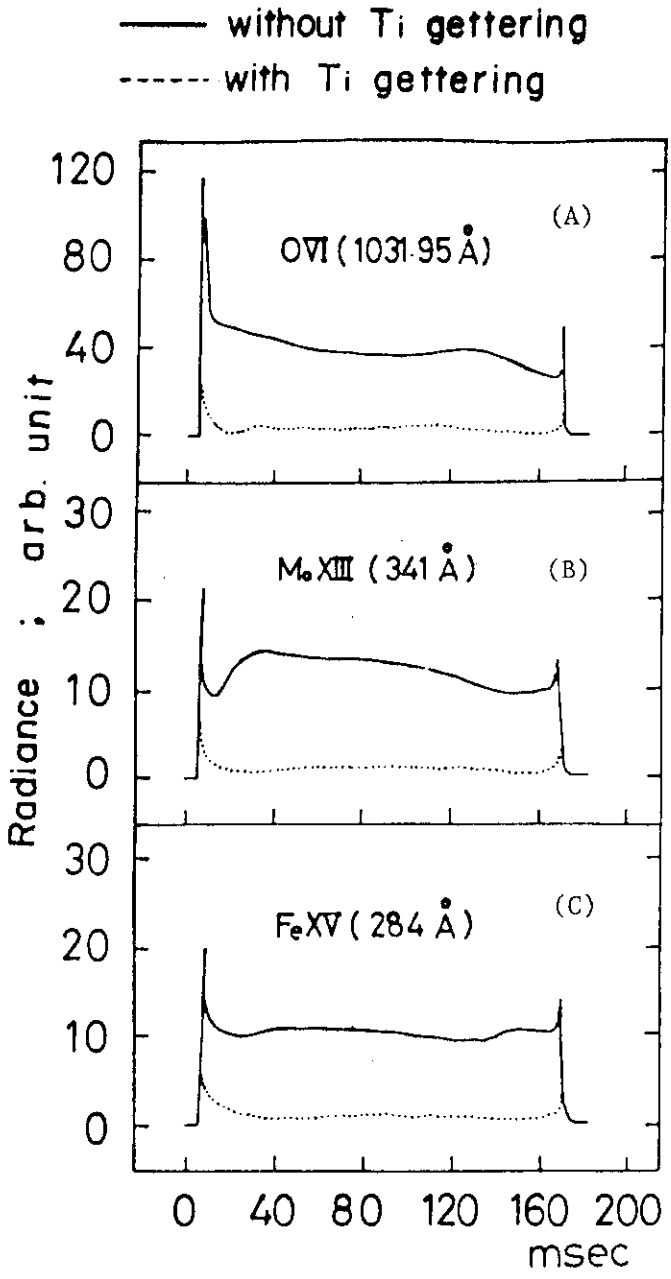

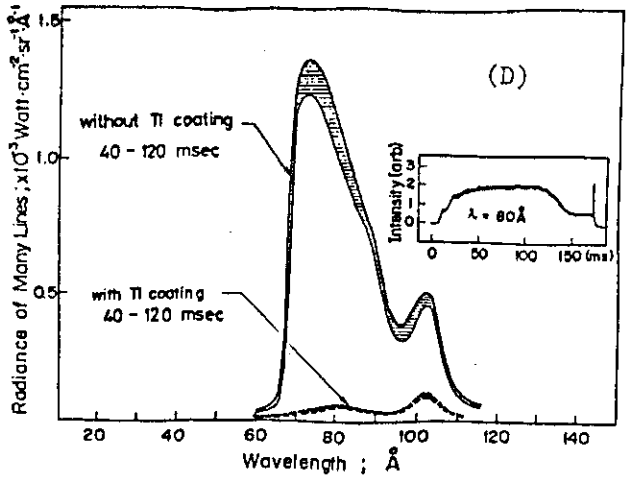

Fig. 2 Reduction of oxygen(A), molybdenum(B,D) and iron(C) impurities by titanium gettering. The figure(D) is the molybdenum pseudo-continuum radiation.

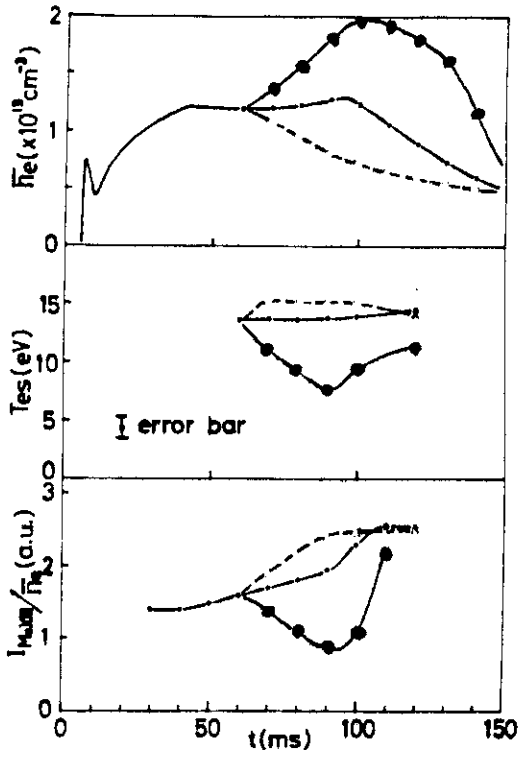

Fig. 3 Relation between scrape-off temperature and molybdenum impurity.

Table 1. Comparison between hydrogen discharges without and with titanium gettering.

V_L (V)	Tes (eV)		Oxygen (cm^{-3})				Zeff	Metal (cm^{-3})		
			O^{7+}	O^{6+}	O^{5+}	O^{4+}		Mo	Fe	Ti
2.7	30	without Ti-gettering	1E12	5E11	3E10	2E9	5.5	~1E9	~1E9	
1.5	30	with Ti-gettering	2E11	9E10	3E9	2E8	2	~1E8	$\lesssim$1E8	~1E8

[e.g. 2E10 should be read as 2×10^{10} cm^{-3}]

Table 2. Comparison among hydrogen, deuterium and helium discharges with titanium gettering.

Working Gas	V_L (Volt)	OVI (a.u.)	MoXIII (a.u.)	Tes (eV)	P_R (a.u.)	Sputtering Yield (atoms/ion)
H_2	1.2	2.3	~1.5	~12	12	$<10^{-4}$
D_2	1.2	2.5	~2.5	~13	15	$<10^{-4}$
He	2.0	2.7	~22	~12	83	$\sim10^{-2}$

3 - 1 Impurity Experiments on JIPP T-II

N. Noda, K. Kadota, K. Sato and J. Fujita
Institute of Plasma Physics, Nagoya University,
Nagoya, Japan

1. Introduction

One of the major subjects in JIPP T-II experiments is to produce low q, high density tokamak plasma free from major disruptions. This has been achieved by a combination of gas-puffing and current-profile control [1]. When strong gas-puffing is applied to raise the plasma density in the JIPP T-II, influx of cold neutral gas cools the outer region, and it causes a peaking of electron temperature profile, which leads to major disruptions (see Fig. 1 a). Additional current-rise has been applied in the density-rising phase (see Fig. 1 b), where skin-current heating with this second current-rise raises the temperature of the outer region again. It has been found that the temperature-profile control with this current-waveform is effective on the suppression of major disruptions. Impurity behaviors have been investigated by means of visible and VUV spectrometers. In this paper, we present some of the data on impurity behavior obtained. We also give brief discussion on mechanism of impurity generation. The machine parameters are given in Table 1. The JIPP T-II has the limiters of two types shown in Table 1. Both of these limiters are made of molybdenum. Time evolutions of plasma parameters are shown in Fig. 1. The figure 1 a) shows that for

the case in which only gas-puffing is applied, 1 b) for the one in which both the gas-puffing and the second current-rise are applied.

2. Experimental Results and Discussion

i) molybdenum (limiter material)

The figure 2 shows the waveforms of line radiations Mo I and Mo II in the case with the second current-rise (see Fig. 1 b). These are observed with a visible spectrometer through a port situated in the vicinity of the diaphragm limiter. There are two characteristic features in the behavior of the Mo I radiation.

a) Intensity of the radiation decreases in a large amount just after the gas-puffing.

b) Intensity after the second current-rise does not return to the level as large as the one before the gas-puffing.

A problem is whether these features are consistent or not with an assumption that the source of the impurity of limiter material is mainly ion-sputtering and/or arcing. If this assumption is true, the molybdenum influx at the limiter surface must depend on electron temperature at the peripheral region. The feature a) is natural since the peripheral temperature measured with Thomson scattering decreases in this phase. Since the temperature reaches as high as before the gas-puffing at the high-density plateau (120 -150 ms in Fig. 1 b), the feature b) is not explained from the above assumption if the line radiation in Fig. 2 a) directly reflects the amount of influx. This will be explained if ionization mean free path is taken into account. The molybdenum neutrals are ionized by electron impact and the neutral density

is reduced with the distance from the limiter surface. The reduction rate becomes large with electron density if temperature is constant. The data of Thomson scattering show that the density at the high density plateau is 3 or 4 times larger than the one before the gas-puffing both in the central region and the outer region of plasma. This means that the mean free path of molybdenum neutrals is reduced by a factor of 3 or 4 in this high density regime. We can explain the difference between the signal level of Mo I before the gas-puffing and the one at the high density plateau as a result of decrease in the ionization mean free path of molybdenum neutrals, that is, the influx rate at the surface of the limiter remains unchanged at the high density plateau compared to the state before the gas-puffing. The situation for radiation of Mo II is not so different from the case of Mo I since the mean free path of Mo^+ ions is about of the same order as that of neutrals.

ii) iron (wall material)

The figure 3 shows the time behaviors of radiations Fe XV and Fe XVI. It is remarkable that the intensity greatly increases after the gas-puffing with the second current-rise. It has been observed that the fast neutral flux due to the charge-exchange process decreases at the location distant from the gas-puffing region. Although we have not observed the fast neutrals at the gas puffing region, the flux must increase in this region. The increase in radiation intensities may be due to the increase in fast neutral flux at the gas-puffing region.

iii) oxygen

The figure 4 and 5 show the time variations of the radiation from oxygen ions. The radiation of O VIII reflects the oxygen density in the central region. The figure 4 a) shows that the amount of increase in O XIII is around factor 3 for the case with the second current-rise. This value is as large as the amount of the density-rise (see Fig. 1 b). On the other hand, the reduction of excitation rate due to lowering of the electron temperature is nearly factor 2. This means the oxygen density in the center increases in some degree. The behavior of radiations O VI, O V (fig. 4 c, d) suggest that the oxygen influx rises at the high density plateau (120 -150 ms in Fig 1 b). This is consistent with the increase of oxygen density in the central region. The increase of the influx may be explained as a result of charge-exchange neutral flux enhanced at the gas-puffing section.

Comparing the case without the second current-rise (fig. 5) to the one with the current rise (Fig. 4), one can fined remarkable difference in the radiations from oxygen of lower ionization states. Those radiations in both cases rise at the first stage after the gas-puffing. In the later stage, however, the radiations in the case without the current-rise continue to increase until disruption occurs. This is contrary to the case with the current rise, where the radiation intensities fall. This is explained as follows; the radiation increase is due to the enhancement of recombination process which is caused by the considerable lowering of electron temperature and the increase of density. The lowering of temperature continues in the case without the current-rise. Contrary in the case with the current-rise, the temperature is

raised again in the later stage, which leads to the reduction of recombination rate. There are some other data which support the contribution of recombination process. Time history of the radiaion increase is one of those data. The radiation from ions in higher ionization states precedes the one from lower state. This is also able to be understood when recombination is taken into account.

3. Summary

The time behavior of the radiation intensity from molybdenum observed in the vicinity of the limiter is consistent with the explanation that an origin of limiter-material impurity is the sputtering by impurity ions and the generation rate rises with peripheral electron temperature.

Both oxygen and iron influxes become large at the high density plateau compared to those before the gas-puffing and the second current-rise are applied. This may be explained as a result of enhanced charge-exchange neutral flux at the gas-puffing region. In the transient phase of density-rise, we observed significant enhancement of radiations from oxygen in lower ionization states. This is not related to influx rate but to recombination process caused by the lowering of temperature and increase of density.

Acknowledgement

The authors are indebted to all the members of JIPP T-II group for the cooperation to the experiments. The authors also thank to operators of the fly-wheel generator for their laborious effort in maintenance and operation of the machine.

Reference

1) K. Toi et al., Nucl. Fusion 19 (1979) 1643

Table 1 Machine Parameters of JIPP T-II

Major Radius	91 cm
Diameter of Diaphragm Limiter	34 cm
Distance of Top-Bottom Rail Limiter	30 cm
Inner Diameter of Vacuum Chamber	40 cm
Toroidal Magnetic Field	26.4 kG

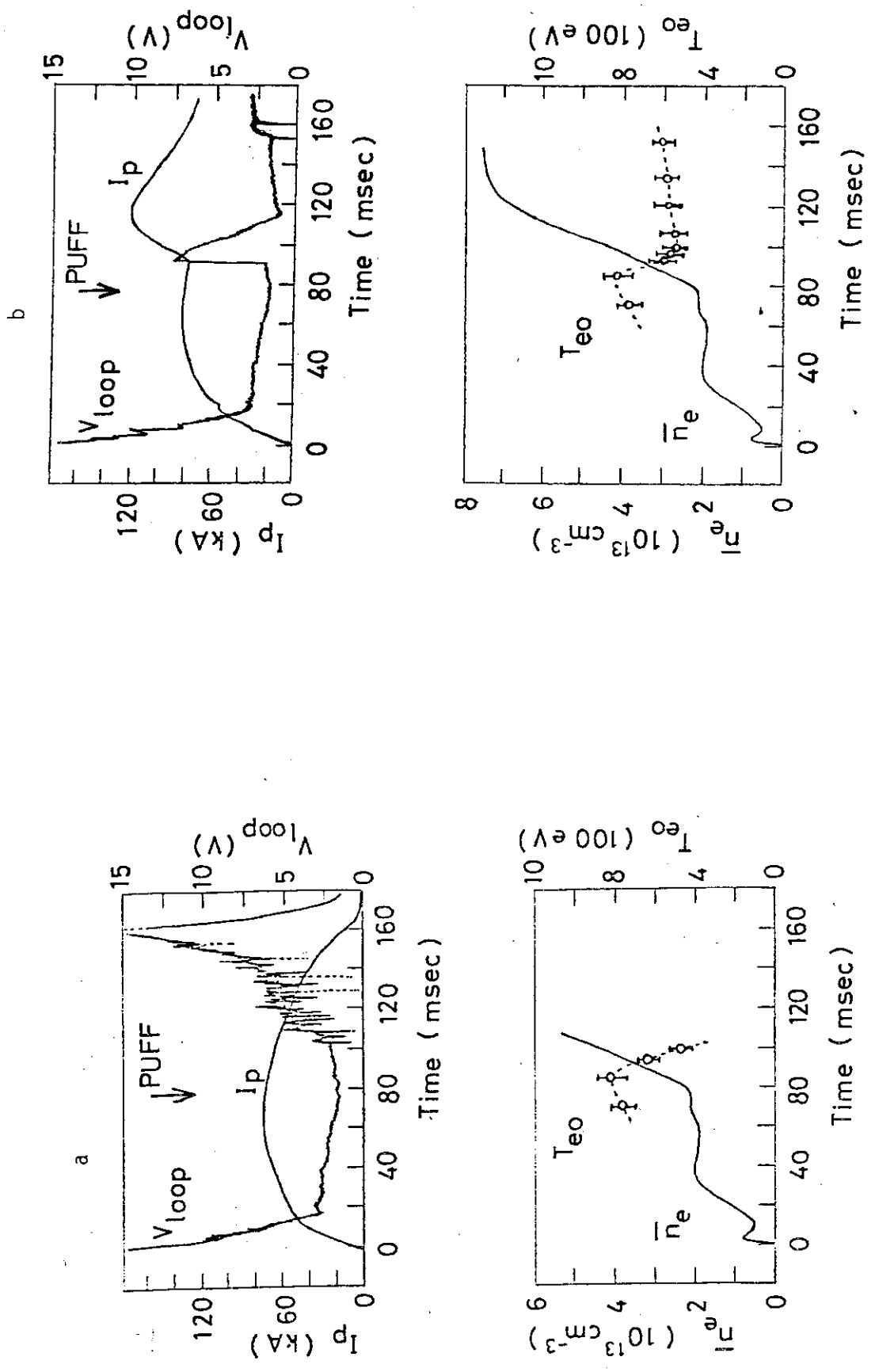

Fig. 1 Time behavior of plasma parameters; a) with gas-puffing only, b) with gas-puffing and second current-rise.

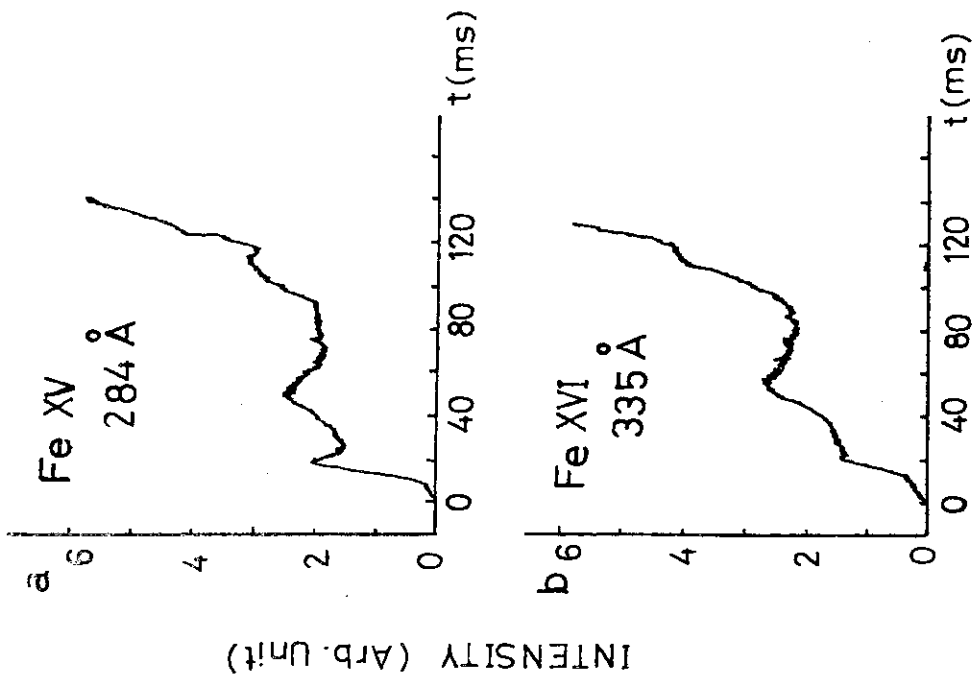

Fig. 3 Radiations of Fe XV and Fe XVI in the case with gas-puffing and current-rise.

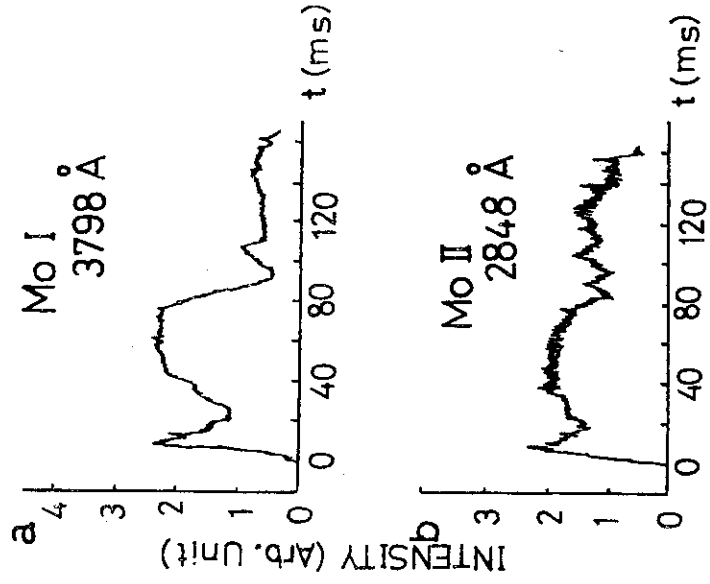

Fig. 2 Radiations of Mo I and Mo II in the case with gas-puffing and current-rise.

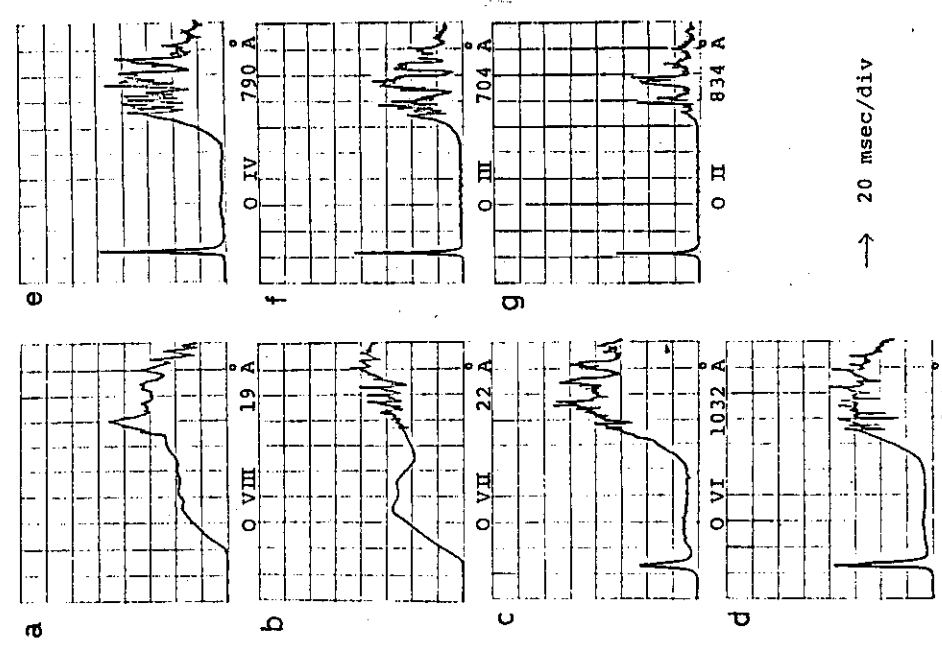

Fig. 4 Radiations from oxygen in the case with gas-puffing and current-rise.

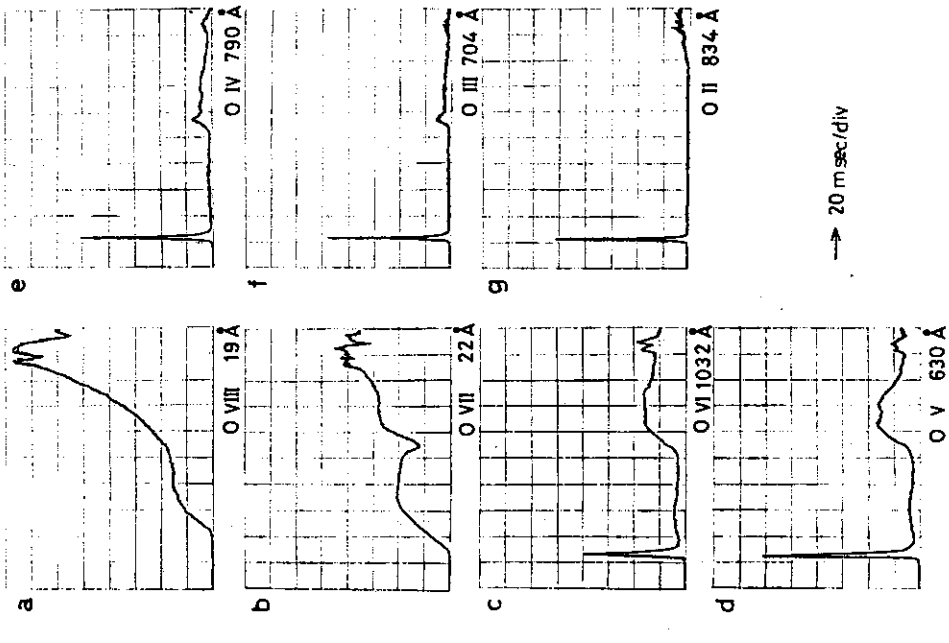

Fig. 5 Radiations from oxygen in the case with gas-puffing only.

3 - 2 Monitoring of Radiation Power from HYBTOK-I Plasma with Microchannel Plate

K. Hayashi, S. Takamura, and T. Okuda
Department of Electrical Eng. Nagoya University,
Nagoya 464 JAPAN

1. Introduction

A study on impurity transport in HYBTOK-I plasma has been made with a visible spectrometer and compared with a computer simulation developed in our laboratory. It is concluded that the impurity transport must be the neoclassical diffusion in Pfirsch-Schlüter region in order to explain the radial profiles of impurity lines, for example CII(426.7 nm) and CIII(464.7 nm). In the present study the radiation power from impurities was measured by using phototubes and a MCP [1] (microchannel plate; Fig.1). MCP can be used not only as a detector of vacuum ultraviolet rays but also as a image detector of plasma cross-section. As the microchannels operate independently and gain is available at each microchannel location in the array ($10^3 \sim 10^4$), the incident radiation pattern is preserved during amplification. The plate can resolve simultaneous events that are spatially separated by distances on the order of the channel size. In such cases the amplified electron output is collected from the channel plate by a multisegment anode or a phosphor screen, appropriately biased with respect to the output electrode of MCP.

The objectives of the present experiment are 1). to measure the radiation power from the plasma, 2). to test the performance of MCP under the practical environment.

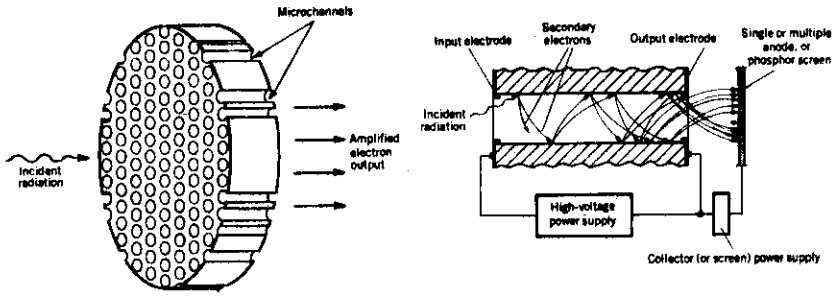

Fig.1

2. Experiment

1). HYBTOK-I

HYBTOK-I [2] is a small tokamak device without conducting shell. Its major radius is 30 [cm] and its minor radius (limiter radius) is 7.5 [cm]. The equilibrium of plasma is attained with an octopole field and a pre-programmed vertical field. The octopole field shapes the magnetic surface and makes the cross-section of plasma noncircular.

2). Measurement with phototube I and MCP

As it is expected that the strongest lines from the plasma lie in the vacuum ultraviolet and the far ultraviolet region, MCP (40～120 nm) and phototube I (115～300 nm) with MgF_2 window are employed. Figure 2 shows their sensitivities. As can be seen in Fig.3 (cross-sectional view of the measurement apparatus), the vertical scanning gives the distribution of the emission coefficient by Abel inversion.

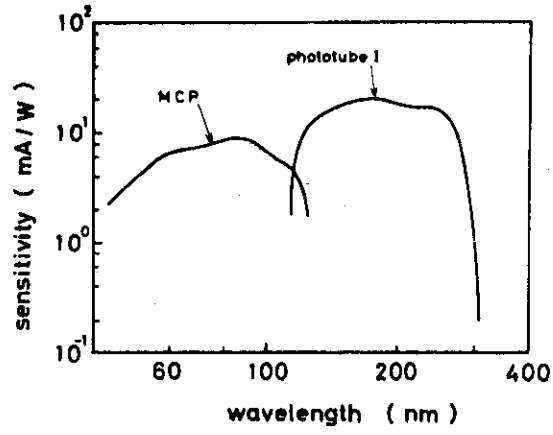

Fig.2

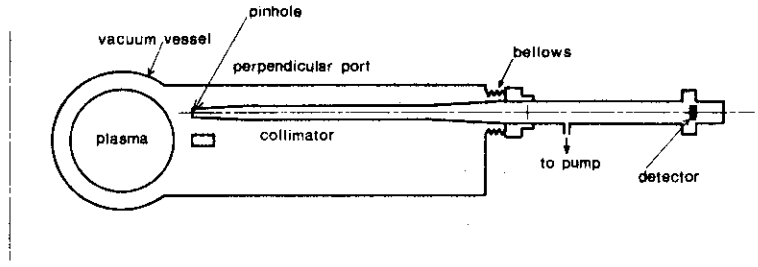

Fig.3

Figure 4 shows one turn voltage, plasma current, horizontal displacement of the current center and output signal of MCP. The emission coefficient is shown in Fig.5. A Joule input is 200 [kW] at t=0.5 [msec] (at the current plateau), while the total radiation power from the plasma is only 200～400 [W].

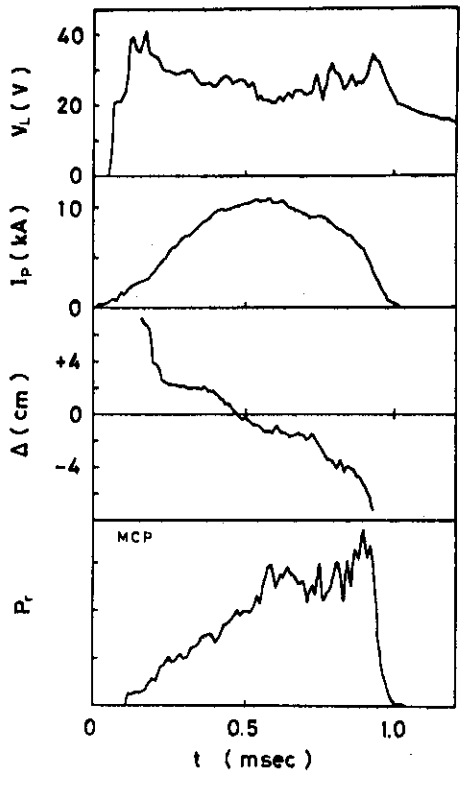

Fig.4

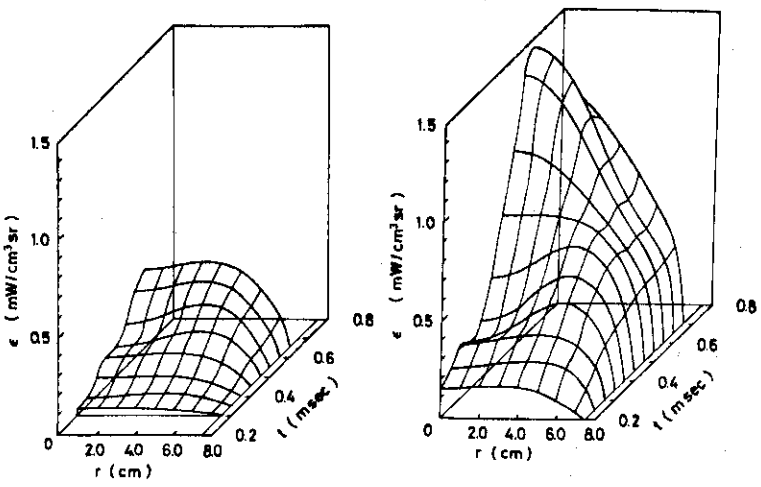

Fig.5

3). Measurement with phototube II and phototube II SS

Two additional experiments are made to verify the experimental results in 2). One is to measure the radiation power with phototube II for the visible radiation and the other is to measure the radiation power in the vacuum ultraviolet and the far ultraviolet region with phototube II SS, prepared by spraying its entrance window with a dilute solution of sodium salicylate in ethyl alcohol. Both sensitivities are shown in Fig.6. As is shown in Fig.7, the radiation power in the visible region is 1/50 ~ 1/100 of the power in the vacuum ultraviolet and the far ultraviolet region, so we can conclude that the visible radiation power is negligibly small compared with a short wavelength emission. Figure 8 shows time evolutions of detected intensities obtained with MCP and phototube I and that with phototube II SS. Both results agree, and the value of total radiation power is 200 ~ 400 [W].

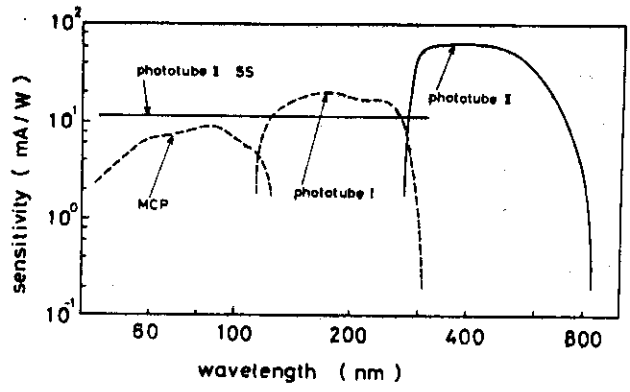

Fig.6

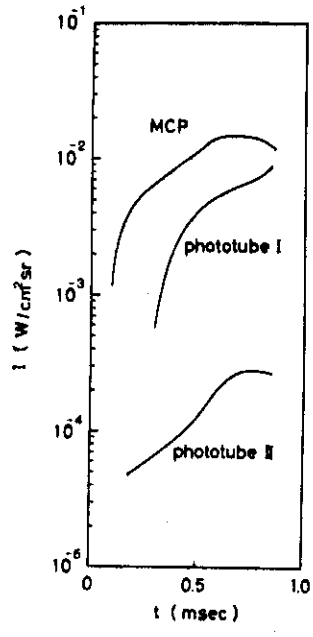

Fig.7

3. Simulation of the Distribution of the Emission Coefficient

The space and time evolution of the emission coefficient is computed with the one-dimensional simulation code [3]. The transport of the impurities (carbon and oxygen) is computed by taking account of both the neoclassical diffusion in Pfirsch-Schlüter region across the magnetic field toward the plasma center and the successive ionization-recombination process.

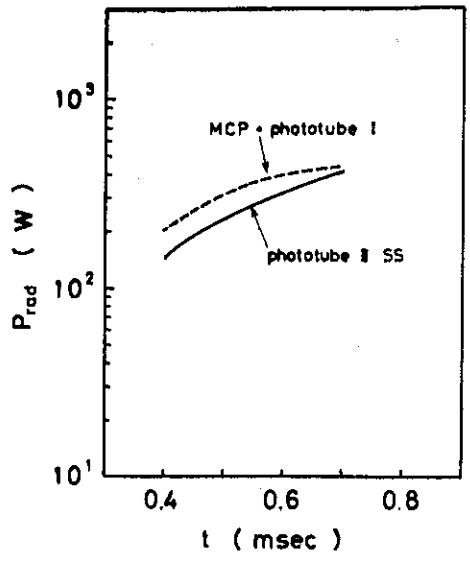

Fig. 8

The equations for the radial diffusion of impurities in various states of ionization are given by

$$-v_1 \frac{\partial n_1}{\partial r} = -n_e \alpha_1 n_1 \qquad (1)$$

$$\frac{\partial n_k}{\partial t} = -\frac{1}{r}\frac{\partial}{\partial r}(r\Gamma_k) + n_e\{\alpha_{k-1} n_{k-1} - (\alpha_k + \beta_{k-1}) n_k + \beta_k n_{k+1}\} \qquad (2)$$

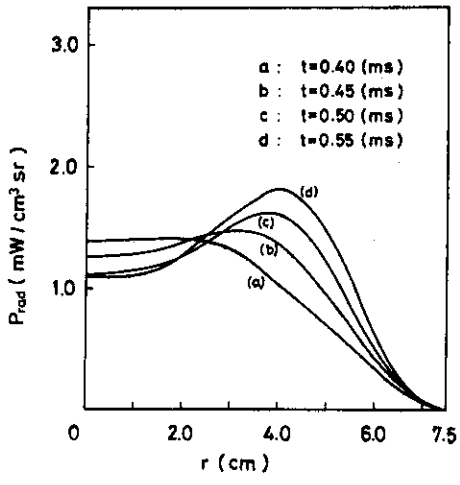

Fig. 9

The first equation gives the radial distribution of the density n_1 of each neutral impurity, which flows into the plasma with a initial velocity v_1. Equation (2) is a rate equation for impurity ions. In these equations n_e is the electron density, n_k is the impurity density of k species in the (k-1)-th ionized state, Γ_k is the particle flux of impurity ions. Coefficients α_k and β_k are ionization and radiative recombination rates, respectively. Both coefficients are given by Hinnov [4]. The radiation power is computed by the following equation.

$$P_{rad} = 3.2 \times 10^{-33} E_H \left(\frac{E_H}{T_e}\right)^{\frac{1}{2}} n_e$$

$$\times \left\{ n_3^c e^{-\frac{12}{Te}} + n_4^c \left(e^{-\frac{8}{Te}} + e^{-\frac{40}{Te}} \right) + 2 n_5^c e^{-\frac{308}{Te}} + 2 n_6^c e^{-\frac{370}{Te}} \right.$$
$$+ n_2^o e^{-\frac{15}{Te}} + n_3^o e^{-\frac{16}{Te}} + n_4^o e^{-\frac{16}{Te}} + n_5^o e^{-\frac{20}{Te}}$$
$$\left. + n_6^o \left(e^{-\frac{12}{Te}} + e^{-\frac{83}{Te}} \right) + 2 n_7^o e^{-\frac{575}{Te}} + 2 n_8^o e^{-\frac{655}{Te}} \right\} \quad [W/m^3] \quad (3)$$

(see Ref. [5])

The simulation result is shown in Fig.9. Before t=0.5 [msec], a peak appears at a radius of r=4 [cm].

4. Conclusions

1). The radiation power from the HYBTOK-I plasma is 200 ~ 400 [W]. The radial shape has a peak at a radius of r=4 [cm] before t=0.5 [msec] and at the center after t=0.5 [msec]. The former distribution is explained to take account of the inward diffusion of impurities, but the latter isn't. The peaking of the radiation may be caused by MHD instability.

2). There is no trouble in using MCP, for example, a breakdown and a rapid decrease of sensitivity. The next stage of monitoring the cross-section of the plasma will be performed as is shown in Fig. 10. A pinhole camera using the MCP as a detector should be installed on the tangential port of HYBTOK-I. The shape of the cross-section and radiating region is seen through vacuum ultraviolet rays. That is to say, vacuum ultraviolet topography.

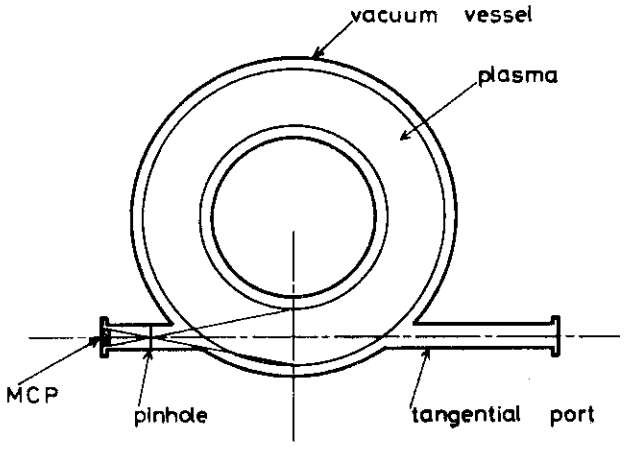

Fig.10

References

[1] B. Leskovar : Phys. Today 30 No.12 (1977) 42.

[2] T. Okuda, Y. Tanaka, K. Sakurai and K. Nakamura : Proc. 8th Europ. Conf. Controlled Fusion and Plasma Physics, Prague, Vol. 1 (1977) 121.

[3] T. Kuzushima et al. : Kakuyugo-Kenkyu Circular in Japanese 39 (1978) 103.

[4] E. Hinnov : MATT-777 (1970)

[5] D. Düchs and H.R. Griem : Phys. of Fluids 9 (1966) 1099

4 - 1 THE DIVA EXPERIMENTS (I)

DIVA GROUP presented by Shin Yamamoto
JAERI, Tokai, Naka, Ibaraki, Japan

ABSTRACT

Divertor actions were quantitatively investigated over a wide range of plasma parameters, with various wall materials, i.e., high(gold), intermediate (titanium) and low(carbon) Z wall.

1. INTRODUCTION

DIVA/JFT-2a was a tokamak device with teardrop-like cross section capable of operating with an axisymmetric divertor[1.2], which was operated from Sept. 1974 to Sept. 1979. In the device, impurities from the wall materials were mainly studied without impurities from absorbed gas, i.e., impurity origin, impurity effects, impurity transport not only in the main plasma but also in the scrape-off layer plasma, impurity control and improvement of energy confinement by reducing impurities. Characteristics of scrape-off layer plasma which are very important to discuss impurity control in fusion devices were also investigated. These results are summarized in this paper.

Table 1. History of DIVA

June 1973 ---	Analysis of configurations R&D Design Construction
Sept. 1974 ---	Operation Divertor configuration Scrape-off layer plasma Gas impurity free plsama Pseudo-continuum Metallic impuruty study Divertor actions
May. 1977 ---	Improvement (1T → 2T) Scaling of scrape-off layer plasma Improvement of plasma confinement Particle and impurity transport Origin of metal impurities ICRF heating Very-low-q discharges Disruption Carbon limiter and carbon wall
Sept. 1979 ---	Shut down

2. DEVICE AND DIAGONOSTICS

The cross-sectional view of DIVA and the typical plasma parameters are summarized in Fig. 1. Various kinds of diagonostic methods including conventional ones were employed and summarized below. Numerical codes, i.e., the tokamak codes, Monte Carlo codes for neutrals, Monte Carlo codes for impurities in the scrape-off layer, mhd code with external coils and tearing code, were applied for analysis.

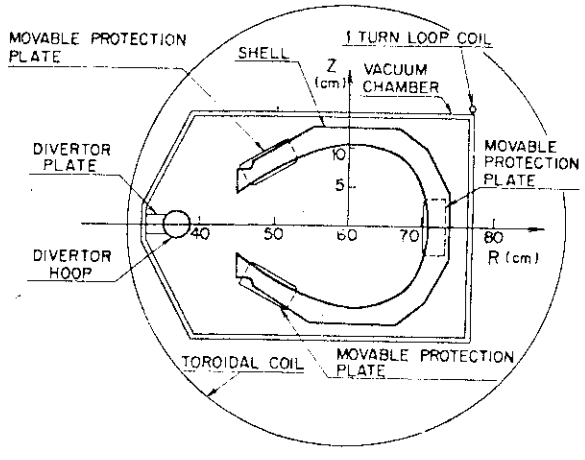

FIG.1. Cross-sectional view of DIVA.

Main Plasma	
Major radius, R (cm)	60
Minor radius, a (cm)	10
Toroidal magnetic field, B_T (T)	0.8 - 2.0
Plasma current, I_p (kA)	10 - 80
Ohmic input power, P_{in} (kW)	40 - 200
Density, n_{eo} (cm^{-3})	$(2 - 14)\times10^{13}$
Electron temperature, T_{eo} (eV)	200 - 700
Ion temperature, T_{io} (eV)	70 - 300 (430 eV, ICRF)
Energy confinement time, τ_E (ms)	0.7 - 5.7
Particle confinement time, τ_p (ms)	0.5 - 3.0
Safty factor, q_a	1.3 - 6.0

Scrape-off Plasma	
Electron temperature, T_{es} (eV)	20 - 100
Ion temperature, T_{is} (eV)	20 - 70
Density, n_{eo} (cm^{-3})	$(2 - 10)\times10^{13}$

Configurations:
B_p, particle and heat flow, potential, high spead camera and Hard X-ray (two dimensional measurements of drift surface of runaway electrons[3], heat flux and particle flux in the scrape-off layer)

Main plasma:
laser, cx, doppler, 2&4 mm, PIN (non-circular cross-section of q=1 magnetic surface[4]), bolometer, X-ray energy analyzer and average particle confinement time (saturation current on various wall and $H_{\alpha,\beta}$[5]).

Scrape-off layer:
$f_{//i,e.}$ (movable small electrostatic analyser[6]), $T_{i\perp}$ (Katsumata probe[7]), v_f (oneside electrostatic probe[5]), $D_\perp$ (combination of movable limiter and one side probe[8]) and heat transport rate (combination of thermocouple and electrostatic probe[6])

Impurities in the main plasma and in the scrape-off layer plasma:
visible, VUV, bolometer, numerical code, impurity injections (laser, arc, gas puff of 100 μs), pseudo-continuum (space and wave-length scan[9])

Fluctuations and disruptions:
$\tilde{B}_p$, PIN, $\tilde{n}_e$, $\tilde{V}_L$, $\tilde{T}_p$, impurity injections and $\tilde{T}_e$ (laser is triggered by sawtooth signals[10])

Surface & impurity origin:
AES, SEM and impurity efflux v.s. limiter temperature or limiter voltage

3. EXPERIMENTAL RESULTS

1) Impurity production

(1) Absorbed gas

It is easy to obtain a plasma free from gaseous impurities by cleaning the first wall surface of Au, Ti or C[11,12,14]. After reducing gaseous impurities, radiation loss due to pseudo-continuum becomes dominant with Au-Wall[13,15].

(2) Wall materials

It was clarified what is the major mechanism of metallic impuriry production[12,16]. Experimental results show that the self-sputtering of the metallic impurity ions accelerated by the sheath potential near the limiter surface is the major mechanism of metallic impurity recycling in the ordinary discharge. The evaporation of the limiter surface occurs by local deposition of high energy electrons in low density discharges and by arcing in the current rising phase or disruptive phase of discharge, or in the case of a dirty limiter surface. Role of runaway electrons in the formation of arcing on the electrically isolated target was discussed[17].

Carbon wall with a carbon limiter was also investigated and it was shown that the chemical sputtering is easily suppressed by pre-bombarding the limiter surface at a high temperature. Consequently, ion sputtering becomes dominant[14].

2) Equilibrium

Stable configurations with a separatrix magnetic surface by using a divertor coil current and a copper shell were obtained[3, 19,20] and dynamic magnetic limiter operations were stably demonstrated[21]. The non-axisymmetric perturbation deforms the old separatrix magnetic surface and there appears an ergodic region around the old separatrix[3].

3) Stability

The separatrix magnetic surface stabilizes the surface mode but separatrix

magnetic surface does not affect the tearing mode[23]. No major disruption is observed in impurity free plasma with and without the divertor. And the major disruption is excited with both of the impurity injection and the internal disruption. The amount of injected impurities exciting the major disruption in the diverted discharge is two times larger than those in non-diverted discharge [22,23]. No major disruption can be excited in non-diverted and diverted discharge with $q_a < 2$ because of no existance of the resonance surface for m=2/n=1 [23]. Ranaway electrons and heat flux are well guided to the divertor even in the disruptive phase[20,23].

4) Confinement

Impurity reduction by the divertor or other method increases the energy confinement by a factor of 2.5 by increasing the radius of the hot column but does not affect diffusion coefficients[13,24]. Therefore the following modified ALCATOR scaling can well describe the observed energy confinement time both with and without the divertor.

$$\tau_E = 1.8 \times 10^{-14} \sqrt{q_a}\, \bar{n}_e a_{half}^2 \text{ sec.} \qquad (q_a \gtrsim 1.3)$$

where q_a, n_e and a_{half} are the safty factor, the mean electron density in cm^{-3}, and the half radius of the electron temperature profile in cm. The divertor increases a_{half} by reducing the impurity level[23]. DIVA was able to operate at low-q and high density simultaneously. High density with the Murakami scaling factor $\bar{n}_e R/B_T (10^{19} m^{-2} T^{-1})$ of 5 was obtained at q_a = 1.7[23].

5) Impurity transport in the main plasma and in the scrape-off layer

Impurity influxes to the hot column are shown in the following figure[13, 25~30].

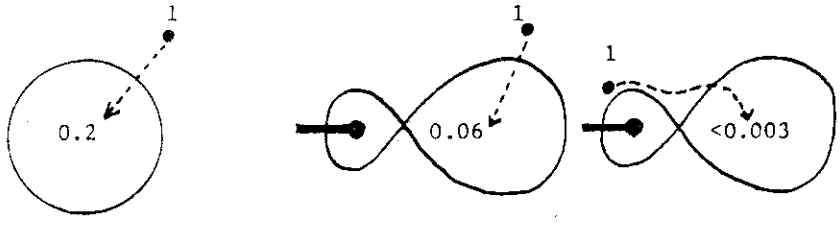

The observed impurity profiles in the main plasma are well described by the combination of neoclassical and anormalous effects. The anormalous diffusion coefficient is almost equal to that of electron energy loss. The transport of impurities in the scrape-off layer is well explained by a Monte Carlo code. Therefore the experimental results shown in the above figure are well described by the tokamak code and the Monte Carlo code.

6) Scrape-off layer

(1) Scaling law[8,24,30]

Essential parameters in the scrape-off layer plasma are v_f, γ and $D_\perp$, where v_f, γ, $D_\perp$ are the particle flow velocity, the heat transport rate and the diffusion coefficient. These parameters were studied. The following results were obtained with B_T = 0.8 - 2.0 T, $n_{es} = (1.5 - 5.0) \times 10^{12} cm^{-3}$, T_{is} =20 - 100 eV and T_{is} = 20 - 70 eV.

$$\begin{cases} v_f \sim 0.3\ C_s \end{cases}$$

$$\begin{cases} D_\perp \sim 0.1\ D_B \\ \gamma \gtrsim 100 \text{ in runaway discharges} \\ \gamma \sim (7 - 15) \text{ in normal discharge} \end{cases}$$

where C_s and D_B are sound velocity and Borm diffusion coefficient. The observed γ in normal discharges is well described by the sheath model including the effects of secondary electrons and epithermal electrons. The results give the following simple equation according to the energy conservation law.

$$\bar{T}_{es} \sim 0.2 \frac{(P_{in} - P_{cx} - P_R)}{P_{in}} (\bar{T}_e + \bar{T}_i) \frac{\bar{\tau}_p}{\tau_E}$$

where $\bar{T}_{es}$, P_{in}, P_{cx}, P_R, τ_p, τ_E, $\bar{T}_e$ and $\bar{T}_i$ are edge temperature, input power, charge-exchange loss-power, radiation loss-power, particle confinement time, energy confinement time, electron temperature and ion temperature, respectively.

This eqation shows that temperature at the edge is extremely high in a high-temperature tokamak with $P_{in} \gg P_{cx} + P_R$ and $\bar{\tau}_p/\tau_E \sim 1$, and it is expected that the surface erosion and the impurity production become serious. Thus, some method of cooling the plasma edge down to a sufficient low temperature, typically several tens of electron-volts or reducing $\bar{\tau}_p$, is required in conventional devices[31].

4. CONCLUDING REMARKS

Clean titanium gettered on the first wall(shell and limiter) was employed to eliminate metal impurities as well as gaseous impurities. Very-low-q discharge has been achieved to q_a = 1.3 with good confinement. Also, DIVA was able to operate at low-q and high density simultaneously, controlling the gas influx during the current build-up phase, and high β plasma was obtained. The high efficiency ICRF heating was also demonstrated with impurity free plasma[32]. For present ohmically heated or low power additionally heated tokamak, intermediate Z material of titanium has been an acceptable altanative.

Carbon is attractive for the first wall in a reactor, because (i) the radiation power density is low in a high temperature plasma and high in a boundary plasma, (ii) thermal properties are as good as those of Cu, Mo and W and (iii) the self sputtering yield is smaller than that of high-Z material such as Mo. In-situ coating carbon wall with carbon limiter was performed in DIVA. Discharge parameters obtained in the carbon wall differed little from those obtained in the regimes with titanium gettering.

Divertor actions as well as divertor effects on impurities and confinements were quantitatively investigated over a wide range of plasma parameters, with various wall materials. The divertor actions were succesfully demonstrated. The divertor configuration does not affects transport coefficients in the confined plasma. The basic characteristics of scrape-off plasma with T_{es} = 20 - 100 eV, T_i = 20 - 70 eV and n_{es} =(1.5 -5) x10^{12} cm^{-3} were investigated. The scrape-off layer plasma with these parameters may simulate the plasma contacting a material surface in a reactor because the plasma has to be cooled down to several tens of electron-volts at the material surface even in a reactor. In addition, thermal properties and self sputtering of gold are worse than those of other materials. Thus, experimental results obtained in DIVA is encouraging for the future high power additional heating experiments with an appropriate first wall material.

ACKNOWLEDGEMENTS

We are grateful to Drs Y. Tanaka, M. Tanaka, M. Yoshikawa, Y. Obata and S. Mori for their continuous encouragement of our works.

REFERENCES

[1] M. Yoshikawa et al., Proc. 6th Europ. Conf. on Controlled Fusion and Plasma Phys. (Moscow, 1973) p.173.
[2] Y. Shimomura et al., JAERI-M 6102 (1975).
[3] S. Yamamoto et al., Nuclear Fusion 18 (1978) 205.
[4] S. Yamamoto et al., to be published in Japan J. Appl. Phys.
[5] H. Ohtsuka et al., Plasma Physics 17 (1978) 1281.
[6] H. Kimura et al., Nuclear Fusion 18 (1978) 1195.
[7] K. Odajima et al., Japan J. Appl. Phys. 17 (1978) 1281.
[8] H. Kimura et al., JAERI-M 6971 (1977).
[9] S. Kasai et al., Nuclear Fusion 19 (1979) 195, J. Phys. Society of Japan 46 (1979) 241 and M. Shiho et al., JAERI-M 7397 (1977)
[10] T. Yamauchi et al., to be published.
[11] M. Nagami et al., Nuclear Fusion 18 (1978) 529.
[12] H. Maeda et al., Plasma Phys. and Controlled Nuclear Fusion Research (Innsbruck, 1978), 1, 377.
[13] S. Yamamoto et al., Proc. 8th Europ. Conf. on Controlled Fusion and Plasma Physics (Prague) 1, 33 and 2, 234 (1977).
[14] S. Sengoku et al., to be published.
[15] H. Maeda et al., Plasma Wall Interaction (Julich, 1976) 537.
[16] K. Ohasa et al., Nuclear Fusion 18 (1978) 874 and J. Phys. Society of Japan 46 (1979) 1635.
[17] S. Yamamoto et al., J. Phys. Society of Japan 48 (1980) 1053.
[18] S. Sengoku et al., JAERI-M 8465 (1979)
[19] Y. Shimomura, Proc. 7th Europ. Conf. on Controlled Fusion and Plasma Physics 1 (Lausanne, 1975) 81.
[20] Y. Shimomura et al., Phys. of Fluids 16 (1976) 1935.
[21] Y. Shimomura et al., Nuclear Fusion 16 (1976) 584.
[22] K. Odajima et al., Symposium on Current Disruption in Toroidal Devices, Garching (1979).
[23] DIVA Group, Nuclear Fusion 20 (1980) No.3, and JAERI-8205 (1979)
[24] DIVA Group, Nuclear Fusion 18 (1978) 12.
[25] H. Maeda et al., Plasma Physics and Controlled Nuclear Fusion Research (Berchtesgaden, 1976) 2, 289.
[26] M. Nagami et al., J. Nuclear Material 76&77 (1978) 521.
[27] S. Sengoku et al., J. Phys. Society of Japan, 45 (1978) 1385.
[28] M. Nagami et al., Nuclear Fusion, 18 (1978) 1347.
[29] M. Nagami et al., Nuclear Fusion 18 (1978) 1217.
[30] Y. Shimomura and H. Maeda, J. Nuclear Materials 76&77 (1978) 45.
[31] Y. Shimomura, Nuclear Fusion 18 (1977) 626 and 1377.
[32] H. Kimura et al., Nuclear Fusion 19 (1979) 1499.

4 - 2 THE DIVA EXPERIMENTS (II)

DIVA Group presented by Seio Sengoku
JAERI, Tokai, Naka, Ibaraki, Japan

I. Introduction

A summary on boundary plasma of a tokamak device is presented. To recognize the "Impurity Control", following closed, cyclic processes are important (Fig.1):

1. The role of plasma on the production of impurities.
2. Impurity transport in the boundary plasma and impurity flow into the main plasma.
3. Influences of accumulated impurities on the main and boundary plasma.

All of these processes and impurity control are made through the "Boundary Plasma". So, following items are discussed here:

1. A summary on boundary plasma characteristics in connection with impurity production and impurtiy transport obtained in DIVA tokamak.
2. Computer simulations modeling the results and deductions obtained in 1.
3. Application to a large fusion device.

II. Boundary Plasmas

First, we begin with some considerations about energy balance. Total input power is balancing with loss powers such that radiation loss and charge-exchange loss to the entire wall and conduction-convection losses mainly onto the limiter or the divertor neutralizer plate. Therefore, it can be expressed as

$$P_S = P_{IN} - P_R - P_{CX} = P_{CC} \qquad (1)$$

Here, the loss power P_S is the integral of local heat flux q as $P_S = \int q\,ds$. Then, the problem is *"How can we evaluate q?"*.

From a normal sheath theory, the heat flux is induced as [1]:

$$q = \gamma f_p T_e \qquad (2)$$

where γ is the heat transmission rate across the sheath including the effects of the sheath, α, secondary electron emission, δ, and the distribution function, F. That is:

$$\gamma = \{2\left(\frac{1}{1-\delta} + 1\right) + \alpha\}F \begin{cases} = 7 - 20 & : \textit{in normal discharges} \\ \gtrsim 100 & : \textit{in ranaway discharges} \end{cases} \qquad (3)$$

$$\alpha = -\ln \frac{\xi\sqrt{m/M}}{1-\delta}, \quad \xi \textit{ is the ratio of the electron-to-ion saturation currents.} \qquad (4)$$

The value αT_e measures the sheath potential. The interest is, now, *"Are these situations realistic still in actual tokamaks?"*. We would like to show the answer is *"Yes"*. Figure 2 shows the results of simultaneous measurements of local heat fluxes, electron temperature and the currents onto a thermo-couple probe located in the scrape-off layer of the DIVA plasma [1]. These curves show that the heat flux decreases with decreasing the average ion energy and increases with the electron flux and energy, and this agrees well with above sheath theory. Furthermore, the heat flux at the floating potential as well as the potential that gives the minimum flux coincide with the theory. These situations are confirmed in DIVA tokamak in

a wide range of plasma parameters (Fig.3)[1]. So, we can conclude that *"The sheath formation is still true in an actual tokamak"*.

As long as the sheath is formed on the material surface, the total power loss onto the material surface is, then, deduced as:

$$P_S = \int q\,ds = \gamma \bar{F}_p \bar{T}_b \qquad (5)$$

where $\bar{F}_p \equiv N_p/\bar{\tau}_p$ and $\bar{\tau}_p$ is overall particle confinement time. Then, the power balance can be rewritten as

$$\gamma \frac{N_p}{\bar{\tau}_p}\bar{T}_b = P_{IN} - P_R - P_{CX} = \frac{3}{2}\frac{N_p}{\tau_E}(\bar{T}_i + \bar{T}_e) - P_R - P_{CX}$$

From this, we can obtain the relation between the boundary temperatures and the bulk temperatures as [2]:

$$\bar{T}_b = 3\,\frac{1}{\gamma}\,\frac{\bar{\tau}_p}{\tau_E}\left(1 - \frac{P_R + P_{CX}}{P_{IN}}\right)\bar{T} \qquad (6)$$

Figure 4 shows that the boundary temperature obtained in DIVA well agrees with calculated one in the wide range of $\bar{T}_b$, say, $\bar{T}_b$ = 20 - 100 eV, with the predicted γ, 7 - 10, in this temperature range [3,4].

Then, summary on scrape-off plasma is as follows: We obtained the relation between the boundary and the main plasma temperatures, eq.(6), and the heat flux onto the material surface, eq.(2). Furthermore, we can deduce following parameters: width of the scrape-off layer d, average boundary electron density $\bar{n}_b$ and particle flux density f_p as [2,4]

$$d = \sqrt{D_\perp L/v_f} \qquad (7)$$

$$\bar{n}_b = \frac{1}{2}\,\frac{L}{v_f d}\,\frac{a}{d}\,\frac{\bar{n}_e}{\bar{\tau}_p} \qquad (8)$$

$$f_p = v_f \bar{n}_b \qquad (9)$$

where L is the path length of the charged particles along the field line in the scrape-off layer. In these parameters, the essential parameters are: γ, v_f, $D_\perp$, and these are reasonably obtained in DIVA as γ = 7 - 15, $v_f \simeq 0.3C_s$ and $D_\perp \simeq 0.1D_{Bohm}$. Moreover, the ratio $\bar{\tau}_p/\tau_E$ plays an important role on eq.(6). Empirical scaling law of the particle confinement time obtained in DIVA [4,5] is found to agree with that of the energy confinement time. The ratio $\bar{\tau}_p/\tau_E$ is less than or around unity with the divertor (Fig.5).

In conclusion up to now, the relation between the main parameters of the main plasma and the boundary plasma is given. The next problem is to reveal the relation between the boundary plasma and the impurities by studying the origin of impurities and the transport of impurities.

III. Impurity

We can now easily decrease the adsorbed or deposited gaseous impurities by cleaning. So the problem is defined about impurities of wall and limiter /divertor neutralizer plate materials. The conclusion of the study on impurity sources are: 1)Evaporation occurs only when heat concentration is unsuccessfuly arise. 2)Arcing is observed in surface conditioning phase and during periods of unstable plasma operations. 3)Ion sputtering is dominant in a normal tokamak discharge [6].

Figure 6 shows an example of sputtering cones observed on the gold limiter of DIVA exposed during $\simeq$ 10,000 of discharges [7]. The reason why the ion sputtering is dominant process even in a low temperature plasma is as follows. The impinging energy of the multi-ionized impurity ions

increases as ionic charge increases as follows,

$$E_M = \alpha T_b Z_M + T_M \qquad (10)$$

where Z_M and T_M are the ionic charge and the impurity temperature. In a normal tokamak, $\alpha \simeq 2$, $T_b \simeq T_M \simeq 50$ eV and $Z_M \simeq 5 - 10$, and this leads to $E_M \simeq (0.5 - 1.0)$ keV. So, in general, the sputtering yeald increases over unity.

The next problem is the impurity transport. Following experiments are made in DIVA to study the impurity transport [8-12]. First, the radial impurity diffusion are examined by methane injection. Transient radial distributions of carbon ions are observed (Fig.7). In order to clarify those processes, computer simulations with an one-dimensional tokamak code is performed, It is shown that "*the radial diffusion is well described with neoclassical diffusion superimposed by anomalous diffusion*" (Fig.8-a), b)). The anomality is set to be consistent with the scaling on energy confinement time and the proton diffusion.

Second, the parallel impurity motions along the scrape-off layer are studied. And it is made clear that there exist the parallel flow of the injected carbon ions being ionized successively during toroidal excursion in the scrape-off layer. Also it was revealed that carbon ions flow into the burial chamber. In the divertor region, carbon-four line radiation is dominant (Fig.9). When alminum atoms are injected in the burial chamber, the accumulation in the main plasma is only less than 0.5 % of the injected aluminum atoms. However, it is around 5 % when it was injected near the main plasma (Fig.10). This shows that the back flow of the impurity from the burial chamber is quite small, because the above mentioned particle flow drives the impurity ions back to the divertor plate.

We perform computer simulations by Monte-Carlo calculation in order to understand these phenomena. In the back ground scrape-off plasma characterized by $\bar{T}_b$, $\bar{n}_b$, v_f and E, test particles (impurity particles) are traced under following processes by Monte-Carlo method: 1)Ionization, 2) Charge-exchange, 3)Coulomb scattering and 4)Perpendicular diffusion.

The results of the simulation with the boundary plasma parameters noted in Fig.11 gives resonable values on average ionic charge and the mean energy of the carbon ions in the burial chamber as shown in Fig.11. Next, the simulation about alminum injection also well describes the experimental results (Fig.12). This simulation shows that the accumulated alminum impurity ions is 0.2 % of the injected aluminum atoms.

IV. Application to a Large Device

Concluding above discussions, following items are clarified: 1)The relationship between boundary plasma and the main plasma, 2)Impurity origin is dominated by ion sputtering and 3)Transport in boundary plasma; this is well described by Monte-Carlo calculation.

Seeing these results, we try to apply these results to a large device, JT-60 [13]. In this calculation, the main plasma parameters are given parameters and the ion sputtering on the limiter or the divertor neutralizer plate is added to the forementioned Monte-Carlo calculation. Figure 13 shows the geometry of JT-60. Assumed parameters are as follows,

$\bar{\tau}_p = \tau_E = 0.7$ *sec*, $T_{e0} = T_{i0} = 7$ *keV*, $n_{e0} = n_{i0} = 7 \cdot 10^{13}/cm^3$ and $B_T = 4.5$ *T*.

and the limiter or the neutralizer plate is made from Molybdenum. The impurity source is only assumed sputtered molybdenum.

The results are as follows. The average ionic charge near the neutralizer plate is around 5 with the divertor and in the case of without the divertor, it becomes up to 10 near the limiter(Fig.14). The average energy of the impinging molybdenum is lessened by a factor of 2 by employing the divertor. These are of several keV (Fig.15). Molybdenum impurities continue to increase when the boundary temperature is above 100 eV without the divertor. Due to radiation cooling, the boundary temperature is balancing within 80 - 160 eV. In opposit to this, the molybdenum impurities continue to decrease in the case of "with the divertor"(Fig.16). In the case of "without the divertor", we must lose a large portion of the input power, 80 - 90 %, by radiation loss or charge-exchange loss(Fig.17).

In conclusion up to now, the relation between the temperature of boundary and main plasma is already obtained (eq.(6)). And the boundary temperature is determined by the calculation on impurity recycling and shown to be rather low in undiverted discharges. We now can deduce the problem to parameter survay, say, $\bar{\tau}_p/\tau_E$ and $(P_R + P_{CX})/P_{IN}$ in eq.(6)(Fig.8). If radiation and charge-exchange power losses are extremly decreased and $\bar{\tau}_p/\tau_E$ is around unity, hot boundary is formed and we must lead out a large portion of the input power by conduction-convection. This situation is shown to be possible with the divertor. If this case is not realistic, the question is *"Is it possible to form cold boundary without giving any deleterious effects on main plasma?"*, that is to say, *"Is it able to radiate a large portion of input power only in the periphery?"* or *"Is it possible to let* $\bar{\tau}_p/\tau_E$ *be extremly small?"*

V. Conclusions

Conclusions are as follows

1) Relation between boundary plasma and main plasma is obtained.
2) Origin of impurities is shown to be dominated by ion sputtering.
3) Impurity transport in boundary plasma shown to be similar to the anomalous proton diffusion.
4) Computer simulations well describe the above described impurity transport.
5) In a large device, two categories of discharge are proposed: hot boundary and cold boundary.

Acknowledgement

We are very grateful to Drs. Y. Tanaka, M. Tanaka, M. Yoshikawa, Y. Obata and S. Mori for their continuous encouragement of our work. We are indebted to the members of DIVA operation group for their assistnace throughout the experiments.

References

[1] H.Kimura, H. Maeda, N. Ueda, M. Seki, H. Kawamura, S. Yamamoto, M. Nagami, K. Odajima, S. Sengoku, Y. Shimomura, Nucl. Fusion, 18 (1978)1195.
[2] Y. Shimomura and H. Maeda, J. Nucl. Mat.,76&77 (1978)45.
[3] DIVA group, Nucl. Fusion, 18 (1978)1619.
[4] DIVA group, Japan Atomic Energy Research Institute Report, JAERI-M 7610,(1978).
[5] T. Sugie, H. Takeuchi, S. Kasai, A. Funahashi, K. Takahashi, H. Kimura, J. Phys. Soc. Japan, 44 (1978)1960.
[6] K. Ohasa, H. Maeda, S. Yamamoto, M. Nagami, H. Ohtsuka, S. Kasai,

K. Odajima, H.Kimura, S. Sengoku, Y. Shimomura, Nucl. Fusion, 18 (1978)872.
/7/ K. Ohasa, H. Maeda, S. Yamamoto, M. Nagami, H. Ohtsuka, S. Kasai, K. Odajima, H.Kimura, S. Sengoku, Y. Shimomura, J. Phys. Soc. of Japan, 46 (1979)1635.
/8/ S. Yamamoto et al., Proc. 8th Europ. Conf. on Controlled Fusion and Plasma Physics. (Prague), 1, 33 and 2, 234 (1977).
/9/ H. Maeda et al., Plasma Physics and Controlled Nuclear Fusion Research (Berchtesgaden, 1976) 2 289.
/10/ M. Nagami et al., J. Nucl. Mat., 76 & 77 (1978) 521.
/11/ M. Nagami et al., Nucl. Fusion, 18 (1978) 1217.
/12/ M. Nagami et al., Nucl. Fusion, 18 (1978) 1347.
/13/ S. Sengoku, M. Azumi, Y. Matsumoto, H. Maeda and Y. Shimomura, Nucl. Fusion, 19 (1979) 1327.

INTRODUCTION

1. IN ORDER TO RECOGNIGE THE "IMPURITY CONTROL" FOLLOWING CLOSED, CYCLIC PROCCESES ARE IMPORTANT:
   - ① THE ROLE OF PLASMA ON THE PRODUCTION OF IMPURITIES
   - ② IMPURITY TRANSPORT IN THE BOUNDARY PLASMA & IMPURITY FLOW INTO THE MAIN PLASMA
   - ③ INFLUENCE OF ACCUMLATED IMPURITIES ON THE MAIN & BOUNDARY PLASMAS
2. ALL OF THESE THREE PROCCESES & IMPURITY CONTROL ARE MADE THROUGH "BOUNDARY PLASMAS"

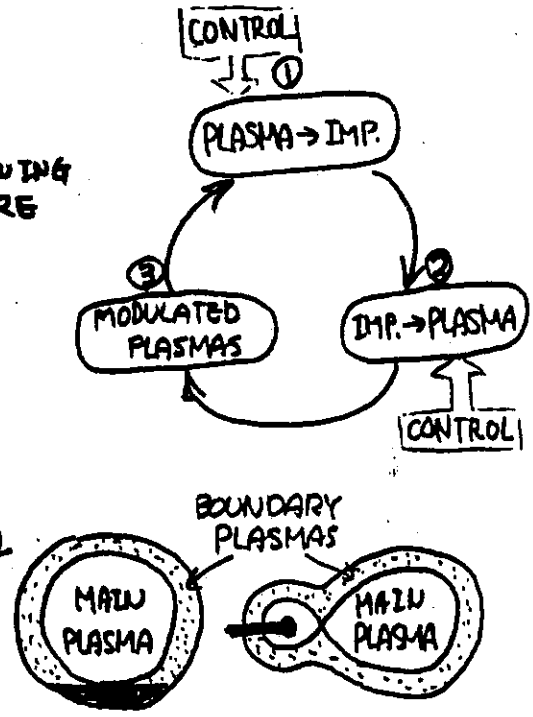

Fig. 1

LOCAL HEAT FLUX
ONTO A THRRMO-
COUPLE PROBE

* SIMULTANEOUS
MEASURMENTS OF

q, Te, i

⇓

CURVES OF i, q
ARE WELL DESCRIBED
BY "THEATH THEORY"

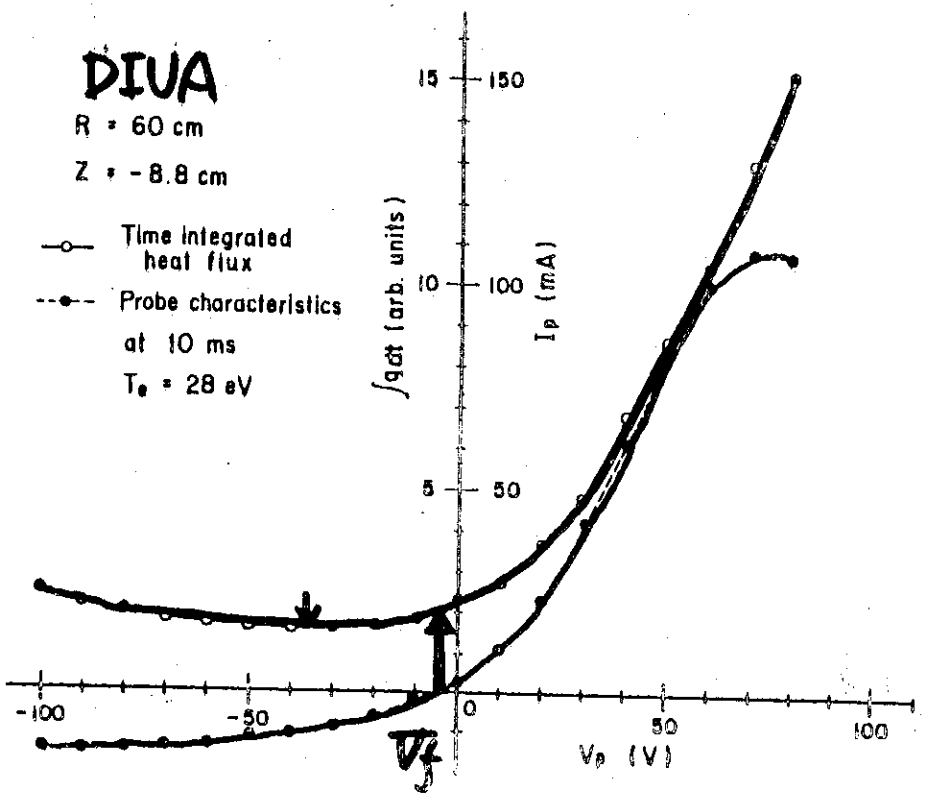

Fig. 2

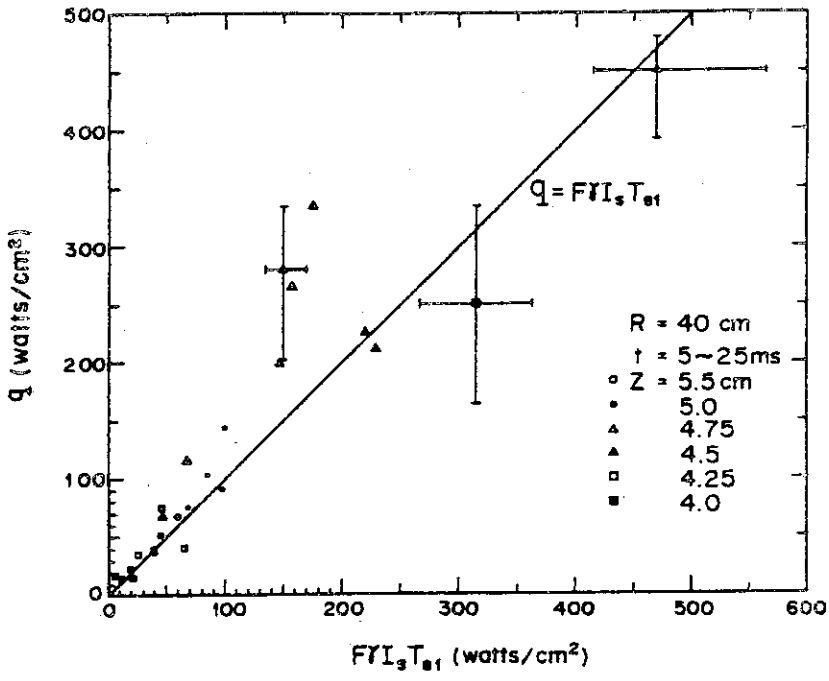

Fig. 3

MEASURED BOUNDARY TEMPERATURE

$$\gamma T_b = 3\frac{\bar{\tau}_P}{\tau_E}\left(1-\frac{P_R+P_{CX}}{P_{LN}}\right)\bar{T}$$

v.s.

T_b (MEASURED)

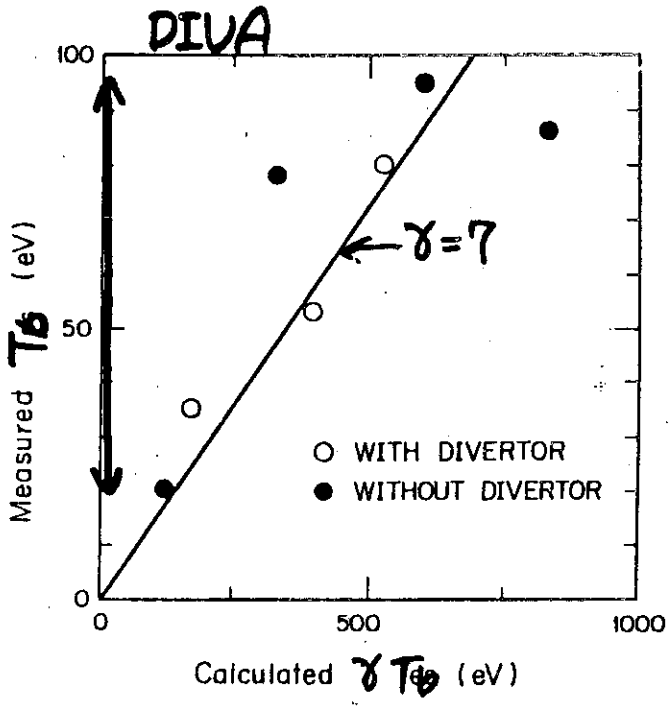

Fig. 4

τ_p/τ_E (DIVA)

- $\tau_p, \tau_E \Longrightarrow$ SAME SCALING LAW $\propto n\sqrt{\beta_a}\, a^2$
- $\tau_p/\tau_E \lesssim 1$

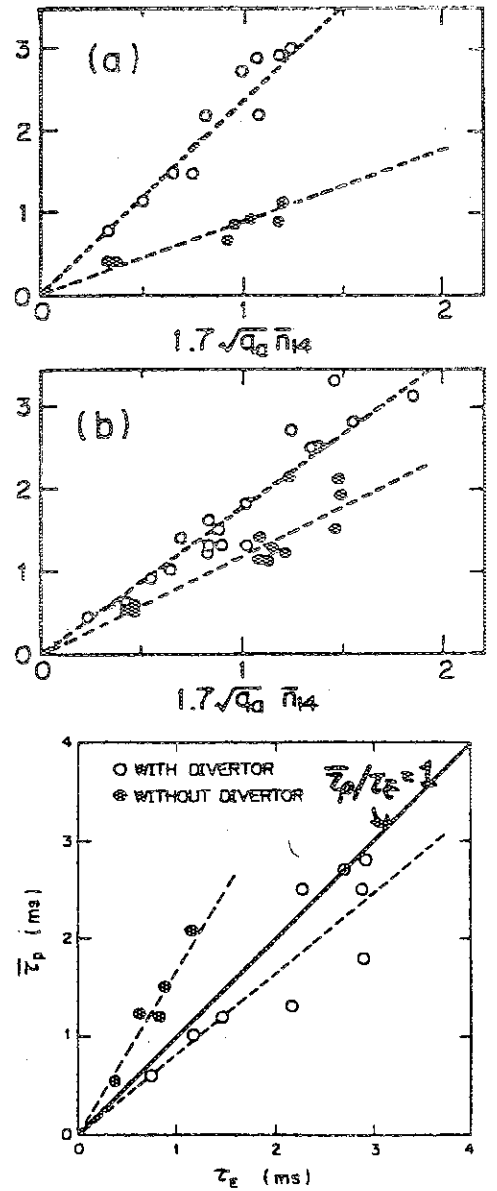

Fig. 5

SPUTTERING CONES (Gold Limiter)

1 μ

~ 10,000 SHOTS

Fig. 6

JAERI-M 8971

COMPUTER SIMULATION 1.

(1-D TOKAMAK CODE)

① RADIAL DIFFUSION

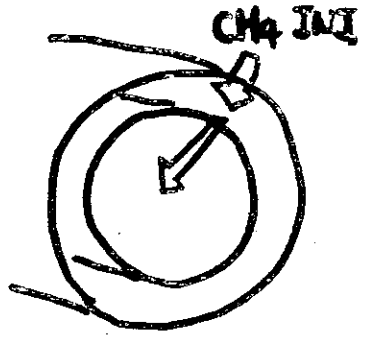

WELL DESCRIBED WITH

"NEOCLASSICAL DIFFUSION SUPERPOSED BY ANOMALOUS DIFFUSION"

ANOMALITY → CONSISTENT WITH THE SCALING ON τ_E

DIVA [CH4 INJ]

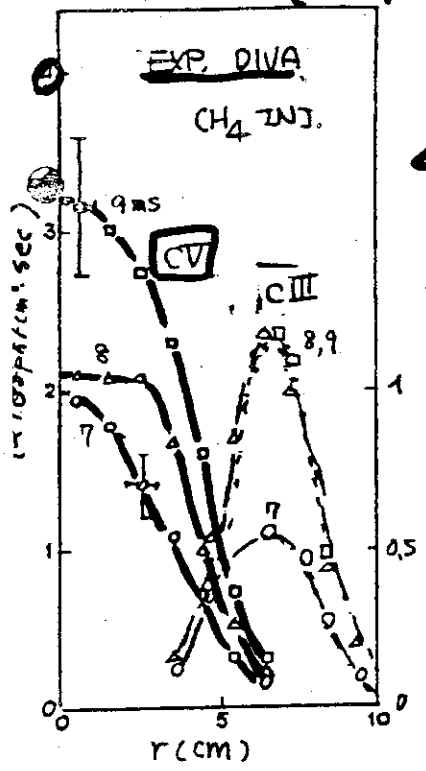

Fig.7

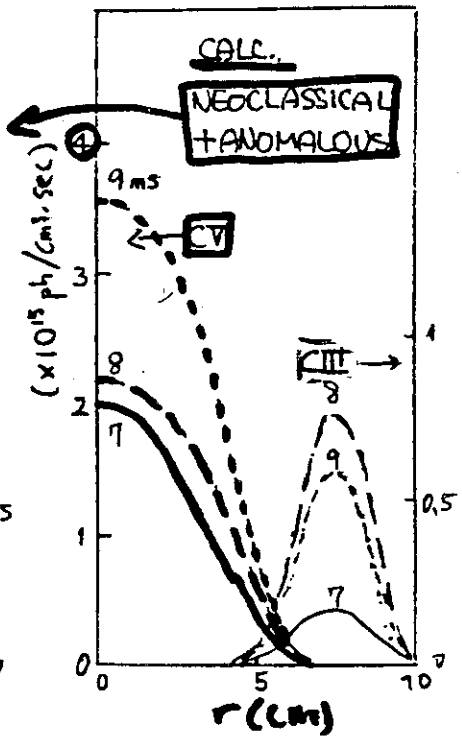

Fig.8 -a)

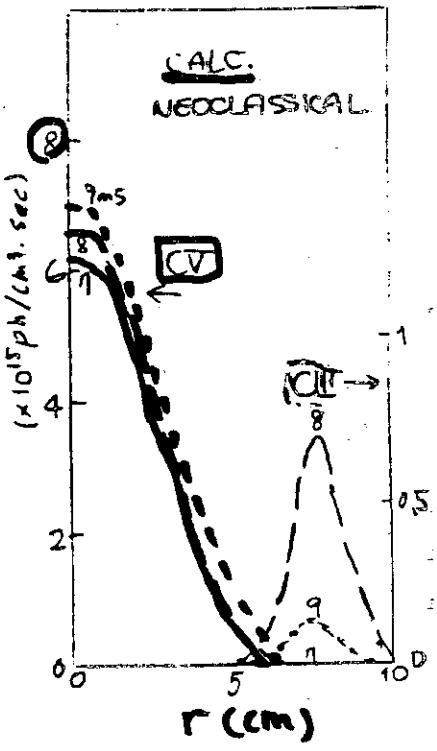

-b)

② PARALLEL MOTION 1

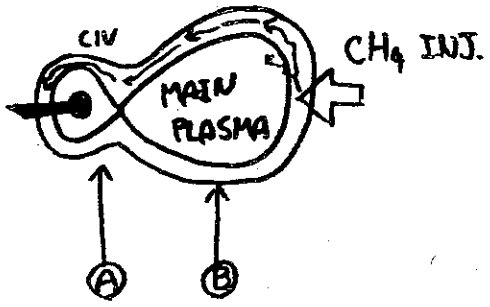

SPECTROMETERS

"PARALLEL FLOW"

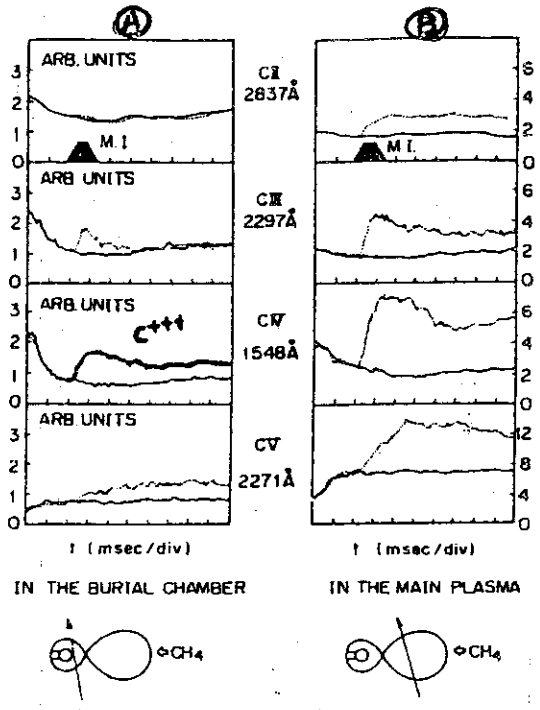

Fig. 9

③ PARALLEL MOTION 2.

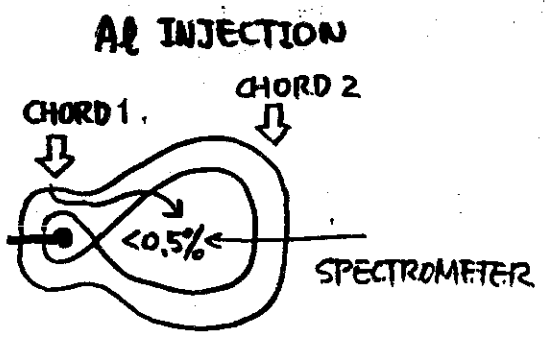

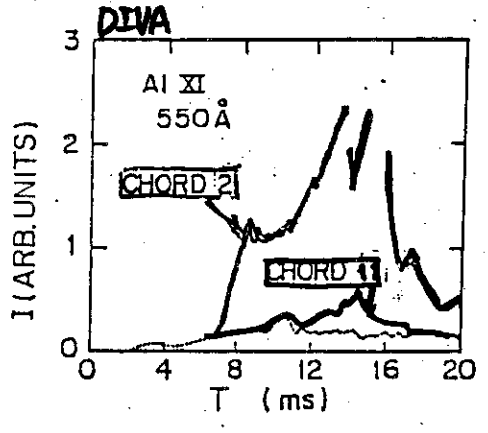

ACCUMULATION IN THE MAIN PLASMA

CHORD 1	< 0.5%
CHORD 2	≈ 5%

Fig. 10

② PARALLEL MOTION 1.

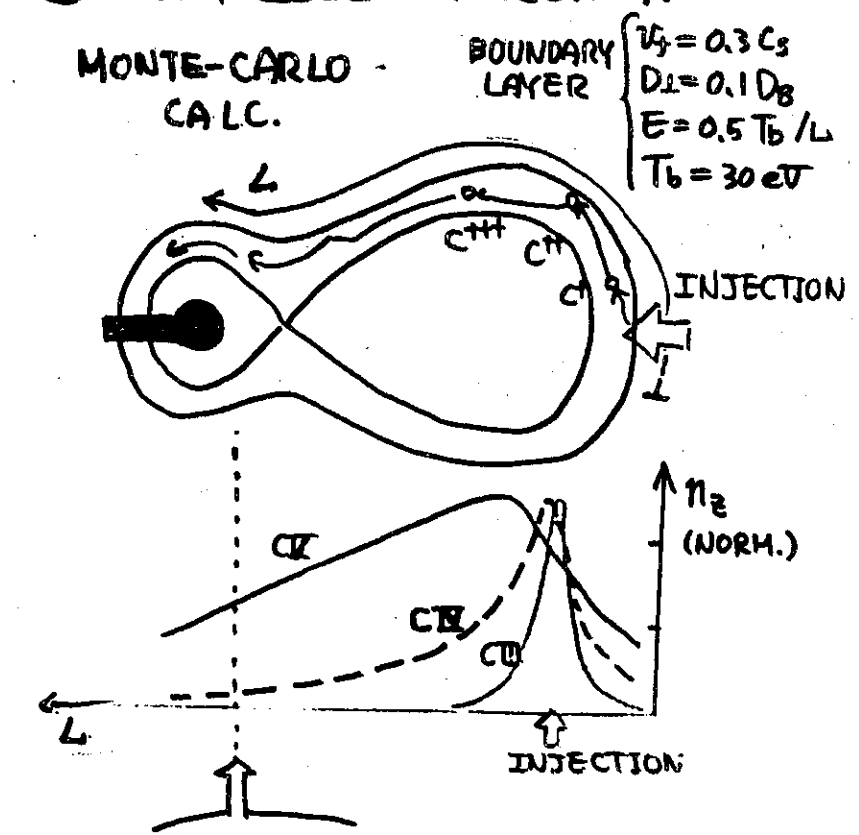

	$\bar{Z}$	T_{CIV}	T_{CV}
EXP.	~3	40 eV	80 eV
CALC.	3.3	50	70

Fig. 11

③ PARALLEL MOTION 2.

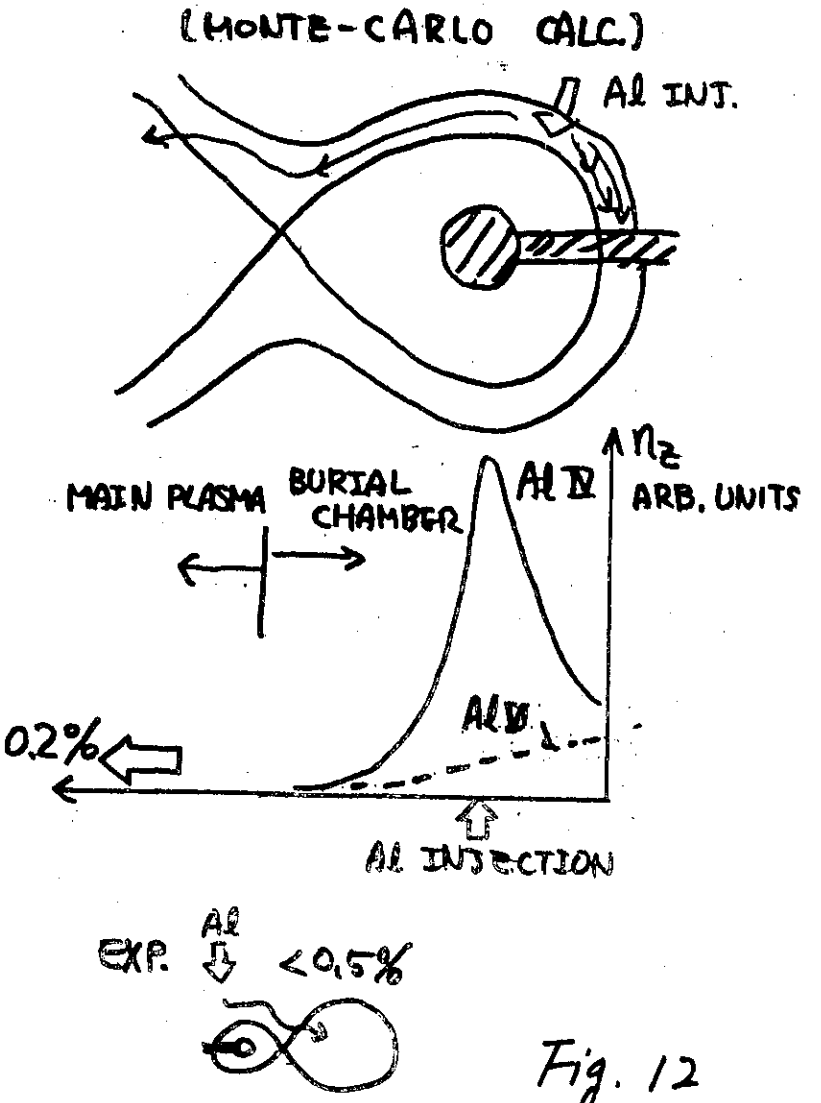

Fig. 12

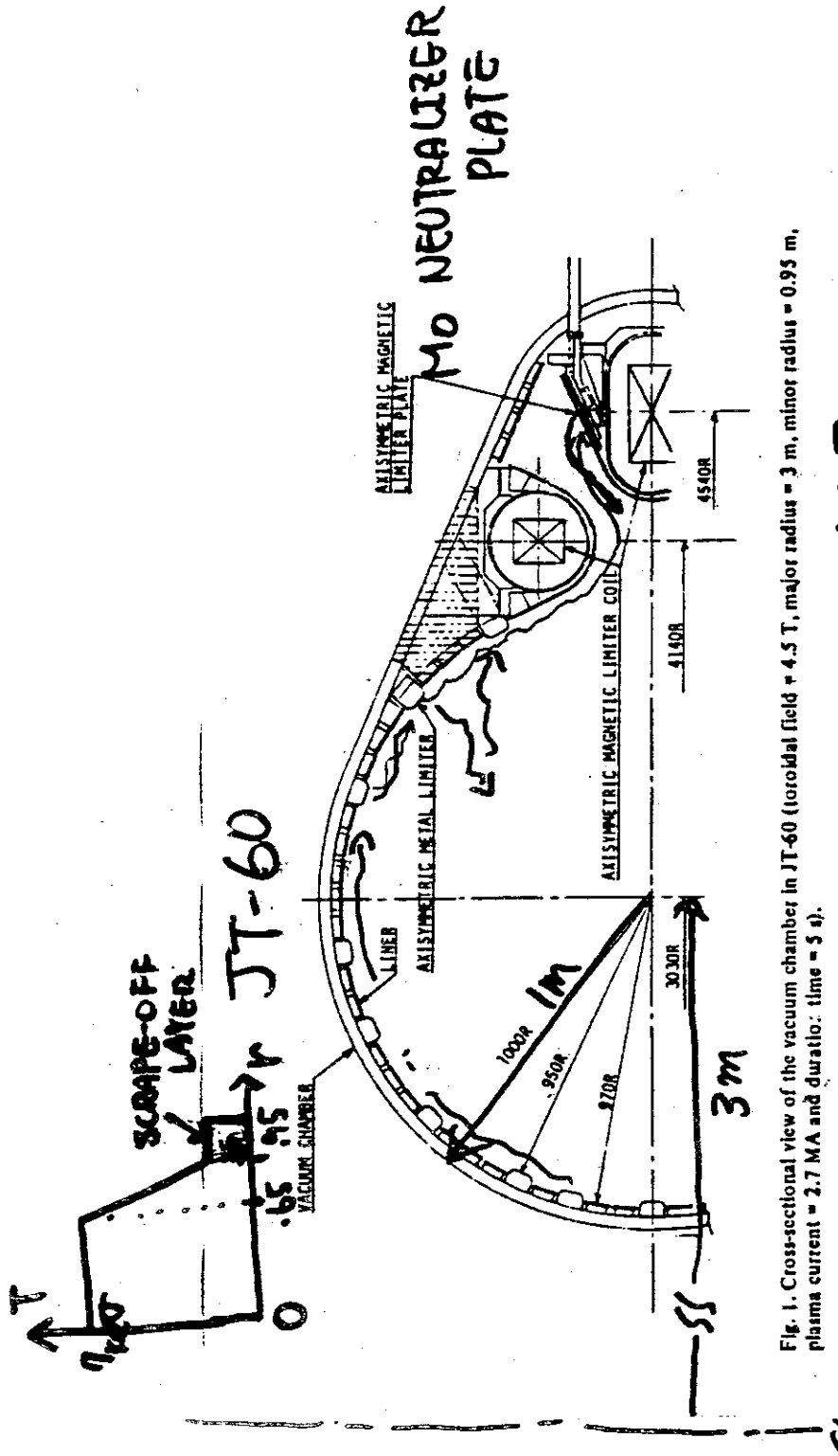

Fig. 1. Cross-sectional view of the vacuum chamber in JT-60 (toroidal field = 4.5 T, major radius = 3 m, minor radius = 0.95 m, plasma current = 2.7 MA and duratio: time = 5 s).

Fig. 13

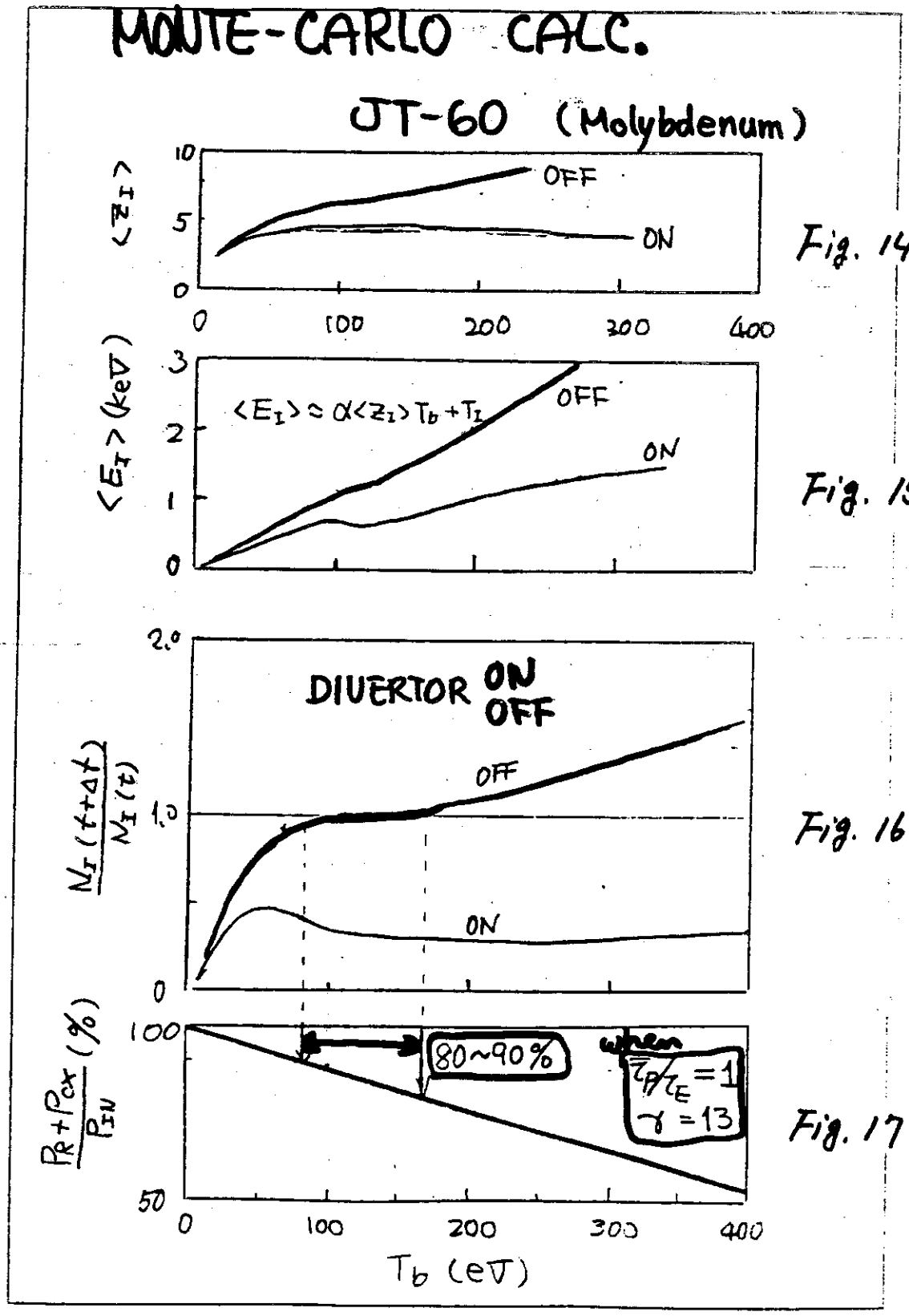

Fig. 14

Fig. 15

Fig. 16

Fig. 17

4 - 3 EXPERIMENTAL RESULTS ON PDX

D. M. Meade

Princeton Plasma Physics Laboratory

PDX DIVERTOR DISCHARGE

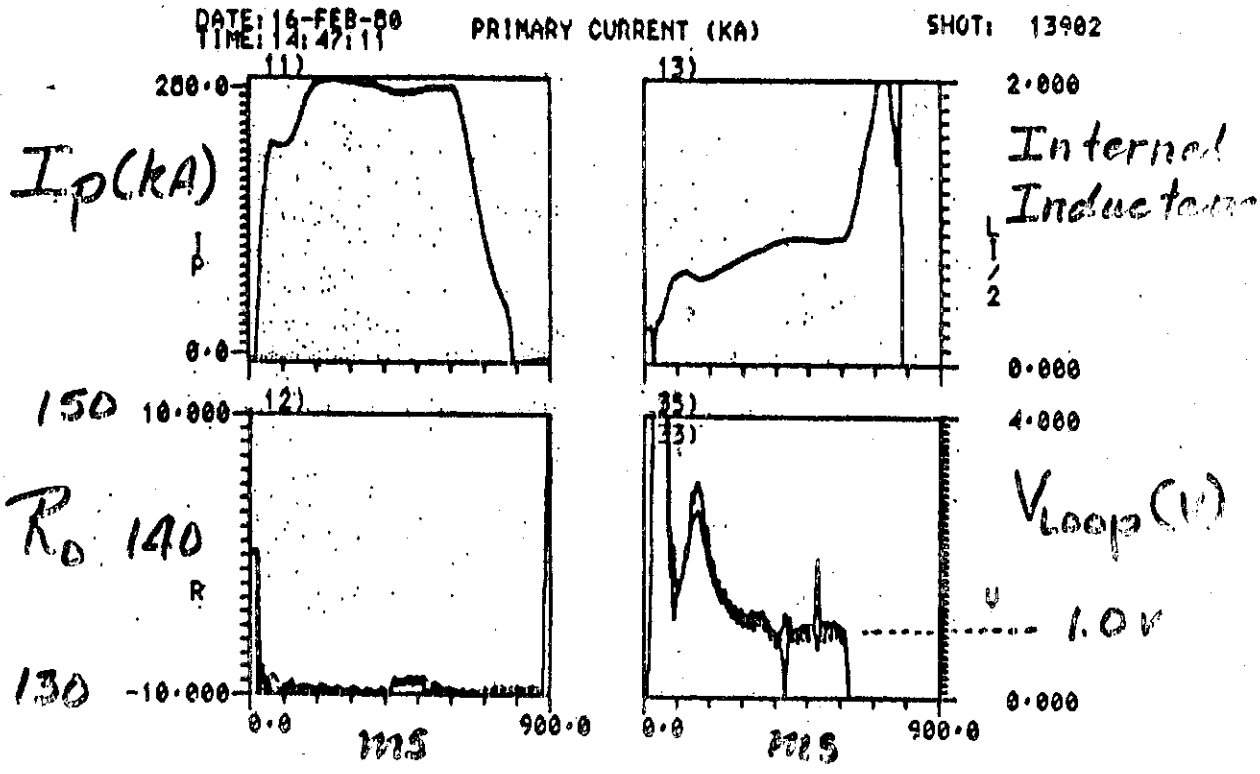

$a \simeq 37$ cm, $R_0 \simeq 130$ cm, $B_T \simeq 17$ kG

$q \simeq 3.5$, $T_e(0) \simeq 1$ keV, $T_i(0) \simeq 900$ eV

$\bar{n}_e \simeq 1-3 \times 10^{13}$ cm^{-3}

FY-80 PDX OPERATIONS RESULTS

1.0 INITIAL DIVERTOR OPERATION (OCTOBER-FEBRUARY)

1.1 DISCHARGE MAGNETIC CHARACTERISTICS

- INITIATION AT OCTOPOLE MAGNETIC NULL
- STABILITY DURING CURRENT-RISE
- LONG PULSE PASSIVE STABILIZATION: DEE SHAPE, INSIDE DIVERTOR INVERSE DEE, OUTSIDE DIVERTOR

1.2 ENERGY BALANCE

- ENERGY DEPOSITION PROFILE ON DIVERTOR PLATE IS WIDE (~3 CM)
- SIGNIFICANT ENERGY FLOW TO DIVERTOR PLATE (50 TO 75% OF INPUT POWER). LIMITED CIRCULAR DISCHARGES HAVE 50 TO 75% OF THE INPUT POWER RADIATED
- INITIAL TiC LIMITER (TFTR) EXPERIMENTS—LIMITER ABSORBS 200 KJ PER PULSE @600°C WITH NO METHANE PRODUCTION (NO REDUCTION IN Ti IMPURITIES), ENERGY SCRAPE-OFF ~1.7 CM

1.3 PARTICLE BALANCE

- Ti GETTER PUMPING IN THE DIVERTOR DOMES ~200 KL/S (1/2 CAPACITY
- GAS PUFFING USING N_E FEEDBACK, MAXIMUM N_E ACHIEVED $3.10^{13}CM^{-3}$ @ B/R ≅ 1 WITH BOTH CIRCULAR AND DIVERTOR. DENSITY SUFFICIENT FOR BEAM INJECTION. DIVERTOR REQUIRES ~8 TIMES AS MUCH GAS AS CIRCULAR
- τ_p ~ 20 MS FROM DENSITY DECAY
- $\int n_e d\ell$ ACROSS DIVERTOR SCRAPE-OFF IS $2.10^{12}CM^{-3}$ IN AGREEMENT WITH EXPECTATIONS

1.4 IMPURITY EFFECTS

- HEAVY IMPURITY REDUCTION (CL, Ti) ~10, Ti BURSTING
- O,C REDUCTIONS ~2, CONSISTENT WITH EXPECTATIONS

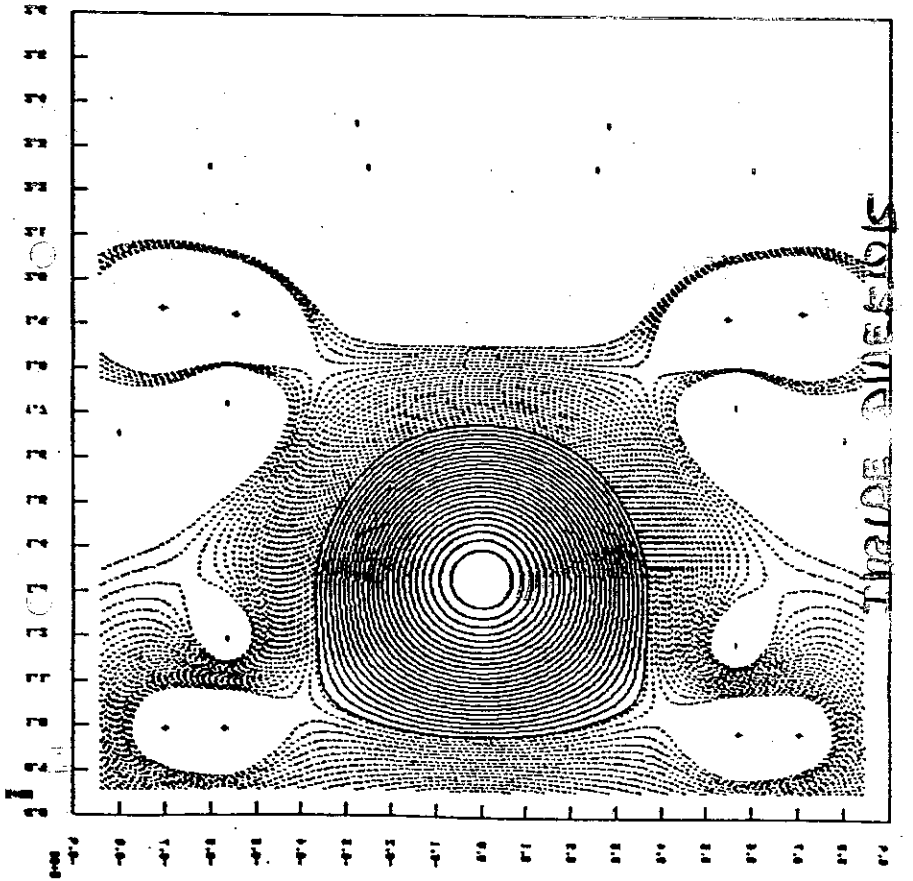

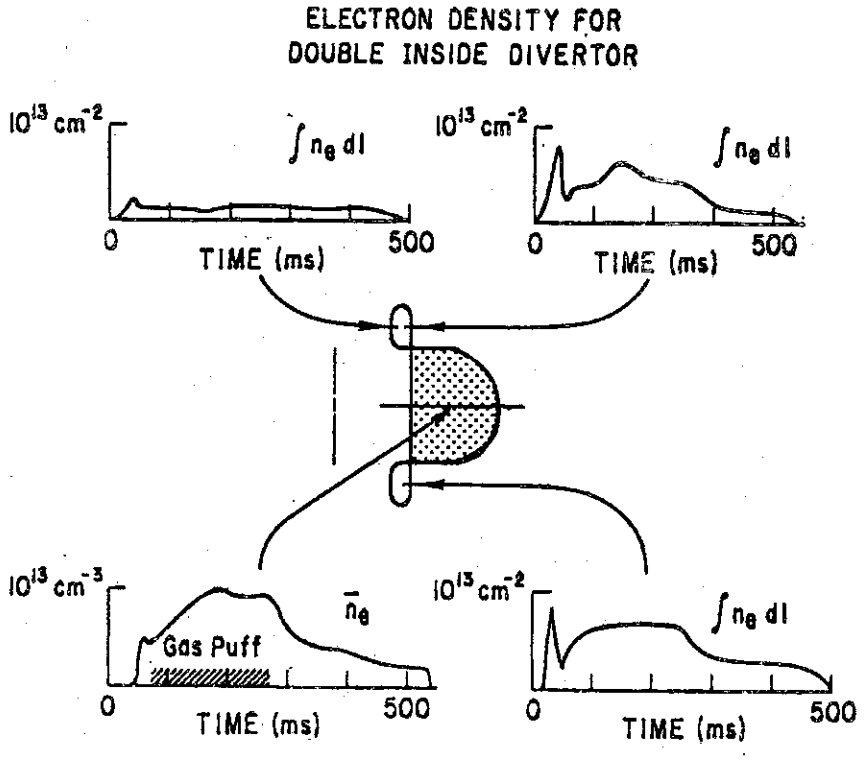
ELECTRON DENSITY FOR
DOUBLE INSIDE DIVERTOR
10^{13} cm^{-2}
$\int n_e\,dl$
0
TIME (ms)
500
10^{13} cm^{-2}
$\int n_e\,dl$
0
TIME (ms)
500
10^{13} cm^{-3}
$\bar{n}_e$
Gas Puff
0
TIME (ms)
500
10^{13} cm^{-2}
$\int n_e\,dl$
0
TIME (ms)
500
Shot 11493 1/18/80

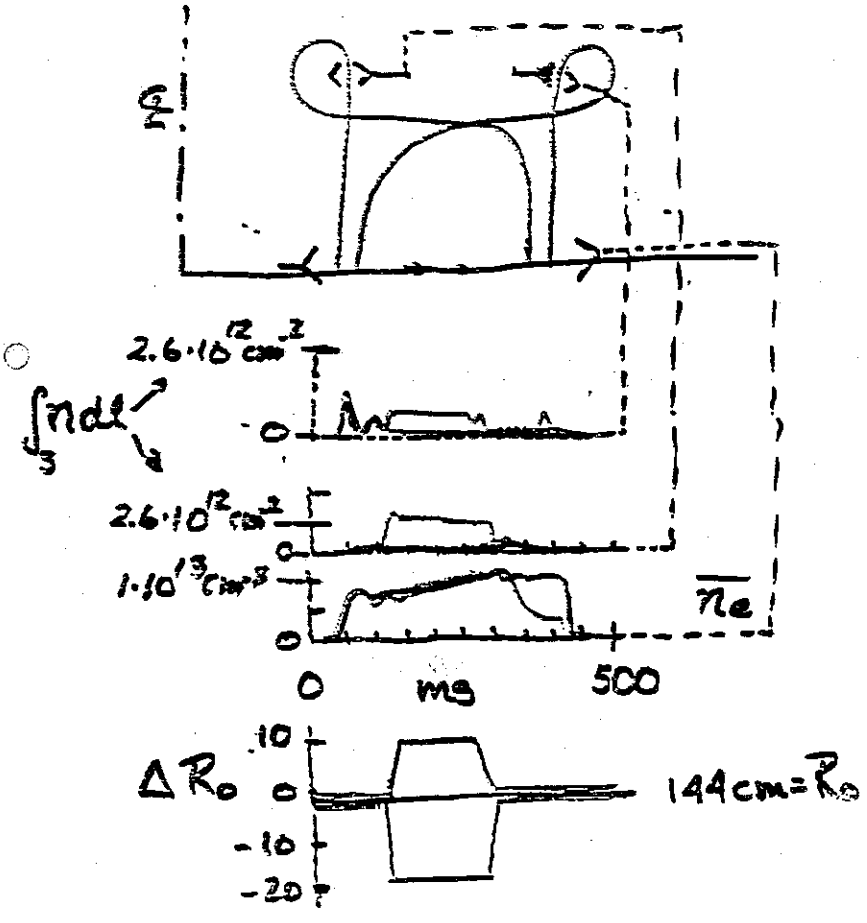
n_e
$2.6\cdot10^{12}$ cm^{-2}
$\int n\,dl$
0
$2.6\cdot10^{12}$ cm^{-2}
0
$1\cdot10^{13}$ cm^{-3}
0
$\bar{n}_e$
0
ms
500
10
ΔR_0
0
-10
-20
144cm=R_0

POWER FLOW IN PDX

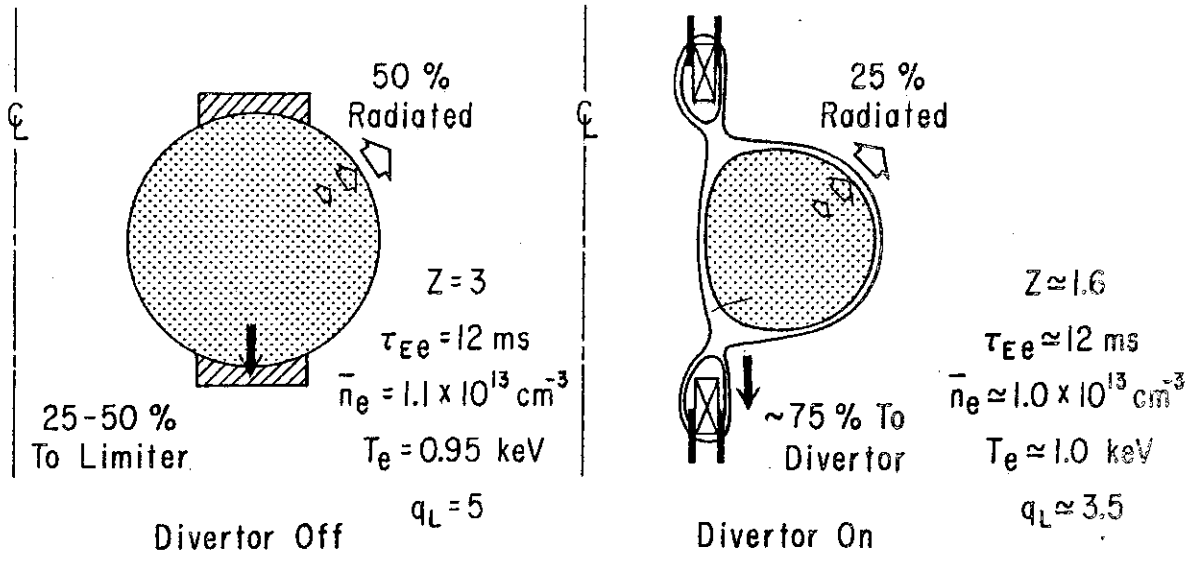

ENERGY DEPOSITION PROFILE (DIVERTOR PLATE)

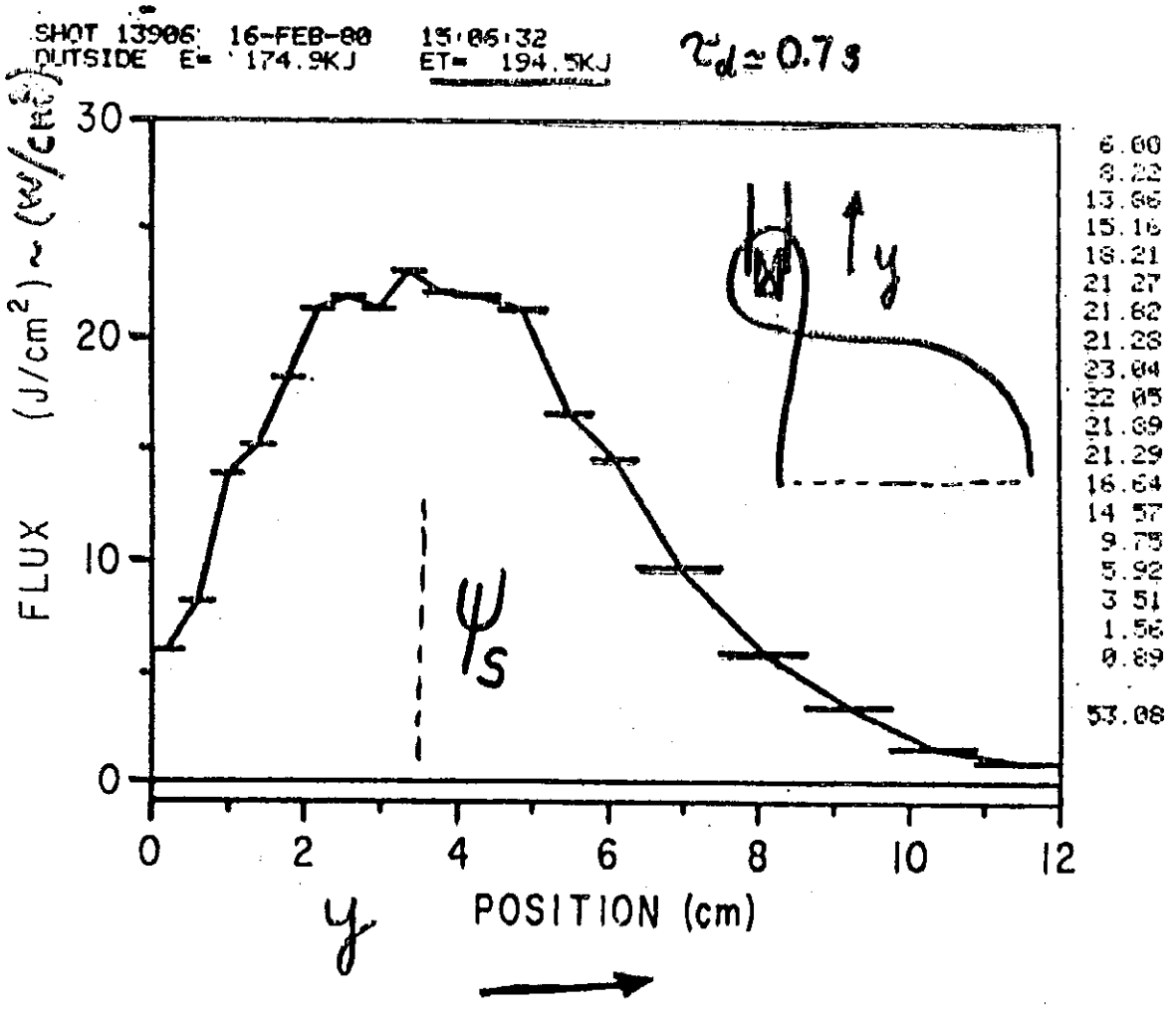

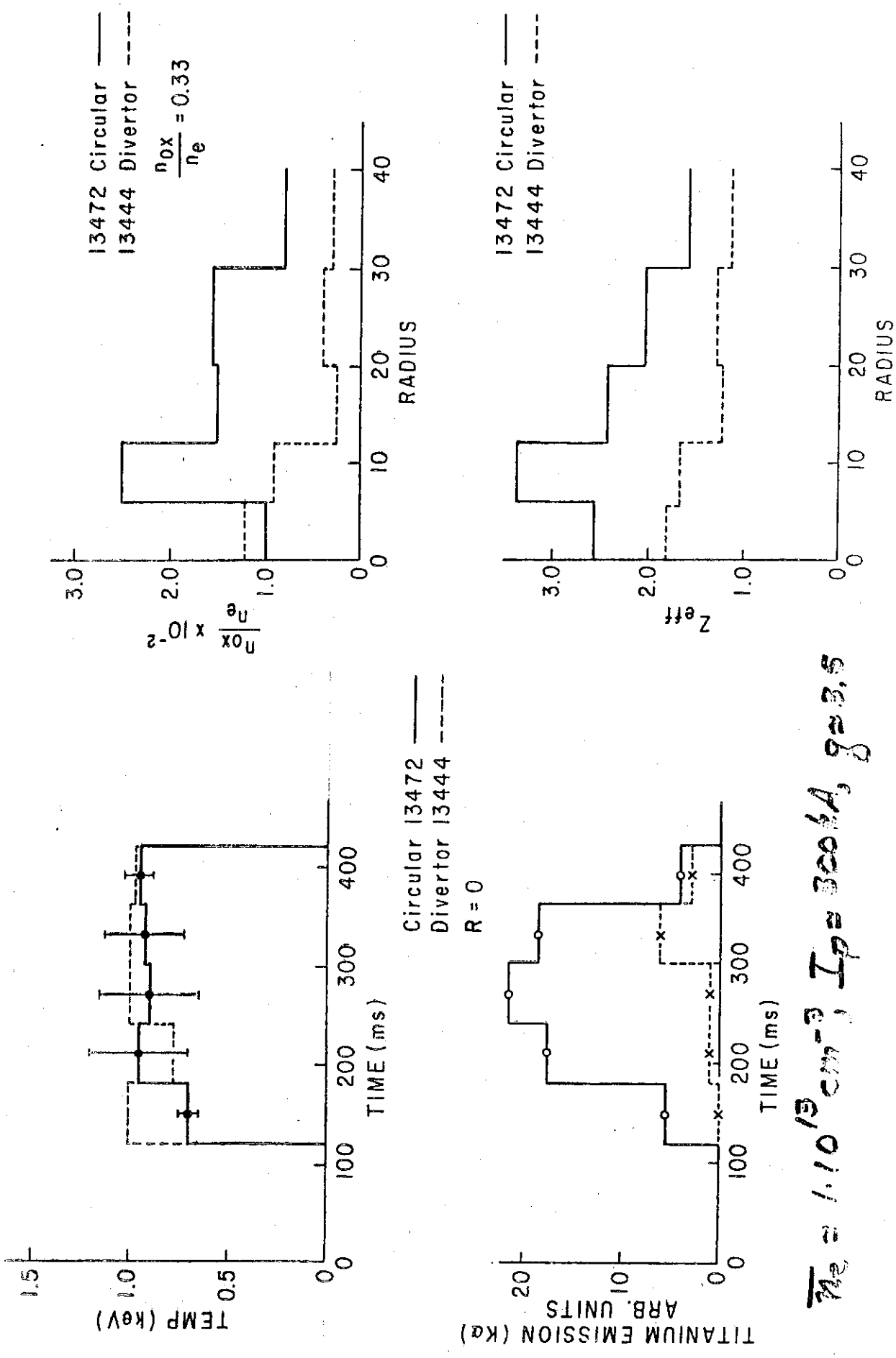
13472 Circular
13444 Divertor
$\frac{n_{ox}}{n_e} = 0.33$
$\frac{n_{ox}}{n_e} \times 10^{-2}$
RADIUS
Z_{eff}
TEMP (keV)
TIME (ms)
Circular 13472
Divertor 13444
R = 0
TITANIUM EMISSION (K_α)
ARB. UNITS
$\bar{n}_e = 1.1 \times 10^{13}$ cm^{-3}, $I_p = 300$ kA, $q_a = 3.5$

IMPURITY ATOM TRANSMISSION

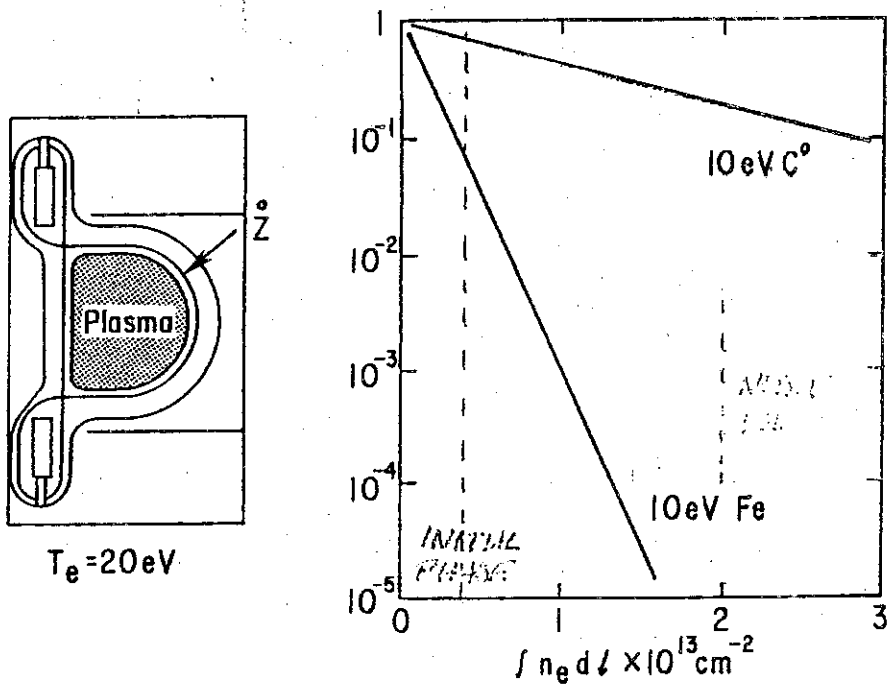

PDX EXPERIMENTAL PROGRAM
(Calendar Years)

FACILITY	1980		1981	1982	1983
B_t	25kG	25kG	25kG	19kg	5sec
I	500 kA	500kA	500 kA	500kA	
Plasma Shape	D,O	D,O	D,O	Optimum	
Divertor	Simple	Simple	Improved	Reactor Prototype	
Neutral Beam	1MW	6 MW H°	6 MW D°	Long Pulse 4MW, 5sec	
ECRH 60 GHz	Design	Fabricate		Install	60 GHz, 1MW
ICRF 55MHz				Install	42 MHz, 1→5 MW
PDX−M	Con. Dsgn.	Proto. Exp.	Fabricate	Install	Operate
PROGRAM					
Divertor Impurity Control	T~1keV	T~5keV	T~10keV	T~5keV, τ~100 τ_E	
MHD Opt	Stability vs Shape and Separatrix				
		High β		High β Long Pulse	
General	Pellet Fueling		Beam Fueling		
			High Neutron Yield Expts.		

4 - 4 BUNDLE DIVERTOR RESEARCH AT ORNL*

R. A. Dory, R. B. Easter, R. H. Fowler, D. H. Gray, H. C. Howe, T. C. Jernigan, V. E. Lynch, J. F. Lyon, B. E. Nelson, J. A. O'Toole,† E. J. Rapperport,‡ J. A. Rome, J. Sheffield, J. E. Tracey,‡ W. R. Wing, R. B. Wysor, T. F. Yang,‡ Y. W. Yarbrough

Oak Ridge National Laboratory
Oak Ridge, Tennessee 37830 USA

*Research sponsored by the Office of Fusion Energy (ETM), U.S. Department of Energy under contract W-7405-eng-26 with the Union Carbide Corporation.

†Grumman Aerospace Corporation, Bethpage, New York.

‡Massachusetts Institute of Technology, Cambridge, MA.

INTRODUCTION

The bundle divertor is a set of coils which locally produces a null in the toroidal magnetic field of a tokamak, and extracts a "bundle" of magnetic flux from the torus. Thus, the plasma can be extracted from the torus and dumped in an external chamber without interacting with any material object within the main vacuum chamber. The bundle divertor appears quite attractive from the engineering view point for fusion reactor designs. The topics included in this paper are the ISX-B bundle divertor design, magnetic field ripple effects of bundle divertors, transport modeling with bundle divertors, and some advanced bundle divertor concepts. Studies have been done modeling DITE, ISX-B, INTOR, ETF, and a new tokamak proposed at ORNL, ISX-C.

DESIGN OF THE ISX-B BUNDLE DIVERTOR SYSTEM

Section 1

The ISX-B bundle divertor module is an advanced two-coil divertor designed[3] and built under the direction of MIT's Plasma Fusion Center. It is based upon earlier work done at Culham[1,2] and Westinghouse Corporation. It consists of two solenoid-like coils mounted in a split stainless steel case (Fig. 1.1). At 18 kG in ISX-B it produces a separatrix at a minor radius of 20 cm with a scrape-off thickness of seven centimeters. The extended, solenoidal coils produce a field ripple of about 1% at the center of the plasma, R = 93 cm.

Plots of the magnetic field lines as they pass through the divertor coils are shown in Figure 1.2. Most of the field lines pass out of the plasma through the coils, and back again into the plasma without striking the structure. This will enable tests to be made of divertor operation without a target in place.

The forces on the divertor coils and the TF coils of ISX-B are shown in Figure 1.3. The overturning moments of the divertor coils are taken within the divertor case. Forces and moments between the divertor and the TF coils are taken by structural links between the TF coils and the divertor case.

The divertor system as it will be installed on ISX-B is shown in Figures 1.4 and 1.5. The divertor coil module is bolted to ISX-B. A target (stainless steel initially, coated graphite eventually) is placed to intercept the magnetic flux bundle. An isolation valve separates the divertor module and target from the pumping chamber. The pumping chamber is pumped by a 150,000 ℓ/s cryocondensation pump at 4.3 K and a 2,000 ℓ/s turbopump.

The divertor is driven by an SCR power supply. The voltage and current waveforms are shown in Figure 1.6. The peak current is 15 kA; the peak voltage is 600 V during the current rise and 220 volts at the end of the flat top. The risetime is 50 ms and the design flat top length is 200 ms.

Cooling of the coils will be achieved by water cooling the double-layer pancakes in parallel from a common coolant source. Thus, for each pancake, coolant entry will be made at a point on the outer diameter and the coolant (inside the conductor) will spiral to the inner diameter of the layer of entry and then change planes ('crossover') to the adjacent layer of the pancake and spiral outward to the exit region at the outside circumference.

This cooling scheme may produce an appreciable shear stress on the epoxy-fiberglass insulation between the two layers of each pancake unless great care is exercised in minimizing the temperature difference between adjacent pancake layers. This shear stress is generated by the thermal shrinkage of the inlet layer compared to the outlet layer in the initial stages of cooling. Initial stress analyses indicate a differential temperature control requirement approaching 6°C.

The cooling water temperature will have to be closely controlled in order to avoid unacceptable shear stresses in the insulation and to cool the coil back to ambient temperatures in the five minutes available. This is a severe requirement and will necessitate very sensitive sensors and controls.

The electrical pulse is calculated to deposit approximately 1.1 MJ in the two coils. The energy will be removed by the temperature programmed flow of coolant water as outlined above.

The design approach selected for analysis is shown schematically in Figure 1.7. The primary components are a coil by-pass valve, a mixing valve (3-way valve as shown or digital valves), and a steam-heated water heater. The proposed operational sequence is as follows:

1. Prior to pulsing, the coils are at temperature TE2 with cold water or a mix of cold/hot water flowing through the by-pass valve depending upon the desired steady state temperature. Only a small quantity flows through the coil because of the low impedance of the by-pass loop.
2. When divertor coils are pulsed, open CV1 and set FCVI for hot water flow.
3. Monitor TE3 and modulate FCV1 until TE1 = TE 3 = TE2.
4. Close CV1.
5. Modulate FCV1 to maintain TE2 6°C less than TE 3.
6. Continue until FCV1 is set for desired initial temperature conditions for the next pulse.

References for Introduction and Section 1

[1]P. E. Stott, C. M. Wilson, and A. Gibson, Nuclear Fusion 17, 3 (1977).

[2]Unpublished design study done by Culham for ORNL. Based upon DITE Mk II divertor design, H. J. Crawley et al, IEEE 8th Symposium on Engineering Problems of Fusion Research 1979. To be published.

[3]R. B. Wysor et al, IEEE 8th Symposium on the Engineering Problems of Fusion Research 1979. To be published.

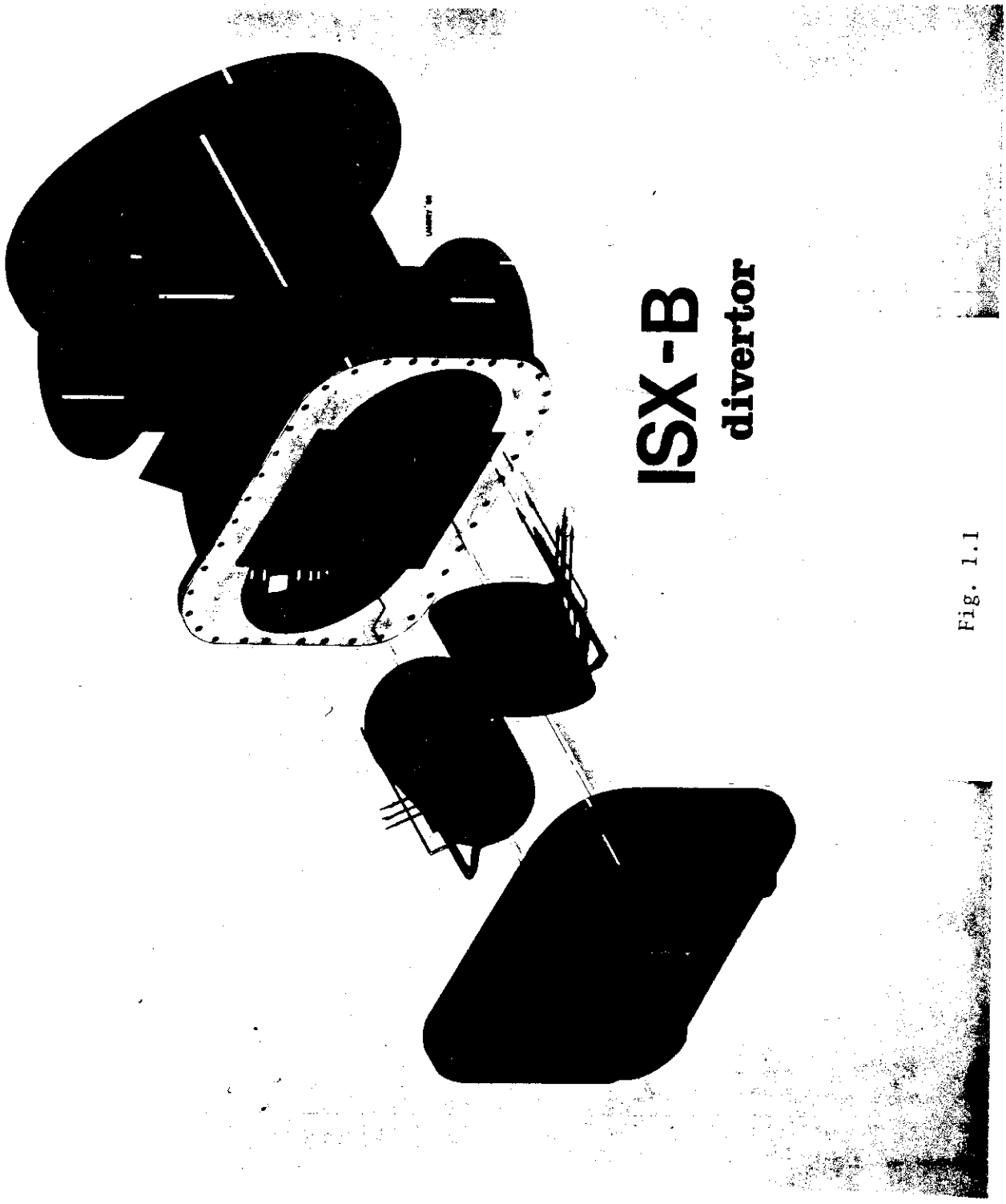

Fig. 1.1

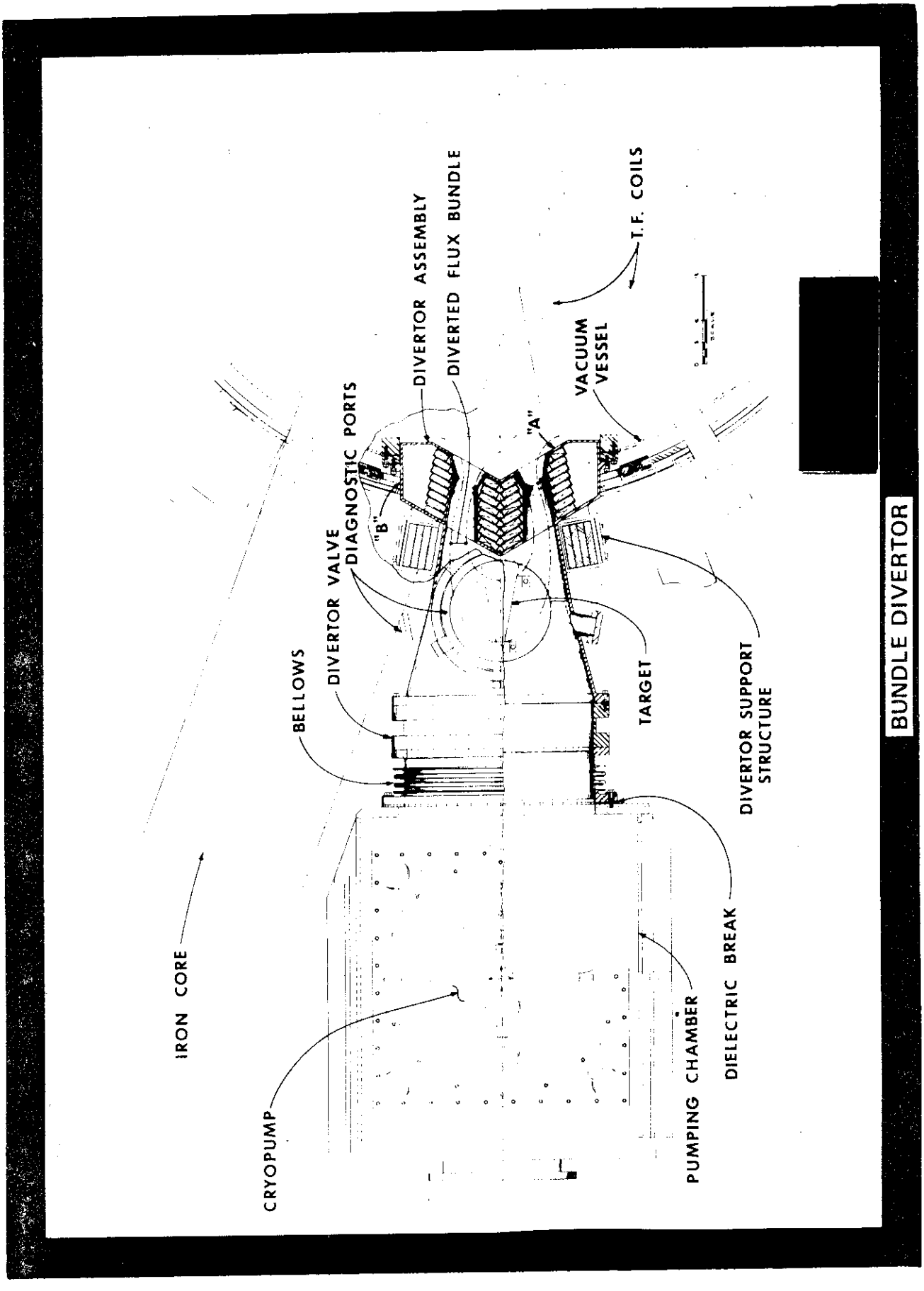
BUNDLE DIVERTOR
IRON CORE
CRYOPUMP
BELLOWS
DIVERTOR VALVE
DIAGNOSTIC PORTS
"B"
DIVERTOR ASSEMBLY
DIVERTED FLUX BUNDLE
"A"
VACUUM VESSEL
T.F. COILS
TARGET
DIVERTOR SUPPORT STRUCTURE
DIELECTRIC BREAK
PUMPING CHAMBER

Fig. 1.4

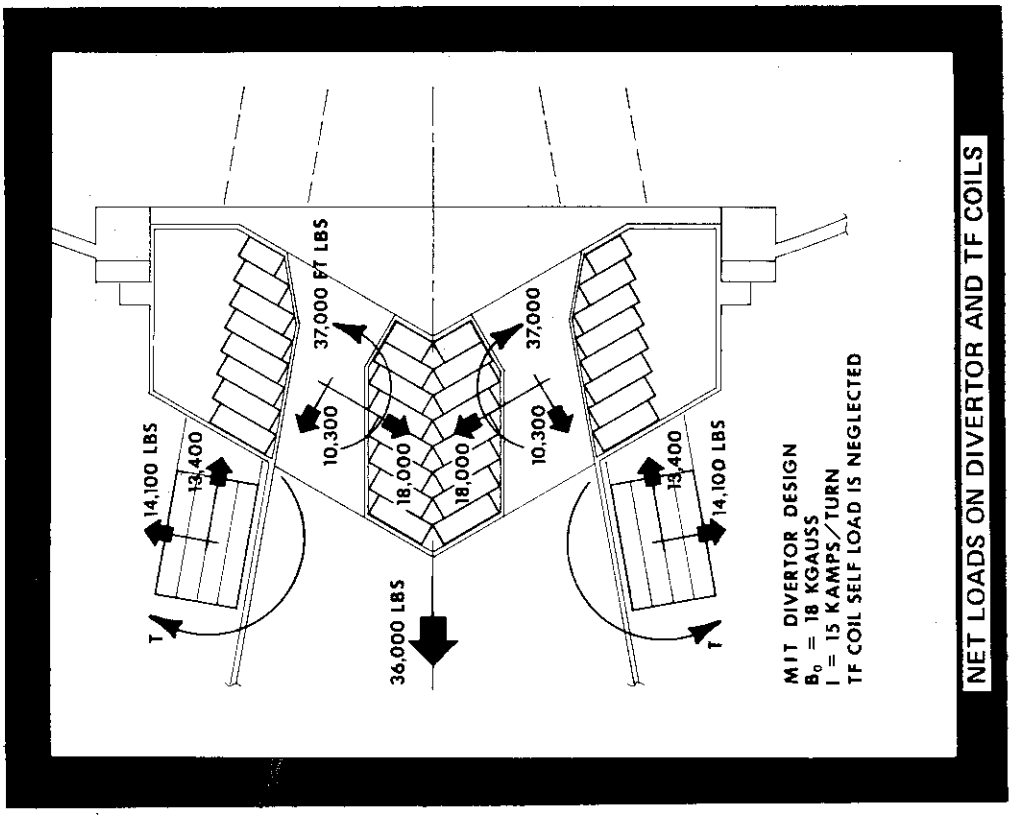
NET LOADS ON DIVERTOR AND TF COILS
MIT DIVERTOR DESIGN
B_0 = 18 KGAUSS
I = 15 KAMPS/TURN
TF COIL SELF LOAD IS NEGLECTED
14,100 LBS
13,400
37,000 FT LBS
10,300
18,000
36,000 LBS
18,000
37,000
10,300
13,400
14,100 LBS
T
T

Fig. 1.3

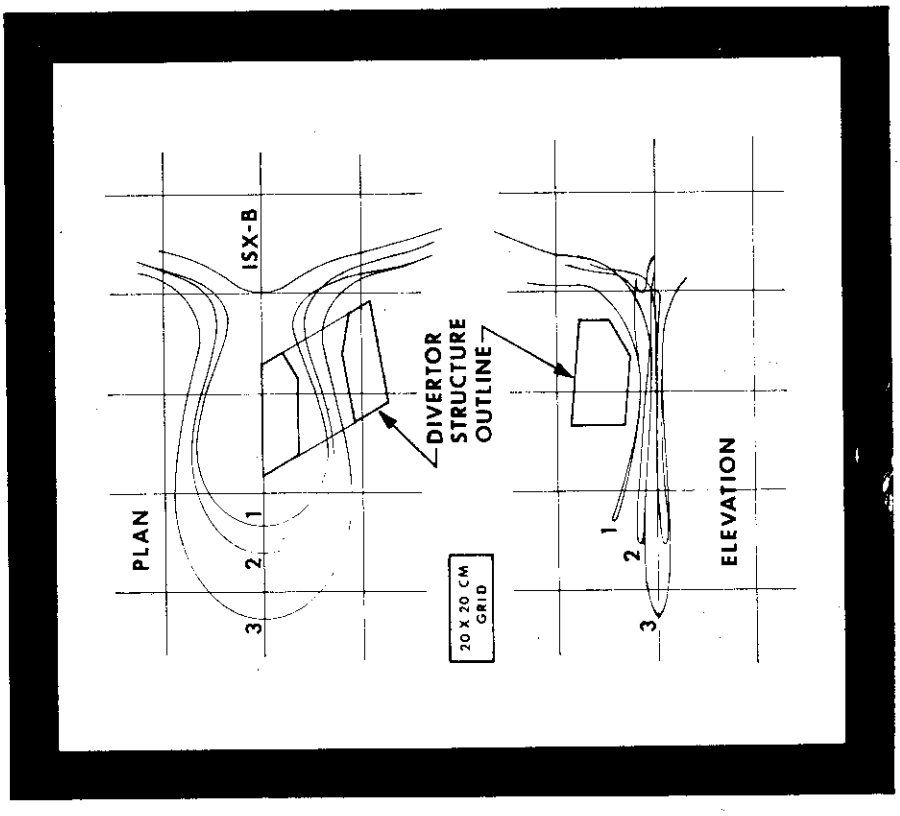
PLAN
ISX-B
DIVERTOR STRUCTURE OUTLINE
20 X 20 CM GRID
ELEVATION
1
2
3
1
2
3

Fig. 1.2

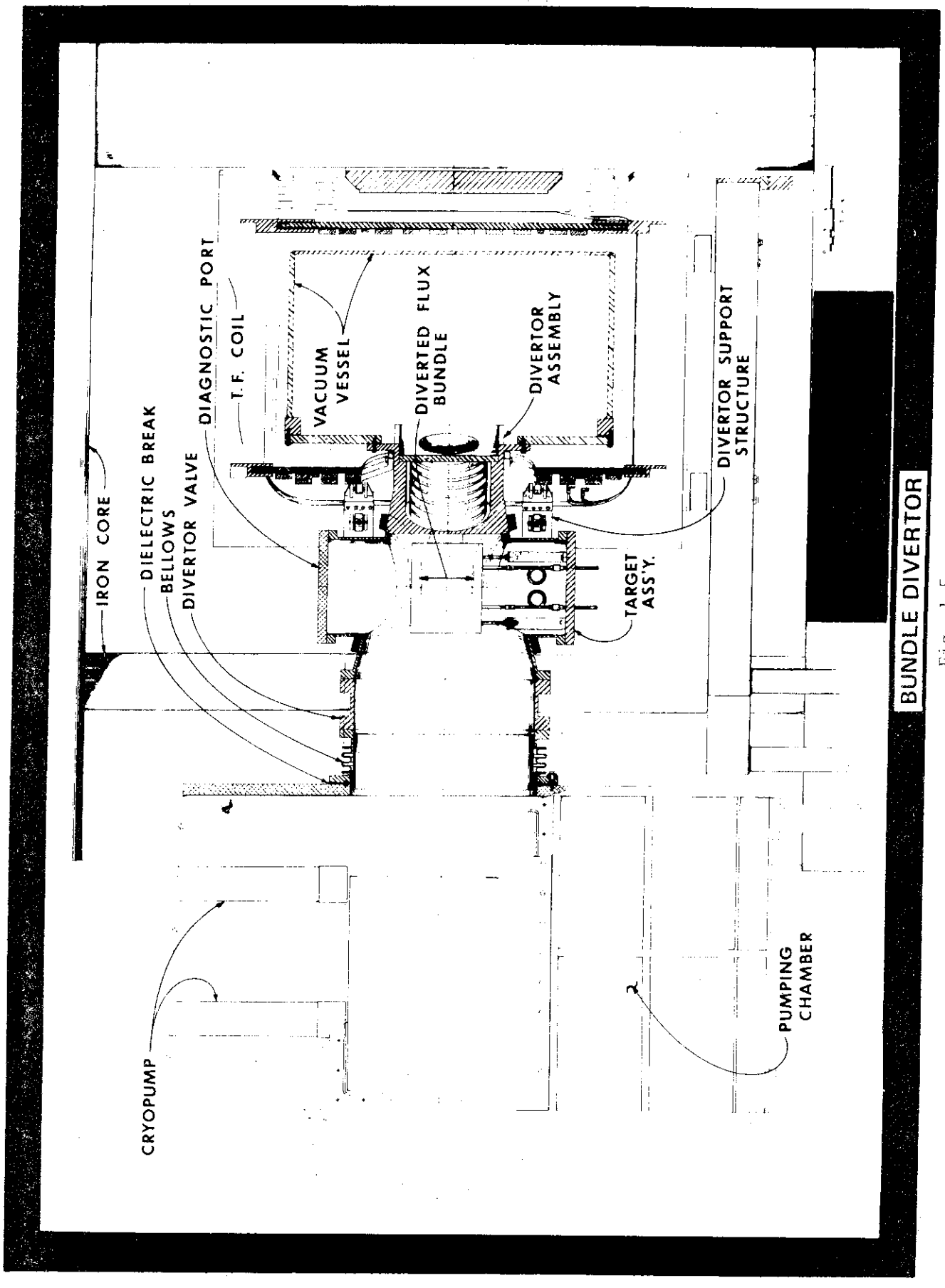
BUNDLE DIVERTOR
IRON CORE
DIELECTRIC BREAK
BELLOWS
DIVERTOR VALVE
DIAGNOSTIC PORT
T.F. COIL
VACUUM VESSEL
DIVERTED FLUX BUNDLE
DIVERTOR ASSEMBLY
DIVERTOR SUPPORT STRUCTURE
TARGET ASS'Y.
CRYOPUMP
PUMPING CHAMBER

Fig. 1.5

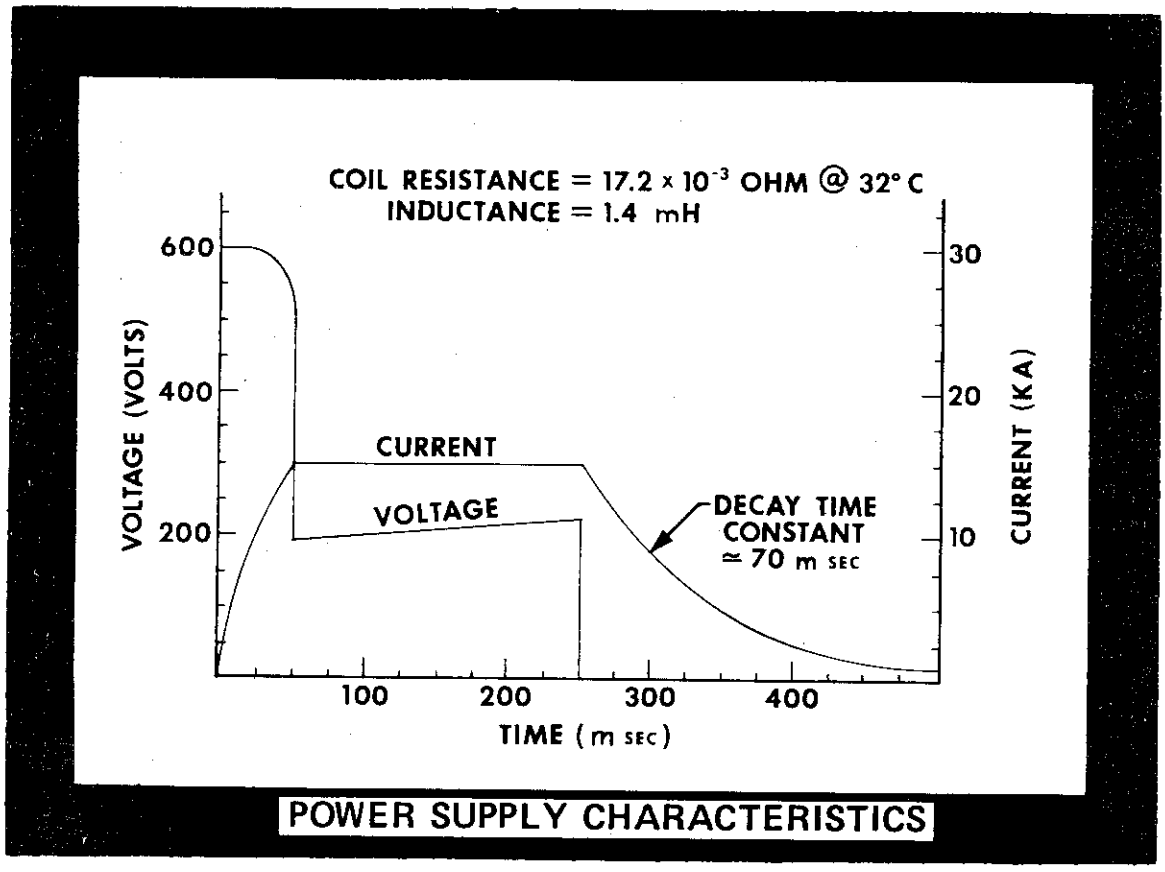
COIL RESISTANCE = 17.2 x 10⁻³ OHM @ 32° C
INDUCTANCE = 1.4 mH
600
400
200
VOLTAGE (VOLTS)
30
20
10
CURRENT (KA)
CURRENT
VOLTAGE
DECAY TIME CONSTANT ≃ 70 m SEC
100
200
300
400
TIME (m SEC)
POWER SUPPLY CHARACTERISTICS

Fig. 1.6

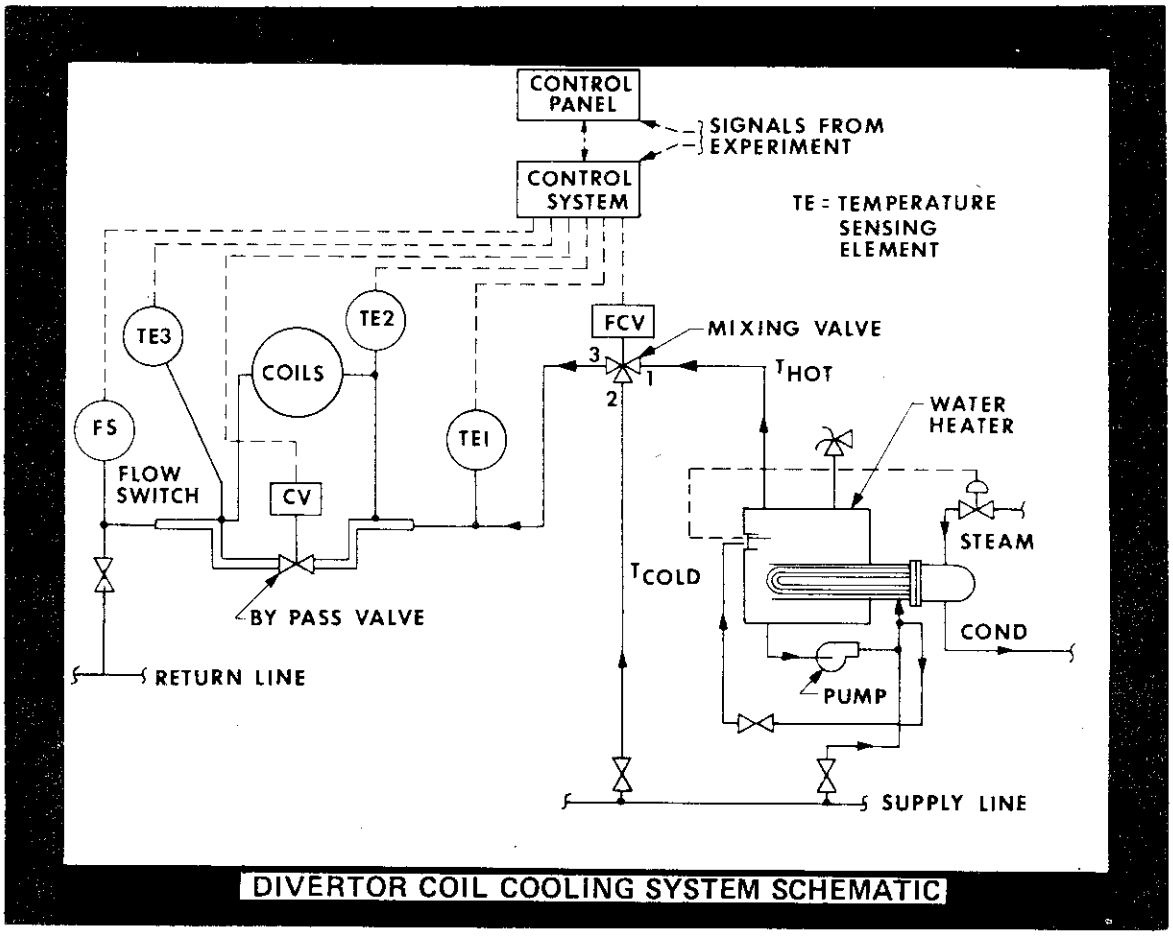
CONTROL PANEL
SIGNALS FROM EXPERIMENT
CONTROL SYSTEM
TE = TEMPERATURE SENSING ELEMENT
TE3
TE2
COILS
FCV
MIXING VALVE
3
2
1
THOT
WATER HEATER
FS
FLOW SWITCH
TEI
CV
STEAM
TCOLD
BY PASS VALVE
COND
RETURN LINE
PUMP
SUPPLY LINE
DIVERTOR COIL COOLING SYSTEM SCHEMATIC

Fig. 1.7

EFFECTS OF BUNDLE DIVERTOR RIPPLE

Section 2

Because bundle divertors destroy axisymmetry, they inherently produce deleterious effects on the flux surfaces, $|B|$ surfaces and particle orbits. One aim of the ISX-B and DITE experiments is to identify and assess the magnitude of these effects. In order for bundle divertors to be reactor relevant, they must allow the suprathermal injected ions and fusion α particles to stay confined long enough to thermalize and heat the background plasma. So far we have concentrated our studies on just these suprathermal ions and have identified a number of potential problems.

The design of bundle divertors has been optimized for low ripple, large spreading of the flux bundle, and keeping the field lines from hitting the wall while under the severe handicap of having to fit into existing tokamaks. These criteria do not guarantee the retention of fast ions deep within the plasma.

Collisionless trapped particles (bananas) are also strongly affected by the shape of the mod B surfaces because the mirror points always lie on the same B surface. Optimizing a divertor for minimum ripple causes the minimum in B (caused by the divertor) to be flanked by two maxima. If these maxima are large, they can prevent the bananas from going toroidally all the way around the machine. The bananas get "hung up" between a maximum and the usual 1/R toroidal fall off of the field and quickly $\bar{B} \times \nabla B$ drift out of the machine. Thus, it appears that the present (basically two-coil) ISX-B and DITE designs will cause most of the injected fast ions which scatter towards the $V_{\parallel}$ axis to be lost. In a reactor, all of the α particles born as bananas ($\sim 1/3$) would also be lost, lowering the expected α heating.

However, it is possible to design a bundle divertor with no maximum in B using a basically four-coil design (Figure 2.1). This will prevent the quick loss of bananas due to the $\vec{B} \times \nabla B$ drifts but there will still be enhanced radial diffusion of these particles due to moving the banana tips around in the divertor region. Also, four-coil divertors have less room for shielding and for flux expansion.

Next, we consider the circulating collisionless ions which may also have problems. Due to the large mirror ratio encountered in going through the divertor coils, these ions may reflect within the divertor and hit the inside of the coils before reaching the collection plate. The process is limited to nearly parallel circulating particles near the outside of the plasma so few α particles should be involved. However, any injected ions born in the outer part of the plasma may meet this fate and they are more likely to mirror and hit the divertor coils than to reach the collector.

Countercirculating fast ions cannot reach the divertor because the orbits are shifted inward (in R) from the flux surfaces. However, if any part of the orbit goes through the scrape-off layer (and even somewhat inside it), the orbit seems to become ergodic and quickly hits the wall. On top of all this, we have also observed islands in the orbit topology the significance of which is unclear.

In Figure 2.2 we show the ISX-B bundle divertor, the $|B| = 1$ T surface, and the resulting flux surfaces. Although the outer surfaces are ergodic, the inner surfaces are well formed.

However, many of the above theoretically predicted effects are model dependent since we assumed that the magnetic field was given by a superposition of the axisymmetric equilibrium plus the vacuum ripple. In reality, the plasma may try to "heal" itself by changing the current distribution in the plasma so that more work to elucidate the true nature of the 3-D equilibrium is required.

Fig. 2.1 a) The $|\bar{B}|$ = 4.4 T surface (dotted) for a divertor on INTOR/ETF which has been designed to eliminate the maximum in $|\bar{B}|$.

b) The same $|\bar{B}|$ surface calculated for various values of toroidal angle and plotted on top of each other. The shape and size of the surface is almost independent of ϕ except at the minimum caused by the divertor (ϕ = 0). In this case, the plasma β is high enough to dig a well in $|B|$ which is why the $|B|$ surface is closed without the divertor present.

Fig. 2.2 a) The ISX-B bundle divertor and the $|B|$ = 1 T contour (dotted). The maximum in $|B|$ near the divertors will cause trapped ions to leave the system quickly.

b) The flux surfaces in this configuration

c) The orbit of a 1 keV banana which escapes from ISX-B due to interacting with the maximum in $|B|$.

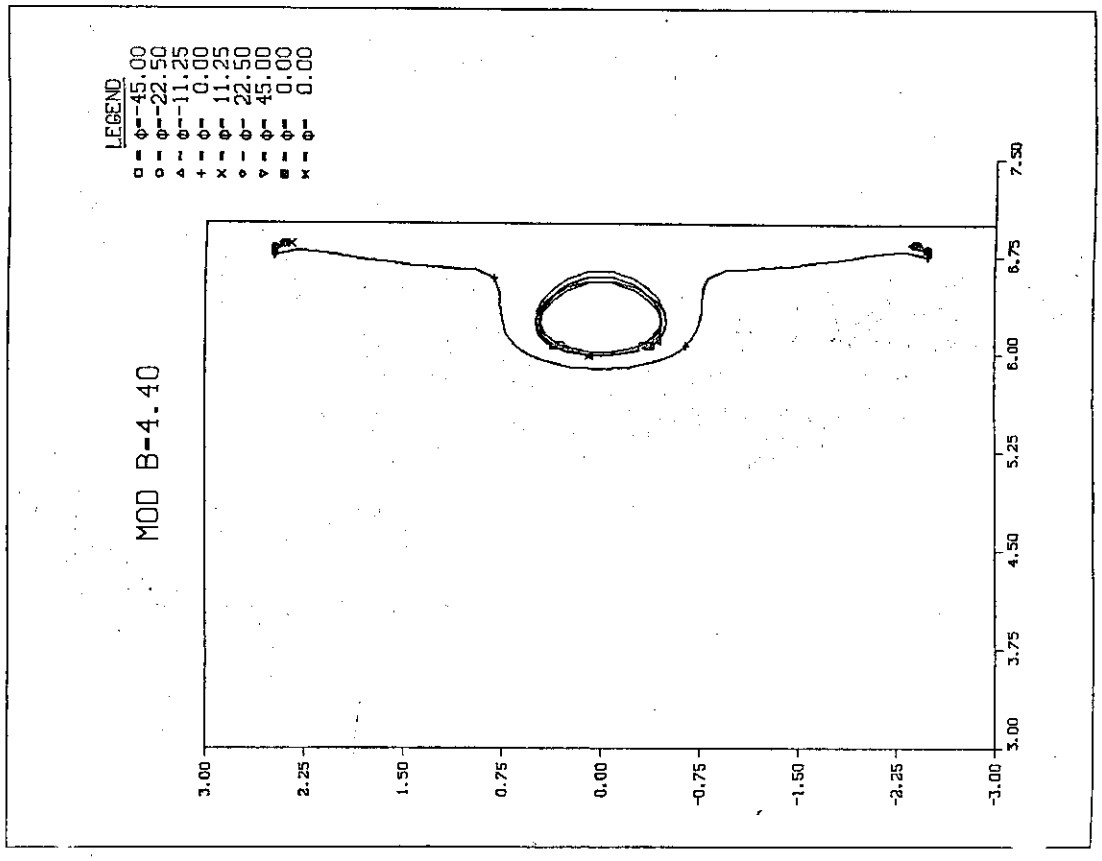

Fig. 2.1(b)

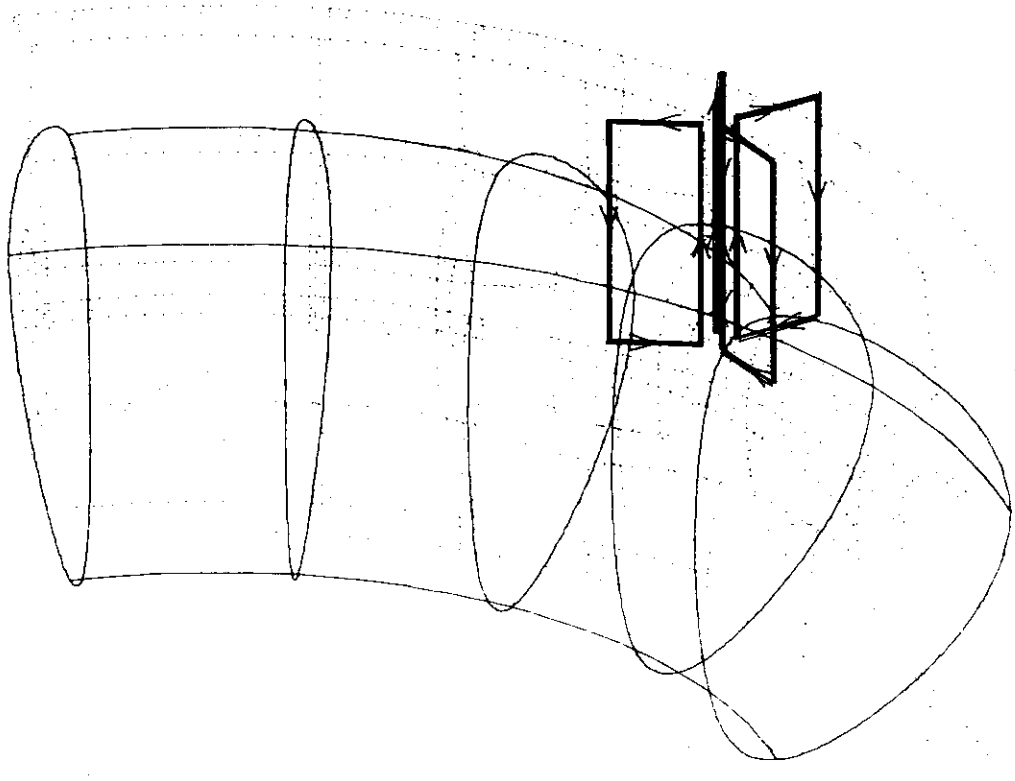

Fig. 2.1(a)

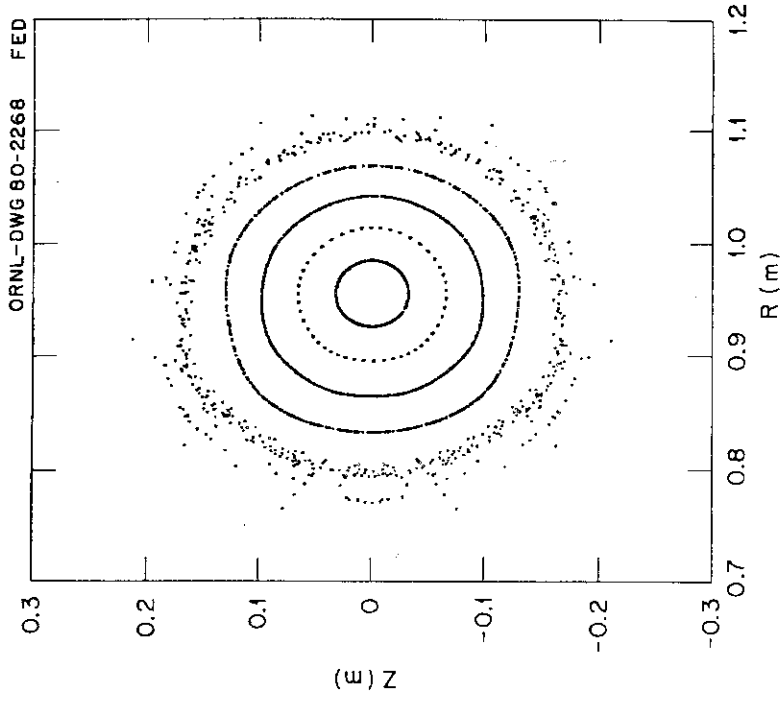

Fig. 2.2(b)

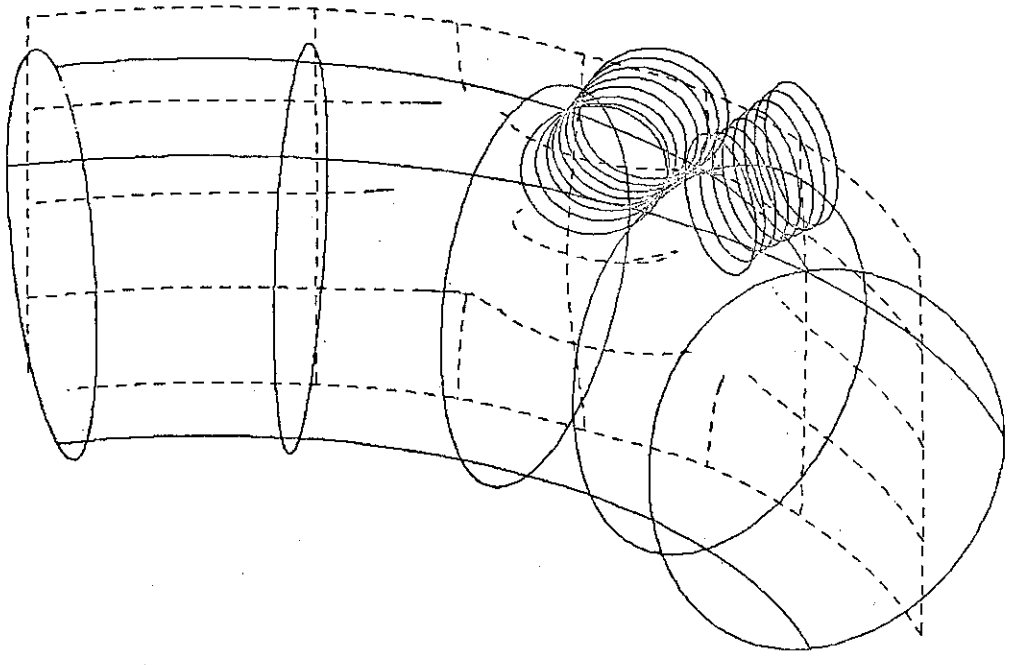

Fig. 2.2(a)

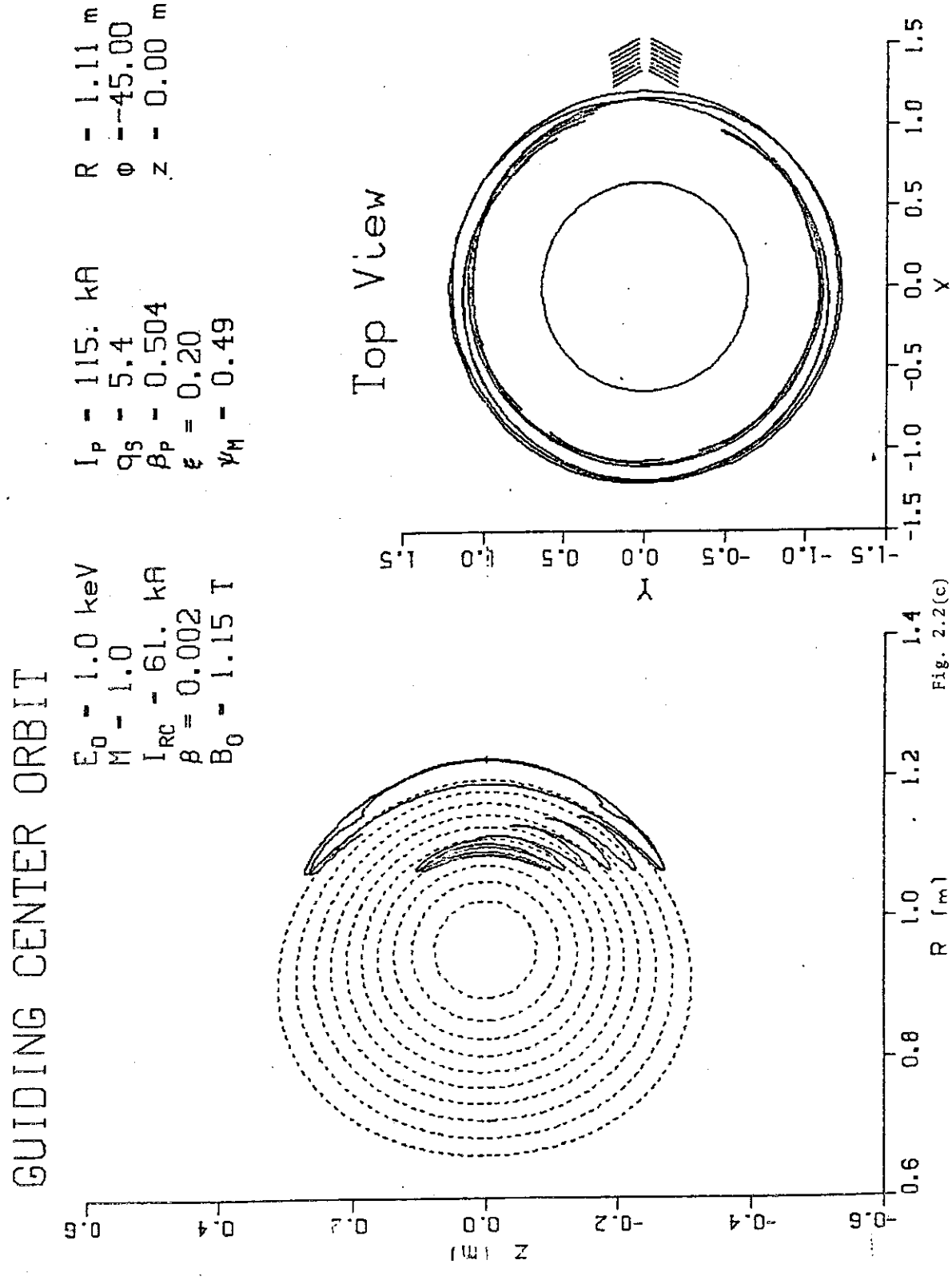
GUIDING CENTER ORBIT
E_0 = 1.0 keV
M = 1.0
I_{RC} = 61. kA
β = 0.002
B_0 = 1.15 T
I_p = 115. kA
q_s = 5.4
β_p = 0.504
ε = 0.20
ψ_M = 0.49
R = 1.11 m
ϕ = -45.00
z = 0.00 m
Top View
Z (m)
R (m)
Y
X

Fig. 2.2(c)

TRANSPORT MODELING OF BUNDLE DIVERTOR

Section 3

Model

Transport modeling of ISX-C predicts the plasma parameters expected, the effect of the bundle divertor, and the saturation time of the wall for hydrogen recycling.

Transport Coefficients

The transport code PROCTR solves a standard set of 1-D plasma transport equations including detailed models for neutral gas transport and neutral beam injection heating. The plasma transport coefficients used are

$$\chi_e = \frac{2 \times 10^{16}}{\overline{n_e}} \left(2 + 20 \left(\frac{r}{a}\right)^2\right) \text{ cm}^2/\text{S}$$

$$D = 1/3\ \chi_e, \quad \chi_i = 1.5\chi_{\text{NEOCLASSICAL}}$$

χ_e and D are enhanced by 1% of Bohm for $q < 1$.

These transport levels give an acceptable fit to present ISX results.[1]
The neoclassical pinch is included in the hydrogen plasma transport equation.
All transport coefficients are enhanced by $10^4 \frac{\text{cm}^2}{\text{S}}$ in the scrape-off.

Divertor Terms

In the plasma scrape-off, the parallel ion flow to the bundle divertor is given by

$$\Gamma = 2\ \alpha\ n_i V_{Ti} \frac{1}{R_m}\ A_D^{-1} F_{CX}^{-1} F_D\ ,$$

$$\alpha = \frac{1}{2\sqrt{\pi}}\ , \quad V_{Ti} = \sqrt{\frac{2T_i}{m_i}}$$

where R_m = upstream divertor mirror ratio

$A_D^{-1} = \frac{1}{q_D} \frac{r - a_s}{a - a_s}$ geometry factor, a = wall radius

a_s = separatrix radius

$q_D = 3$

$F_{CX}^{-1} = 1 + \frac{R_m A_D 2\pi R_o}{\lambda_{CX}}$ effect of c-x drag on parallel flow to divertor

and F_D = empirical factor used to fit experiments.

From modeling of data from DITE, we find $F_D = \frac{1}{5}$ is needed to fit the results, and we use this factor for all calculations here.

The energy fluxes to the divertor are:

$Q_{\parallel}^{i} = 2T_i\Gamma$,

$Q_{\parallel}^{e} = 2\gamma T_e\Gamma$,

where $\gamma = \frac{1}{1-\sigma_s} + \frac{1}{4} \ln \left(\frac{1}{4} \frac{m_i}{m_e} \frac{T_e}{T_i} (1-\sigma_s^2)\right)$

and σ_s = secondary electron emission coefficient.

Recycling

In estimating fueling requirements in the presence of a divertor, a realistic recycling model is required. In these calculations, all ions which diffuse to the limiter (or wall) are recycled as a cold neutral flux. A fraction of this cold flux (~40%) returns to the wall as hot c-x neutrals and a fraction (50-90%) of this hot flux is reflected. The c-x neutrals which are not reflected stop in the wall and may subsequently diffuse through the metal to the surface and be desorbed. In our calculations, we include a time-dependent 1-D Fick's law diffusion equation for hydrogen in the wall to calculate the desorption flux

and the buildup of hydrogen in the wall. We use the model of Wilson and Baskes[2] for wall diffusion assuming loaded traps and a room temperature (T = 20°C) wall diffusion coefficient ($D_{Wall} = 3 \times 10^{-12} \frac{cm^2}{s}$). We also assume an initial concentration of zero for the mobile hydrogen density in the wall before each shot. A detailed description of this model will appear shortly[3].

Results

Machine Parameters

The ISX-C parameters we use for our calculations are,

a_{wall} = 45 cm, a_{sep} = 35 cm, R_o = 125 cm (circular),

B_T = 18 kG, I_T = 400 kA, (q_{sep} = 2.2, q_{wall} = 3.8),

E_{inj} = 45 keV, a_{BEAM} = 15 cm, $R_{TANGENT}$ = 105 cm.

For the density, we have a feedback control algorithm which continually adjusts the cold gas or pellet feed rate to maintain the volume average electron density at $\langle n_e \rangle = 4 \times 10^{13}$ for which $4.5 \times 10^{13} \leq \bar{n}_e \leq 6 \times 10^{13}$ depending on the density profile. We assume $Z_{eff} = 1.5$ and $n_e = n_i + n_B$ where n_B = fast ion density. The upstream mirror ratio for the divertor is $R_m = 2.5$.

Calculated Plasma Parameters

Plasma parameters which result from the model described above for P_{inj} = 0, 1.5, 3.0 MW are given in Table 1. We see that simple extrapolation (in size and heating power) from the present ISX experiment predicts a plasma with high enough temperatures (5 keV) and β_T (2.6%) to satisfy the objectives of the ISX-C experiment. Higher β_T at lower temperatures would be obtained at higher densities, since $\langle n_e \rangle = 4 \times 10^{13}$ is well below the penetration limit of the 45 keV beams.

Divertor Energy and Power Flows

The integrated power and particle balances for the ohmic and for the P_{inj} = 3 MW cases are shown in Figure 1. The interesting result from DITE is that a small fraction of the total heating power and an even smaller fraction of the total fueling (recycle + gas feed) flux are diverted. This is also evident in the ohmic ISX-C case in Figure 3.1a, where 13% of the particle and 41% of the transport energy loss are diverted. These fractions increase to 31% and 76% with P_{inj} = 3 MW (Figure 3.1b) primarily because the ion temperature in the scrape-off and hence the parallel flux to the divertor increase. Thus, these calculations indicate that

1) the bundle divertor will be only a partial divertor with much of the recycle and heat flux still going to the limiter, and
2) the divertor efficiency increases with P_{inj}.

Long-Pulse Saturation of Wall

One purpose for a long-pulse experiment is to allow complete saturation of the vacuum vessel walls so that all the pumping of gas is by the divertor. We estimate the saturation with a 10 sec simulation for P_{inj} = 1.5 MW. The plasma profiles (Figure 3.2) reach steady state within the first 2 sec. of the run. The volume source term for hydrogen in the wall due to nonreflected c-x neutrals from the plasma (Figure 3.3) is also constant after the first 2 sec. The density of hydrogen in the wall, however, evolves continually and, after 10 sec, is still far from equilibrium. The ratio of flux diffusing out of the wall into the plasma to the total rate of deposition in the wall (Figure 3.4) reaches 90% in 1 sec and 95% in 10 sec indicating that 10 sec time scales are relevant for full wall saturation. The net pumping rate of the wall after 10 sec is 1.5×10^{20} H/sec which is 2.5% of the divertor pumping rate; thus, most of the external fueling is replacing

loss to the divertor with only a small fraction going to replace wall absorption. The peak wall density at 10 sec is 1.5% atomic fraction of the wall metal (Fe) density.

Ripple

For all our calculations, we assume a toroidal field ripple of

$$\delta(r) \equiv \frac{B_{max}-B_{min}}{B_{max}+B_{min}} = 1.42 \times 10^{-2} e^{r/14.9(cm)}$$

which gives $\delta(a) = 2.9\%$ at the plasma edge ($r = 45$ cm). Using the formulation of Stringer, we find that the enhancement of the ion heat conduction due to toroidal field ripple above the neoclassical value is negligible for all cases considered here.

Pellet Fueling

It is evident from the particle balance shown in Figure 3.5 that most of the gas used for fueling is stopped in the scrape-off. Direct fueling of the plasma may only be achieved with pellets. To simulate pellet fueling, we calculate the deposition profile of the pellet ions from a pellet ablation model[4]. The fuel is then added continually rather than at discrete times. This allows us to calculate time-average plasma and wall profiles without the rapid transients associated with discrete pellet fueling. This approximation becomes more valid as the pellet rate increases; for the case studied here, the equivalent rate is sufficiently high (1 pellet every 6.5 ms) to justify this method.

We assume a pellet velocity $v_{pel} = 1$ km/s and an initial pellet radius of 0.5 mm. The resulting plasma parameters for a 10 sec simulation with $P_{inj} = 1.5$ MW are shown in Table 1. No external cold gas feed was used. The fueling rate by pellets is 60 tl/s (equivalent to 1 x 50 pellets/sec) which is a factor of 25% less than the gas feed rate of 80 tl/s which was needed for the gas fueling

cases described above. The total fueling (pellet + recycled gas) profile is shown in Figure 3.5. Because the large recycle flux is reduced by pellets, the pumping efficiency of the divertor (Table 1) is greatly increased, both for energy and particles. The reduced neutral level also lowers the charge exchange flux absorbed in the wall so that at t = 10s, the amount of hydrogen in the wall is 50% of the amount with gas puffing. Similarly, the desorbed flux is 90% of the absorbed flux.

We conclude that pellet fueling

1) does not significantly alter the plasma parameters (temperatures, β, etc.), which are obtained with gas fueling,
2) improves the divertor efficiency by lowering the hydrogen recycle interaction with the limiter and
3) increases the hydrogen saturation time of the wall.

Impurity Shielding of Scrape-off

By integrating over the fast c-x neutral spectrum incident on the wall, we find the erosion rate of the wall due to sputtering to vary from 1.32×10^{11} $Fe^{\circ}/cm^2/s$ for the ohmic case to 5.75×10^{13} $Fe^{\circ}/cm^2/s$ for the P_{inj} = 3 MW case. Pellet fueling at P_{inj} = 1.5 MW increases the rate slightly from 1.2×10^{13} $Fe^{\circ}/cm^2/s$ with gas fueling to 1.6×10^{13} $Fe^{\circ}/cm^2/s$, primarily because the increase in T_i in the scrape-off and edge plasma increases the average sputtering yield from $\tilde{Y} = 2.6 \times 10^{-4}$ to 1.5×10^{-3}.

In all cases, this sputtering flux is ionized completely in the scrape-off (for $E_{Fe} \equiv 20$ eV) and the impurity influx to the plasma will depend on the balance between the inward cross-field transport of the various charge states of the Fe and the parallel loss to the divertor. The transport code PROCTR does not yet have an impurity transport equation; however, we note that if a flux of 5×10^{13} $Fe/cm^2/s$

is deposited uniformly in the scrape-off, the Fe density reaches $10^{12}/cm^3$ in 200 ms in the absence of losses. Thus, for a 10s pulse, the divertor will have to be effective to screen the plasma from this relatively large impurity influx.

References for Section 3

[1]Murakami, et al., Phys Rev. Lett., 42, 655 (1979).

[2]Wilson, K. L. and M. I. Baskes, J. Nucl. Mat., 76-77, 296, 1978.

[3]Howe, H. C., Hydrogen recycle modeling and measurements in Tokamaks and EBT, to appear in J. Nucl. Mat.

[4]Houlberg, et al., ORNL/TM-6549, 1979.

ISX-C

TABLE 1

P_{inj}(MW)	0	1.5		3.0
		Gas	Pellets	
τ_E(ms)	92	85	82	92
$T_e(0)$, eV	1100	2530	2200	4000
$T_i(0)$, eV	990	3100	2400	5100
$n_e(0)$, cm^{-3}	6×10^{13}	6.9×10^{13}	8.5×10^{13}	9.7×10^{13}
$\bar{n}_e$, cm^{-3}	4.6×10^{13}	4.9×10^{13}	5×10^{13}	5.7×10^{13}
β_T(%)	0.33	1.2	1.3	2.5
β_p	0.34	1.3	1.3	2.6
S_G(t-l/s)	40	80	60*	90
ξ_p	0.13	0.22	0.50	0.31
P_{DIV}	105 kW	675 kW	1000 kW	1.31 MW
ξ_E	0.41	0.65	0.80	0.76

S_G = cold gas or equivalent pellet fueling rate. 1 t-l/s = 7.07×10^{19} $\frac{\text{particle}}{\text{sec}}$

ξ_p = divertor particle pumping efficiency = ($\frac{\#}{\text{sec}}$ to the divertor)/(total ionization rate due to fueling and recycling)

ξ_E = divertor energy efficiency = (power flow to divertor)/(total input power - radiation power - c-x loss)

*Equivalent gas rate. Corresponding pellet rate = 152 pellets/sec.
= 6.6 ms between pellets.

Fig. 3.1 Integrated power and particle balances for ISX-C for (a) P_{inj} = 0 and (b) P_{inj} = 3 MW. The increase in divertor loss due to injection is evident. Divertor terms outlined in red.

3.2 Plasma Profiles for a 10 sec simulation with P_{inj} = 1.5 MW. The plasma reaches steady state within 2 sec.

3.3 Wall profiles for a 10 sec simulation with P_{inj} = 1.5 MW. The density of hydrogen in the wall is still evolving after 10 sec and is far from steady state.

3.4 Ratio of flux out of wall to flux into wall for P_{inj} = 1.5 MW, t_{max} = 10 s case.

3.5 Local particle balance for fueling by (a) gas and (b) pellets for P_{inj} = 1.5 MW at t = 10 sec.

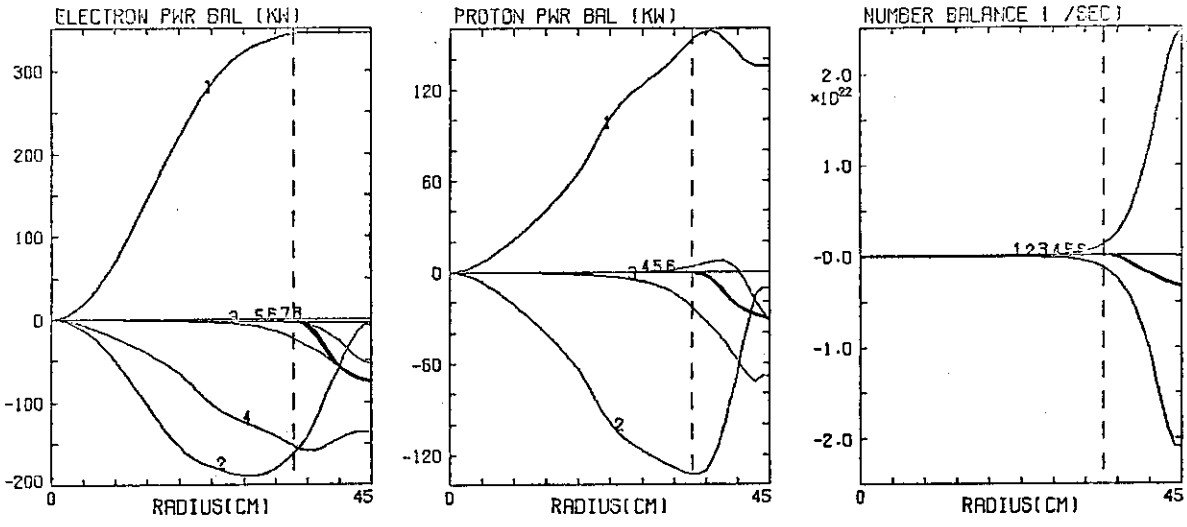

Fig. 3.1(a)

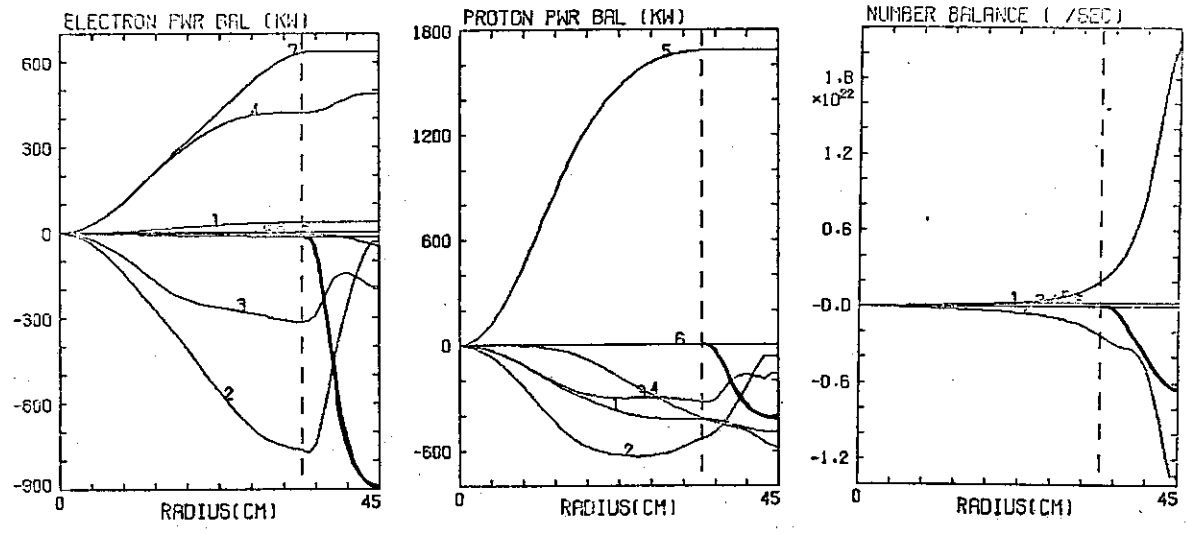

Fig. 3.1(b)

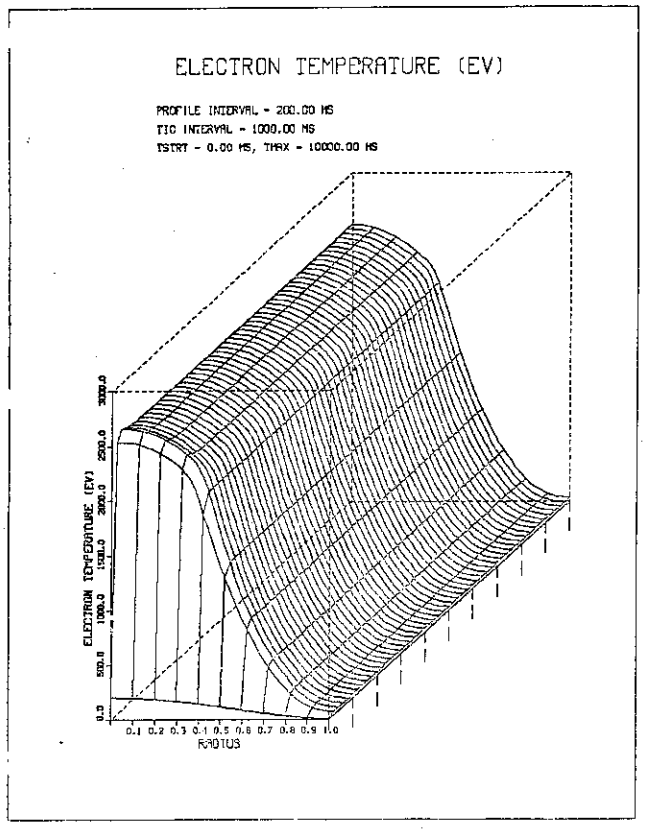

Fig. 3.2(a)

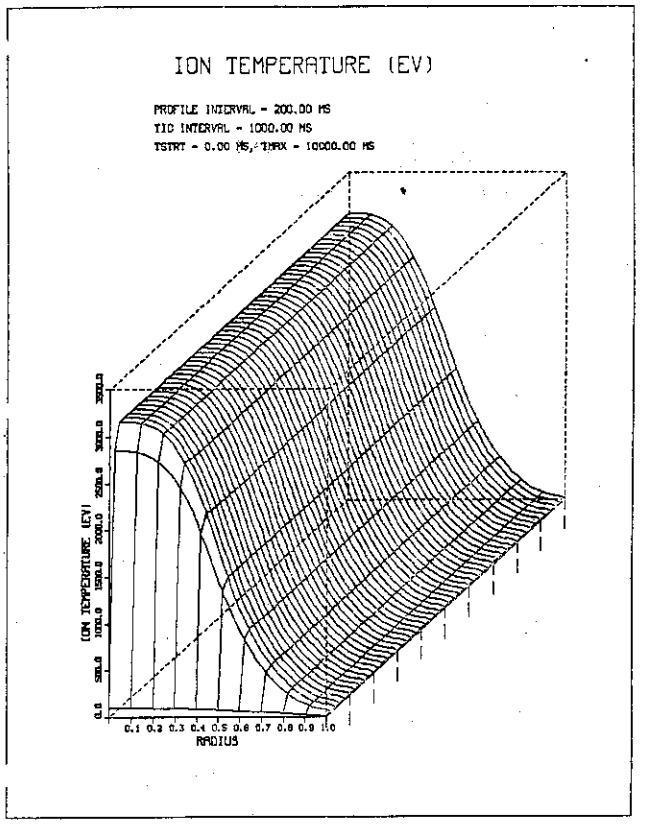

Fig. 3.2(b)

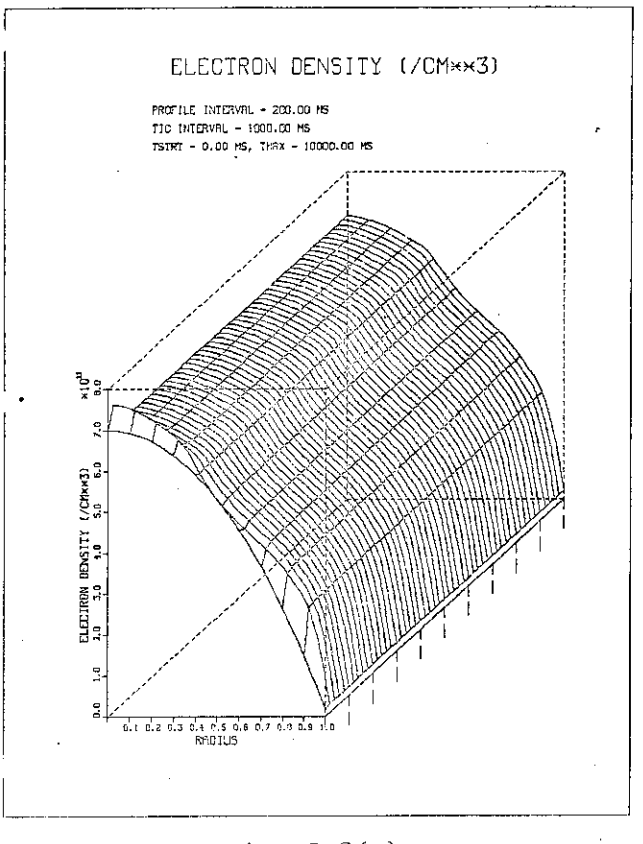

Fig. 3.2(c)

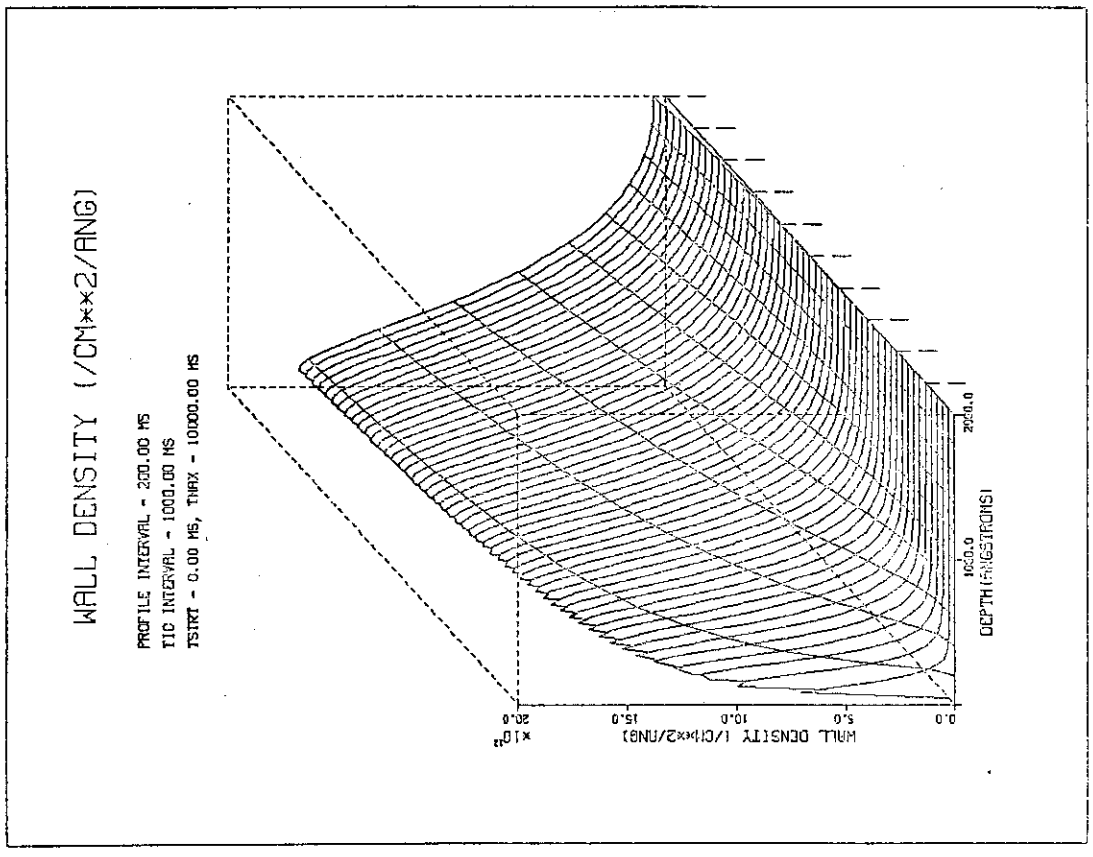

Fig. 3.3(b)

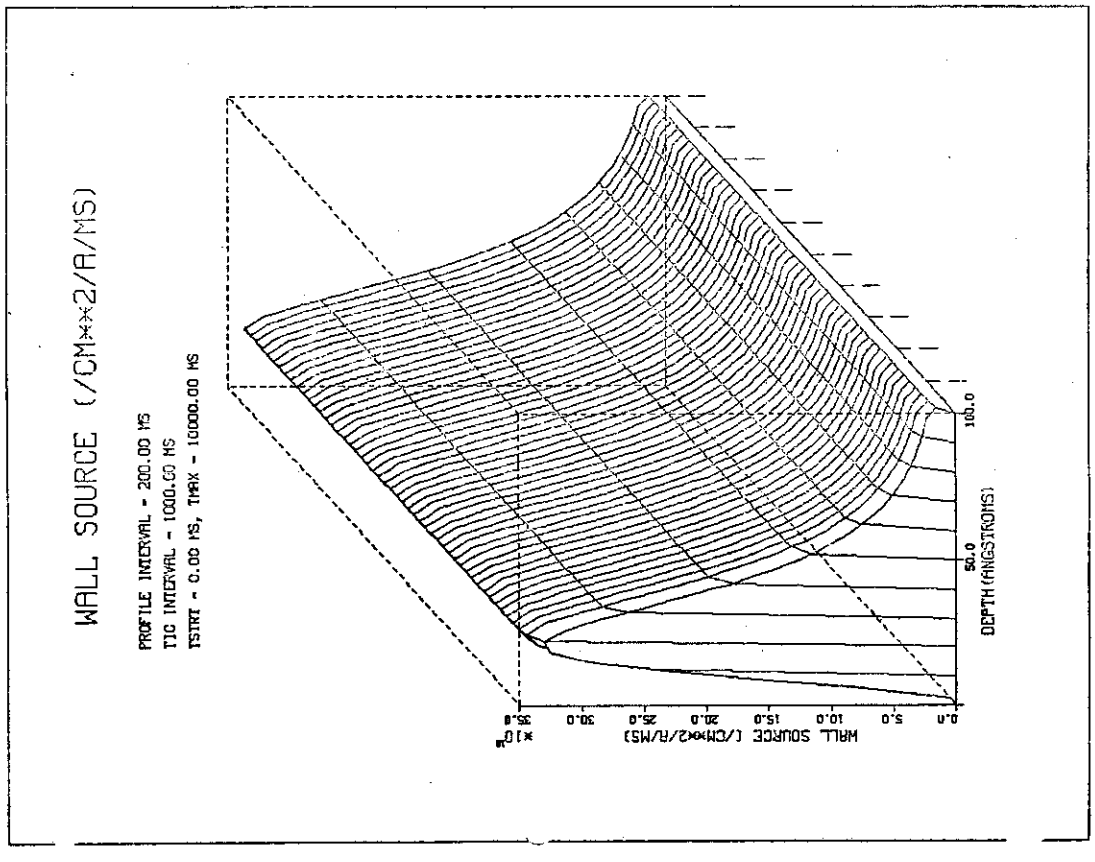

Fig. 3.3(a)

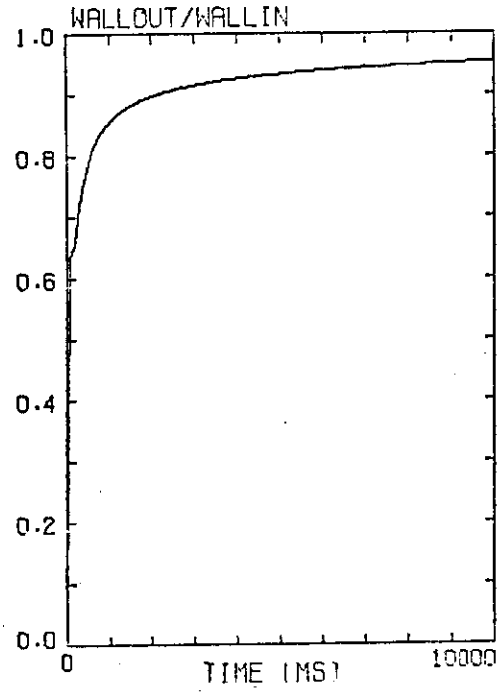
WALLOUT/WALLIN
1.0
0.8
0.6
0.4
0.2
0.0
0
TIME (MS)
10000

Fig. 3.4

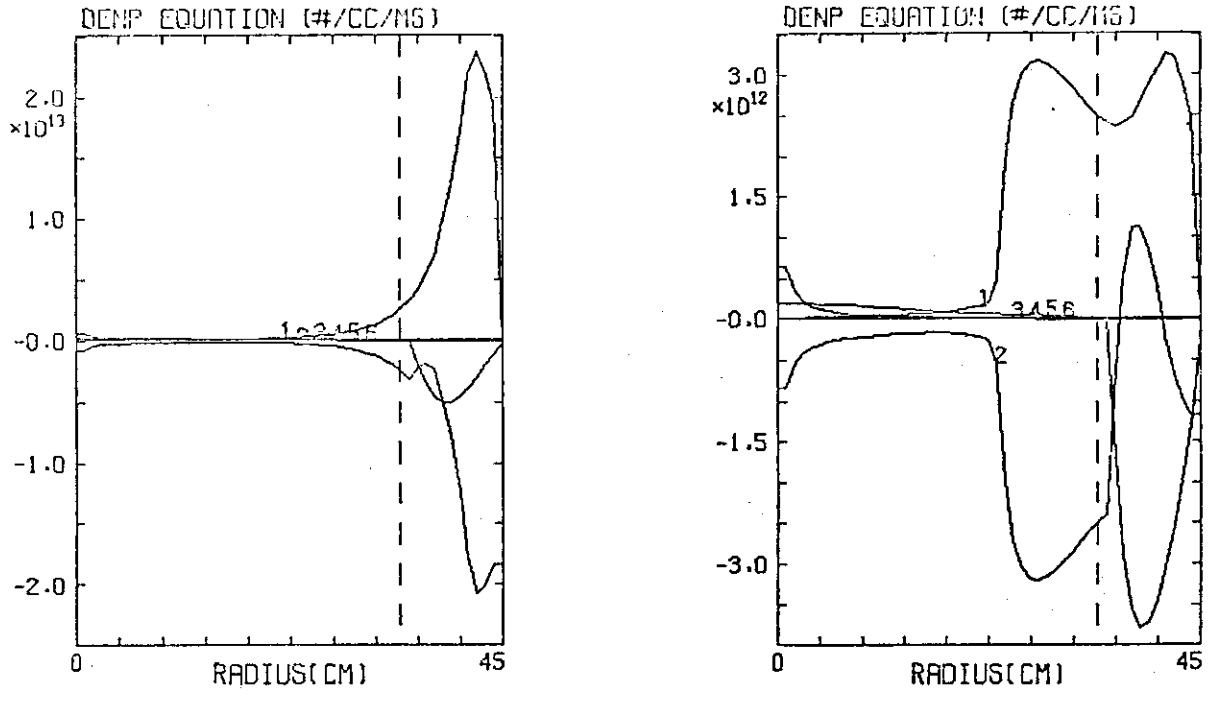
DENP EQUATION (#/CC/MS)
2.0
×10^13
1.0
-0.0
-1.0
-2.0
0
RADIUS(CM)
45
DENP EQUATION (#/CC/MS)
3.0
×10^12
1.5
-0.0
-1.5
-3.0
1
2
0
RADIUS(CM)
45

Fig. 3.5

BUNDLE DIVERTOR POSSIBILITIES FOR ISX-C

Section 4

Introduction

A major reason for the modifications of the ISX device which lead to ISX-C is the capability of testing various advanced divertor options for the ETF. These include advanced bundle divertors and external poloidal divertors.

In this section we present briefly the results of preliminary optimization studies of octupole bundle divertors. Generally, the octupole divertor gives $\sim$ 3 times less ripple than a conventional (quadrupole) bundle divertor. In these studies, we adjust the configuration in order to minimize the field perturbation at the plasma center. The results will guide the more complete optimization that will be done for the eventual final engineering design.

The ripple δ is defined as $(B_{max}-B_{min})/(B_{max}+B_{min})$ taken along a field line of the toroidal field (TF) plus divertor coil system. A bundle divertor naturally has 100% toroidal ripple at the plasma surface (separatrix). However, the ripple will fall off rapidly with distance from the divertor and it is possible to hold $\delta(0)$, the ripple at the magnetic axis, to quite low values. The divertor induced ripple can be as low as the inherent TF coil ripple, in this case $\delta^{TF}(0) \sim 0.2\%$.

The study uses a simple field-line-following code in which coils are assumed to be circular filaments. In order to represent distributed currents, arrays of filaments are spread over the region of actual conductors. Since the proposed ISX-C coils are rectangular rather than circular we use TF coil parameters which are not strictly the same as the real ones, but which give the design value for $\delta^{TF}(0)$.

Figure 4.1 presents a top view of the tokamak midplane, with small squares representing the location of the current filaments. Dimensions are in cm, and several parameters are defined pictorially. Of these, optimization has been carried out on X_{REF}, the distance in direction X_1 between the inner and outer solenoids of the divertor and on Θ_2, the tilt of the individual inner solenoid coils with respect to the X_1 direction. The angle Θ, determines the line of centers of the elements of the solenoid and has not been optimized to minimize δ_o. In fact, lower values of Θ_1 reduces δ_o but also reduce the clear bore through the solenoid and therefore restrict the amount of flux diverted. Other cases will also be presented.

The figure also shows the current in kiloamperes in each of the four solenoids making up the octupolar array, so the current through the "private flux" of the divertor is four times this, or 6 Megamperes. The field line encircling the four solenoids has an area of about $\pi \cdot 20 \cdot 22$ cm^2, so the average current density in the "center post" of the octupolar array is about 4500 Amp/cm^2 in this example. The coil radius is comparable with the EBT-S coils which operate in steady state with 6500 A/cm^2 in the copper, thus this assembly should have an adequate pulse length for ISX-C ($\sim$ 30 s).

Other printed values include the toroidal field in Gauss evaluated at R_c, the radial distance to the center of the nominal circular TF coils. In all the examples presented, R_c is 152 cm and a_c, the mean radius of the TF coils is 92.5 cm. The nominal area of the TF conductor is 19 cm by 28 cm so the inner bore of the TF coil is 235 cm − 69 cm = 166 cm. Again, these parameters have only approximately the proposed ISX-C design values, and are chosen to model the value δ_o^{TF} = 0.2% expected from the actual rectangular coils in the proposal.

For all the cases presented here, the TF coils are excited to a level where B_{TF} = 12.29 kG at R = 130 cm, and 12.00 kG at R = 133.1 cm.

The parameter E_{LONG} takes values 1 or 3, depending on whether the divertor solenoids are to be circular, or to have approximately 3:1 elongation out of the plane of the figure in order to increase the total flux diverted. In the latter case, the elongated coils are modeled by a stacked set of 3 circular coplanar coils with separation of 1.8 times their radius, known as a_{DC}.

In all the examples shown here, a_{DC} has the value, 12 cm, chosen as a compromise between reducing ripple by means of small a_{DC} and increasing the total amount of diverted flux by means of large a_c. With this value, the entire divertor module has a width in the X_2 direction of approximately the planned 70 cm width of the ISX-C large ports.

The parameters X_{DIV} are the distances in X_1 and X_2 directions from the major axis of the tokamak to the innermost filament of the divertor coil set. The value of Y_{DIV} is 20-22 cm, and X_{DIV} is varied to ensure that the separatrix X-point falls at X_2 = 0 and X_1 = 185 cm. The latter value leads to an outer plasma edge (separatrix) which falls at R ≃ 175 cm in the area away from the divertor. With nominal magnetic axis at 130 cm, the plasma minor radius would then be a = 45 cm except near the separatrix where it would bulge to 55 cm. In the several cases presented, it is the location of the X-point which is fixed, not ap.

In an example to be shown later the X point is placed at R = 180 cm to yield a reduced plasma radius a = 40 cm.

Figure 4.2 shows the variation of B along the field lines of Figure 1 and the resulting ripple profile $\delta(r)$ in the midplane through the divertor.

Trade Studies

The number of input parameters is large and the criteria for judging the results are still diffuse, so that we do not yet present a single recommended design. In fact, one key attribute of ISX-C will be the capability of accepting and testing various divertor versions.

Criteria for judging the apparently most desirable cases for experimental test will be the ripple profile induced, amount of space (or flux) available for the diverted plasma layer, the currents, the shielding and other structures, resulting field line spread at the divertor layer, and the extent of mirror trapping of particles in the divertor region. The cases presented establish that for each of these factors there is a range of acceptable values within the design envelope of ISX-C.

It should be noted that for larger, next generation devices the design of a bundle divertor may in fact be easier, provided the initial device parameters are chosen with this divertor in mind. An important factor requiring further study for any bundle diversion scheme is whether the influence of plasma currents at high beta will be such as to reduce the ripple in the hot plasma region so that higher ripple levels are tolerable in the vacuum field configuration. If this conjecture proves true, then the applicability of bundle divertors to ETF's and INTOR's is greatly enhanced.

In the present study we have focused upon δ as the primary indicator of merit for divertor combinations. This allows us to determine a narrower range of study for the more complete analysis which is necessary to determine the effects of the divertor on energetic particle losses and to minimize these. It is likely that the overall "best" case will have slightly more than the absolute minimum ripple in order to provide the least perturbation of the ion distribution

functions. For example, J. A. Rome has observed that minimizing the "magnetic mountain" at each side of the divertor region may be more important than minimizing $\delta(0)$ itself. Determination of these factors is possible within the analysis pioneered by J. A. Rome, J. F. Lyon and R. H. Fowler, and their codes will be applied to the potential designs presented here.

Figure 4.3 presents the divertor field pattern from an octupolar array of solenoids, which yields quite rapid falloff of perturbing field in the far-field region in which the bulk of the discharge lies. When TF coils are energized, the X-point lies in the near-field region.

Figure 4.4 presents the pattern for a flattened version of the previous arrangement, having a strong quadrupole component as well as the octupolar behavior. The two multipole moments can be played off against one another in a way that minimizes perturbations at the plasma center, and in this example there is a null of the divertor field caused by the balancing of the two moments. Taking into account the spatial profiles of both divertor and TF fields, a low value of the total ripple can be achieved throughout an entire region, as will be seen.

Figure 4.5 presents a case with nearly pure octopole field, and elongation of 3. The resulting $\delta(0)^{total}$ is 0.51%, $\delta(0)^{div}$ = 0.31% and there is clearly adequate space for currents, support structure and a diverted plasma layer which is approximately 10 cm thick in the region away from the divertor.

Figure 4.6 presents an intermediate case with a significant quadrupolar component and somewhat reduced ripple values, $\delta(0)^{total}$ = 0.44% and $\delta(0)^{div}$ = 0.24%.

Figure 4.7 shows the flattened case which has $\delta(0)^{total}$ = 0.41% and $\delta(0)^{div}$ = 0.21%. The extreme tilt of the coils reduces the diverted flux and the field line spread at the divertor plate region.

Figures 4.8 – 4.10 show the same three cases with $E_{LONG} = 1$, in which examples it is necessary to increase the divertor current to 1.5 MA per solenoid. If this is not done, then the private flux region within the separatrix is too small and the separatrix passes through the conductors. Even with the increased current, the values of $\delta(0)^{total}$ are reduced from the elongated cases, but of course the total diverted flux is also reduced. The decision between the cases (or an intermediate one) rests on the acceptable level of heat flux to the divertor plate and will require further analysis. In each of the three cases X_{REF} has been "tuned" to minimize $\delta(0)$; the rather curious private flux pattern of Fig. 8 could be modified by re-optimization with respect to Θ_2.

Another area in which the present examples could be improved is in optimization of the energy flux to the divertor plate by "splaying out" the outer solenoids in order to spread the field lines at the outside (large R) of the divertor. For example, if the outermost coils of the outer solenoid had progressively larger radii and corresponding minor changes to Θ_1, Θ_2 and X_{sep}, then the divertor plate power density will fall while the balancing of the multiple moments will maintain control of the ripple in the hot plasma region.

Some simple scaling of the present results of ETF/INTOR sized plasmas suggests that similar bundle divertors could be used there if the number and size of the TF coils is chosen with this in mind (not necessarily the presently envisaged conceptual design parameters). The requirements would be significantly eased if it proved possible to operate at lower q values and/or higher β than present "conservative" assumptions posit, so that B may be reduced. This would of course improve safety factors in other engineering elements of the advanced tokamak designs.

Figure 4.11 which should be compared with Figure 4.6 since the parameters are otherwise similar, shows the effect of reducing the radius of the X-point from 185 to 180 cm in order to reduce the plasma radius away from the divertor to 40 cm rather than 45 cm as in all the other examples. Unless the coil radius is also reduced, the value of $\delta(0)$ rises from 0.44% to 0.52% because the divertor must be pushed nearer the magnetic axis.

TABLE OF RUN PARAMETERS FOR ISX-C BUNDLE DIVERTOR APPENDIX

Fig	X_{DIV}	Y_{DIV}	Θ_2	Θ_2	X_{REF}	E_{LONG}	R_{SEP}	δ_o
1, 2	190.4	20	45°	55°	12.5	1	185	0.63%
3	185	21	45°	45°	12.5	1	185	-
4	185	21	0°	50°	12.5	1	185	-
5	190.9	20	45°	55°	8.0	3	185	0.51%
6	191.0	20	30°	50°	10.0	3	185	0.44%
7	190.6	22	0°	46°	12.5	3	185	0.41%
8	192.4	20	45°	45°	19.0	1	185	0.33%
9	191.3	20	30°	50°	10.0	1	185	0.32%
10	191.0	22	0°	46°	13.3	1	185	0.32%
11	185.6	20	30°	50°	10.0	3	180	0.51%

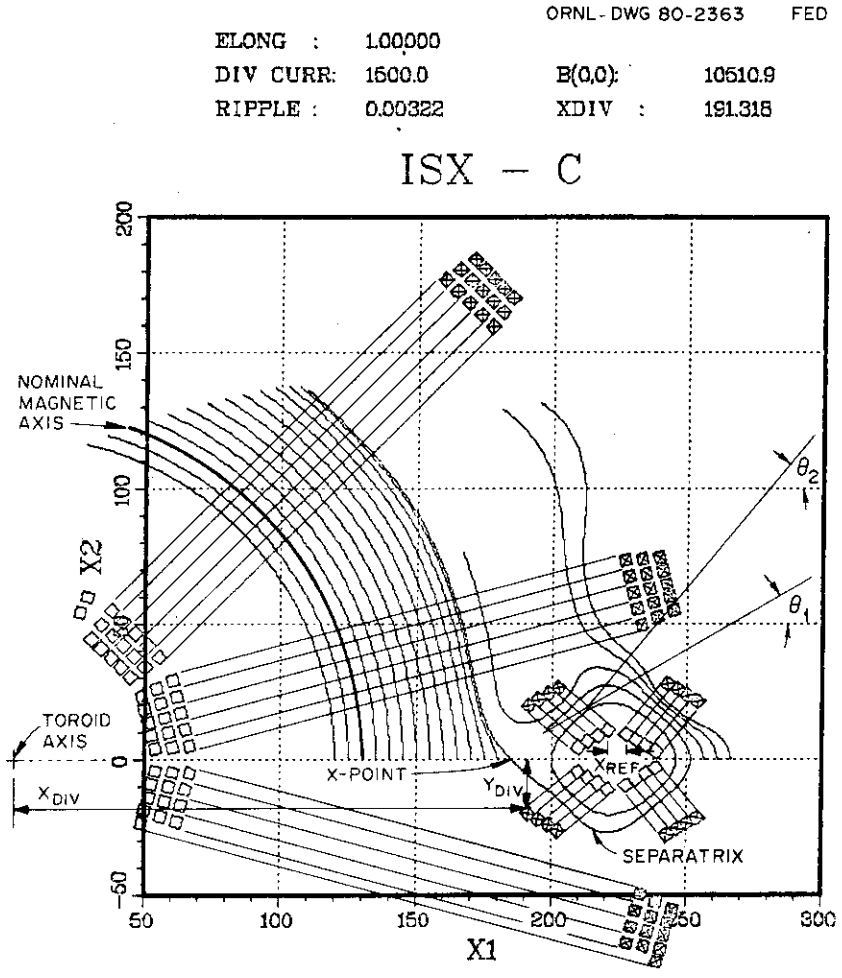
ORNL-DWG 80-2363 FED
ELONG : 1.00000
DIV CURR: 1600.0
RIPPLE : 0.00322
B(0,0): 10510.9
XDIV : 191.315
ISX – C
NOMINAL MAGNETIC AXIS
TOROID AXIS
X-POINT
SEPARATRIX
X1
X2

Fig. 4.1

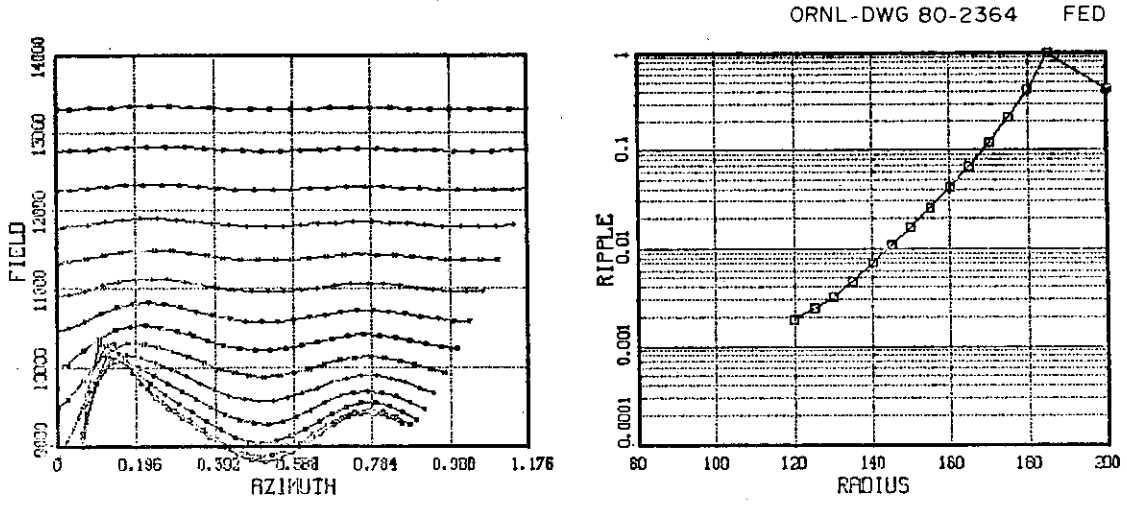
ORNL-DWG 80-2364 FED
FIELD
AZIMUTH
RIPPLE
RADIUS

Fig. 4.2

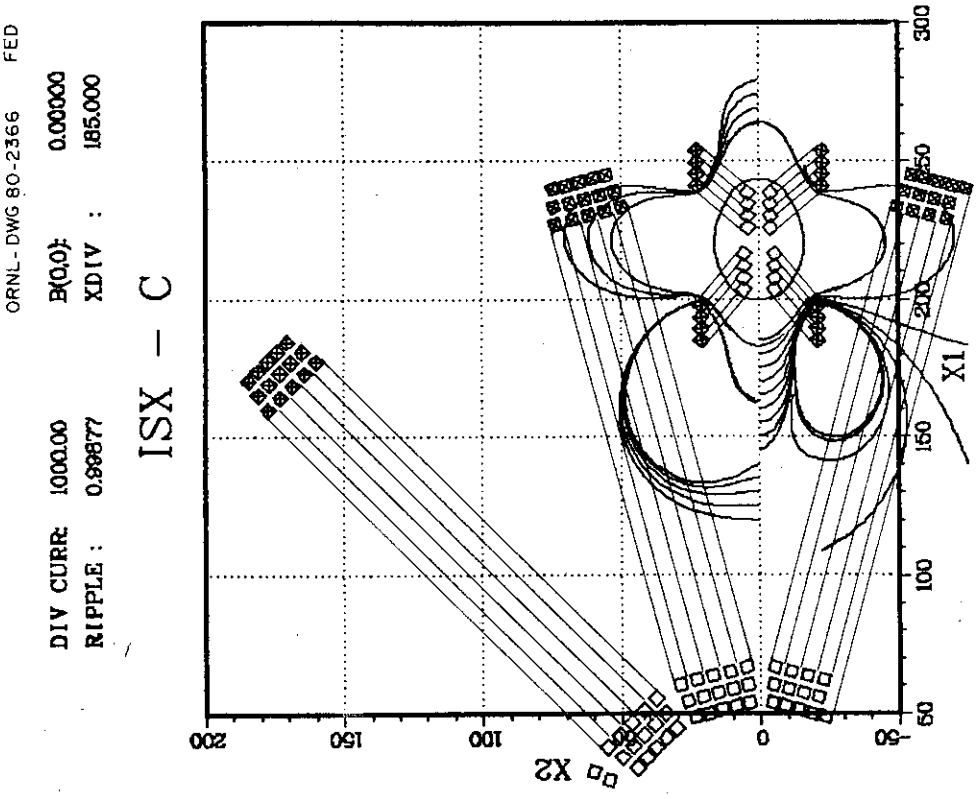
ORNL-DWG 80-2366 FED
ISX – C
DIV CURR: 1000.00 B(0,0): 0.00000
RIPPLE : 0.99877 XDIV : 185.000
X1
X2
300
250
200
150
100
50
200
150
100
0
-50

Fig. 4.4

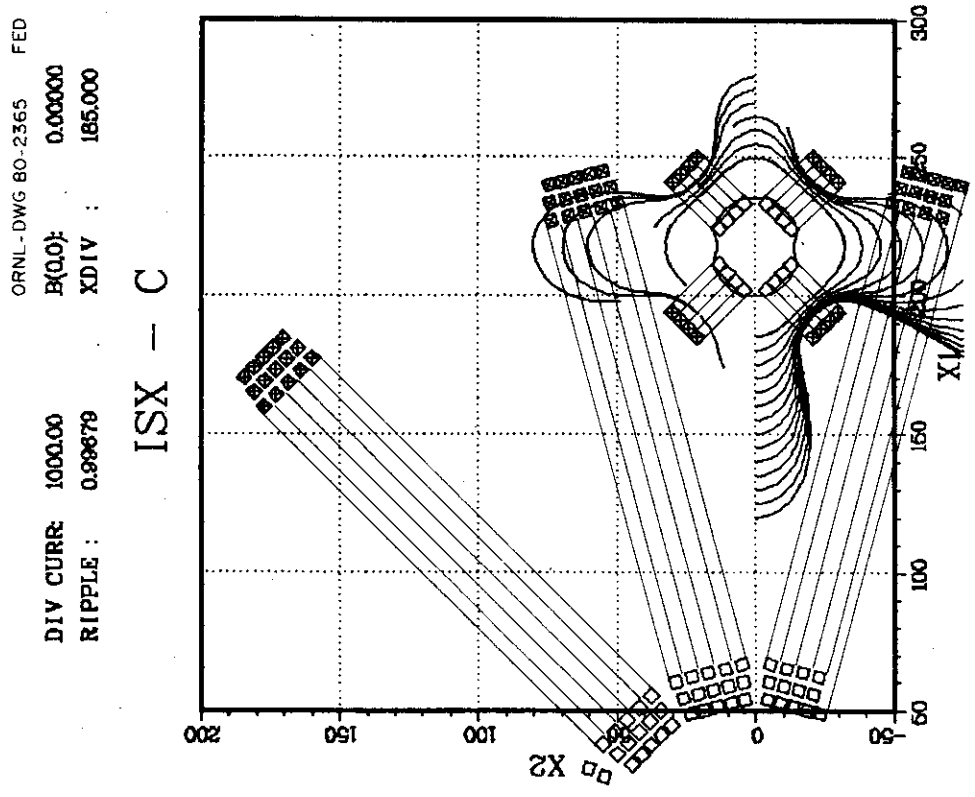
ORNL-DWG 80-2365 FED
ISX – C
DIV CURR: 1000.00 B(0,0): 0.00000
RIPPLE : 0.99879 XDIV : 185.000
X1
X2
300
250
200
150
100
50
200
150
100
0
-50

Fig. 4.3

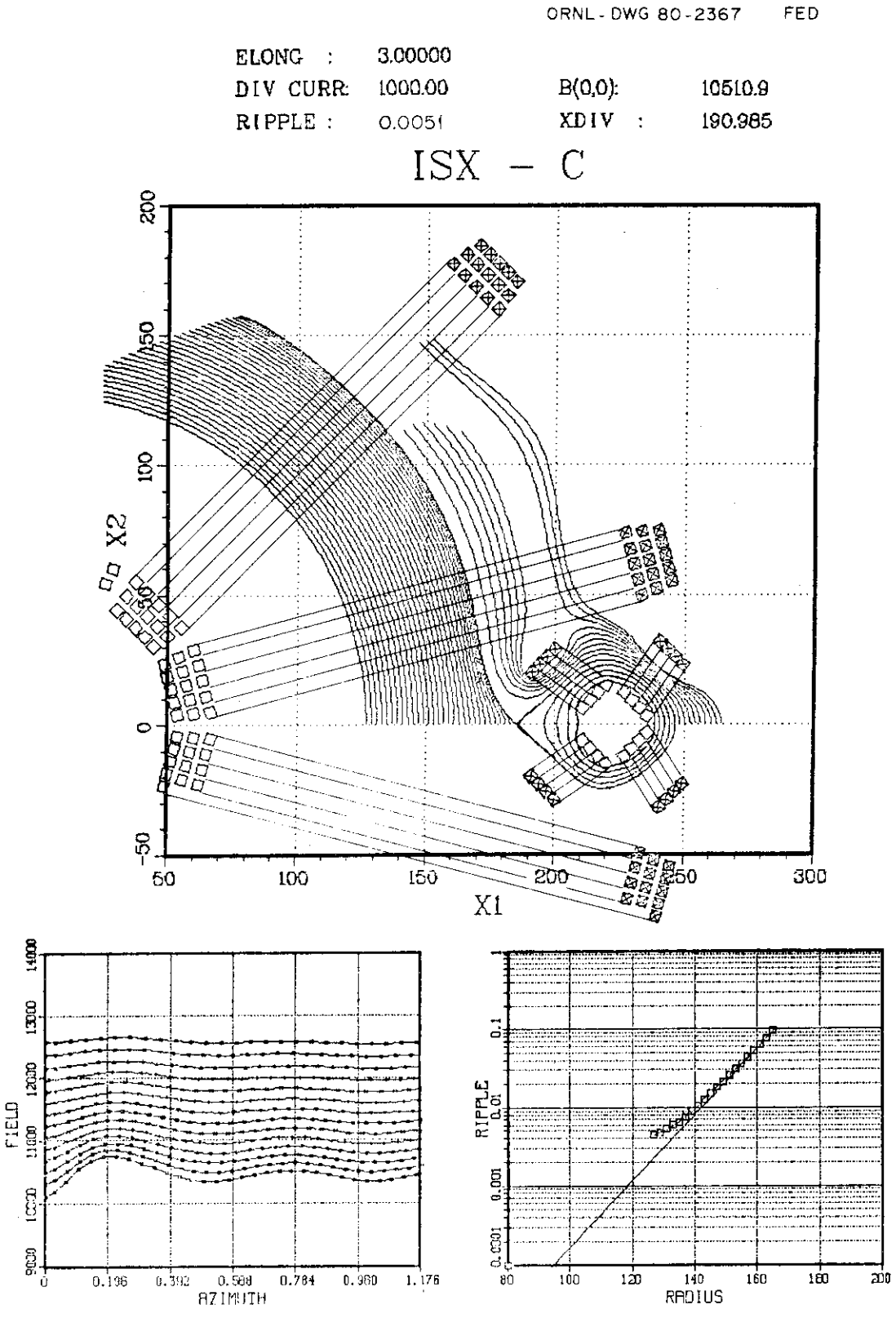
ORNL - DWG 80-2367 FED
ELONG : 3.00000
DIV CURR: 1000.00
B(0,0): 10510.9
RIPPLE : 0.0051
XDIV : 190.985
ISX - C
X2
X1
FIELD
AZIMUTH
RIPPLE
RADIUS

Fig. 4.5

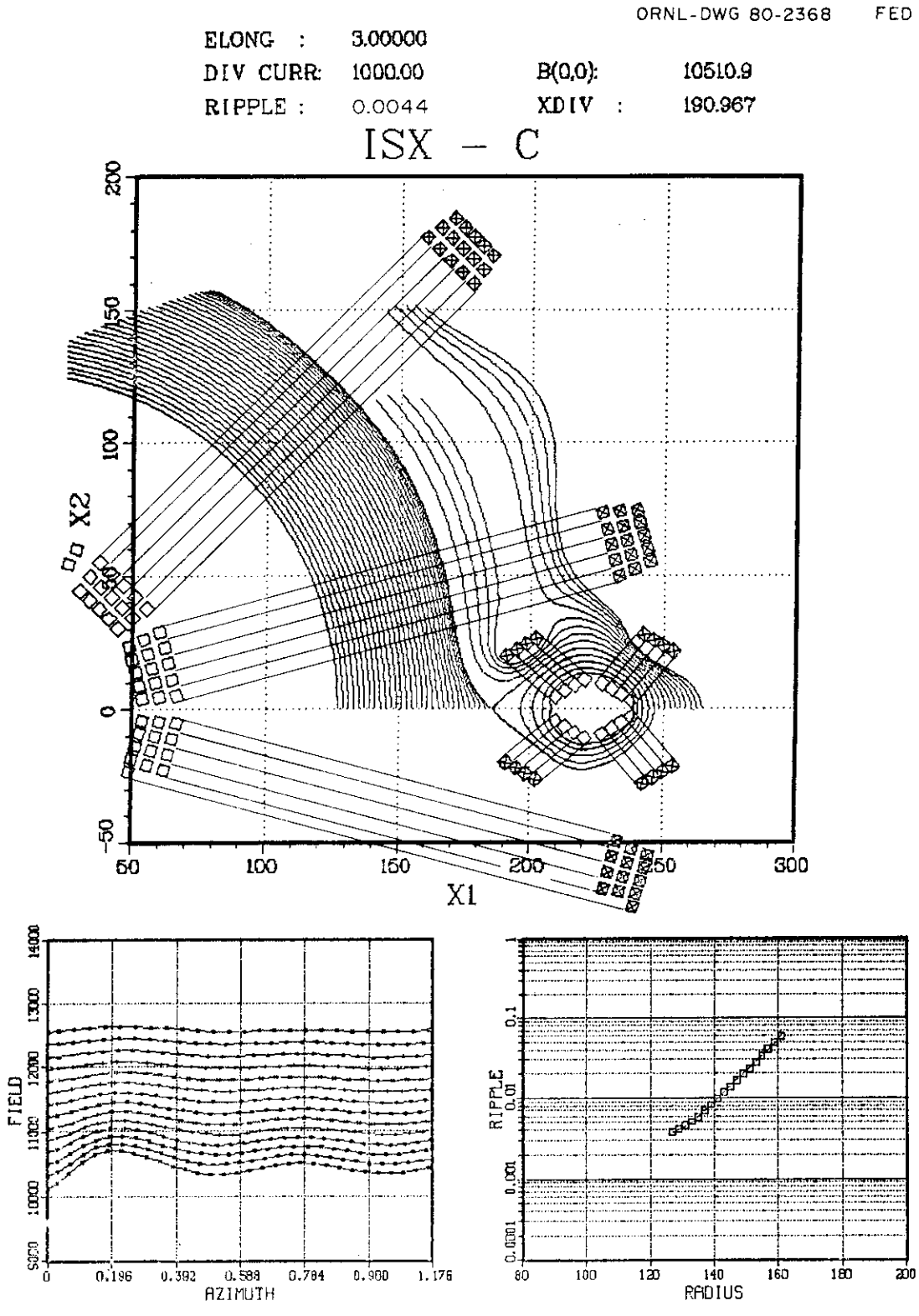
ORNL-DWG 80-2368 FED
ELONG : 3.00000
DIV CURR: 1000.00
RIPPLE : 0.0044
B(0,0): 10510.9
XDIV : 190.967
ISX - C
X2
X1
FIELD
AZIMUTH
RIPPLE
RADIUS

Fig. 4.6

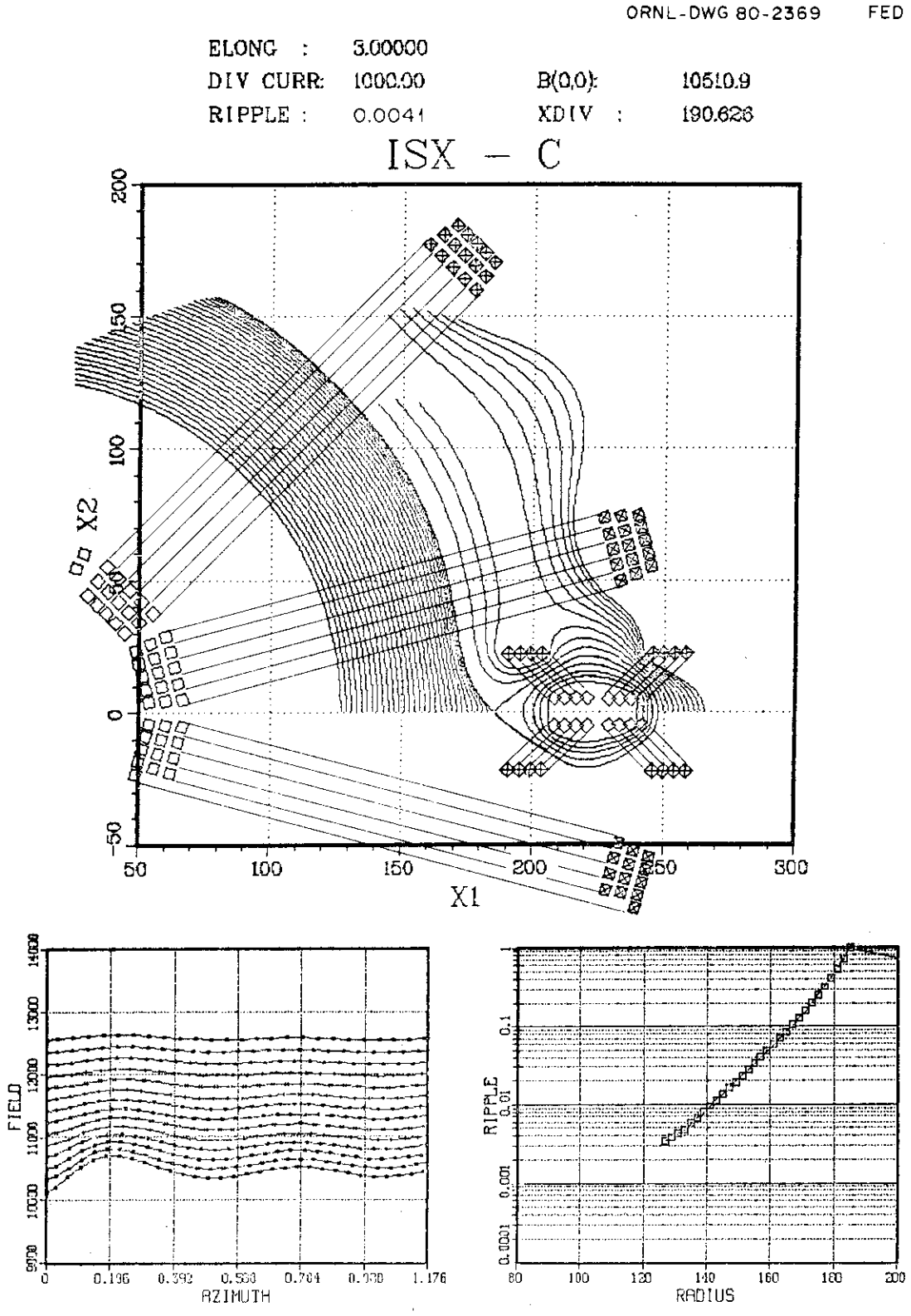
ORNL-DWG 80-2369 FED
ELONG : 5.00000
DIV CURR: 1000.00
B(0,0): 10510.9
RIPPLE : 0.0041
XDIV : 190.628
ISX - C
X2
X1
FIELD
AZIMUTH
RIPPLE
RADIUS

Fig. 4.7

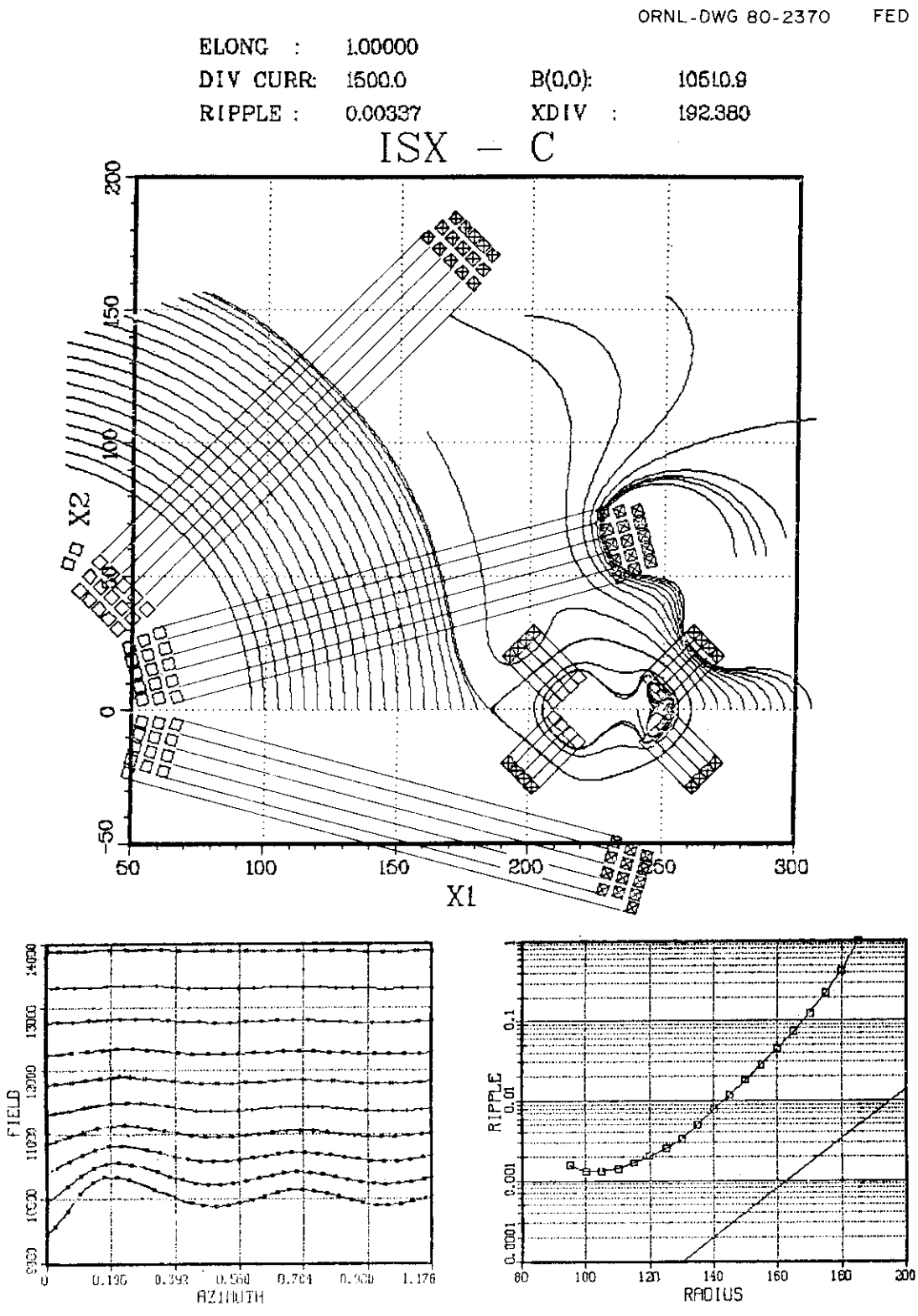
ORNL-DWG 80-2370 FED
ELONG : 1.00000
DIV CURR: 1500.0
B(0,0): 10510.9
RIPPLE : 0.00337
XDIV : 192.380
ISX - C
X2
X1
FIELD
AZIMUTH
RIPPLE
RADIUS

Fig. 4.8

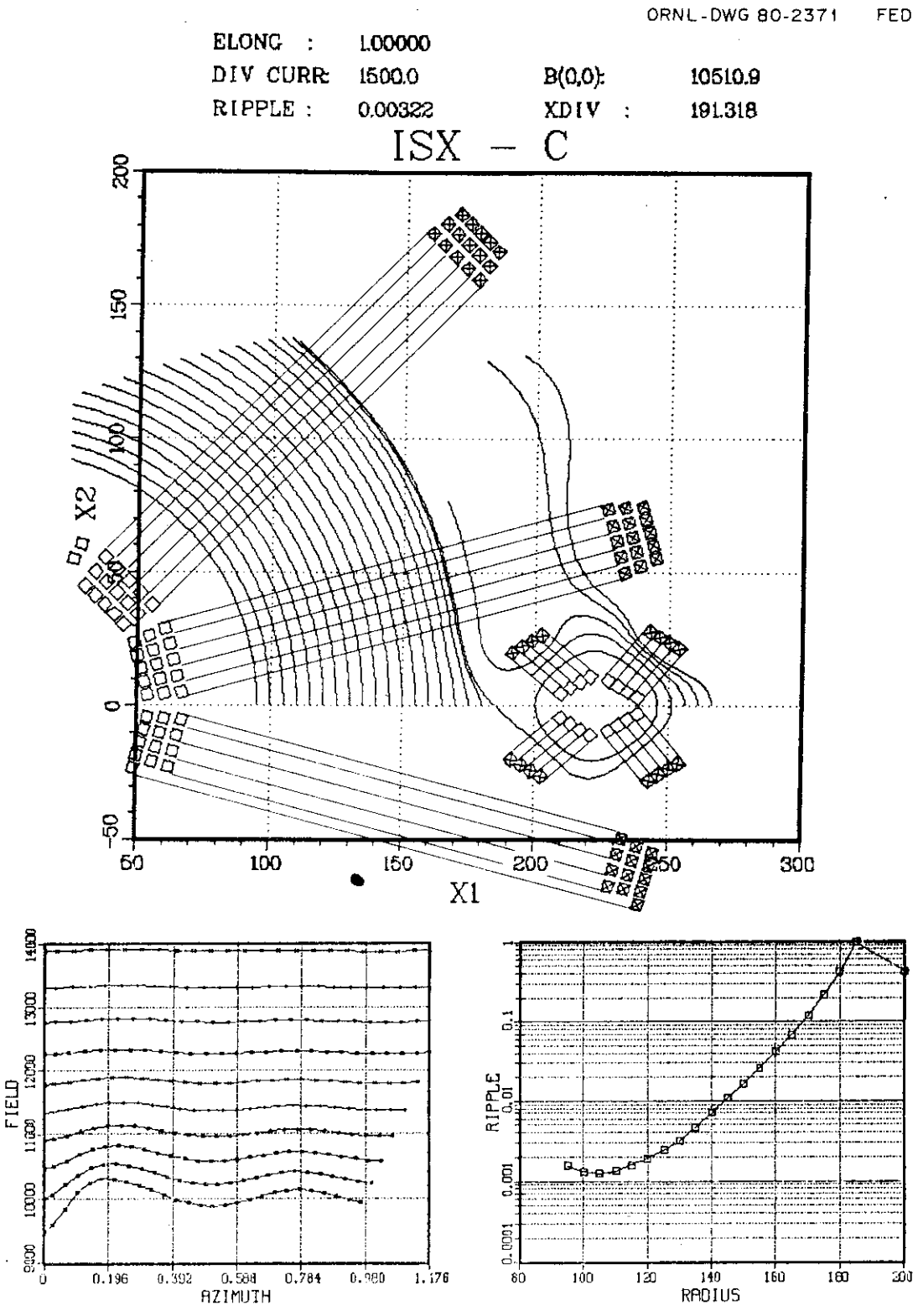
ORNL-DWG 80-2371 FED
ELONG : 1.00000
DIV CURR: 1500.0
B(0,0): 10510.9
RIPPLE : 0.00322
XDIV : 191.318
ISX - C
X2
X1
FIELD
AZIMUTH
RIPPLE
RADIUS

Fig. 4.9

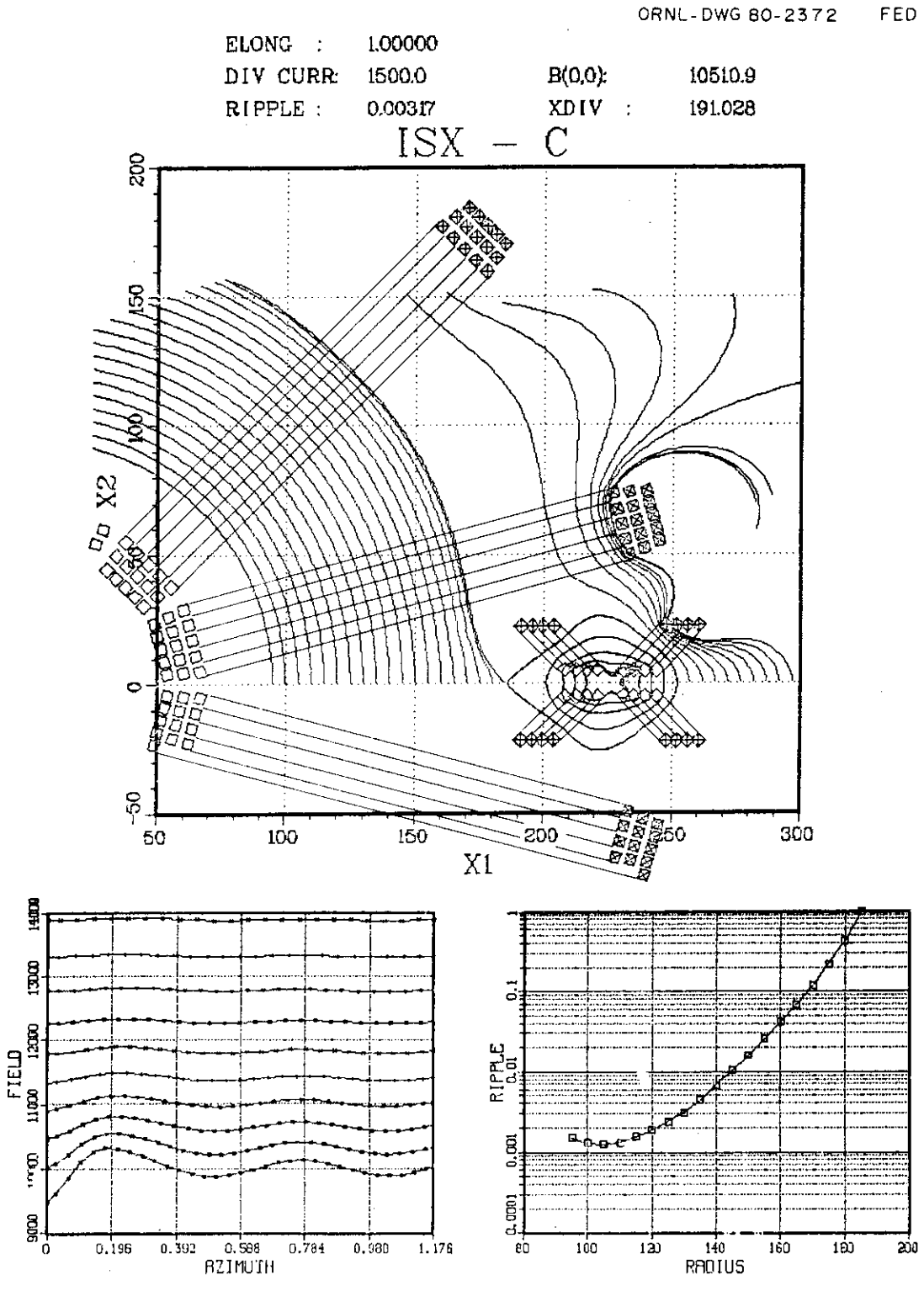
ORNL-DWG 80-2372 FED
ELONG : 1.00000
DIV CURR: 1500.0
B(0,0): 10510.9
RIPPLE : 0.00317
XDIV : 191.028
ISX - C
X2
X1
FIELD
AZIMUTH
RIPPLE
RADIUS

Fig. 4.10

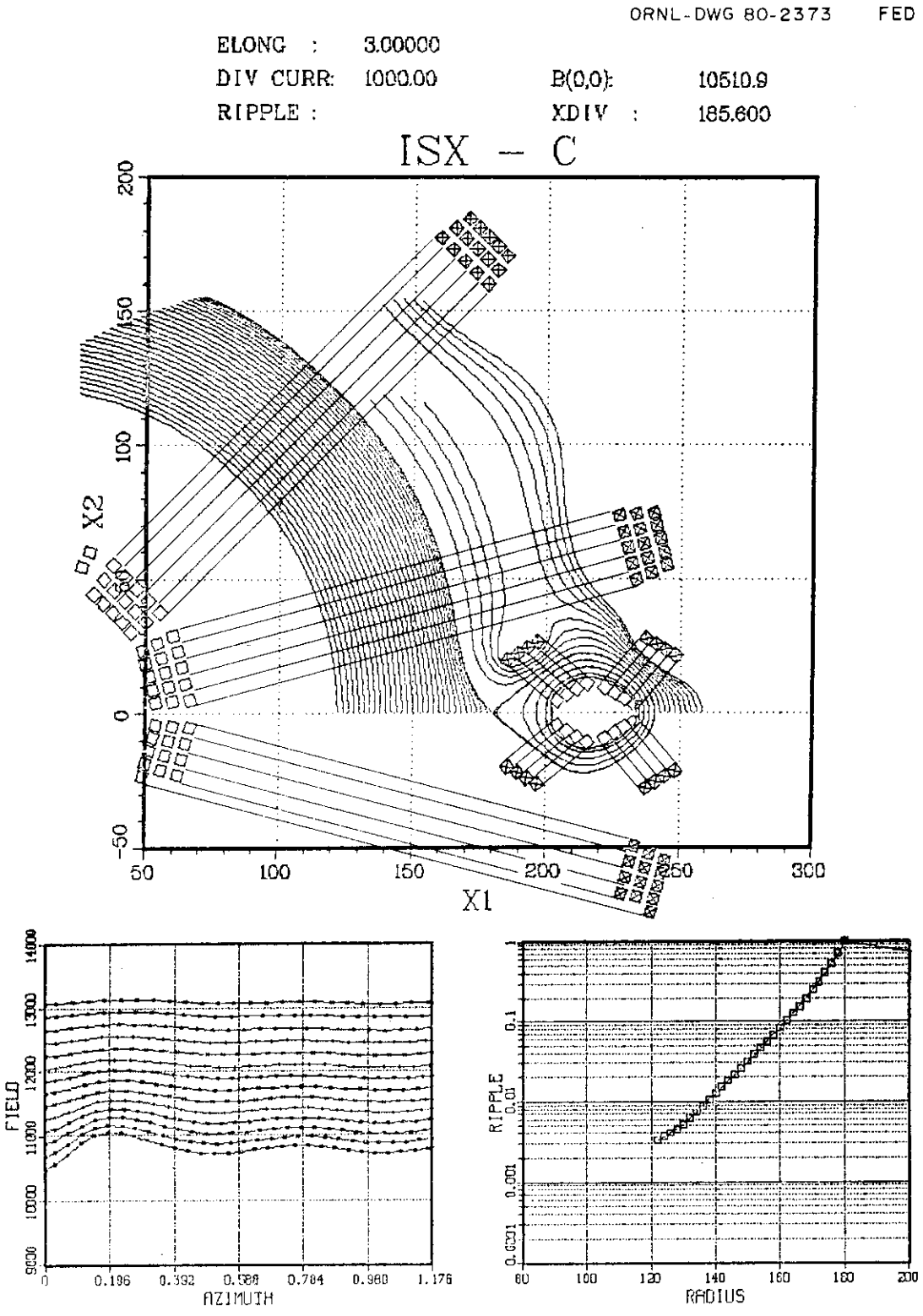
ORNL-DWG 80-2373 FED
ELONG : 3.00000
DIV CURR: 1000.00
B(0,0): 10510.9
RIPPLE :
XDIV : 185.600
ISX - C
X2
X1
FIELD
AZIMUTH
RIPPLE
RADIUS

Fig. 4.11

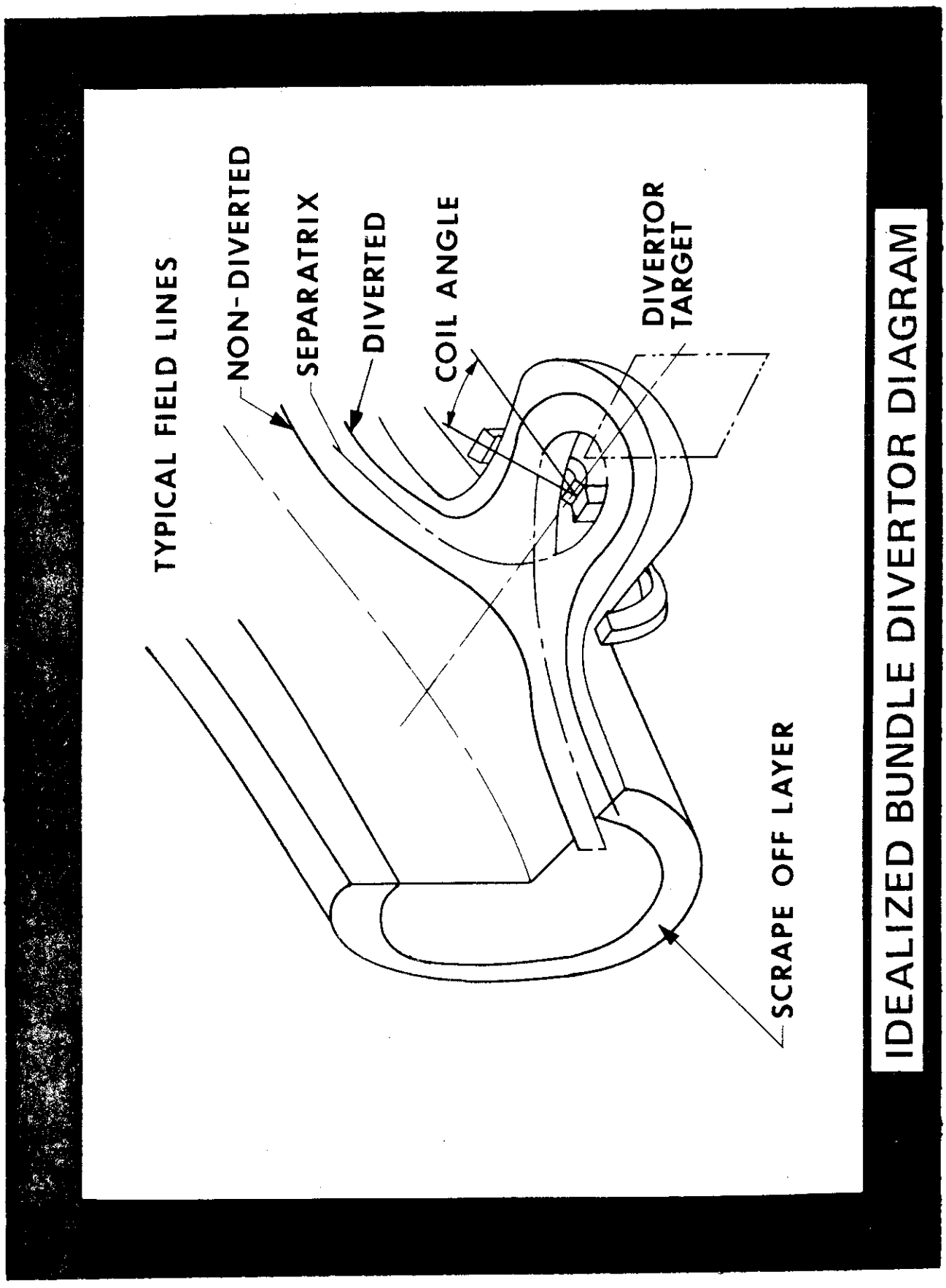
IDEALIZED BUNDLE DIVERTOR DIAGRAM
TYPICAL FIELD LINES
NON-DIVERTED
SEPARATRIX
DIVERTED
COIL ANGLE
DIVERTOR TARGET
SCRAPE OFF LAYER

ISX-B

GUIDING CENTER ORBIT

E_0 = 40.0 keV
M = 1.0
I_{RC} = 61. kA
β = 0.002
B_0 = 1.15 T

I_p = 115. kA
q_s = 5.4
β_p = 0.504
ϵ = 1.00
ψ_M = 0.84

R = 1.17 m
ϕ = -45.00
z = 0.00 m

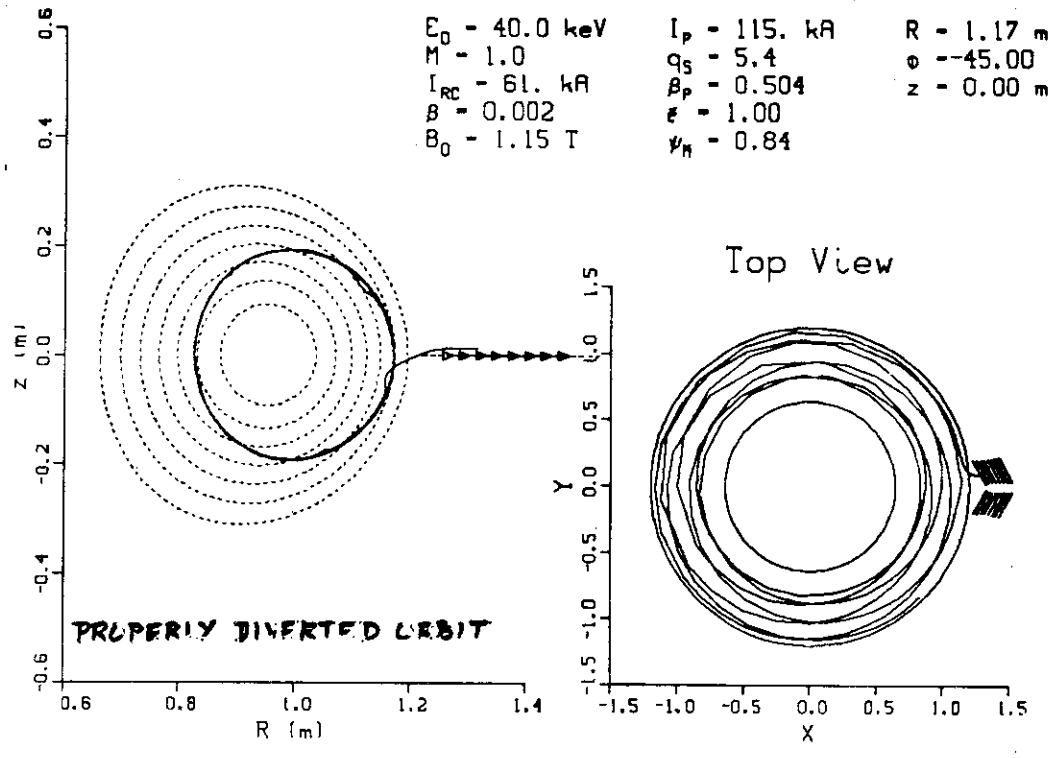

ISX-B

GUIDING CENTER ORBIT

E_0 = 40.0 keV
M = 1.0
I_{RC} = 61. kA
β = 0.002
B_0 = 1.15 T

I_p = 115. kA
q_s = 5.4
β_p = 0.504
ϵ = 0.50
ψ_M = 0.84

R = 1.17 m
ϕ = -45.00
z = 0.00 m

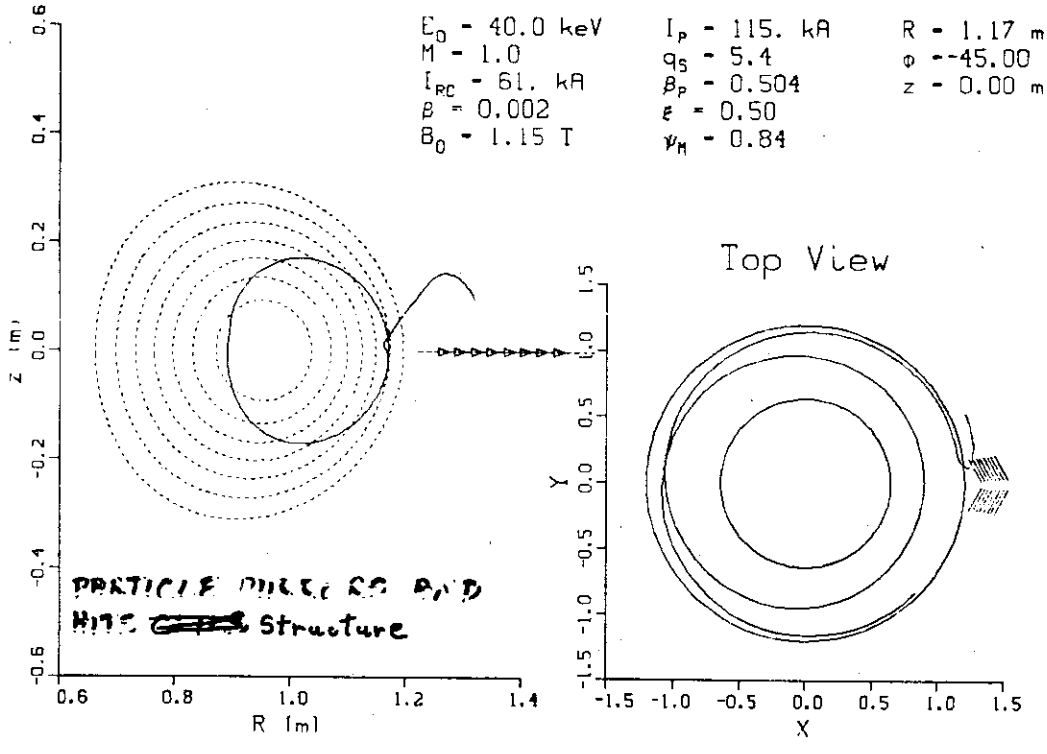

ISX-B

GUIDING CENTER ORBIT

E_0 - 40.0 keV
M - 1.0
I_{RC} - 61. kA
β - 0.002
B_0 - 1.15 T

I_p - 115. kA
q_s - 5.4
β_p - 0.504
ε - 0.80
ψ_M - 0.84

R - 1.17 m
ϕ --45.00
z - 0.00 m

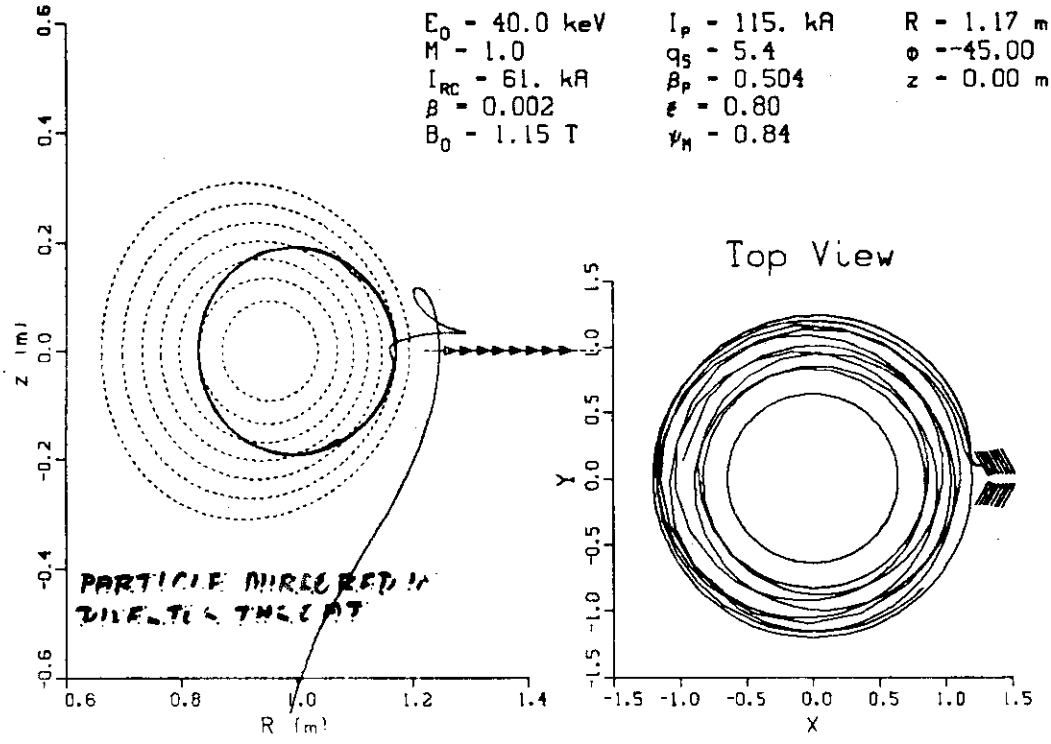

ISX-B

GUIDING CENTER ORBIT

E_0 - 40.0 keV
M - 1.0
I_{RC} - 61. kA
β - 0.002
B_0 - 1.15 T

I_p - 115. kA
q_s - 5.4
β_p - 0.504
ε - 0.30
ψ_M - 0.49

R - 1.11 m
ϕ --45.00
z - 0.00 m

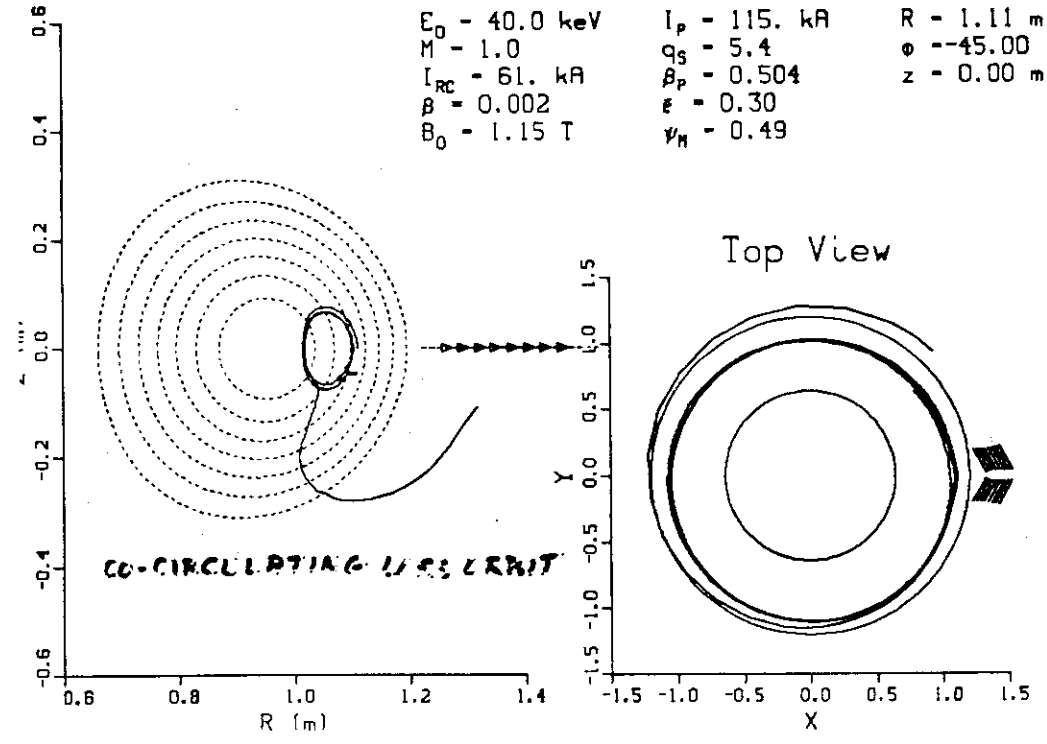

INTOR

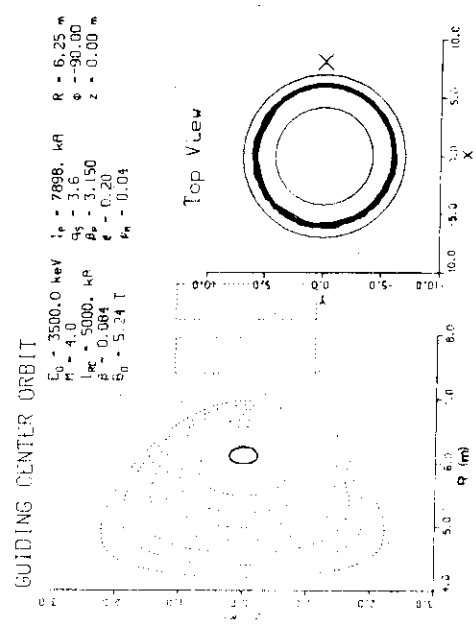
GUIDING CENTER ORBIT
Top View
X
Y
R (m)

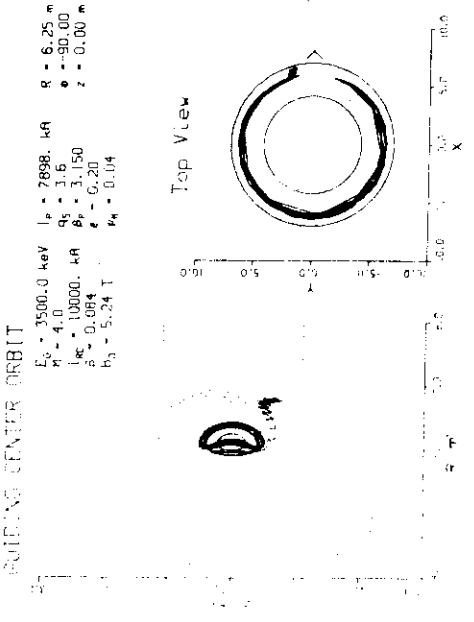
Top View
X
Y

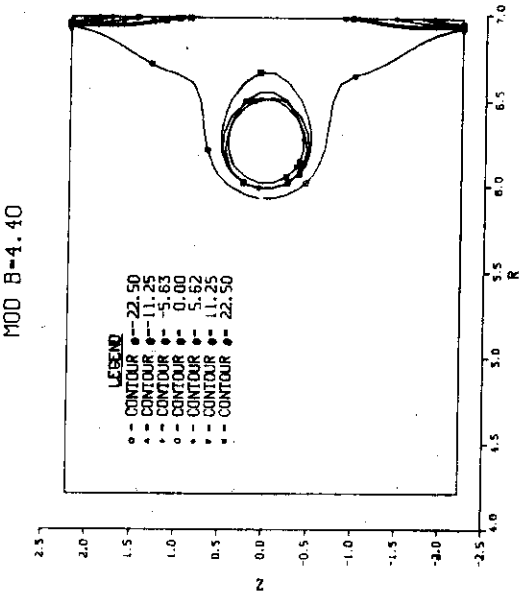
MOD B=4.40
LEGEND
CONTOUR -22.50
CONTOUR -11.25
CONTOUR -5.63
CONTOUR 0.00
CONTOUR 5.62
CONTOUR 11.25
CONTOUR 22.50
Z
R

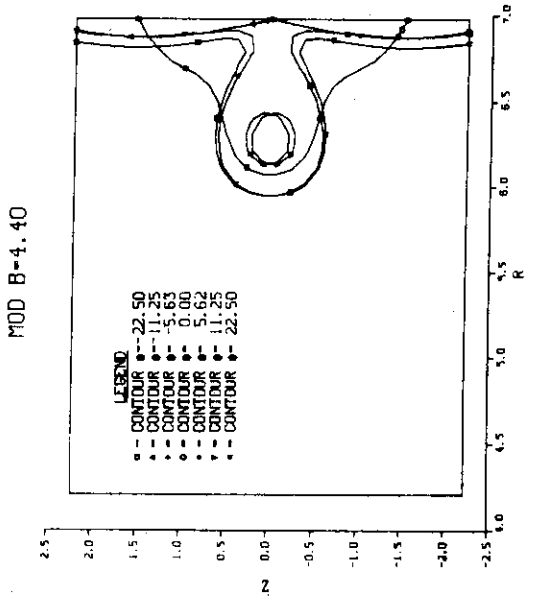
MOD B=4.40
LEGEND
CONTOUR -22.50
CONTOUR -11.25
CONTOUR -5.63
CONTOUR 0.00
CONTOUR 5.62
CONTOUR 11.25
CONTOUR 22.50
Z
R

THE EFFECTS OF LOCAL RIPPLE FROM BUNDLE DIVERTORS

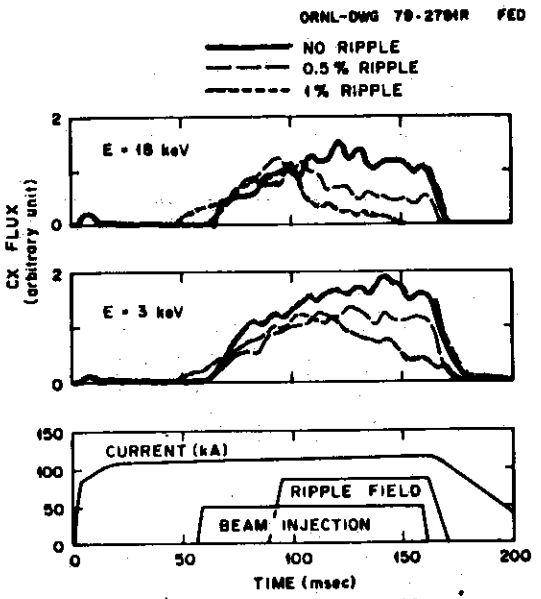

⊥ cx flux decreases with increasing ripple. This is not inconsistent with the presence of a loss region.

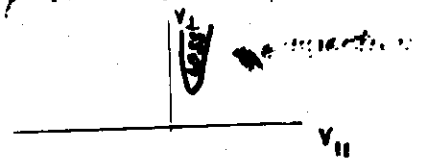

OUR STUDIES SHOW THAT

- IONS TRAPPED IN THE RIPPLE (MINIMUM) ARE ALWAYS LOST - HOWEVER, THIS IS A SMALL FRACTION OF THE IONS
- CIRULATING IONS ARE RELATIVELY UNAFFECTED
- BANANA ORBITS AFFECTED NEAR THEIR TIPS, FAST IONS BOUNCE OFF MAXIMA IN FIELD AND RAPIDLY WALK OUT - LARGEST ION LOST EFFECT.
- SINGLE DIVERTOR MAY DESTROY FLUX SURFACES
- MULTIPLE DIVERTORS HEAL FLUX SURFACES BUT FAST IONS ARE LOST FASTER IF MAXIMUM IN |B| OCCURS.
- HIGH BETA INCREASES THE EFFECT OF LOCAL RIPPLE.
- FULL 3-D NATURE OF RIPPLE CRUCIAL.
- BANANA TRAPPED IONS ARE LOST IF |B| SURFACES ARE BLOCKED TOROIDALLY, PERCENT OF CROSS-SECTIONAL AREA NOT AFFECTED IS NEW DESIGN FIGURE OF MERIT.

5 - 1

Divertor Concept for INTOR-J and its Engineering Feasibility

Y. Shimomura and K. Sako
Japan Atomic Energy Research Institute, Tokai, Naka, Ibaraki, Japan

The next fusion device has been studied related to IAEA INTOR Workshop.[1] The guiding parameters are very similar to those of INTOR and its temporal name is INTOR-J. The expected thermal output is 500 M watts and the burning time is 200 sec as shown in Table 1. Therefore it is very important to control ash and impurities.

Non divertor concept is the most attractive reactor because of its simplicity. In the non divertor concept, the edge plasma temperature has to be kept very low, e.g. 50 eV in order to employ a mechanical ash-exhaust system. By this time, however, we did not demonstrate a reliable edge cooling method without adverse effects on plasma confinement characteristics. These studies will be done in a large device. If the edge temperature is very low only with poor confinement, a magnetic divertor has to be employed in INTOR-J.

Various kinds of divertor configurations have been proposed. The effectiveness of the poloidal divertor was demonstrated in DIVA/JFT-2a,[2] D-III with Dee operations[3] by JAERI Team and so on. Therefore the polidal divertor is the most promissing method for impurity control. The classical poloidal divertor whose coils are installed inside the vacuum chamber seems unrealistic for its serious technological difficulties and we need to make it simple (Fig.1).

Divertor coils can be located outside the toroidal coils, since we employ D-shape and the additional current of the poloidal coils for the divertor is small.[4] In this case, the length of the divertor throat becomes short and the width becomes wide. The problem is whether the short and wide throat can control impurities and ash or not. All the above experiments were done with a wide and short throat and some results are shown in Fig.2. In the all experiments, the divertor controlled impurities and the following conclusions were obtained. Sputtered impurities from the neutralizer plate flow hardly into the main chamber and some of them directly thrust out the scrape-off layer and stick to the wall surface of the divertor region. Therefore an artificial pumping system is necessary only for the ash exhaust. Concerning the ash-exhaust, behavior of the ash particles is numerically simulated by a Monte-Carlo method.[5] This model explained well impurity behavior in DIVA as shown in Session IV - (4-2) and the detailed discussion is shown in Session VI- (6-2). A typical result is shown in Fig.3. Almost all the reflected helium atoms are ionized and flow back to the neutralizer plate, or

freely into the pumping region. Therfore the ash particles flow hardly into the main chamber. The fuel particles, however, can easily flow back into the main chamber. In other words, the scrape-off layer plasma reduces the throat conductance for ash backflow by a large factor, e.g. 10. From these results, we can conclude that the simple poloidal divertor controls impurities and ash by enriching and pumping them.

The other problems are wall erosion and high heat load of the neutralizer plate. Heat load to the neutralizer plate can be reduced down to 150 W/cm^2 by adding following methods. A small non-axisymmetric magnetic field from artificial coils and/or plasma perturbations forms the ergotic region near the old separatrix and consequently spread the scrape-off layer. The mirror effect may increase the width. The expected width is about 10 cm or 20 cm. It seems necessary to swing the flux line by 10 cm as employed in JT-60 to unify peaked heat fluxes in this layer. And the neutralizer plate can be put almost parallel to the scrape-off layer. Consequently the neutralizer plate can be designed. The wall erosion rate is around 100 kg/year. If we can control the edge plasma, these problems become more easy.

An engineerig design of the device including the poloidal divertor was also done and demonstrated its feasibility.[6] The cross-sectional view of INTOR-J is shown in Fig.4.

When we discuss the engineering feasibility of divertor, not only divertor design itself but also its maintenance method must be considered. A design study on poloidal divertor and its maintenance method has been conducted by Hitachi Ltd. under contract with JAERI. Base on the result of the study, the engineering feasibility of the divertor is briefly discussed.

(1) Divertor plate design

Total of 50 MW of plasma energy was assumed to be deposited on the divertor plate in our design. A concept of divertor plate assembly is shown in Fig. 5. The plate consists of copper (Cu) tube assembly as shown in Fig. 6. Tapered tube is selected to allow a small deformation of tubes. Temperature distribution in a typical tube is shown in Fig. 7. The tube is cooled by 5 kg/cm^2, 100°C water. Heat fluxes on the tube surface are 140 W/cm^2 for the flat part and 400 W/cm^2 for the tapered part. Heat flux of cooling surface is 450 W/cm^2 which is near the burnout heat flux of water.

Thermal stress induced in the tube cross section is estimated to be 4 kg/mm^2 and in a total tube system 5 $\sim$6 kg/mm^2. We analyzed a case of swinging the separatorix 10 cm by 1 Hz. Because of the time constant of cooling tube is small, cyclic temperature change of the tube seems to be very severe. Further investigations are required.

Design problems of the divertor plate are as follows;

1) Temperature changes due to reactor start up and shut down are very large. Thermal cycle fatigue seems to be very severe.

2) High thermal conductivity material should be used for cooling tube because of very high heat flux. We tentatively selected copper. There are no useful data on the neutron irradiated material properties.

3) Errosion by ion sputtering for Cu is estimated to be very high. Once some errosion result in irregular shape, heat flux concentration and hence high local thermal stress in the cooling tube and break down of the tube are expected.

4) A method to overcome this problem may be to braze M-alloy (eg. TZM) pieces on the Cu cooling tube. This idea should be experimentally tested.

5) Electro-magnetic force induced in divertor plate in case of plasma disruption is a very severe problem. Careful considerations are necessary for the material selection of the tube assembly and support structure.

6) Protection from very high heat flux in case of the disruption should be provided.

(2) Repair and maintenance of divertor

Divertor plate replacement should be performed without disassembly of the reactor. Accurate reinstallation of the divertor plate by fully remote operation is a difficult problem. This is entirely new technology, so extensive R & D is required. Our design study is faily detailed including a survey of the procedure by using a 1/20 scale model. The study includes the design of repairing machines and failure detecting technics. By a preliminary estimate, total required time is 10∿20 days to replace the failed divertor plate after inspecting all of the plates.

Reference

1) IAEA INTOR Workshop Report, JAERI-M 8621,8710,8622,8623,8624,8625,8711,8510, 8511,8512,8513,8514,8503,8518 (1970)

2) S. Yamamoto, Session IV - (4-1).

3) S. Seki, private comunication.

4) Y. Shimomura, K. Sako and K. Sinya, JAERI-M 8294 (1979).

5) Y. Seki, et al., to be submitted to Nuclear Fusion, Session VI- (6-2).

6) K. Sako et al., JAERI-M 8518 (1979).

7) M. Koizumi et al., Annual Meeting, Japan Atomic Energy Soc., D33, Mar. 1980.

Table I Parameters of INTOR-J

Major radius	R	5	m
Minor radius	a/b	1.2/1.8	m
Plasma volume	V	200	m^3
Plasma surface area	S	300	m^2
Toroidal field	B_t	5	T
Plasma current	I_p	4.75	MA
Thermal out put	P_{th}	450	MW
α-particle out put	P_α	90	MW
Mean temperature	$\bar{T}$	10	keV
Mean fuel density	$\bar{n}_f$	1.2×10^{20}	m^{-3}
Mean ash density	$\bar{n}_\alpha$	1.2×10^{19}	m^{-3}
Energy confinement time	τ_E	1.5	s
Average particle confinement time	$\bar{\tau}_p$	0.5	s
Total particle loss flux	F_p	5.4×10^{22}	s^{-1}
Ash flux to pump	$F_{\alpha o}$	1.6×10^{20}	s^{-1}
Burning duration	τ_B	200	s

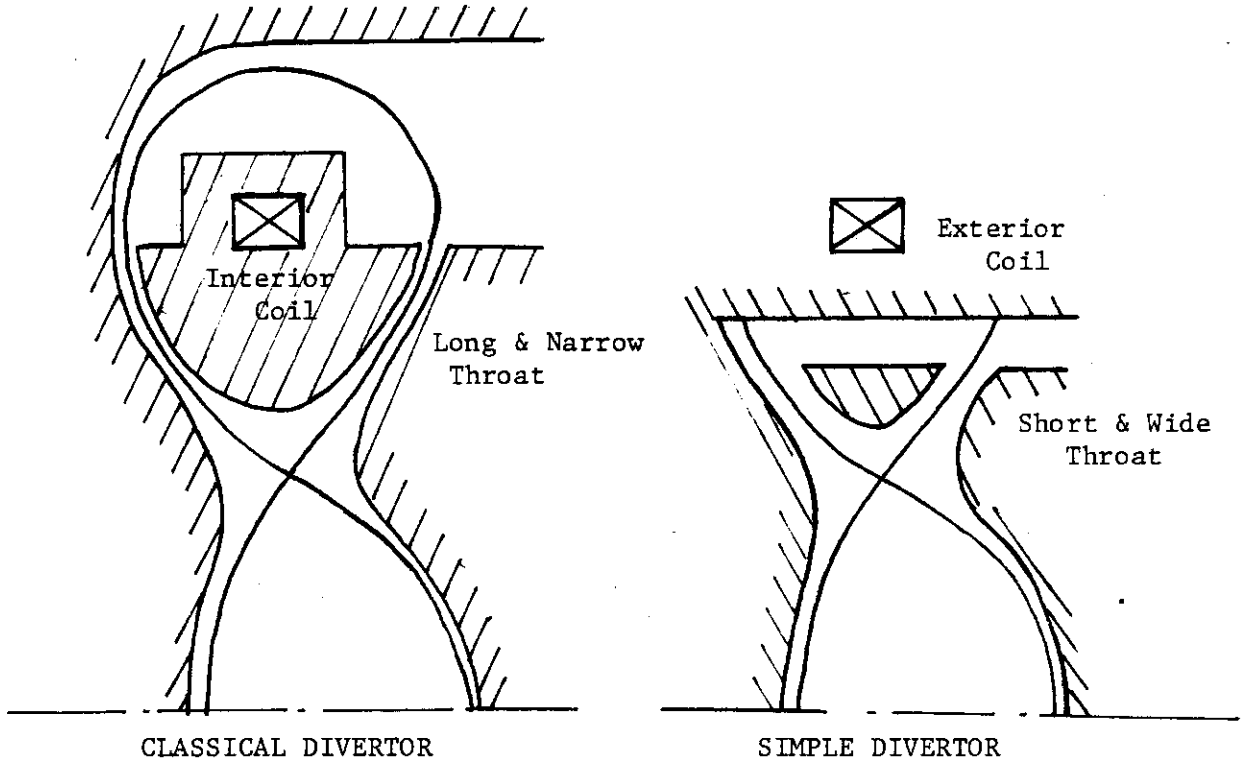

Fig.1 Classical and simple poloidal divertor.

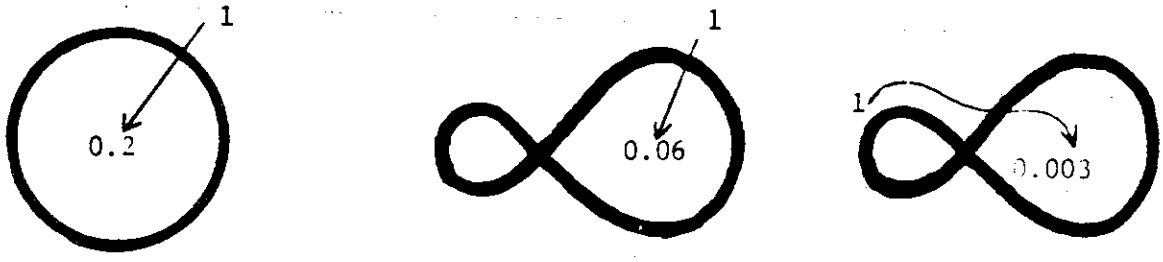

(a) DIVA/JFT-2a (a_p = 0.1 m, 0.05 s.). Impurity flow into the main plasma from various impurity source positions.

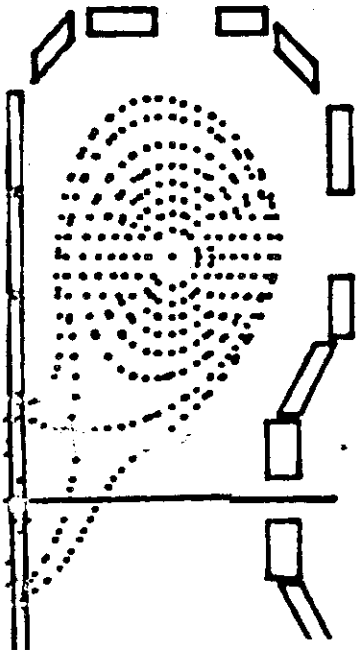

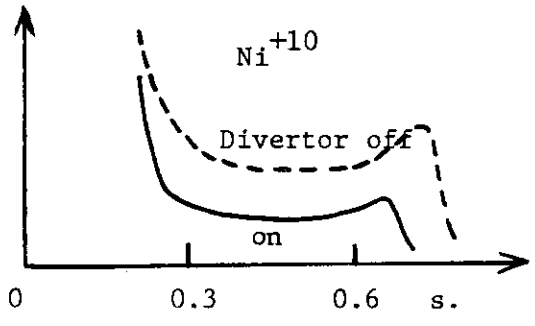

(b) D-III (a_p=0.5 m, 0.5 s.). Dee operation with a magnetic limiter operated by JAERI Team.

(c) JT-60 (a_p= 1 m, 10 s.)

Fig.2 Poloidal divertor experiment with a short and wide divertor throat.

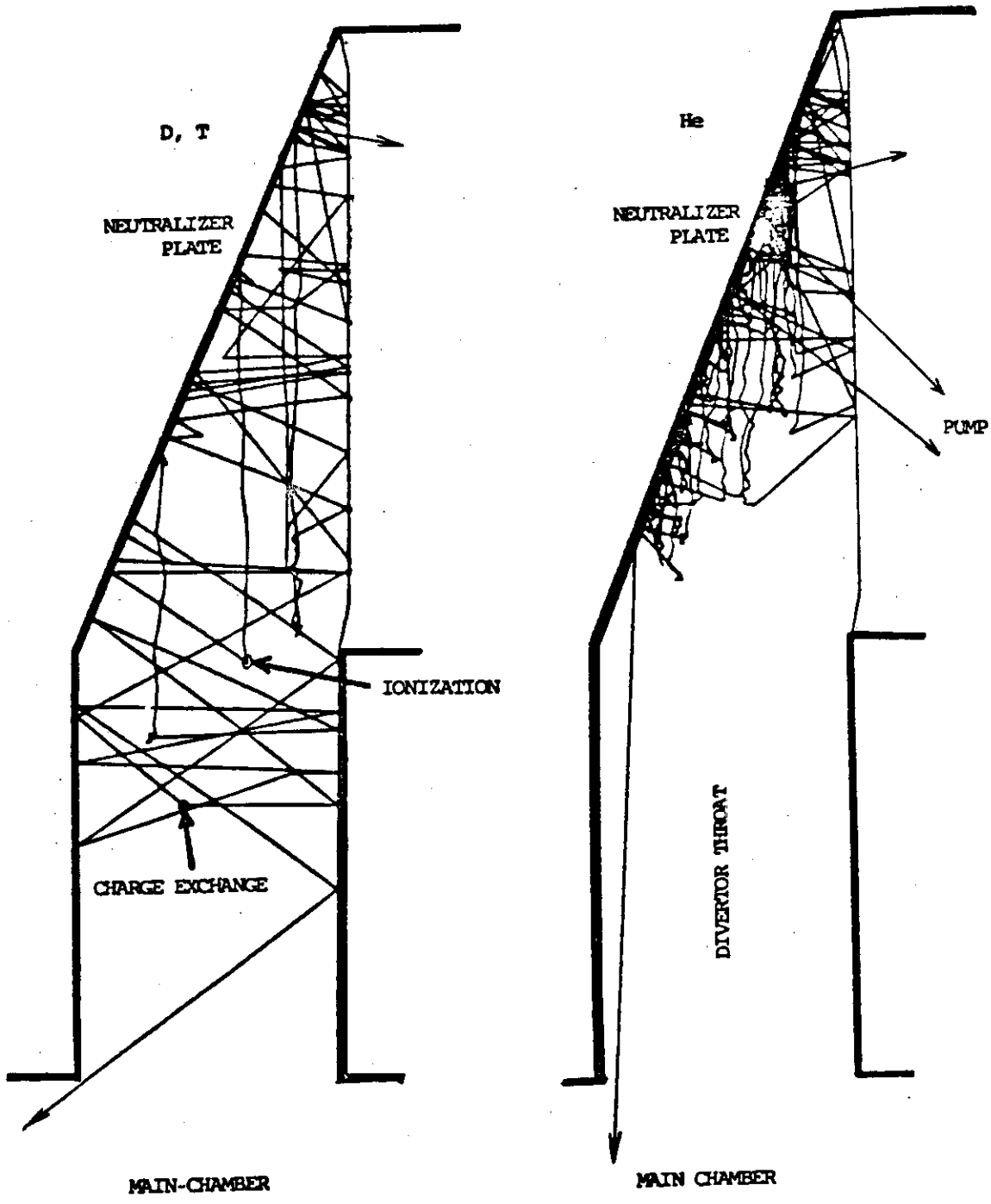

Fig.3 Behavior of fuel and ash particles in the divertor region.

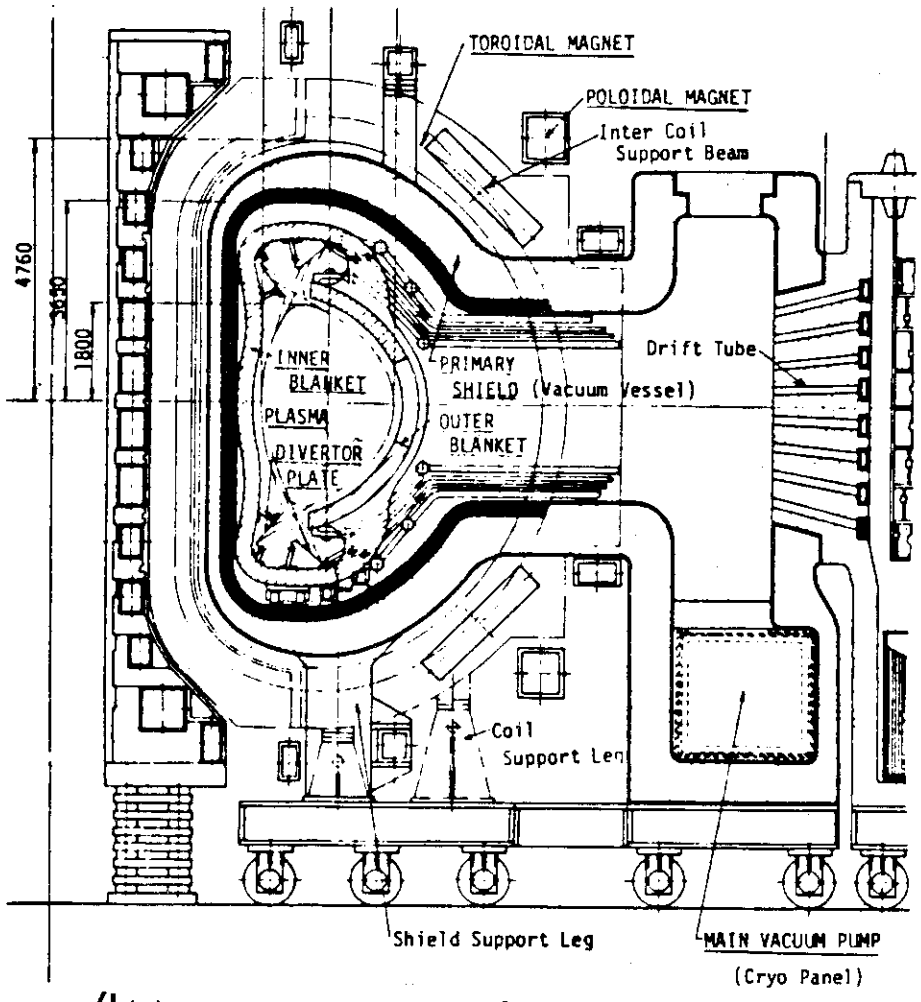

Fig. 4(a) A design example of a poloidal divertor with exterior coils.

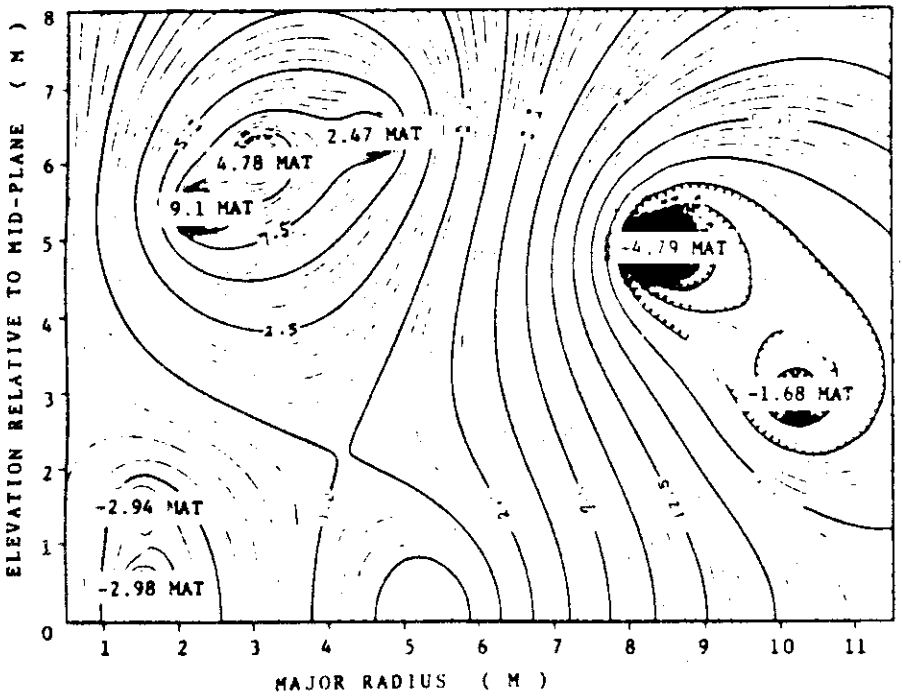

Fig. 4(b) A computed result of free boundary equilibrium of a poloidal divertor.

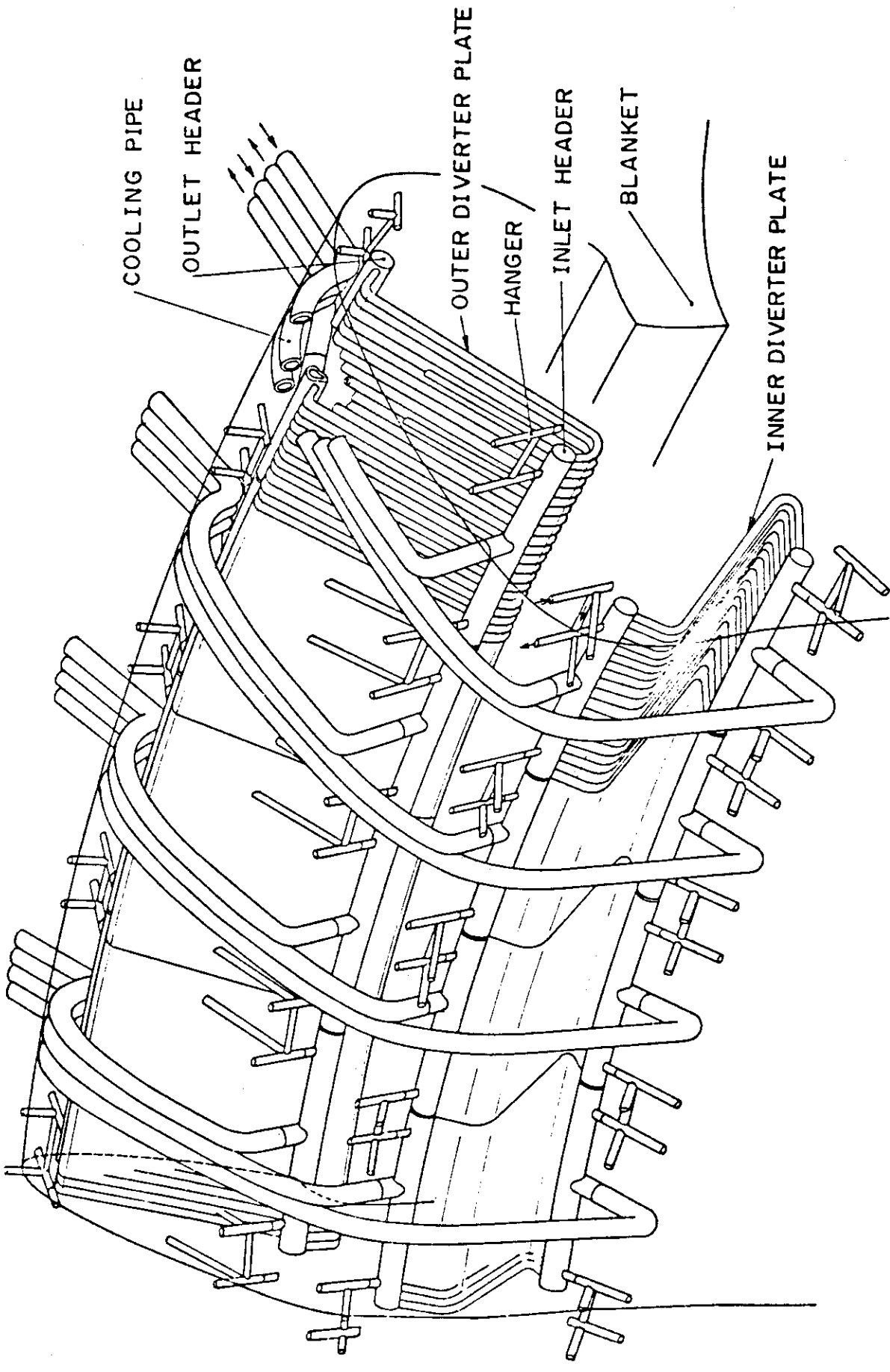

Fig.5 Divertor plate assembly

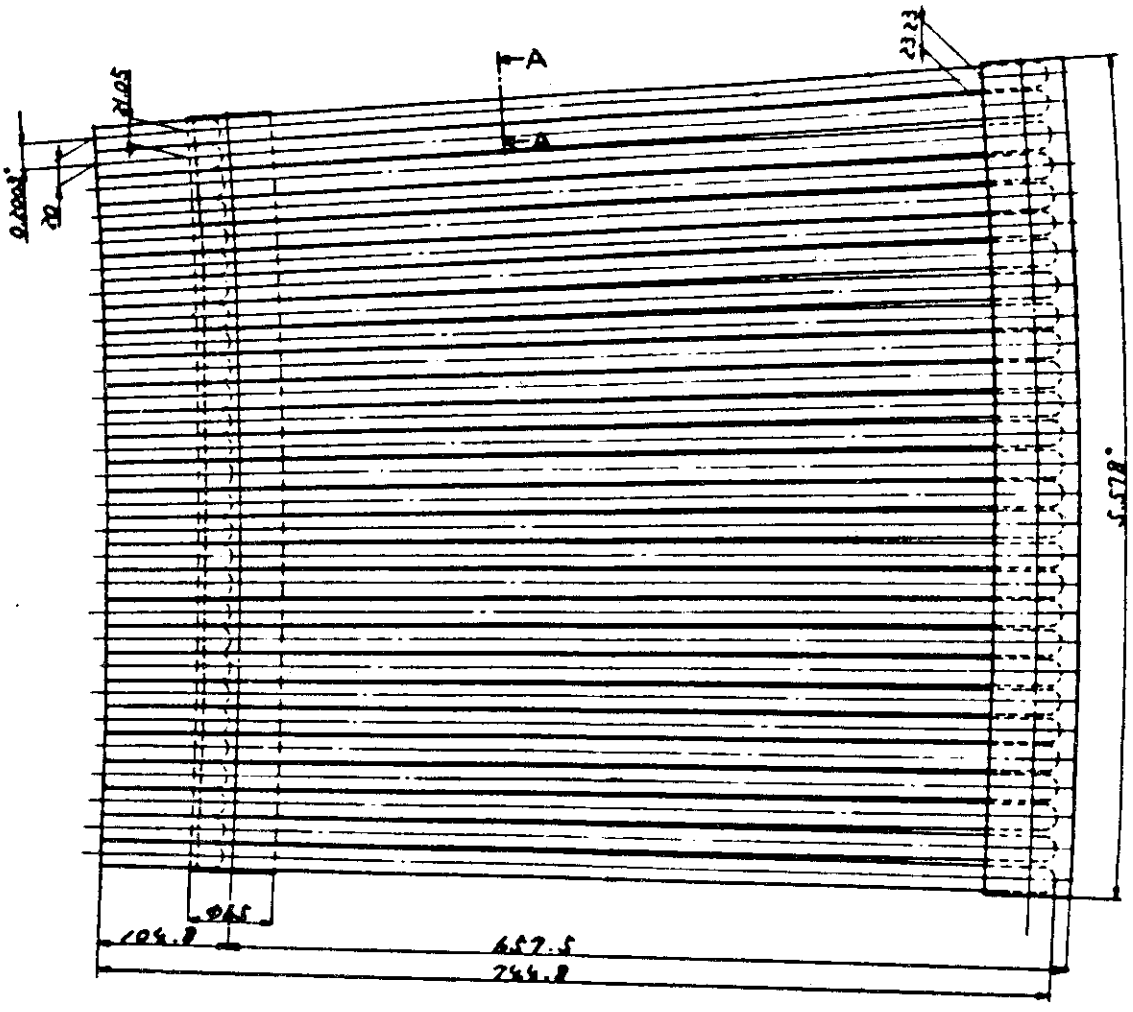

Fig.6(a) Divertor plate

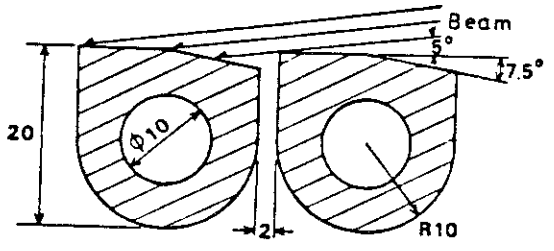

Fig.6(b) Cross section of cooling tube

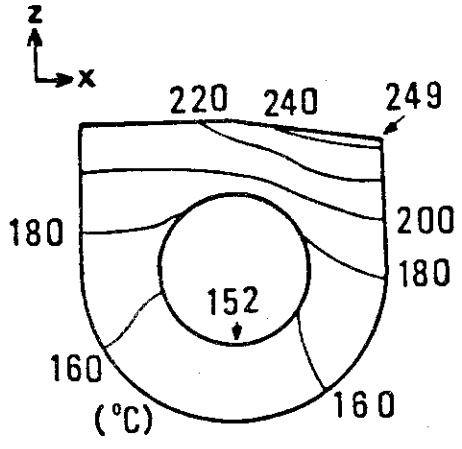

Fig.7 Temperature distribution in cooling tube[7]

5 - 2 POLOIDAL DIVERTORS FOR REACTORS AND A REVIEW OF INTOR DIVERTOR STUDIES

D. M. Meade

Princeton Plasma Physics Laboratory

REACTOR GOALS

1. NO MAJOR CHANGEOUTS DURING 20 YEAR LIFETIME

   E.G. STRUCTURE-NEUTRONS

   DIVERTOR/LIMITER-SPUTTERING

   IMPLIES - OPERATION AT MUCH LESS THAN FLAT OUT PERFORMANCE

2. STEADY-STATE

3. SIMPLE - TOUGHEST

EXTERNAL COIL POLOIDAL DIVERTOR

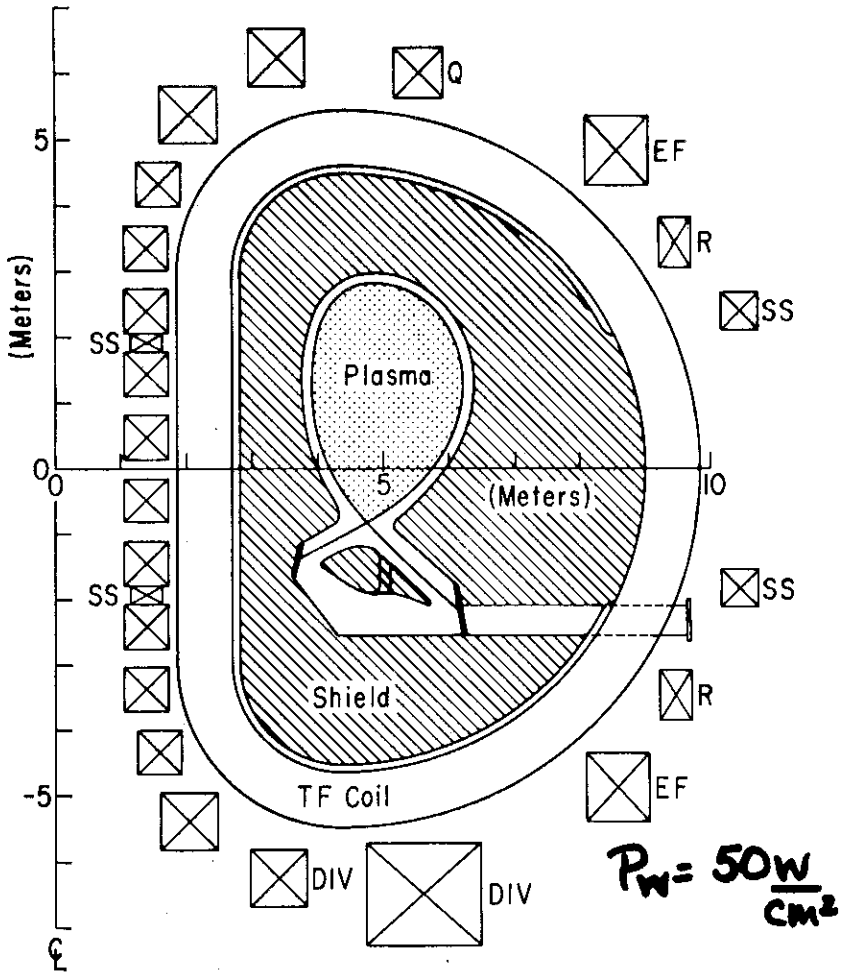

POLOIDAL DIVERTOR CONFIGURATIONS

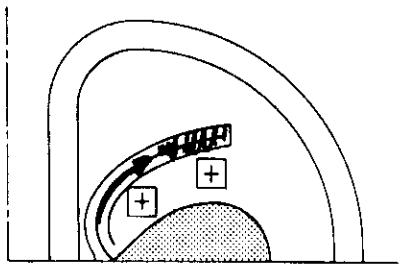

Standard Coil

1. Long Exhaust Channels
2. Divertor & Toroidal Coils Are Linked

(Large TF coil)

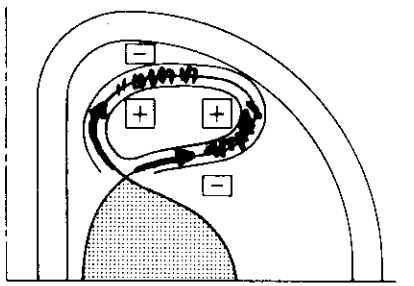

Segmented Coil

1. Long Exhaust Channels
2. Internal Divertor Coils (Unlinked With Toroidal Coils) $\Sigma NI = 0$

(only 30 cm shielding for INTOR)

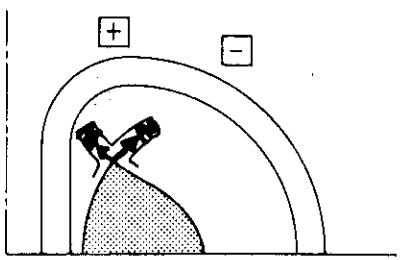

External Coil

1. Short Exhaust Channels
2. External Divertor Coils

POLOIDAL DIVERTOR ISSUES

PRIMARY ADVANTAGES -

- o GLOBAL - AXISYMMETRIC - NO DELETERIOUS PHYSICS EFFECTS
- o MODEST ENERGY DENSITY IN EXHAUST CHANNEL

MAJOR CONCERNS -

- o ENERGY DEPOSITION INSIDE BLANKET
- o REQUIRED LENGTH OF EXHAUST CHANNELS
- o COMPLEXITY OF INITIAL DESIGNS

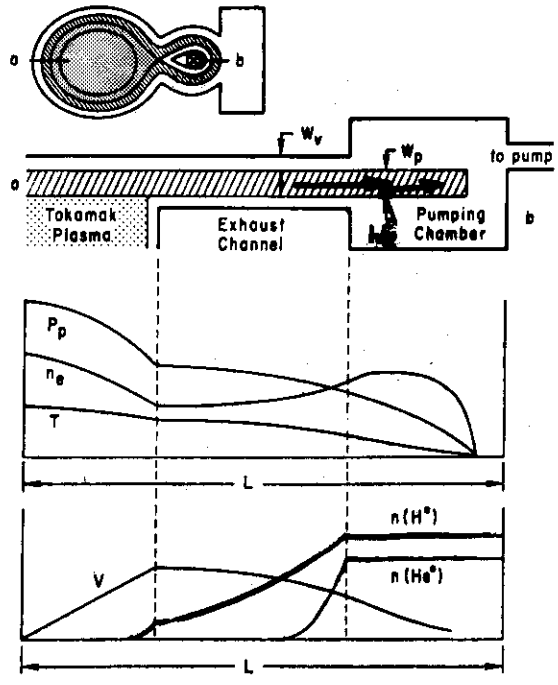

REMOTE GAS BLANKET

1. DISTRIBUTES THE PLASMA ENERGY OVER LARGE AREA (~ .1 kW/cm^2 FOR INTOR)
2. COOLS THE DIVERTOR SCRAPE-OFF TO ~ 50 eV (REDUCING IMPURITY GENERATION AND SURFACE EROSION)
3. INCREASES PLASMA DENSITY IN THE SCRAPE-OFF PROVIDING GREATER IMPURITY SHIELDING
4. RECYCLES THE D^0 AND T^0 BACK THROUGH THE EXHAUST CHANNEL (REDUCING T^0 INVENTORY)
5. OBTAINS POSSIBLE HELIUM ENRICHMENT IN THE PUMPING CHAMBER
6. REDUCES PUMPING REQUIREMENTS

PARTICLE FLOW

$$\tau_E \simeq \frac{(a/2.4)^2}{K_\perp(\text{center})}$$

$$\tau_p \simeq \frac{a\lambda}{2 D_\perp(\text{edge})}$$

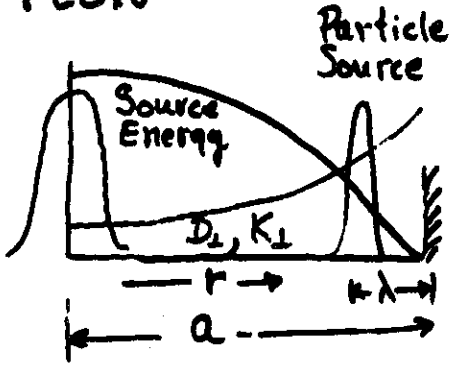

Typical Numbers for Intor

$\tau_E \sim 2$ sec

$\tau_p \sim 50$ ms

implies $T_b \sim 50$ eV

$\Phi_p = 3 \cdot 10^{23}$ p/s

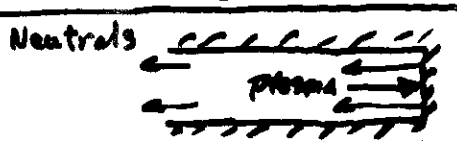

$$n_{02} = \frac{\Phi_p L}{V_n A^2/B} \sim 10^{14}\,\text{cm}^{-3}, \quad L=1\text{m}, W=0.1\text{m}$$

$$n_{01} = 4\Phi_p/AV_n \sim 10^{13}\,\text{cm}^{-3}$$

Neutral Density Required to cool Intor Divertor Channel to 50 eV

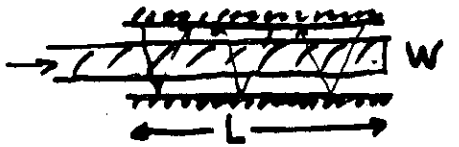

$$2\pi R L N W n_e n_0 \sum \langle \sigma_{cx} v_i \rangle kT + \langle \sigma_i v_0 \rangle U_i$$

$$= 100\ \text{MW}$$

$W n_e = 3 \cdot 10^{13}\,\text{cm}^{-2}$ shielding

$T \sim 50$ eV 1) no sputtering 2) good thermal conduction

FOR INTOR $R = 5$m, $N = 2$ channels

$$\boxed{n_0 L \gtrsim 10^{15}\,\text{cm}^{-2}}$$

JAERI-M 8971

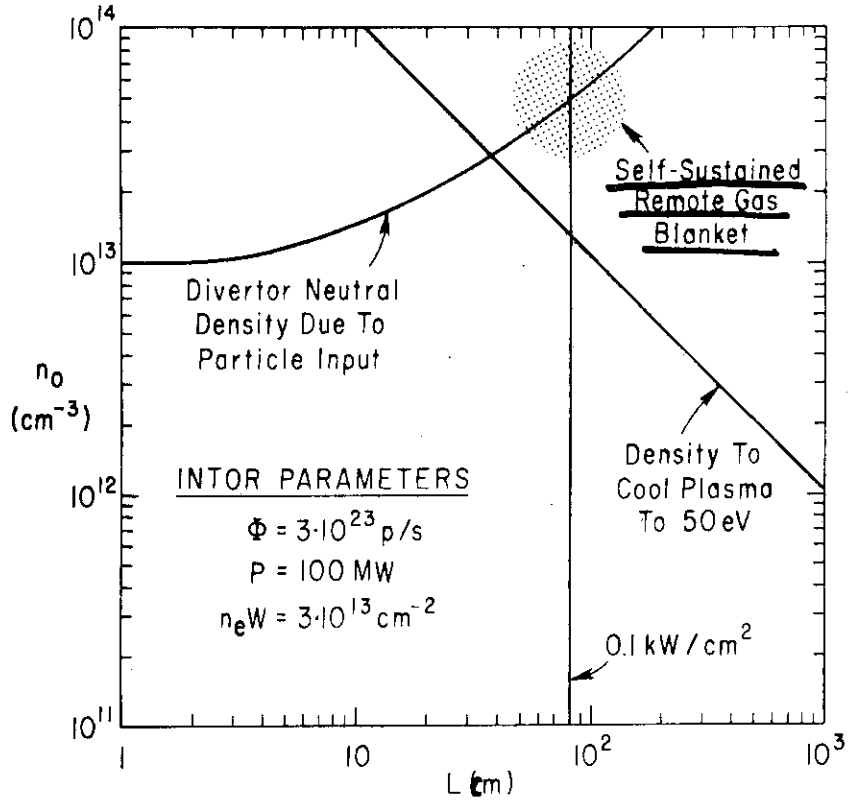

↝ Exhaust plasma can sustain the remote gas blanket (and plasma is refueled by cold gas from divertor chamber)

GASEOUS NEUTRALIZER (REMOTE GAS BLANKET) CONCEPT

F. TENNEY (1971)

BASIC PHYSICS TESTS

1. STABLE NEUTRALIZATION - YAMADA, ET AL, 1978
2. PLASMA PUMPING - YAMADA, ET AL, 1979
3. HELIUM ENRICHMENT - IN PROGRESS

SMALL SCALE TESTS ON PDX

FULL SCALE TESTS ON PDX

QED-I GETTERING CONFIGURATION

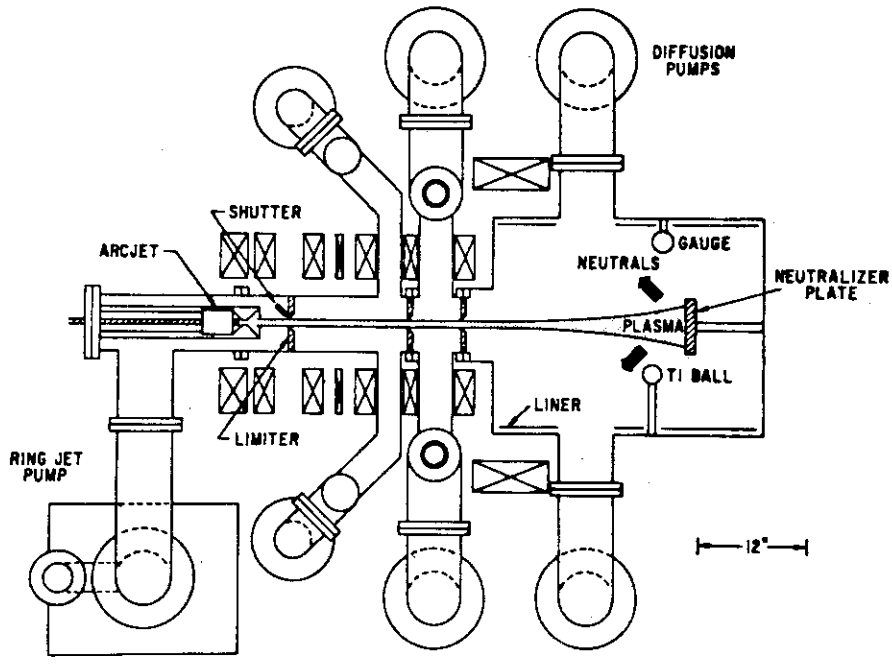

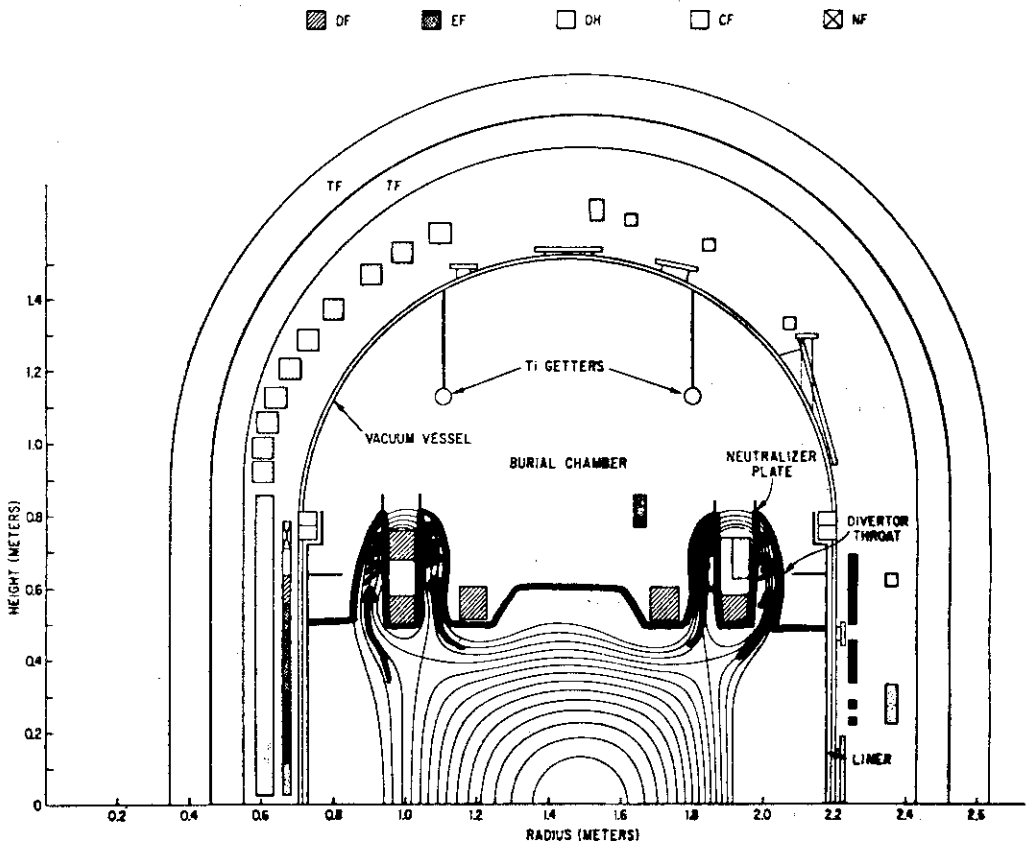

5 - 3 BUNDLE DIVERTOR MAGNETICS FOR ISX-B, ETF AND REACTORS

T.F. YANG

Plasma Fusion Center
Massachusetts Institute of Technology
Cambridge, Massachusetts 02139

SUMMARY

In this report the detailed magnetics and the methods of designing the ISX-B bundle divertor are presented. A preliminary result of a new bundle divertor configuration for ETF will also be presented. This divertor will reduce the current requirement and the size of the divertor significantly such that the whole assembly can be withdrawn from the tokamak easily. The plasma instabilities in the divertor and their implications on target and particle removal will also be discussed.

1. Introduction

Due to the experimental success of DITE bundle divertor [1] and the success of designing such a divertor for reactor, there is a vast interest in bundle divertor. Many improvement concepts have been proposed in the past year.[2,3] To understand the physics in the higher β regime the ISX-B bundle dibertor was proposed and to be built at ORNL. A very detailed design has been done by the Culham Laboratory.[4] A brief design study has been carried out by Westinghouse.[5] These two studies form the basis for the present final design at MIT. The conventional two coil configuration was chosen because of the existing tight space of ISX-B. The final configuration was chosen based on the considerations of lower magnetic field ripple, larger flux expansion and better engineering design without paying the penalty for additional complexity. Such details will be discussed in section 2.

The ripple due to the two coil system is still unsatisfactorily

high. A four coil system will reduce the ripple on the axis drastically. This system is under extensive study at ORNL.[6] At present the two coil and preliminary result of four coil system appear to be difficult for maintenance. A T-shaped divertor coil configuration developed for ETF appears to give the best solution for maintenance. A four T-shaped coil system and other detailed study are also underway at MIT. A brief discussion is given in section 3.

In section 4 the instability of the plasma in the bundle divertor will be discussed. The estimate of the effect of the local field ripple on the critical β_c due to the ballooning mode is also given and appears to be small. If the instability and ballooning mode effect are observed to be correct on ISX-B then the particle collection will be easy and the bundle divertor may be a very attractive system.

2. ISX-B Bundle Divertor

The plane view of the ISX-B TF coil and bundle divertor coil layout is shown in Figure 1. The key parameters of ISX-B are R_o = 92 cm, a = 20 cm and the scrape-off layer thickness is 7 cm. The designed value of B_o is 1.8 T. The selection of this final magnetic configuration is described below.

The original DITE divertor is two solenoid system. The current density is 25 kA/cm^2/Tesla. Consequently the magnetic stress concentration is very higher. The new Culham design uses large radius to reduce the current requirement thus the current density has been reduced to 7.6 kA/cm^2/Tesla. However, the ripple is still above 2%. The use of toroidal ripple has also been proposed by ORNL. This is not

desirable because the periodical toroidal ripple is found to have a deleterious effect on the confinement of energetic particles. A pair of vertical axiliary coils to reduce the field intensity to be nulled by the divertor was suggested in the Westinghouse study. This will add the undesirable complexity. The method used here is to spread out the conconductor to reduce the current density. This can be accomplished by increasing the radius of each turn while being moved away from the null point. Each divertor coil is now a sectional conical shape instead of solenoid. A current density of 7.6 kA/cm^2/Tesla has also been achieved. The ripple is lowest among all the methods discussed. It is generally conceded that the optimal divertor angle is 45° when adequate space is available. Because of the very limited space in ISX-B a 30° angle was chosen. The consideration of such a choice is given below.

In search for the flux pattern given in Figure 1, a series of configurations for various coil sizes and angles have been computed. Three typical flux patterns are presented in Figure 2. The corresponding divertor angles are 40°, 35°, and 30°. The radius of the coils is constrained by placing the outside edge of the coils along the center lines through the TF coils while the front corner closest to the first wall is fixed at R = 122 cm. For the angle larger than 40° or larger radius the fluxes will run into structure. This figure demonstrates that a very thick scrape-off layer in the divertor can be produced as long as space is available. The fluxes in figures 2a and b are still interfering with the structures. Figure 2c is the best choice. For

angles less than 30° the expansion is too small and the current requirement and ripple will go up.

As has been pointed out in the culham design[4] the poloidal field will cause the diverted flux bundle drifted upward and partially intercepted by the coil structure. To study the plasma stability in the divertor we would like to correct this deviation. The resultant field lines were computed by taking into account of poloidal field coil and plasma current. The poloidal field coil arrangement and filamentary representation of the plasma current are shown in Figure 3. The bundle divertor is interfering with the neighboring EF coils. they are bent locally to bypass the divertor as shown by the side view. The typical field lines projected on the midplane, on the vertical plane on the divertor center line and on the R-θ plane are shown in Figure 4. To see whether they will interfere with the structure the points of intersection of the field lines with the cross sectional planes at five locations as shown in Figure 4 are plotted in Figure 5. The circles in Figure 5 represent the inner structures of the divertor assembly. None of the points actually falls on the structure. More detailed study of the scrape-off layers in the tokamak and divertor are in progress. The divertor assembly structure and assembly method are shown by Figure 7. The divertor coils are inserted into the housing and sealed by a cover from the back side.

4. Bundle Divertor for ETF and Reactors

As was pointed out earlier the conventional two coil divertor system is not suitable for reactor without further modification. The current density is still too high and the maintenance is still difficult because the trace of stagnation points bends toward the divertor coils.[1]

The shielding space is not of equal thickness and may not be enough between the center limb and the null trace above or below the midplane. A pair of vertical auxiliary coils will make the null trace vertical.[5] However the Auxiliary coils are 10 m tall and it adds to the complexity.

The T-shaped coil evaluated for the proposed long pulse device LPTT which was under consideration by ORNL is shown in Figure 7. The cross-sectional view is shown by Figure 8. The null trace is now vertical and the space between the null and the center limb is now large and uniform. The application of this T-shaped coil system to ETF is illustrated by the isometric Figure 9. The computed magnetic flux and the engineering layout are shown in Figure 10. The key plasma parameters are R_0= 5.6m, a = 1.35 m, B_0 = 5.5 T. There are 12 TF coils. The divertor assembly consists of two L-shaped divertor coils each of which carried a current of 8 MA-T and an expansion coil set each of which has a current of 4 MA-T. Because of the large TF coil bore an expansion coil set is needed to bring the flux to the outside of the TF coils system. The current in the divertor coils is only half of what will be expected from the conventional circular coil design. A series of expansion coils can be added to carry the flux further out. The magnetic intensities due to divertor alone, due to divertor and TF coils and the 1/R variation are plotted in Figure 11. The expanded field error is shown in the upper left corner. The error is actually zero on the axis and slightly positive for $R < R_0$. As can be seen from Figure 10 the divertor assembly can be inserted or withdrawn in between the TF coils. Therefore the maintenance is easy. The shielding space in front of the outer limbs is 50 cm which has to be increased for superconducting coils. The optimization and detailed analyses of this system will be carried in the coming months.

5. Plasma Instabilities and Particle Collection

It was found that the plasma becomes unstable in the divertor when the plasma is not intercepted by a target or collector.[7] Because the plasma density and temperature profiles in the scrape-off layer peak at the separatrix. The target technology was considered to be very difficult. A conducting neutralizing plate will actually stabilize the plasma. Because of bad curvature of the magnetic field lines as shown by Figure 12 and large field and pressure gradients the plasma is unstable to the local interchange mode. The plasma will probably disperse toward the chamber wall. The wall can then be used as collector. The surface area is large. The thermal and particle flux will be uniform and low. Thus the collector and vacuum systems will be much easier to design.

The condition for instability for a closed field lines is

$$\left(\frac{d}{d\psi}\int_{(1)}\frac{dl}{B}+\frac{d}{d\psi}\int_{(2)}\frac{dl}{B}\right)\frac{dp}{d\psi} \tag{1a}$$

$$\left(\frac{d}{dr}\int_{(1)}\frac{dl}{B}+\frac{d}{dr}\int_{(2)}\frac{dl}{B}\right)\frac{dp}{dr}<0 \tag{1b}$$

where (1) indicates the region of integration inside the tokamak and (2) the region inside the divertor as shown in Figure 12. The plot of $\int_{(1)}\frac{dl}{B}$ is shown in Figure 13. It was found that[7]

$$\frac{d}{dr}\int_{(1)}\frac{dl}{B}<0, \tag{2}$$

inside the tokamak and the plasma is stable since $\frac{dP}{dr}<0$. On the other

hand $\frac{d}{dr}\int_{(2)} \frac{dl}{B} \frac{dp}{dr} < 0$ so that the plasma is not stable in the divertor.

The growth rate of the interchange instability modes is approximately

$$\gamma_{inst.} \cong V_S/\sqrt{R_c R_p} \quad , \tag{2}$$

where $V_S = \sqrt{T_e/M_i}$ is the sound speed, $\frac{1}{R_c} = \frac{1}{p}\frac{dp}{dr}$. The inverse of the transit time of the plasma flowing through the divertor is

$$\gamma_{transit} \cong V_S/2\pi R_{div} \quad , \tag{3}$$

where R_{div} is the mean radius of the divertor flux loop. Then we see that it is possible that

$$\gamma_{inst} \geq \gamma_{transit}$$

for $R_c \geq R_{div} \geq R_p$. The cross-field diffusion coefficient of the turbulent transport is approximately

$$D_{\perp} \lesssim V_S \sqrt{R_c R_p} \quad . \tag{4}$$

The scrape-off layer thickness is approximately

$$\Delta X \sim \sqrt{D_{\perp} \tau_{||}} \geq R_{div} \tag{5}$$

The scrape-off layer thickness is as large as the mean radius of the diverted flux loop. Therefore, the plasma may be turbulently dispersed over the entire bundle divertor chamber, thereby leading to a low power loading and particle flux on the chamber wall. The relationship given in Equation (5) indicates that it is better to obtain a flux pattern with a larger radius of curvature. Such a configuration is shown in Figure 11b with an appropriate choice of divertor coil angle and location. The mean radius of the loop, R_{div}, is about doubled.

6. Ballooning Mode with Local Field Ripple

The effect on the ballooning modes of instability of the tokamak due to the presence of a bundle divertor may be estimated using the potential energy associated with small perturbations from equilibrium[8]

$$2\delta W = \int d\tau \left[Q_{\perp}^2 + \left(\vec{Q}_{\parallel} - B \frac{\vec{\xi}\cdot\vec{\nabla}p}{B^2} \right)^2 + \gamma p (\vec{\nabla}\cdot\vec{\xi})^2 + \frac{\vec{J}\cdot\vec{B}}{B^2} \vec{B}\times\vec{\xi}\cdot\vec{Q} - 2(\vec{\xi}\cdot\vec{\nabla}p)(\vec{\xi}\cdot\vec{k}) \right] \tag{6}$$

Based on the balancing of the shear term of $Q_{\perp}^2$ with the curvature term of $2\vec{\xi}\cdot\vec{\nabla}p\vec{\xi}\cdot\vec{k}$, a limit on β was given in Reference (8) by $\beta^* \leq a/q^2R$ for axisymmetry. Better estimates on the β limit have been given elsewhere. We will use the method given in Reference (8) to estimate the relative change in β due to the local field ripple created by a bundle divertor. The approximate connection length and radius of curvature are qR and R in the axissymmetric case and become $q \cdot (R + \Delta R)$ and $(R - \Delta R)$ respectively with a bundle divertor. Here, R is the local deviation in radius as shown in Figure 2-1. By the comparison of the shear and curvature terms we found that the change to critical β_c is

$$\frac{\Delta\beta_c}{\beta_c} \leq \frac{\Delta\phi}{\pi} \frac{4\Delta\beta}{\beta} \qquad (7)$$

The ratio $\frac{\Delta\phi}{2\pi}$ is approximately the inverse of the number of TF coils which is typically less than 1/16. The ratios $\frac{\Delta R}{R}$ and $\frac{\Delta B}{B}$ are a few percent. Therefore, the β limit is reduced only by a few tenths of a percent due to the local ripple created by a bundle divertor.

7. Conclusion

If the divertor physics is confirmed by ISX-B experiment and there is no deleterious effect on the confinement and stability due to the field perturbation created by the divertor, the bundle divertor would be very attractive as has been demonstrated by the magnetic system for ETF. The bundle divertor can essentially be treated as a plug-in unit. The thermal and particle handling problems would also be relatively simpler if the plasma instabilities in the divertor do exist and do not cause deleterious effect on tokamak.

8. Aknowledgement

This work is supported in part by the U.S. Department of Energy under the contract number AC02-80ER52057 and by ORNL Fusion Energy Division. The engineering designs of ISX-B were performed by E. Rapperport and Jack Tracey.

1. P.E. Stott, C.M. Wilson, A. Gibson, Necular Fusion 475(1977) and references cited.

2. J. Sheffield, R.A. Dory, ORNL-TM6220 (1978).

3. T.F. Yang et al., WFPS-TME-104 (1978).

4. K.M. Plummer et al. Culham Report, CLM/02/1 (1979).

5. T.F.Yang, WFPS-TME-075 (1978).

6. U.S. INTOR Report (1979).

7. T.F. Yang, J.D. Callen, Submitted to Nuclear Fusion (1979).

8. A.M. Todd, M.S. Chance, J.M. Greene, R.G. Grimm, J.L. Johnson, and J. Mamikan, Phys. Rev. Lett. 38, (1977) 826.

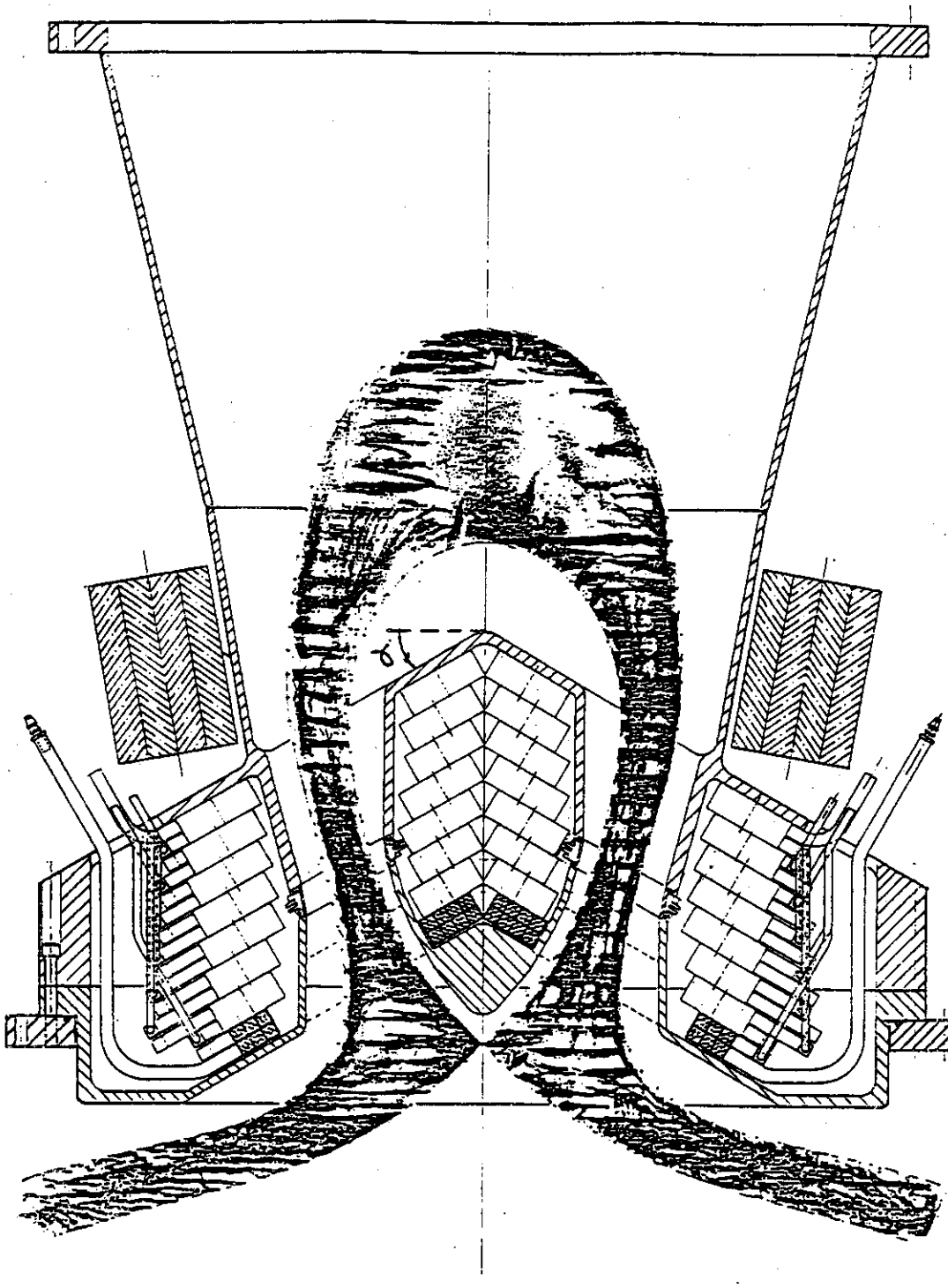

Figure 1. ISX-B Bundle divertor projected on midplane divertor angle α = 30°.

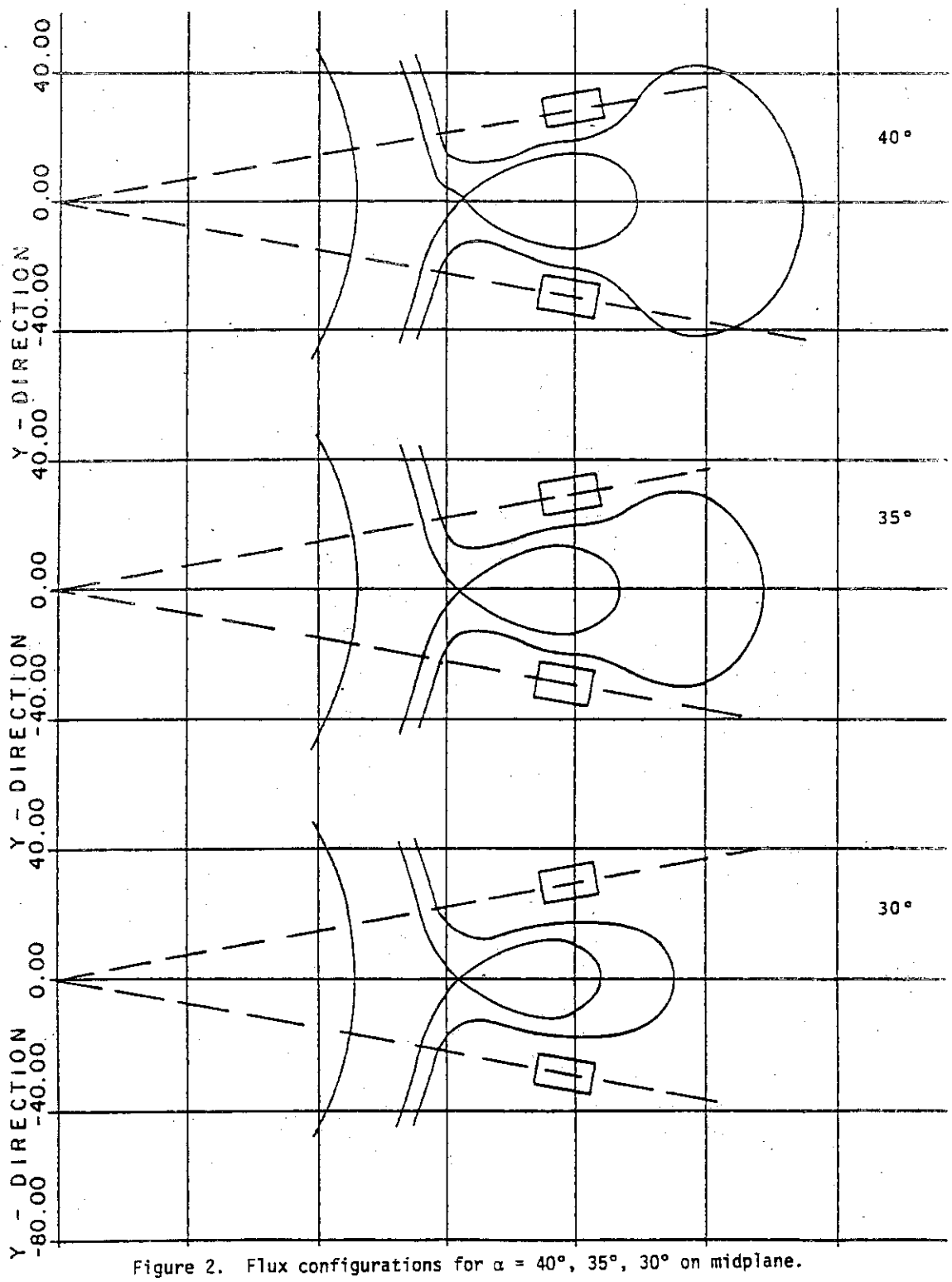

Figure 2. Flux configurations for α = 40°, 35°, 30° on midplane.

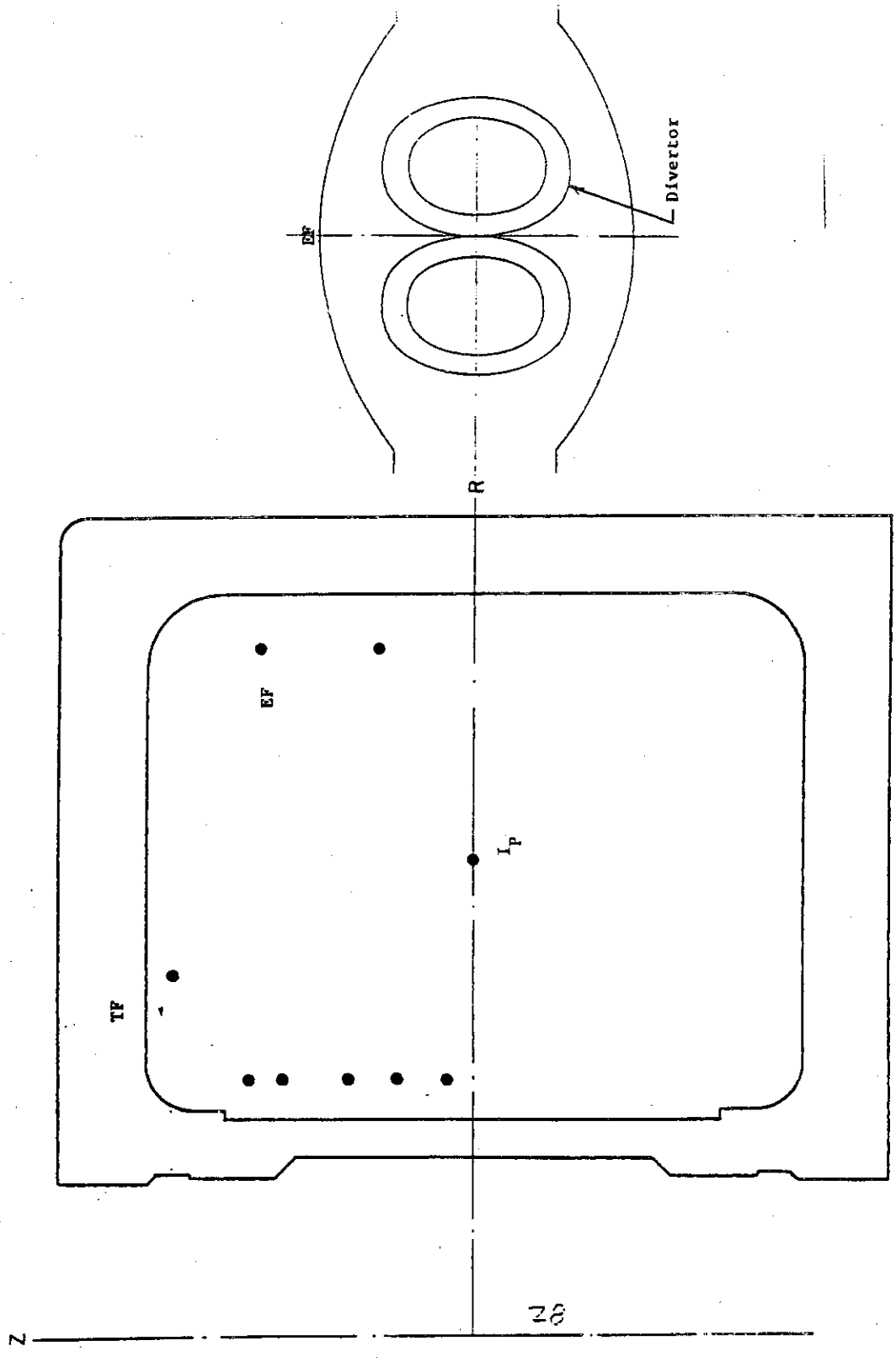

Figure 3. Model of the Equilibrium Field coils (cross-sectional view)and the section of the equilibrium coils around divertor (side view) for computation.

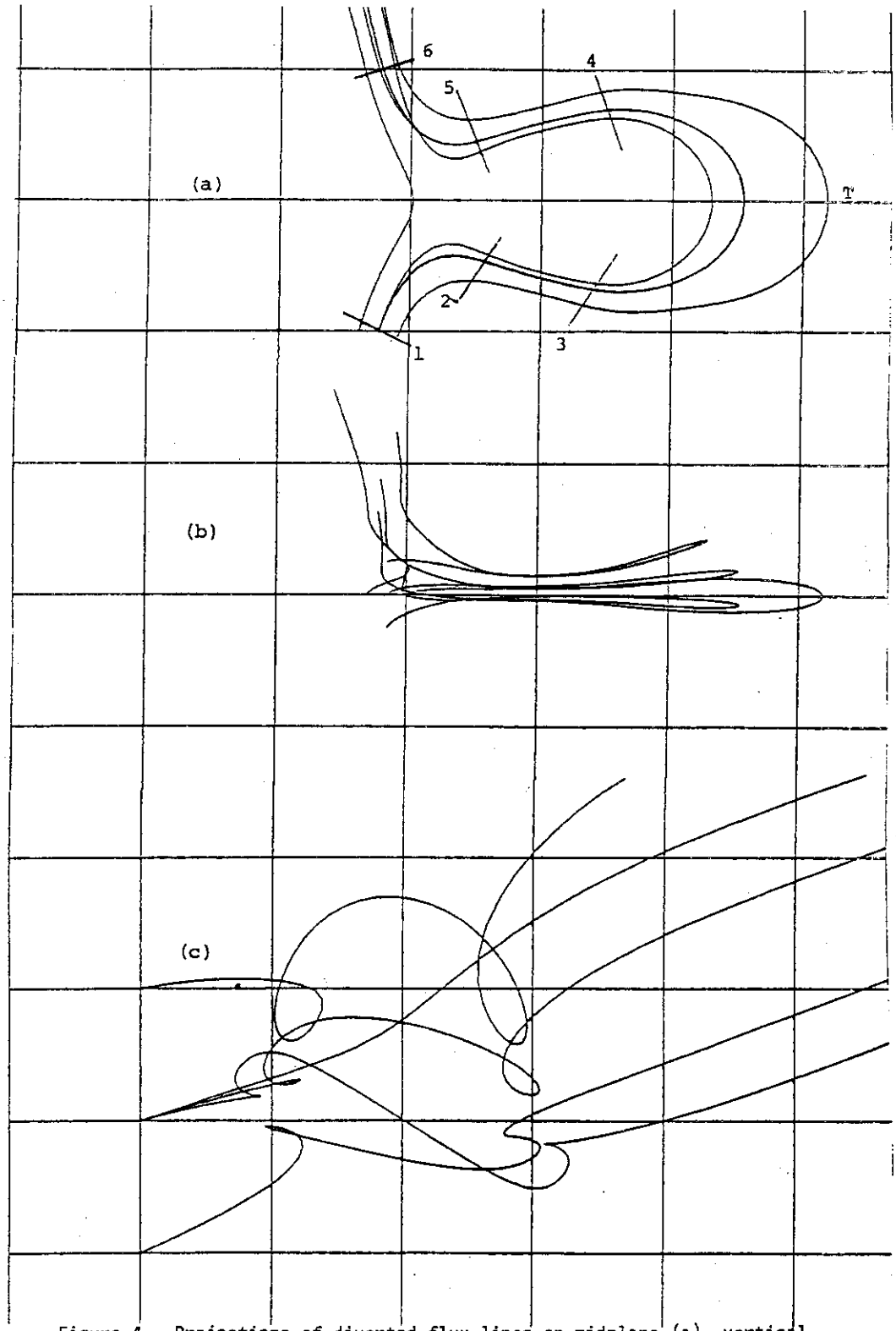

Figure 4. Projections of diverted flux lines on midplane (a), vertical plane (b) and R-θ plane.

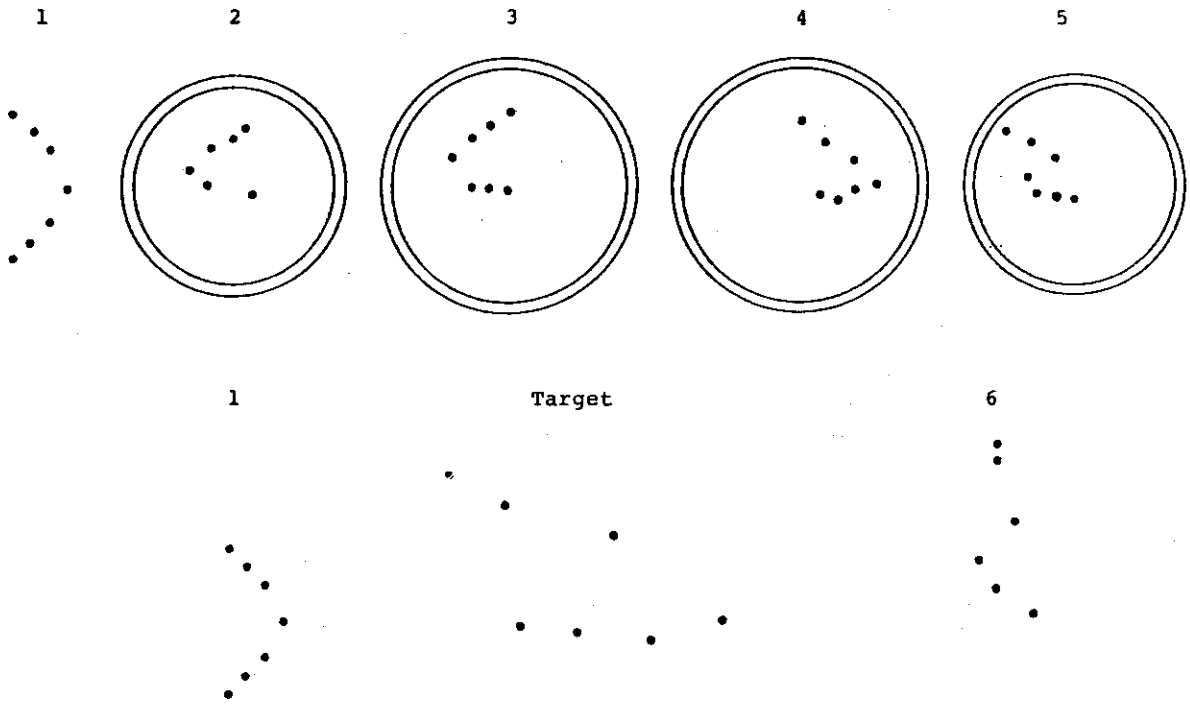

Figure 5. Intersections of the flux lines with cross-sectional planes 1 through 6 of Figure 4a.

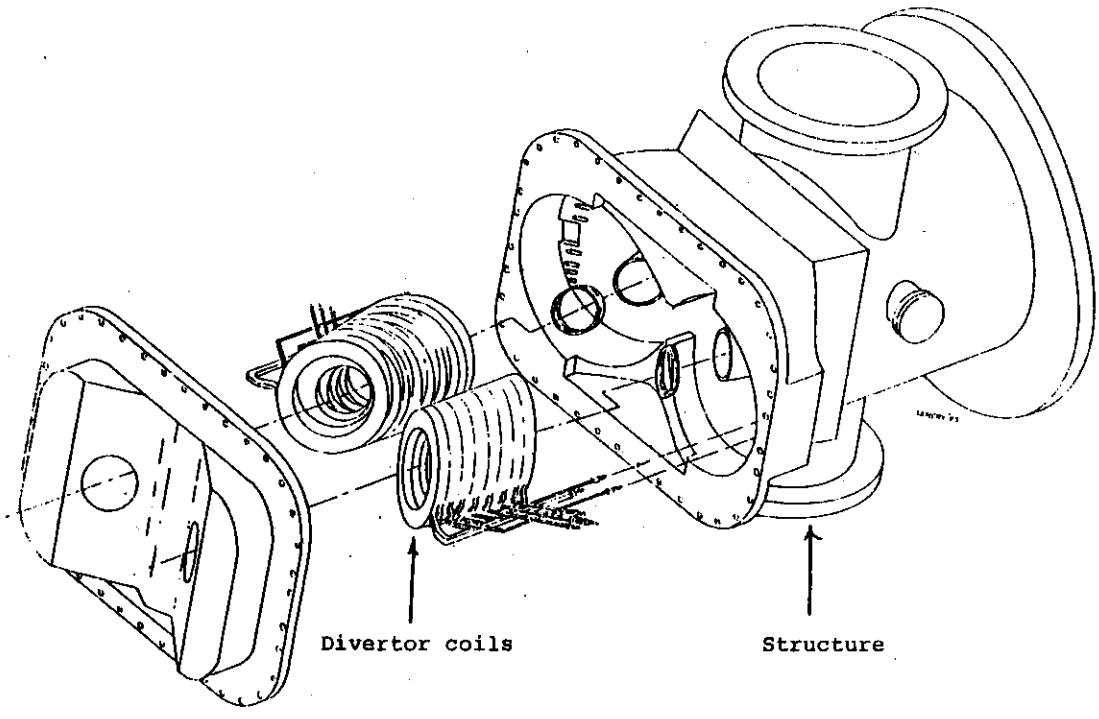

Figure 6. Divertor coil and structure assembly.

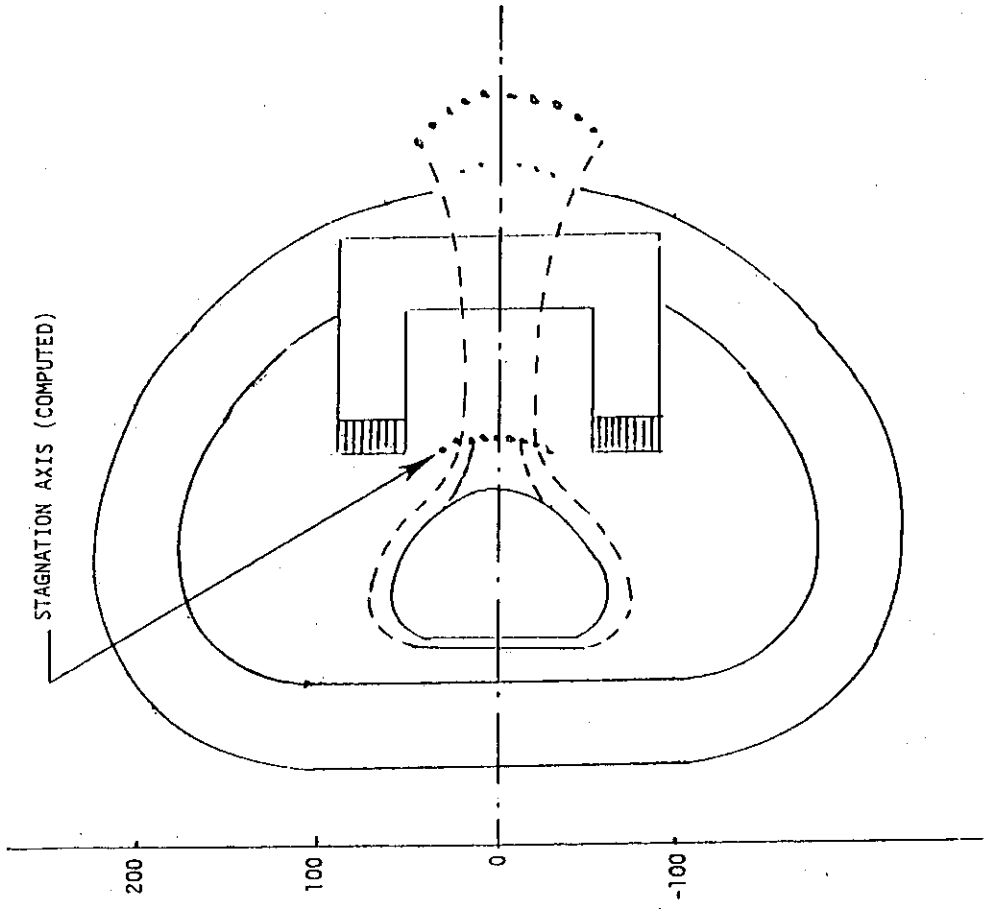

Figure 8. CROSS-SECTIONAL VIEW OF LPTT DIVERTOR (FLUX LINES ARE PREDICTED)

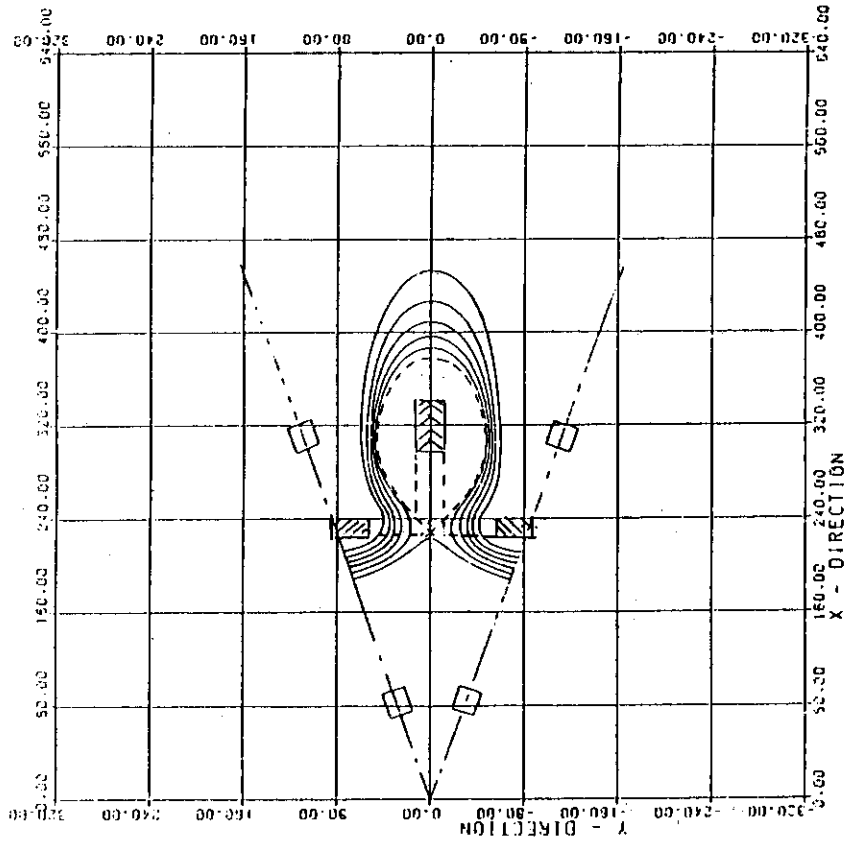

Figure 7. Magnetic Flux Configuration of the Efficient Bundle Divertor for ORNL/LPTT.

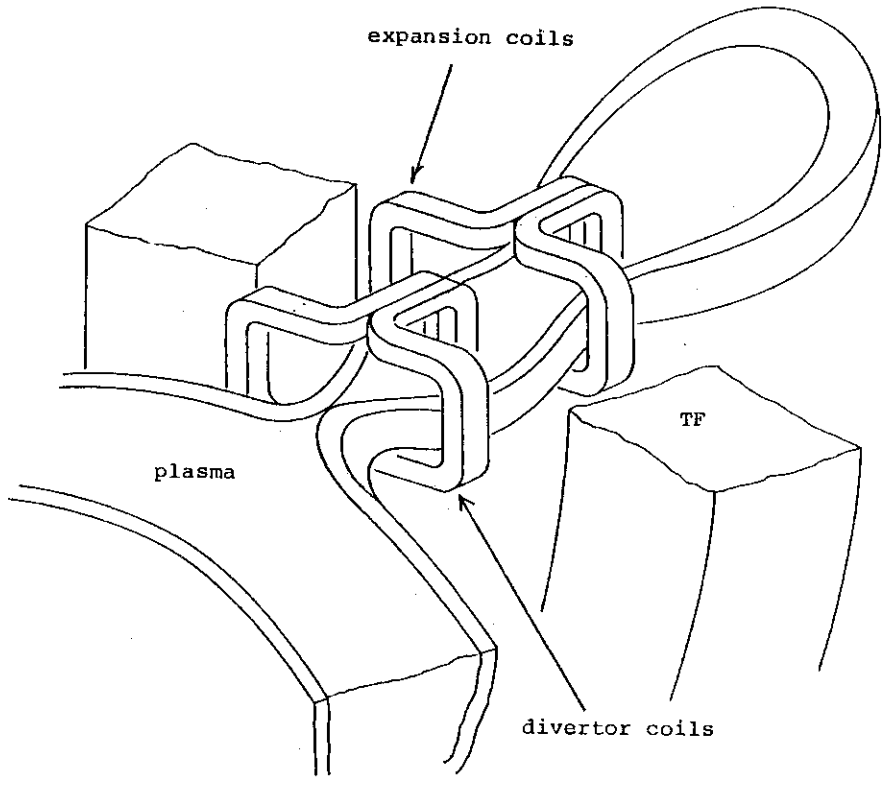

Figure 9. Isometric illustration of the ETF Bundle Divertor.

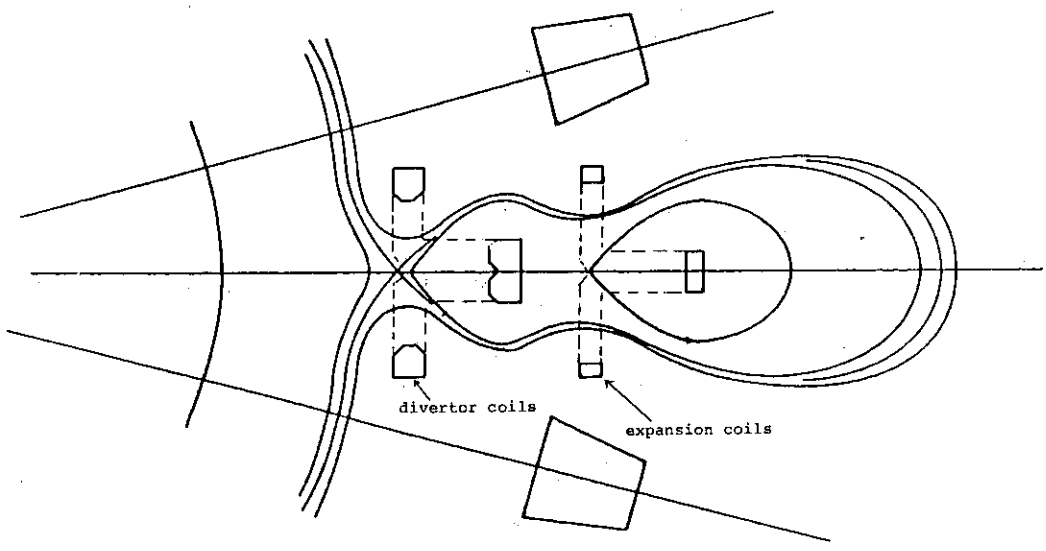

Figure 10. Project of ETF bundle divertor on the midplane

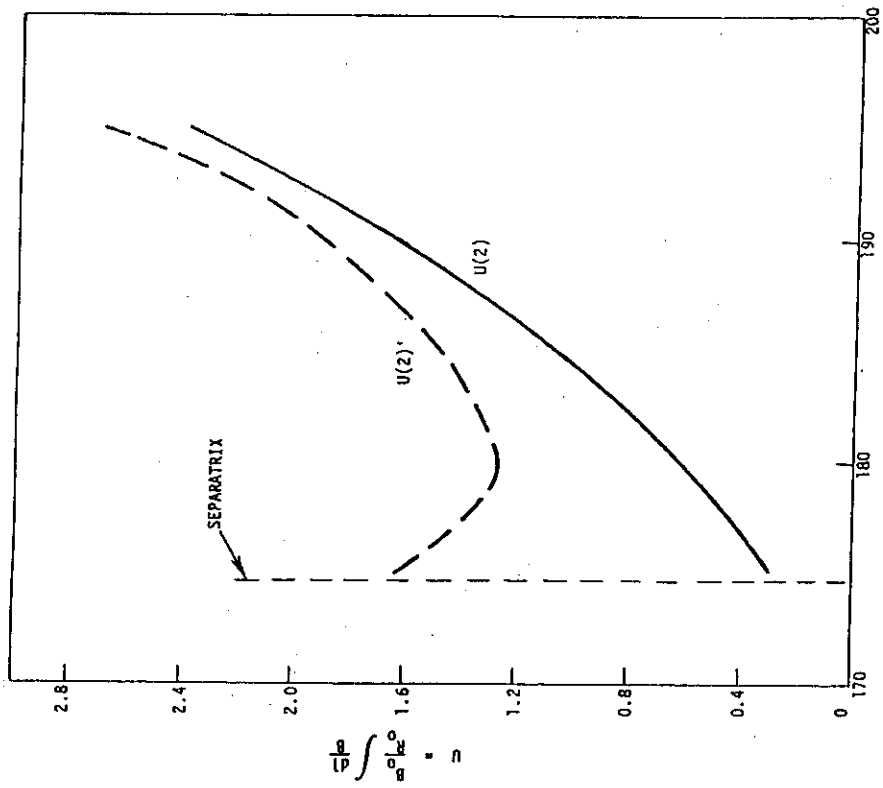

Figure 13. Plots of the integrals $U(2) = \frac{B_0}{R_0}\int_M^N \frac{d\ell}{B}$ and $U(2)' = \frac{B_0}{R_0}\int_{M'}^{N'} \frac{d\ell}{B}$.

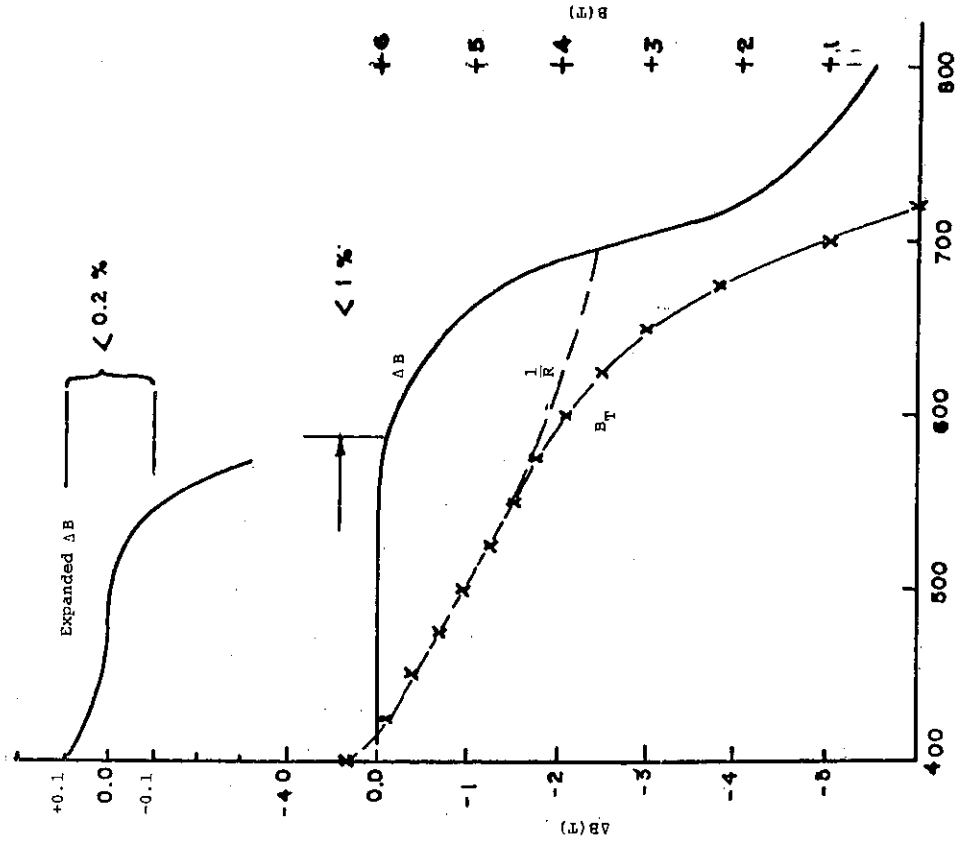

Figure 11. Plot of eaxisymmetric B_T (dashed line), resultant B_T (line with X) and perturbation field ΔB due to divertor.

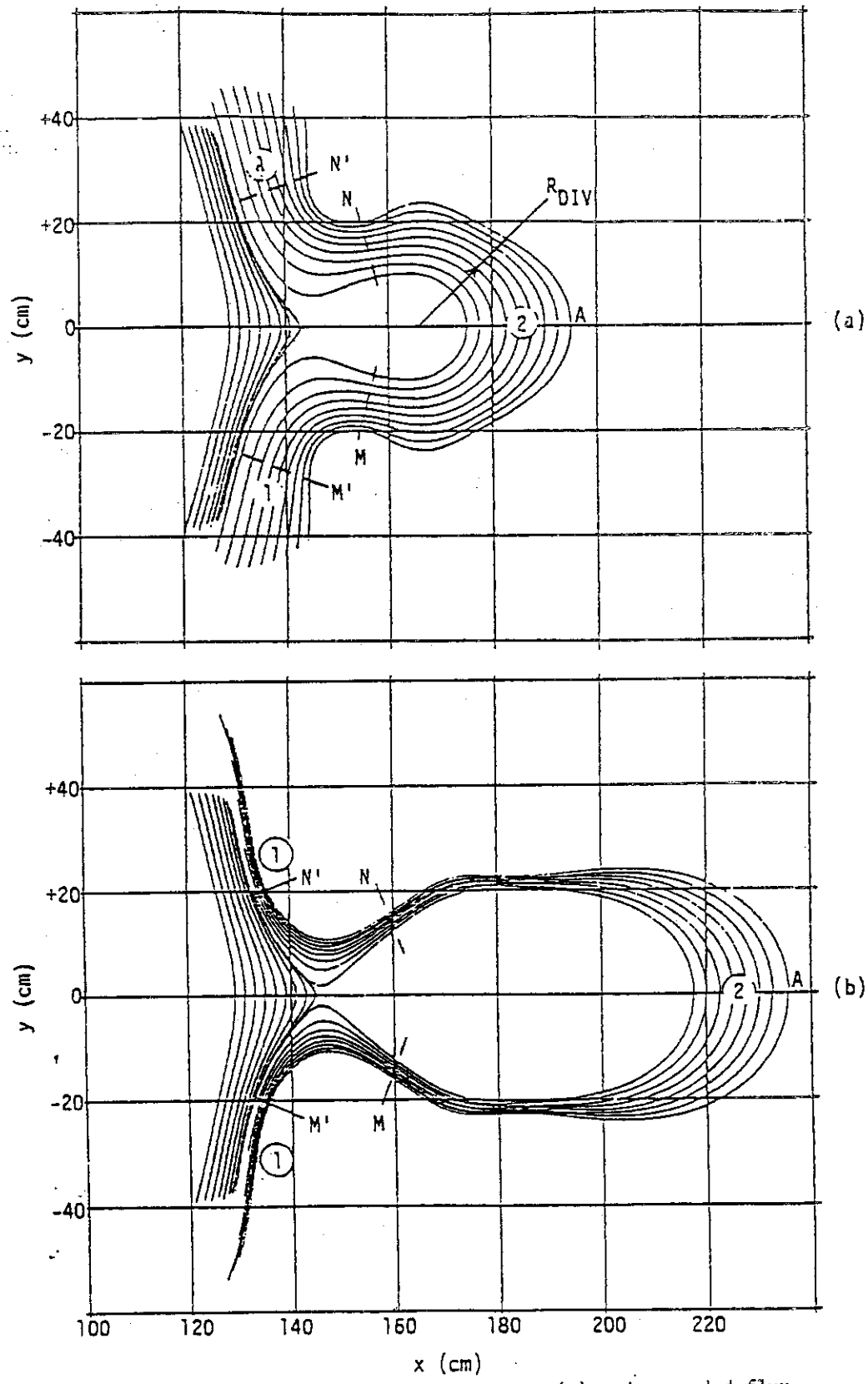

Figure 12. Reproduced flux patten of DITE(a) and expanded flux pattern (b).

5 - 4 "WALL LAPPING PLASMA" WITH ROTATING HELICAL RESONANT ISLANDS FOR IMPURITY CONTROL AND MECHANICAL VALVES FOR ASH EXHAUST IN A REACTOR-GRADE TOKAMAK WITHOUT A DIVERTOR

Teruhiko TAZIMA and Masayoshi SUGIHARA

Division of Large Tokamak Development
Tokai Research Establishment, JAERI

An alternative conception of the divertor, called "Wall Lapping Plasma" is proposed for impurity control and ash exhaust which are one of the most serious problems in reactor-grade tokamaks. Resonant helical islands formed in the boundary region rotate when we add rotating helical field by two sets of external helical coils whose current changes alternately. Consequently the plasma surface in contact with the wall by the islands rotates along the whole wall surface, so that the plasma contamination by evaporation of wall surfaces due to local heat deposition can be avoided.

Plasma particles flow along the magnetic force lines intersecting the wall by islands. Intersecting angle is very small, so that mechanical valves with small height of opening located on the wall can exhaust ash easily, since backflow of neutralized helium is small because of the narrow opening.

The necessary helical field is only 1/500 of the toroidal magnetic field, the total valve area is less than several percent of the wall surface area: besides the valves are easily repairable. "Wall Lapping Plasma" will be interesting as an alternative of the divertor because of the simple technology.

1. INTRODUCTION

At present, we have no perfectly reliable method from both physical and technological view points for impurity control and ash exhaust even in a machine with the divertor. We propose a following new conception called "Wall Lapping Plasma" with rotating helical resonant islands for impurity control and mechanical valves for ash exhaust in a reactor-grade tokamak without the divertor.

Resonant islands are formed at the rational surface when we add a small helical field (e.g. 1 - 2% of the poloidal field) by external helical coils (Fig. 1). This configuration is used for a divertor called "Resonant Helical Divertor" proposed by F. Karger and K. Lackner . Helical divertor plates and helical shielding plates are installed inside the islands in this divertor. However, it seems complicated structure to install these helical plates inside the vacuum chamber, and it also seems dangerous that the heat load to the edge of the shielding plates will amount to over several kW/cm^2 which may cause severe evaporation, since besides the primary islands, islands of higher mode numbers are formed on the corresponding surfaces owing to the toroidal curvature and setting errors of poloidal and toroidal coils, so that these islands may overlap and the field lines are ergodized .

More simple structure avoiding extremely large heat deposition can be imagined as follows. In order to rotate these islands, two sets of helical coils are located and each current is changed alternately at 1∿10 Hz. Consequently, the plasma surface contacting with the wall rotates along the whole wall surface. Therefore, we can avoid the evaporation of the first wall by local heat deposition. Ergodization of the field lines can help above effect, since high heat conduction flows along the primary islands will be decreased.

As to the ash exhaust, simple pumping through ports adjacent to the plasma periphery seems very difficult, since machine structures limit the pumping conductance to a level at which equilibrium can be achieved only at high ash pressure at the periphery. We employ simple mechanical valves located on the first wall for the ash exhaust (Fig. 2). Plasma and helium ions flow into the narrow valve openings along the magnetic force lines and only a small fraction of these particles can backflow to the bulk plasma . The most important point to design these valves is what a kind of shape is preferable to avoid evaporation by local heat deposition on valve edges as described in section 3.

The other difficult problem in this system is a countermeasure to the plasma contamination by the first wall material due to sputtering by plasma particles and self sputtering by impurity ions. The low Z first wall with low chemical sputtering yield is preferable except the case where most of the energy losses carried by particles from the bulk plasma (i.e. conduction and convection losses) is converted into radiation in the boundary region and consequently the edge temperature is cooled down to 50∿100 eV, or the case where the boundary temperature is reduced by high electron heat conduction along the field lines to the wall.

2. HELICAL RESONANT ISLANDS FOR IMPURITY CONTROL

2.1 Width of Manetic Island by Externally Applied Helical Field

$$x^2 = \Delta^2 \left[k^2 - \sin^2 \frac{\zeta}{2} \right] ,$$

$$\Delta^2 = \frac{4r_s}{m} \left| \frac{\tilde{b}_{rs}}{\psi''_{0s}} \right| = \frac{4R}{n} \frac{q(r_s)}{q'(r_s)} \left| \tilde{b}_{rs} \right| .$$

Here Δ represents a half width of the magnetic island. This result agrees with the expression obtained by Matsuda, Yoshikawa except for a numerical factor. For INTOR plasma, $\Delta \sim 20$ cm when $\tilde{b}_{rs} \sim 1/500$ (i.e. $b_{rs} \sim 100$ Gauss). Thus, considerably large helical islands can be formed by the resonant helical field with relatively small amplitude but fairly high coherency. Arbitrary error field may contain the resonant component, so that this error field can also form magnetic islands. However, since arbitrary error field with high coherency may not be expected, total amplitude of the error field will become so large that the performance of the plasma will be deteriorated.

2.2 Helical Coils

$$\phi_h = \frac{2\mu_0 J \alpha n r_0}{\pi} \sum_{p=0}^{\infty} K'_N (N\alpha r_0) I_N (N\alpha r) ,$$

$$N = (2p + 1)n$$

We assume $q(r) = 3$ surface is located at the plasma edge surface. For INTOR plasma, $a = 1.2$ m. Since $q = 3$ and $n = 3$, $N = 3$ ($m = 3$, $n = 1$) is the fundamental component of the helical field and $N = 9$ ($m = 9$, $n = 3$) is the second harmonics. We assume INTOR size plasma and $r_0 = 2$ m. From this equation, we can evaluate that J=40 50 kA is sufficient for the radial component b_r by only fundamental component of ϕ_h to be 100 Gauss at the $q = 3$ surface. It can also be shown that the fundamental component of the helical magnetic field falls by $(r/a)^{m-1}$, so that inner hot plasma will not be affected by this helical field.

3. MECHANICAL VALVE FOR ASH EXHAUST

3.1 Valves

In order to operate a burning plasma for a long time under the critical beta, ash exhaust is necessary to prevent the density excess. Recycling flow of particles near the plasma boundary can be expected to be larger than that in the bulk plasma by $10 \sim 20$ times, so that it is sufficient to exhaust $5 \sim 10\%$ of the recycling helium through the exhausting ports. By simple opening ports, of which area is $5 \sim 10\%$ of

(1) The valves stick out into the plasma to guide the recycling particles into the exhausting ports. Since B_r is much smaller than B_z, the shadow area of the valve is B_z/B_r times larger than that of the valve itself. For INTOR plasma, $B_z/B_r \sim 500$ and A_w (first wall surface area) ~ 300 m^2. Thus, about 20 valves, of which opening height is about 1 cm and opening area is 0.5 m^2, are shown to be sufficient to collect 5 $\sim$ 10% of recycling particles.

(2) Since the plasma contacts with whole wall surface almost uniformly by means of rotating the helical resonant islands, heat load of the first wall can be suppressed well below to bearable level for evaporation (at most 30 W/cm^2 for INTOR plasma). However, when the valves are put perpendicularly to magnetic field lines, the heat load on the front edges are expected to be quite large. Let us estimate the heat flux w along the magnetic field lines.

In wall lapping plasma, the magnetic field line intersects with the first wall by radial component of the field line B_r. Thus, when the total heat flowing from the main plasma P_α is sustained uniformly by all of the first wall with the area A_w,

$$w A_w \frac{B_r}{B_z} = P_\alpha \quad ,$$

For INTOR plasma, $B_r/B_z \sim 1/500$, $A_w \sim 300$ m^2 and $P_\alpha \sim 90$ MW so that $w \sim 15$ kW/cm^2. The edge of the valve perpendicular to the field line will suffer this heat load, which will cause serious evapolation. In order to mitigate the heat load to the edge, the valve is bent down slightly as shown in Fig. 2. As a result, the front edge does not suffer heat load directly. The heat load on the front surfaces of the valves is naturally equal to that on the first wall, i.e. under 30 w/cm^2, while that on the inner back surfaces, onto which guided particles flow and are neutralized, is under 150 - 300 w/cm^2. The heat load on the side edges of the valves w_v is most serious. However, these valves are easily repaired owing to their structural simplicity, and this is one of the major advantages of these valves comparing with the divertor plates of the poloidal divertor.

An example of the valve, which can meet these requirements, is shown in Fig. 2.

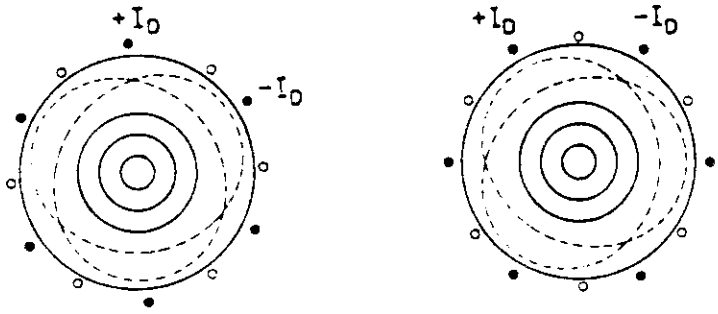

Fig. 1 Schematic pictures of the cross section of a helical island with resonance at q = 3. Two sets of helical coil currents are quickly changed alternately.

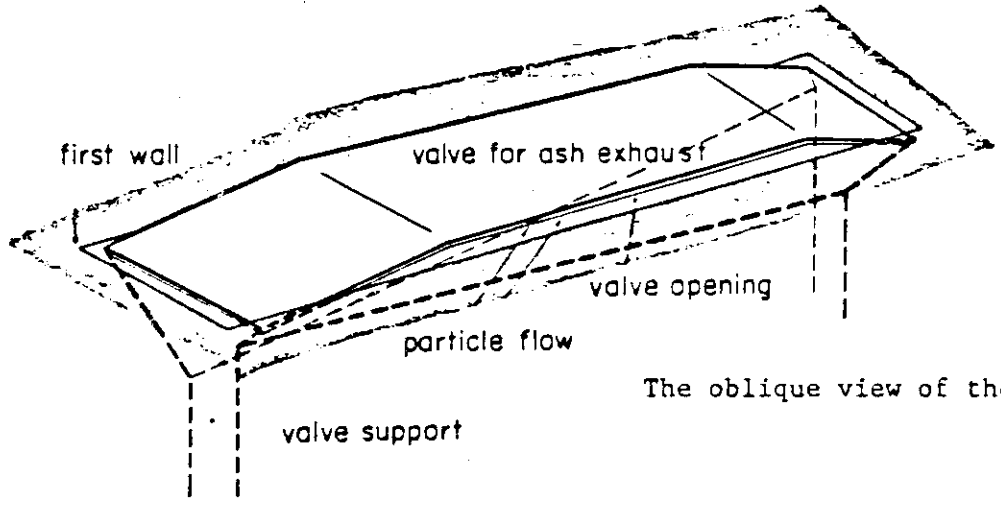

The oblique view of the valve.

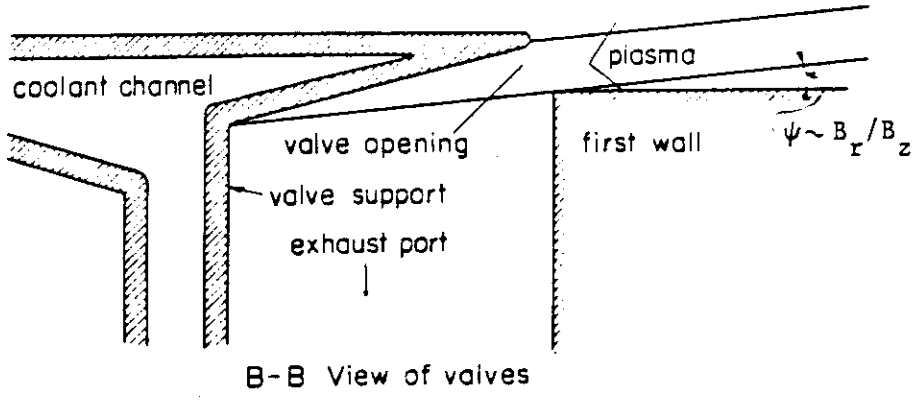

B-B View of valves

Fig. 2

5 - 5 EVALUATION OF MECHANICAL DIVERTORS

K.OKAMOTO, ULVAC CORPORATION, 2500, HAGISONO,
CHIGASAKI, KANAGAWA-PREF.,JAPAN. 253

Mechanical divertor which was proposed by W.Bieger et al.[1] is a specially structured limiter combined with pumping chamber. Figure 1 shows the schematic diagram given in the ref. 1), and Fig.2 is a sketch where the direction AA' is poloidal one. Several mechanical divertors are distributed along the toroidal circumference. The basic concept is to direct a substantial fraction of neutral particles produced at the limiter surface into a pumping chamber which is closely connected to it and is used as a piping space for blanket. This situation is brought about by making the angle α small, where α is the angle between the limiter surface which is hit by the scrape-off layer plasma and the magnetic surface. They took α of 45° and assumed the flux density of the charged particles hitting the limiter decays linearly to zero within the scrape-off layer and the intensity distribution of reflected or sputtered neutral particles obey the cosine law. Then the unloading capacity ζ, that is, the probability of neutral particles from the limiter which penetrate the entrance aperture of the pumping port is about 0.4. The unloading efficiency η, that is, the unloading percentage of helium gas which is produced at the limiter surface is given by the relation

$$\eta = \zeta \times S / (S + C) \qquad (1)$$

where S (l/s) is the effective pumping speed for helium gas at the place of the pumping chamber, and C (l/s) is the conductance between the pumping chamber and the plasma region. They expressed the disposal of heat power into the limiter is a difficult

problem to be solved.

In this paper we evaluate the mechanical divertor in connection with the application to JAERI Experimental Fusion Reactor. JEXR has the following parameters: minor radius of plasma is 150 cm, major radius 675cm, thickness of blanket and piping space are both 80cm and the size of pumping aperture in blanket is 120cm in both the toroidal and poloidal directions. The walls of the pumping duct have to be cooled by water to cool down hot fuel and helium gases. The situation is shown schematically in Fig.3. The values of ζ, C and S neccessary for demanded η values are estimated as functions of parameters α, T and s, where T is the thickness of the scrape-off layer and s is the distance between the edge line of the limiter and the intersection line of a plane formed by extending entrance aperture perpendicularly to the toroidal magnetic field and the surface of the scrape-off layer. At the distance s_0 the plane which is formed by the edge lines of limter and entrance aperture becomes perpendicular to the limiter surface.

Figure 4 shows the contours of ζ as function of α and s/s_0. The contours do not change with T. The values of ζ increases with decreasing α and increasing s/s_0 values.When α =25° and s/s_0=1, ζ is 0.75.

The conductance C is shown in Fig.5-a,b as functions of s/s_0 and T.

Now, equation (1) gives the neccessary pumping speed S for helium gas at the place of the pumping chamber. Figure 6-a,b show the value of S for η's of 0.2 and 0.3, and α's of 25° and 35° as functions of T and s/s_0. It is evident that for α of 25° required S is smaller and insensitive to s/s_0. For non-gasous

impurities emitted from the limiter, larger value of ζ is desirable, and so s/s_0 of 1 has to be taken. Figure 7 shows α of 25° is a good choice for s/s_0 of 1. Figures 8-a,b are the relation between S, η, and T for α of 25° and s/s_0 of 1 and show effective pumping speed for helium gas of several 10^5(l/s) is required.

As a solution of the problem of disposal of heat power input to the limiter surfaces, adoption of heat pipe whose working fluid is sodium is suitable. Figure 9 is a sketch of the interior of the limiter, and Fig.10 is the cross-section. The surface faced to the hot plasma is cooled by thin rectangular heat pipes, and the surfaces hit by the scrape-off layer plasma are cooled by cylindrical heat pipes. The heat pipes are cooled by water which flows in and out of the limiter through the upper and lower rectangular ducts. The ducts also support the limiter and extend to a vacuum flange equipped with bellow. Exchange and ajustment of the position of the limiter are done with these ducts, and the sketch of the setting is shown in Fig.11.

In conclusion, the mechanical divertor may be one of the candidates of divertors in fusion reactor.

(reference)

1) W.Bieger, K.H.Dippel, G.Fuchs, G.H.Wolf; "On Mechanical Divertors (Scrape-Off-Limiter)", Proc. Int. Symp. on Plasma Wall Interaction, 18-22 Oct. 1976, p.609.

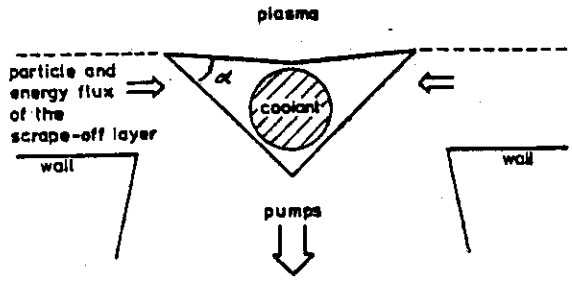

Fig.1

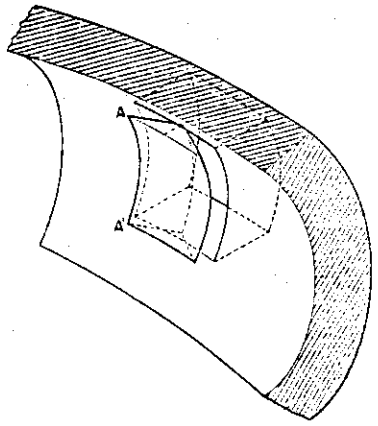

Fig.2

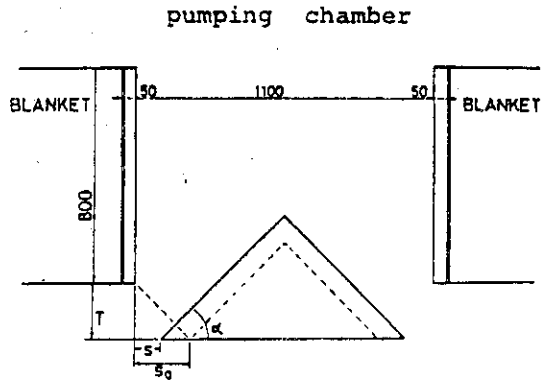

Fig.3

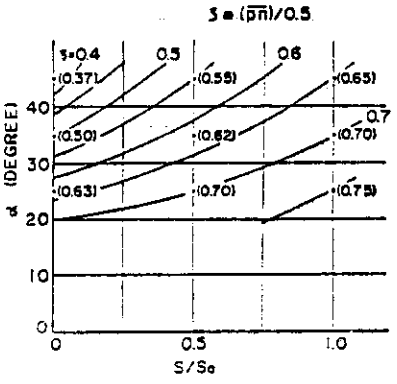

Fig.4

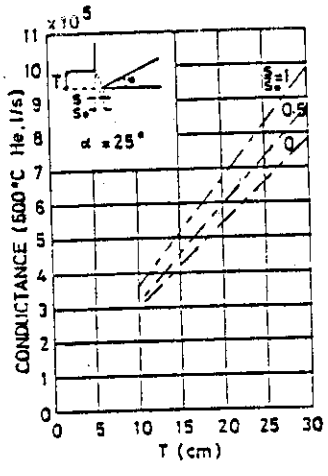

Fig.5-a

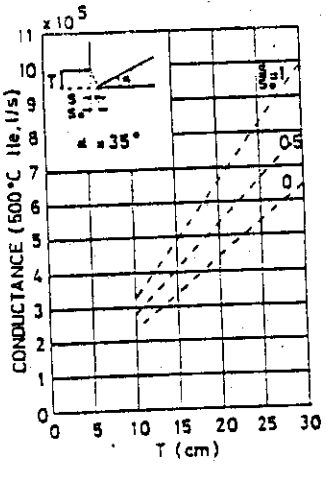

Fig.5-b

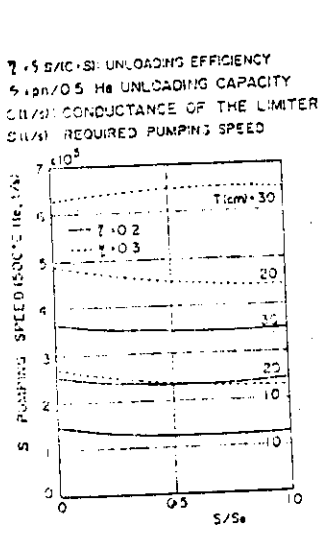

Fig.6-a

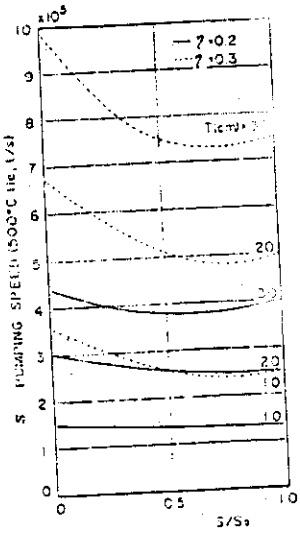

Fig.6-b

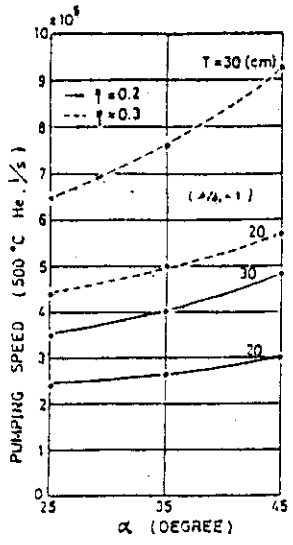

Fig.7

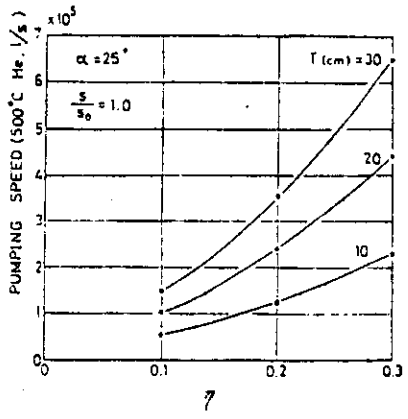

Fig.8-a

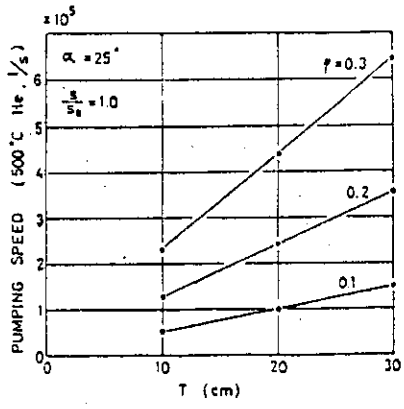

Fig.8-b

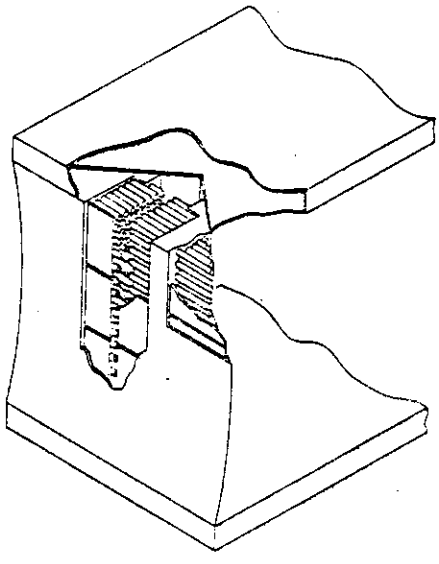

Fig.9

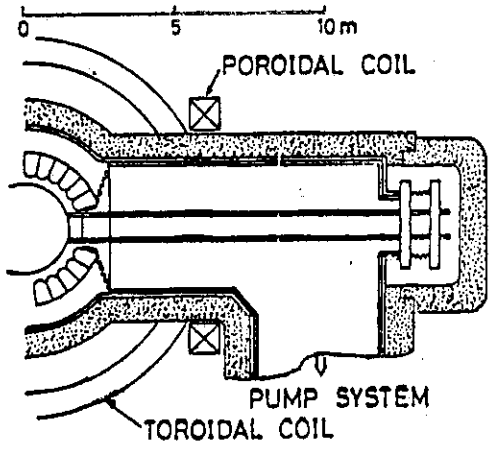

Fig.11

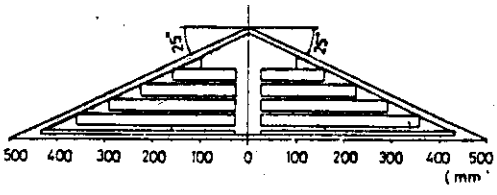

Fig.10

6 - 1 Numerical Simulation of Impurity Transport in Tokamaks

T. Amano

Plasma Physics Laboratory, Faculty of Engineering

Osaka University

§1. Introduction

It is of critical importance to understand correctly the impurity transport in tokamaks for the realization of efficient fusion reactors. In this paper, we describe our attempts to understand impurity behaviors in tokamak plasmas by utilizing an impurity transport simulation code[1),2)]. In the code, we solve the coupled rate and diffusion equations for the impurity ions. For the neoclassical diffusion coefficients, we adopt Hirshman's calculation[3),4)] in which the impurity ions are in the Pfirsh-Schlüter collisional regime while the plasma ions are either in the Pfirsh-Schlüter or in the plateau banana regime. We add an empirical anomalous diffusion flux proportional to the impurity density gradients. We can use the code to solve the impurity transport equations when the plasma profiles such as Ne(r,t), Te(r,t), Ti(r, t) are specified externally. Alternatively, the code can be combined with a tokamak transport code which solve the plasma density, current and temperature equations taking into account of impurity radiation energy losses.

§2 describes the results of simulation of the Argon injection experiment in T-4 tokamak[5),6)]. §3 desctibes the analysis of the behavior of oxygen impurity in JIPPT-2 tokamak[7),8)].

§ 2. Argon injection in T-4 tokamak

In T-4 tokamak[1], neutral Argon atoms were injected into a helium plasma and the several Argon line radiations were measured. Especially, Ar 16^+ line was measured both temporally and spatially. Behavior of such a highly ionized ion is relatively insensitive to the change of the plasma edge density and temperature, which usually is not measured well, and thus is suited for the comparison between theory and experiment.

We assume the coronal equilibrium for the oxygen ions, and the amount of oxygen is determined from the experimentally estimated $Ze_{ff}=3$. Experimentally measured Te, Ti, Ne are used; $Te(r)=1100(1-r^2/17^2)^3$, $Ne(r)=2.1 \times 10^{13}(1-r^2/17^2)$, $Ti(r)=400x(1-r^2/15.5^2)+10$. We puff the neutral Argon into the Helium plasma for an interval of 1 msec.

In Fig.1 is shown the comparison between the measured and computed profiles of Ar 16^+(3Å) line. The lower three curves correspond to t=20 msec after the injection and the upper three curves to t=40 msec. From Fig.1, it is seen that the neoclassical diffusion alone cannot explain the experimentally observed peaking of Ar 16^+ line. The addition of small anomalous diffusion coefficient $D_A=10^3 cm^2/sec$ contributes to the flattening of Ar 16^+ distribution near the center with leading to the peaking of 3Å line whose excitation energy is about 4 KeV. To check sensitivity the computed results on the reaction rates, the ionization rate was doubled and the recombination was reduced by factor 5. In this case, Ar 16^+ line did not peak for purely neoclassical diffusion coefficient.

Figs.2a, 2b, 2c show the time behavior of the experimental and computed Ar 15^+(362Å), Ar 15^+(23Å), Ar 16^+(4Å) lines integrated along the line of sight, respectively. The dasned curves are the experimental results, △ curves are calculated ones with purely neoclassical diffusion coeffisients and ○ curves are calculated ones with the neoclassical and anomalous diffusion coefficients, $D_A=10^3 cm^2/sec$. In Fig.2c, we find that for purely neoclassical case, the rise time of Ar 16^+ line is slow in the beginning, but the line intensity continues to rise without saturation. By including anomalous diffusion, we can explain the quick rise and the subsequent saturation of experimental profile. In Figs.2 x-curves are the result computed without the temperature screening term and without the anomalous diffusion. The ▽ curves are computed ones by assuming all the plasma ions are in Pfirsh-Schlüter regime.

§ 3. Analysis of oxygen impurity behavior on JIPPT-2

In JIPP T-Ⅱ tokamak experiment, resonance lines of oxygen ions (OⅡ - OⅧ) are observed by a 2 m grazing incidence spectrometer which covers the wavelength range from 15 to 1300 Å along a chord passing through the plasma axis. Spatial profiles of OⅣ, OV and OⅥ lines are also measured in the UV region[1]. We investigate numerically the radial behavior of these lines by means of the impurity transport code. We specify the total amount of oxygens by an effective ionic charge that is estimated from the experiment. In order to obtain a stationary state the outflux at the edge is replaced by the same amount of neutral atom influx, whose velocity cannot be known from the observation.

The computation taking account of neoclassical transport only cannot explain the observed line intensities. This is because the

oxygens concentrate to the center in this case and low ionized ions remain very few at the edge region. It is interpreted by little outward diffusion flux, in other words, by a slow recycling. Including of an anomalous diffusion improves the numerical results. We adopt the anomalous diffusion coefficient proportional to the inverse of electron density. The magnitude of this diffusion coefficient D_a and the neutral atom influx velocity V_0 are used as our simulation parameters. Fig.3 shows chord-integrated line intensities in the steady state obtained from computations with a fixed value of D_a, which is found to give reasonable results, and several values of V_0. The measured line intensities are also shown by filled circles.

Computed results with V_0=50 - 100 eV agree the measured ones within a factor of 2 except the line from OII which actually is very weak to measure. It is seen that the line intensities from low ionized ions are high when the influx velocity is low. This is considered that the constant influx requires higher neutral atom density for lower velecity; hence more amount of low ionized ions is produced near the edge to yield more line intensities from these ions. The lines from highly ionized ions are irrespective of the change in V_0 since those ions occupy most part of ionized oxygens. Spatial distributions of each ionized ion are shown Fig.4.

References

1) M.Okamoto and T.Amano, Computational Physics 26 (1978) 80.

2) T.Amano and E.C.Crume, ORNL/TM-6363.

3) S.P.Hirshman: Physics of Fluids 20 (1977) 589.

4) R.J.Hawryluk et al: Nuclear Fusion 19 (1979) 607.

5) V.A.Abramov et al: Controlled Fusion and Plasma Physics (Proc.

8th Europ. Conf. Prague) Vol.1 (1977) 30.

6) T.Amano, M.Kako and E.C.Crume: to be presented at International Conference on Plasma Physics -1980 April, Nagoya.

7) K.Toi et al: IPPJ-372 March 1979.

8) T.Kato et al: to be presented at International Conference on Plasma Physics -1980 April, Nagoya.

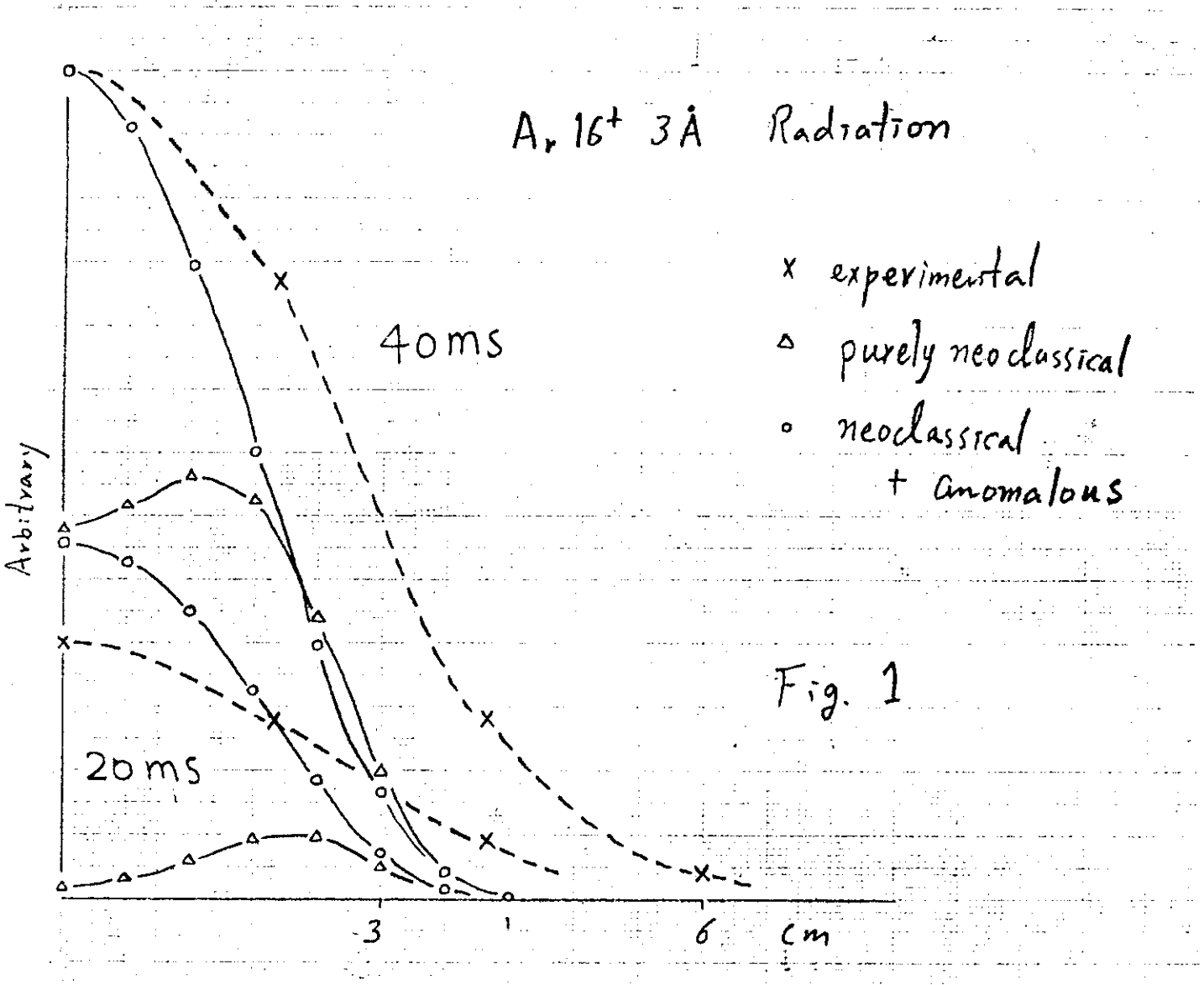

Fig. 1

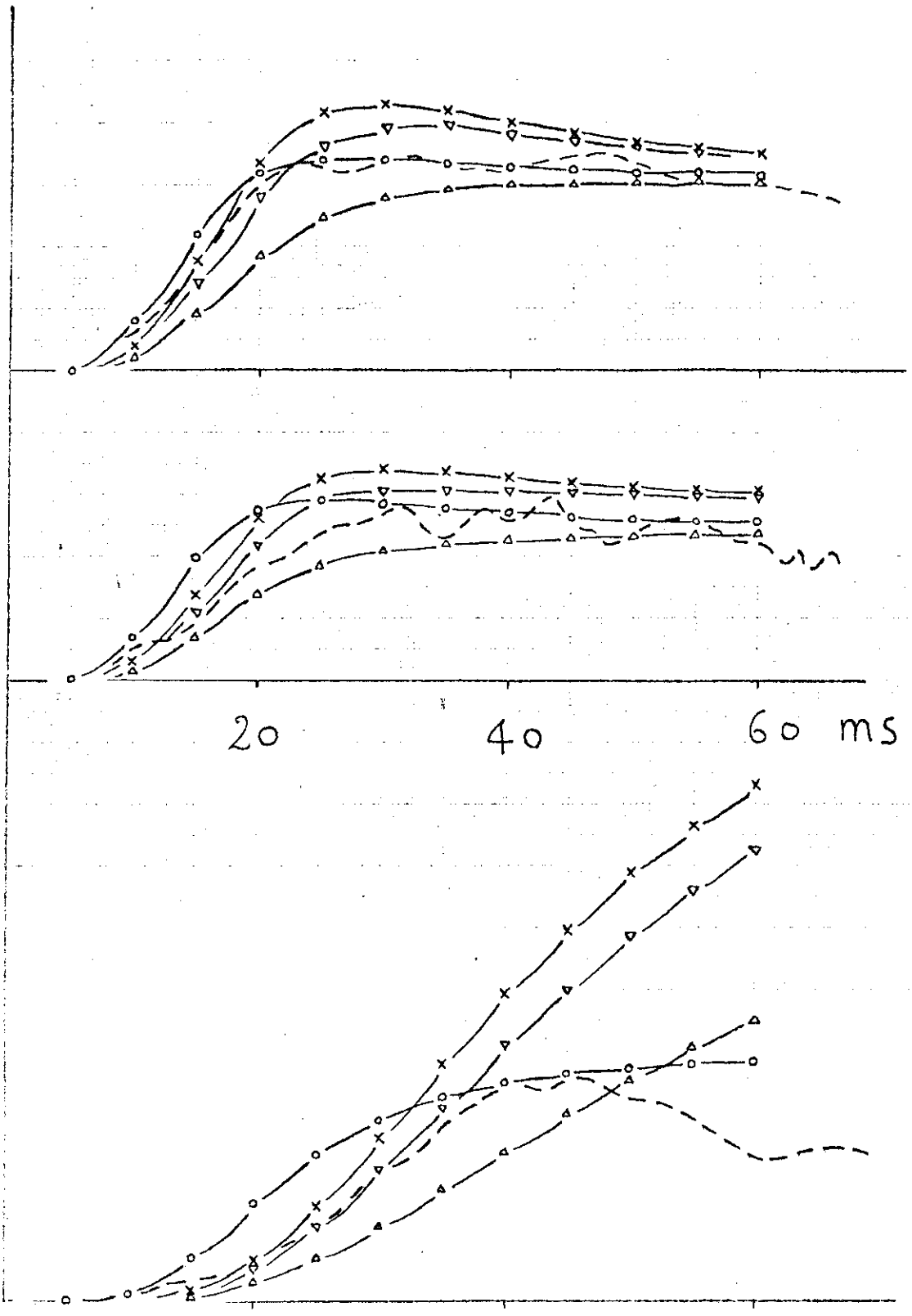

Fig. 2

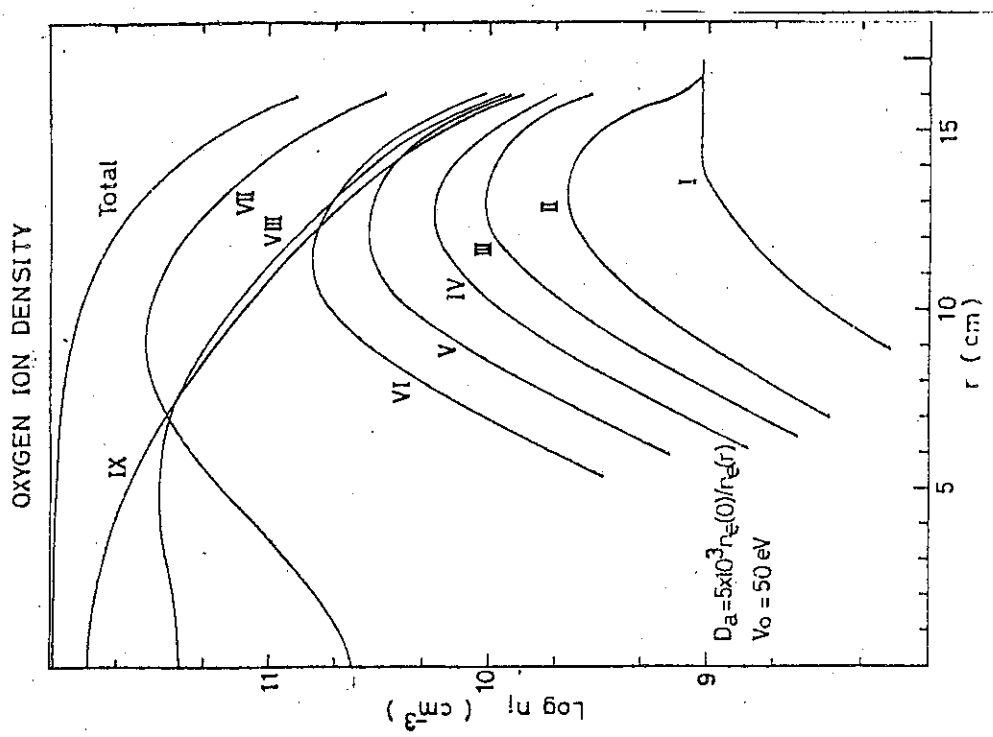

Fig.4 Spatial density profiles of oxygens

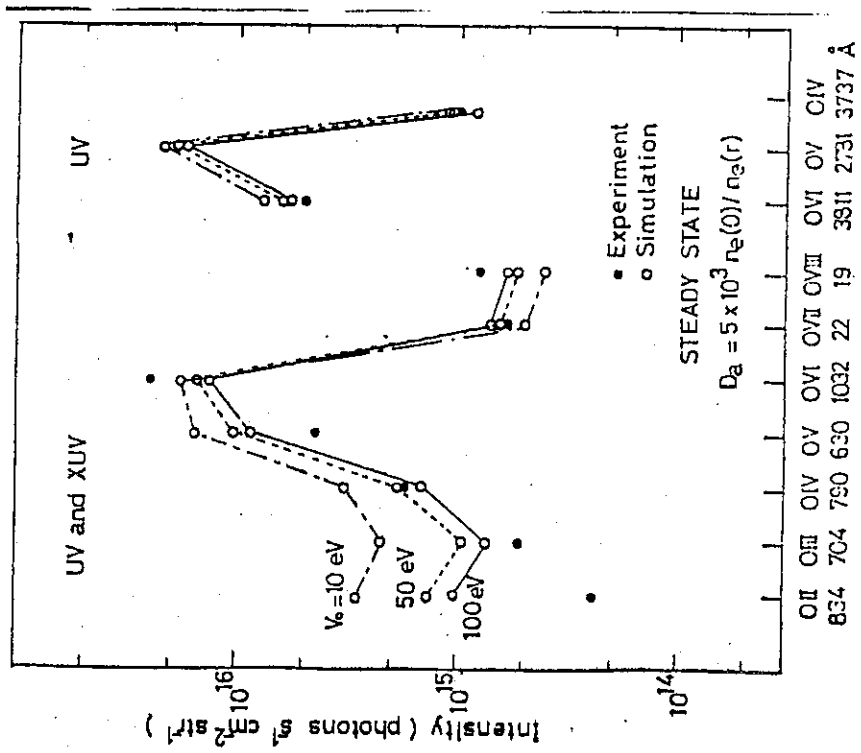

Fig.3 Line intensities from oxygen ions

6 - 2 Numerical Calculations of Helium Ash Enrichment and Exhaust by a Simple Divertor

Yasushi SEKI, Yasuo SHIMOMURA, Koichi MAKI* and Masafumi AZUMI

Japan Atomic Energy Research Institute,

Tokai-mura, Naka-gun, Ibaraki-ken,

Japan

ABSTRACT

A simple poloidal divertor which can enrich and exhaust helium ash has been proposed for an INTOR size reactor. Monte Carlo simulations are carried out to investigate the motion of DT fuel and He ash particles after they are re-injected from the divertor neutralizer plate. Helium ash exhaust was shown to be feasible with a modest pumping speed of 5×10^5 ℓ/s for most of the conceivable plasma particle containment conditions.

* On leave from Energy Research Laboratory, Hitachi, Ltd., Hitachi, Japan

6-3 Particle Simulation of Scrape-off Plasmas in a Poloidal Divertor Tokamak

T. Takizuka & M. Azumi
Japan Atomic Energy Research Institute

—

- Potential distribution
- Density "
- Flow velocity "
- Velocity distribution function

→
- Analysis of experimental results
- Monte Carlo calculations of impurities

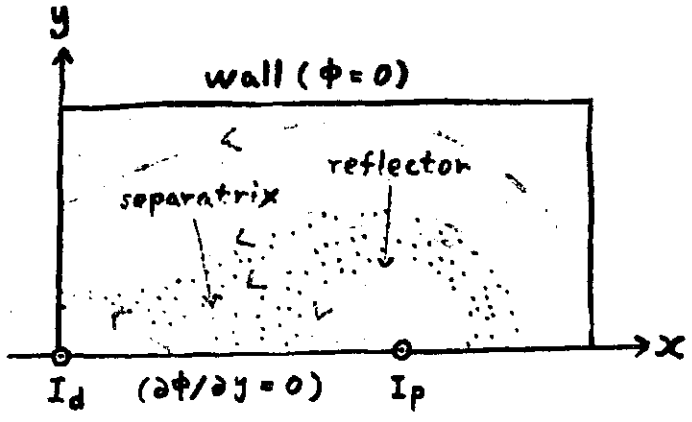

- neglect the toroidicity B_ξ = const.
  up-down symmetry
- 2 dimension : poloidal divertor
- line plasma current + divertor current

$$B_x \propto -\left(\frac{I_d}{I_p}\frac{y}{x^2+y^2} + \frac{y}{(x-x_p)^2+y^2}\right)$$

$$B_y \propto \frac{I_d}{I_p}\frac{x}{x^2+y^2} + \frac{x-x_p}{(x-x_p)^2+y^2}$$

$$\sqrt{B_x^2+B_y^2}\Big|_{\text{reflector}} \ll B_\xi$$

(reflector is set artificially)

• Motions parallel to B and Electrostatic field are self-consistently calculated by using PIC method (collisionless)

$$\frac{dv_{\parallel}}{dt} = -\frac{e_j}{m_j}\frac{\vec{B}}{B}\cdot\vec{\nabla}\phi \qquad \frac{d\vec{r}}{dt} = \frac{\vec{B}}{B}v_{\parallel}$$

$$-\nabla^2\phi = \frac{e}{\epsilon_0}(n_i - n_e)$$

★ Particle In Cell method

- spacial grid

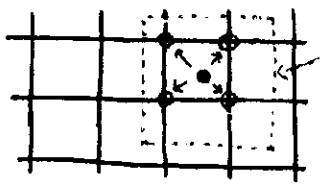

· Finite Sized Particle

- sharing the charge density
- Poisson's equation (difference equation)

$$\frac{\partial^2\phi}{\partial x^2} \rightarrow \frac{1}{\Delta^2}(\phi_{i+1} - 2\phi_i + \phi_{i-1})$$

$$\frac{\partial\phi}{\partial x} \rightarrow \frac{1}{2\Delta}(\phi_{i+1} - \phi_{i-1})$$

- averaging the electric field

• Cross field diffusions are simulated by using a Monte Carlo method

$$D_{\perp} = \frac{\langle\delta^2\rangle}{\Delta t}$$

δ : nearly Gaussian random valuable ($\langle\delta\rangle = 0$)

$$\delta_x = \frac{B_y}{\sqrt{B_x^2 + B_y^2}}\delta \qquad \delta_y = \frac{-B_x}{\sqrt{B_x^2 + B_y^2}}\delta$$

t=0 Initial condition

↓

Sharing the change

↓

Poisson's equation

↓

Parallel motions

↓

Cross field diffusions

↓

$t \leftarrow t + \Delta t$

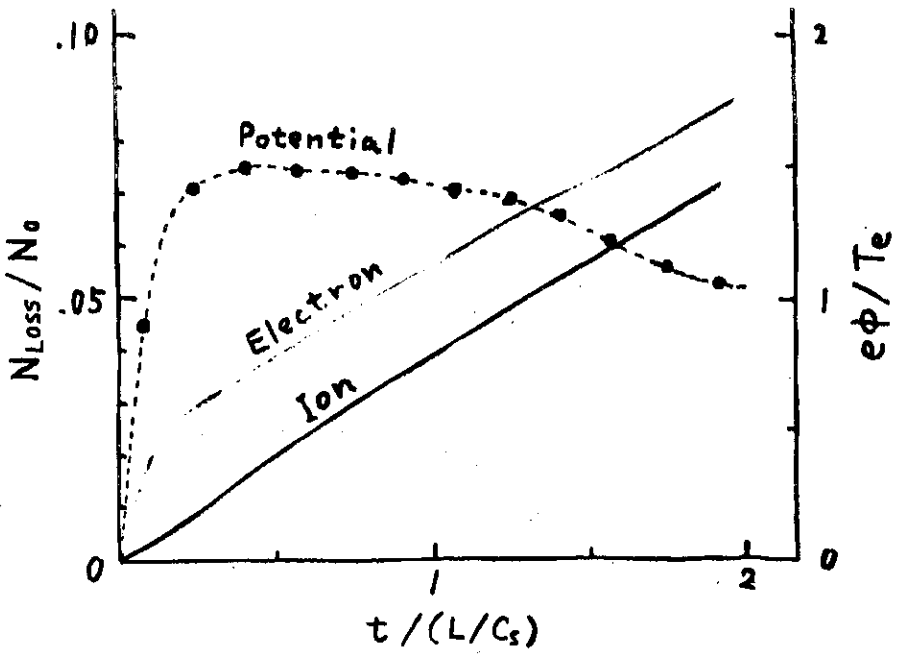

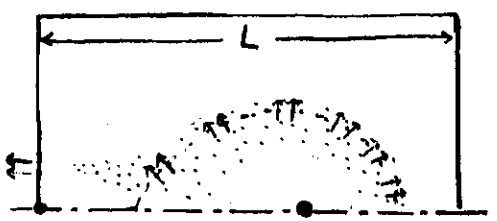

- boundary condition for particles absorbed into wall (2ndary emition etc. are neglected)

Simulation parameters

$L/\lambda_D = 64$	→ 128	
$I_d/I_p = 0.5$		
$T_i/T_e = 0$		· $T_i/T_e \neq 0$
$m_i/m_e = 100$		· $m_i/m_e > 100$
$D_\perp \simeq 10^{-3} L C_s$		· some $D_\perp$
$N_0 = 5000$	→ ~20000	

• Equi- Potential Curve $(t \sim 2L/C_s)$

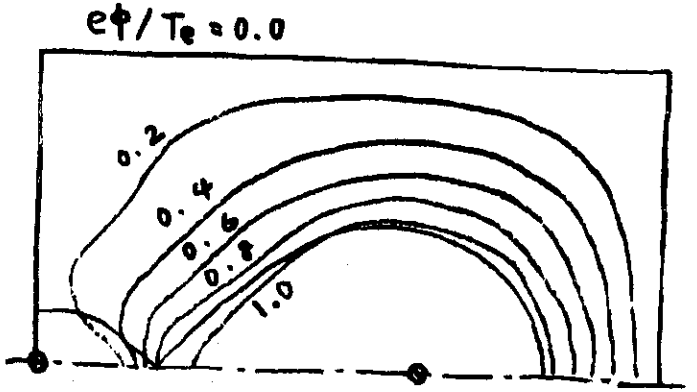

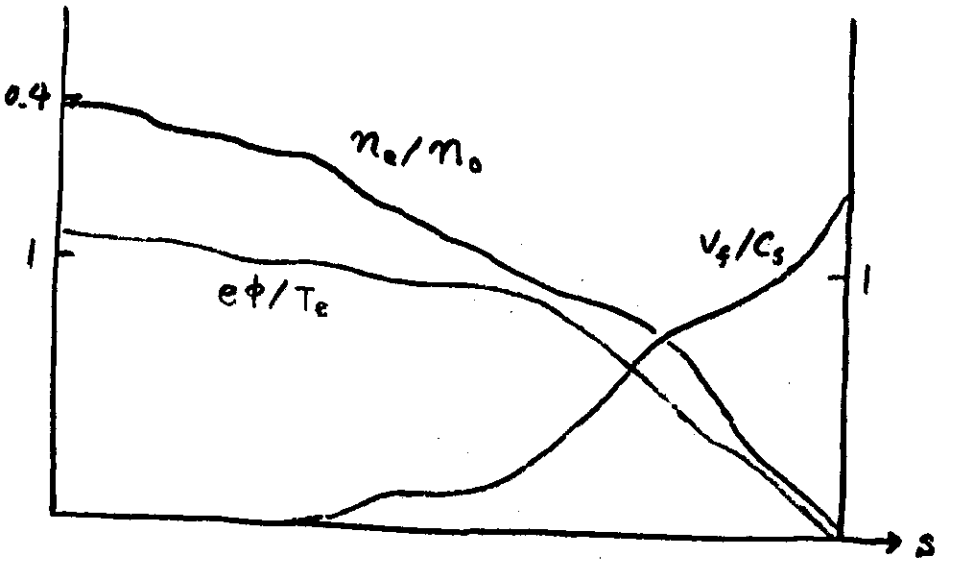

• Flow Velocity $(t \sim 2L/C_s)$

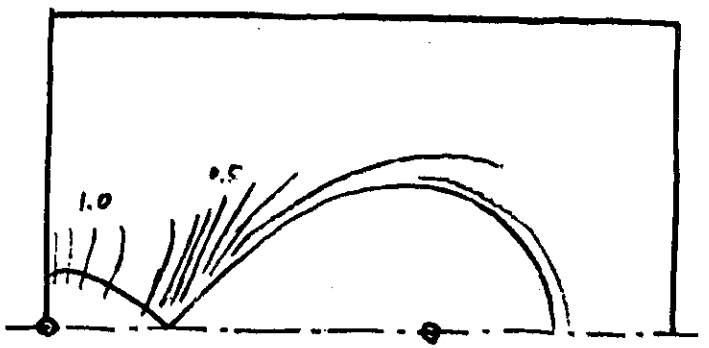

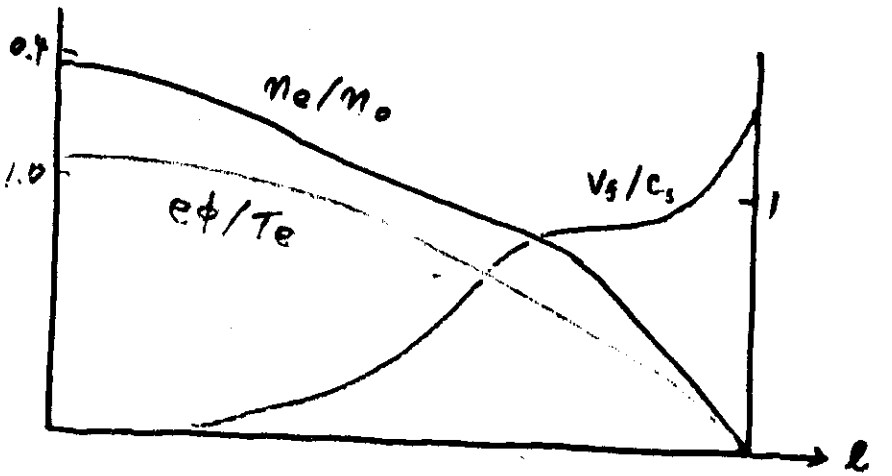

along a magnetic line of force near the separatrix

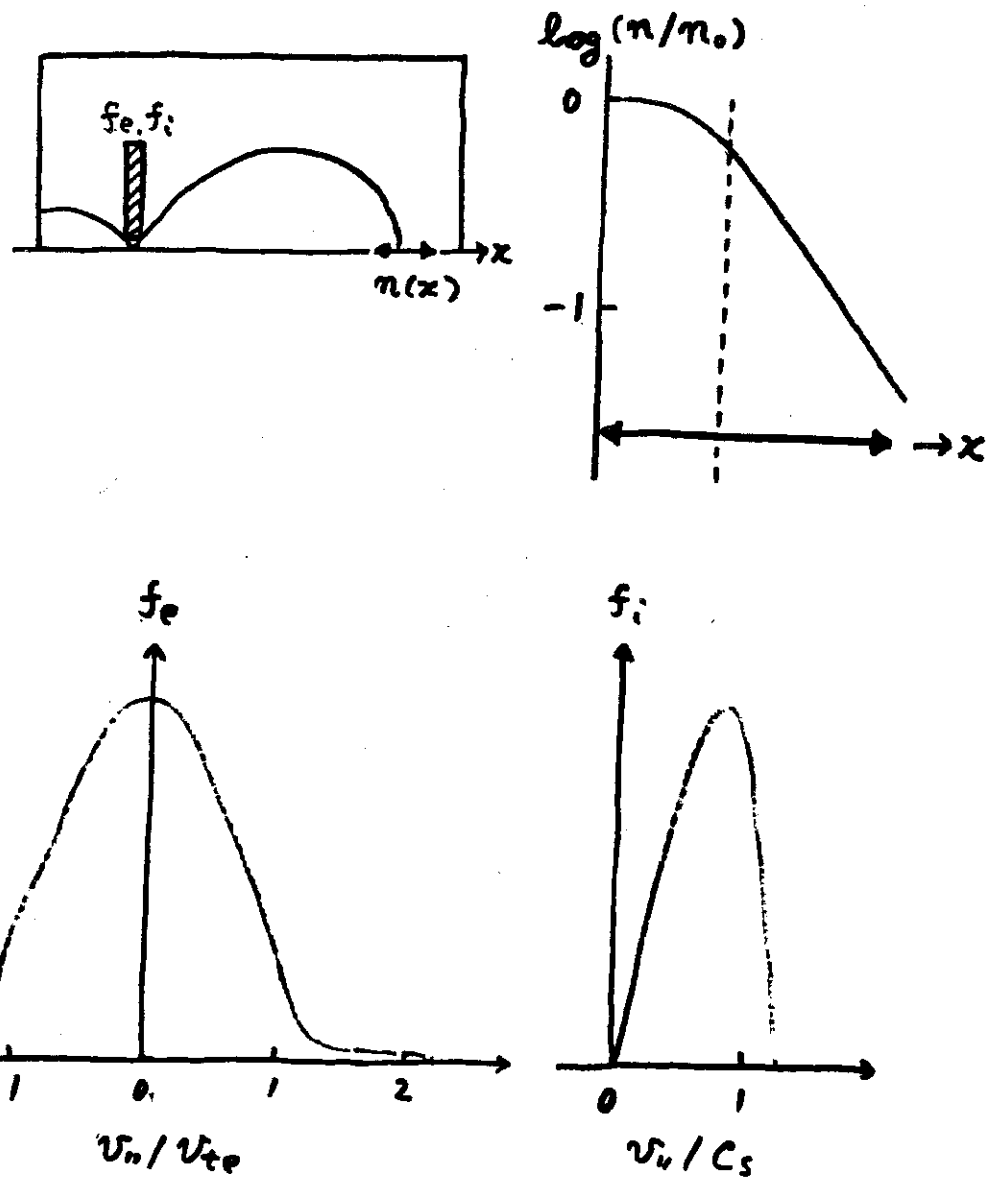
f_e, f_i
x
n(x)
log (n/n₀)
0
-1
x
f_e
-1
0
1
2
v_n / v_{te}
f_i
0
1
v_u / C_s

6 - 4 Analysis of Impurity and α-Particle Recyclings in a Tokamak Plasma with Particle Balance Equations

T. Kawamura, A. Miyahara and K. Okamoto*

Institute of Plasma Physics, Nagoya University, 464 Nagoya, Japan

* ULVAC Corporation, 253 Kanagawa, Japan

Abstract

Stationary concentration of impurities and α-particles in a Tokamak fusion plasma is investigated on the basis of the particle balance model. The relations between some system parameters and the fractions of impurities and α-particles relative to the fuel ions are calculated and the effects of the limiter on plasma contamination are analysed.

§1. Introduction

The recyclings of fuel particles (D and T), impurities and α-particles between the plasma and the first wall or the limiter are important problems for long time operation in a magnetic fusion device, because the particle confinement time is finite in any case of a magnetic fusion experiment owing to the particle diffusion across the magnetic field.

In this work the particle fluxes of fuel ions, impurities and α-particles to the first wall in the stationary state are calculated on the basis of the particle balance model,[1] and the steady fractions of impurities and α-particles relative to the fuel particles are estimated, and the effects of the limiter on the plasma contamination are also clearified.

§2. Recycling of Fuel Particles

The loss flux of fuel ions ϕ_D^+ from the plasma to the wall

owing to the diffusion across the magnetic field is expressed as

$$\phi_D^+ = \frac{n_D}{\tau_D} \cdot \frac{V}{S} \quad , \qquad (1)$$

where n_D and τ_D is the average DT density and the particle confinement time for fuel ions, and V and S are the total plasma volume and the total plasma surface area that is assumed to be nearly equal to the first wall area. Because the scrape-off layer exists between the plasma surface and the first wall, a fraction ε_D of the flowing fuel ions to the wall is guided to the limiter along the magnetic lines of force, and a fraction ζ_D of fuel particles comes back to the plasma from the limiter as neutrals. Therefore a fraction $1-\varepsilon_D$ of fuel particles reaches the first wall and is considered to go back to the plasma from the wall as a low energy neutral flux with a multiplication factor r_D owing to backscattering, evaporation or other processes. A fraction ε_D' of this returning neutral flux is ionized and guided to the limiter within the scrape-off layer. A neutral fuel particle coming back to the palsma from the wall or the limiter produces a high energy neutal from the plasma to the wall owing to the charge exchange process with a probability A.

The refuelling current, which is necessary because of the finiteness of the confinement time of fuel ions in the plasma, also produces additional contribution to the charge exchange neutral flux to the wall with a probability A_R that is distiguished from A considering the different refuelling conditions.

Using these system parameters the fuel particle influx ϕ_D^{in} to the first wall in the stationary state is obtained from the particle balance equations as[2)]

$$\phi_D^{in} = K_D \phi_D^+ \tag{2}$$

with

$$K_D = \frac{1 - \varepsilon_D\{1 - A\zeta_D - A_R(1 - \zeta_D)\} + A_R f_b}{1 - A\{1 - \varepsilon_D'(1 - \zeta_D)\}r_D - A_R\{1 - r_D + \varepsilon_D'(1 - \zeta_D)r_D\}} \tag{3}$$

where f_b is the burning fraction of DT ions relative to the loss flux ϕ_D^+ and is given by $f_b = n_D \tau_D \langle\sigma v\rangle_{DT}/2$ in which $\langle\sigma v\rangle_{DT}$ is the DT reaction rate for equal densities of D and T ions.

In the following analyses we take $r_D = 1$ and $\varepsilon_D = 1$ assuming the steady wall deposition of fuel particles and the sufficiently broad limiter, and also take $A_R << A$ assuming the high energy neutral injection, and $A = 0.4$ for $T_e = T_i \simeq 10$ keV, then we have $K_D \simeq 0.7\ \zeta_D/\{1 + 0.7\varepsilon_D'(1 - \zeta_D)\}$. The other system parameters strongly depend on the scrape-off layer plasma condition and the ability of the exhaust system. The fuel particle current F_D^L into the limiter is given by $F_D^L = (1 + \varepsilon_D' K_D)\phi_D^+ S$ ($K_L \equiv 1 + \varepsilon_D' K_D$).

§3. Generation and Recycling of Impurities

The impurity particles are generated by sputtering due to fuel particles and other erosion processes at the first wall as well as the solid limiter in case. We distinguish the impurities originated from the wall and those from the solid limiter. For respective loss flux from the plasma we have $\Phi_W = (n_W/\tau_W)(V/S)$ and $\Phi_L = (n_L/\tau_L)(V/S)$, where the suffix W stands for the wall impurities and L does for the limiter impurities. The system parameters for impurities like as descrebed in §2 for fuel particles are also introduced and indicated by the suffix W or L. We also assume $\varepsilon_W = \varepsilon_L = 1$ for the sufficiently broad limiter. Then, at the stationary state we have the following results for the fractions of impurities relative to the fuel ion density from the particle balance equations:

$$\frac{n_W}{n_D} = K_W K_D S_{D,W} \frac{\tau_W}{\tau_D} \quad , \quad \left(K_W = \frac{1}{1 - \zeta_W} - \varepsilon'_W \right) \quad , \tag{4}$$

$$\frac{n_L}{n_D} = \frac{\zeta_L}{1 - \zeta_L S_{L,L}} \left(K_L S_{D,L} + \frac{1}{1 - \zeta_W} K_D S_{D,W} S_{W,L} \right) \frac{\tau_L}{\tau_D} \quad , \tag{5}$$

where $S_{D,W}$ is the average sputtering yield of wall impurities due to a fuel particle at the wall, $S_{D,L}$ and $S_{w,L}$ are the ones of limiter materials due to a fuel particle and due to a wall impurity particle at the limiter respectively, and $S_{L,L}$ is the average self-sputtering yield at the limiter. If we consider the magnetic limiter with a divertor, we may use Eq.(4) only for the impurities originated from the wall materials.

The characteristic features for the solid limiter[3] are as follows. If $\zeta_L S_{L,L} \geq 1$, the stationary state of the limiter impurities does not exist. The condition that ζ_W should be as small as possible is necessary for the wall impurities as well as for limiter impurities, because the limiter material sputtering due to the wall impurities becomes serious if ζ_W is not so small.

§4. α-particles

The α-particles from the DT reaction could be treated as a sort of impurities so far as the sputtering at the wall and the limiter if they would be well confined and thermalized until they rise to the plasma surface. The effect of the burning fraction f_b on K_D is small if we assume $A_R << A$. We may take $\phi_\alpha = (n_\alpha/\tau_\alpha)(V/S)$ for the α-particle loss flux from the plasma, we have

$$\frac{n_\alpha}{n_D} = K_\alpha \frac{\tau_\alpha}{\tau_D} \quad ; \quad K_\alpha = \frac{f_b/2}{1 - \zeta_\alpha \varepsilon_\alpha - (1 - \varepsilon_\alpha)\{1 - \varepsilon'_\alpha(1 - \zeta_\alpha)\} r_\alpha} \tag{6}$$

where the meanings of system parameters are same as in §2. In the case that $\varepsilon_\alpha = 1$ for the broad limiter the fraction of α-particles in the plasma becomes

$$\frac{n_\alpha}{n_D} = \frac{f_b}{2(1 - \zeta_\alpha)} \frac{\tau_\alpha}{\tau_D} \quad . \tag{7}$$

The sputtering due to α-particles appears as an additional term $K_\alpha S_{\alpha,L}$ in the brackets of Eq.(5). The serious effect of thermalized α-particles is the nuclear power diminution when the fraction n_α/n_D becomes a considerable value.

§5. Discussion

In the steady state of the plasma the neutral fuel particles of high energies due to charge excharge bombard the wall even if the limiter has sufficiently broad width and generate the impurities of the wall origin. The impurity-impurity sputtering at the solid limiter is much serious if it is in case. Therefore, the values ζ_W and ζ_L which depend on the exhaust ability become very important for suppression of heavy impurities.

The impurity and α-particle concentrations have the power dimunution effects other than the radiation cooling. The suppression and exhaust of impurities and α-particles are urgent problems for the fusion studies.

References

1) R. Behrisch and B. B. Kadomtsev, Plasma Physics and Controlled Nuclear Fusion Research, 1974 Tokyo, IAEA (1975) 2, 229.
H. Vernickel et al. Proc. of the Int. Symp. on Plasma-wall Interaction, 1976 Jülich, Pergamon Press, 208.

2) T. Kawamura et al. Kakuyugo-kenkyu, 43 (1980) 145 in Japanese.

3) Y. Gomay et al. Japan. J. of Appl. Phys. 18 (1979) 1317.

7 - 1

Overview of U.S. Program on Plasma/Material Interaction*

Robert A. Langley

Oak Ridge National Laboratory†
Oak Ridge, Tennessee 37830 U.S.A.

The U.S. plasma/material interaction program is a coordinated effort involving many institutions. The community underwent a self-study and evaluation in 1977. The product of this study was a program plan that attempted to deal with the orientation of the program for the succeeding five years by defining the problem and setting major milestones.[1] This was accomplished through the use of a task group arrangement. The present members of the task group and their responsibilities are shown in Fig. 1 along with the sub task group members and their affiliations. Subsequent to the publication of the program plan, workshops were held on relevant topics. These were:

- the First Wall Coating Workshop,[2]
- the Arcing Phenomena in Fusion Devices Workshop,[3]
- the Workshop on New Diagnostics Related to Impurity Release,[4]
- the Workshop on Sputtering Caused by Plasma (Neutral Beam)-Surface Interaction,[5] and
- the Workshop on Hydrogen Recycling.[6]

This paper briefly describes these workshops and illustrates relevant areas of work by examples of ongoing studies. The ongoing studies are presented as copies of the viewgraphs after the numbered figures. The coating program is described in an accompaning paper[7] and is not covered here.

*Research sponsored by the Office of Fusion Energy (ETM), U. S. Department of Energy.

†Operated by Union Carbide Corporation under contract W-7405-eng-26 with the U. S. Department of Energy.

The purpose of the Arcing Phenomena in Fusion Devices Workshop is shown in Fig. 2, while Figs. 3 and 4 answer the question "What do we know from observations of arcing in tokamaks and ion sources?" Figures 5, 6, and 7 attempt to answer the questions "What can be inferred from vacuum arc observations?" and "What are the unresolved questions concerning arcing phenomena in fusion devices?", respectively. The objectives of the Workshop on New Diagnostics Related to Impurity Reslease are shown in Fig. 8. While the first two objectives were attained, the third was not completed in detail. The objectives of the Workshop on Sputtering Caused by Plasma (Neutral Beam)-Surface Interaction are shown in Fig. 9, and the priorities for future experimental and theoretical work are shown in Fig. 10. The Workshop on Hydrogen Recycling detailed problem areas that require further attention; these are shown in Fig. 11.

In summary, the U.S. plasma/material interaction community has attempted to focus its efforts on the study of relevant phenomena and to continually evaluate its performance in accomplishing this goal.

REFERENCES

1. The Fusion Reactor Materials Program Plan. Section III: Plasma Material Interaction, DOE/ET-0032/3, U.S. Department of Energy (July 1978).

2. First Wall Coating Workshop, held at Albuquerque, New Mexico, January 31-February 1, 1978.

3. Arcing Phenomena in Fusion Devices Workshop, held at Oak Ridge, Tennessee, April 5-6, 1979.

4. Workshop on New Diagnostics Related to Impurity Release, held at Germantown, Maryland, May 31-June 1, 1979.

5. Workshop on Sputtering Caused by Plasma (Neutral Beam)-Surface Interaction, held at Argonne, Illinois, July 9-10, 1979.

6. Workshop on Hydrogen Recycling, held at Dublin, California, October 17-18, 1979.

7. R. A. Langley, "Review of U.S.A. Low-Z Coating Development Program," to be presented at this workshop.

(References 1 and 3-6 can be obtained from:

National Technical Information Service,
U. S. Department of Commerce,
5285 Port Royal Road,
Springfield, Virginia 22161.)

PLASMA MATERIALS INTERACTION TASK GROUP

Walter Bauer, SLL - Chairman
Klaus Zwilsky, U.S. DOE - OMFE Representative
Kenneth Wilson, SLL - Secretary

Sub-Task Group Committees

1. Walter Bauer, SLL -	H Recycle: Reflection, Re-Emission/Trapping Desorption & Surface Chemistry	Tom Picraux, SLA Bob Clausing, ORNL David Lichtman, U of W Ed Thomas, GI of T
2. Sam Cohen, PPPL	Plasma Devices: Wall Conditioning & Wall Fluxes	Keith Burrell, GA Dick Colchin, ORNL Gil Emmert, U of W Alan Krauss, ANL Earl Marmar, MIT Bob Taylor, UCLA
3. Bob Conn, U of W	Plasma Impurity Effects & Reactor Requirements	Wayne Houlbert, ORNL Dick Post, PPPL Jahn Kahn, LLL
4. Mark Davis, SLA	Wall Modification: Coatings Development	John Tien, C U Mike Ulrickson, PPPL Maurice Sabado, GA S. Fixler, Grumman Aero George Fuller, McDD
5. Manfred Kaminsky, ANL	Erosion: Sputtering & Blistering	Joe Smith, GA Dieter Gruen, ANL Joe Cecchi, PPPL Lee Haggmark, SLL George Thomas, SLL Fred Vook, SLA
6. Bob Langley, ORNL	Diagnostics, Neutral Beam Effects & Special Surfaces	Keith Burrell, GA Will Stirling, ORNL Bill Cooper, LBL Charles Moeller, GA Bill Hooke, PPPL Bill Wing, ORNL

ARCING WORKSHOP

PURPOSE

THE WORKSHOP ON ARCING PHENOMENA IN FUSION DEVICES WAS ORGANIZED TO:

1) REVIEW THE PRESENT STATUS OF OUR UNDERSTANDING OF ARCING AS IT RELATES TO CONFINEMENT DEVICES,

2) DETERMINE WHAT INFORMATION IS NEEDED TO SUPPRESS ARCING AND

3) DEFINE BOTH LABORATORY AND IN-SITU EXPERIMENTS WHICH CAN ULTIMATELY LEAD TO REDUCTION OF IMPURITIES IN THE PLASMA CAUSED BY ARCING.

THE WORKSHOP WAS ATTENDED BY EXPERTS IN THE AREA OF VACUUM ARC ELECTRODE PHENOMENA AND ION SOURCE TECHNOLOGY, MATERIALS SCIENTISTS, AND BOTH THEORETICIANS AND EXPERIMENTALISTS ENGAGED IN ASSESSING THE IMPORTANCE OF "UNIPOLAR" ARCING IN TODAY'S TOKAMAKS.

REVIEW OF DISCUSSIONS

WHAT DO WE KNOW FROM OBSERVATIONS OF ARCING IN TOKAMAKS AND ION SOURCES?
AT THE CLOSE OF THE FORMAL PRESENTATIONS AN ATTEMPT WAS MADE TO LIST THINGS THAT WE COULD ALL AGREE WERE KNOWN ABOUT THE ARCING PHENOMENA IN FUSION DEVICES.

1. IT WAS AGREED THAT ARCING IS WIDELY OBSERVED IN TOKAMAKS AND THAT IT IS A NORMAL RATHER THAN AN UNUSUAL OCCURRENCE.
2. IT CAN BE SHOWN THAT THE VOLUME OF MATERIALS EJECTED FROM ARC CRATERS CAN PRODUCE ENOUGH IMPURITIES TO ACCOUNT FOR ALL OF THE METAL IMPURITIES IN THE PLASMA. IT CANNOT BE STATED, HOWEVER, THAT THE METAL IMPURITIES IN THE PLASMA ARE DERIVED FROM ARCING PHENOMENA SINCE LITTLE IS KNOWN ABOUT THE TRANSPORT OF MATERIALS FROM THE PLASMA EDGE TO ITS CENTER AND THUS FAR THERE HAS BEEN NO CORRELATION OF THE PRESENCE OF IMPURITIES IN THE CENTRAL PLASMA WITH ARCING PHENOMENA.
3. DATA FROM TIME-RESOLVED EXPERIMENTS IN THE DITE TOKAMAK AND ISX-B INDICATE THAT ARCING IS MOST LIKELY TO OCCUR DURING PERIODS OF PLASMA INSTABILITY AND MHD ACTIVITY AT THE BEGINNING OR END OF DISCHARGES, ALTHOUGH THE STEADY STATE PORTION OF THE TOKAMAK PULSES IS NOT IMMUNE TO ARCING PHENOMENA.
4. THERE SEEMS TO BE GENERAL AGREEMENT, ALTHOUGH LITTLE PROOF, THAT CONDITIONING PROCESSES DO OCCUR IN TOKAMAKS AND THAT ARCING GENERALLY DIMINISHES AS A FUNCTION OF TIME AND PLASMA OPERATION. THERE IS DATA FROM LABORATORY EXPERIMENTS WHICH CLEARLY SHOWS THAT CONDITIONING CAN OCCUR.
5. THERE ARE A NUMBER OF SIMILARITIES BETWEEN VACUUM ARCS AND "UNIPOLAR ARCS," AND THE RATHER EXTENSIVE LITERATURE ON VACUUM ARCS CAN THUS SUPPLY USEFUL GUIDANCE FOR THE STUDIES OF "UNIPOLAR" ARCS IN TOKAMAKS.

6. BOTH VACUUM ARCS AND ARCS OBSERVED IN TOKAMAKS APPEAR TO MOVE IN A RETROGRADE DIRECTION, I.E., THE ARC COLUMN MOVES IN A DIRECTION OPPOSITE TO THE ELECTROMOTIVE FORCE $\vec{J} \times \vec{B}$).
7. ARC CRATERS CAUSED BY VACUUM ARCS AND "UNIPOLAR" ARCS APPEAR TO BE VERY SIMILAR IN SIZE AND SHAPE. ARC CURRENTS (PER CATHODE SPOT) ARE APPARENTLY ABOUT THE SAME (FROM < 10 A TO ~100 A MAX). CURRENT DENSITIES IN THE ARC CRATERS ARE IN THE RANGE FROM 10^4 TO 10^9 A/cm^2.
8. UNIPOLAR ARCING IS A SERIOUS PROBLEM IN THE ION SOURCES OF NEUTRAL BEAM INJECTORS. SOURCE "CONDITIONING" IS ALWAYS REQUIRED AND IS A TIME CONSUMING NUISANCE AT BEST. SOMETIMES THE PROBLEMS ARE SO SEVERE THAT THEY COMPLETELY PREVENT THE OPERATION OF AN ION SOURCE.

WHAT CAN WE INFER FROM VACUUM ARC OBSERVATIONS?

BASED ON THE SIMILARITIES BETWEEN VACUUM ARCS AND THE ARCS OBSERVED IN ION SOURCES AND TOKAMAKS, THE WORKSHOP CONCLUDES THAT THE FOLLOWING INFORMATION OBTAINED FROM VACUUM ARC STUDIES IS PROBABLY APPLICABLE TO ARCING IN FUSION DEVICES.

1. ARCS WILL PRODUCE AT LEAST ONE ION PER 20 ELECTRONS IN THE ARC COLUMN. THE MAXIMUM YIELD OF IONS AND IMPURITY ATOMS MAY BE MUCH HIGHER THAN THIS AND DEPENDS UPON THE PROPERTIES OF THE MATERIAL. ALTHOUGH IONS ARE EJECTED PERPENDICULAR TO THE SURFACE, DROPLETS TEND TO BE EJECTED PARALLEL TO THE SURFACE.
2. TOPOGRAPHY AND SURFACE CONDITIONS ARE IMPORTANT AND INFLUENCE BOTH THE ARC INITIATION AND PROPAGATION PROPERTIES.
3. THERE SEEMS TO BE GENERAL AGREEMENT THAT ARC INITIATION IS PROBABLY EASIER ON DIRTY SURFACES BUT THAT DAMAGE TO THE DIRTY SURFACES MAY BE LESS.
4. THERMAL AND ELECTRICAL PROPERTIES ARE IMPORTANT MATERIALS' PARAMETERS, BECAUSE JOULE HEATING OF THE REGION IN THE BULK JUST BELOW THE CATHODE SPOT SEEMS TO BE VERY IMPORTANT IN CRATER FORMATION AND ARC PROPAGATION [SEE KIMBLIN'S PAPER (WESTINGHOUSE)].
5. THE MAXIMUM CURRENT PER ARC SPOT IS PROBABLY 100 A OR LESS AND THE MINIMUM VOLTAGES NEEDED TO SUSTAIN ARCS FOR VARIOUS MATERIALS ARE KNOWN [SEE KIMBLIN'S PAPER (WESTINGHOUSE)].

UNRESOLVED QUESTIONS CONCERNING ARCING PHENOMENA IN FUSION DEVICES

WE HAVE LISTED A NUMBER OF QUESTIONS WHICH SHOULD BE ANSWERED BY EXPERIMENTS AND MODELING. THEY ARE LISTED BELOW:

1. WHAT FRACTION OF IONS AND NEUTRALS FROM ARCS GET INTO THE PLASMA?
2. HOW FAR DO THESE IONS AND NEUTRALS PENETRATE INTO THE PLASMA; DO THEY GET INTO THE CENTRAL CORE?
3. IS THE ROLE OF DROPLETS EJECTED FROM ARC CRATERS A SIGNIFICANT IMPURITY INJECTION MECHANISM?
4. WHY DO ARCS MOVE IN A RETROGRADE DIRECTION IN MAGNETIC FIELDS?
5. WHAT ARE THE DISIMILARITIES BETWEEN VACUUM AND "UNIPOLAR" ARCS? WE KNOW THE DRIVING SOURCES ARE DIFFERENT, BUT DOES THIS PRODUCE SIGNIFICANT DIFFERENCES IN ARC INITIATION OR PROPAGATION?
6. HOW DOES ARC INITIATION DEPEND UPON MAGNETIC FIELD, SURFACE CONDITIONS, ELECTRIC FIELDS, TEMPERATURE, INHOMOGENEITIES IN THE SURFACE, CLEANLINESS, ADSORBED GASES, ETC.?
7. WHAT MECHANISMS ARE IMPORTANT IN ARC INITIATION?
8. WHAT ARE THE "CHOPPING" LEVELS FOR ARCS AND HOW DOES THE MINIMUM CURRENT OR VOLTAGE REQUIRED TO SUSTAIN AN ARC DEPEND UPON MAGNETIC FIELDS AND MATERIALS PARAMETERS?
9. HOW IS THE ARC CURRENT (AS A FUNCTION OF TIME) RELATED TO THE TOPOGRAPHIC STRUCTURE WHICH IS SEEN AS FOSSIL EVIDENCE IN THE ARC TRAILS?
10. WHAT CAUSES THE TERMINATION OF ARCS?
11. WHAT HAPPENS TO THE ARC COLUMN AS IT GOES INTO THE TOKAMAK PLASMA, i.e., WHAT IS THE CURRENT PATH IN THE CENTRAL PLASMA; WHAT DOES THE COMPLETE CIRCUIT LOOK LIKE; WHAT ARE CURRENT DENSITIES AND VOLTAGES?
12. WHAT ARE THE MECHANISMS OF SURFACE CONDITIONING WHICH RESULT IN DECREASED FREQUENCY OF ARCING AS A FUNCTION OF TIME FOR CONSTANT EXPOSURE CONDITIONS IN THE LABORATORY; DO THESE SAME MECHANISMS OPERATE EFFECTIVELY IN A TOKAMAK?
13. IS THERE AN UPPER LIMIT TO THE AMOUNT OF CONDITIONING WHICH OCCURS ON THE SURFACE AND IF SO WHAT IS IT, HOW CAN WE DESCRIBE IT, AND WHAT DETERMINES THIS LIMIT?

SPUTTERING WORKSHOP

OBJECTIVES:

- COMPARISON OF EXISTING DATA WITH THE DATA NEEDS DERIVED FROM KNOWLEDGE OF FLUXES TO FIRST WALLS, LIMITERS, AND DIVERTOR TARGETS SHOULD IDENTIFY AREAS FOR FURTHER STUDY.
- PRODUCE DATA COMPILATION USEFUL TO THOSE CONDUCTING CONFINEMENT EXPERIMENTS AND DESIGN STUDIES.

PRIORITIES FOR FUTURE EXPERIMENTAL AND THEORETICAL SPUTTERING WORK:

(1) DETERMINE TOTAL YIELD VALUES FOR A LIMITED NUMBER OF ELEMENTAL MATERIALS AND, IN ADDITION, DIFFERENTIAL YIELD VALUES FOR THE CONSTITUENTS OF SELECTED ALLOYS AND COMPOUNDS (E. G. COATINGS AND CLADDINGS MATERIALS) UNDER ENERGETIC LIGHT ION BOMBARDMENT (1 KEV-200 KEV, H AND D, AND TO KEV TO 4 MEV ^{4}HE). THE EXPERIMENTALLY DETERMINED YIELD VALUES SHOULD HELP TO ESTABLISH SCALING LAWS AND BE USEFUL FOR PLASMA-WALL INTERACTION MODELING.

(2) DETERMINE BOTH TOTAL AND DIFFERENTIAL YIELD VALUES FOR LOW ENERGY IONS (0.1 TO 1 KEV/AMU FOR H, D, HE, B, C, O) FOR SELECTED SPECIAL MATERIALS SUCH AS COATINGS AND CLADDINGS.

(3) FOR A LIMITED NUMBER OF ELEMENTAL MATERIALS AND OF ALLOYS AND COMPOUNDS (E.G. COATINGS, CLADDINGS) DETERMINE FOR THE IRRADIATION CONDITIONS LISTED ABOVE UNDER (1) AND (2) THE FOLLOWING PARAMETERS AND/OR QUANTITIES:

   (A) THE ANGULAR AND ENERGY DISTRIBUTION OF SPUTTERED SPECIES AS A FUNCTION OF THE ANGLE OF INCIDENCE AND OF THE PRIMARY ION ENERGY (AT LEAST FOR NORMAL INCIDENCE AND FOR AN ANGLE BETWEEN 70° AND 80° WITH RESPECT TO NORMAL). IT WAS FELT THAT IN THE DETERMINATION OF THE ENERGY DISTRIBUTION THE ACCURACY FOR THE MEASUREMENT OF THE PEAK INTENSITY AND FOR THE INTENSITIES OF THE HIGH ENERGY TAIL WOULD NOT HAVE TO BE BETTER THAN A FACTOR OF TWO.

   (B) THE DIFFERENT TYPES OF SPUTTERED SPECIES RELEASED (BOTH CHARGED AND UNCHARGED, ATOMIC AND MOLECULAR).

   (C) THE EFFECT OF SURFACE ROUGHNESS ON TOTAL YIELDS, DIFFERENTIAL YIELDS, AND THE ANGULAR DISTRIBUTION OF SPUTTERED SPECIES (FOR EXAMPLE, USE POLISHED SURFACES AND "TECHNOLOGICAL" SURFACES WHICH ARE CHARACTERISTIC OF THOSE USED IN PLASMA DEVICES).

   (D) THE EFFECT OF GAS LOADING OF MATERIALS (E.G. GAS TRAPPING OF INCIDENT H, D, HE IONS) ON YIELD VALUES AND ENERGY DISTRIBUTIONS.

(4) DETERMINE FOR A VERY LIMITED NUMBER OF MATERIALS SELF-SPUTTERING YIELDS FOR THE ENERGY REGION OF 0.1 TO 1.0 KEV/AMU.

(5) DETERMINE FOR A SELECTED NUMBER OF MATERIALS THE YIELDS AND VELOCITY DISTRIBUTIONS OF PARTICLES SPUTTERED BY PLASMA RADIATIONS IN EXISTING DEVICES. FOR THESE MEASUREMENTS THE USE OF IN-SITU TECHNIQUES IS RECOMMENDED (DSLFS).

(6 DETERMINE THE OVERALL SURFACE EROSION YIELDS (CAUSED BY THE SIMULTANEOUS OCCURRENCE OF SPUTTERING, BLISTERING, FLAKING) FOR THE SELECTED SYSTEMS AND CONDITIONS DESCRIBED ABOVE UNDER (1), (2), AND (3).

(7) ESTABLISH IF THE EROSION YIELDS OF FIRST WALL COMPONENT SURFACES UNDER EITHER ION BEAM AND/OR PLASMA IRRADIATIONS ARE AFFECTED BY CHECMICAL SURFACE REACTIONS. SOME OF THESE STUDIES SHOULD BE CONDUCTED IN THE PRESENCE OF HYDROGEN GAS AND WITH IN-SITU MONITORING DEVICES.

(8) INCORPORATE MORE ADEQUATELY THE ANGULAR-ENERGY DISTRIBUTIONS OF SPUTTERED PARTICLES INTO EXISTING THEORETICAL APPROACHES.

(9) IMPROVE THE MODELING OF PLASMA-WALL INTERACTIONS BY INCORPORATING MORE ADEQUATELY THE ANGULAR AND ENERGY DISTRIBUTIONS OF SPECIES SPUTTERED FROM "TECHNOLOGICAL" SURFACES.

OBJECTIVES FOR WORKSHOP ON NEW DIAGNOSTICS RELATED TO IMPURITY RELEASE

- PUBLICIZE THE NEED FOR DEVELOPING EXPERIMENT TECHNIQUES TO STUDY THE QUESTIONS OF IMPURITY GENERATION AND TRANSPORT.
- PROVIDE A PUBLIC FORUM WHERE SEVERAL NEW APPROACHES, INCLUDING FLUORESCENCE SPECTROSCOPY, INFRARED PHOTOMETRY, AND SURFACE ANALYTIC TECHNIQUES COULD HAVE THEIR RELATIVE ADVANTAGES DISCUSSED.
- ARRIVE AT A CONCENSUS AS TO WHAT QUESTIONS RELATED TO IMPURITY RELEASE WERE OF CRITICAL IMPORTANCE.

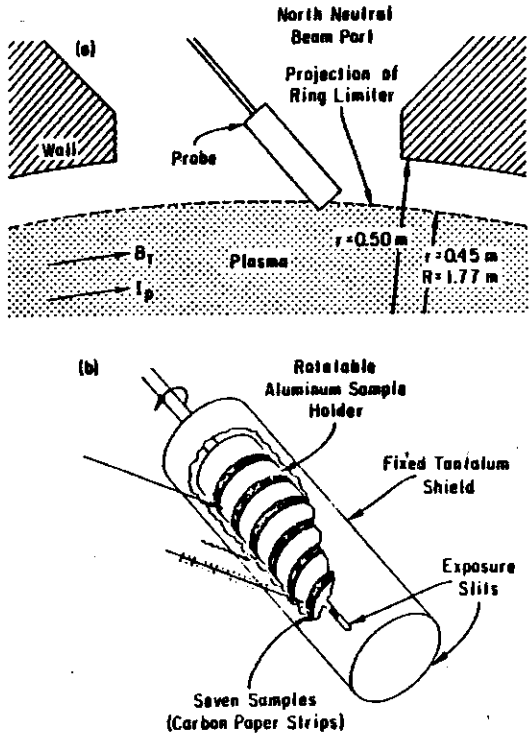

FIGURE 1.

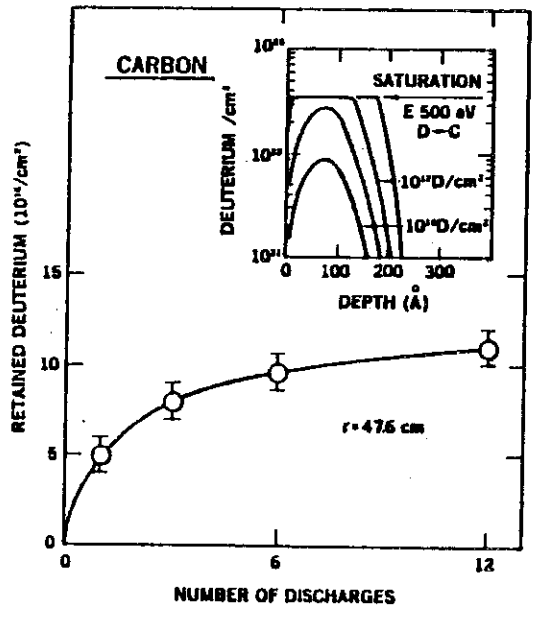

FIGURE 2.

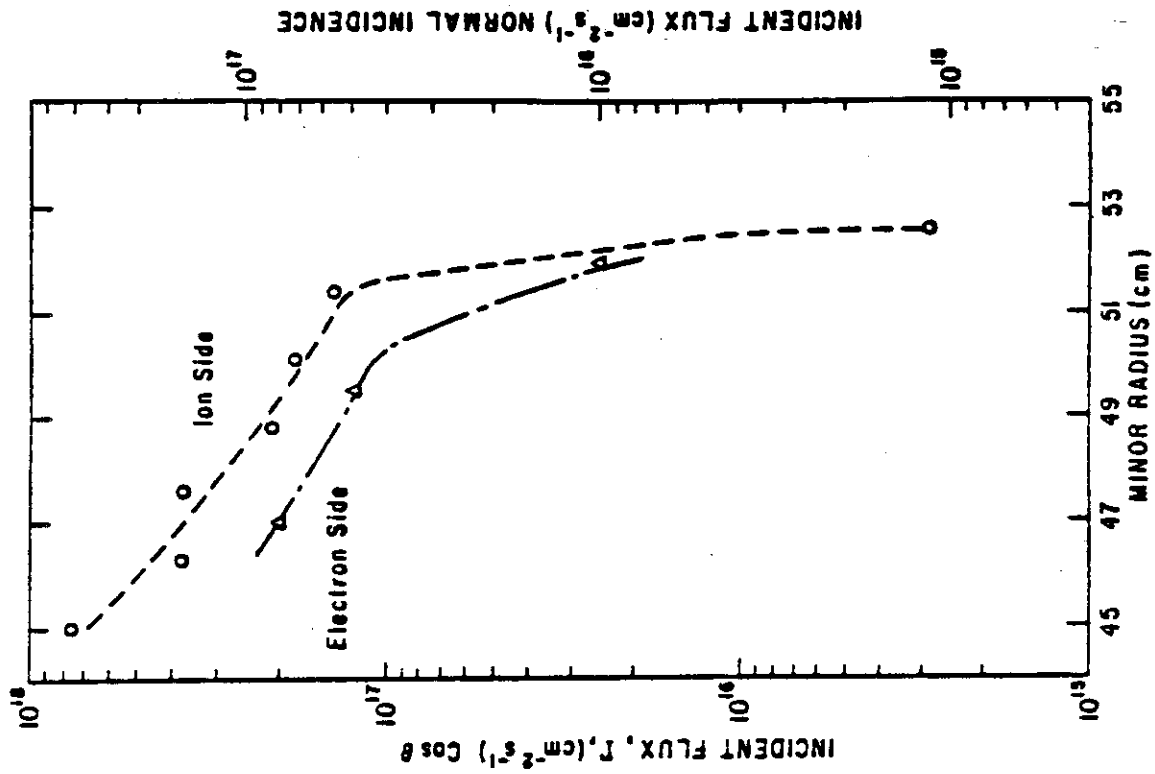

FIGURE 6.

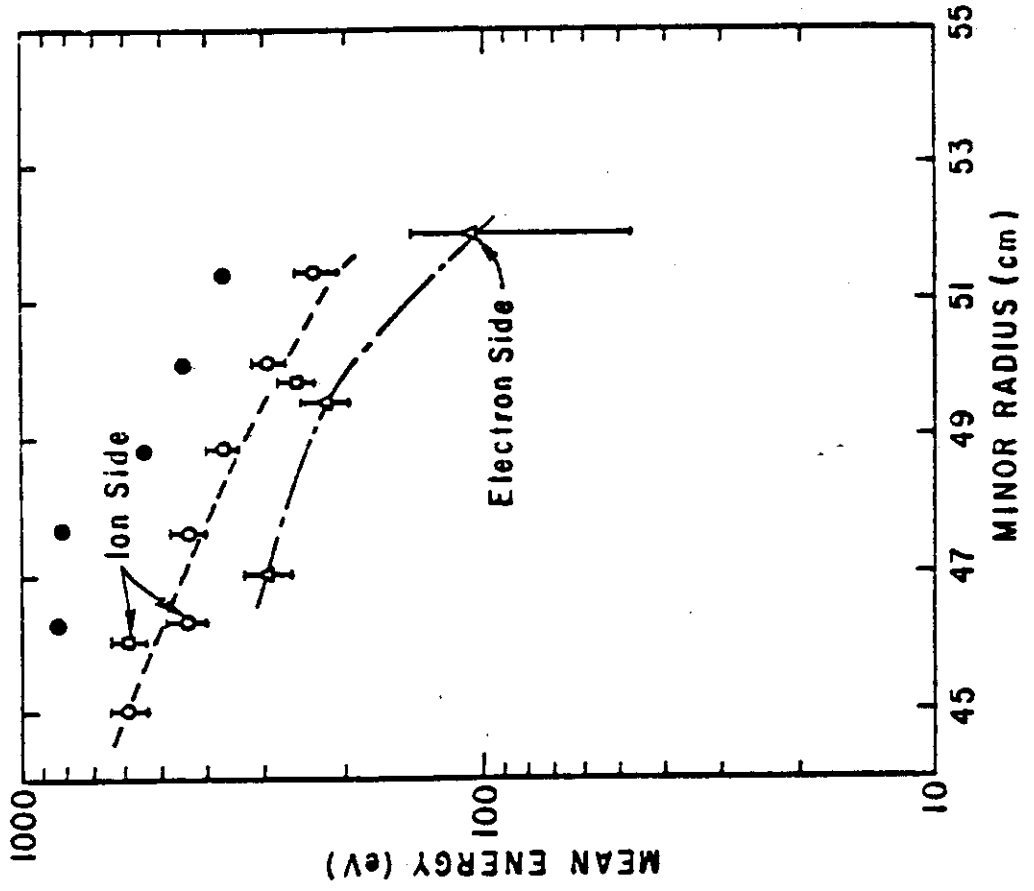

FIGURE 5.

WAMPLER, SLA

DEVICE	radius (cm) Limiter	radius (cm) wall	probe	$\bar{E}$ (ev)	Γ (10^{16} cm^{-2}/discharge)	T_e (0) (kev)	N_e(0) (10^{13} cm^{-3})
PLT[1]	45	50	45-52.5	170±30- 600±50	80- 2	1.1	1.5
TFR[3]	20	26	20.1 23.6	50±10- 20(±5 10)	12- 0.4	1.2	4.0
ISX-B[2]	27	35	29	40	3	n.a.	1.4

Table 1: Comparison of recent measurements of the mean energy ($\bar{E}$) and Fluence (Γ) of hydrogen in the edge-plasma of three tokamaks. The measurements were made with hydrogen retention probes and analyzed according to the model given in Ref[5].

LASER FLUORESCENCE SPECTROSCOPY

- MEASUREMENT OF

  PARTICLE DENSITY, n_{METAL}

  VELOCITY DISTRIBUTION FUNCTION, $F(v)$

  FLUX DENSITY, $\phi = n \langle v \rangle$

- ADVANTAGES: HIGH SENSITIVITY

  HIGH TIME AND SPACE RESOLUTION

  INDEPENDENCE OF n_E AND T_E

- PROBLEMS: CALIBRATION

  PLASMA RADIATION

- MEASURES NEARLY ALL METALS WITH PULSED DYE LASER SYSTEMS:

  . λ = 380 NM - 700 NM

  λ = 240 NM - 350 NM (FREQUENCY DOUBLING)

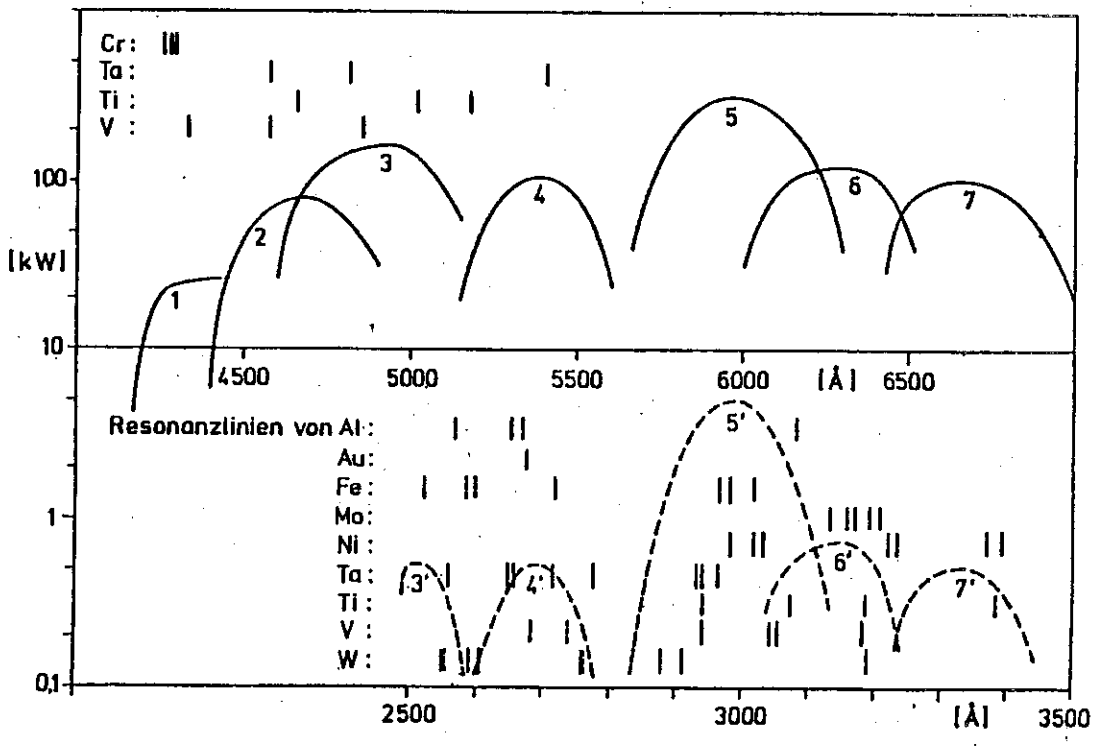

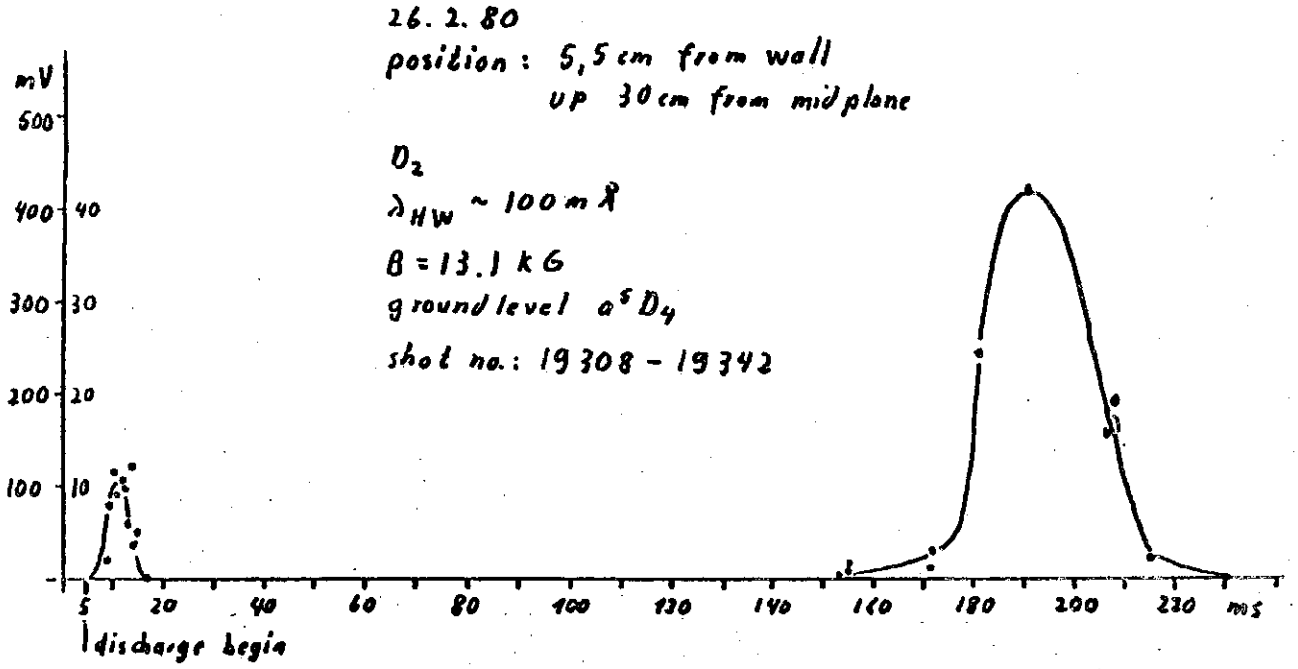
26. 2. 80
position : 5,5 cm from wall
up 30 cm from midplane
D_2
λ_{HW} ~ 100 mÅ
B = 13.1 kG
ground level a^5D_4
shot no.: 19308 - 19342
mV
500
400
300
200
100
40
30
20
10
5
20
40
60
80
100
120
140
160
180
200
220
ms
discharge begin

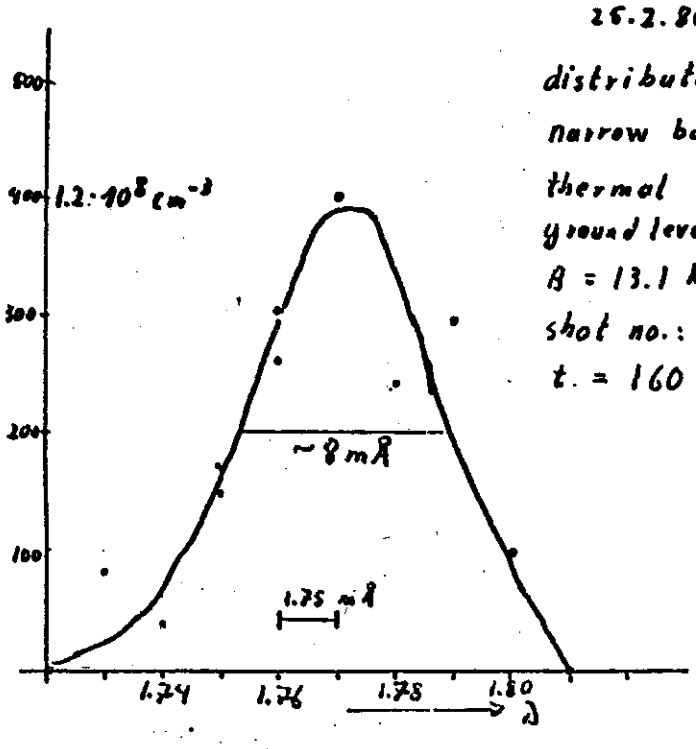
26.2.80
distribution function f(v)
narrow bandwidth ~ 6 mÅ = λ_{HW}
thermal
ground level a^5D_4
B = 13.1 kG
shot no.: 19291 - 19303
t = 160 ms
500
400
300
200
100
$1.2 \cdot 10^8$ cm^{-3}
~ 8 mÅ
1.75 mÅ
1.74
1.76
1.78
1.80
λ

HYDROGEN RECYCLE WORKSHOP

- HYDROGEN RECYCLE MODELS AND METHODS FOR CONTROL IN NEW EXPERIMENTS
- IN-SITU MEASUREMENTS
- FUNDAMENTAL PROCESSES

HYDROGEN RECYCLE MODELS AND METHODS FOR CONTROL IN NEW EXPERIMENTS

- DEVELOPMENT OF GETTERS FOR RECYCLE CONTROL WHICH CAN BE REGENERATED AT MODEST TEMPERATURES.
- EXPERIMENTS IN THE PLASMA EDGE REGION TO DETERMINE NEUTRAL HYDROGEN PROFILES AND SPECTRA, IMPURITY TRANSPORT, AND RECYCLING RATES.
- IMPROVED MODELS OF THE PLASMA-EDGE AND PLASMA (NEUTRAL)-SURFACE INTERACTIONS INCLUDING MODELS OF THE NEAR SURFACE REGION OF THE WALL.
- EXPERIMENTS WITH SPECIALLY DESIGNED LIMITERS AND DIVERTORS AS METHODS FOR PUMPING, IMPURITY CONTROL AND ADEQUATE HEAT REMOVAL.

FUNDAMENTAL PROCESSES

- REFLECTION
- DESORPTION
- PLASMA-SURFACE SIMULATION STUDIES
- TRAPPING AND MIGRATION
- GETTERING

HYDROGEN RECYCLING IN TFTR

- LIMITED TRITIUM INVENTORY NECESSITATES USING MATERIALS WHICH HAVE LOW HYDROGEN RETENTION AND READILY DESORB HYDROGEN WHEN HEATED.

- OPTIMIZING THE DEUTERIUM TRITIUM DENSITY RATIO REQUIRES REDUCED RECYCLING AND SELECTIVE PULSED GAS FEED.

TRITIUM LIMITATIONS

MAXIMUM ON SITE INVENTORY	50 kCi
MAXIMUM ON LINE	25 kCi
QUANTITY/FULL POWER PULSE	270 Ci
MAXIMUM IN READILY RELEASEABLE FORM	2.3-23 kCi

CECCHI, PPPL

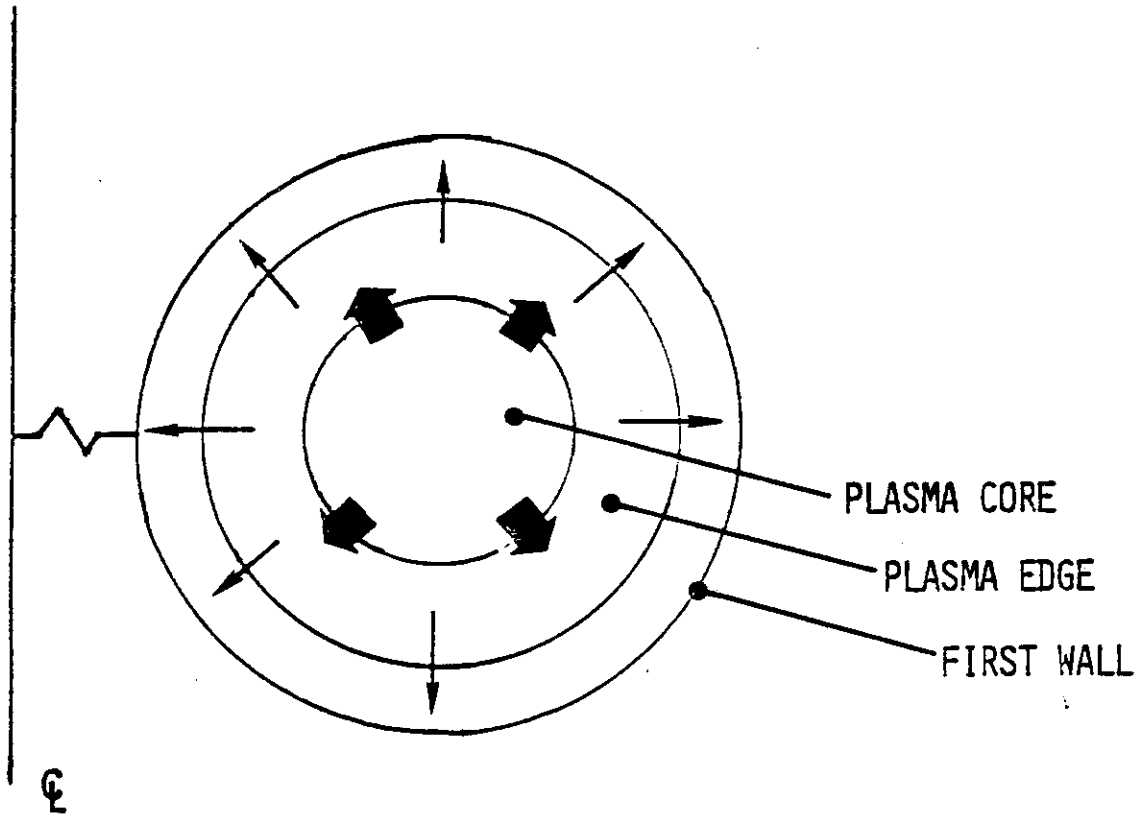

PLASMA EDGE EFFLUXES WITH VARIOUS RECYCLING AND RADIATION ASSUMPTIONS

(Helium outflux rate is always - 1-2 × 10^{20}/sec, 3 torr liters/sec, before ash buildup.)

U. S. INTOR

	No Recycling Negligible Radiation	99% Recycling Negligible Radiation	99.9% Recycling Negligible Radiation	99% Recycling 90% Radiation
Particle Efflux (particles/sec)	10^{22}	10^{24}	10^{25}	10^{24}
Average Particle Energy (keV)	40	0.4	0.04	0.04
Diffusive Power Efflux (W/cm^2)	30	30	30	3
(MW)	100	100	100	10

J. N. Brooks/D. L. Smith
ANL Fusion Power Program

Hydrogen Recycling Workshop
Dublin, California
October 17-18, 1979

HELIUM RETENTION AS AN IMPURITY CONTROL METHOD FOR FUSION REACTORS

PURPOSE:

RETAIN SOME OF THE IMPINGING HELIUM IONS ON FIRST SURFACE DURING THE BURN — PUMP OUT AFTER BURN — PERMIT A NONIMPURITY-LIMITED BURN IN FUSION REACTORS.

ADVANTAGES:

(1) PASSIVE SYSTEM — NO DIVERTORS, COILS, ETC.

(2) NO PUMPING DURING BURN:

- REDUCED NEUTRON STREAMING IN VACUUM DUCTS.
- MINIMIZES TRITIUM INVENTORY.

KEY MATERIAL PROPERTIES:

(1) HELIUM SATURATION LEVEL

(2) HELIUM REFLECTION COEFFICIENT/STICKING PROBABILITY.

(3) POST-BURN RELEASE RATE — TEMPERATURE DEPENDENCE.

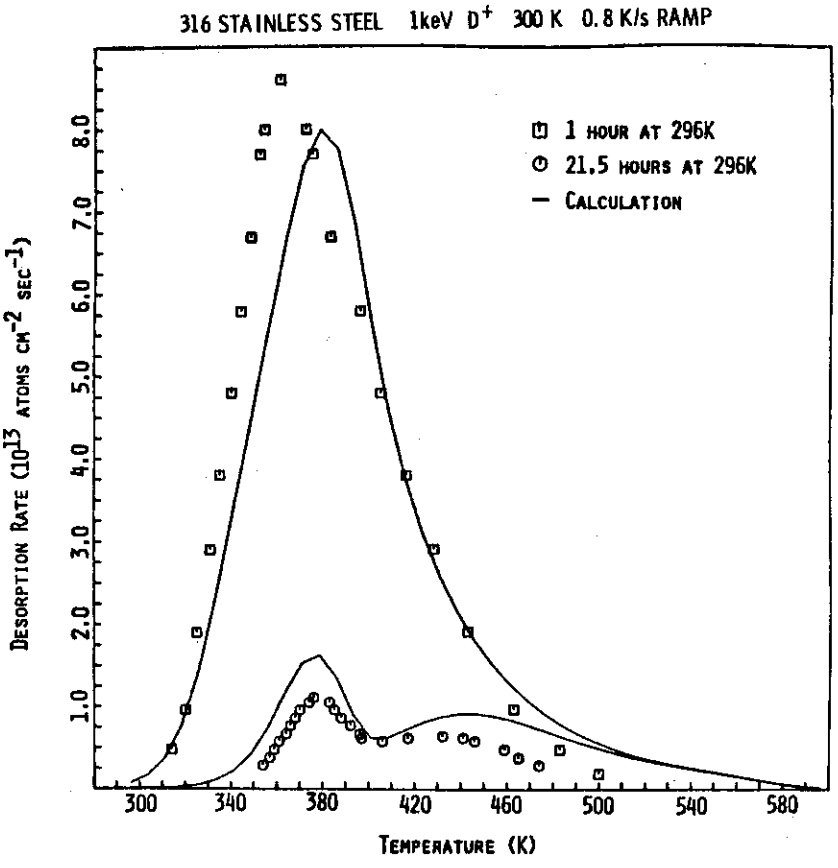

WILSON SLL

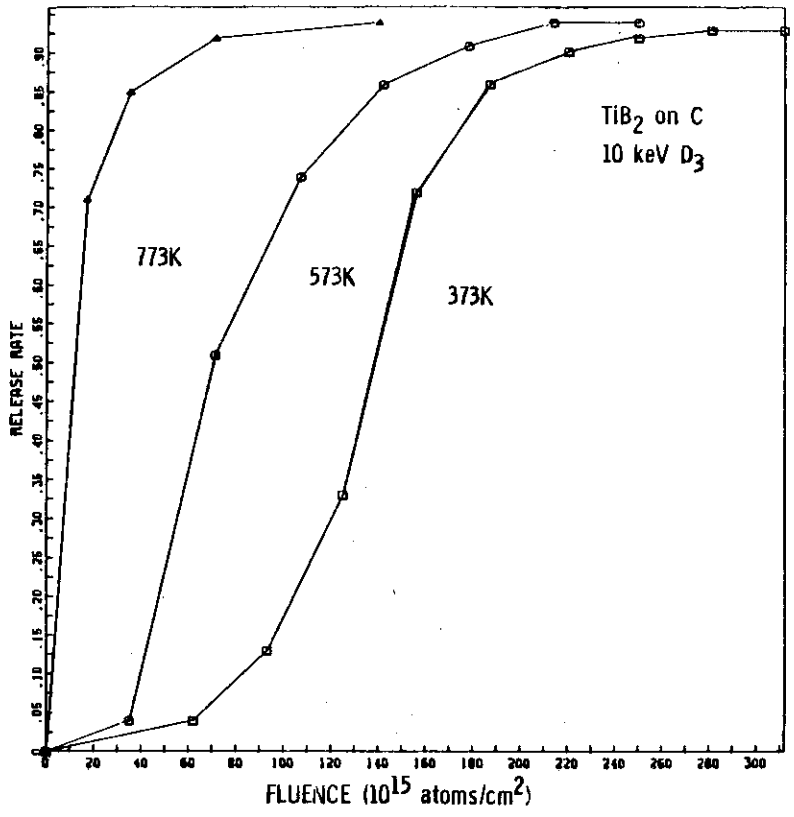

K. L. Wilson, SLL

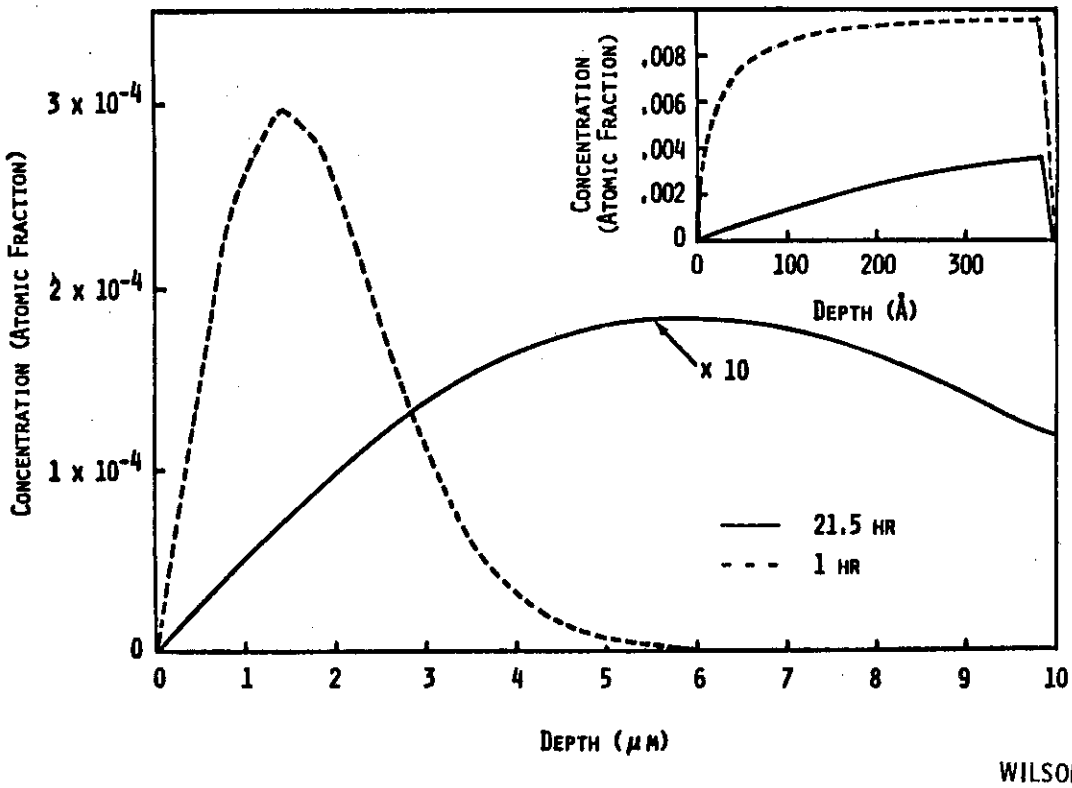

WILSON SLL

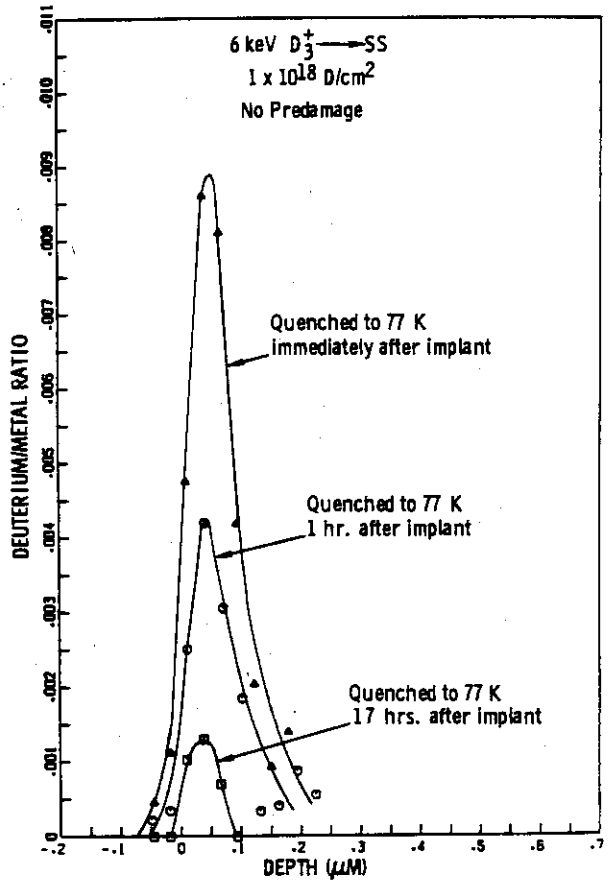

WILSON SLL

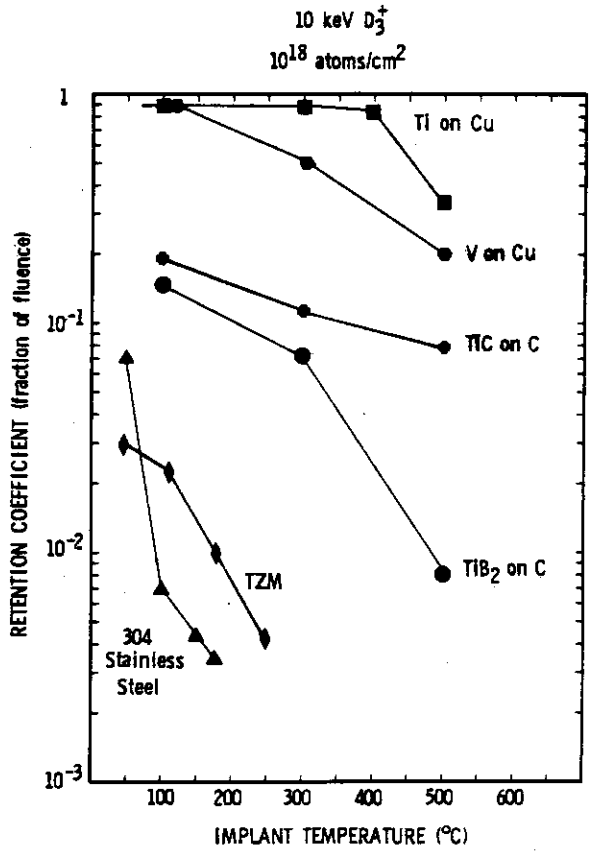

K. L. Wilson, SLL

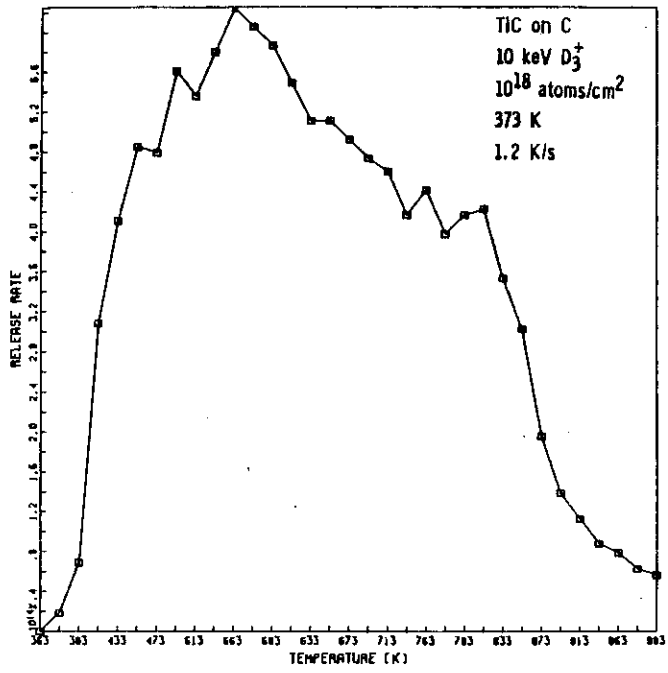

K. L. Wilson, SLL

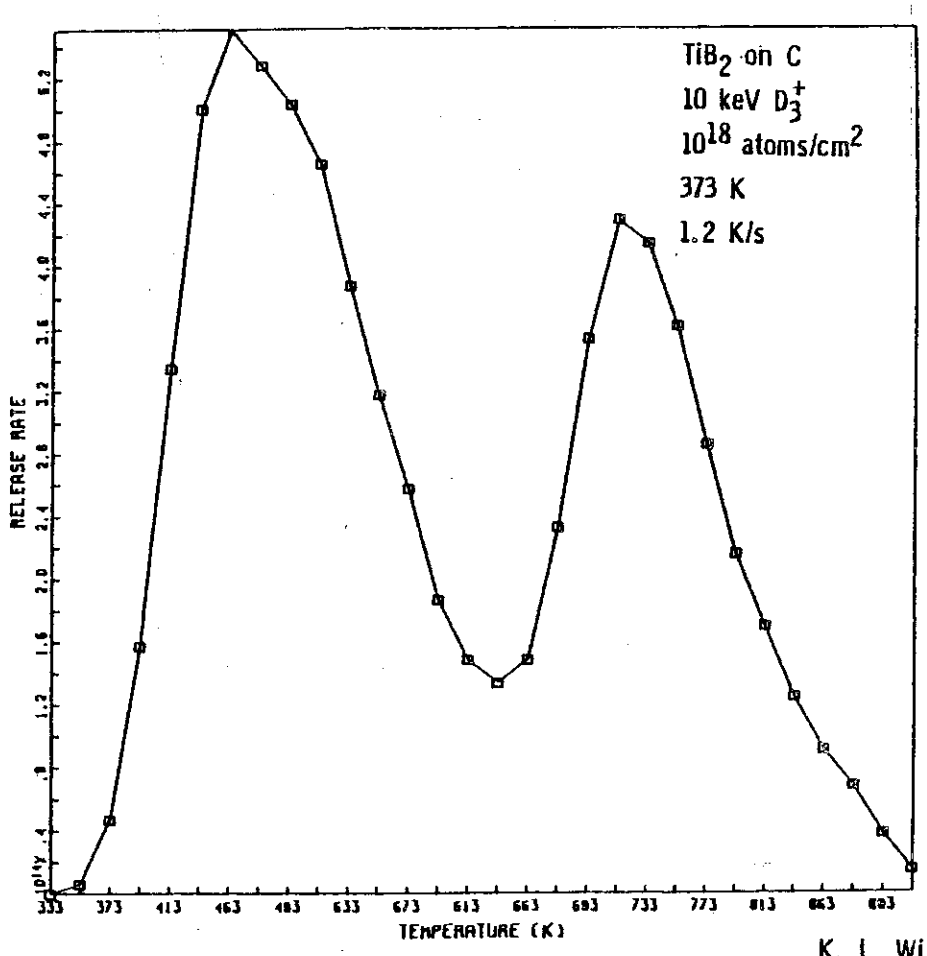

K. L. Wilson, SLL

ITER MATERIALS

STRUCTURE	MATERIAL	APPROXIMATE SURFACE AREA	INCIDENT FLUX†
VACUUM VESSEL PLATE SECTIONS	STAINLESS STEEL 304 LN	10^6	CX, EP,
VACUUM VESSEL BELLOWS	INCONEL 625	10^6	(COLD GAS)
BUMPER LIMITER*	C, V, Ti-V ALLOY TiB_2, TiC, B_4C, Mo	10^5	CX, EP, MP, NB
MOVEABLE LIMITER*	C, V, Ti-V ALLOY, TiB_2, TiC, B_4C, Mo	10^4	CX, EP, MP
PROTECTIVE PLATES*	C, V, Ti-V ALLOY TiB_2, TiC, B_4C, Mo	10^5	CX, EP, NB

* MATERIAL NOT DETERMINED - CANDIDATE MATERIALS LISTED.

†CX - CHARGE EXCHANGE NEUTRALS
EP - EDGE PLASMA IONS
MP - MAIN PLASMA IONS
NB - NEUTRAL BEAM

7 - 2 REVIEW OF FUNDAMENTAL IMPURITY STUDIES IN JAERI

Y. Murakami

Division of Thermonuclear Fusion Research
Tokai Research Establishment, JAERI

1. Introduction

The fundamental impurity studies program in thermonuclear fusion research of JAERI was started in 1975, and has been continued in close connection with the JT-60 project and with the JFT-2 and DIVA experiments. The main objectives of this program are to investigate the individual phenomena in plasma-wall interaction which can occur in present and near-term tokamaks and to develop vacuum techniques for surface conditioning and near-surface modification.

This review presents an outline of the progress and program of the impurity studies and a summary of the results on sputtering, adsorption and desorption, surface conditioning and near-surface modification, and blistering. Results from recent plasma experiments with additional heatings raise serious questions about the use of conventional, high-Z liners and limiters in forthcoming experiments. Therefore, an emphasis is laid on low-Z materials and low-Z surface coatings for the first wall.

2. Progress and Program

In 1975 and 1976, two ion accelerators named LSP and HSP were designed and constructed. LSP was intended to measure the physical and chemical sputtering yields of first wall materials by light ions, especially by protons, in the energy range of 0.1 - 6 keV.[1] In this apparatus the ion beam is formed by a duoplasmatron ion source and beam transport optics with a mass analyzer. The base pressure in the target chamber is maintained in the 10^{-7} Pa range by using a sputter-ion pump and a cryocondensation pump. Measuring instruments include an Auger electron spectrometer, an electro-microbalance, a quadrupole mass spectrometer and their calibration systems (see Fig.1).

HSP is a 400 kV Cockcroft-Walton accelerator.[2] The incident ion energy is variable from 50 to 400 keV. In 1978, a special scanning electron microscope with a newly developed solid-state detector for detecting back-scattered electrons was installed in an exclusive beam line of HSP.[3] This enables us to observe sample surfaces under ion bombardment.

A high-current, duoPIGatron ion source was constructed in 1979. This is used to measure the surface erosion rate of low-Z materials by hydrogen and deuterium ions. The current density of this apparatus is about one order of magnitude higher than that of LSP. A design study of the ion source for refractory materials has been performed for self-sputtering measurement. Construction of the source is planned for 1980.

In order to provide a vacuum technological data base for the impurity problem, outgassing rate measurements were made on first wall materials. Some preliminary considerations were made on adsorption and desorption characteristics of gases on low-Z materials.

An atomic hydrogen experiment has been carried out to study the wall cleaning procedures since 1978. In the experimental apparatus atomic hydrogen is produced on rhenium hot filaments and flows through a Teflon-coated glass tube from the atomizer into a reaction vessel.

The design and construction of a vacuum experiment apparatus named JVX-I is now under way. This is intended to use mainly for the optimization of in-situ coatings of low-Z materials and for the demonstration of their cleaning procedures. The apparatus will consist of a cylindrical vacuum vessel made of Inconel 625, 0.36 m in diameter and 1.5 m long, an insertible coating device, an RF discharge equipment, and a turbomolecular pumping system. Two diagnostics

will be installed to monitor plasma and wall condition. The surface monitor station is capable of exposing a sample substrate to the wall position. After exposure, the sample can be retracted to an attached UHV system for Auger and secondary ion mass analysis.

At present, our fundamental impurity studies are especially concerned with the following items; (1) surface erosion of first wall materials in actual and probable conditions, (2) vacuum and surface properties of carbon and low-Z compounds as a tokamak first wall, and (3) surface conditioning and near-surface modification of the first wall. Table 1 shows the time schedule of the program during FY 1979 through FY 1981 in Fusion Research and Development Center. Studies on sputtering and blistering are also pursued by Division of Nuclear Fuel Research and Division of Physics in JAERI.

3. Summary of Results

3.1 Sputtering

The experiments on sputtering in JAERI are summarized in Table 2. In 1976 and 1977, proton sputtering yield of molybdenum was determined in the energy range of 0.15 - 6 keV by using LSP.[4,5] According to the measurement, the yields at 0.3 and 1 keV are 1×10^{-4} and 2×10^{-3}, respectively, as shown in Fig.2.

When technical materials are subjected to ion bombardment, the surface topography gradually changes and may influence the sputtering yield and the angular distribution of the sputtered atoms. In order to demonstrate the effect, various polycrystalline molybdenum samples were bombarded with neon ion beams at two different angles of incidence. The surface was found to be gradually covered with facets of protuberances and depressions.[6] Many microscopic hills were formed on the bombarded surfaces in case of oblique incidence. The angular distribution of emitted particles was influenced by grain size of the material, incident ion energy, angle of incidence, and total dose.[7] At oblique incidence the more forward emission was observed as the grain size became smaller (see Fig.3).

In 1979, chemical sputtering yield of various types of carbon was measured with hydrogen ions in the energy range of 0.1 - 6 keV.[8] In the early stage of bombardment, the methane formation rate changes with fluence depending on the initial condition of the samples. After the fluence exceeds 10^{18} ions$\cdot$cm^{-2}, however, the reaction reaches a steady state. The methane formation rate at steady states is shown in Fig.2. It has a maximum of 0.07 CH_4/H^+ at an incident energy of 1 keV and 500°C.

The usefulness of a honeycomb structure was proposed as a simple means of reducing the number of sputtered particles. In order to make sure experimentally of the concept, a measurement was made on the ratio of the sputtering yield of molybdenum honeycomb walls to that of a flat wall.[9] In case of normal incidence of argon ions, the sputtering ratio was found to decrease drastically with increasing the depth-to-width ratio.

3.2 Adsorption and Desorption

In 1977, outgassing rate from various wall materials was measured at both room temperature and 500°C under a contract with ULVAC.[10] The rate from unbaked pyrolytic graphite is normally in the range 10^{-5} - 10^{-7} Pa$\cdot$m$^3\cdot$sec$^{-1}\cdot$m^{-2}, depending on the pretreatments and the time for which it has been maintained under vacuum. The main desorbed species is H_2O, with lesser quantities of H_2 and CO. After baking for 100 - 200 hours at 500°C in vacuum, however, the outgassing rate decreases to less than 10^{-9} Pa$\cdot$m$^3\cdot$sec$^{-1}\cdot$m^{-2} at room temperature.

The adsorption and desorption characteristics for oxygen containing gases indicate that the sticking probability of these gases on carbon and graphite is extremely low. This may retard the oxygen accumulation on the wall in spite of the inevitable introduction of the gases into the vacuum vessel due to leaks and outgassing in the system.[11] The fact that the adsorbed oxygen can be

removed as CO_2 and CO at relatively low temperatures is another desirable characteristic of the materials. A carbon wall experiment on DIVA supported the idea, in which once clean surface was obtained stable discharges with a small quantity of oxygen were reproduced for a number of shots without any additional cleaning procedure.[12] Figure 4 shows typical Auger spectra of carbon and titanium films deposited on the first wall in DIVA. The spectrum from the carbon film scarcely changed during 500 shots, while that from the titanium film gradually changed within early several shots and indicated the oxygen accumulation on the wall.

3.3 Surface Conditioning and Near-Surface Modification

A surface conditioning process of carbon and graphite was determined by measureing the surface reaction rate with atomic hydrogen.[13] Figure 5 shows a measurement of methane formation rate from pyrolytic graphite exposed to atomic hydrogen. The sample was heated up in steps of 100 degrees from 100 to 900°C. In the first run a peak in the methane formation rate was observed between 500 and 600°C. However, the rate decreased and the peak disappeared in the measured temperature range after the sample had been exposed to hydrogen atoms to a fluence in excess of 10^{18} atoms·cm^{-2} at about 500°C.

As to near-surface modification, JAERI has been developing carbon surface coatings by a magnetron sputtering method in cooperation with ANELVA. Low-Z surface coatings on refractory metals by ion plating and CVD are pursued by National Research Institute for Metals in cooperation with JAERI.

3.4 Blistering

A number of experiments have been carried out in the field of blistering and flaking by using HSP. The special scanning electron microscope was concurrently used to examine the behavior of polycrystalline molybdenum as a function of implanted helium dose.[14] Practically, it is important to find out how to reduce the surface erosion by blistering and flaking in actual and possible conditions. Experiments on surface roughness effects on blister formation showed that blistering can be effectively reduced in molybdenum surfaces with a multigroove microstructure.[15,16] Experiments were also made on the helium ion bombardment with multiple energies from 60 to 400 keV.[17] (See "Summary of the Works on Blistering and Related Erosion Phenomena in JAERI", reviewed by K. Kamada.)

References

[1] T. Narusawa, et al, Proc. 7th Intern. Vac. Congr. & 3rd Intern. Conf. Solid Surfaces (Vienna, 1977) p.371.
[2] K. Obara, et al, JAERI-M 7250 (1977) (in Japanese).
[3] K. Obara, et al, JAERI-M 7797 (1978) (in Japanese).
[4] K. Sone, et al, Proc. Intern. Symp. Plasma Wall Interaction (Jülich, 1976) p.323.
[5] H. Ohtsuka, et al, J. Nucl. Materials 76 & 77 (1978) 188.
[6] R. Yamada, et al, J. Nucl. Materials 82 (1979) 155.
[7] R. Yamada, et al, J. Nucl. Materials 84 (1979) 101.
[8] R. Yamada, et al, this seminar, paper 9-2.
[9] T. Abe, et al, J. Nucl. Sci. Technol. 15 (1978) 471.
[10] H. Yoshikawa, et al, Proc. 7th Intern. Vac. Congr. & 3rd Intern. Conf. Solid Surfaces (Vienna, 1977) p.367.
[11] Y. Murakami, et al, private communication.
[12] S. Sengoku, et al, to be presented at 4th Intern. Conf. Plasma Surface Interactions in Controlled Fusion Devices (Garmisch-Partenkirchen, 1980); this seminar, paper 2-2.
[13] T. Abe, et al, to be published in J. Nucl. Materials; this seminar, paper 9-4.
[14] M. Saidoh, et al, JAERI-M 7997 (1978) (in Japanese); this seminar, paper 9-1.
[15] M. Saidoh, et al, JAERI-M 7182 (1977).
[16] K. Sone, et al, J. Nucl. Materials 76 & 77 (1978) 240.
[17] M. Saidoh, et al, private communication.
[18] K. Kiuchi, et al, to be published in JAERI-M report.
[19] K. Sone, et al, private communication.

Table 1 The time schedule of fundamental impurity studies during FY 1979 through FY 1981

Experimental Apparatus	FY 1979	FY 1980	FY 1981
LSP		Experiment →	
HSP (incl. SEM)		Experiment →	
High current, light-ion source	Construction →	Experiment →	
SSP		Design & Construction →	Experiment →
Atomic hydrogen source		Experiment →	
JVX-I	Construction →	Installation ⇢	Experiment →

Table 2 List of experiments on sputtering in JAERI

Target Material	Incident Particle	Angle of Incidence	Energy (keV)	Dose and Dose Rate* (cm^{-2} and $cm^{-2}\cdot s^{-1}$*)	Temperature (°C)	Notes
Mo (Polycrystalline)	H^+	Normal	0.1 - 6		RT	Energy dependence
	Ne^+	Normal	2	1.5×10^{19}	RT	Dose effect
		Normal, 45°	0.6, 1.5	2×10^{19}	RT	Angular distribution of sputtered atoms
	Ar^+	~Normal	~1		RT	Honeycomb structure
	Ar^+, O^+	45	0.5 - 5	$2\text{-}6 \times 10^{15}$*	RT - 1500	Secondary ion emission [18]
C (Pyrolytic, isotropic, glassy, and vacuum deposited)	H^+	Normal	0.1 - 6	$3\text{-}7 \times 10^{14}$*	RT - 650	Chemical sputtering (Energy and temperature dependence)
	H^0	Random	Thermal	$10^{13} - 10^{14}$*	RT - 900	Surface conditioning
SiC (Ion-plated)	H^+	Normal	1.5	2×10^{20}, 2.5×10^{15}*	500	Total erosion, Chemical composition dependence [19]

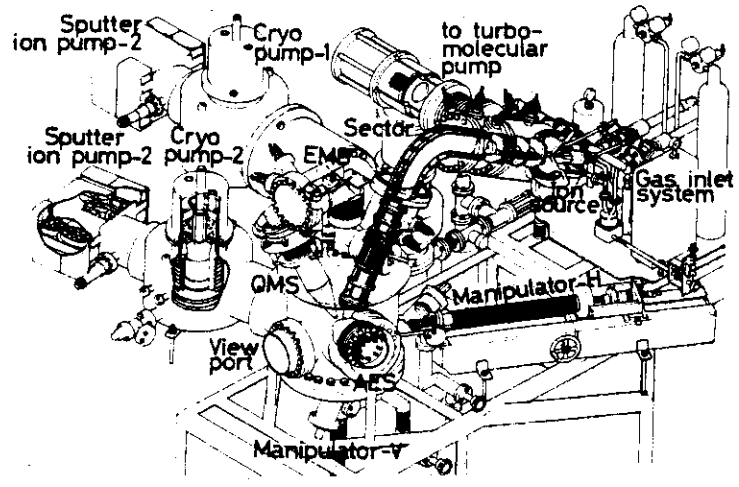

Fig.1 The whole view of LSP.

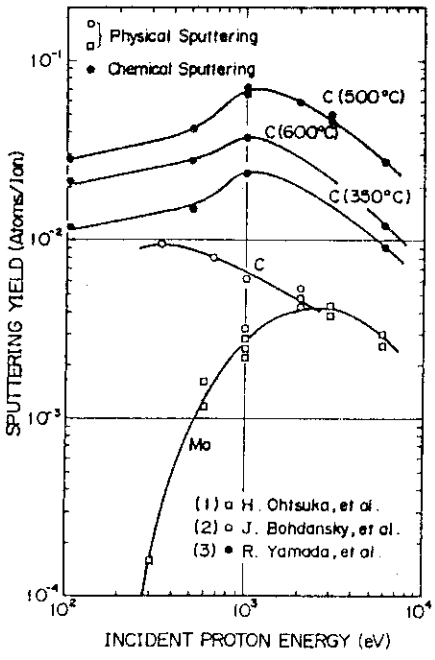

Fig.2 Sputtering yield of molybdenum and pyrolytic graphite by protons.

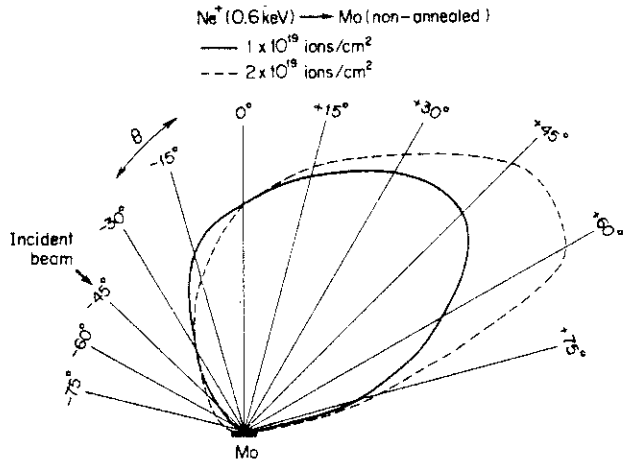

Fig.3 Angular distribution of sputtered atoms from non-annealed polycrystalline molybdenum bombarded with 0.6 keV neon ions at 45° angle of incidence.

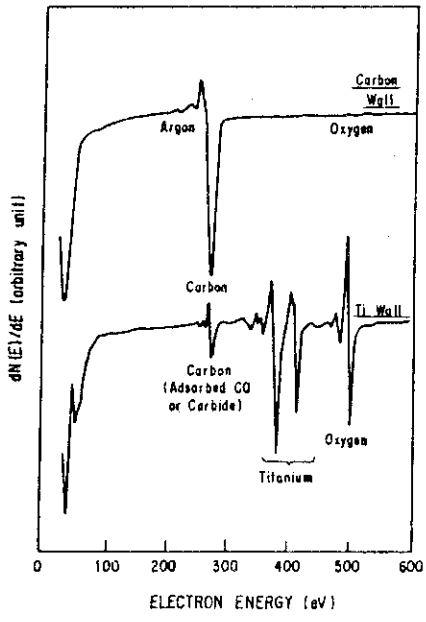

Fig.4 Typical Auger spectra from carbon and titanium films deposited on the first wall in DIVA.

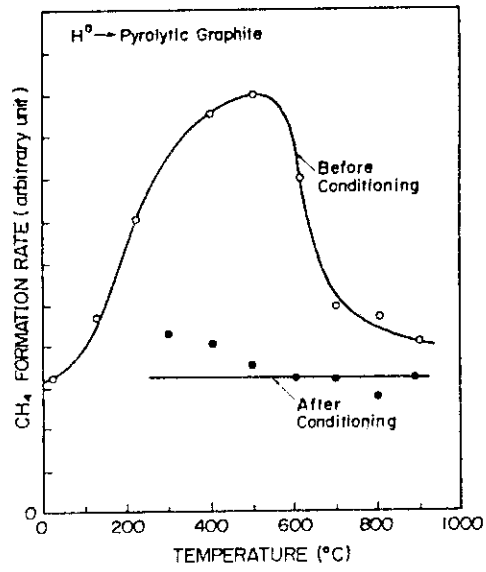

Fig.5 Methane formation rate from pyrolytic graphite exposed to atomic hydrogen.

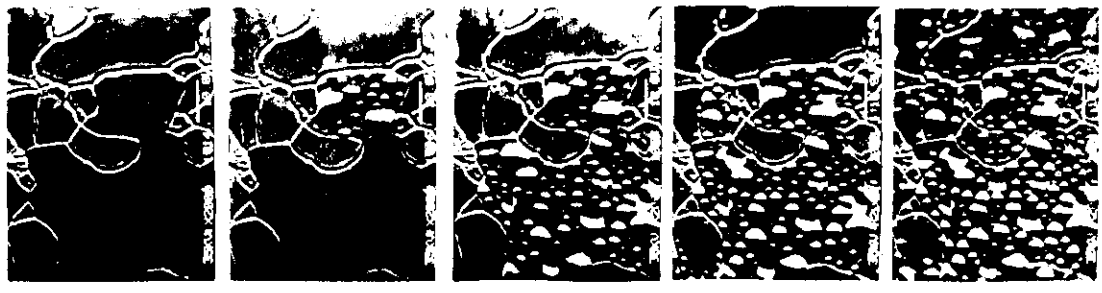

Fig.6 A series of scanning electron micrographs showing developments of surface erosion in polycrystalline molybdenum.

7 - 3 Surface Study Program in IPP, Nagoya University

K. Akaishi

IPP, Nagoya

I. Abstract

The objectives and tasks of surface study program are summarized in following items.

1. Development of diagnostics for measurement of sputtering yield

1-1 vacuum microbalance

1-2 ion scattering spectrometer (ISS)

2. Surface observation by ISS

2-1 cleaning process of stainless steel (baking, ion bombardment)

2-2 surface impurities on Mo limiter (sample test in UHV, ISS system)

2-3 effect of Ti-gettered surface

3. Ion impact gas desorption
(measurement of desorption cross section)

3-1 ISS technique
H_e^+, $Ar^+ \rightarrow O_2$ and CO on Mo

3-1 AES technique
He^+, Ne^+, $Ar^+ \rightarrow O_2$ on Mo

4. Preliminary coating experiments of TiB_2 and TiC on Mo and SS substrates

5. Plasma Wall Interaction in JIPP T-Ⅱ tokamak
(collaboration with Prof. Yamashina's group, Hokkaido Univ.)

The typical experimental results and outline of coating experiments, and the sample transfer device going to apply to JIPP, T-Ⅱ tokamak are shown in Ⅱ. The summary and publication list derived from above works are given in section Ⅲ.

Ⅱ. Typical results

1-1 The sketch of the microbalance is shown in Fig.1. The sputtering yields for Cu and Nb samples measured by the balance are shown in Fig.2 and Fig.3, respectively.

1-2 ISS technique is now investigated as a new diagnostics for sputtering yield measurement. Fig.4 is a demonstration of the technique, where the Ti film on Mo substrate is bombarded with Ar ion and the changes of ISS signals from Ti film and Mo substrate are shown as a function of bombarding time. The principle for yiled determination in this technique is explained in Fig.5. The film thickness Δt can be readly determined from the point that the Ti signal starts to decay. But for accurate measurement of the thickness it has to study the interface region of the film in detail.

2. Surface observation by ISS. Effect of Surface conditionings (baking, Ar ion bombardment) for SS and Mo Samples, and effect on gas impurity (CO) emission control of Ti gettered surface are investigated. Fig.6 and 7 are typical results for Mo sample and Ti gettered surface.

3. The cross section data measured by ISS are shown in Fig.8. For CO adsorption on Mo two cross sections are measured.

This shows that there are two different adsorption state in CO adsorption. The other cross sections for different adsorbing gas and metal samples are shown in Fig.9. The cross sections of Fig.10 are measured by AES technique. Here the cross sections obtained with ISS are plotted on for comparison.

4. The coating experiments of TiB_2 and TiC on SS and Mo plates are carried out in the magnetron sputtering source. In the constructed small magnetron source the coating film of the film thickness up to 10 μm is achieved. The surface characterization for TiB_2 film will be reported at 4th international conference on plasma surface interaction in Garmisch-Partenkirchen.

5. The sketch of the sample transfer system is shown in Fig. 11, which is the first design for plasma wall interaction study.

Ⅲ. Summary

1-1 a. microbalance is a suitable technique for absolute measurement of sputtering yield.

b. sensitivity of 7×10^{-8} g/mv can be routinly obtained in the construction of balance.

c. In the S. Y. measurement for materials with low S. Y. (< 1 atoms/ion), it is necessary to irradiate the target with high ion dose ($\gtrsim 10^{18}$ ions/cm^2) because of reliable data production.

1-2 a. ISS is a promising technique for S. Y. measurements of

metalic thin films and low-Z compounds.

b. The calibration of this method can be done with the balance.

2. ISS is very useful to observe the contaminating state of surface with oxygen atoms. However, for surface characterization of various candidated reactor materials (low-Z compounds) in future, a hybrid surface analyzer must be designed and constructed.
3. We are going to continue the data accumulation for ion induced gas desorption.
4. Low-Z compound coating and their characterization will be started.
5. The simple sample transfer system is just constructed.

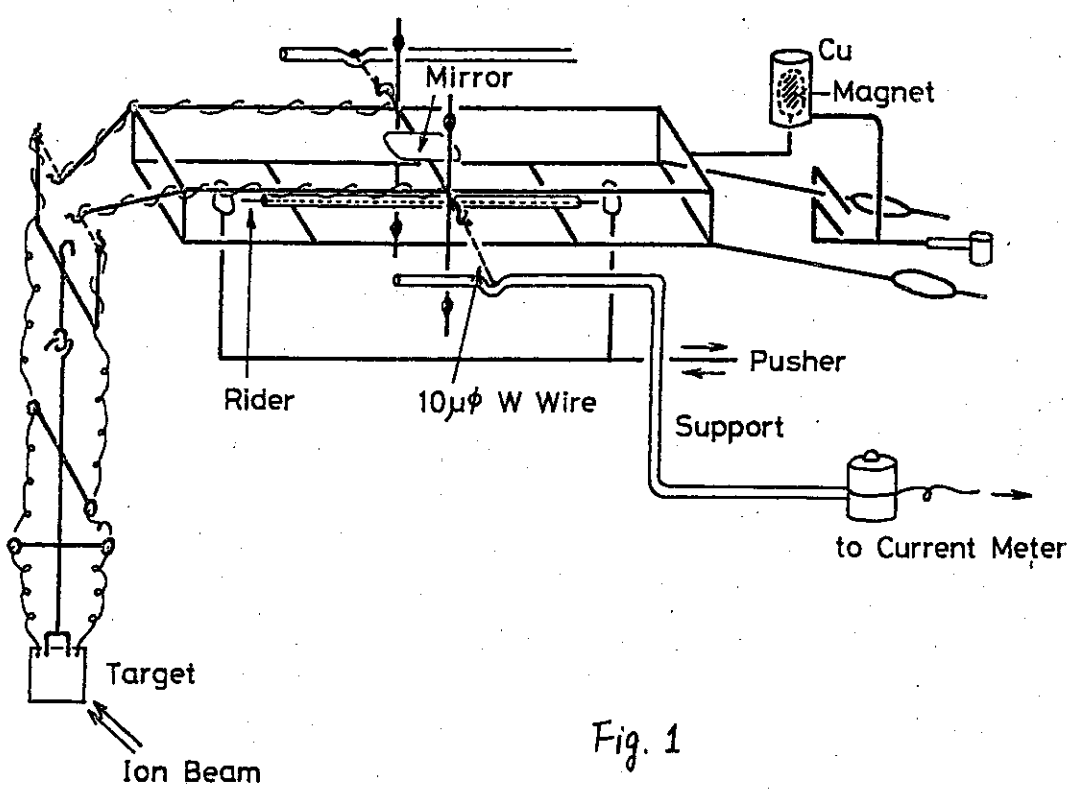
Mirror
Cu
Magnet
Pusher
Rider
10μφ W Wire
Support
to Current Meter
Target
Ion Beam

Fig. 1

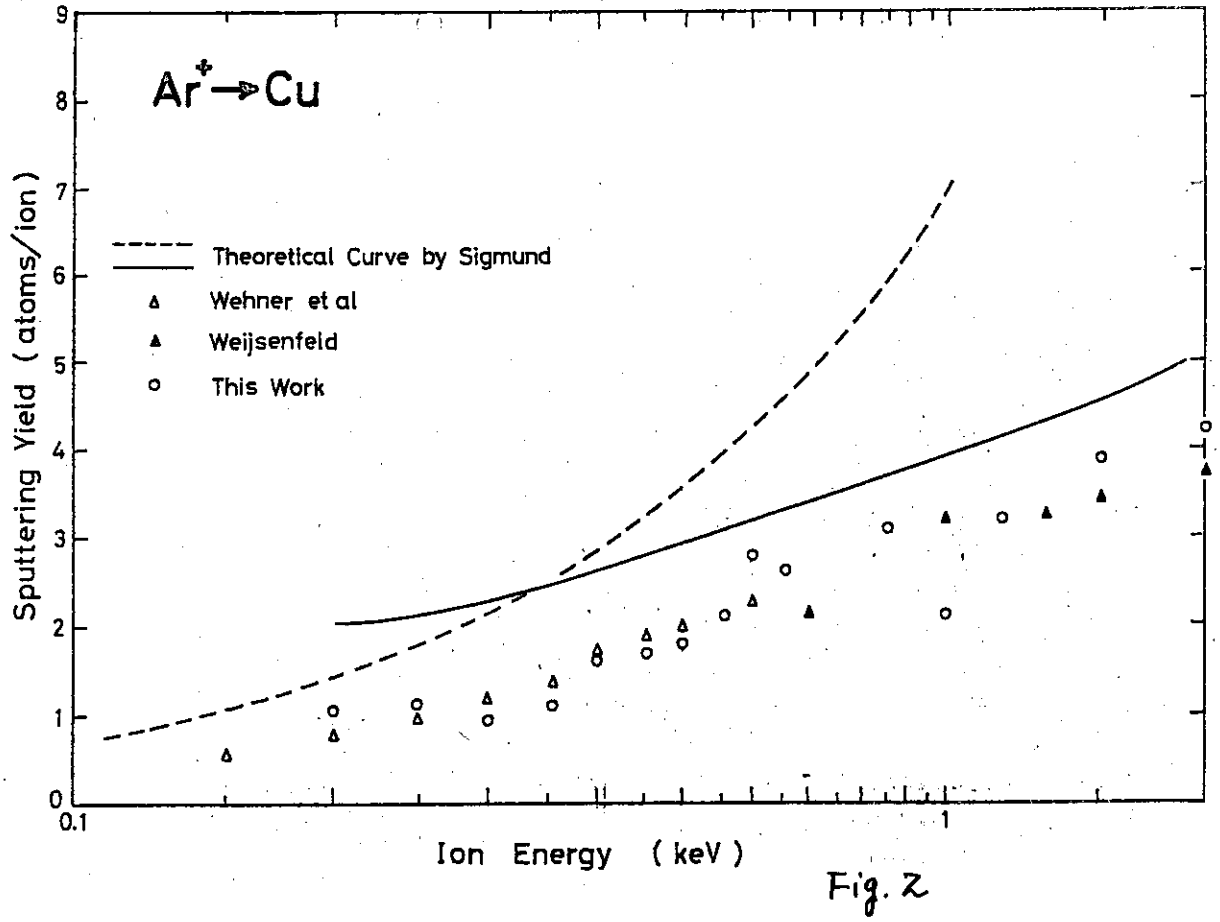
Ar+ → Cu
Theoretical Curve by Sigmund
Wehner et al
Weijsenfeld
This Work
Sputtering Yield (atoms/ion)
Ion Energy (keV)
0
1
2
3
4
5
6
7
8
9
0.1
1

Fig. 2

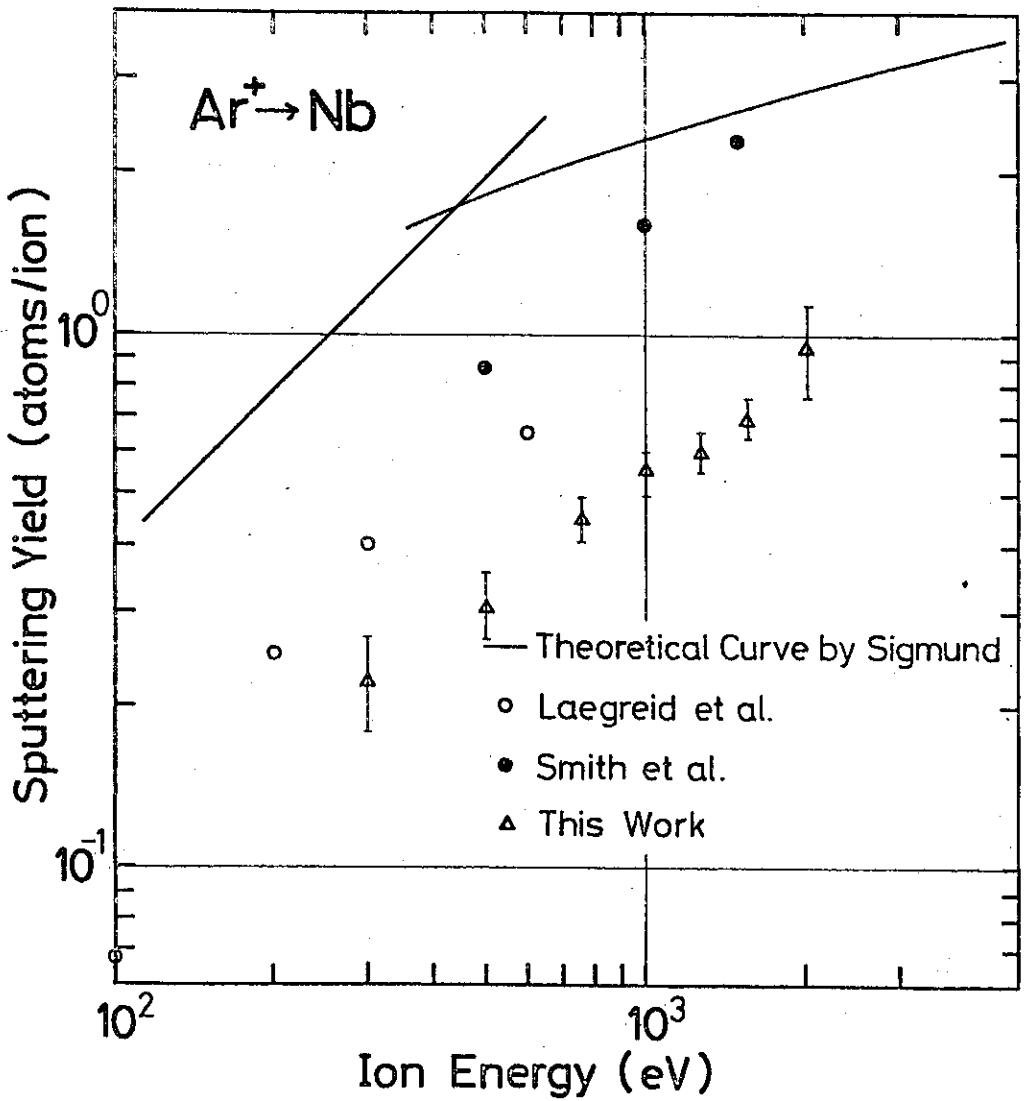

Fig. 3

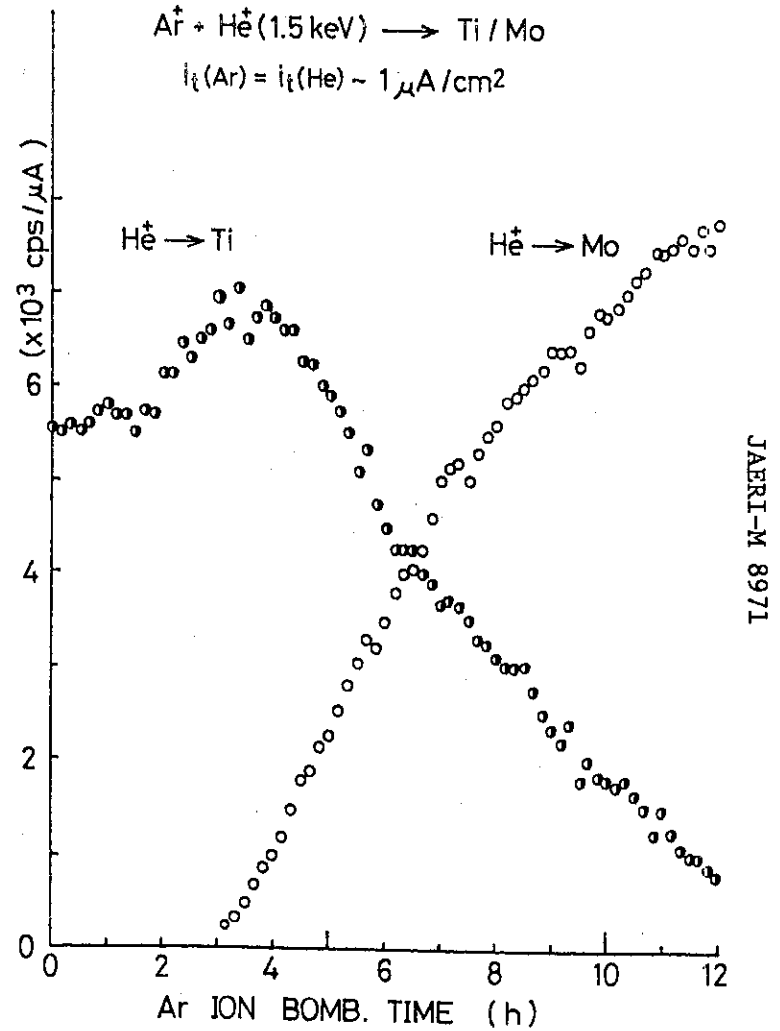

Fig. 4

JAERI-M 8971

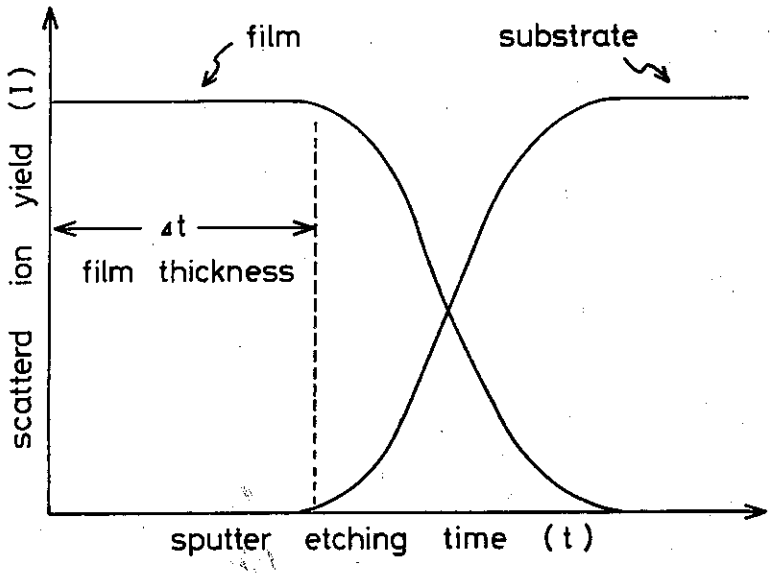
film
substrate
scatterd ion yield (I)
Δt
film thickness
sputter etching time (t)

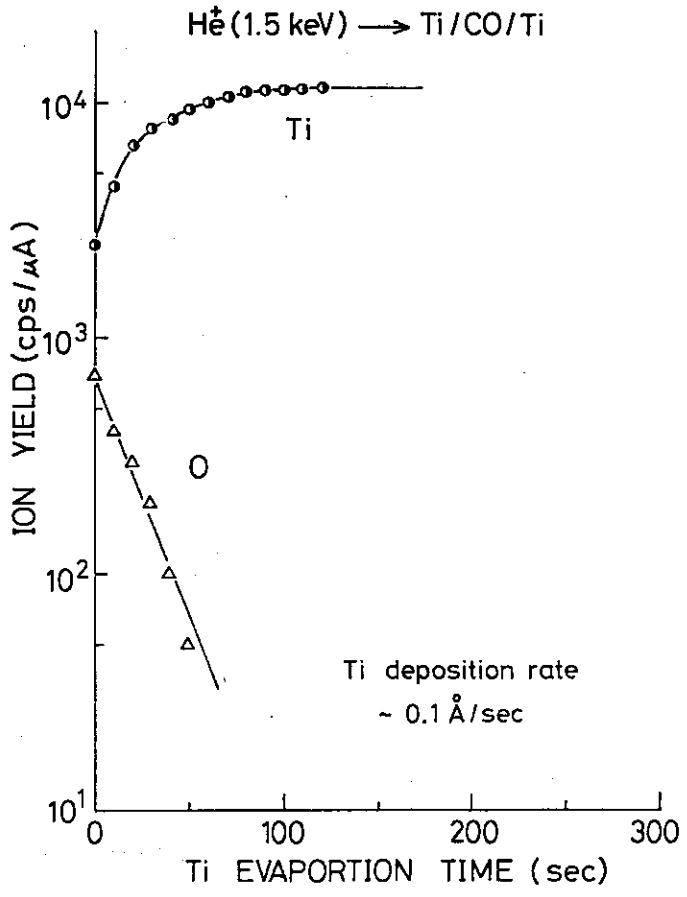
He+ (1.5 keV) ⟶ Ti/CO/Ti
Ti
O
ION YIELD (cps/μA)
10^4
10^3
10^2
10^1
Ti deposition rate
~ 0.1 Å/sec
0
100
200
300
Ti EVAPORTION TIME (sec)

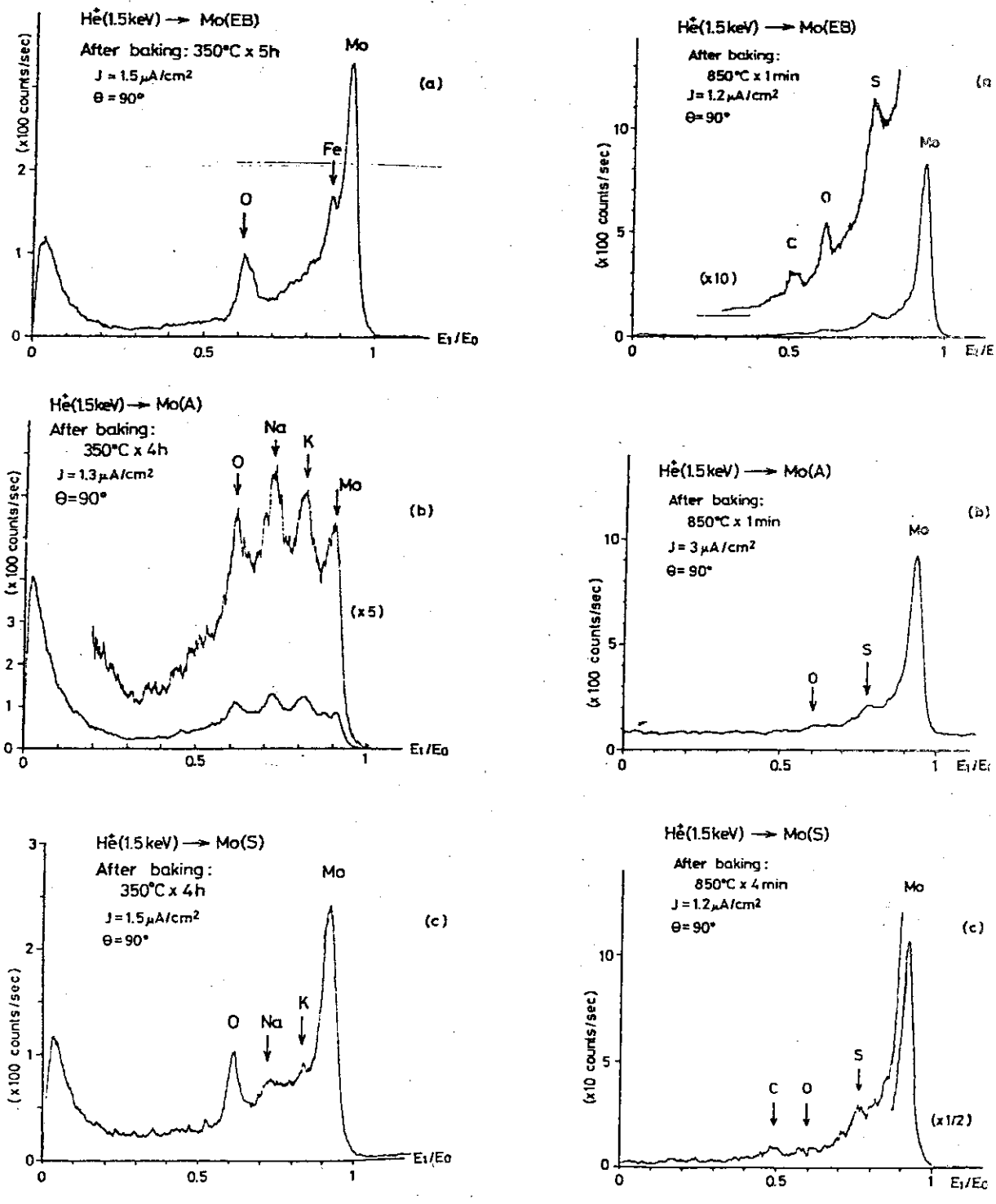
He+(1.5keV) → Mo(EB)
After baking: 350°C x 5h
J = 1.5 μA/cm²
θ = 90°
(a)
Mo
Fe
O
(x100 counts/sec)
E1/E0
He+(1.5keV) → Mo(EB)
After baking:
850°C x 1min
J=1.2 μA/cm²
θ=90°
S
Mo
O
C
(x10)
He+(1.5keV) → Mo(A)
After baking:
350°C x 4h
J = 1.3 μA/cm²
θ=90°
(b)
O
Na
K
Mo
(x5)
He+(1.5keV) → Mo(A)
After baking:
850°C x 1min
J= 3 μA/cm²
θ= 90°
(b)
Mo
S
O
He+(1.5keV) → Mo(S)
After baking:
350°C x 4h
J=1.5 μA/cm²
θ=90°
(c)
Mo
O
Na
K
He+(1.5keV) → Mo(S)
After baking:
850°C x 4min
J=1.2 μA/cm²
θ=90°
(c)
Mo
S
C
O
(x1/2)

Fig. 7

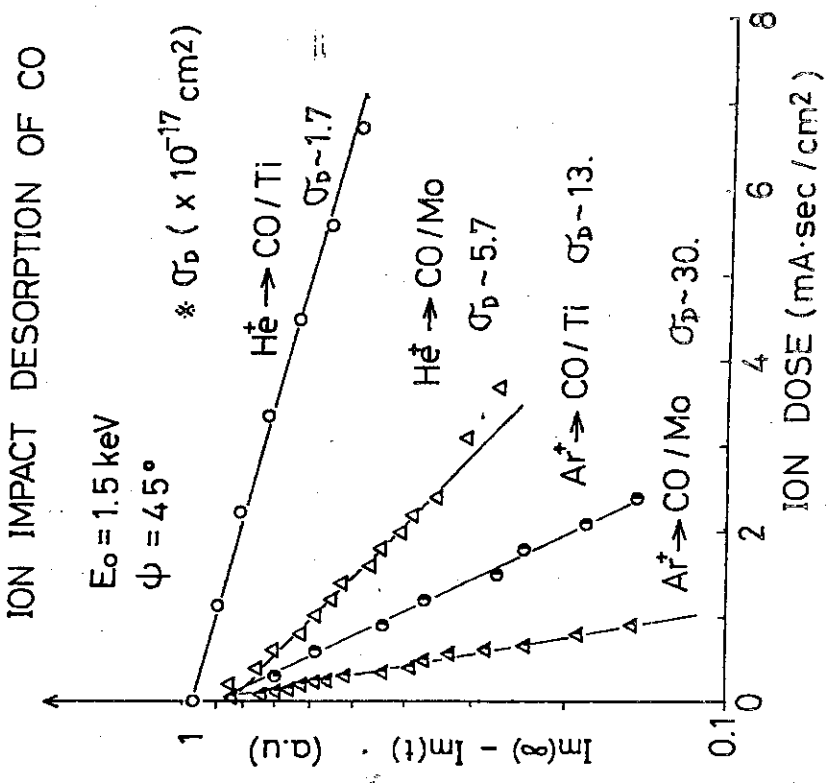
ION IMPACT DESORPTION OF CO
E₀ = 1.5 keV
ψ = 45°
* σD (x 10⁻¹⁷ cm2)
He+ → CO / Ti
σD ~ 1.7
He+ → CO / Mo
σD ~ 5.7
Ar+ → CO / Ti σD ~ 13.
Ar+ → CO / Mo σD ~ 30.
Im(∞) - Im(t) · (a.u)
ION DOSE (mA·sec / cm2)

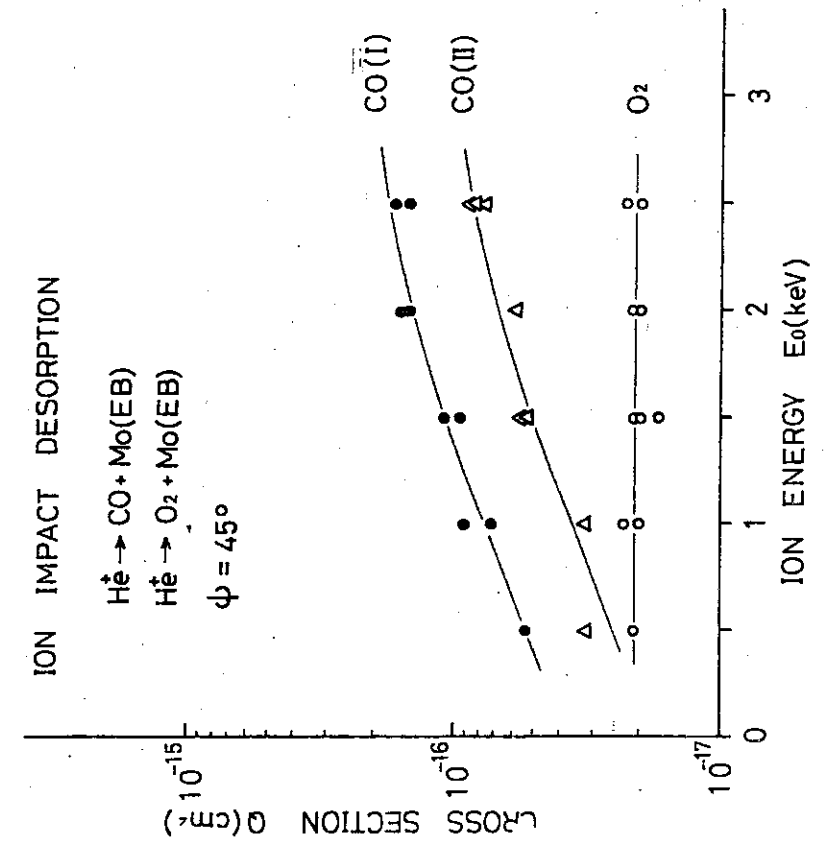
ION IMPACT DESORPTION
He+ → CO+ Mo(EB)
He+ → O₂ + Mo(EB)
ψ = 45°
CO (I)
CO(II)
O₂
CROSS SECTION σ (cm²)
ION ENERGY E₀(keV)

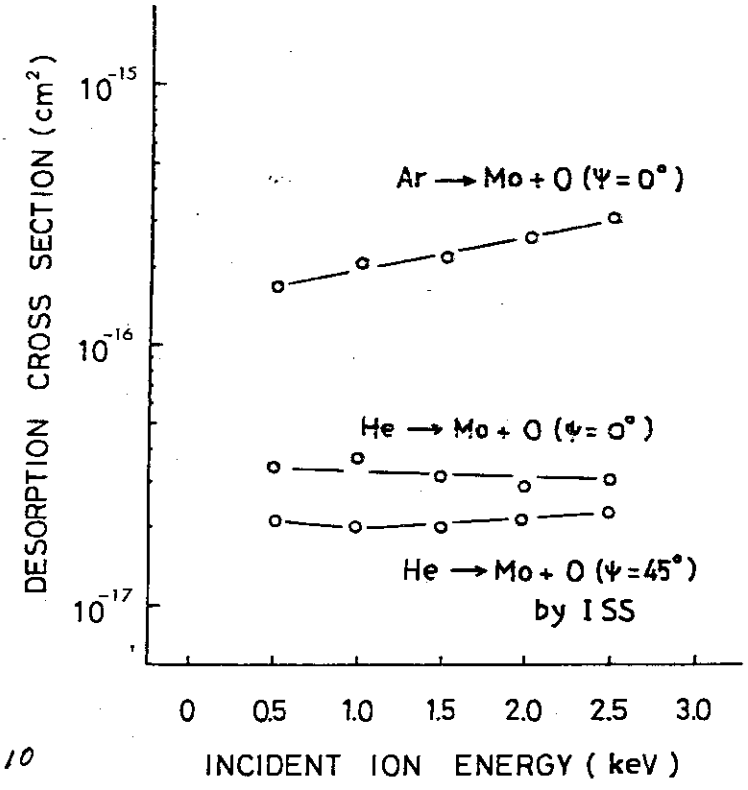

Fig. 10

5. P-W-I in JIPP. T-II

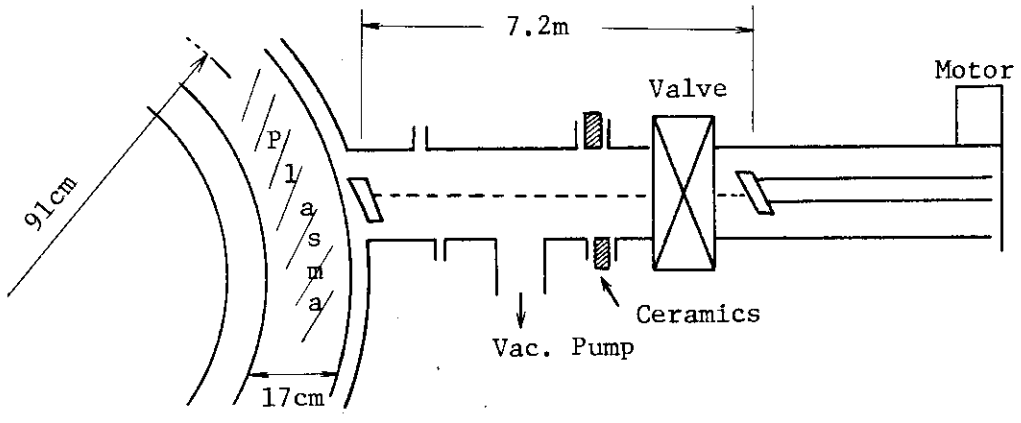

Bt∿30 kG
n ∿3×10^{13} cm^{-3}
Te 0.8∿1.3 KeV
Ti 0.4∿0.6 KeV
T_E 5∿14 m Sec

Construction of sample transfer system

7 - 4 Studies on Low-Energy Ion Sputtering at Faculty of Engineering of Nagoya University

K. Morita

Department of Crystalline Materials Science, Faculty of Engineering,
Nagoya University, Nagoya, Japan

I. Introduction

Ion Sputtering from the first wall materials of controlled thermonuclear fusion devices is known to cause plasma contamination. Therefore, it is important to understand the sputtering phenomena and to develope materials which have a low sputtering yield for atoms with high atomic numbers and at the same time have a high thermal conductivity and a high mechanical strength. The refractory metals and their compounds such as alloys, carbides and oxides have been pointed out to be candidates of the first wall materials.

In this review, the two works concerning the ion sputtering are reported, which have been carried out by the members of the Prof. Itoh's laboratory at Nagoya University; one is a work on derivation of a semi-empirical formula for the sputtering yield[1] and another is an experimental study on the ion sputtering of refractory carbides.[2]

II. A semi-empirical formula for energy dependence of the sputtering yield[1]

A compilation of a great number of sputtering yield data of monatomic metals and semi-conductors and derivation of an empirical formula fitting to them have been carried out. The sputtering yield data for 193 ion-target combinations were collected. They were fitted to a simple semi-empirical formula:

$$Y = P \cdot S_n(E)\{1 - (E_{th}/E)^{1/2}\} , \quad E > E_{th} , \qquad (1)$$

with

$$P = \frac{0.42}{U_s} \alpha ,$$

where E is the incident ion energy, $S_n(E)$ is the nuclear stopping cross-section, U_s is the heat of sublimation and α is a factor depending mainly on M_2/M_1. The last factor in Eq (1) indicates that a threshold energy is necessary for the replacement collision cascade to be created.

It is to be noted that Eq (1) is transfered into the Sigmund's formula[3] by putting $E_{th} = 0$. Both α and E_{th} were used as fitting parameters. An example of the fitting curve of $Y/P \cdot S_n$ vs E/E_{th} for nickel target is shown in Fig. 1. The parameters of α and E_{th} for each ion-target combination were determined so that Eq (1) is fitted to the experimental data. The best fit values of α and E_{th} divided by U_s are plotted as a function of M_2/M_1 in Fig. 2 and Fig. 3, respectively. In both figures, the solid curves show the averaged values of α and $\xi = E_{th}/U_s$ and dashed curves show 30 % deviation from the average. From both figure it can be seen that most of data points of α and ξ fall between ± 30 % values (dashed lines) of the solid curve.

III. Reduction of partial sputtering yield of vanadium atoms by ion-induced segregation of carbon layer at the surface of MeV He^+-preirradiated vanadium carbide[2]

We studied the effect of keV Ar^+ bombardment on vanadium carbide films on the glassy carbon. For vanadium carbides which contain excess carbon atoms and are pre-irradiated with 2 MeV He^+ the carbon enrichment at the surface was observed. The partial sputtering yield of vanadium atoms is found to be reduced to the carbon enrichment maintained during irradiation.

The specimens of vanadium carbide were prepared by heating vanadium-deposited glassy carbon substrates at 800°C or at 900°C for 20 hours. The composition of the specimens prepared at 800°C and 900°C was determined to be

$VC_{0.83}$ and $VC_{0.87}$, respectively, by means of Rutherford backscattering. The lattice constants of these specimens, determined by X-ray diffraction measurements, agree with those of $VC_{0.83}$ and $VC_{0.87}$ obtained by Storms and McNeal.[4] Sputtering of the specimens by 1 ~ 5 keV Ar^+ ions at a normal incidence was carried out and their thickness before and after the Ar^+ bombardment was measured by means of Rutherford backscattering of 2 MeV He^+. The sputtering uield was determined from the thickness cahnge. In order to obtain the effect of the irradiation on the sputtering yield a part of the specimen was pre-irradiated with 2 MeV He^+ before the Ar^+-bombardment.

The partial sputtering yields by 5 keV Ar^+ of vanadium atoms are shown in Table I, it can be seen that the partial sputtering yield from the pre-irradiated part of $VC_{0.87}$ is much less than those for other cases. Examination of the backscattering energy spectrum showed that at the surface of the pre-irradiated part of $VC_{0.87}$ the carbon atoms are enriched by the Ar^+ bombardments. Such carbon enrichment was not observed for other cases. Thus we consider that the reduction of the sputtering yield of metal atoms is due to the coverage of the surface with segregated carbon layers.

It is known that $VC_{0.87}$ contains excess free carbon. Thus the excess carbon appears to be responsible for the carbon enrichment. Since the segregated carbon layer is also sputtered by Ar^+ bombardment, the rate of the segregation should be larger than the rate of the sputtering for the carbon layers to remain on the Ar^+-bombarded surface. It appears that the bombardment with He^+ enhances the diffusivity of carbon in $VC_{0.87}$ in such a degree that the segregation rate surpasses the sputtering rate.

REFERENCES

1) N. Matsunami, Y. Yamamura, Y. Itikawa, N. Itoh, Y. Kazumata, S. Miyagawa K. Morita and R. Shimizu, Radiation Effects Letter (to be published).

2) K. Morita, H. Nakamura and N. Itoh, submitted to Symposium on Sputtering (Wien, 1980).

3) P. Sigmund, Phys. Rev. 184, 383 (1969).

4) E. K. Storms and R. J. McNeal, J. Phys. Chem. 66, 1401 (1962).

TABLE I. Sputtering Yield by 5 keV Ar^+ of metal atoms from $VC_{0.83}$ and $VC_{0.87}$ on glassy carbon. The column "non-preirradiated" shows the result for the as-prepared part of the specimens and that "preirradiated" shows that the result for the part of the specimen irradiated with 2 MeV He^+ at a dose of 4×10^{15} ions/cm^2.

	non-preirradiated	preirradiated with He^+
$VC_{0.83}$	0.40 ± 0.08	0.35 ± 0.08
$VC_{0.87}$	0.44 ± 0.08	0.03 ± 0.01

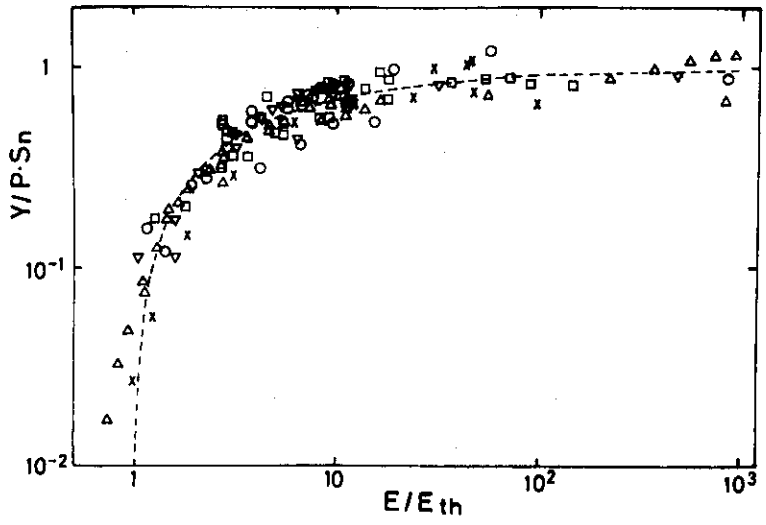

FIGURE 1, Energy dependence of the sputtering yield of Ni targets for H (x), He (□), Ni (o), Ar (Δ) and Xe (▽) ions. The yield and energy are normalized by $P \cdot S_n$ and E_{th}, respectively. The values of P and E_{th} are given in Table I. The dashed line is obtained with Eq (4).

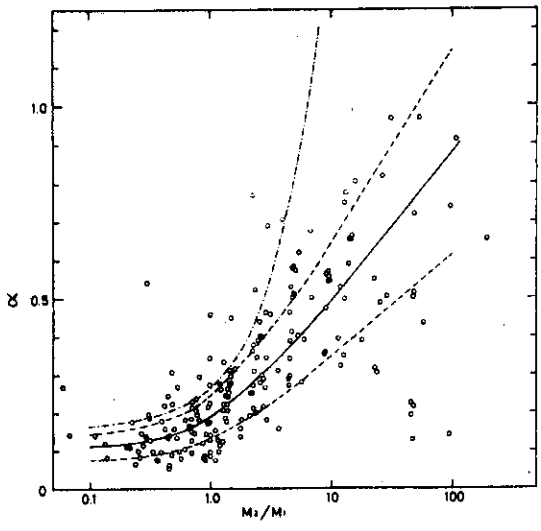

FIGURE 2, The α-parameter as a function of the mass ratio M_2/M_1, where M_2 and M_1 are the masses of target atoms and incidnet ions, respectively. The solid line is drawn by smoothing the averaged values by 1.3 and 0.7, broken lines are drawn. The theoretical values are shown by the dot-dashed line.

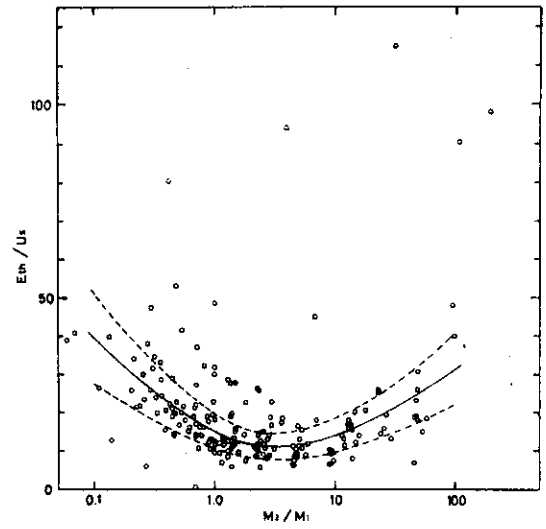

FIGURE 3, The $\xi = E_{th}/U_s$ parameter as a function of the mass ratio M_2/M_1, where M_2 and M_1 are the masses of target atoms and incident ions, respectively. The solid line is drawn by smoothing the averaged values. Multiplying the averaged values by 1.3 and 0.7, broken lines are drawn.

7 - 5

Studies on Plasma-Wall Interaction at the Institute of Physical and Chemical Research (IPCR).

Y. Sakamoto

The Institute of Physical and Chemical Research
Wako-shi, Saitama 351, Japan

1. Introduction

Studies on plasma-wall interaction at IPCR have the origin in ones on degassing of metal wall by electron and ion bombardment. We are now interested in ECR discharge cleaning by using hydrogen, after experiments of reduction of oxide layers on metal surface by using 1) hydrogen atom flux from dissociation of H_2 on a rhenium hot filament, and 2) low temperature ECR plasma of hydrogen.

Here are reported the main results of these experiments and recent ones concerning discharge cleaning of JFT-2 which was executed under the collaboration with the JFT-2 group. Future plans will be also presented.

2. Basic experiments

2-1 Degassing by electron beams[1)]

A straight wolfram filament is coaxially surrounded by a stainless steel (JIS-316L) cylinder. Test surfaces are 1) that of the mother material itself (stainless steel) and 2) that gold-plated on the cylinder (gold). After evacuation under baking at 200°C, the residual gas pressure (H_2) becomes 6.7×10^{-6} Pa. A high current density electron beam (several mA/cm^2) with an

energy between $10^{-1} \sim 10^{0}$ KeV bombards the test surface. After the bombardment, a very low current density electron beam (50 $\mu A/cm^2$), which is called the probing beam, is applied to search layers near the surface. Figure 1 shows the gas yield from the test surface of stainless steel as a function of probing beam energy, taking the degassing beam energy as a parameter. The gas yield increases steeply when the probing beam energy increases over the degassing beam one. This means that the treatment depth is determined only by the degassing beam energy, because it determines the penetration depth of the electrons.

The bombarding electrons excite the carbon and oxygen atoms on the surface to make CO and CO_2 molecules. It is expected that species of the resultant molecules (CO or CO_2) are determined by the surface density of oxygen atoms. This is evidenced by Fig.2 which shows the time evolution of the partial pressure ratio Pco/Pco_2 in both cases of gold and stainless steel, where one supplies several times, Air, O_2 and CO gas. Introduction of air and O_2 naturally increases the surface density of oxygen, which leads to the increase of CO_2 production rate, therfore, to the decrease of Pco/Pco_2. Without doubt, introduction of CO raises Pco/Pco_2.

2-2 Glow discharge cleaning

Results of glow discharge cleaning are similar to those obtained at CERN ; addition of 10 % of O_2 into Ar is very efficient in removal of carbon on the surface.

2-3 Reduction of oxide layers by thermally dissociated hydrogen beams[2)]

Oxide layers of molybdenum are reduced by hydrogen atoms produced by thermal dissociation of H_2 on a hot rhenium filament. Test surfaces are provided by 1) high temperature oxidation and

2) exposure to air. In both cases, the test surfaces are kept at 300°C and O-H reaction probability (γ) are measured, by means of H_2O trapping and by measuring the change of H_2 flow rate. Figure 3 shows the dependence of the reaction probability on the H-atom dose (D_H), where open circles and crosses present γ's in the cases of the exposure to air and the high temperature oxidation, respectively. In both cases in the dose region below 2×10^{16} cm^{-2}, γ's rest constant and above the value, they show the dependence as $\gamma \propto D_H^{-1.4}$. In the former region, the reduction takes place only in the adsorped oxygen layer, but in the latter region, in the oxide layers. The value 1.4 is not yet explained.

2-4 Reduction of oxide layers by ECR hydrogen plasma[3)]

The essential idea of discharge cleaning is that the dominant light impurities, carbon and oxygen, can be transformed into CH_4 and H_2O by hydrogen plasma and pumped out. In general, oxygen can be removed more hardly than carbon.

We tried to reduce oxides of metals which are familiar in the CTR ; Cu, Ni, Fe, Ti and Al. Figure 4 is the schematic drawing of the experimental device. A hydrogen plasma is produced by ECR method. The test pieces are made by oxidation in air (Cu, Ni, Fe, Ti) and anodic oxidation (Al). The oxide layers show interference colors, and we can know approximate thickness of the layers if the refractive indexes are known.

Table 1 shows the thickness of oxide layers and the time necessary to reduce them, along with the measured plasma parameters. The estimated flux ($H^+ + H^o$) is 2.6×10^{16} cm^{-2} sec^{-1} and the reaction probabilities are $\gamma \simeq 0.4$ for Cu_2O and $10^{-3} < \gamma < 10^{-2}$ for other oxides. We were encouraged by these data to carry out real discharge cleaning of a Tokamak device.

3. ECR discharge cleaning of JFT-2[4)]

The advantages of ECR discharge cleaning are as follows :

1) continuous operation.
2) easy control of Te by appropriate combination of microwave power density and gas pressure,
3) low operation cost,
4) no problem for introduction of superconductor coils.

we show schematically in Fig.5 the experimental setup of JFT-2 discharge cleaning. A microwave (2.45 GHz, 2kW CW) is launched by a helix launcher (VSWR $\leqq$ 1.14). Plasma parameters are measured by Langmuir probes P_A & P_B. Resultant gases are analyzed by a quadrupole mass analyzer (QMA). Figure 6 shows the dependence of the electron density on the hydrogen pressure, taking the microwave power as a parameter. We find the maximum density at a pressure. In the higher pressure region, the electron temperature decreases and the lower pressure side, the gas density decreases, this may be the reason why the maximum is observed. The increase of the power shifts the maximum toward the higher pressure side.

Figure 7 shows the dependence of the electron temperature on the gas pressure. The electron temperature is found in the range of several electron volts, which is suitable for discharge cleaning. It is interesting that the pressures which give (Ne) max and (QMA singal for H_2O) max coincide.

Finally, we show, in table 2, partial pressures of resultant gases under quasi-equilibrium condition, comparing those of ECR-DC and Taylor-DC. They have comparable cleaning effect.

4. Future plans

1. Refinement of observation of discharge cleaning, applying in situ surface observation.
2. Measurement of particle fluxes : (Plasma → wall) and (wall → Plasma).
3. Study on hydrogen trapping into metals, as a basic research of a divertor.

References

1) Y. Ishibe : KAKUYUGO KENKYU (in Japanese) 31 Supplement 4 (1974) 2.
Y. Ishibe, H. Oyama : HODEN KENKYU (in Japanese) 69 (1976) 2.
2) Y. Ishibe and H. Oyama : J. Nucle. Mater. 85 & 86 (1979) 1191.
3) Y. Sakamoto and Y. Ishibe : submitted to Jpn. J. Appl. Phys.
4) Y. Sakamoto, Y. Ishibe, K. Yano, H. Oyama, Y. Tanaka, N. Fujisawa, Y. Matsuzaki, N. Suzuki, K. Maeno, T. Yamamoto and K. Yokokura : to be presented in the 4th Intern. Conf. Plasma Surface Interractions in Controlled Fusion Devices, Garmisch -Partenkirchen, FRG (1980).

Figure Captions

Fig 1. Gas yield as a function of probing electron beam energy.

Fig 2. Ratio of partial pressures P_{CO}/P_{CO_2} as a function of electron dose, for test surfaces of gold and stainless steel.

Fig 3. Dependence of reaction probability on hydrogen atom dose for a test surface of stainless steel.
o → exposure to air at room temperature, x → oxidation at high temperature in vacuum.

Fig 4. Experimental device for reduction of metal oxides by using hydrogen plasma.

Fig 5. Experimental set-up of ECR discharge cleaning of JFT-2.

Fig 6. Dependence of electron density on hydrogen pressure.

Fig 7. Dependence of electron density and temperature and QMA output signal ($^{m}/e = 18$) on hydrogen pressure.

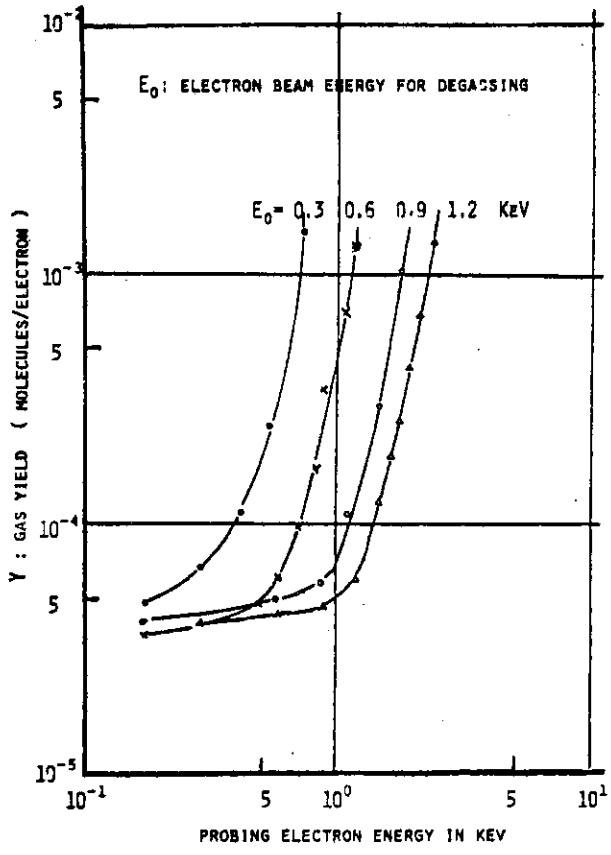

Fig.1

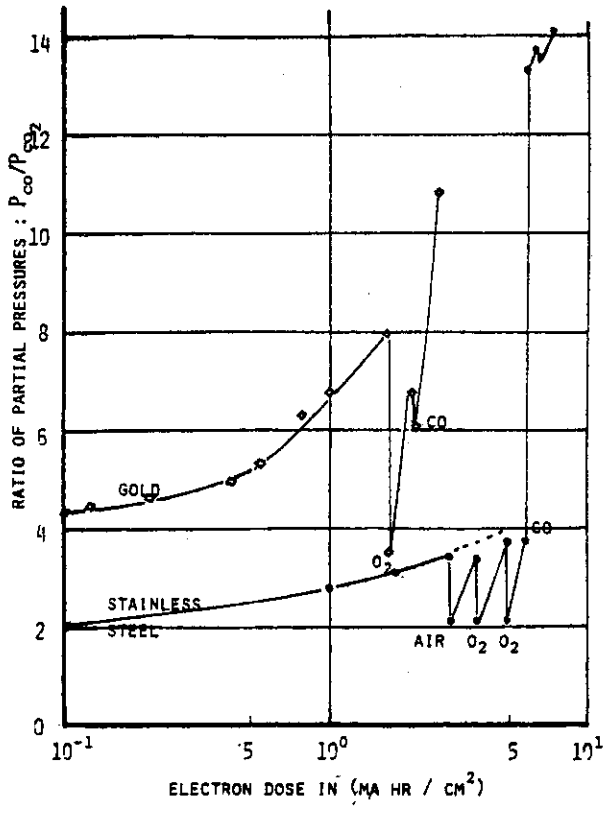

Fig.2

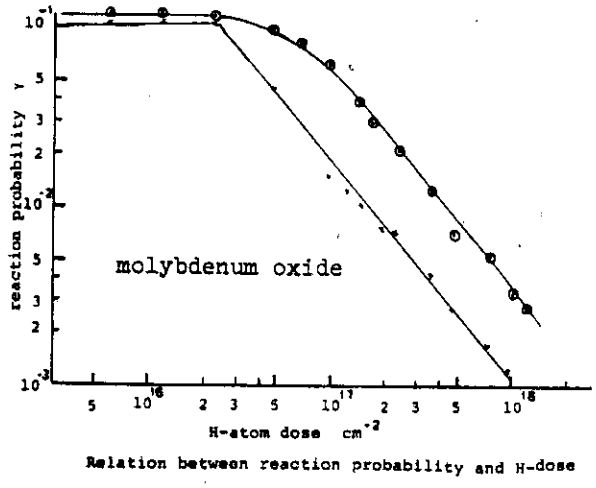

Relation between reaction probability and H-dose

Fig.3

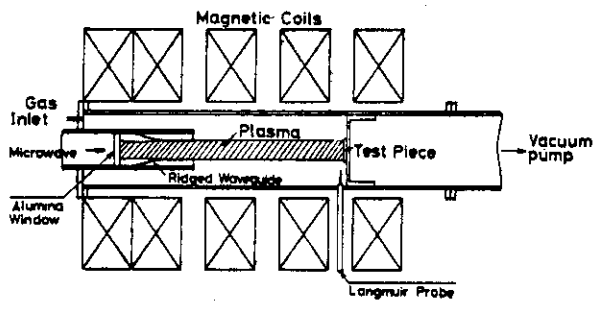

Fig.4

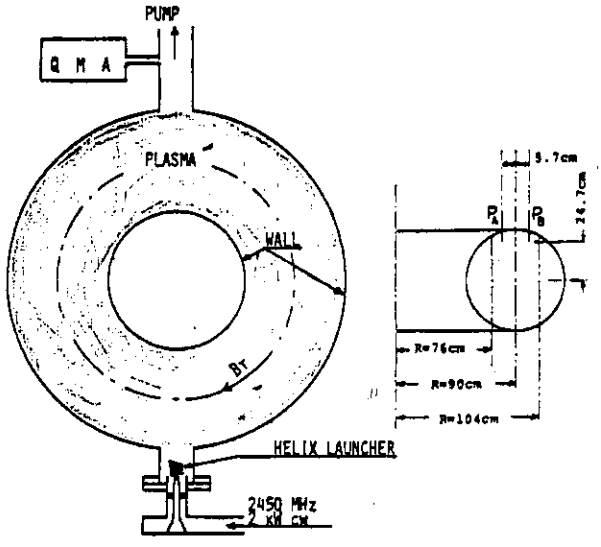

Fig.5

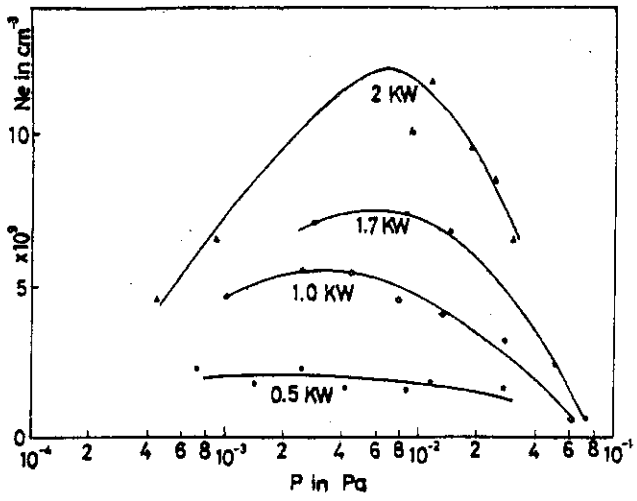

Fig.6

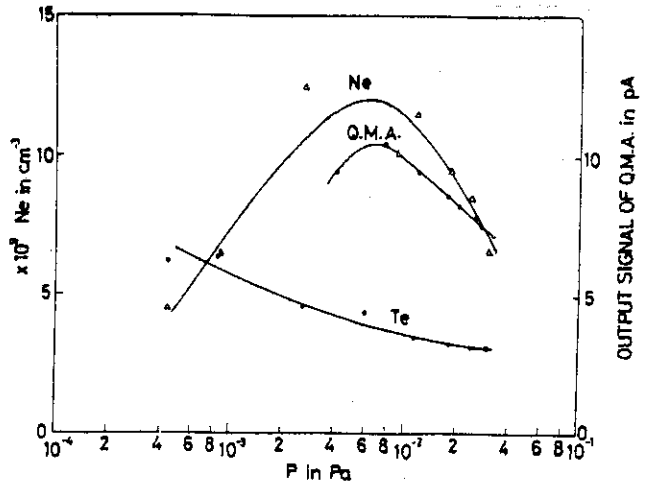

Fig.7

OXIDS	THICKNESS	REDUCTION TIME
Cu_2O	171 nm	72 sec
NiO	209	3 hr
Fe_2O_3	153	5
TiO_2	177	15
Al_2O_3	150	34
$P_{H_2} = 2.7 \times 10^{-2}$ Pa Te = 12 eV Ni = 4×10^{10} cm^{-3}		

Table 1. Necessary reduction time for a given thickness of an oxide by the hydrogen plasma whose parameters are given in the botom space.

PARTIAL PRESSURES OF RESULTANT GASES IN THE CASES OF E C R - D C AND T D C			
GASES	ECR-DC (2 kW) Tw = 60 ~ 100°C	TDC (2 kW) Tw = 80 ~ 180°C	BACKGROUD PRESSURE
CH_4	3.3×10^{-6} Pa	6.6×10^{-6} Pa	2.7×10^{-7} Pa
H_2O	8.6×10^{-6} "	9.3×10^{-6} "	1.3×10^{-6} "
CO	3.4×10^{-6} "	3.1×10^{-6} "	4×10^{-7} "
PUMPING SPEED (N_2) 620 ls^{-1}			

Table 2. Comparison between partial pressures of produced gases when ECR-DC and TDC are carried out.

7 - 6 Research at Vacuum Science Laboratory Hokkaido Uneversity

Vacuum Science Laboratory
Department of Nuclear Engineering
Hokkaido University, Sapporo

presented by M. Mohri

Principal Research Staffs

Toshiro Yamashina, Professor Dr.
Kuniaki Watanabe, Associate Professor Dr.
Mamoru Mohri, Research Associate Dr.
and
two Technical Scientists, five Graduate Students and four Undergraduate Students (Senior).

Research Projects 1980 - 1981

In this laboratory, research works are in progress on the following subjects,

1. Sputtering Processes of Low-Z Compounds as the First Wall
   1) AES-SIMS-XPS study of surface segregation of low-Z compounds (TiC, SiC, TiN, B_4C, BN, etc.) with energetic ion bombardment
   2) Physical and chemical sputtering of low-Z compounds by ion probe microanalysis technique
   3) Implantation-desorption experiments of energetic ions on low-Z materials
   4) "in situ measurement of sputtering yield by high sensitive microbalance.
2. Coatings of Low-Z Materials onto Metals and Alloys
   1) TiC and SiC coatings onto C, Mo and stainless steels by means of r.f.sputtering and electron beam
   2) Quantitative in-depth profile of coating layers of low-Z materials
   3) Roughness factor measurement of coating layers of ion bombardment.
3. Selective Sputtering and Segregation of Binary Alloy Surfaces
   1) Selective sputtering and altered layers of Cu-Ni and

Ag-Au alloys with ion bombardment

2) Quantitative surface analysis of stainless steels with ion bombardment and discharge cleaning.

Cooperation with Other Institutes

In the several subjects described above, we have been cooperating with Institute of Plasma Physics, Nagoya University, Government Industrial Development Laboratory, Hokkaido, Central Laboratory, Hitachi Ltd. and ISR Section, CERN, Geneva. Especially with the collaboration of Professor A.Miyahara's group, a surface station for the plasma-wall interactions to be connected with JIPPT-II Tokamak device of Nagoya University is expected to complete shortly.

7 - 7 SUMMARY OF THE WORKS ON BLISTERING AND RELATED EROSION PHENOMENA IN JAERI

Kohji KAMADA

Physics Division,JAERI.

Works in JAERI on blistering and related erosion phenomena on materials surface have been aiming at both studies on the fundamental blistering mechanism and on the erosion of the first wall of future fusion devices.

The first kind of works have been carring out in Physics Division, in both theoretical and experimental aspects. Theoretical studies were concerned with blistering and flaking mechanisms from the stand point of pressure driven models. Theoretical tools exploited were dislocation theory and fracture mechanics.

Results of the theoretical studies are as follows: (1) blistering takes place when the condition

$$[0.30(\frac{a}{h})^{3.28} + 0.14(\frac{a}{h})^{3.69} + 0.03(\frac{a}{h})^{4.10}](\frac{P}{\sigma_{ys}})^2 = 1$$

is satisfied, provided the ratio h/a<0.3. In the region h/a>0.3, another formulation, but on the same footing, is obtained. In the above formula, a=blister radius, h=depth from a free surface, P=internal pressure of the blistter, and σ_{ys}=mechanical yield stress of the sub-surface layer. Employing an appropriate value for σ_{ys}, satisfactory agreement with experimental result was obtained. (2) assuming ductile crack propagation in the ion irradiated subsurface layer, due to the presence of small spherical bubbles, blistering and flaking are reasonably discriminated on the basis of a single mechanism of gas driven model.

Experimentally, in-situ observations of blistered surface were carried out in a scanning electron microscope, which was connected to a 2 MeV Van de Graaff accelerator. Target materials were single crystalline metals, such as Nb,Mo,Cu and Al, in which Nb was most extensively examined. Ion species were He^+,Ne^+ and Ar^+ of relatively high energy more than 300 keV. One of the aims of this experiment was precise measurement of the critical fluence of blistering, together with further developement of surface erosion due to the blistering as a function of ion dose. Studies of blistering due to heavier ions than He^+ were another purpose of the experiment. Actually, bombardment by Ne^+,

which is presumed to situate at interstitial site, but less mobile than He^+, in BCC structure, shows differnt aspects of blistering in comparison with He^+ blistering. Further, bombardment by Ar^+, which is larger than Ne^+ and presumably situates at substitutional site at room temperature and below, shows quite a differnt aspects, being necessary the post irradiation annealing for blistering to appear.

Flaking in pyrolytic graphite due to He^+,Ne^+,Ar^+ and N^+ ion bombardments, and hole-formation in glassy carbon by Ne^+ ion bombardment were also studied experimentally. As for the flaking, theoretical explanations were given on the basis of elastic theory of strongly anisotropic materials. The results are in satisfactory agreements with experimental results.

In-situ observations of blistering and subsequent exfoliations during 100 keV He^+ ion bombardment on polycrystalline Mo surface were carried out in Fusion Research Division. Facilities for this experiment were 400 keV Cockcroft-Walton type ion accelerator and specially designed scanning electron microscope connected with it. Critical fluence of blistering together with its dependence on crystal orientation, subsequent exfoliation of the surface layer, and the speed of the exfoliation were successfully measured.Incidentally, anticipating the thermal cycling for the first wall of future fusion devices, post irradiation annealing experiments were also undertaken.

In anticipation of reducing the surface erosion due to ion bombardment, experiments on multi-grooved polycrystalline surface were carried out. The multi-groove structure consists of a number of rectangular parallel grooves, the width and depth of which were 3-7 and 2-3 μm, respectively. It was found by scanning electron microscopy that surface erosion due to blistering is effectively reduced by this structure.

A phenomenon named grain ejection was found, by bombardment with pulsed intense beam of 25 keV H^+, as well as H_2^+, in the temperature range of 150-250°C. The averaged ion beam intensity was 1.7×10^{17} ions/cm^{2}sec. The surface erosion observed was presumed by original authors to be due to the exfoliations along grain boundaries. However, its physical mechanism is not well explored yet.

LIST OF EXPERIMENTS ON BLISTERING AND FLAKING IN JAERI

	Materials and Pre-Treatments	Ion and Energy Range	Dose and Dose-Rate	Temperature ^{o}C	Comments	Reference
1.	Mo(Poly.) 1300°C 1h.ann.	He^{+} 100 keV	$<9.0\times10^{17}/cm^{2}$	R.T.	In-situ observations under irradiation.	1
2.	Mo(poly.) 500-600°C 10h ann.	He^{+} 100 keV 400 keV	5×10^{18}, $1\times10^{19}/cm^{2}$ 1.9×10^{14}-$3.8\times10^{14}/cm^{2}sec$	R.T.– 850°C	On multi-grooved surfaces.	2
3.	Mo(110) 1500°C 48h ann.	Ar^{+} 300 keV	1, $6\times10^{17}/cm^{2}$ 1, $3\times10^{18}/cm^{2}$	-130°C	Room temperature annealing effects.	3
4.	Mo(poly.) 1400°C 1h ann.	Ar^{+} 450 keV	1×10^{16}-$4\times10^{18}/cm^{2}$ 8.8×10^{13}, $3.5\times10^{14}/cm^{2}sec$	<200°C	Post-irr. annealing effects in 500-1200°C.	4
5.	Mo(poly.)	H^{+}, H_{2}^{+} 25 keV	6×10^{18}-$1.3\times10^{19}/cm^{2}$ <$1.7\times10^{17}/cm^{2}sec$>*	100-500°C	Grain ejection in 150-260°C. With pulsed ion beam.	5
6.	Mo(poly.) 1300°C 1h ann. 800°C 1h ann.	He^{+} 60-400 keV	$<10^{19}/cm^{2}$ $5\times10^{14}/cm^{2}sec$	R.T.	Multiple energy irradiation.	6
7.	Nb(100) 1100°C 48h ann.	Ne^{+} 450 keV	2.4×10^{17}-$1.2\times10^{18}/cm^{2}$ $2.6\times10^{14}/cm^{2}sec$	R.T.	In-situ observation; blistering.	7
8.	Nb(111) 1100°C ann.	He^{+} 300 keV	7.2×10^{17}-$1.1\times10^{18}/cm^{2}$ 1.1, $2.3\times10^{14}/cm^{2}sec$	R.T.	In-situ observation; flaking.	7
9.	Nb(100) 1500°C 48h ann.	Ne^{+}	$10^{18}/cm^{2}$ $9\times10^{13}/cm^{2}sec$	-130°C	Blistering and exfoliation.	8

	Materials and Pre-Treatments	Ion and Energy Range	Dose and Dose-Rate	Temperature	Comments	Reference
10.	P-graphite, on basal plane.	450 keV Ar^+ 1.1 MeV N^+ 1.9 MeV He^+	$2x10^{13}$-$3x10^{17}$ Ar^+/cm^2 $2x10^{13}$-$2x10^{16}$ N^+/cm^2 $1x10^{14}$-$2x10^{17}$ He^+/cm^2	-153°C	Flaking.	9
11.	P-graphite, on basal plane.	Ne^+ 350 keV 850 keV	$1x10^{14}$-$4x10^{18}/cm^2$ $9.4x10^{13}/cm^2$sec	-153°C	Flaking.	10
12.	Glassy cargon.	Ne^+ 850 keV	$1x10^{14}$-$4x10^{18}/cm^2$ $9.4x10^{13}/cm^2$sec	-153°C	Hole.	10
13.	P-graphite, on basal plane.	He^+ 100 keV	$1x10^{17}$-$5x10^{18}/cm^2$ 1.9-3.1$x10^{14}/cm^2$sec	R.T.	Flaking and cone structure.	11
14.	P-graphite, on basal plane. Mechanical polish.	H_2^+ 200 keV	$5x10^{16}$-$2.5x10^{18}/cm^2$ $1.3x10^{14}/cm^2$sec	R.T.	Blistering at $1x10^{18}/cm^2$.	11
15.	Ge(110)	Ar^+ 450 keV	$<8x10^{17}/cm^2$	<40°C	Blister cut-off and amorphization.	12

* < > denotes mean value.

REFERENCE

1/ M.Saidoh,K.Sone,R.Yamada and H.Ohtsuka:
Simultaneous and continuous observations of He bombarded surface of polycrystalline Mo.
JAERI-M 7997 (in Japanese).

2/ K.Sone,M.Saidoh,R.Yamada and H.Ohtsuka:
Reduction of erosion by blistering in Mo surface with a multi-groove microstructure.
J.Nucl.Mat.76/77(1978)240.

3/ K.Kamada,H.Naramoto and Y.Kazumata:
Room temperature aging effects of blistering and surface roughening after Ar^+ ion bombardment on Mo single crystal.
J.Nucl.Mat.71(1978)249.

4/ M.Tanaka,K.Fukai and K.Shiraishi:
Observation of blistering formed on the surface of Mo irradiated with Ar^+ ion at ambient temperature.
JAERI-M 6585 (in Japanese).

5/ Y.Nakamura,T.Shibata and M.Tanaka:
Grain ejection from the surface of polycrystalline Mo irradiated by intense H^+ and H_2^+ ion beams.
J.Nucl.Mat.68(1977)253.

6/ M.Saidoh et al.
To be published.

7/ K.Kamada and H.Naramoto:
Flaking and blistering on He and Ne bombardments.
Rad.Effects 42(1979)209.

8/ H.Naramoto and K.Kamada:
Blister formation in Nb single crystal on Ne^+ bombardment.
J.Nucl.Mat.74(1978)186.

9/ Y.Kazumata:
Surface topography of pyrolytic graphite crystals bombarded with Ar^+,N^+ and He^+ ions.
J.Nucl.Mat.68(1977)257.

10/ Y.Kazumata:
Surface erosion of pyrolytic graphite and glassy carbon by ion bombardment.
J.Nucl.Mat.71(1977)178.

11/ K.Sone,T.Abe,K.Obara,R.Yamada and H.Ohtsuka:
Graphite surface erosion by 100 keV He and H bombardments.
J.Nucl.Mat.71(1977)82.

12/ K.Kamada,Y.Kazumata and K.Kubo:
Observation of blistering and amorphization on Ge surface after 450 keV Ar^+ iom bombardment.
Rad.Effects 28(1976)43.

THEORETICAL PAPERS

1/ Y.Higashida and K.Kamada:
Mechanism of flaking in pyrolytic graphite on ion bombardments.
I. Stress fields around a penny-shaped crack in the sub-surface layer.
J.Nucl.Mater.73(1978)30.

2/ K.Kamada and Y.Higashida:
Mechanism of flaking in pyrolytic graphite on ion bombardments.
II. Numerical discussions in relation to the flaking.
J.Nucl.Mater.73(1978)41.

3/ K.Kamada and Y.Higashida:
A fracture model of radiation blistering.
J.Appl.Phys.50(6)(1979)4131.

7 - 8 Radiation Damage on Low Z Ceramics of the First Wall in Near-Term Fusion Reactors

Y. ATO, M. KOBAYAKAWA and K. YASUDA

Government Industrial Research Institute, Nagoya, Nagoya, Japan

Low Z ceramics are required for a number of applications in fusion systems. One of the important application of ceramics is as a first walls or liners. The low Z ceramics,e.g. carbides, silicides, oxides, nitrides and borides, are suitable candidate materials as a first walls with following major advantages: low plasma impurity effects, low induced radioactivity, high operating temperature, and inexpensive raw material supply. First wall ceramics will be exposed to intense radiation from plasma (light ions, impurity ions, neutral fuel gases, fast neutrons, photon, electrons). Such energetic radiations can cause a variety of surface phenomena, e.g. sputtering, chemical erosion, blistering, arcing, vaporization and cracking. At present, there is insufficient information on these phenomena for ceramics.

In our institute the irradiation effects on inorganic materials has been researched using facilities of a Van de Graaff accelerator (1.2－2.0 MeV, He^+ 30 μA), an electron linear accelerator (10 MeV, 300 μA) and a RF (exchangeable for hot cathode) type ion implanter (20－200 keV, He^+ 300 μA) Recently, in order to obtain the fundamental data of first wall materials in near-term fusion reactors, investigation of radiation damage for low Z ceramics was begun under co-operation with the division of ceramics engineering in this institute.

The ceramics examined in this work are coated films of SiC, TiC, TiN and Al_2O_3 as well as bulks of SiC, Si_3N_4, B_4C and C. The strategy of this study are as follows: 1) invesitgation of surface damage by

sputtering, blistering, flaking and of other surface changes due to heavy bombardments, 2) investigation of surface damage due to synergistic ion-bombardments and multiple-energy-ion bombardments, 3) production of surface coatings by low Z ceramics and characterization for the coated films.

Results so far are as follows: 1)The topographic changes in low Z materials due to He^+ and H^+ ion bombardments have been investigated using a scanning electron microscope (SEM) as functions of energy, ion dose, temeperature of the samples. The critical ion doses for blistering on CVD and Refel SiC were of the order of $2\text{-}7\times10^{17}$ ions/cm^2 for He^+ and H^+ ion bombardments with 100 keV. The range of blister diameters on CVD and Refel SiC was about 2-28 μm. There was a good agreement between the blister skin thickness and the projected range of He^+ and H^+ ions, but in case of H^+ ion bombardment under 30 keV energy the skin thickness was larger than the projected range. 2) The significant increase in the critical ion dose for blistering due to He^+ ion on SiC have been obtained by pre-bombardment of C^+ ions. 3) The sputtering yield of CVD SiC for 30 keV He^+ ion bombardment at ambient temperature was 3×10^{-3} atoms/ion, which was measured by weight loss mehtod. Electron-beam evaporated boron films were bombarded by He^+ ion (30-150 keV) and the sputtering yields were measured for doses of 10^{17}-10^{18} ions/cm^2, using the nuclear resonance reaction near 163 keV in $^{11}B(p,\alpha)^{8}Be$. No significant difference was found the between experimental values and the theoritical predictions by Sigmund, et al.. 4) The change of surface composition by H^+ ion bombardment at ambient temperature and 700 °C was measured using AES. At ambient temperature SiO_2 layers were formed on the CVD SiC surface. 5) SiC films were deposited on glassy carbon by

reactive sputtering in acetylene-argon atmosphere. The film composition, measured by 1.8 MeV He^+ backscattering, varied considerably with the acetylene pressure. The morphology of the film surface was examined with SEM, and it was found that the surface of Si rich film was rough and that of C rich film was flat.

In future, plasma-material interaction for low Z ceramics and low Z coatings are extensively investigated through the following process: 1)blistering, flaking, physical and chemical sputtering, 2) compositional change of surface, 3) effects of synergistic bombardment of light and impurity ions, 4) effects of multiple-energy-ion bombardment, 5) structual modification effects of surface (cracked and porous), 6) effects on critical ion doses due to heavy ion pre-bombardment, 7) production of surface coatings by plasma CVD, 8) characterization of surface coatings (composition, density, porosity, surface morphology,texture, compatibility with substrate), 9) production of multilayer composite coatings by plasma CVD, 10) examination of candidate coating system (adhesion under thermal loading in hydrogen plasma, capability of coating refomation).

8 - 1 Research on Low-Z Material Coatings in National Research Institute for Metals

Masatoshi OKada, Masao Fukutomi, Masahiro Kitajima
Tatsuo Shikama, and Ryoji Watanabe

National Research Institute for Metals, Tsukuba Branch
Sakuramura, Niiharigun, Ibaraki 305 Japan

Introduction

The coating of low-Z materials on the surface of the wall which faces the confined plasma is one of the important problems in the research and development of the tokamak fusion reactor. At the present stage in the field of research on plasma control, this problem has become a very serious one.

As for the coating materials, it is essentially required that they have high resistivity to surface irradiation, stability for thermal cycle, shock and evaporation, and adherence between the coating films and the substrate metals.

On the other hand, requirements of the coating technique are that the temperature of coating process be as low as possible so as not to deteriorate the mechanical properties of the substrates, that the technique be applicable to the coating of a large area with fairly homogeneous film, and further that the regeneration of repair of the coated film be available during operation by so-called in-situ coating.

From these points of view, we have been studying low-Z coatings by means of the ion-plating and the chemical vapor deposition. Among the several coating methods such as chemical vapor deposition(CVD), physical vapor deposition(PVD), plasma spray and diffusion coating, the PVD including ion-plating and plasma assisted CVD is considered to be the most suitable method to satisfy the requirements described above.

Research in National Research Institute for Metals

Outline of the Research

An outline of our research is presented in Figure 1. Among the coating materials such as SiC, Si_3N_4, AlN, C, Si-C-Al-O and Si-N-Al-O which have been chosen in our experiment, we have especially tried to accumulate data on SiC coating because it has a thermal expansion coefficient very close to that of Mo substrate.

We have taken Mo as a substrate metal at our first choice, because it is to be used as a liner of JT-60 and a protective plate of JXFR in the respective designs proposed by JAERI.

The purpose of this research is to obtain knowledge concerning the characters of coated films and their behavior under some environments in regard to the difference of coating methods between the CVD and PVD, the ion-plating in our case.

Coating Methods; CVD and Ion Plating

The CVD coating used in our study has been previously described in detail.[1] SiC was deposited by the hydrogen reduction and/or thermal decomposition of ethyltrichlorosilane($C_2H_5SiCl_3$). The substrates, sintered Mo, were polished on emery paper, and some of them were undercoated with boron of approximately 1 μm thickness or 0.1 μm thick carbon. During the coating process, the substrates were heated to a temperature between 1050-1300°C.

Details of the ion-plating used in our study are described elsewhere.[2] The vapors of Si from molten Si pool and of the introduced acetylene(C_2H_2) were glow discharged by a RF coil. The total reactant gases have a varied pressure in the range from 4.0×10^{-3} to 9.0×10^{-3} torr, and the substrate was heated to a temperature between 250 and 1000°C. A fairly high deposition rate, 0.1- 1 μm/min, could be obtained in this experiment.

As will be described later, in the case of ion-plating some content of Al_2O_3 was added to SiC or Si_3N_4 to improve the thermal stability of the coatings.

In this case, two kinds of source materials of Al_2O_3 were used: (1) direct evaporation from Si and Al_2O_3 mixture molten by an electron beam, (2) dual source from aluminum-isopropoxide, $Al(OCH(CH_3)_2)_3$, and Si.

The CVD method appears to have a disadvantage compared with the ion-plating in that it needs a higher temperature of the substrate. Above 1000°C, recrystallization of Mo proceeds and it becomes brittle.

Characterization of the Coated Film

(1) Appearance of the cross section.

Scanning electron microscopy revealed that the CVD SiC was homogeneous in microstructure and it coated with almost equal thickness along the edge of the substrate. On the contrary, the ion-plated SiC film is laminar in structure and the coating along the edge is poor. These distinctions are considered to be attributable to the difference of the directional throwing power and of flux-fluctuation of the reactant gases between the two methods.

(2) Surface morphology

SEM observation presents that the surface of the CVD SiC is composed of dense nodule-like grains and the cross section of the film has columnar structures, while the ion-plated SiC has a rather flat and smooth surface with lesser density of the nodule and its cross section appear glass-like.

(3) Chemical composition

The ion-plated film made at 800°C has a composition very close to stoichiometry but in those made at lower or higher temperature, the composition shifts to Si or C rich region respectively. This seems to be due to the decomposition rate of acetylene. The CVD film prepared at 1150°C has an almost stoichiometric composition as dose the ion-plated at 800°C.
The calculated composition of the ion-plated Si-C-Al-O composit film is $Si_{0.21}Al_{0.37}O_{0.31}C_{0.11}$ (Si: not SiO_2, probably SiC, Al: Al_2O_3, Al_4C_3?, C: Carbide, O: Al_2O_3) from auger electron spectroscopy.

(4) Chemical bonding

The Si-C bond in the film of the CVD and ion-plated at 800°C is much more accomplished than in the ion-plated at 250°C. The CVD films had a relatively deep SiC bond in infrared spectra, which probably resulted from the small water content of the source material ETCS. (Figure 2)

(5) Crystalline state

X-ray diffraction analysis revealed that the ion-plated SiC was easily crystallized by heat treatment at 1400°C for 5 min though the degree of its crystallization was quite small. The CVD film was obtained as crystalline.

(6) Pinhole defect

The pinhole defect in the as-coated film was detected by the electrographic method, details of which were described previously.[3] The density of pinhole decreases with the increase of the film thickness in the case of the ion-plated Si_3N_4. Compared to the results of the CVD SiC, it may be concluded that the density of the pinhole in the CVD film is generally less than that of the ion-plated. It may be reasonable if we take account of the difference of growth mechanism of the deposited film between the two methods. (Figures 3(a) & 3(b))

The results of the characterization presented above are listed in Table 1.

Non-irradiation test

(1) Thermal cycle test

The stability of the CVD SiC coating under thermal cycle condition was evaluated in air using a thermogravimeter. The coating defects formed during the heat cycle could be sensitively detected by the weight loss of the evaporated molybdenum trioxide. The underlayer of boron seems to be effective to obtain heat resistance. A thermal cycle with much steeper temperature rate which simulated the burn cycle of JXFR was also applied in argon or vacuum environment. The ion-plated SiC had a tendency to easily lose the weight by exfoliation and evaporation of the film, while the CVD SiC is fairly stable. The improvement of the heat resistance of the ion-plated SiC was tried by the addition of Al_2O_3 to SiC by means of the methods previously described, and fairly good results were obtained though the number of cycle was too small to estimate life time.

(2) Oxidation test

Oxidation tests using a thermogravimeter were carried out in the air or in argon containing 1% oxygen. From these tests we can estimate the density of defects or micropores which channel to the Mo substrate. It may be considered that CVD film has less defect- or micropore-density and deposits more densely than the ion-plated film. This conclusion is also supported by the results of pinhole detection.

Irradiation test[4)]

The ion-plated SiC and carbon film on the Mo substrate were irradiated by proton and helium ions of energies of 25KeV and 100KeV up to the total dose of 3×10^{18} ions/cm^2 at ambient room temperature. The SiC coating was carried out at the substrate temperature of 800°C and the characters of the film was described. As for the carbon film, no X-ray diffraction line was observed distinctly. The specimen size is a disk of 3 mmϕ of 0.3 mm in thickness. The thickness of the film was about 10 μm. The ion beam is accelerated by the small Van der Graaff, deflected 30°C by analyzer magnet, defocussed to the circular shape of about 30 mmϕ and then introduced into the target chamber. The total dose of irradiation could be measured by a Faraday cup behind the specimen holder.

Half the specimen surface was masked with Mo foil during irradiation. After irradiation the coated films changed in color in the irradiated area and the boundary between this area and the masked one could be easily observed.
In irradiation area, unevenness of the coated film caused by roughness of the substrate surface was smoothed, while the projection of nodules became clearer. The reduction of the thickness of SiC film by the irradiation was roughly estimated from the profile to be about 0.4 μm in the case of H^+ with the dose of 3×10^{18} ions/cm^2. The erosion yield thus evaluated was about unity. No indication of blistering could be noticed in the present study.

The present results have some discrepancies compared with the results obtained about the CVD SiC by other researchers. Atoh et al. have shown that marked blistering occurred in the CVD SiC film by the irradiation of helium ion up to the dose of less than 1×10^{18} ions/cm^2 at room temperature. SiC used in their study was coated on fairly smoothed graphite surface and was polished after coated. Kaminsky and Das reported the observation of blistering at the top of some nodules of as-deposited TiB_2 prepared by the CVD method.

The present authors assumed that the sputtering yield of SiC would depend strongly on the crystallographic structures. As mentioned in a section of the characterization, in the as-coated condition, the CVD SiC is fully crystallized while the ion-plated SiC is amorphous or poorly crystallized. Further, the chemical bond between Si-C is stronger in the CVD film than in the ion-plated one. It might be speculated that the nodules observed by SEM would have a well crystallized structure and the flat region around the nodules observed in the ion-plated SiC would have a poorly crystallized structure. As a result of irradiation, the flat regions in the ion-plated film would be sputtered strongly with the results of the reduction of such a large thickness and of leaving a clear projection of the nodules, while the CVD film composed of the dense nodules would be less susceptible to sputtering. As for blistering, the ion-plated film would have less tendency to form a blister from the view points of the defects and micropores mentioned before.

As for the interpretation of the irradiated test, we think we need much more data including the CVD prepared specimens to make the above discrepancy clearly explicable.

Conclusion

Comparisons between the CVD and the ion-plated techniques, and between the materials prepared by the two methods were conducted, mainly concerning the SiC coating on molybdenum substrate.

As for the coating technique, the CVD provides film superior to the ion-plated film in uniformity of structures and thickness along the substrate, though its coating temperature exceeds 1000°C. The CVD film also has superiority in the degree of crystallization, strenght in Si-C bonding, control of stoichiometry and the defects of the coated film.

These differences of characters affect the non-irradiation properties of the two kinds of coated materials. The CVD coating lasted longer in the thermal cycle

test and bore to higher temperature in the oxidation test than the ion-plated one. It might be also considered from our irradiation experiments, although they were not sufficient to yield a clear conclusion, that the sputtering and blistering behaviors would be different between the two kinds of coated materials.

Taking account of the fact that the ion-plated does not need such a high substrate temperature as the CVD and that it will be more applicable to the in-situ coating in future, intensive research will be necessary to improve the PVD techniques including ion-plating. As an example, it was shown that the ion-plated Si-C-Al-O or Si-N-Al-O complex compound coatings improved the resistance to thermocycles.

References

(1) M.Fukutomi, M.Kitajima, M.Okada,& R.Watanabe, "Silicon Carbide Coatings on Molybdenum by Chemical Vapor Deposition and Its Stability under Thermal Cycle Conditions" J. Nucl. Mater. 87 (1979) 107

(2) M.Fukutomi, M.Kitajima, M.Okada,& R.Watanabe, "Silicon Nitride Coatings on Molybdenum by RF Reactive Ion Plating" J. Electrochem. Soc., 124 (1977) 1420

(3) M.Kitajima, M.Fukutomi, M.Okada,& R.Watanabe, "Electrographic Detection of Pinholes in Ion-Plated Silicon Nitride Film on Molybdenum" DENKI KAGAKU(J.Electrochem. Soc. Japan) 47 (1979) 214

(4) T.Shikama, M.Fukutomi, M.Kitajima, M.Okada,& R.Watanabe, "Surface Radiation Damage of Silicon Carbide and Carbon Films Coated on Molybdenum" Porc. 5th Domestic Meeting on Fusion Reactor Materials. at IPP Nagoya Univ. to be published

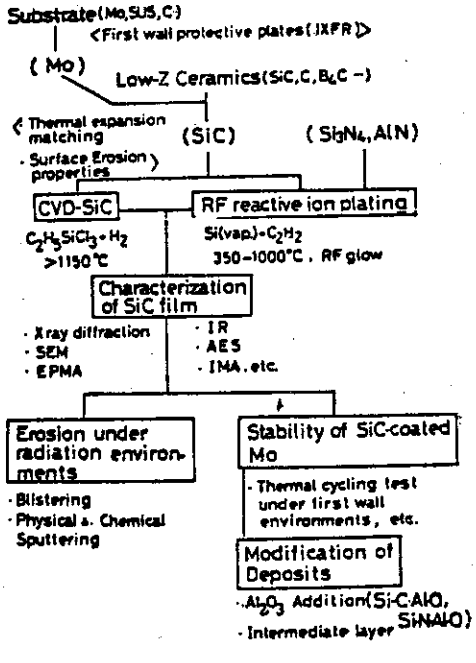

Figure 1 Coatings of low-Z materials on molybdenum
(National Research Institute for Metals)

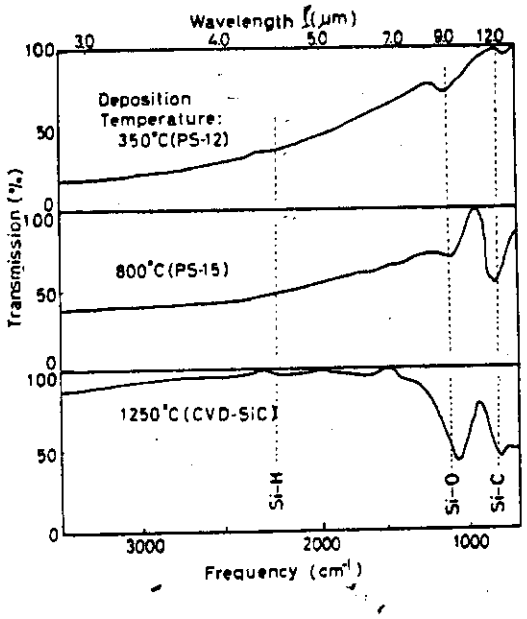

Figure 2 Typical infrared spectra of reactive ion-plated and chemically vapor deposited silicon carbide film

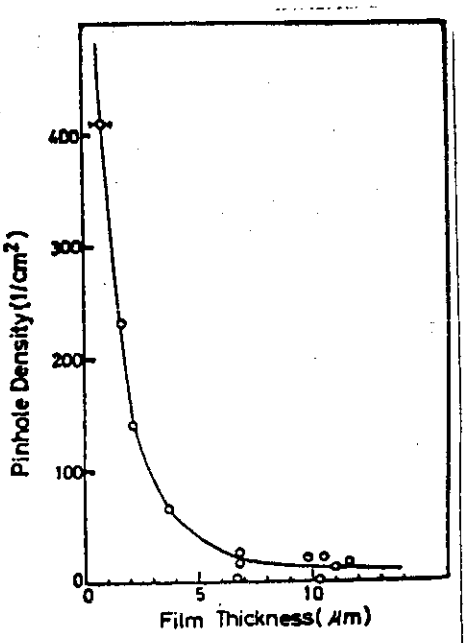

Figure 3(a) Defect density vs. film thickness by electrograph method.

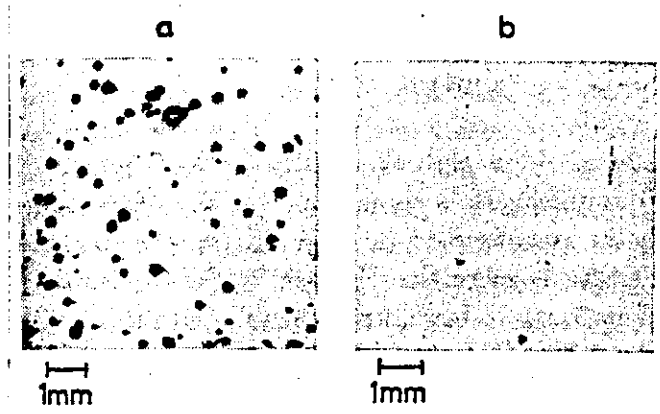

Figure 3(b) Photographs of electrograph for silicon nitride films
a: film thickness 2 μm, b: film thickness 10 μm

		CVD-SiC	PVD-SiC			
		(1150)*	SiC(250)	SiC(800)	SiC(1000)	Si-C-Al-O(800)
SURFACE MORPHOLOGY	optical metalograph, SEM	domed crystalline	small nodule	small domed crystalline	rough, lusterless	smooth, small nodule
COMPOSITION STOICHIOMETRY	EPMA AES	stoichiometric SiC	Silicon rich SiC	nearly Stoichiometric SiC	carbon-rich SiC	Si,C, Al,O,
CRYSTALLINITY	X-ray diffraction	α-,β-SiC(s) SiO_2(w)	amorphous	α-SiC(w) β-SiC(vw)	α-,β-SiC (m), C(s)	amorphous
CHEMICAL BOND	I.R.	Si-C(s) Si-O(w)	Si-C(w) Si-O(vw)	Si-C(s) Si-O(vw)	-	unidentified absorption(w)
THERMOCYCLING STABILITY						
600-1200°C,20°C/min		~1500h	-	-	-	-
900-1200°C,~130°C/min 10 times		good	poor(film separation, vaporization)			good

* seposition temperature, °C

	SiC(800)**	Si_3N_4(900)	AlN(350)	Si-Al-O-N(800)
SURFACE MORPHOLOGY	small domed crystalline	large grains composed of many small grains	domed crystalline	smooth
COMPOSITION STOICHIOMETRY	nearly stoichiometric SiC	nearly stoichiometric Si_3N_4	nearly stoichiometric AlN	Si-Al-O-N
CRYSTALLINITY	α-SiC(w) β-SiC(vw)	amorphous	AlN(s) Al (w)	amorphous
CHEMICAL BOND	Si-C(s) Si-O(vw)	Si-N(s) N-H,Si-H(vw)	Al-N(s)	unidentified absorption(s)
THERMOCYCLING STABILITY 900-1200°C ~130°C/min 10 times	poor		good	good

** deposition temperature, °C

Table 1 Characteristics of SiC coatings deposited by CVD and reactive ion-plating (PVD), and various low-Z coatings by reactive ion-plating(PVD)

8 - 2

Review of U.S.A. Low-Z Coating Development Program*

Robert A. Langley

Oak Ridge National Laboratory
Oak Ridge, Tennessee 37830 U.S.A.

The U.S.A. coating development program was implemented in 1976 with the initiation of a feasibility study; the development program was funded in 1977. The initial study tried to answer the following questions: (1) is there a need for a first wall coating in an experimental power reactor application? (2) what are the appropriate factors for the selection of a coating? (3) how should the development program be formulated? These questions were answered in Ref. 1 and 2. The focus of the program was changed as a result of a workshop held in January 1978.[3] The new focus was a shorter-term goal of providing appropriate materials for limiters, beam dumps, and protective plates for present-day and near-term tokamaks, with a long-range interest in solving the EPR first wall problem.

The attached copies of the viewgraphs summarize the work to date. They describe Sandia Laboratories' development results and preliminary testing results in the Impurity Study Experiment (ISX-B). At present, TiC and TiB_2 coated graphite limiters have been tested in ISX-B, and TiC limiters are being evaluated in the Poloidal Divertor Experiment (PDX) and Alcator-C.

---

*Research sponsored by the Office of Fusion Energy (ETM), U. S. Department of Energy under contract W-7405-eng-26 with the Union Carbide Corporation and contract DE-AC04-76-DP00789 with Sandia Laboratories.

REFERENCES

1. M. J. Davis, R. A. Langley, and T. S. Prevender, Sandia Laboratories, Albuquerque, New Mexico, SAND77-1027, (August 1977).

2. R. A. Langley and T. S. Prevender, Thin Solid Films 45, 235 (1977).

3. Proc. First Wall Coating Workshop Ed. by D. M. Mattox, Sandia Laboratories, Albuquerque, New Mexico, January 31-February 1, 1978.

BIBLIOGRAPHY

D. M. Mattox, Thin Solid Films 63, 213 (1979).

M. J. Davis, J. Nucl. Mater. 85 & 86, 1063 (1979).

A. W. Mullendore, J. B. Whitley, D. M. Mattox, and R. K. Thomas, paper presented at the 8th Symposium on Engineering Problems in Fusion Research, to be published.

B. L. Doyle and F. L. Vook, J. Nucl. Mater. 85 & 86, 1019 (1979).

H. O. Pierson and E. Randich, and D. M. Mattox, "The Chemical Vapor Deposition of TiB_2 on Graphite," paper presented at the 6th International Symposium on Boron and Borides, Drubzha, Bulgaria, October 1978, (proceedings to be published in J. Less Common Metals).

H. O. Pierson and A. W. Mullendore, "The Chemical Deposition of Boron from Diborane," Proc. 7th International Conf. on Chemical Vapor Deposition, p. 360 (1979).

D. M. Mattox and D. J. Sharp, "Application of a Kaufman Ion Source for Low Energy Hydrogen Ion Bombardment Studies," Proc. First Wall Coating Workshop (1978).

D. M. Mattox and D. J. Sharp, "Low Energy Hydrogen Ion Erosion Yields as Determined with a Kaufman Ion Source," Sandia Laboratories Report SAND78-1029 (October 1978).

D. J. Sharp, J. K. G. Panitz, and D. M. Mattox, "Applications of a Kaufman Ion Source to Low Energy Ion Erosion Studies," to be published in J. Vac. Sci. Technol. (Proceedings of the 15th Symposium on Electron, Ion, and Photon Beam Technology, May 30-June 1, 1979, Boston, MA).

J. B. Whitley and D. M. Mattox, "Erosion of Refractory Metals and Coatings by Arcing," paper presented at the 1979 TMS-AIME Meeting, Milwaukee, Wisconsin, September 16-20, 1979.

J. B. Whitley and D. M. Mattox, "Plasma Arcing of Low Z Coatings," Proc. Arcing Phenomena in Fusion Devices Workshop, April 5-6, 1979, Knoxville, TN, Edited by R. A. Langley, ORNL, DOE Contract 7405-eng-26.

LONG RANGE DEVELOPMENT PLAN AND STRATEGY

- SELECTING THE MOST IMPORTANT EPR COATING PROPERTIES.
- DEVELOPING SCREENING TESTS TO RANK MATERIALS IN TERMS OF THESE PROPERTIES.
- SCREENING MATERIALS, COATINGS AND PROCESSES.
- VERIFYING THE IMPORTANCE OF THE PROPERTIES SELECTED AND MEASURING COATING PERFORMANCE IN A TOKAMAK.
- ESTABLISH MATERIALS, PROCESS AND DESIGN STANDARDS FOR BETTER COATINGS, SUBSTRATES AND PROCESSES.

MATERIALS SELECTION

- CHEMICAL STABILITY IN A HYDROGEN PLASMA AND DURING DISCHARGE CLEANING.
- LOW PHYSICAL AND PHYSICO CHEMICAL EROSION RATES.
- LOW VAPOR PRESSURE AT OPERATING TEMPERATURES.
- LOW HYDROGEN AND HELIUM RETENTION.
- RADIATION DAMAGE RESISTANCE.

SCREENING TESTS

- CHEMICAL EROSION
- PHYSICAL EROSION
- SPUTTERING
- MECHANICAL ADHESION
- THERMAL FATIGUE

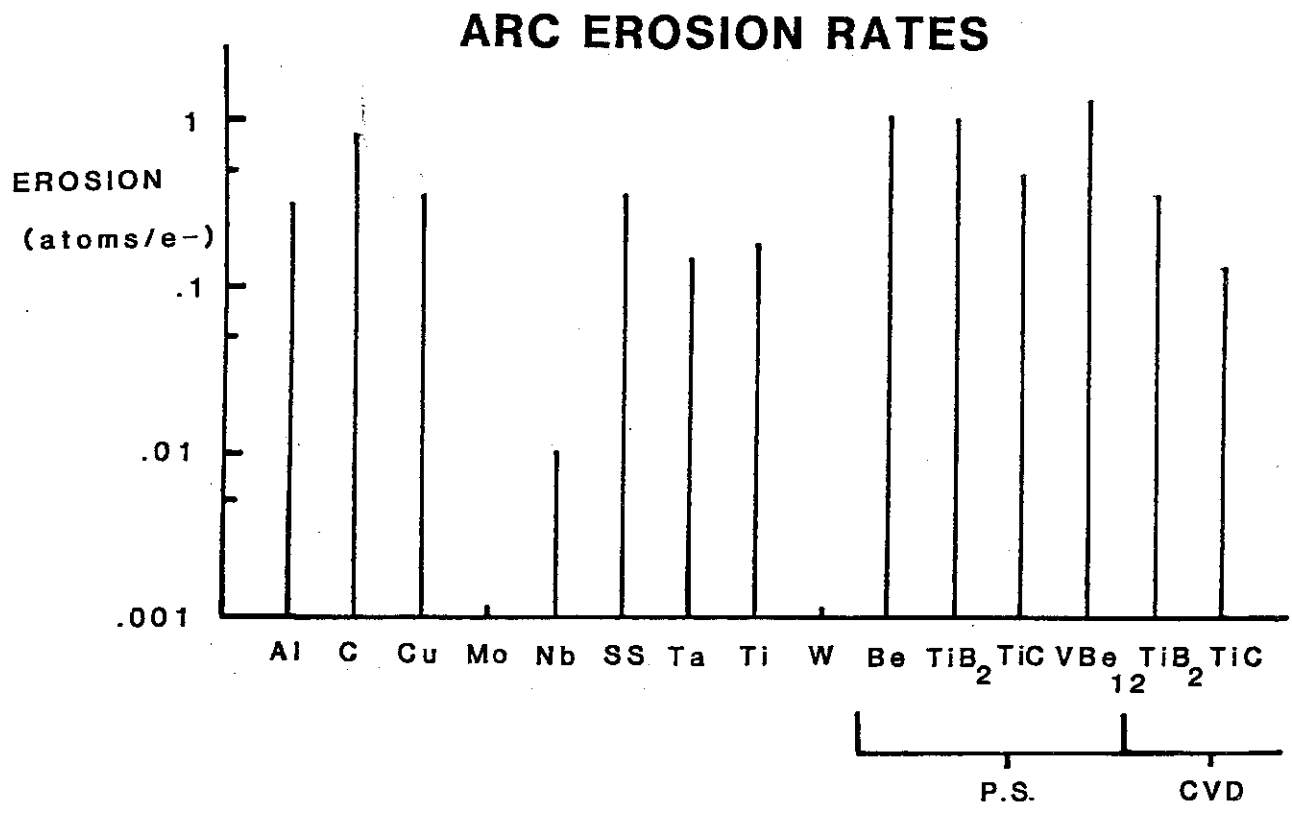

COATINGS PROGRAM - ACCOMPLISHMENTS

(February 1980)

A number of materials and coatings have been screened as to

Sputter erosion
Thermal fatigue resistance
Arcing susceptibility

Desirable candidates have been identified.

Several coating technologies have been evaluated as to ability to provide desirable coatings.

(CVD, Plasma Spray, explosive bonding, pack boriding)

Physical and mechanical properties of selected coatings have been determined.

Coating technologies are being refined for specific applications.

Thermal fatigue test unit has been assembled with the following capabilities

20 kW e-beam gun
Optical pyrometry
Thermocouple thermometry
Video taping/viewing
Residual gas analysis (mass spectrometer)
2-axis sample positioning (TFM study)
Programmable e-beam pulsing/sample positioning (TFM study)

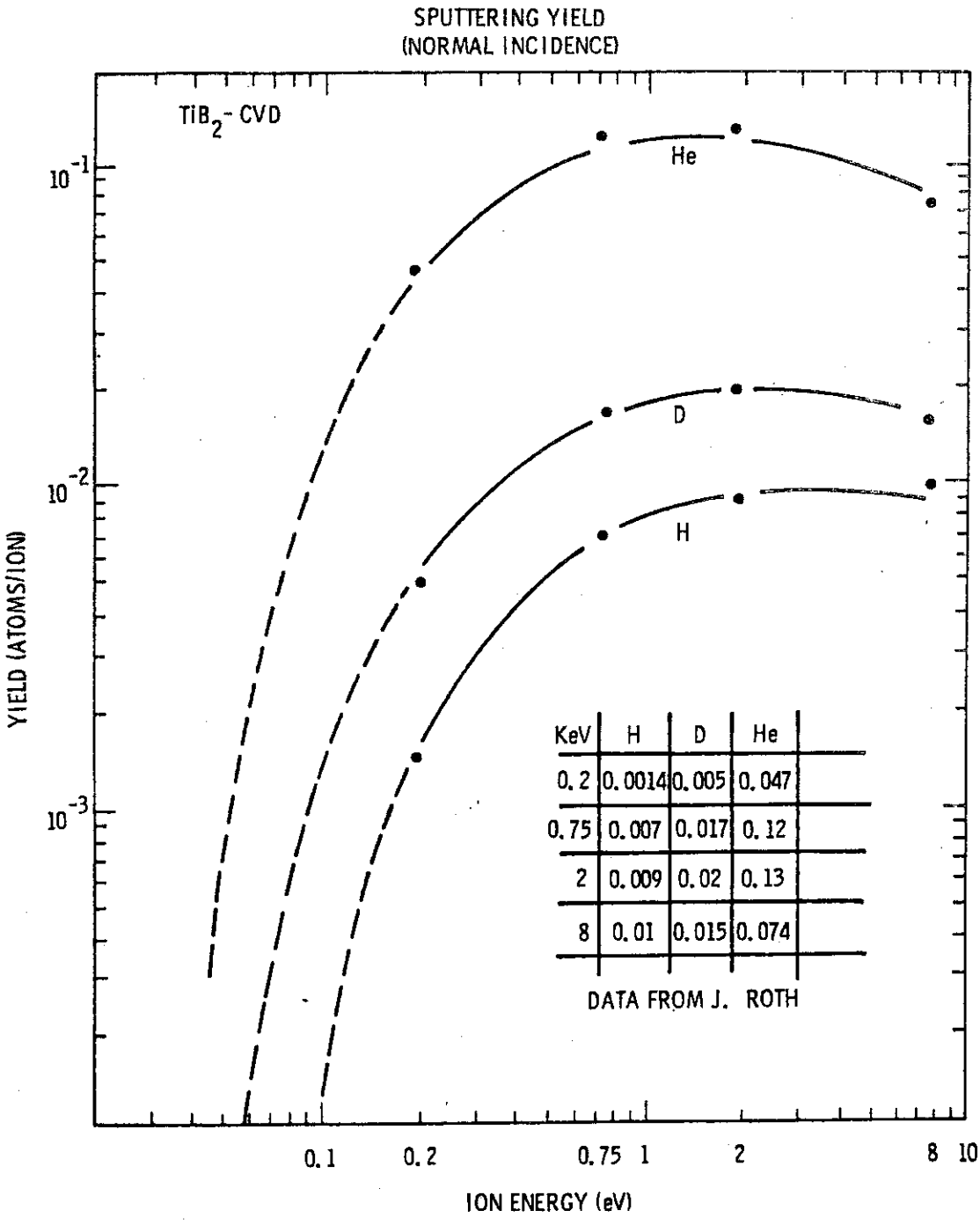
SPUTTERING YIELD
(NORMAL INCIDENCE)
TiB2 - CVD
He
D
H
YIELD (ATOMS/ION)
10-1
10-2
10-3
0.1
0.2
0.75
1
2
8
10
ION ENERGY (eV)
KeV | H | D | He
0.2 | 0.0014 | 0.005 | 0.047
0.75 | 0.007 | 0.017 | 0.12
2 | 0.009 | 0.02 | 0.13
8 | 0.01 | 0.015 | 0.074
DATA FROM J. ROTH

TABLE 1

TYPICAL OPERATING AND FAULT ENVIRONMENTS

MODERATE SIZE (EPR) FUSION REACTOR

		First Wall	Neutral Beam Injector Armor	Limiter
Normal Operation (200 MJ Plasma)	Fast Neutrons >13 MeV	5-10 x 10^{13} cm^{-2}/s	5-10 x 10^{13} cm^{-2}/s	5-10 x 10^{13} cm^{-2}/s
	Total Neutrons	1-5 x 10^{14} cm^{-2}/s	1-5 x 10^{14} cm^{-2}/s	1-5 x 10^{14} cm^{-2}/s
	D, T, He	5-10 x 10^{15} cm^{-2}/s ($\bar{T}$ = 0.2 - 3 KeV)	Shinethrough 10^{16} - 10^{18} cm^{-2}/s ($\bar{T}$ = 60 - 200 KeV D^o)	10^{18} - 10^{19} cm^{-2}/s ($\bar{T}$ = 0.2 - 3 KeV)
	e^-	----	----	10^{18} - 10^{19} cm^{-2}/s ($\bar{T}$ = 0.2 - 3 KeV)
	Radiation	10^{-2} - 10^{-3} Kw/cm^2	10^{-2} - 10^{-3} Kw/cm^2	10^{-2} - 10^{-3} Kw/cm^2
	Total Thermal Load	0.01 - 0.5 Kw/cm^2	0.05 - 1 Kw/cm^2	0.5 - 5 Kw/cm^2
	Unipolar Arcing	?	?	?
Fault Conditions	D, T, e^-	10^{19} - 10^{21} cm^{-2}/s ($\bar{T}$ = 5-10 KeV)	5-50 x 10^{17} cm^{-2}/s (D^o)* ($\bar{T}$ = 60-200 KeV)	Same as Wall
1. Plasma Dump in 10-100μs	Thermal Load	10^4 - 10^6 Kw/cm^2 (Local - 1/3 Wall)	5-10 Kw/cm^2 (D^o)*	Worse than Wall
2. Runaway Electrons	e^-			10^{18} - 10^{19} cm^{-2}/s >1 MeV

*With no plasma, the neutral beams will strike the armor for 0.1 sec. If the plasma dumps onto the armor, these values would be in addition to the first wall parameters.

FAILURE SUMMARY

SAMPLE COATING	NUMBER TESTED	SUBSTRATE	PREPARATION TECHNIQUE	200 CYCLE, RADIATION COOLED 1 kW/cm^2	200 CYCLE, ACTIVELY COOLED 2 kW/cm^2	1000 CYCLE, ACTIVELY COOLED 2 kW/cm^2
TiB_2	4 (8)[1]	Poco[2]	CVD	NF	NF	NF
TiC	4 (8)[1]	Poco[2]	CVD	NF	NF	NF
TiB_2	4	Poco[2]	CVD	NF	NF	
B	4	Poco[2]	CVD	NF	NF	
TiB_2	4 (8)[1]	Cu	PS	NF	NF	NF
V	4	Cu	EB	EM	NF	
Ti	4	Cu	EB	NF	EM	
VB_2	4 (8)[1]	Cu	EB Boriding	NF	NF	SM

(1) Number in 1000 cycle test.

(2) AXF/5Q graphite.

Key

CVD - Chemical Vapor Deposition

PS - Plasma Sprayed

EB - Explosively Bonded

NF - No Failures

EM - Coating Edge Melt

SM - Substrate Melt

ISX TOKAMAK TESTS

- HV TRANSFER CHAMBER
- TiC/GRAPHITE AND TiB_2/GRAPHITE BEHAVED WELL IN OHMICALLY-HEATED PLASMAS; Z_{EFF} <3 FOR FIRST DAY OF OPERATION.
- MAXIMUM HEAT LOAD CORRESPONDS TO AN AVERAGE POWER DENSITY OF 0.5 kW/cm^2 (THIS IS ~x 10 LESS THAN THE MAXIMUM EXPECTED IN BEAM HEATED DISCHARGES).
- VISUAL INSPECTION OF THE TiC/GRAPHITE LIMITER SHOWED SOME CHANGE IN THE COATING SURFACE, MAINLY ARCING, BUT MORE DETAILED METALLOGRAPHICAL EXAMINATION IS UNDERWAY.

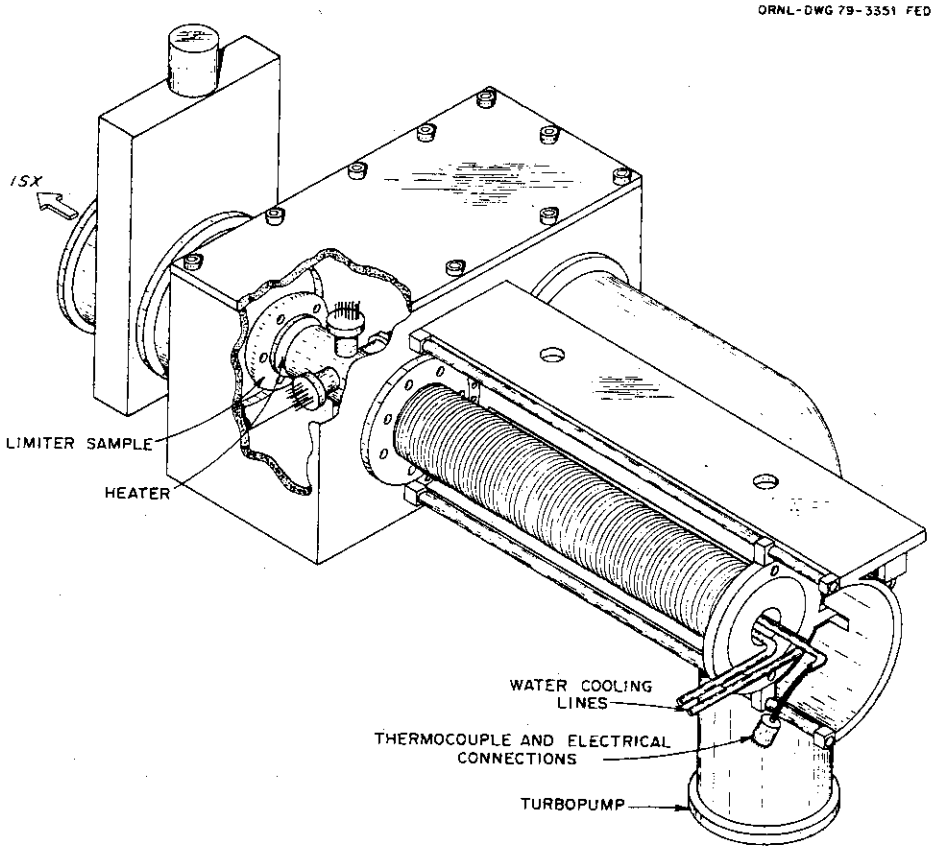

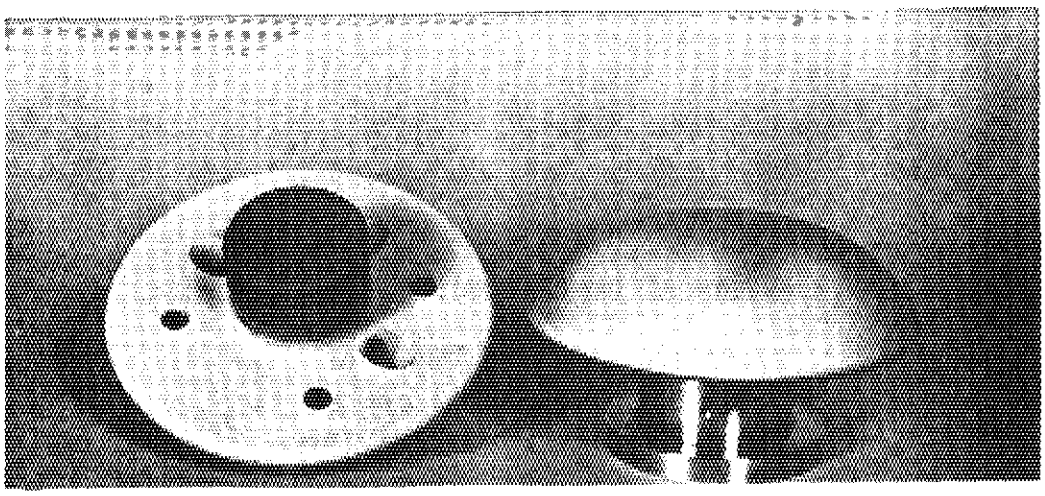

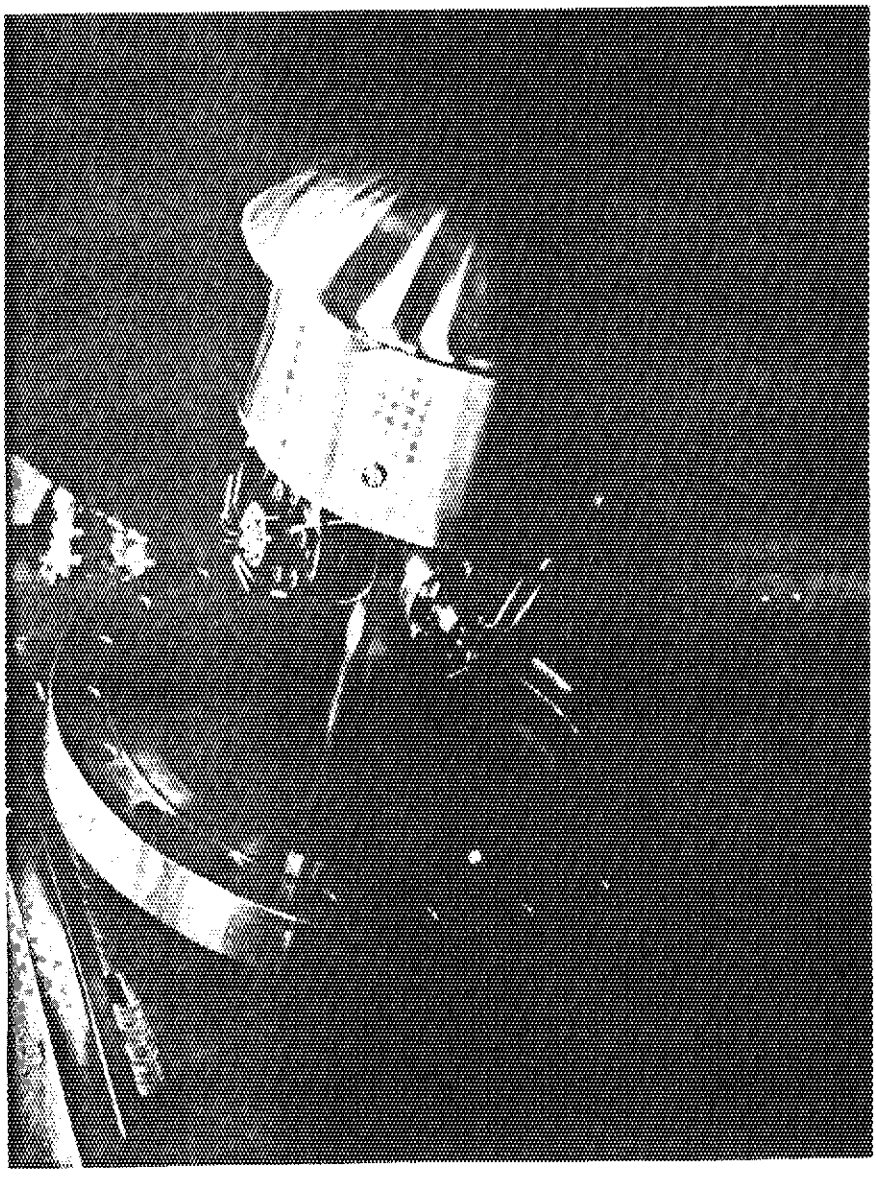

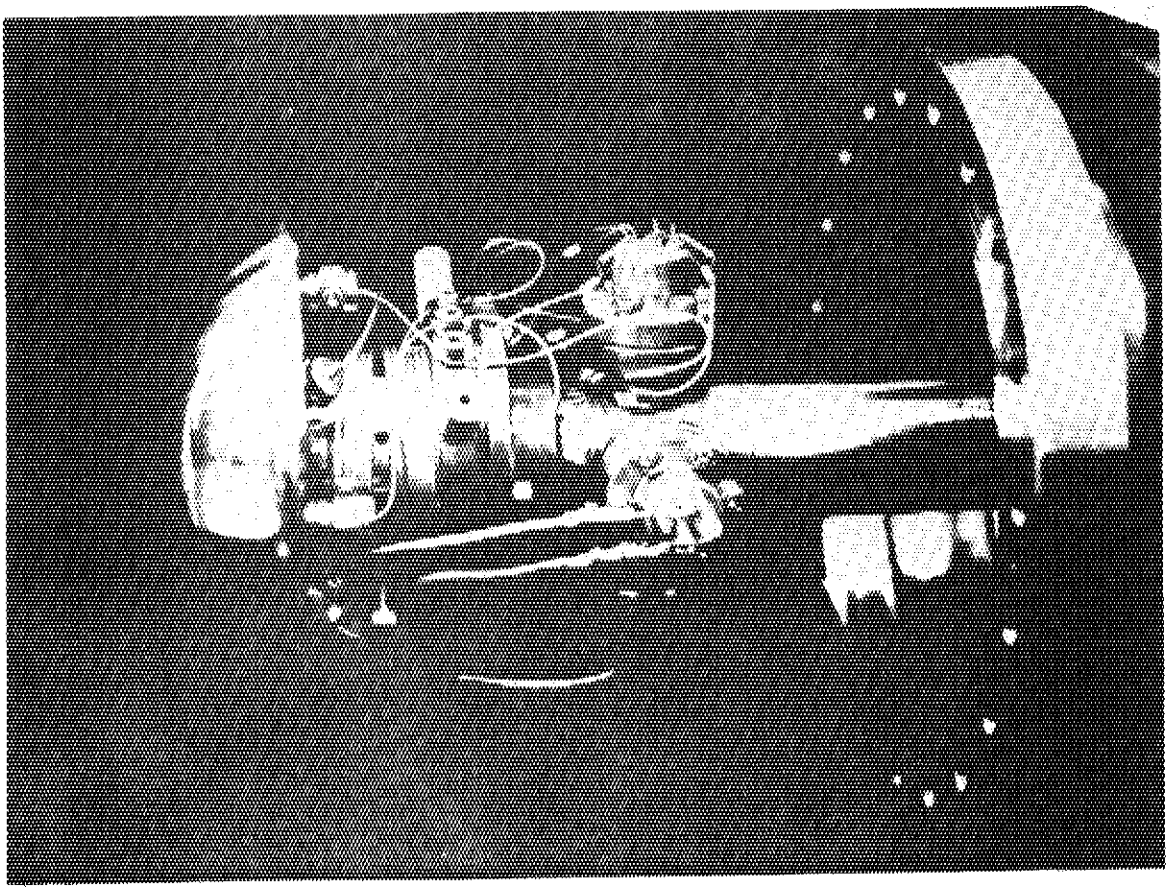

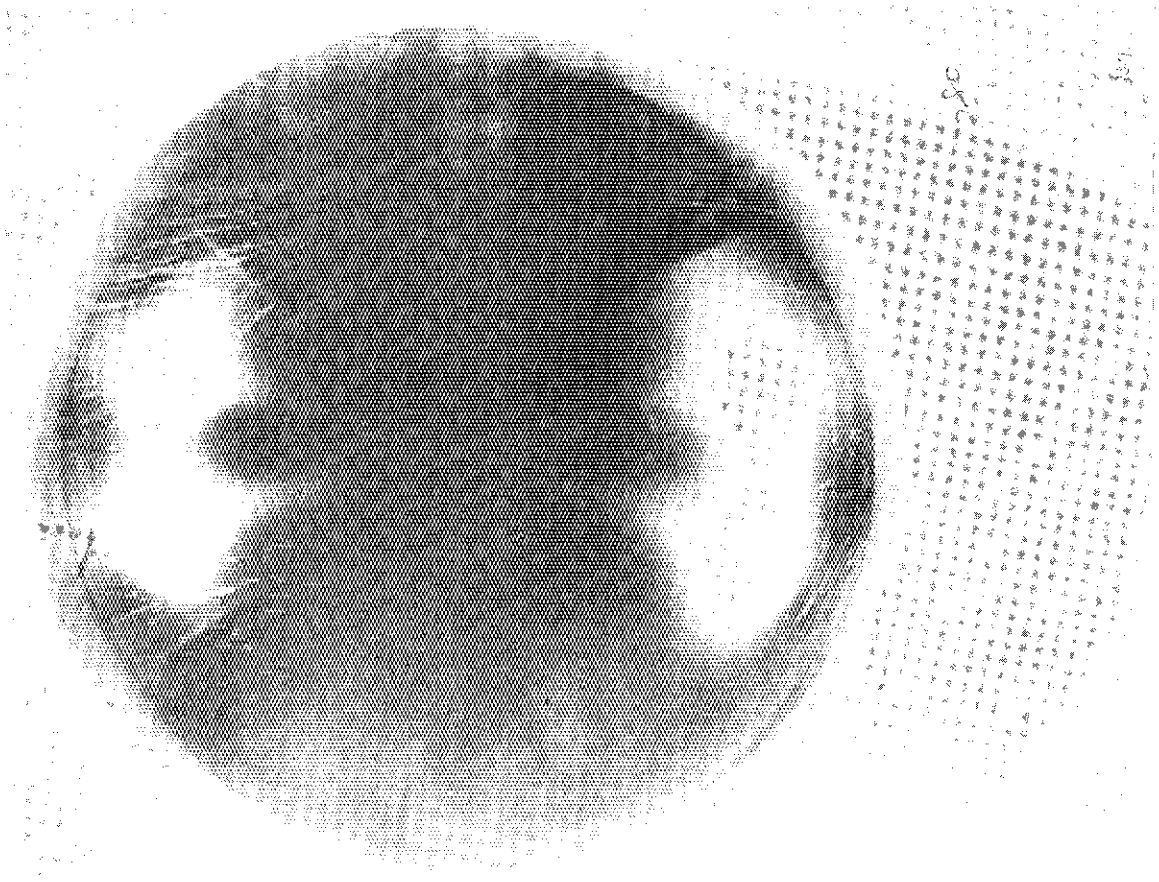

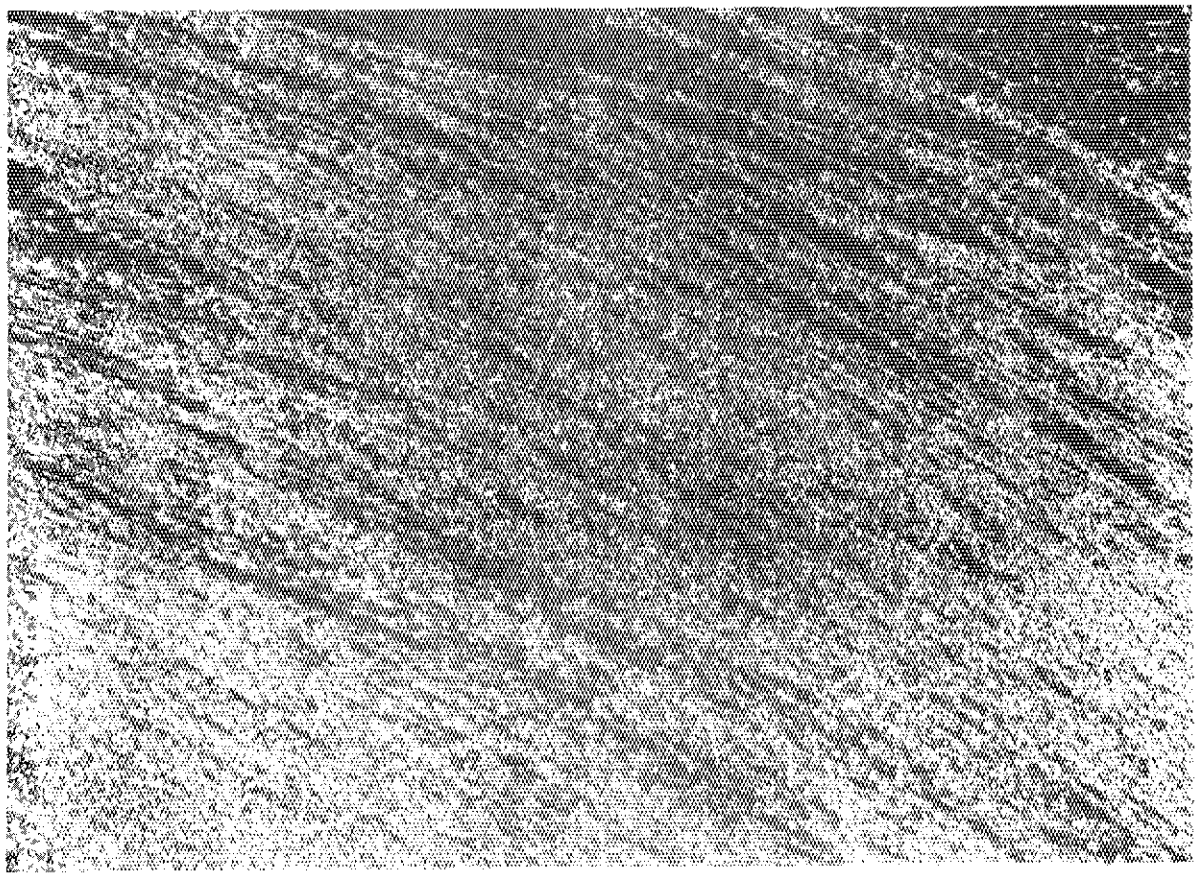

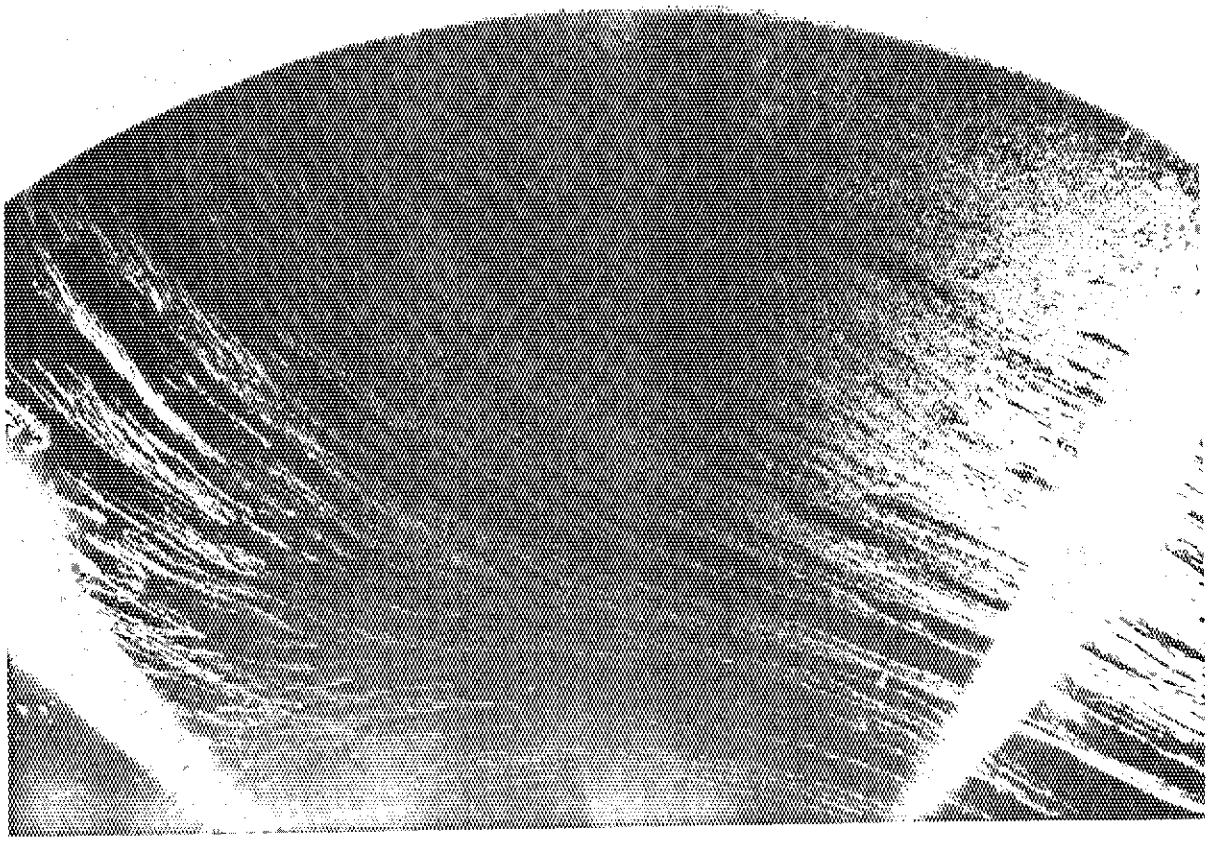

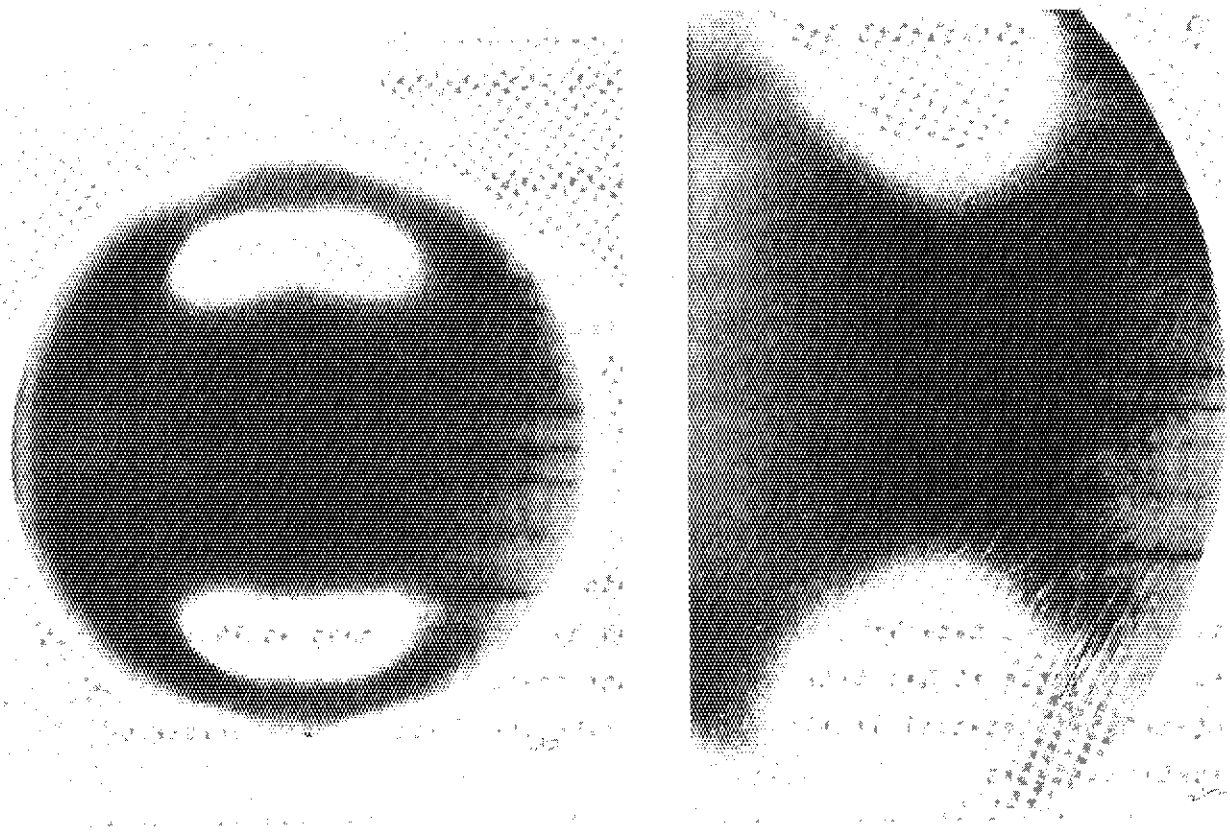

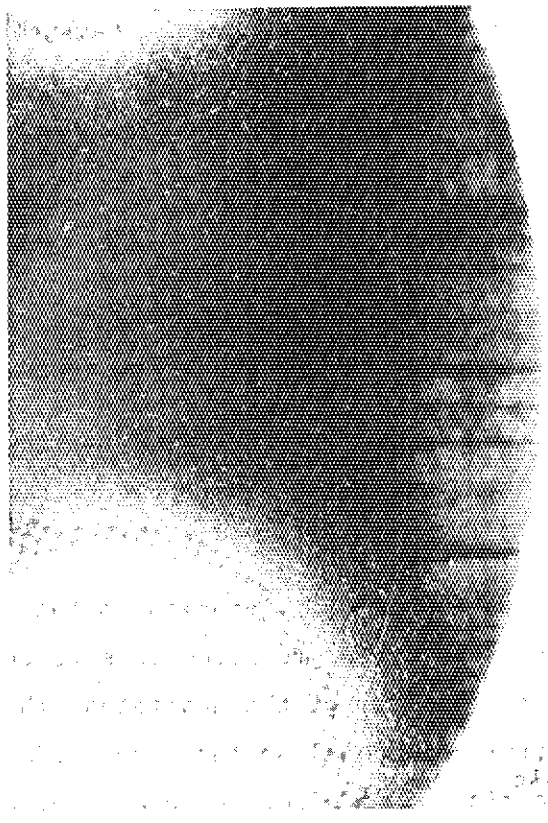

9 - 1 SIMULTANEOUS AND CONTINUOUS OBSERVATION OF SOLID SURFACES UNDER HELIUM ION BOMBARDMENT

M. SAIDOH, K. SONE, R. YAMADA and K. NAKAMURA

Division of Thermonuclear Fusion Research
Tokai Research Establishment, JAERI

1. Introduction

A number of works on surface erosion of solids caused by ion bombardment have been made by using helium and hydrogen isotopes as impinging ion species, since it has been expected that energetic plasma particles and α-particles created by D-T burning strike the first wall materials of fusion reactors.

The change of surface topography induced by ion bombardment, so far, has been observed in a scanning electron microscope (SEM) after specific dose levels were attained and the samples removed to a SEM. Therefore the dose dependence of the development of the surface erosion has not been examined in detail. In order to gain insight into these dynamic processes, we have made SEM observations during ion bombardment of solid surfaces using an in-situ facility. A detail description of the experimental apparatus has been reported previously[1].

In this report we describe the experimental apparatus briefly and show the film which recorded the development of the surface erosion of polycrystalline molybdenum under helium ion bombardment.

2. Experimental

A JEOL JSM-35 SEM was mechanically coupled to the beam line of a 400 kV Cockcroft-Walton type accelerator to allow in-situ observations. Figure 1 shows a schematic diagram of the apparatus. The sample surface is inclined up to 60° from horizontal so that the surface can be simultaneously probed by the microscope electron beam and the ion beam from accelerator. The microscope must be correctly positioned to assure that

the electron beam can be scanned in the ion beam spot on the sample surfaces.

Backscattered electrons were detected by P-N junction type detector for image contrast. Aluminum coated mica film was placed in front of the P-N junction type detector in order to eliminate the secondary electrons produced by ion beam. The detector could be rotatable around the sample stage so that it could be positioned properly to make a good image contrast. The maximum usable magnification of backscattered electron image operation was attained to about x 6000 under helium ion bombardment. Most data were taken at a magnification of x 4000 or below.

A Faraday cup consisted of a cylindrical tube with a 5 mm diameter beam-defining aperture and of a movable shutter and a 8mm diameter beam-defining aperture were placed at the entrance to the microscope to measure a beam current during surface observation. The sample was bombarded with the ion beam through two apertures and an impinging current was obtained by measuring the ion beam which hit the aperture of 5 mm in diameter during bombardment. The beam was scanned two-dimensionally by applying potential with a frequency of 1000 Hz on two sets of deflection plates. The scanning area was approximately 10 mm x 10 mm on the aperture of 8 mm in diameter. The integrated ion beam current was converted into digital display of which signal was synchronized to the respective electron beam scanning modes so that the surface states as well as the accumulated ion fluence could be recorded in each frame.

Video recorder (SONY AV-8750) was used for continuous recording. Film shown here was made from video tapes by means of kinescope-recording system. Rapid scan (a half speed of video scan) could be selected to get a photograph with a better resolution under ion bombardment. Typical SEM micrograph taken from rapid scanned frames was shown in Fig. 2. In the figure electron accelerating voltage, magnification, numbering, micron indicator and ion fluence were displayed.

Polycrystalline molybdenum from Plansee Co. was used and target samples were annealed at 1300 °C for one hour after mechanically polished.

3. Contents in the film

Followings were filmed.

(1) Details of the experimental apparatus

(2) 200 keV helium ion bombardment

(3) 100 keV helium ion bombardment

(4) 200 keV helium ion bombardment after pre-bombardment of 100 keV helium ion.

The bombardment conditions, critical fluences and surface deformation modes are summarized in table 1. It was found that the formation of the blisters and the exfoliation of the surface layer were strongly dependent on the crystal grains. Typical SEM micrographs taken from the video frames were shown in Figs. 3 and 4. In Fig. 3 blisters of 2-3 μm in diameter as well as exfoliation of around 10 μm in size were observed. Individual exfoliation developed at a rate faster than the video scan rate (16.6 msec). Dramatic development of surface deformation was observed as a result of pre-implantation shown in Fig. 4. Exfoliation occured continuously once the critical fluence was achieved. This type of surface deformation was reported previously[2] and the effect of the pre-implantation on the surface erosion will be published[3].

References

(1) K. Obara, T. Abe and K. Sone : JAERI-M 7797 (1978) (In Japanese)

(2) M. Saidoh, K. Sone, R. Yamada and H. Ohtsuka : JAERI-M 7997 (1978) (In Japanese)

(3) M. Saidoh et al. : To be published.

Table 1 Surface deformation of molybdenum caused by helium ion bombardment

Irradiation Mode	Energy (keV)	Fluence (He^+/cm^2)	Critical Fluence (He^+/cm^2)	Deformation Mode
Single	100	9.2×10^{17}	6.0×10^{17}	Blister
	200	12.3×10^{17}	8.9×10^{17}	Exfoliation + Blister
Single Sequence	100 200	4.4×10^{17} 12.3×10^{17}	(a) 8.6×10^{17}	Exfoliation

(a) Fluence after initiation of 200 keV helium ion bombardment.

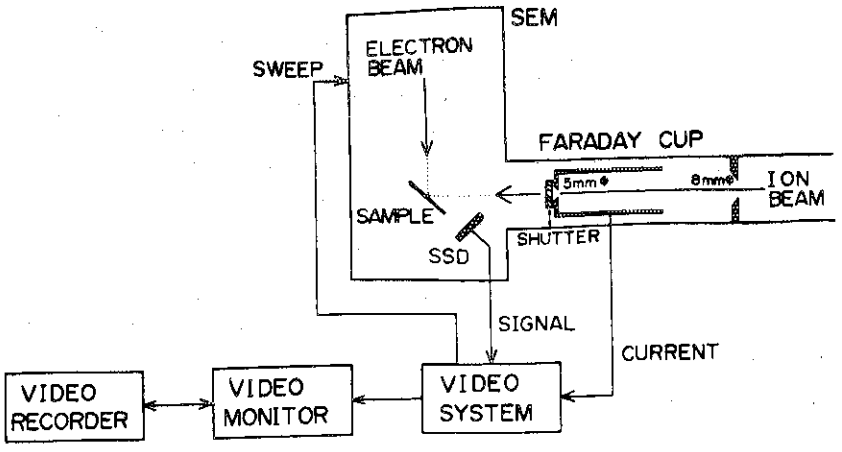

Fig. 1 Schematic representation of experimental apparatus.

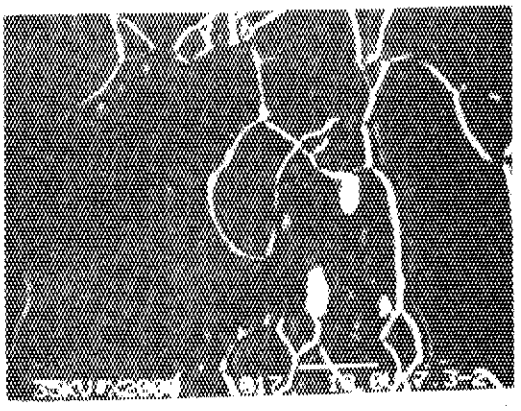

1 2 3 4 5

Fig. 2 SEM micrograph taken from rapid scanned frames:
1 - electron accelerating voltage, 2 - magnification,
3 - numbering, 4 - micron indicator and 5 - ion fluence.

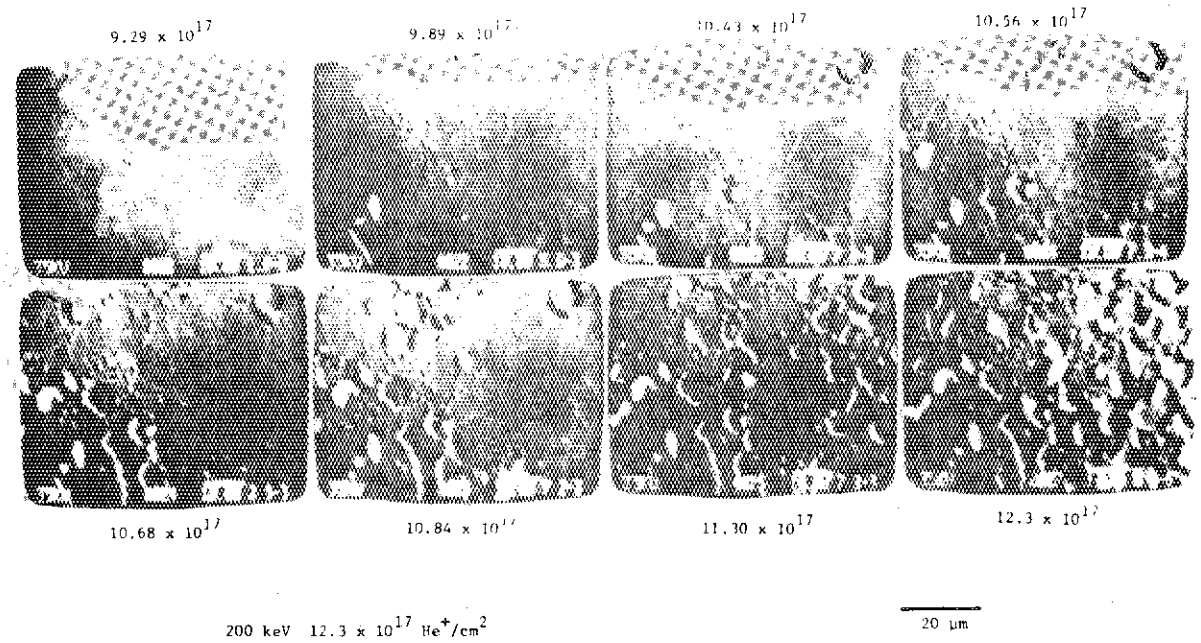

Fig. 3 A series of SEM micrographs showing the development of surface erosion in 200 keV helium ion bombarded molybdenum with irradiation dose up to a fluence of 12.3×10^{17} He^+/cm^2 at ambient room temperature.

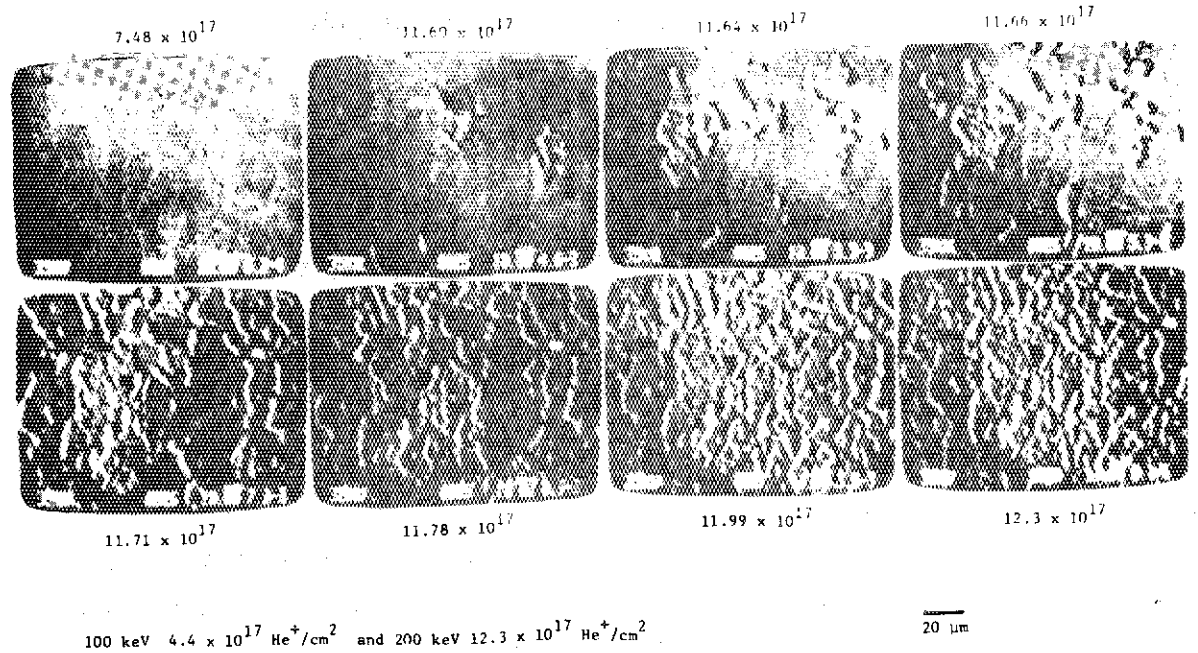

Fig. 4 A series of SEM micrographs showing the development of surface erosion in 200 keV helium ion bombarded molybdenum with irradiation dose up to a fluence of $12.3 \times 10^{17} He^+/cm^2$ at ambient room temperature. Prior to the 200 keV helium ion bombardment the target was bombarded with 100 keV helium ion up to a fluence of 4.4×10^{17} He^+/cm^2.

9 - 2 MEASUREMENT OF CHEMICAL SPUTTERING YIELDS OF VARIOUS TYPES OF CARBON

R. YAMADA, K. NAKAMURA, K. SONE AND M. SAIDOH
Division of thermonuclear Fusion Research,
Tokai Research Establishment, JAERI

1. Introdution

Methane formation from carbon due to the bombardment with hydrogen ions have been studied by several laboratories[1-5]. Most of the studies used more than 5 keV for the incident energy. The recent study of plasma impurity control reveals the most probable energy of impinging ions exists less than 1 keV for a carbon limiter and less than 0.1 keV for a carbon liner in Tokamak devices[6]. The importance of chemical sputtering during bombardment of hydrogen ions with less than 1 kev have been developing now. The agreements of chemical sputtering yields are not so well between the different studies[1-5] even if the same incident energy and target temperatures. One of the reasons is that properties of carbon samples used were thought to be more or less different from each other even if they were produced by the same method such as pyrolytic graphite[1]. The other reason is that pretreatments of sample were incomplete. The suggestion of the importance of pretreatment was given by the preliminary experiment at this laboratory[3] which showed the hysteresis of chemical sputtering of carbon to be caused by the pretreatment before the bombardment.

We have investigated how dose of incident ions and various types of carbon have influence on methane production rate under careful pretreatments of carbons. The incident energy range of hydrogen ions used was 0.1-6 keV for the purpose of filling the lack of chemical sputtering coefficents for low energy hydrogen ions.

2. Experimental

The schematic diagram of experimental appratus is shown in Fig.1. Details of the ion beam apparatus have been described in the previous paper[3]. the background pressure in the target chamber was 1×10^{-8}Torr and the pressure during bombardment was 5×10^{-8}Torr. The samples used were two kinds of pyrolytic graphite which were delivered from Nippon Carbon, Japan named as PG-A and Union Carbide, USA named as HPG. Both basal and edge planes which were cut perpendicular and parallel to c-axis, respectively, were used as surfaces of targets for bombardments with H^+ ions. The another kinds of carbon also used were the isotropic atomic grade graphite named as 7477PT from Le Carbone , France and the glassy carbon named as GC-30 from Tokai Carbon, Japan. The typical properties of the six kinds of carbon are listed in Tab.1.

The treatments of targets before the bombardment were as follows, The target were annealed at 1700 C for 2hrs at a vacuum furnace which was evacuated

under $1x10^{-6}$Torr during annealing. After the targets were cooling down in the furnace, the target was moved to the target chamber and sticked to a tantalum strip heater which was 0.05mm thick. The target whose dimension was 10x10x1 mm^3 was heated by direct heating more than 1hr at 700 C under the vacuum of $1x10^{-8}$Torr prior to the bombardment. The target temperature was monitored by a thermocouple which was inserted between the target and the heater. The surfaces of each sample were not particularly polished.

The incident energies of H^+ ions ranged between 0.1 and 6 keV. The beam current was measured at a target with a pasitive vias for suppression of secondary electron emission and the current density ranged from 50 to 200 uA/cm^2 depending on the primary energy of H^+ ion. The methane formation formed from carbon targets by bombardment with H^+ ions were measured by a quadrupole mass spectrometer(QMS). For the improvement of QMS signal to noise ratio of methane the position of target was enclosed by a small chamber whose volume was about $200cm^3$. The H^+ ion beam was mass-analyzed and defined by a hole with 4mm diameter of its chamber. The head of QMS was directly attached to a hole with 15 mm diamter of its chamber. The calibration of methane signal of QMS to produtions rate of methane by H^+ ion bombardment was achived by the orifice conductance method.

3. Results

The dose dependence of methane production rates for the virgin samples were shown in Fig.2 where PG-A targets were bombarded at 525 C with H^+ ions whose energies were 0.1-6 keV. Fig.2 shows that the methane prodution rate increases with dose and gradually reaches a constant value. There is no decline of methane production rate after reaching of the equilibrium state. Samples which were pre-bombarded by hydrogen ions showed very different dose depeddence of methane production rate when the following bombardment was done with hydrogen ions. The results of them are shown in Fig.3. The features of methane production rates less than $1x10^{18}/cm^2$ are quite different each other for three cases. In all cases of such anomalous rates they become the constant value when the targets were bombarded up to $5x10^{18}/cm^2$. These anomalous rates can be explained by patticle induced desorption of super-saturated hydrogen concentration in the target. The methane production rates dependent on incident energies, target tempearures and types of carbon are shown in Figs,4-9 which were measured rates become constant. These results indicate that the energy and temperature dependences of methane production rates are almost same for the various carbon materials even though they have very differnt properties as shown in Tab.1. The maximum rate is 0.08+0.02 atom/ion in the conditon of about 525 C and 1 keV H^+. The temperature dependence of rate becomes smaller when incident energy is smaller as similar as the rate itself.

References

[1] J. Roth, J. Bohdansky, W. Poschenrieder and M.K. Sinha, J. Nucl. Mater. 63 (1976) 222.

[2] N.P. Busharov, E.A. Gorbatov, V.M. Gusev, M.I. Guseva and Yu.V. Martynenko,

[3] K. Sone, H. Ohtsuka, T. Abe, R. Yamada, K. Obara, O. Tsukakashi, T. Narusawa, T. Satake, M. Mizuno and S. komiya, Proc. International Wall Interaction, Julich, 1976 (Pergamon press,1977) p323.

[4] C.M. Braganza, S.K. Erents and G.M. McCracken, J. Nucl. Mater. 75 (1978) 220.

[5] J.N. Smith Jr. and C.H. Meyer Jr., J Nucl. Mater. 76&77 (1978) 193.

[6] S. Sengoku, Private commnucation

Table 1. Typical Properties of carbons[a)]

	Density	Electric Resistivity	Thermal Conductivity	Tensile Strength
	g/cm^3	cm	Kcal/mhrC	kg/cm^2
PG-A Basal	2.2	4.5×10^{-6}	350	1500
Edge	2.2	4.0×10^{-3}	20	30
HPG Basal	2.2	6.0×10^{-3}	300	1000
Edge	2.2	4.4	1.5	30
GC-30	1.45	3.5×10^{-5}	15	500[b)]
7477/PT	1.80	1.7×10^{-5}	70	200

a) These data were obtained from the catalogue data published by the deliverers.

b) Flexural strength

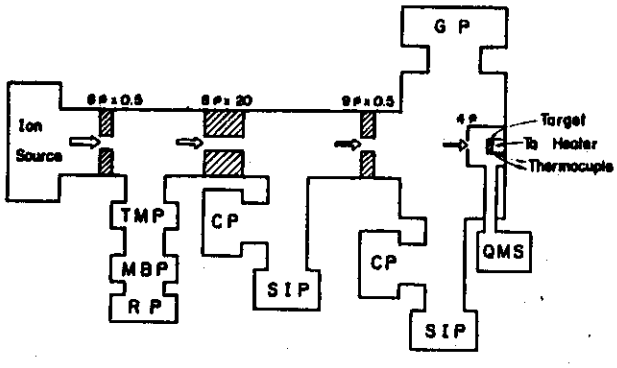

Fig.1 Schematic representation of experimental apparatus.

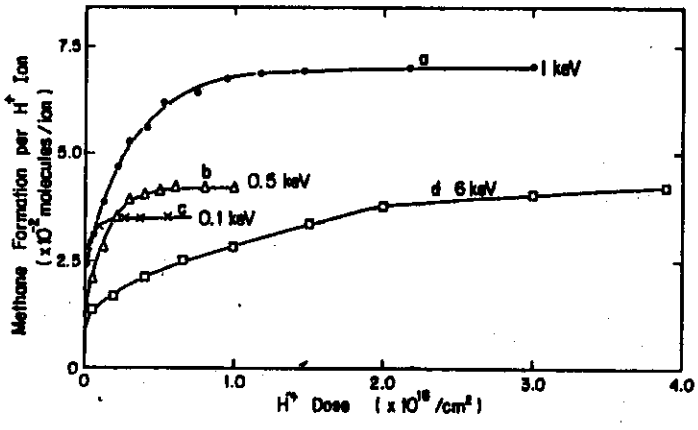

Fig.2 Dose dependence of methane formation for virgin samples.

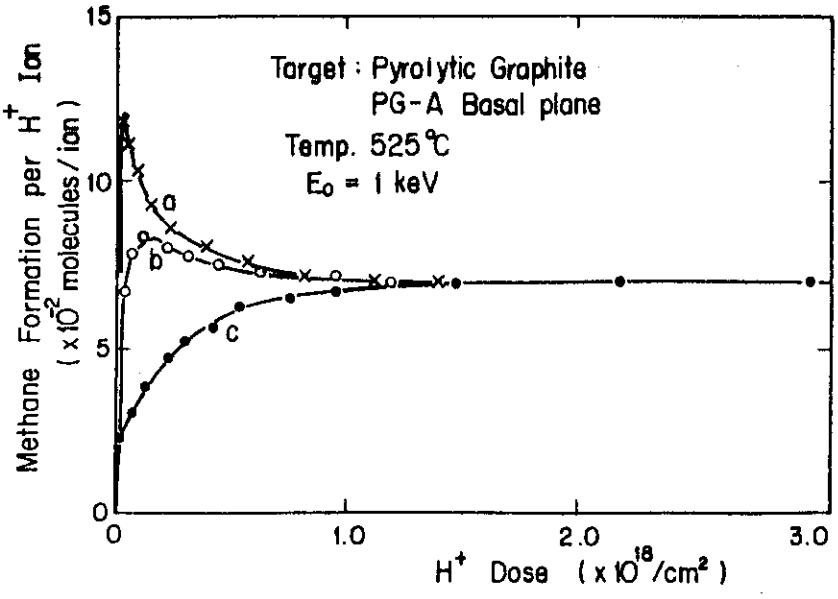

Fig.3 Dose dependence of methane formation for pre-bombarded samples. The individual treatment of targets before the bombardment at 525 C were as follows
a) Pre-bombardment of 9×10^{17}/cm^2 with 1 keV at R.T.. The heat cycle of taget was R.T. and 525 C.
b) Pre-bombadment was the same as a). The heat cycle was R.T., 700 C and 525 C.
c) Without pre-bombardment at room temperature.

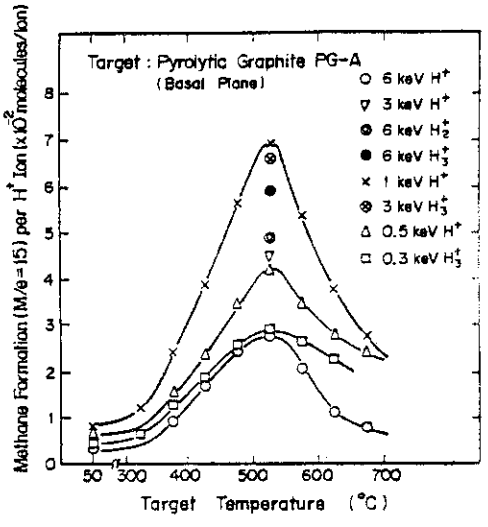

Fig.4 Methane production rate of basal plane of PG-A.

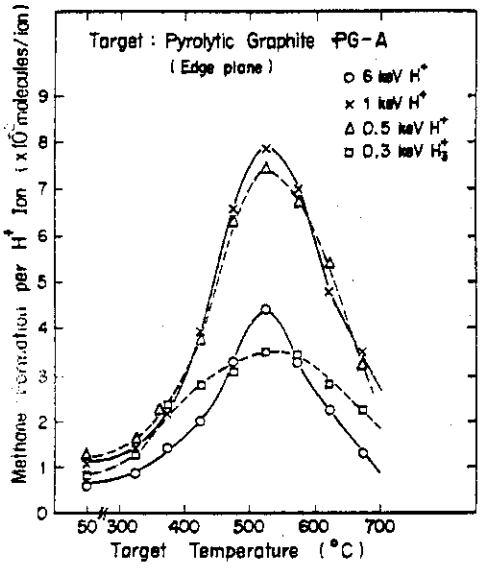

Fig.5 Methane production rate of edge plane of PG-A.

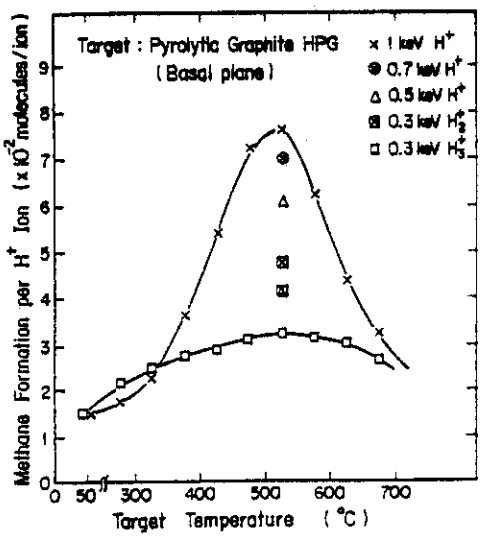

Fig.6 Methane production rate of basal plane of HPG.

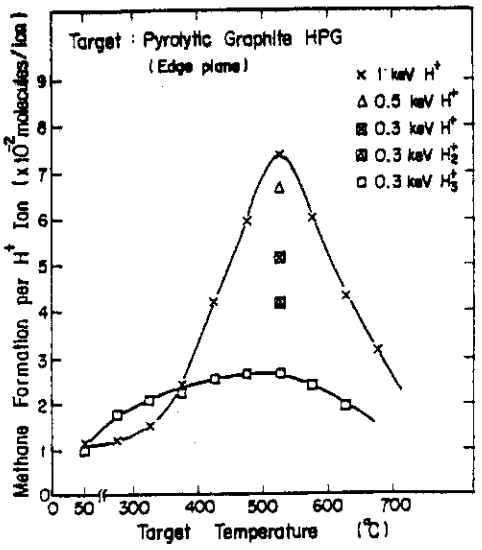

Fig.7 Methane production rate of edga plane of HPG.

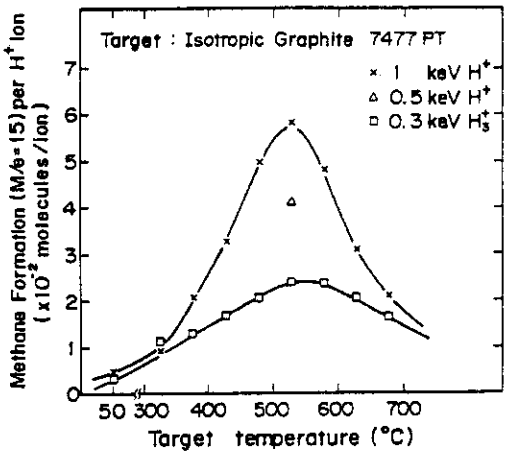

Fig.8 Methane production rate of 7477PT.

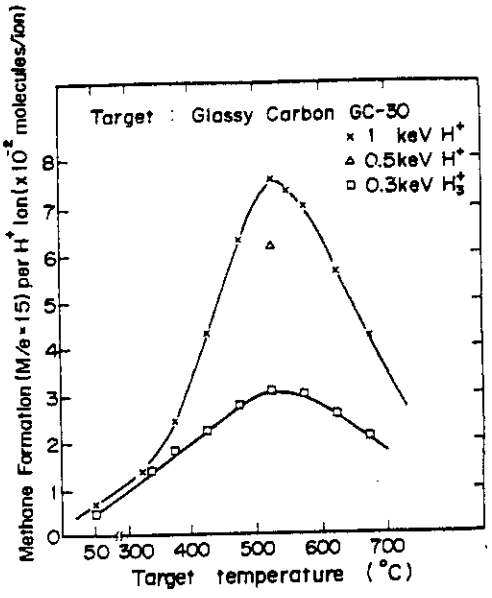

Fig.9 Methane production rate of GC-30.

9 - 3 Reduction of Partial Sputtering Yield of Metal Atoms from VC and NbC by Ion Induced Precipitation of Carbon Layer at the Surface

K. Morita

Department of Crystalline Materials Science, Faculty of Engineering,
Nagoya University, Nagoya, Japan

see 7 - 4

9 - 4 CONDITIONING OF GRAPHITE SURFACE BY ATOMIC HYDROGEN

T. Abe, K. Obara and Y. Murakami
Division of Thermonuclear Fusion Research
Tokai Research Establishment, JAERI

I INTRODUCTION

The incidence of energetic and/or chemically active hydrogen particles on the first wall surface gives rise to the introduction of impurities into the tokamak plasma by particle-surface interaction. These impurities will lose energy by line and recombination radiation and bremsstrahlung. Generally, the higher atomic number impurities will radiate greater amounts of power. Therefore, there is increasing interest in the use of low-Z materials and low-Z surface coatings for the first wall.

Graphite has been proposed as a candidate low-Z material for the first wall due to its high heat conductivity and low volatility at high temperatures. However, the bombardment of graphite with hydrogen ions and atoms is well known to produce gaseous hydrocarbons such as methane and acetylene[1-4].

II EXPERIMENTAL

In this connection, we have studied the possibility of conditioning graphite surfaces by atomic hydrogen shower. The measurement of the graphite erosion rate by thermal atomic hydrogen was made in the surface temperature range of 100-900 °C. The experimental arrangement is shown schematically in Fig.1. It consists of a gas inlet, a hydrogen atomizer, a reaction vessel, a quadrupole mass analyzer (ANELVA, type 515B), and a pumping system. The atomizer is made of a rhenium filament 0.025 cm in diameter and 36 cm long. In this arrangement some of the hydrogen molecules impinging on the rhenium hot filament are dissociated into atoms[5]. The atomic hydrogen produced flows through a Teflon-coated glass tube from the atomizer into the reaction vessel because a very small amount of atomic hydrogen can recombine on Teflon[6]. Thus, the pressure of atomic hydrogen in the reaction

vessel could be varied from 10^{-8} to 10^{-7} Torr, which corresponded to the fluxes from 2×10^{13} to 2×10^{14} atoms·cm^{-2}·sec^{-1}. The partial pressures of atomic hydrogen, molecular hydrogen and methane were measured with the quadrupole mass analyzer. The methane pressure was read from m/e = 15 in order to avoid any error which might arise from the presence of H_2O, CO_2, and CO. The reaction vessel was made of quartz. Graphite samples (pyrolytic graphite and nuclear grade graphite obtained from Nippon Carbon) 2 cm in diameter and 0.1 cm thick were heated with an infrared lamp and their temperature was measured with a chromel-alumel thermocouple. Prior to the measurement, the samples were baked in high vacuum at 1000°C for 60 minutes.

Since the actual surface area of the graphite is unknown, the areas referred to are geometric areas.

III RESULTS and DISCUSSION

Figures 2(a)-2(c) show variations in methane production rate in the reaction vessel with a pyrolytic graphite sample exposing to atomic hydrogen as a function of exposure time and sample temperature. The pressure of atomic hydrogen in the vessel was about 1×10^{-7} Torr and the sample was heated up in steps of 100 degrees from room temperature to 900 °C. Before time a the system reached a steady state flow of molecular hydrogen by adjusting the gas inlet valve. At time a, the rhenium filament was heated to a very high temperature so that a considerable rate of the molecular hydrogen impinging on the filament were dissociated into atoms. The increase in methane production rate at time a was due to the reaction of atomic hydrogen with wall contaminants and it was constant during each run. Figure 3 summarizes the methane production rates from the pyrolytic graphite sample during three runs. In the first and second runs a peak was observed between 500 and 600 °C, but the rate at the second run was relatively lower

than that at the first run. In the third run where the sample had been exposed to atomic hydrogen shower to a fluence of about 10^{17} atoms·cm^{-2} at above 500 °C, the methane production rate further decreased and the peak disappeared in the measured temperature range.

This experimental result implies that the graphite surface can be made passive to atomic hydrogen by a surface treatment. The time dependence of methane production rate at above 500 °C also supports the phenomenon (see Fig.2(a)). On the other hand, the inactive graphite surface has been found to be restored again to the former state if it is exposed to an oxygen containing gas such as air.

The effect of atomic hydrogen on nuclear grade graphite was also similar to that on pyrolytic graphite. The experimental results are shown in Figs.4(a)-4(c) and 5.

Recently, similar effects have been demonstrated in a tokamak experiment using DIVA, where a pyrolytic graphite sample is exposed in the divertor plasma[7]. The surface conditioning of graphite may be attributed to the depletion of free radicals on the surface, or to the decrease in the ratio of the production rate of methane to the rate of recombination of hydrogen on the surface. For the satisfactory explanation, however, a direct measurement of the adsorbed state on the surface will be necessary.

REFERENCES

[1] R.K. Gould, J. Chem. Phys. 63 (1975) 1825.

[2] R. Behrisch, et al, J. Nucl. Materials 60 (1976) 321.

[3] J. Roth, et al, J. Nucl. Materials 63 (1976) 222.

[4] K. Sone, et al, Proc. Internl. Symp. Plasma Wall Interactions, Jülich, 1976 (pergamon, 1976) P.323.

[5] Y. Murakami, J. Vac. Sci. Technol. 10 (1973) 359.

[6] P.W. Zitzewitz and N.F. Ramsey, Phys. Rev. A3 (1971) 51.

[7] S. Sengoku, et al, JAERI-M 8465 (1979).

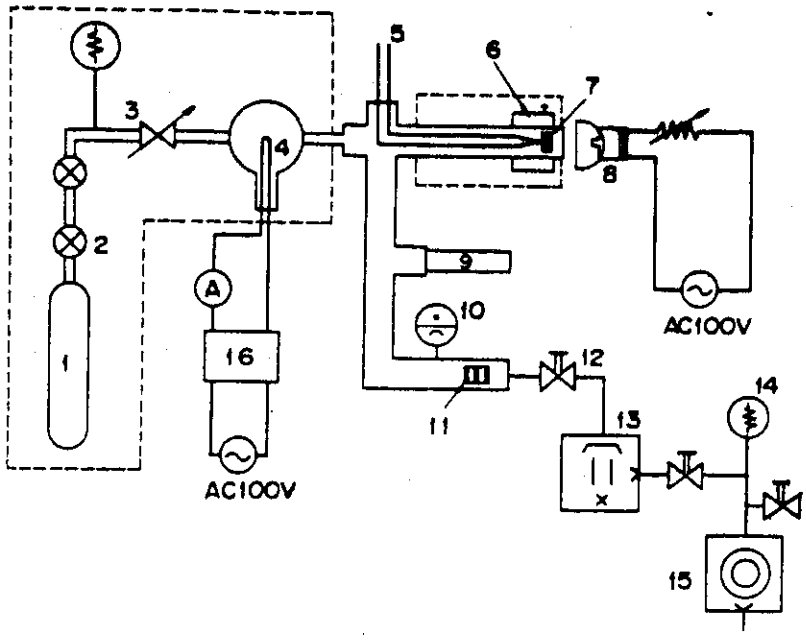

Fig.1 Experimental set-up for measurement of erosion rate of carbon by thermal atomic hydrogen; 1-3 gas inlet, 4 hydrogen atomizer, 7 reaction vessel, 9 quadrupole mass analyzer, and 11-15 pumping system. The parts enclosed by the dotted line is made of quartz.

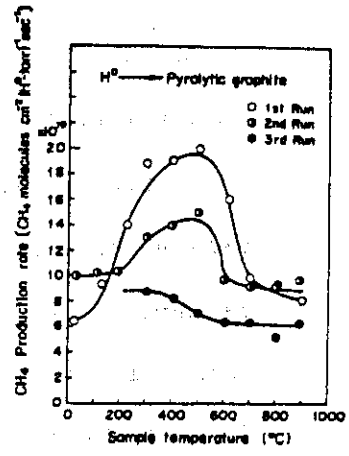

Fig.3 Measured methane production rate from pyrolytic graphite as a function of sample temperature.

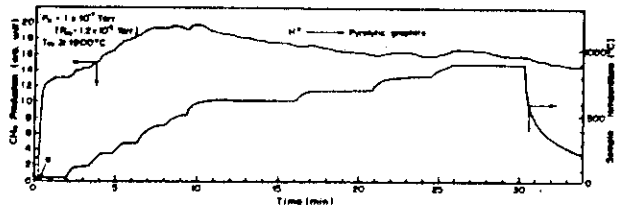

Fig.2(a)

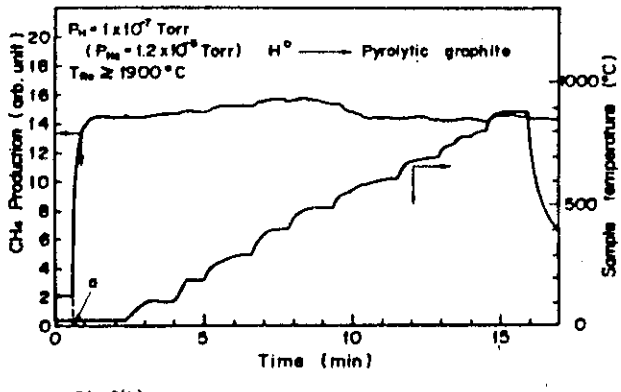

Fig.2(b)

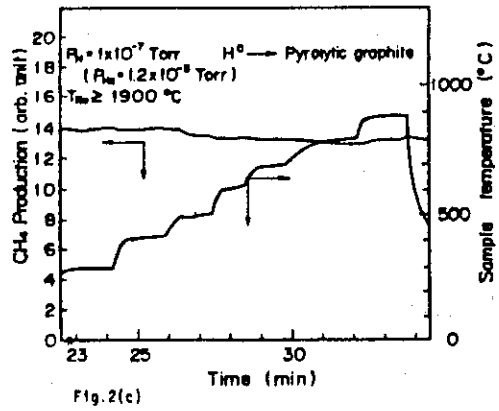

Fig.2(c)

Fig.2 Variation in methane production from pyrolytic graphite exposing to atomic hydrogen as a function of exposure time and sample temperature. First, second and third runs are 2(a), 2(b) and 2(c), respectively.

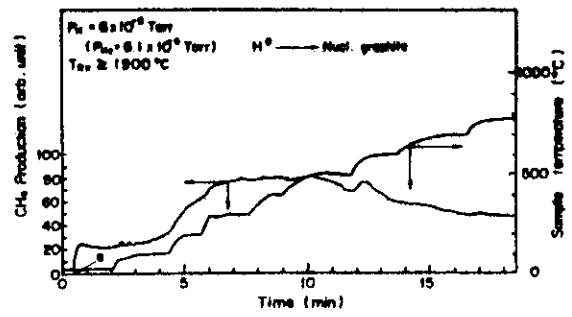

Fig.4(a)

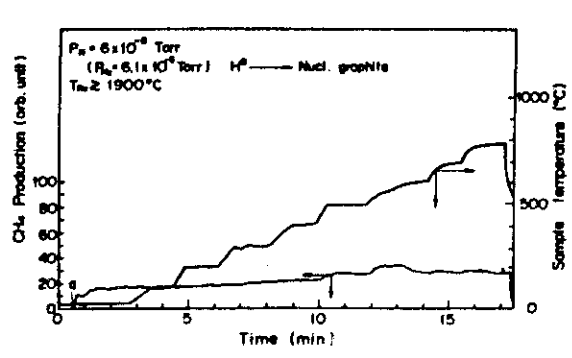

Fig.4(b)

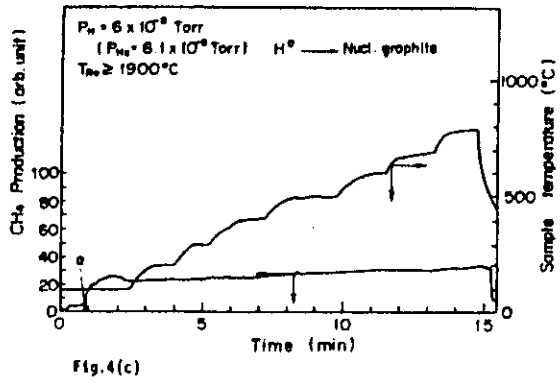

Fig.4(c)

Fig.4 Variation in methane production from nuclear grade graphite exposing to atomic hydrogen as a function of exposure time and sample temperature. First, second and third runs are 4(a), 4(b) and 4(c), respectively.

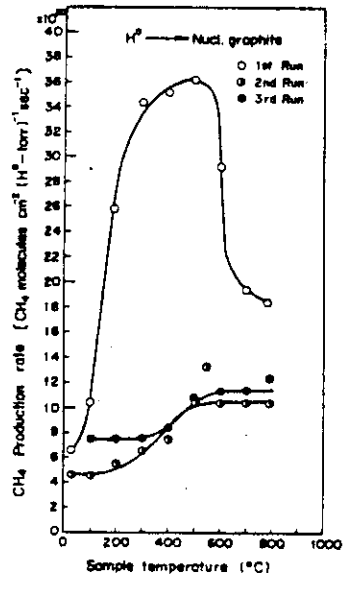

Fig.5 Measured methane production rate from nuclear grade graphite as a function of sample temperature.

9 - 5

Conditioning of Graphite Surface by Atomic Hydrogen Shower

K. Akaishi and A. Miyahara

Institute of Plasma Physics, Nagoya University, Nagoya, Japan

The effect of carbon coating on first wall in tokamak machine is recently tested, and it is reported that the carbon coated surface has the same effect on emission control of gas impurity as in titanium gettered surface[1]. As an interpretation for the achievement of gas impurity free plasma by the carbon coating, we can assume that the carbon film surface is passivated by discharge cleaning with hydrogen plasma. This work is carried out to examine, from stand point of elementary process, whether the carbon or graphite surface can be passivated with atomic hydrogen irradiation.

A nuclear graphite sample is set in the UHV system which is pumped by a turbo-molecular pump, and is irradiated with thermally dissociated hydrogen atoms by hot tungsten filaments. During the irradiation of hydrogen atoms, the sample is heated from room temperature to 900°C, and desorbed gases from the sample are analyzed by a quadrupole mass filter. From the thermal desorption spectra, CH_4 formation on the graphite surface is not expected, rather gas formation such as H_2O and CO due to chemical reaction of H_2 gas with hot tungsten filaments is predominant. Therefore in this experimental set-up it is difficult to appreciate the passive state of the graphite surface.

9 - 6 PHYSICAL VAPOR DEPOSITION OF LOW Z MATERIALS.

Souji Komiya and Chikara Hayashi
ULVAC Corporation
2500, Hagisono, Chigasaki, Kanagawa-Pref. 253. Japan

Modern techniques of physical vapor deposition can be utilized for low atomic number material coating on removable components such as limiters and wall armors of magnetically confinement fusion experimental devices. Deposition by using hollow cathode discharge evaporation is a prominent candidatefor refractory compounds of combination of low Z elements including B, C, N, Al, Si and Ti.

Low voltage high current plasma beam emitted from a HCD gun produces a considerable fraction of ions and energetic neutrals of evaporating material out of thermally moved vapor atoms. Low pressure reactive gas introduced either through the hollow cathode or to the proximity in the evaporation zone during deposition serves to form highly adhesive, dense, ductile and chemically pure compound films, even in a relatively low substrate temperature.

In the preliminary experiments done in ULVAC laboratory for binary systems of Ti-C and Ti-N, the following experimental set-up is successfully used; a HCD gun produces a bent beam which is deflected into a water cooled copper button hearth. Argon is introduced through a tantalum cathode tube. Approximately 50 V and upto 130 A is applied between a water cooled anode and the cathode. The electron beam is extracted through the anode hole and is bent toward the copper hearth by a weak magnetic field. A titanium button of 30 g is placed in a praphite liner 6 mm thick which sits on the hearth. Typical operating parameters are; argon flow rate, 23 cm^3(STP)min^{-1}; argon pressure, 0.1 Pa; discharge parameters, 40 V and 80 A. A typical deposition rates for titanium carbide and nitride films are 0.25 $\mu m\, min^{-1}$ measured with a thickness monitor 14 cm from the hearth. Reactive gas(CH_4, C_2H_4 or C_2H_2 for Ti-C system and N_2 for Ti-N system) is fed through a fine control variable leak valve. Substrate temperature is kept around 923K.

The similar technique will be hopefully applicable to Al-C, Al-N, Si-C and Si-N systems. Some modefication, however, will be required on the experimental apparatus to form films of B-C, B-N and Ti-B systems.

REFERENCES for the investigations of the hollow cathode discharge evaporation done in ULVAC laboratory.

1) S.Komiya and T.Tsuruoka, Jpn. J. appl. Phys. Suppl. 2 Pt.1. (1974) 415. "Production and measurement of dense metal ions for physical vapor deposition by a hollow cathode discharge."

2) S.Komiya and K.Tsuruoka, J. Vac. Sci. Technol. 12 (1975) 589. "Thermal input to substrate during deposition by hollow cathode discharge."

3) S.Komiya and K.Tsuruoka, J. Vac. Sci. Technol. 13 (1976) 520. "Physical vapor deposition of thick chromium and its carbide and nitride films by hollow cathode discharge."

4) K.Nakamura, K.Inagawa, K.Tsuruoka and S.Komiya, Thin Solid Films 40 (1977) 155. "Applications of wear resistant thickfilms by PVD processes."

5) S.Komiya, S.Ono and N.Umezu, Thin Solid Films 45 (1977) 473. "Hardness and grain sizerelations for thick chromium films deposited by hollow cathode discharge."

6) S.Komiya, S.Ono, N.Umezu and T.Narusawa, Thin Soild Films 45 (1977) 433. "Characterization of thick chromium-carbon and chromium-nitrogen films deposited by hollow cathode discharge."

7) S.Komiya, T.Tsuruoka, S.Ono and H.Yoshikawa, Proc. 7th Intern. Vac. Congr. &3rd Intern. Conf. Solid Surfaces (Vienna 1977) Vol. 1, p.367. "Production of metal ions and energetic neutrals by HCD deposition."

8) S.Komiya, H.Yoshikawa and S.Ono, J. Vac. Sci. Technol. 14 (1977) 1141. "Mass and energy analysis of incident ions to substrate during deposition by hollow cathode discharge."

9) S.Komiya, N.Umezu and T.Narusawa, Thin Solid Films 54 (1978) 51. "Formation of thick titanium carbide films by the hollow cathode discharge reactive deposition process."

10) S.Komiya, N.Umezu and C.Hayashi, Thin Solid Films 63 (1979) 341. "Titanium nitride films as a protective coating for a vacuum deposition chamber."

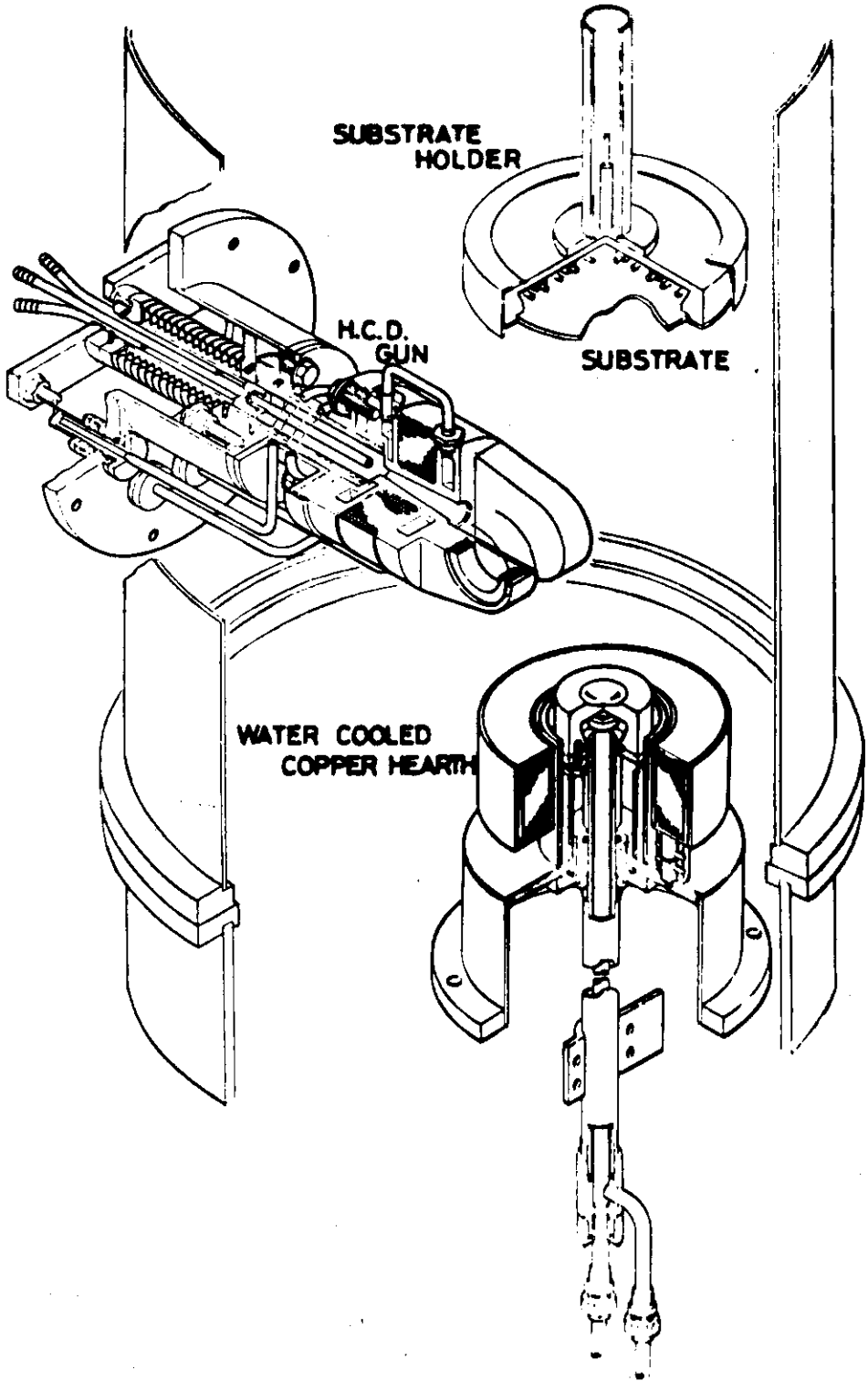
SUBSTRATE
HOLDER
SUBSTRATE
H.C.D.
GUN
WATER COOLED
COPPER HEARTH

9 - 7 Preparation and Properties of Carbon Films with Magnetron Sputtering

Hiroaki Kitahara, Akio Konishi and Naokichi Hosokawa
Anelva Corporation, 5-chome, Yotsuya, Fuchu-shi, Tokyo 183

Hajime Hiratsuka and Katsuo Annoh
Japan Atomic Energy Research Institute, Tokai Research Establishment, No. 2, Shirane, Tokai-mura, Naka-gun, Ibaragi-ken 319-11

Because of low atomic weight and low sputtering yield, carbon could be a suitable material of the first wall of fusion reactors. The possibility of carbon coating of the inner wall has been examined using rf magnetron sputtering with graphite target. Special interest has been taken in the adhesion of sputtered carbon film, and in the deposition rate.

Fundamental relationship between film properties and sputtering conditions were studied using a small sputtering system with a 10 cm diameter planar magnetron electrode. Carbon films were prepared at a target/substrate distance of 3.8 cm and varying sputtering argon pressure from 1×10^{-3} to 2×10^{-1} Torr, deposition rate from 50 to 700 Å/min, and substrate temperature from room temperature to 300°C. Plates of SUS-304 and glass were used as substrates. It was found that the most effective factor which influenced adhesion was sputtering pressure. Adhesion of the films prepared at pressures below 6×10^{-3} Torr was very poor. It was also clarified that the adhesion was degraded by increasing film thickness. Topographic variation of the films was obviously observed with a SEM. Films on SUS-304 substrate were found to change their structure from agglomerate, sooty state prepared at lower pressures to continuous, smoother state prepared at higher pressures.

Film appearance on glass substrate was different from that on SUS-304 substrate. Sooty state was not observed. However, after the films were prepared at lower pressures and taken out from the vacuum chamber to atmosphere, gradually progressive self-flaking was observed. SEM observation showed that these flakes hanged over each other at their peripheries. This could

suggest that large compressive stress in the film was released so as to increase the total area of the film. It was also observed that the film became transparent as the sputtering pressure was increased. No influence of the deposition rate and substrate temperature on the adhesion was found within the conditions of this work.

In order to apply magnetron sputtering of carbon to tokamak reactor, spatial distribution of the deposition rate was studied using a relatively large sputtering system with a cylindrical electrode of 5 cm in diameter and 30 cm in length. Magnetic field was generated by permanent magnet cores inserted in the electrode. Experiment was carried out mainly at a sputtering pressure of 7×10^{-4} Torr. Approximate relationship of $D = K\, d^{-3/2}$ was found, where D, d, and K are deposition rate, distance between target and substrate, and constant, respectively. Some interpretation has been given about the discrepancy between experimental results and calculated deposition rates based on cosine distribution of sputtered atom flux. The deposition rate of about 5 Å/min was obtained at a distance of 80 cm, and at an rf input power of 2.7 kW.

Table I Calculated mass absorption coefficient of carbon films prepared on glass substrate at different powers and pressures with a planar magnetron electrode.

sputtering pressure (x 10^{-2} Torr)	6					10
rf input power (W)	75	150	300	600	900	300
deposition rate (Å/min)	46	153	265	546	704	255
mass absorption coefficient (cm^2/g)	1900	2800	16000	23000	36000	3600

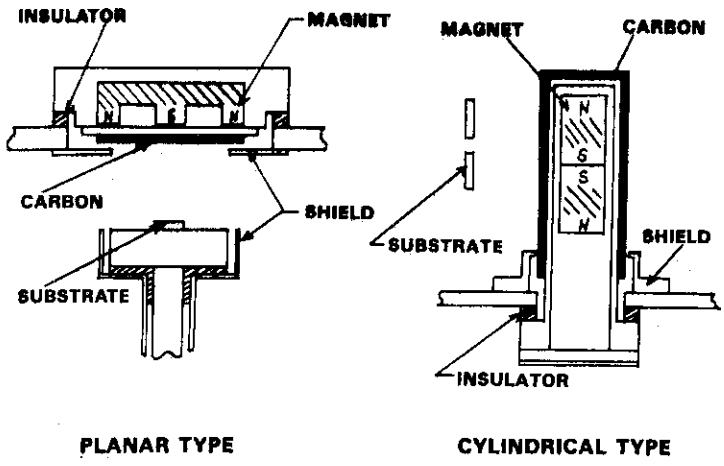

Fig. 1 Schemata of sputtering systemes. planar magnetron electrode with 10 cm diameter target (left) and cylindrical magnetron electrode with 5 cm diameter and 30 cm length target (right).

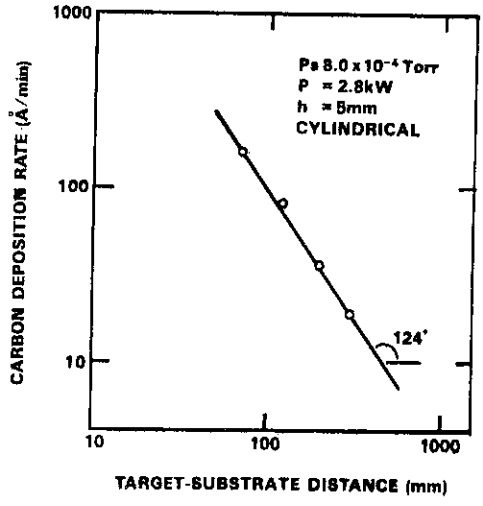

Fig. 4 Deposition rate as a function of distance between target and substrate on a equatorial plane of cylindrical magnetron sputtering system.

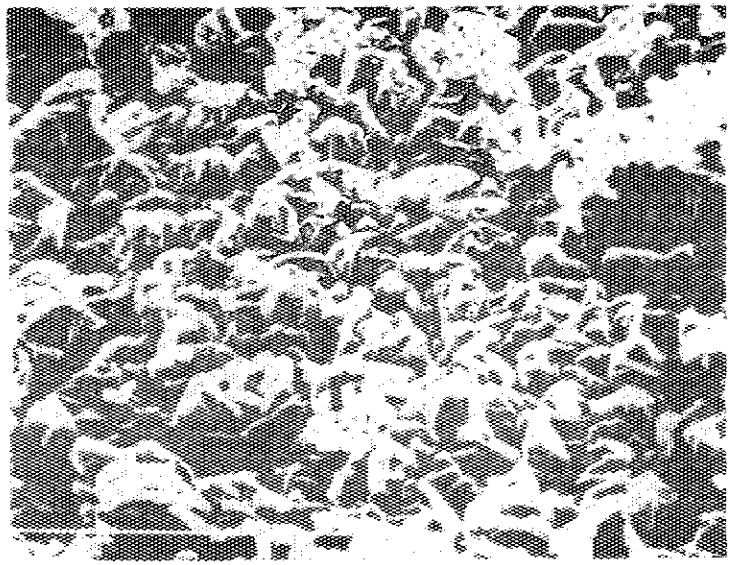

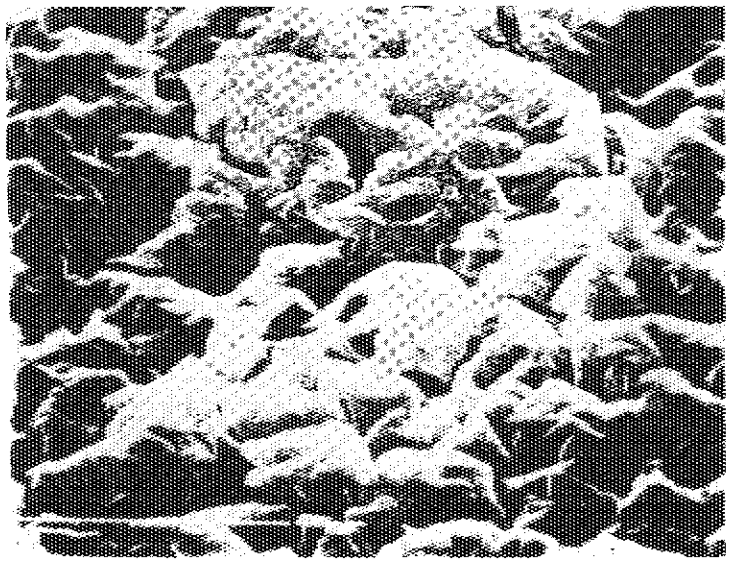

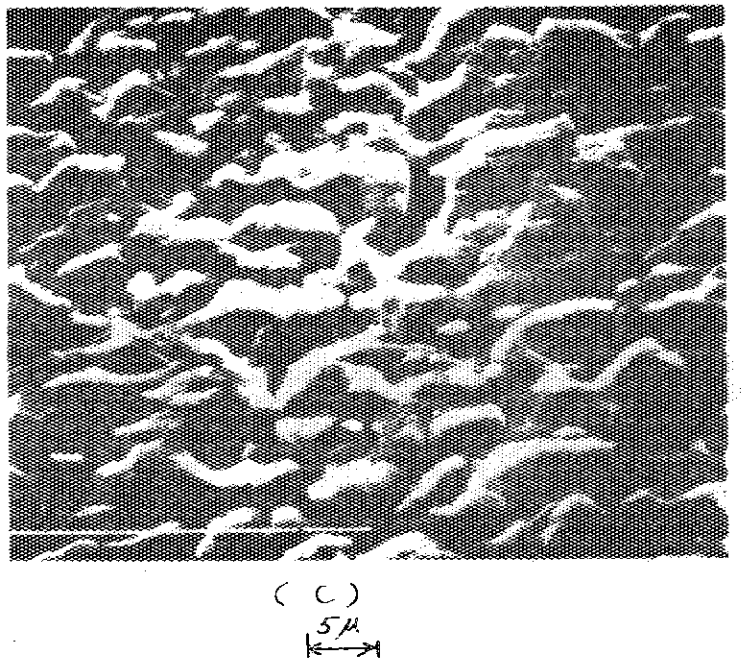

Fig. 2 SEM photos of carbon films on SUS-304 substrates prepared at sputtering pressures of (a) 1×10^{-3} Torr, (b) 1×10^{-2} Torr, and (c) 1×10^{-1} Torr at an rf input power of 300 W with the planar magnetron electrode.

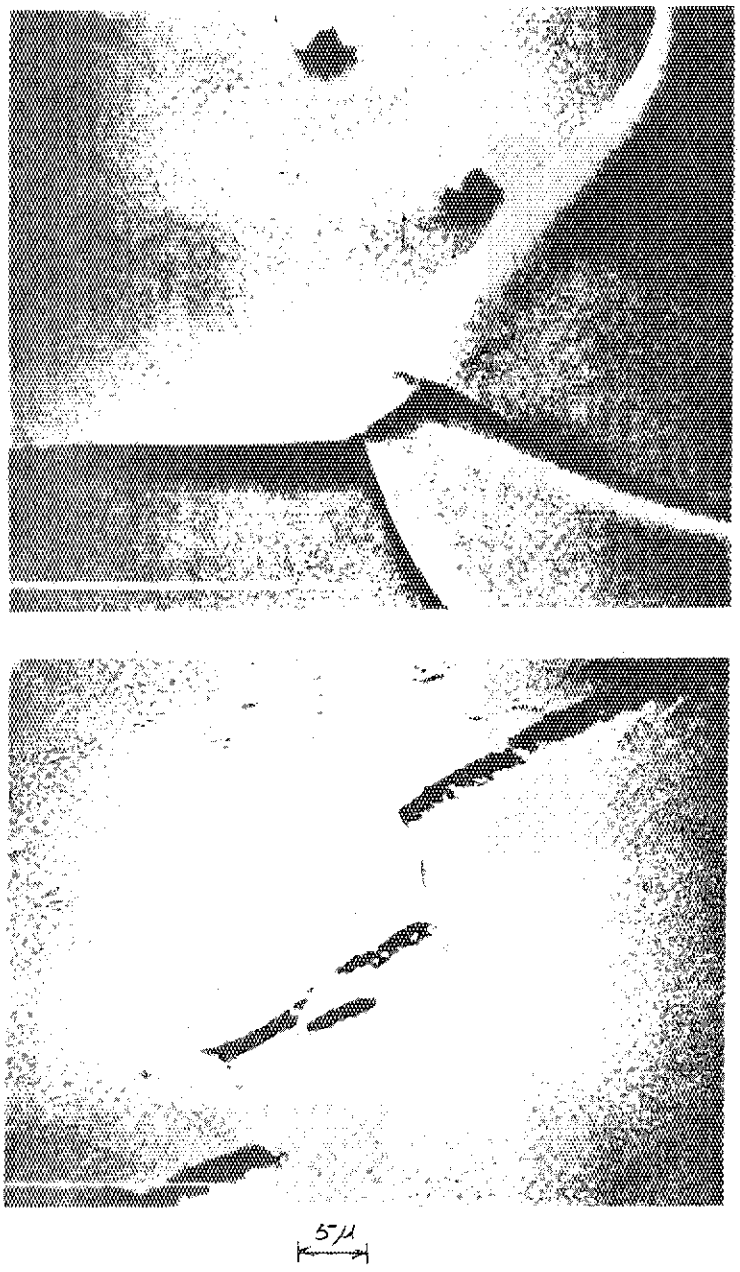

Fig. 3 SEM photos of carbon film on glass substrates prepared at sputtering pressures of (a) 6×10^{-3} Torr, and (b) 6×10^{-2} Torr with the planar magnetron electrode.

10 - 1 MATERIAL STUDIES RELATED TO DIVERTOR OPERATION AND THE TFTR FIRST WALL

M. Ulrickson
Plasma Physics Laboratory, Princeton University
Princeton, New Jersey 08544 USA

ABSTRACT

As the input power to tokamaks has increased in each generation of machines, the need for careful selection of the material to be used as the primary heat sink has increased. The impurity control part of the Tokamak Flexibility Modification (TFM) program for TFTR has supported research to control impurities through proper material selection. The effort has consisted of two parts; base material selection, and selection of coatings or claddings to improve the performance of the base material. The tests are being conducted using electron beams, neutral beams, and exposure on PDX. At this point in the study the most interesting material choices are TiC coated on POCO graphite and vanadium cladding on copper.

I. INTRODUCTION

As the input power and energy content of tokamaks has increased with each generation of machines, the need for careful selection of the material to be used as the primary heat sink has increased. This is due in large part to the success there has been in reducing the impurity content of the plasma. The result of impurity reduction is a decrease in radiated power with an attendant increase in heat conduction to the primary heat sink. If the material and/or design of the primary heat sink is not adequate to accept this increased fraction of the heat load of the plasma, then the material will reach a temperature sufficient to emit enough impurities to limit the heat flow to an acceptable level. Recognizing this fundamental relationship, the impurity control study under the Tokamak Flexibility Modification (TFM) Program of the Tokamak Fusion Test Reactor (TFTR) included material studies.

The material studies conducted under TFM were divided into two major divisions. One was a study of base materials to be used as the primary structural elements of the primary heat sink. The second was a study of coatings and claddings to be used on the base material to improve the surface properties. The desired improvements in surface properties are reductions in sputtering, chemical erosion, sublimation, and outgassing. The coatings must also have low hydrogen retention characteristics consistent with tritium inventory requirements for TFTR. The studies in the second phase were conducted jointly by Princeton, Argonne National Laboratory, Sandia Laboratories

in Albuquerque and Livermore. The results of the study of base materials have been previously reported.[1] The results of the coatings and claddings study done at Princeton will be reported here. While the studies were primarily aimed at limiters and first walls for TFTR, the results are easily generalized for applications to divertor plates.

In TFTR the peak heat loads on the bumper limiter (see Fig. 1) under TFM operation are anticipated to be about 1.0 kW/cm^2 maximum for a scrape-off thickness λ = 0.43 cm and 0.5 kW/cm^2 for λ = 2.5 cm both for pulse lengths of 1.5 s. These heat loads are based on a model[2] which has power flowing along field lines to the bumper limiter using the geometry shown in Fig. 2. The variation of these heat loads with poloidal angle θ is shown in Figs. 3 and 4. These heat loads are based on neutral beam heating of 33 MW. The heat load estimates for the moveable limiters (see Fig. 1) are much more sensitive to the plasma scrape-off thickness and the operating mode. The estimates vary from 1 kW/cm^2 to 10 kW/cm^2. The latter is for the strong compression plasma on the tips of the inner two moveable limiters. This heat load estimate is one of the major reasons for the installation of the bumper limiter. The heat loads and pulse lengths used in the material studies were within the limits discussed above.

II. EXPERIMENTAL TECHNIQUE

The material combinations being studied have been subjected to three types of heat loads: electron beam irradiation, neutral beam irradiation, and exposure to plasma bombardment in PDX. The electron beam apparatus is a standard evaporation unit which operates at 10 kV and has a maximum current capability of 1.9 A. The area of the beam is about 1 cm^2, which implies a power density of up to 19 kW/cm^2. The maximum pulse length of the power supply is 1.5 s. The neutral beam operates at 40 kV and has a maximum current of about 60 A. The maximum pulse length is 0.3 s. The beam power profile is Gaussian with a 1/e half width of about 10 cm. The maximum power density is 2.5 kW/cm^2. The neutral beam is identical to those used on PLT. In the plasma exposures done on PDX the maximum heat flux has been about 500 W/cm^2 for pulse durations of about 0.5 s. Further exposures at higher powers are planned in the future.

The samples used in the electron beam irradiation were 2.5 cm × 2.5 cm × 1.3 cm. The samples used in the neutral beam tests were 10 cm × 10 cm × 1.3 cm. This latter size was chosen because it is approximately the size of tiles in the conceptual design for the bumper limiter. The sample exposed to plasma in PDX was one half of a cylinder 15 cm in diameter and 25 cm long. This size is similar to the titanium limiters on PDX.

In the electron and neutral beam irradiations the surface temperature of the material was monitored using infra-red emission in the 2.0 to 2.5 μm wavelength band. In addition,

the bulk temperature was monitored using thermocouples. The surface temperatures were used to deduce the heat flux in those cases where it could be monitored. In the plasma irradiation the heat flux was inferred from the energy deposited during the pulse and the measured plasma scrape off width.

Two types of tests were done in the electron beam irradiations. The materials were first subjected to heat fluxes high enough to cause failure of the surface (i.e., melting, spalling, or cracking) in a single pulse. Those materials which showed high flux limits in the thermal shock tests were subjected to at least 1000 pulses at heat fluxes and pulse lengths similar to those expected in TFTR to determine their fatigue behavior.

The samples tested were produced with four different methods: chemical vapor deposition (CVD), explosion bonding (EB), plasma spray, and pack boriding. The CVD samples were titanium carbide on POCO graphite, titanium diboride on POCO graphite, and boron on POCO graphite. The EB samples were titanium on copper, vanadium on copper, and vanadium on molybdenum on copper. The titanium diboride on copper was produced by plasma spray. The vanadium diboride on vanadium was produced by pack boriding.

III. RESULTS AND DISCUSSION

The flux limits for 0.5 s and 1.5 s pulse lengths determined for the coating/cladding systems subjected to the electron beam thermal shock tests are shown in Table I. The surface damage caused by each sample is shown in Fig. 5. The flux limits listed in Table I were set by melting of the surface of

the sample for TiC on graphite, boron on graphite, vanadium on molybdenum on copper, and titanium on copper. The flux limit for vanadium on copper, TiB_2 on copper, and VB_2 on vanadium on copper was set by melting of the substrate under the coating or cladding.

For TiB_2 on graphite the flux limit was set by spalling of the coating. The melting that is seen for the TiB_2 is only on the edges of severely spalled areas. In the cases of the VB_2 coating, the TiB_2 coating on copper, and the B coating there is evidence that spalling occurred at approximately the same time as melting of the surface or substrate.

The melting of the substrate under a coating results in a very sudden failure of the coating since the heat transfer from the coating to the substrate is severely reduced when the melting occurs. This could result in a very rapid influx of impurities due to the melting of the entire coating. This phenomenon can be eliminated by proper choice of coating thickness. As an example, consider the vanadium cladding on copper (the other two cases are not considered because of lack of knowledge about the thermal properties of plasma sprayed TiB_2 and pack borided VB_2). Figure 6 shows the effect of vanadium cladding thickness on the surface temperature of the vanadium and the temperature of the copper at the interface. The optimum thickness is when the temperature drop across the cladding is slightly greater than the difference in the melting temperature of the two materials. From Fig. 6 this optiumum thickness is seen to be about 2.3 mm for 1 kW/cm^2 and a pulse length of 1.5 s. The optimum thickness depends strongly on pulse length and

heat flux. Thus the optimum must be adjusted to match the conditions expected in a given case. The 2.3 mm optimum thickness needed for TFTR presents very severe production difficulties because such thick pieces are difficult to purchase in large sizes. The three layer combinations such as V on Mo on copper represent an attempt to decrease the thickness of the vanadium. While the combination with the molybdenum worked well, the high Z of Mo poses potential plasma contamination problems so that other intermediate layers have been considered. The most interesting candidate at this time is stainless steel (SS) since it has a melting point intermediate between vanadium and copper and is readily available. The temperature profile for a V/Cu combination is shown in Fig. 7 and for a V/SS/Cu combination is shown in Fig. 8. The power flux is 1 kW/cm^2 for 1.5 s in both cases. It can be seen from these figures that about the same temperature drop across the cladding is achieved in each case. This triple combination will be tested as soon as samples are available.

Thermal fatigue tests using the electron beam have been performed on TiC on graphite, vanadium on copper, titanium on copper, and TiB_2 on copper. The minimum number of cycles of irradiation was 1000. The TiC on graphite was subjected to 5000 pulses. The heat flux in each case was 1 kW/cm^2 for 0.5 s for all samples and 1.5 s for the TiC/graphite only. The Ti on Cu showed severe cracking and deformation of the surface which was attributed to the crystal phase transition that Ti has around 800 C. Melting of the tips of the most severely deformed

areas was observed even at those low fluxes. For this reason Ti on copper is not a strong candidate material. The TiB_2 on copper showed a 0.05 mm deep crater after 1000 cycles which appeared to be due to slight spalling of the surface under irradiation. Again, this is not considered a suitable fatigue behavior. The vanadium on copper showed very slight surface cracking after irradiation. There was no evidence of melting or surface distortion around the cracks. It is unlikely that such surface cracks will cause any problem, and this material is still considered a viable candidate. The TiC on graphite showed a slight amount of surface discoloration after 5000 cycles. The damage was so minimal that this material is also a viable candidate.

Four of the materials tested in the electron beam test have been subjected to neutral beam tests: TiC on graphite, TiB_2 on graphite, V on copper, and TiB_2 on copper. The TiB_2 on graphite sample showed the same spalling problem as in the e beam tests, except the behavior was seen at about a factor of two lower flux, i.e., 1.5 kW/cm^2 for 0.3 s. This adhesion problem with the TiB_2 coating makes it unacceptable. The V cladding on copper failed in the neutral beam test because the cladding was not bonded near the edge of the sample. This problem can be eliminated with proper screening of the bonded plates. In addition, the use of more ductile and hence easier to bond alloys of vanadium (V10%Ti or V15%Ti) is being investigated to alleviate the quality control problem for this combination. The TiB_2 coating on copper showed no damage from

300 neutral pulses. The TiC on graphite also showed no damage from about 500 neutral beam pulses.

The only coating system that has been exposed to plasma on PDX is TiC on graphite. Figure 9 shows the variation of energy deposited on a test limiter as a function of minor radius. Using the scrape-off thickness inferred from Fig. 9, the measured energy deposited, and the pulse length, the peak heat flux is estimated to be 0.5 kW/cm^2. This would result in a peak surface temperature of about 500 C. After about 30 discharges, the limiter was removed from PDX. The only damage observed was two areas of surface discoloration about 3 mm in diameter. There were two disruptions while the limiter was in the machine. While this short plasma test is not complete, it is encouraging that no damage was observed. There was no increase in Ti or C radiation from the plasma during these tests. Further exposures are planned.

IV. CONCLUSIONS

Based on the tests carried out at this time, the most promising of the coating/cladding systems for use as limiters, wall armor, first walls, or divertor neutralizer plates are TiC on POCO graphite and a vanadium titanium alloy (e.g., V10Ti) on stainless steel on copper. These two materials have very similar thermal flux limits. However, their electrical and thermal conductivities are very different, which impacts on the forces exerted on a plate of these materials during disruption and the temperature gradients expected during long pulses.

The thermal flux limits determined in the e beam tests are only relevant for fault conditions. The limiting heat flux for normal operation is determined by the allowable vapor pressure of the surface material and/or physical or chemical sputtering yields. The sputtering yields are being considered separately from the thermal tests and the results are not yet complete. The vapor pressure of the materials being considered are shown in Fig. 10. Using the area of the bumper limiter and the volume of TFTR together with an assumed particle confinement time and a maximum allowed concentration of medium Z atoms of ~0.1%, the vapor pressure limit is calculated to be about 10^{-5} Torr. This limits the surface temperature of vanadium to about 1400 C and that of TiC to 1800 C. This implies that the flux limits are 1.65 kW/cm^2 for V and 1.35 kW/cm^2 for TiC for 1.5 s pulses.

Further tests of coated/cladded limiters are planned for PDX. Tests of prototype designs for TFTR bumper limiter will be tested on the neutral beam test stand. In addition, options for lower Z coatings are being examined in case the medium Z of Ti or V is not acceptable.

ACKNOWLEDGEMENTS

I would like to acknowledge the many helpful suggestions from and discussions with J. Cecchi, J. Schmidt, and R. Budny. This work was supported by U. S. Department of Energy Contract No. DE-AC02-76-CHO-3073.

REFERENCES

[1] M. Ulrickson, Journal of Nuclear Materials 85&86, 231 (1979).

[2] J. A. Schmidt, TFTR Physics Report No. 12 (May, 1979).

TABLE I

THERMAL SHOCK TEST RESULTS

Coating/ Cladding	Thickness (mm)	Base Material	Thermal flux Limit (kW/cm^2)	
			0.5 s*	1.5 s*
TiC	2×10^{-2}	POCO Graphite	4.0	2.45
TiB_2	2×10^{-2}	POCO Graphite	2.5	1.45
B	2×10^{-2}	POCO Graphite	2.6	1.7
V	0.5	Copper	5.0	2.4
V/Mo	0.5/1.5	Copper	5.0	3.0
VB_2/V	2×10^{-2}/0.5	Copper	5.0	2.4
Ti	0.5	Copper	4.1	2.5
TiB_2	0.1	Copper	5.0	2.45

*Pulse length

FIGURE CAPTIONS

Fig. 1. A cross section of TFTR showing the location of the bumper limiter and the moveable limiter blades. The moveable limiter is at one toroidal location only while the bumper limiter completely encircles the machine toroidally on the small major radius side of the machine.

Fig. 2. A schematic diagram of the bumper limiter showing the relation of the plasma and the limiter. The curve on the left is typical of the power distribution expected on the limiter.

Fig. 3. The anticipated bumper limiter heat loads for λ = 0.43 cm. The total heat load is the sum of the loads shown from the plasma and the neutral beam shine through.

Fig. 4. The anticipated heat load for λ = 2.5 cm.

Fig. 5. Results of thermal shock tests on coated/clad materials. These tests were done with electron beams.

Fig. 6. The surface temperature of the vanadium and the surface temperature of the copper substrate as a function of the thickness of the vanadium cladding. The heat flux was 1 kW/cm^2 and the pulse length 1.5 s with a starting temperature of 20 C.

Fig. 7. The temperature variation through the thickness for 2.3 mm thick vanadium on copper. The heat flux was 1 kW/cm^2 for 1.5 s with a starting temperature of 20 C.

Fig. 8. The temperature variation through the thickness for 0.5 mm vanadium on 0.7 mm 304 stainless steel on copper. The heat flux was 1 kW/cm^2 for 1.5 s with a starting temperature of 20 C.

Fig. 9. The energy deposited on the TFTR test limiter on PDX as a function of the position of the limiter in minor radius. A fit to the points yields a scrape off thickness of λ = 1.7 cm.

Fig. 10. The vapor pressure of selected materials as a function of the inverse of the absolute temperature.

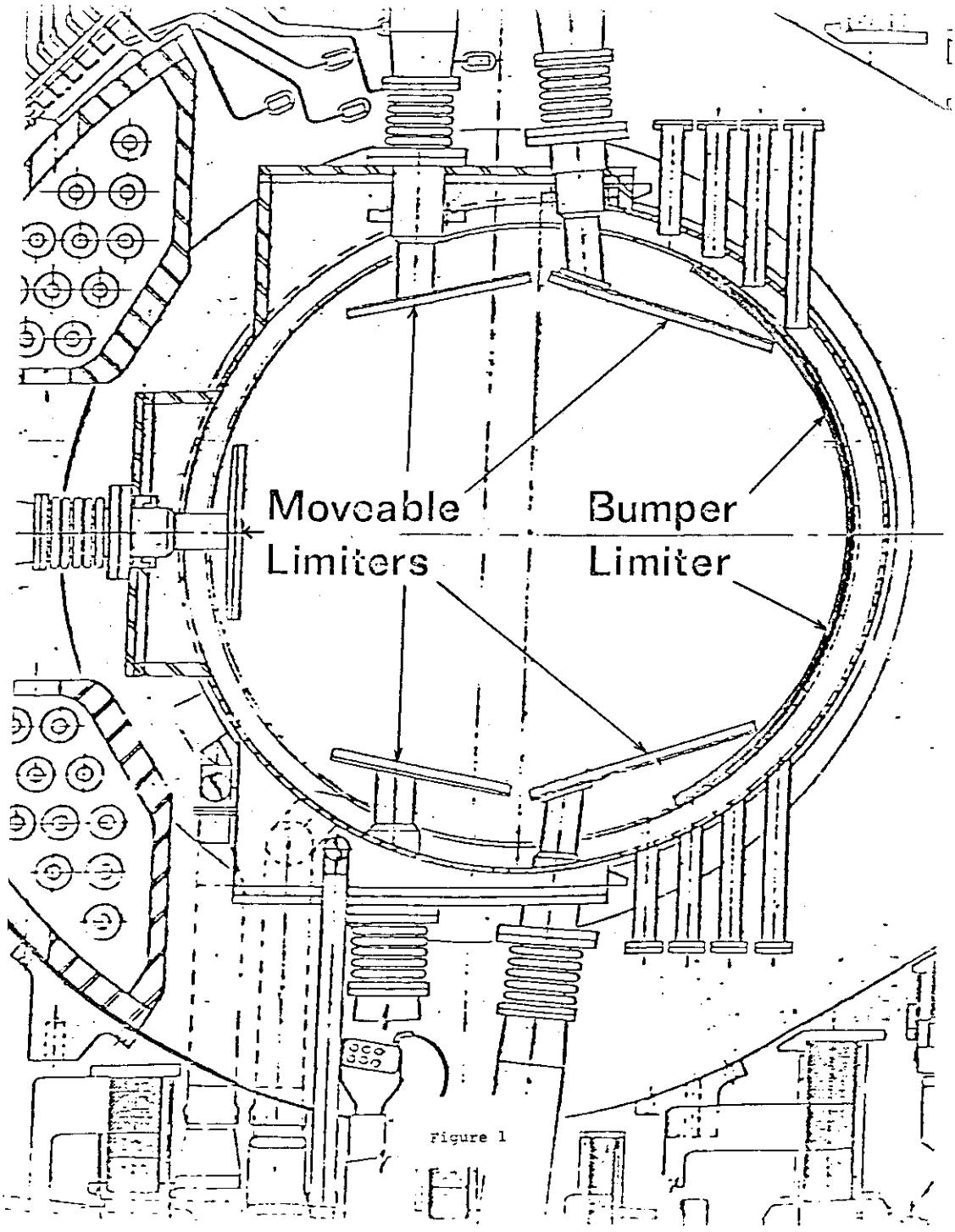

Figure 1

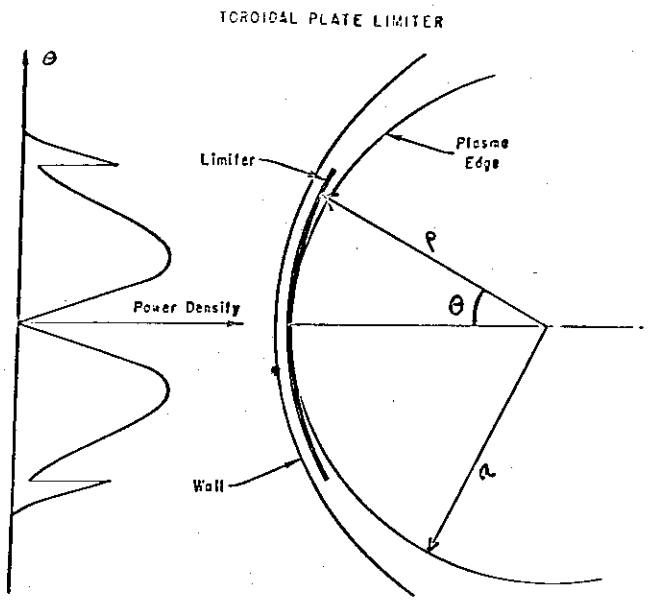

Figure 2

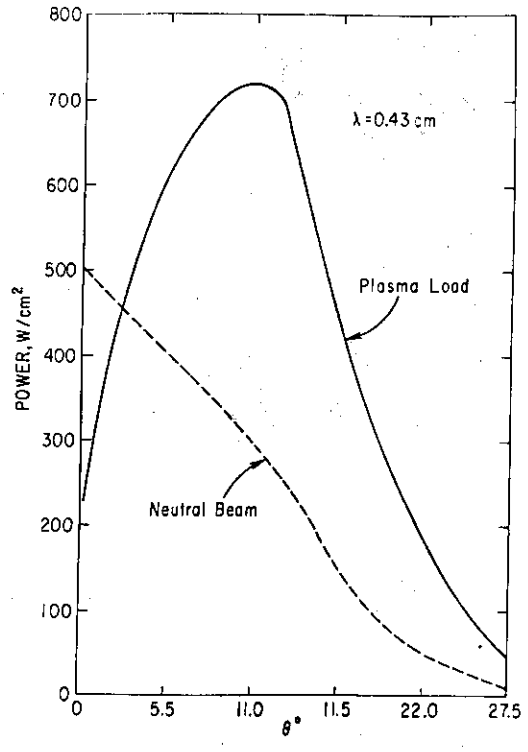

Figure 3

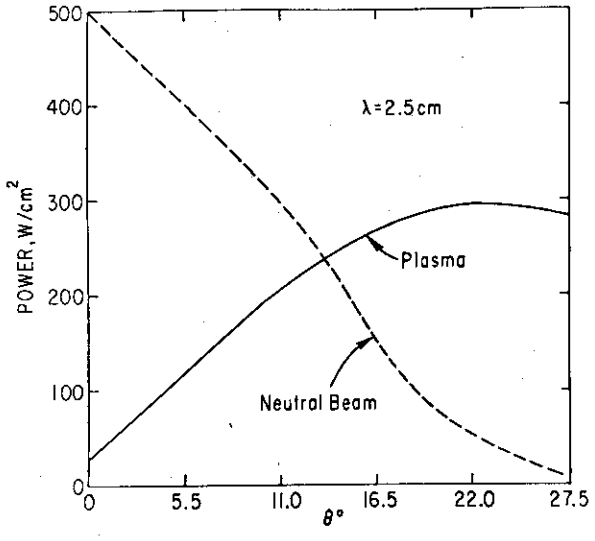

Figure 4

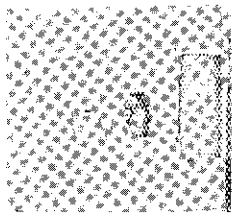

TiB_2/C

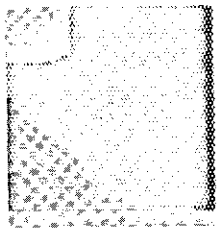

TiC/C

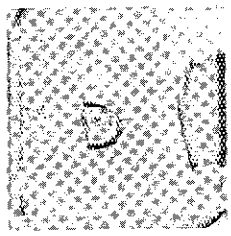

B\C

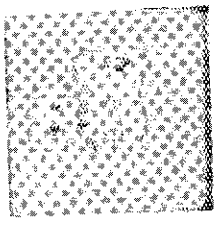

V/Cu

V/Mo/Cu

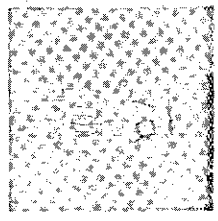

Ti/Cu

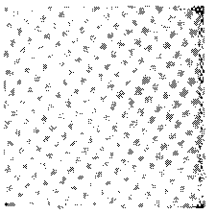

$VB_2/V/Cu$

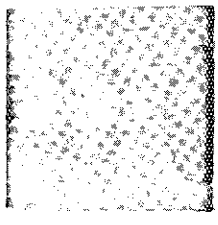

TiB_2/Cu

Figure 5

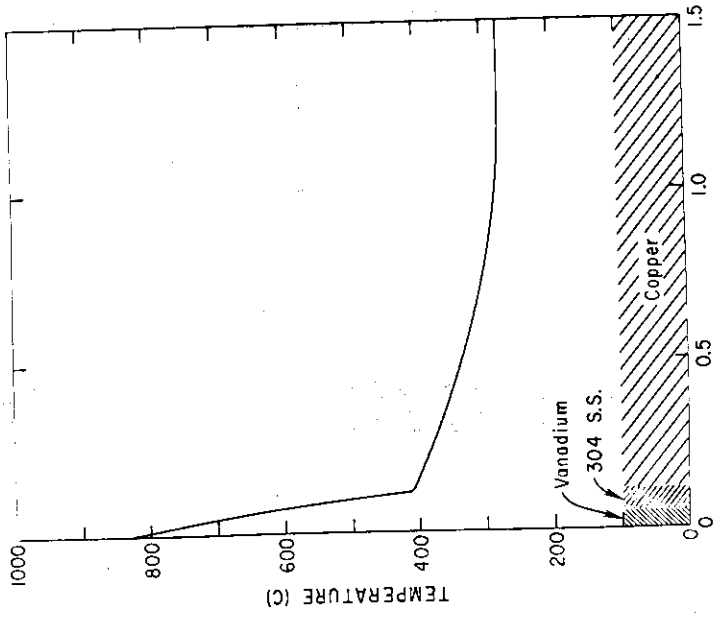

Figure 8

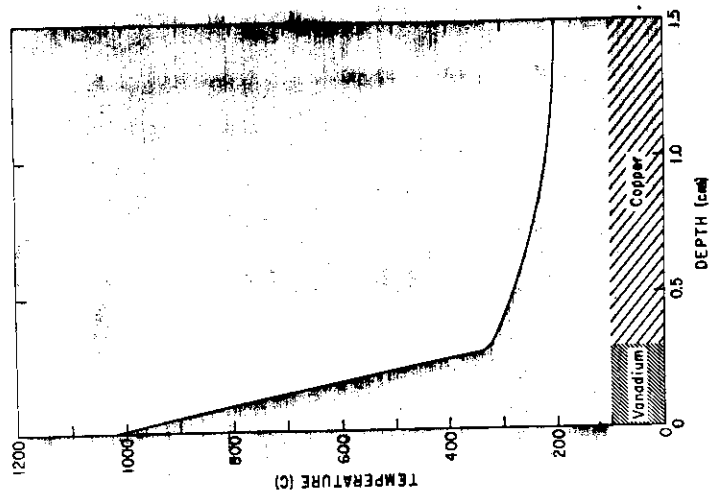

Figure 7

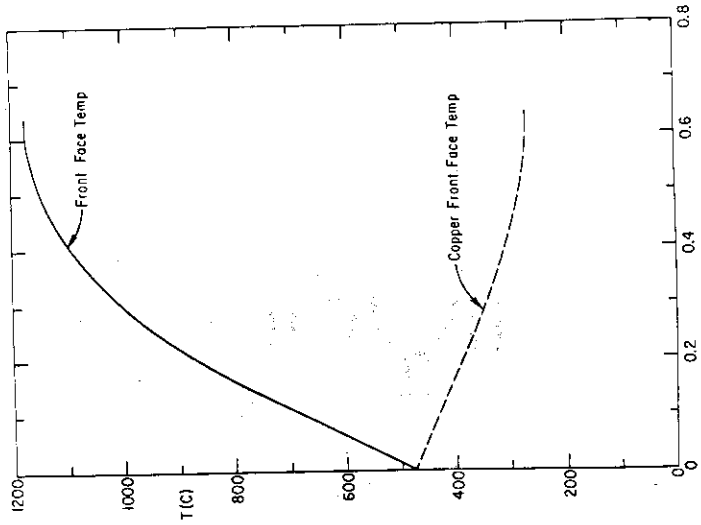

Figure 6

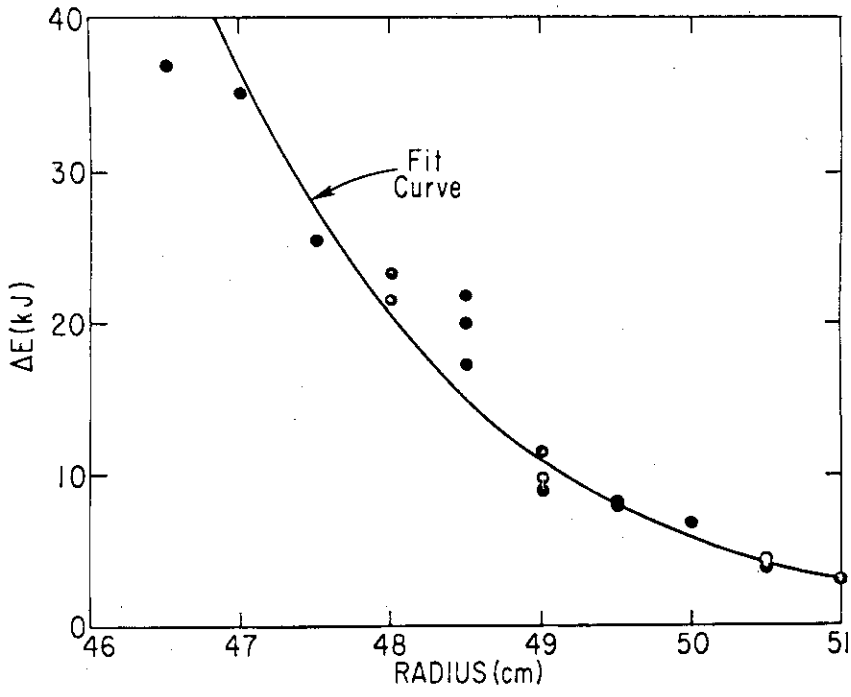

Figure 9

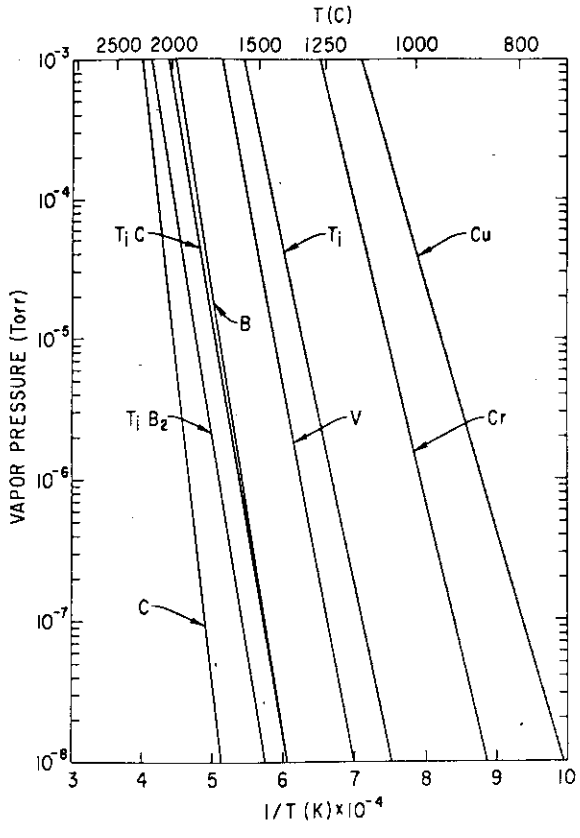

Figure 10

10 - 2 JT-60 FIRST WALL DEVELOPMENT PROGRAM

by HIROO NAKAMURA

Division of Large Tokamak Development, JAERI
Tokai-Mura, Naka-Gun, Ibaraki-Ken, Japan

In recent years, impurity control has become one of the most serious problems in Tokamak research. Impurity controls are classified into two groups: light impurity control and wall material impurity control. Light impurity contamination can be reduced to acceptable limits by providing proper treatment of the wall surfaces before assembly, and in-situ conditioning after assembly.

On the other hand, to suppress the influx of wall material impurity has become important, as the interaction between plasma and first wall(especially limiter) increases in the presence of strong neutral beam heating(as in PLT,for example). PLT experiment showed that graphite limiter was more successful than a metallic one.

Therefore, the development of low-Z material first wall is neccessary to reduce the detrimental effect of wall material impurity.

IMPURITY CONTROL

LIGHT IMPURITY ---------- ADSORBED AND ABSORBED GAS SUCH AS C,O,N

WALL MATERIAL IMPURITY ---------- W,Mo,SS (METAL WALL)
----- C,SiC (LOW-Z WALL)

LIGHT IMPURITY CONTROL

LIGHT IMPURITY CONTAMINATION CAN BE REDUCED TO ACCEPTABLE LEVEL BY PROVIDING PROPER TREATMENT OF WALL SURFACE BEFORE AND AFTER ASSEMBLY

BEFORE ASSEMBLY -----
- GLOW DISCHARGE CLEANING
- BUFFPOLISHING
- ELECTROPOLISHING

AFTER ASSEMBLY -----
- BAKING
- DISCHARGE CLEANING
- OXYGEN AND HYDROGEN TREATMENT (IN CASE OF Mo WALL)
- IN-SITU COATING

WALL MATERIAL IMPURITY CONTROL

TO SUPPRESS THE INFLUX OF WALL MATERIAL IMPURITY HAS BECOME IMPORTANT, AS THE INTERACTION BETWEEN PLASMA AND FIRST WALL(ESPECIALLY LIMITER) INCREASE IN THE PRESENCE OF STRONG NBI.

CONTROL OF IMPURITY GENERATION

- SELECTION OF WALL MATERIAL ---------- LOW-Z MATERIAL
- CONTROL OF BOUNDARY PLASMA ---------- EDGE COOLING

CONTROL OF IMPURITY INFLUX TO MAIN PLASMA

- IMPURITY SHIELDING AND REDUCTION OF PLASMA WALL INTERACTION ---------- MAGNETIC LIMITER

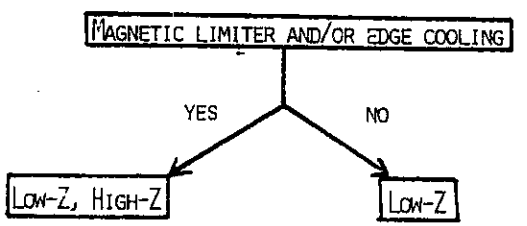

JT-60 FIRST WALL

1. LINER
2. FIXED LIMITER (FL)
3. MAGNETIC LIMITER PLATE (MLP)

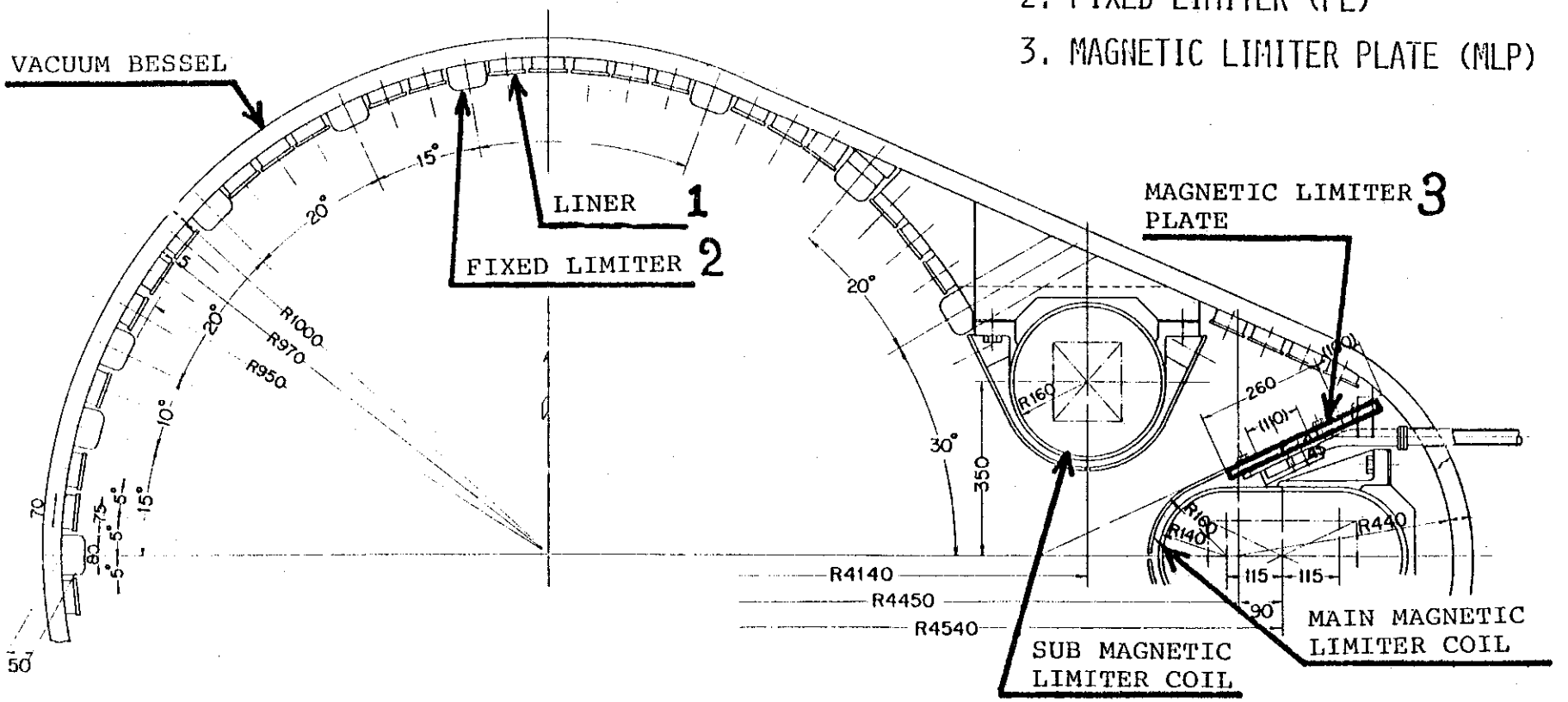

SECTIONAL PLAN OF JT-60 VACUUM VESSEL

HEAT FLUX TO JT-60 FIRST WALLS

NORMAL CONDITION

- LINER---------- 10MW x 10SEC $100M^2$ · $10W/CM^2$
- FIXED LIMITER-- 10MW x 10SEC $3M^2$(1) $333W/CM^2$
- MAGNETIC-LIMITER PLATE-- 20MW x 5SEC $5.7M^2$(2) $350W/CM^2$

(1). HEAT FLUX DEPOSIT TO 3 TOROIDAL LIMITERS UNIFORMLY
(2). 10 CM WIDTH ON MLP

NBI PENETRATION

- LINER----------$1000W/CM^2$ x (LESS THAN 1 SEC)

RUNAWAY ELECTRON, DISRUPTION

- FIXED LIMITER, MAGNETIC LIMITER PLATE --- 10-100 KW/CM^2

TEMPERATURE OF FIRST WALLS AT NOMAL OPERATION

FIRST WALL	EQUILIBRIUM BASE TEMPERATURE	TRANSIENT TEMPERATURE RISE
LINER	100-200°C	~20°C
FL	500-1000°C*	600-800°C
MLP	~650°C	~500°C
	ΔT_1	ΔT_2

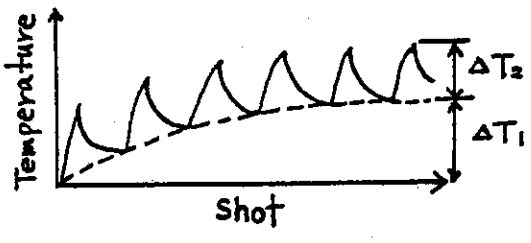

* To reduce this value to several hundreds °C, N_2 gas cooling is under design modification.

JT-60 FIRST WALL DEVELOPMENT PROGRAM

AT THE PRESENT SITUATION, SELECTION OF THE FIRST WALL MATERIALS SUITABLE FOR FUSION REACTOR IS DIFFICULT BECAUSE THE DETAILS OF REACTOR PLASMA CONDITIONS ARE NOT CLEAR.

THEREFORE, JT-60 FIRST WALL DEVELOPMENT PROGRAM IS DIVIDED INTO THE FOLLOWING TWO STAGES.

JT-60 FIRST WALL DEVELOPMENT PROGRAM

→ FIRST STAGE DEVELOPMENT

--------- DEVELOP THE FIRST WALL MATERIALS INTENDED TO IMPROVE THE PLASMA PARAMETERS, BY THE START OF JT-60 OPERATION.

→ SECOND STAGE DEVELOPMENT

--------- DEVELOP THE FIRST WALL MATERIALS WHICH ARE SUITABLE AND APPLICABLE TO FUSION REACTORS, CONSIDERING THE FIRST STAGE DEVELOPMENT RESULT.

WE DESCRIBE ONLY THE FIRST STAGE DEVELOPMENT PROGRAM, BECAUSE THE SECOND STAGE ONE HAS TOO MUCH UNCERTAINTIES TO DISCUSS AT PRESENT. THE SECOND STAGE ONE IS ONE OF THE SUBJECT FOR FUTURE STUDY.

SCHEDULE OF JT-60 FIRST WALL DEVELOPMENT PROGRAM

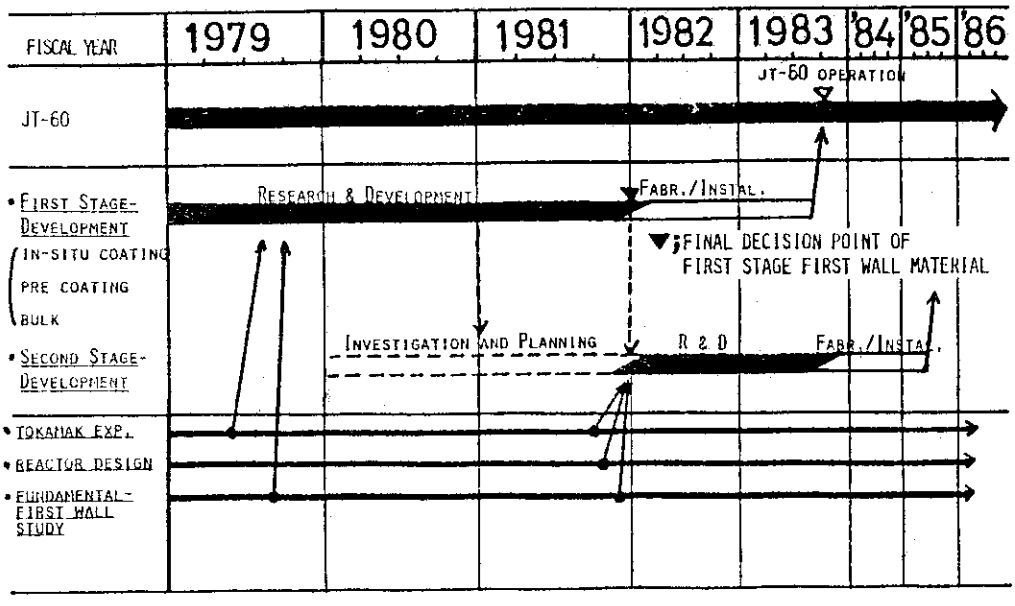

APLLICATION METHOD FOR FIRST STAGE DEVELOPMENT

I. IN-SITU COATING/Mo SUBSTRATE

II. PRE COATING/Mo SUBSTRATE

III. BULK

I,II COATING TECHNIQUE

A. PLASMA SPRAY
B. CHEMICAL VAPOR DEPOSITION (CVD)
C. EXPLOSION BONDING
D. PHYSICAL VAPOR DEPOSITION (PVD)

WE SELECTED PVD METHOD AS JT-60 FIRST WALL COATING METHOD IN THE FIRST STAGE DEVELOPMENT.

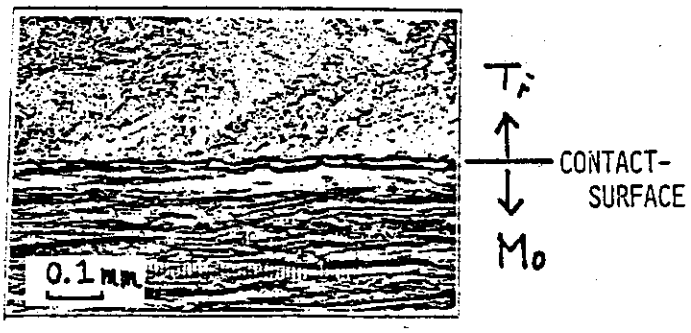

Ti/Mo CLAD MATERIAL BY EXPLOSION BONDING METHOD

- CRACKING IN Mo SUBSTRATE
- LOW ADHESION STRENGTH

PVD COATING PROCESS

1. VACUUM DEPOSITION------- · JOULE HEATING METHOD**
  (EX. Ti-BALL)
  · EB HEATING METHOD**
  · ARE METHOD*

2. SPUTTER DEPOSITION------ · MAGNETRON SPUTTER**
  (CO-AXIAL TYPE)

3. ION PLATING ------------ · RF ION PLATING*
  · HOLLOW CATHODE DISCHARGE*

* PRE COATING

** IN-SITU COATING, PRE COATING

SUITABLE PROCESS TO JT-60 FIRST WALL COATING WILL BE SELECTED AFTER THE SCREENING TESTS.

- ADHESION TEST(MECHANICAL TEST, THERMAL SHOCK TEST, THERMAL FATIGUE TEST)
- PHYSICAL SPUTTERING MEASUREMENT
- CHEMICAL SPUTTERING MEASUREMENT
- LIMITER EXPERIMENT IN TOKAMAK
- SURFACE CLEANING
- STABILITY IN PLASMA CONDITION

FIRST STAGE DEVELOPMENT (IN-SITU AND PRE COATING)

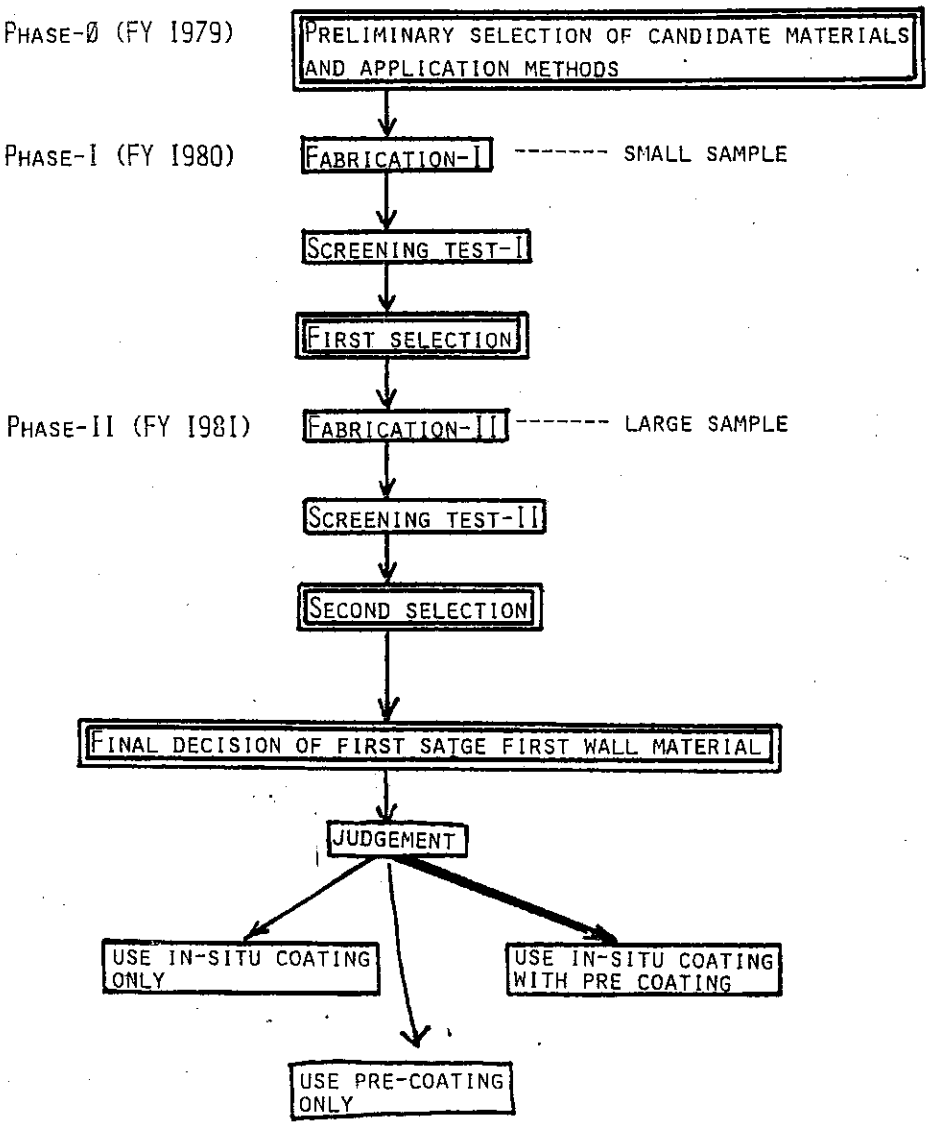

PRELIMINARY SELECTION OF CANDIDATE MATERIALS FOR THE FIRST STAGE FIRST WALL DEVELOPMENT

THE SELECTION OF CANDIDATE MATERIALS ARE BASED ON LARGELY ON THE FOLLOWING PROPERTIES.

- ATOMIC NUMBER
- MELTING POINT
- VAPOR PRESSURE
- THERMAL CONDUCTIVITY (BULK)
- PHYSICAL SPUTTERING YIELD
- CHEMICAL SPUTTERING YIELD

MATERIALS WHICH WERE USED IN THE TOKAMAK LIMITER EXPERIMENTS
OR INVESTIGATED IN THE FUNDAMENTAL FIRST WALL MATERIAL STUDIES

Atomic number		4	5	6	13	14	22	23	26	28
Single element		Be	B	C	Al	(Si)	Ti	V	Fe *	Ni**
Compound	Carbide	Be_2C	B_4C			SiC	TiC	VC		
	Nitride		BN		AlN	Si_3N_4	TiN	VN		
	Boride						TiB_2	VB_2		
	Oxide	BeO			Al_2O_3					

* FE IS REPRESENTATIVE OF STAINLESS STEEL

** NI IS REPRESENTATIVE OF INCONEL ALLOY

→ CANDIDATE FIRST WALL MATERIALS IN FIRST STAGE DEVELOPMENT

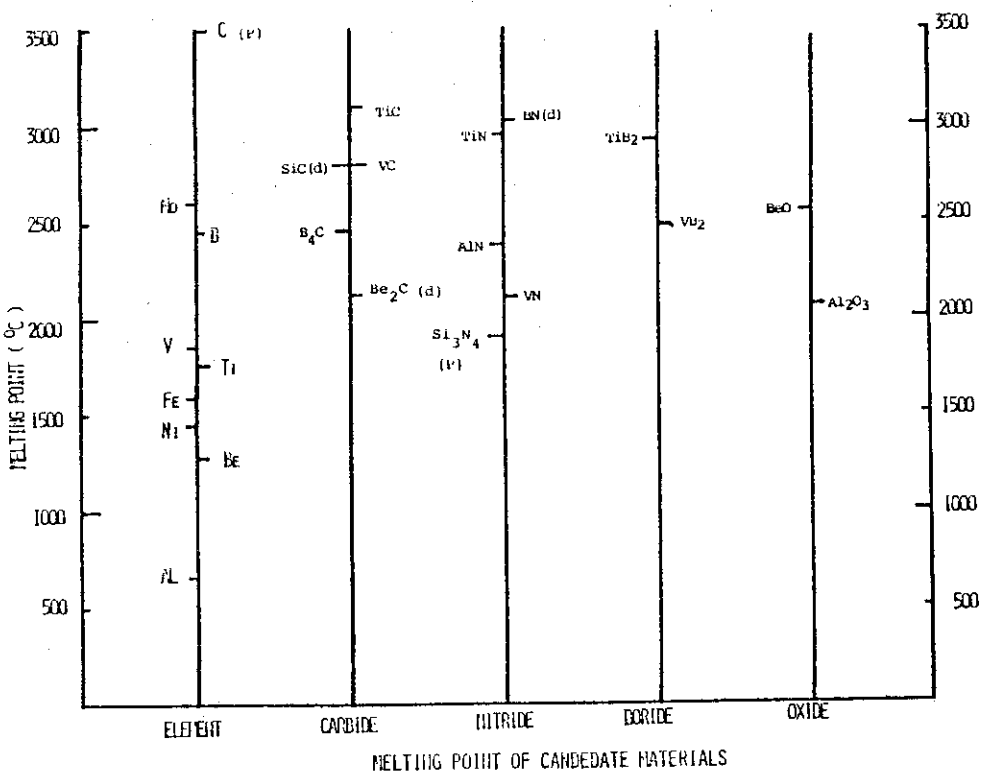

MELTING POINT OF CANDIDATE MATERIALS

VAPOR PRESSURE

TEMPERATURE WHICH VAPOR PRESSURE EXCEED 10^{-5}Torr

MATERIALS	TEMPERATURE ($^{\circ}$C)
Be	897
Be_2C	1100
BeO	1700
B	1637
B_4C	1800
BN	1280
C	1997
Al	902
SiC	1687
Si_3N_4	950
Ti	1317
TiC	1847
TiN	1427
TiB_2	1767

MATERIAL ⟶ THE TEMPERATURE WHICH VAPOR PRESSURE EXCEED 10^{-5}Torr IS HIGHER THAN 1500°C.

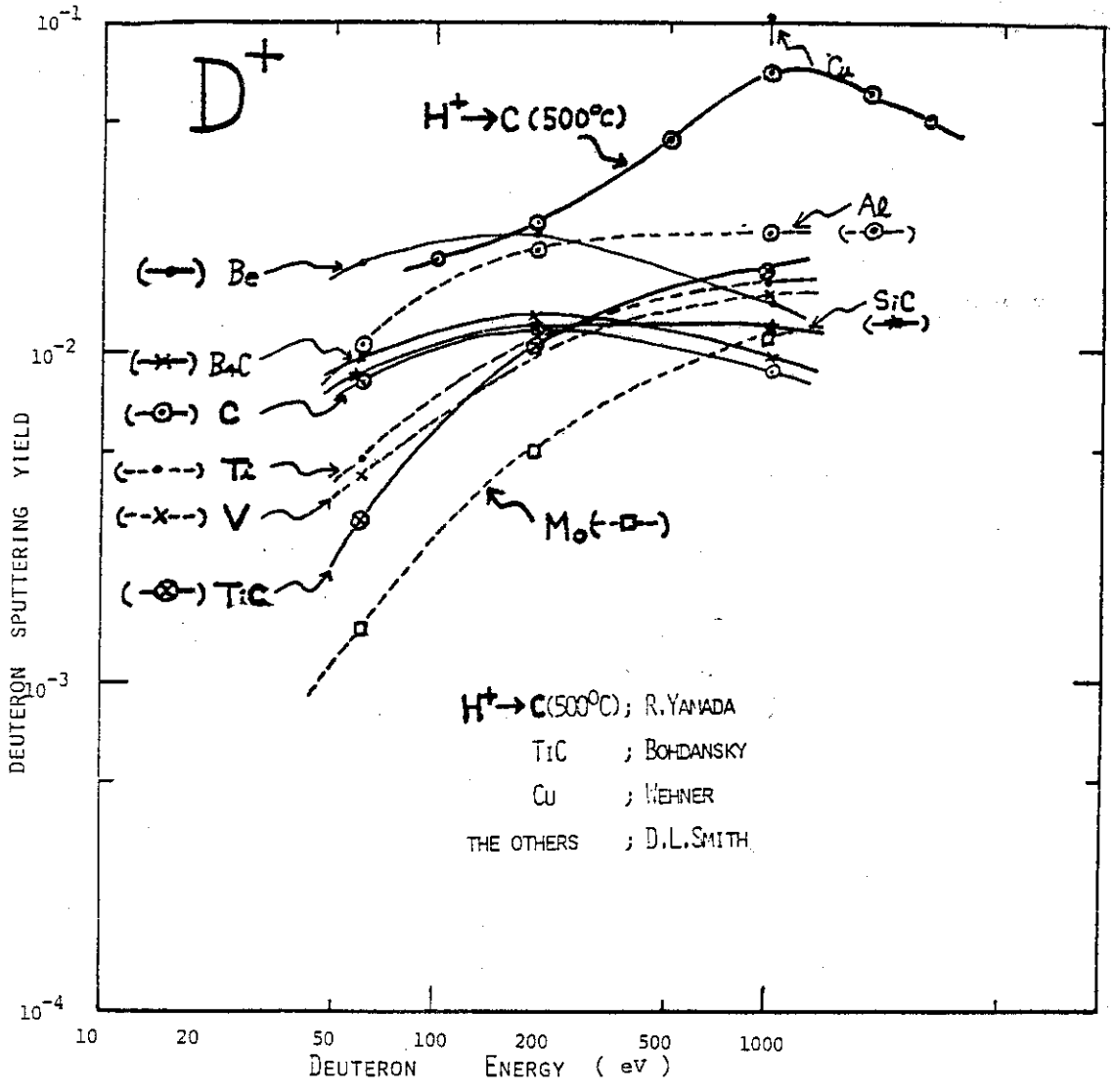

MAXWELLIAN AVERAGED SPUTTERING YIELD

THE DATA OF D.L.SMITH——THE INTEGRATED PHYSICAL SPUTTER YIELDS OF INTEREST HAVE BEEN OBTAINED BY AVERAGING THE CALCULATED MONO-ENERGETIC SPUTTER YIELDS WITH A MAXWELLIAN DISTRIBUTION OF INCIDENT-PARTICLE ENERGIES.

FOM VALUE

$$\text{FOM VALUE} = \frac{\text{CRITICAL IMPURITY CONCENTRATION}}{\text{SPUTTERING YIELD}}$$

CRITICAL IMPURITY CONCENTRATION

THE VALUE AT 7 KeV BY K.V.JENSEN PPPL-1350(1977)

MAXIMUM ALLOWABLE IMPURITY CONCENTRATIONS FOR IGNITION OF A D-T PLASMA AS A FUNCTION OF THE PLASMA TEMPERATURE, ASSUMING ZERO RADIATION LOSS

SPUTTERING YIELD

THE VALUE OF DEUTERON SPUTTERING

BY D.L.SMITH J.NUCL.MATER. 75(1978)20

MAXWELLIAN AVERAGED SPUTTERING YIELD

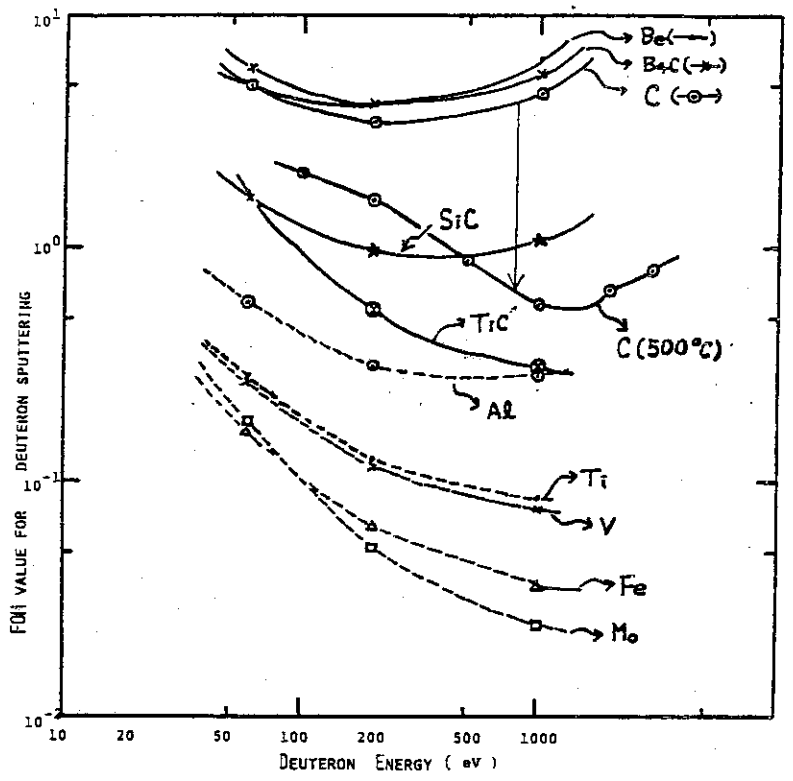

RATIO OF CRITICAL IMPURITY CONCENTRATIONS OVER SPUTTERING YIELDS VERSUS DEUTERON ENERGY OF THE INCIDENT DEUTERON

$$\text{FOM VALUE} = \frac{\text{CRITICAL IMPURITY CONCENTRATIONS}}{\text{SPUTTERING YIELD}}$$

III. BULK TECHNIQUE

IN BULK METHOD, PYROLYTIC GRAPHITE IS ONE OF THE ATTRACTIVE MATERIALS FROM THE VIEWPOINT OF THERMAL PROPERTIES BECAUSE OF ITS HIGH THERMAL CONDUCTIVITY ALONG THE BASAL PLANE.

HOWEVER, CONSIDERABLE DEVELOPMENT IS NEEDED FOR SUITABLE STRUCTURE OF PYG LIMITERS OR MAGNETIC LIMITER PLATES.

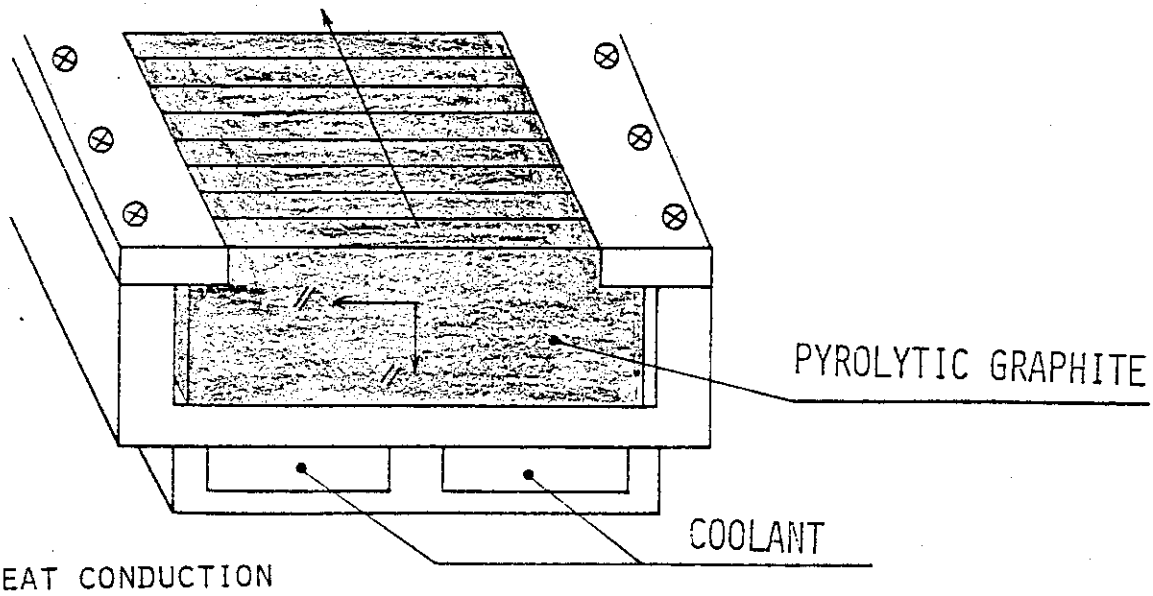

//; HIGH HEAT CONDUCTION PLANE

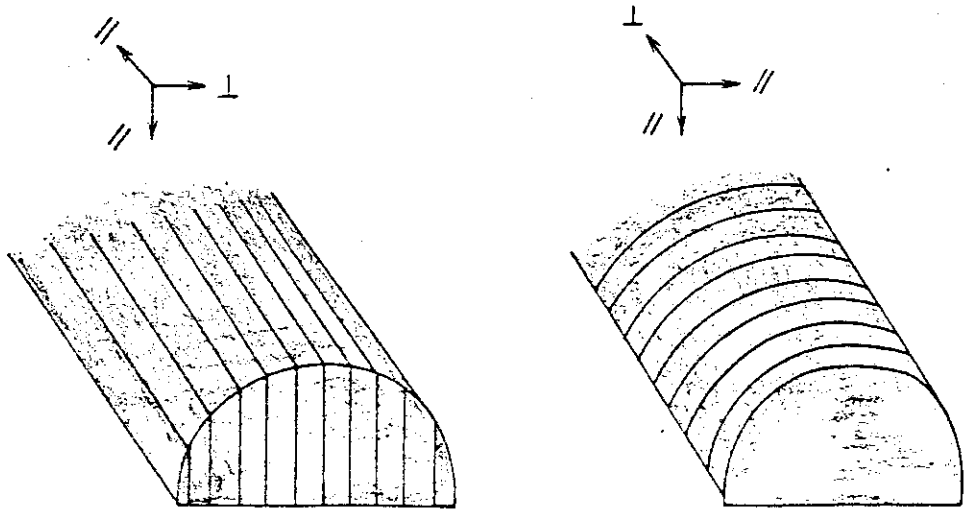

Type A Type B

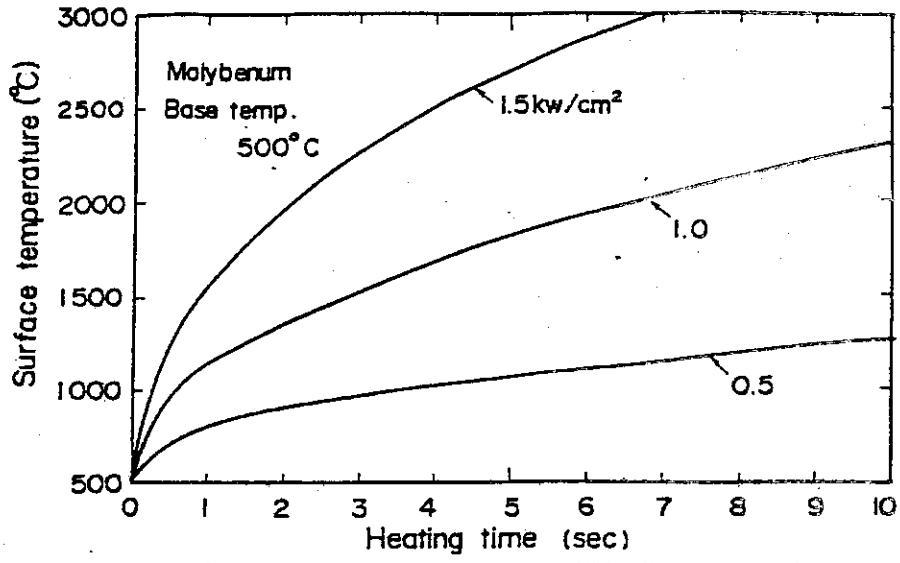
Molybenum
Base temp.
500°C
1.5kw/cm²
1.0
0.5
Surface temperature (°C)
Heating time (sec)

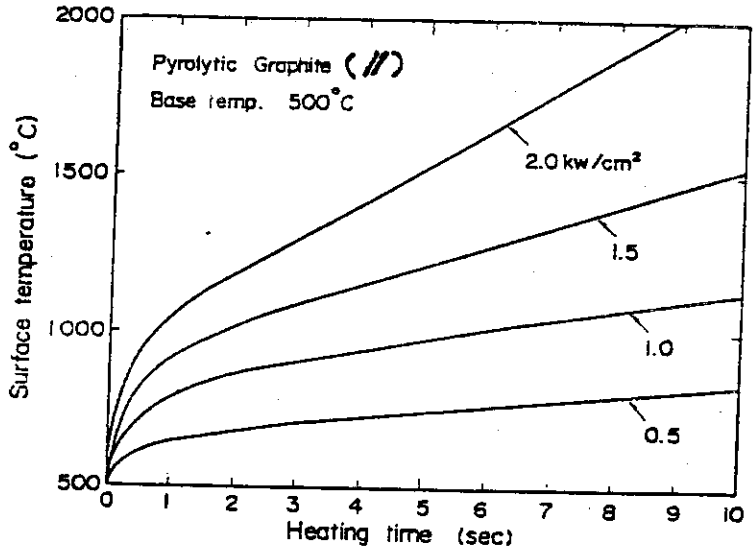
Pyrolytic Graphite (//)
Base temp. 500°C
2.0 kw/cm²
1.5
1.0
0.5
Surface temperature (°C)
Heating time (sec)

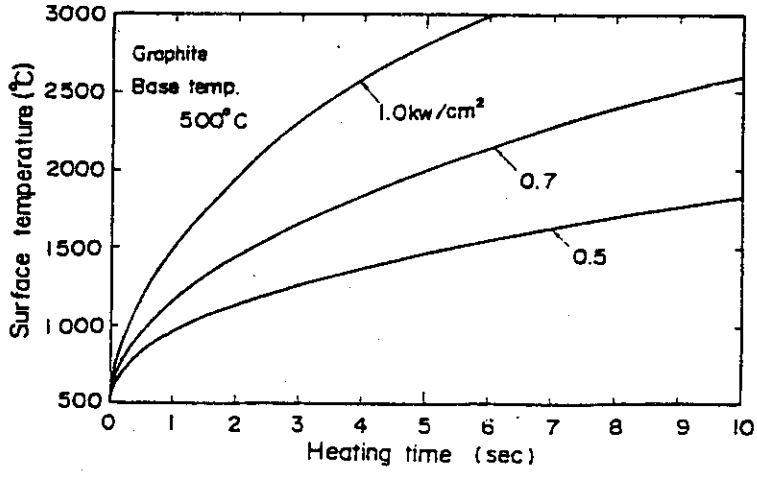
Graphite
Base temp.
500°C
1.0kw/cm²
0.7
0.5
Surface temperature (°C)
Heating time (sec)

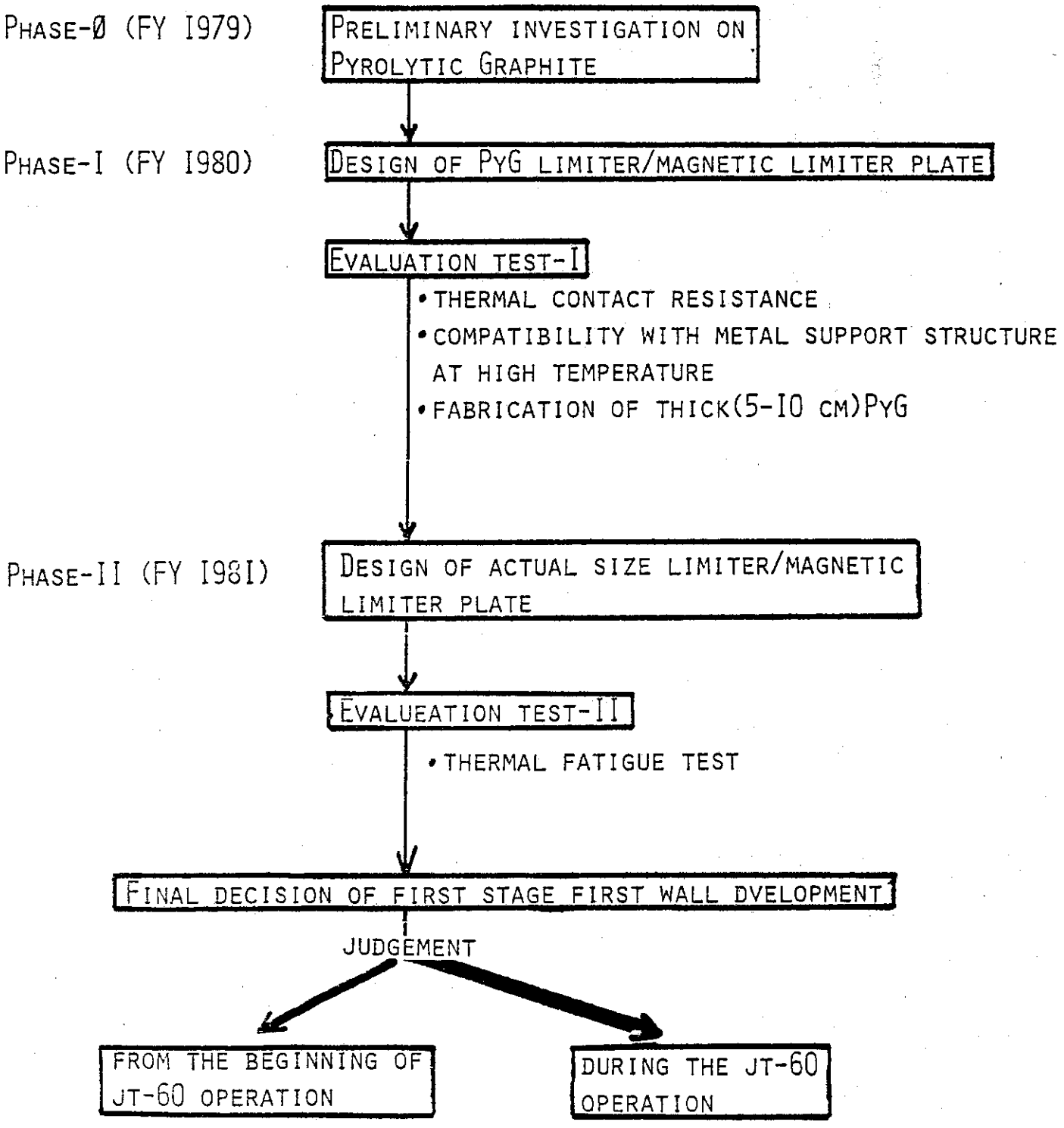
FIRST STAGE DEVELOPMENT (BULK)
PHASE-Ø (FY 1979)
PRELIMINARY INVESTIGATION ON PYROLYTIC GRAPHITE
PHASE-I (FY 1980)
DESIGN OF PyG LIMITER/MAGNETIC LIMITER PLATE
EVALUATION TEST-I
• THERMAL CONTACT RESISTANCE
• COMPATIBILITY WITH METAL SUPPORT STRUCTURE AT HIGH TEMPERATURE
• FABRICATION OF THICK(5-10 CM)PyG
PHASE-II (FY 1981)
DESIGN OF ACTUAL SIZE LIMITER/MAGNETIC LIMITER PLATE
EVALUEATION TEST-II
• THERMAL FATIGUE TEST
FINAL DECISION OF FIRST STAGE FIRST WALL DVELOPMENT
JUDGEMENT
FROM THE BEGINNING OF JT-60 OPERATION
DURING THE JT-60 OPERATION

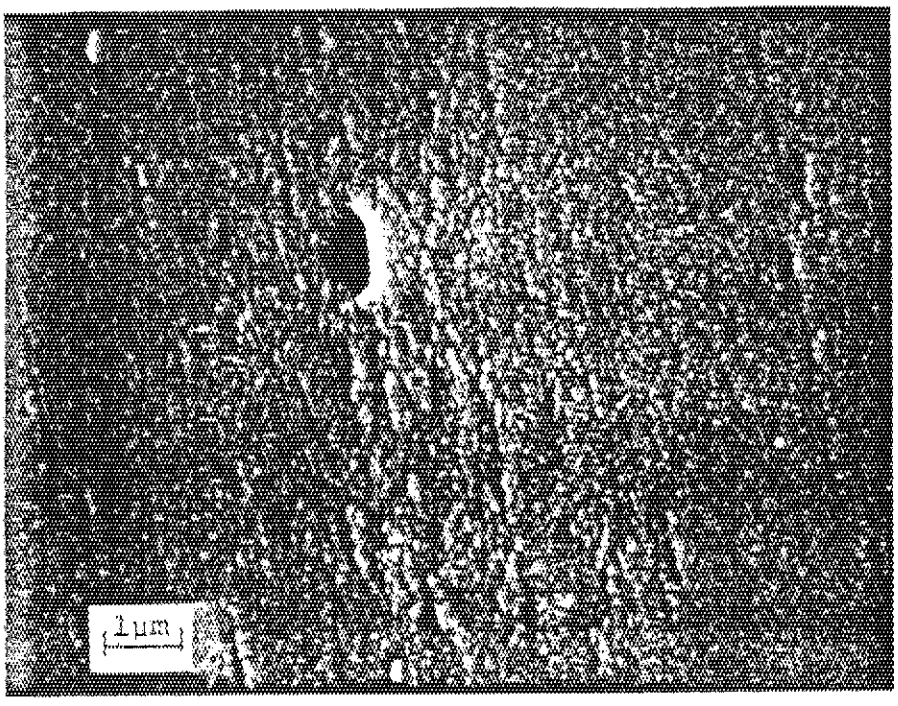

SEM PICTURE OF CARBON COATING SURFACE PRODUCED BY CO-AXIAL MAGNETRON RF SPUTTERING

(350°C BAKING, Ar PRE-BOMBARDMENT)

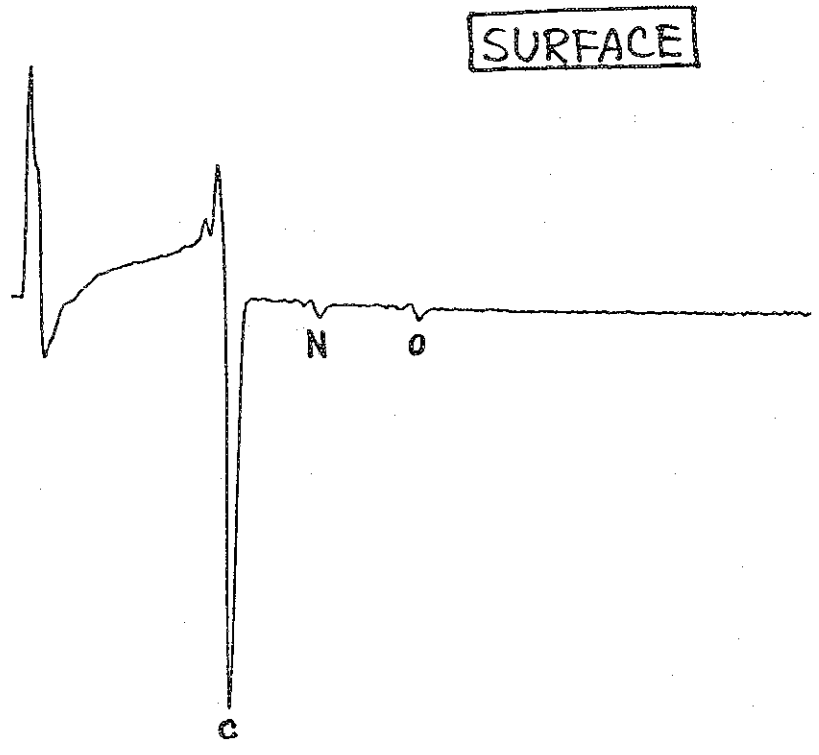

CLOSING

M. Tanaka (JAERI)
E. Oktay (DOE)

Now we have completed all the scheduled agenda of the workshop Before closing I would like to ask Dr. Oktay of DOE to give us a few minutes talk.

Dr. Oktay's speech*

In framing the agenda of the present workshop, we, Dr. Murakami of JAERI and myself, did not prepare any special summary talk. However Dr. Oktay just gave us a nice summary, which indicates also key issues in this area remained to be pursued in coming dates. I would like to add some remarks now.

Impurity control in fusion device has been recognized as a key problem to improve the plasma parameters toward ignition. Several methods to reduce the impurity content in the plasma have been proposed and tested especially in tokamak devices. I can say steady progress both in physics and technoloty has been made in recent years.

As an example I would like to mention here on divertors. The pioneer works on DIVA at JAERI and DITE at Culham have revealed many significant findinds on the function of divertors in tokamak device, and also on the underlying physics of the scrape-off plasmas. On the basis of these experiments divertor concepts feasible for INTOR or ETF like device are now actively discussed. Of course the tests should be continued on more large and powerful plasmas. These are now carried out or scheduled on PDX and ISX-B in United States and also ASDEX in Federal Republic of Germany.

Here in Japan DIVA was shutdowned last year and there exist no device with divertor at present time. We have to wait the start of the JT-60 operation more than four years. I would like remind you that the JT-60 program has put a special emphasis on impurity study, namely the magnetic limiter and long pulse discharge.

In this connection I have also to mention on the Heliotron E device of Kyoto University, which is, as you know, a torsatron stellarator with

* To our regret we could not reproduce here (M.T. & Y.M.)

built-in helical divertor. I had asked Professor Iiyoshi to deliver a talk at the present workshop. To my regret the device is now under the final test and he could not participate in the workshop.

Anyway Heliotron E will be only device with divertor in Japan for coming few years until JT-60 operates. Therefore I sincerely hope more close collaboration with United States, which operates PDX, ISX-B, and also Doublet III. Namely personnel exchange, workshop like this and others. I believe these collaborations will be quite beneficial for both sides.

Finally Dr. Murakami and myself deeply appreciate the collaborations of all the participants as well as administration staff of STA and JAERI. in carrying out the present workshop successfully. Dr. Oktay of DOE, Professor Miyahara of IPP, and Dr. Yoshikawa of JAERI provided helpful advices in framing the workshop. The speakers summarized their works nicely in limited time , the participants join in active discussions. Thank you for your collaboration.

LIST OF PARTICIPANTS

US

T. Jernigan	- Oak Ridge National Laboratory
R. A. Langley	- Oak Ridge National Laboratory
D. M. Meade	- Princeton Plasma Physics Laboratory
E. Oktay	- US Department of Energy
J. Ulrickson	- Princeton Plasma Physics Laboratory
T. Yang	- Massachusetts Institute of Technology

Japan

T. Abe	- JAERI
K. Akaishi	- IPP, Nagoya
T. Amano	- Osaka Univ.
T. Aochi	- JAERI
T. Asaoka	- JAERI
Y. Ato	- IRI, Nagoya
K. Doi	- JAERI
N. Fujishima	- STA
K. Fukutomi	- NRIM
A. Funahashi	- JAERI
Y. Gomay	- Toshiba
Y. Hamaguchi	- JAERI
R. Hasiguti	- Science Univ. of Tokyo
K. Harada	- JAERI
K. Hayashi	- Nagoya Univ.
T. Iijima	- JAERI
K. Inoue	- JAERI
N. Inoue	- Univ. of Tokyo
T. Iwata	- JAERI
K. Kamada	- JAERI
T. Kawamura	- IPP, Nagoya
A. Kinbara	- Univ. of Tokyo
H. Kitahara	- ANELVA Corp.

List of Participants (Cont'd)

S. Komiya	- ULVAC Corp.
T. Kondo	- JAERI
Y. Kurihara	- STA
Y. Maejima	- ETL
A. Miyahara	- IPP, Nagoya
K. Miyamoto	- Univ. of Tokyo
M. Mohri	- Hokkaido Univ.
H. Momota	- IPP, Nagoya
K. Mori	- IPCR
S. Mori	- JAERI
K. Morita	- Nagoya Univ.
Y. Murakami	- JAERI
R. Nagasaki	- JAERI
Y. Nakai	- JAERI
H. Nakamura	- JAERI
N. Noda	- IPP, Nagoya
Y. Obata	- JAERI
K. Ogawa	- ETL
M. Ohta	- JAERI
M. Okada	- NRIM
K. Okamoto	- ULVAC Corp.
T. Oku	- JAERI
M. Ono	- ETL
M. Saidoh	- JAERI
Y. Sakamoto	- IPCR
K. Sako	- JAERI
Y. Seki	- JAERI
S. Sengoku	- JAERI
T. Shikama	- NRIM
J. Shimokawa	- JAERI
Y. Shimomura	- JAERI
K. Shiraishi	- JAERI
M. Sugihara	- JAERI
S. Takamura	- Nagoyo Univ.
T. Takizuka	- JAERI
T. Tamaru	- ETL

List of Participants (Cont'd)

M. Tanaka	- JAERI
Y. Tanaka	- JAERI
G. Tominaga	- Univ. of Tokyo
H. Toyama	- Univ. of Tokyo
Y. Tuzi	- Univ. of Tokyo
M. Wakatani	- Kyoto Univ.
R. Yamada	- JAERI
S. Yamamoto	- JAERI
M. Yoshikawa	- JAERI

ETL: Electrotechnical Laboratory
IPCR: Institute of Physical and Chemical Research
IPP, Nagoya: Institute of Plasma Physics, Nagoya University
IRI, Nagoya: Industrial Research Institute, Nagoya
JAERI: Japan Atomic Energy Research Institute
NRIM: National Research Institute for Metals
STA: Science and Technology Agency